Improved modelling of disperse multi-phase transport based on numerical simulation and PDF analysis

Christopher Stafford

School of Engineering

Newcastle University

September 2020

Submitted in partial fulfilment for

the degree of Doctor of Philosophy

To my parents

"These motions were such as to satisfy me, after frequently repeated observation, that they arose neither from currents in the fluid, nor from its gradual evaporation, but belonged to the particle itself."

[Summary of Brownian motion]
— **Robert Brown**

Abstract

In this work probability density function (PDF) models are used as a method for studying the statistical distribution of particles in turbulent flows, which is of interest in many industrial and environmental processes. This approach involves derivation of a transport equation for describing the evolution of the joint PDF of particle variables. In different flow configurations the PDF approach identifies various contributions to the particle phase mass flux that act as additional drift and diffusion terms. These terms, which are critical in the formulation of two-fluid models, require closure. In order to evaluate the effect of the different flux contributions arising in the various flow configurations, these terms are considered in the context of both homogeneous and inhomogeneous flows. In the case of homogeneous flows the enhancement of the settling rate of inertial particles under an applied body force, specifically gravity, is investigated. Inhomogeneous turbulence is used to study the clustering of particles in a framework associated with the behaviour of particle pair dynamics in homogeneous flows. Existing closures based on simple local approximations are shown to neglect the contributions of interest to the particle phase mass flux, and an improved methodology is proposed which takes into account underlying physical mechanisms behind the observed behaviour, and consists of modelling various correlations that arise from the PDF formulation. The performance of this closure strategy is evaluated making use of particle trajectory simulations in a synthetic flow field generated using Kinematic Simulation (KS). The Eulerian two-point, two-time fluctuating velocity correlations for the continuous phase are central to the modelling, and these are determined in the specification of the flow field. Similarly the particle response tensor to perturbations in the continuous phase is computed allowing for exact evaluation of the unclosed terms. A linear drag law is used in the particle equation of motion, and the influence of both Stokes number and applied body forces on the increase in particle settling rate and clustering is investigated. In agreement with previous work it is seen that the mechanism responsible for these effects can be quantified in terms of the preferential sampling of strain over rotation by inertial particles due to interaction with the structures in the flow field.

Acknowledgements

First and foremost I wish to express my gratitude to my supervisory team, to whom I am eternally grateful for providing me with the opportunity to pursue research in this area. In particular, the guidance from my principal supervisor Dr David Swailes has been invaluable throughout the course of this research. His sharp eye for detail, insight into the various problems encountered along the way, and continual encouragement to seek answers to the fundamental questions which arise have enabled me to develop a true appreciation for the modelling of dispersed particle transport. I am also very thankful for the support from my secondary supervisor Professor Nilanjan Chakraborty, both through sharing his expertise in numerical simulation and turbulence theory during the initial stages of the project, along with his assistance in facilitating access to the computational facilities required for undertaking this research.

Additionally, I would also like thank Professor Michael Reeks, with whom some enlightening discussions concerning the modelling aspects of this work have been very helpful. The continued morale and rapport of my colleagues in office T4 has been indispensable, and of course also the plentiful supply of refreshments; the constant offers of freshly ground coffee have in large part been responsible for my departure from being exclusively a tea drinker. Finally, I have to thank my family for their unconditional encouragement, belief, and support throughout my studies, without which I would not have been able to complete this research.

I further wish to acknowledge Newcastle University for providing the funding for this project, and the Rocket and Topsy High Performance Computing facilities on which the simulations in this work were carried out.

Contents

List of Figures

List of Tables

Nomenclature

Roman Characters

$2\mathcal{L}$ Length of the simulation domain in one coordinate direction

$\boldsymbol{c}(t)$ Particle fluctuating velocity

$\boldsymbol{r}_p(t';t)$ Spatial separation vector along particle trajectories, defined as $\boldsymbol{r}_p(t';t) = \mathbf{x} - \boldsymbol{x}_p(t')$

$\boldsymbol{v}_p(t)$ Inertial particle velocity

$\boldsymbol{x}_f(t)$ Fluid element trajectory

$\boldsymbol{x}_p(t)$ Inertial particle trajectory

$\boldsymbol{z}(t)$ Phase-space trajectory

$\boldsymbol{\mathcal{B}}$ Uniform simulation domain 'box'

$\boldsymbol{\mathcal{G}}[t;t']$ Phase-space response tensor

$\boldsymbol{\mathcal{H}}[t;t']$ Particle response tensor

$\boldsymbol{\mathcal{J}}(\mathbf{x}^0,t)$ Jacobian of the Eulerian-Lagrangian transformation

$\boldsymbol{\mathcal{V}}(\mathbf{x},t)$ Particle velocity field

$\mathbf{a}(\boldsymbol{\xi},t)$ Phase-space deterministic mean field

$\mathbf{b}(\boldsymbol{\xi},t)$ Phase-space zero-mean stochastic field

$\mathbf{D}(\boldsymbol{\xi},t)$ Phase-space diffusion tensor

$\mathbf{d}(\boldsymbol{\xi},t)$ Phase-space drift tensor

$\mathbf{F}(\mathbf{x},\mathbf{v},t)$ Mean particle acceleration

$\mathbf{f}(\mathbf{x},t)$ Zero-mean fluctuating particle acceleration

$\mathbf{g}$ Gravitational acceleration

$\mathbf{k}$ Fourier space modes

$\mathbf{K}^n$ n^{th} cumulant of a given probability distribution

$\mathbf{m}$ Mean of a given probability distribution

$\mathbf{n}$ Number of Fourier space modes used in each direction to generate the velocity field

$\mathbf{Q}(\mathbf{r})$ Eulerian two-point one-time fluid velocity correlation tensor

$\mathbf{R}(\mathbf{x}', t'; \mathbf{x}, t)$ Eulerian two-point two-time correlation tensor of the fluctuating particle acceleration $\mathbf{f}(\mathbf{x}, t)$

$\mathbf{r}$ Spatial separation vector in phase-space, defined as $\mathbf{r} = \mathbf{x}_2 - \mathbf{x}_1$

$\mathbf{U}(\mathbf{x}, t)$ Synthetic velocity field produced using kinematic simulation

$\mathbf{u}(\mathbf{x}, t)$ Continuous phase fluid velocity

$\mathbf{v}$ Fixed velocity in phase-space

$\mathbf{V}_g$ Stokes settling velocity vector

$\mathbf{w}(\mathbf{x}, t)$ Wiener process

$\mathbf{x}$ Fixed location in phase-space

$\mathcal{P}(\mathbf{x}, \mathbf{v}, t)$ Fine-grained joint PDF of particle position and velocity

$\mathrm{E}_\omega(s)$ Eulerian temporal decorrelation function for the velocity field

q Radial coordinate in the polar frame of reference

r Magnitude of separation between two points in physical space

$\overline{\mathbf{ccc}}(\mathbf{x}, t)$ Particle kinetic stress flux

$\overline{\mathbf{cc}}(\mathbf{x}, t)$ Particle kinetic stresses

$\overline{\mathbf{F}}(\mathbf{x}, t)$ Velocity averaged form of $\mathbf{F}(\mathbf{x}, \mathbf{v}, t)$

$\overline{\mathbf{v}}(\mathbf{x}, t)$ Mean particle velocity

A_p Projected cross sectional area of a particle in the direction of the relative velocity $|\mathbf{u} - \boldsymbol{v}_p|$

C_D Corrective drag coefficient

d Number of physical spatial dimensions ($\in \{2, 3\}$)

d_p Particle diameter

$f(\mathrm{r})$ Normalised longitudinal fluid velocity correlation coefficient

Fr Froude number

$g(\mathrm{r})$ Normalised transverse fluid velocity correlation coefficient

$J(\mathbf{x}^0, t)$ Elemental volume deformation along a particle trajectory

k Magnitude of Fourier space mode

L_{11} Longitudinal integral lengthscale

l_{ref} Reference lengthscale

m_p Mass of an individual particle

$p(\mathbf{x}, \mathbf{v}, t)$ Averaged joint PDF of particle position and velocity

P Continuous phase pressure

P_d Dispersed phase pressure

Re Continuous phase Reynolds number

Re_p Particle Reynolds number

Ro Rouse number

St Stokes number

u' Continuous phase root mean square velocity fluctuation

u_{ref} Reference velocity

V_g Stokes settling velocity

V_p Particle volume

m Turbulence structure parameter

Greek Characters

α_d Dispersed phase volume fraction

β Particle inertia parameter ($= \tau_p^{-1}$)

$\boldsymbol{\alpha}$ Rate scales representing the decorrelation timescales for the normalised fluctuating fluid velocity along particle trajectories

$\boldsymbol{\Gamma}(t)$ Standard Gaussian white-noise process

$\boldsymbol{\kappa}(\mathbf{x}, \mathbf{v}, t)$ Particle dispersion tensor for spatial convection

$\boldsymbol{\lambda}(\mathbf{x}, \mathbf{v}, t)$ Particle dispersion tensor for spatial diffusion

$\boldsymbol{\mu}(\mathbf{x}, \mathbf{v}, t)$ Particle dispersion tensor for velocity diffusion

$\boldsymbol{\Phi}(\mathbf{k})$ Velocity spectrum tensor

$\boldsymbol{\sigma}$ Continuous phase stress tensor

$\boldsymbol{\sigma}_d$ Dispersed phase stress tensor

$\boldsymbol{\tau}$ Continuous phase viscous stress tensor

$\boldsymbol{\tau}_d$ Dispersed phase viscous stress tensor

$\boldsymbol{\Theta}$ Covariance of a given probability distribution

$\boldsymbol{\Xi}(\mathbf{b}(\boldsymbol{\xi}^0, t_0))$ Initial distribution of the trajectory $\boldsymbol{z}(t_0)$

$\boldsymbol{\xi}$ Phase-space coordinate vector

Δk Fourier mode spacing

Δt Computational timestep

η Kolmogorov lengthscale

μ Continuous phase dynamic viscosity

μ_d Dispersed phase dynamic viscosity

$\overline{\boldsymbol{\kappa}}(\mathbf{x}, t)$ Velocity averaged form of $\boldsymbol{\kappa}(\mathbf{x}, \mathbf{v}, t)$

$\overline{\boldsymbol{\lambda}}(\mathbf{x}, t)$ Velocity averaged form of $\boldsymbol{\lambda}(\mathbf{x}, \mathbf{v}, t)$

$\overline{\boldsymbol{\mu}}(\mathbf{x}, t)$ Velocity averaged form of $\boldsymbol{\mu}(\mathbf{x}, \mathbf{v}, t)$

$\rho(\mathbf{x}, t)$ Averaged particle number density

ρ_f Continuous phase density

ρ_p Dispersed phase density

σ_k Magnitude of the Fourier modes corresponding to the peak of the energy spectrum $E(k)$

τ_η Kolmogorov timescale

τ_{eddy} Eddy turnover time

τ_E Eulerian fluid integral timescale

τ_f Characteristic response time of the continuous phase

τ_{Lp} Lagrangian fluid decorrelation timescale along inertial particle trajectories

τ_L Lagrangian fluid integral timescale along fluid element trajectories

τ_p Characteristic response time of the particle to changes in the local fluid velocity

θ Angular coordinate in the polar frame of reference

$\varrho\,(\mathbf{x}, t)$ Fine-grained particle number density

u_η Kolmogorov velocity scale

Other Symbols

$\langle\cdot\rangle$ Ensemble average taken over all realisations

$\langle\cdot\rangle_{\boldsymbol{z}=\boldsymbol{\xi}}$ Conditional ensemble average based on the subset of realisations for which $\boldsymbol{z}(t) = \boldsymbol{\xi}$

Subscripts

p Evaluation of a quantity along the inertial particle trajectory $(\boldsymbol{x}_p(t), \boldsymbol{v}_p(t))$

Superscripts

0 Initial value of a variable at time t_0

Acronyms / Abbreviations

AB4 Four-step explicit Adams-Bashforth method

AM3 Three-step implicit Adams-Moulton method

BBO Basset-Boussinesq-Oseen

BCM Box Counting Method

BIT Backward-in-Time

CFD Computational Fluid Dynamics

DNS Direct Numerical Simulation

FFT Fast Fourier Transform

FIT Forward-in-Time

FLM Full Lagrangian Method

FN Furutsu–Novikov

FRS Fully Resolved Simulation

GLM Generalised Langevin Model

HIT Homogeneous Isotropic Turbulence

HPC High Performance Computing

KM Kinetic Model

KS Kinematic Simulation

LES Large-Eddy Simulation

LHA Local Homogeneous Approximation

LHDI Lagrangian History Direct Interaction

MEF Mesoscopic Eulerian Formalism

PDF Probability Density Function

PSA Passive Scalar Approximation

PVF Particle Velocity Field

RANS Reynolds-Averaged Navier-Stokes

RDF Radial Distribution Function

RGT Random Galilean Transformation

RK4 Fourth-order Runge-Kutta method

RMS Root Mean Square

TKE Turbulent Kinetic Energy

Chapter 1

Introduction

1.1 Background

The transport of droplets and particles in turbulent flows is an area of considerable interest in the context of both engineering applications and scientific understanding, with widespread occurrences arising in natural and artificial systems in addition to the many theoretical questions which remain unanswered. The need for greater understanding of particle behaviour in both environmental and industrial applications encompasses situations including cloud formation in the atmosphere [138], particle transport in pipelines [131], spray combustion of fuel droplets [47], and atmospheric dispersion of emissions [136].

To better understand the physics involved in such processes, the study of particle transport in turbulence has evolved into an important research topic since the mid 20^{th} century. Almost without exception, the motion of disperse particles is highly dependent on the behaviour of the underlying fluid flow, meaning that the statistical treatment required for describing turbulence is also inherent in characterising the behaviour of particles within such flows [181]. Specifically, it is the various averaged quantities that are associated with particles in a given flow configuration that is of most interest, chief among which is the physical distribution of particles in space and how this evolves over time. Being able to accurately describe such statistics makes it desirable to investigate the behaviour of these multiphase flows within a general framework, and accordingly two distinct approaches have emerged to enable the development of accurate models for this purpose [90].

Firstly, development of a mathematical framework can be achieved by modelling the

Figure 1.1: Asperatus clouds demonstrating the interaction between the atmospheric conditions at different physical scales and the distribution of water droplets that constitute the cloud. Image credit and copyright: Witta Priester via NASA

particles as a continuum in a fixed Eulerian frame of reference, with average particle behaviour governed by transport equations which are analogous to those for the continuous phase (conservation of mass, momentum, energy, etc.). Such an approach is referred to as a *two-fluid model*, however due to the continuous phase not having a closed form mathematical solution in the context of turbulent flows, this is also the case for the corresponding particle phase transport equations. Consequently the two-fluid approach will result in unknown terms that require closure, which is subsequently addressed by further modelling.

The alternative method is *particle tracking*, which entails the modelling of individual particles within a moving Lagrangian frame of reference. Calculation of particle trajectories is possible by the numerical solution of the governing equation of motion in conjunction with the transport equations for the fluid velocity field. Due to the high variability of individual particle trajectories, many such realisations are needed in order

to achieve a sufficient ensemble size from which average particle statistics which are sufficiently noise-free can be obtained. As a result, particle tracking naturally lends itself to computational fluid dynamics (CFD) simulations, which can be performed using various methods that resolve the underlying fluid flow to different levels. Despite being conceptually simple, the limitation to particle tracking is the availability of computational resources and time which are needed in order to obtain a sufficient level of accuracy in simulations. The advance of modern high performance computing (HPC) facilities has seen the use of such simulations become increasingly feasible, and for research purposes it is currently possible to obtain a high level of detail within a reasonable amount of time by using particle tracking.

1.2 The Role of Computational Fluid Dynamics

Due to the closure problem which remains an inherent part of two-fluid models, the need arises for not only capturing the appropriate physical behaviour of particles in various flow configurations by developing accurate closures within a mathematical framework, but also a methodology for validating such closures. One approach is obtaining the true physical behaviour of a given flow from particle tracking simulations, which can be used to quantitatively assess closure strategies based upon how much of the observed particle behaviour they capture. The alternative to using simulations for these purposes is to make use of experimental data. Whilst this would arguably provide behaviour which can be considered more realistic physically, if the required data does not already exist it can be a time-consuming process to obtain it experimentally, due to the level of precision that is required to ensure that measurement errors which could compromise the validity of results are minimised. Furthermore, the ability to obtain experimental data for certain physical conditions can often be considerably more complicated than the equivalent computational approach. This demonstrates the efficacy of numerical simulation at both handling complex setups including geometry, boundary conditions, and physical interactions, and also providing the required data in a straightforward manner without the need for complicated measuring apparatus and procedures. For these reasons numerical simulation provides a suitable way of substantiating closure models, and has accordingly become the third means of investigation within scientific research alongside the traditional avenues of theory and experiment.

It is important to note however that even though numerical simulation provides a way of testing the capabilities of models developed using either theoretical or empirical

means, it does not guarantee that they are able to accurately represent the behaviour that is present in the full physical reality of a certain configuration. For this reason it is essential to validate the performance of models using data obtained from a rigorous experimental setup before true confidence in the accuracy of a model can be had, and scale-up to scientific and engineering applications can be done. Nonetheless, this does not detract from the usefulness of numerical simulation as an efficient means of model development, but highlights the need to ensure compatibility of the model with the environmental or industrial applications which it is intended to address.

1.3 Aims of the Current Work

One method of closure for two-fluid models is the use of probability density function (PDF) models [181, 97], which are a useful means of studying the statistical distribution of particles in a turbulent flow. In addition to their use in the modelling of single-phase fluid flows, PDF models provide a basis for constructing the transport equations for the particle phase of a two-fluid model, however due to the PDF description containing unclosed quantities these will also appear in the corresponding two-fluid model. The aim of the present work is to apply the PDF modelling approach to different flow configurations in order to identify various contributions that act as additional convection and diffusion terms, and are therefore critical in the formulation of two-fluid models.

The flow configurations under consideration in this study are simple cases of both homogeneous and inhomogeneous flow fields, which are constructed such that the contributions to the particle phase mass flux can be easily identified. In the case of homogeneous flows the enhancement to the settling rate of inertial particles under an applied body force, specifically gravity [91, 163], is the focus. Inhomogeneous turbulence is used to study the clustering of particles in a framework associated with the behaviour of particle pair dynamics in homogeneous flows, and notably the balance of forces upon particles which results in the radial distribution function [31, 179]. Existing closures based on both local [151, 127] and non-local [142, 13] approximations are shown to not adequately capture the contributions of interest to the particle phase mass flux, with the aim of the present work then being to propose improved closure methodologies which are able to include the characteristic behaviour of these terms based upon the underlying physical effects experienced by particles.

In addition to using specific flow configurations to more easily study the required contributions to the particle mass flux, this work also utilises simple physical representations

for both the flow field and the particles which contain enough information to study the desired phenomenon, but do not include all the physics that such systems would contain in reality. Specifically, the fluid flow is constructed as a synthetic flow field which is representative of the large scale motions of turbulence, and is taken to be Newtonian, isothermal, incompressible, isotropic, and statistically stationary. The particles are assumed to be small enough that their mass can be modelled as acting entirely at their centre of mass, and although this is a vast simplification of the various forces that would act non-uniformly over the particle surface in reality, the forces which are taken into account in this work are sufficient to reproduce the particle behaviour which is of interest. In this way the investigation of such simplified systems can be more easily approached, and understanding of the phenomenological behaviour in question developed, leading to the possibility of studying more realistic representations in the future.

To summarise, the main objectives of this research are to:

- Demonstrate through the use of numerical simulation that PDF models are capable of providing an exact representation of the contributions of interest in the particle phase mass flux
- Show that existing PDF model closures do not capture the behaviour of interest in the specific flow configurations used in this work
- Develop novel closure methodologies that account for the additional convective terms in the particle mass flux through consideration of non-local effects
- Analyse the PDF framework as applied to the flow configurations under consideration in order to further understand the underlying physics responsible for observed particle behaviour

1.4 Scope of the Thesis

This thesis is structured to introduce and review the essential concepts that underpin the research, followed by detail of the findings. Chapter 2 outlines various aspects of particle-laden flows including their classification, description of the carrier flow and the distinct approaches to simulation, description of the particle phase in both Lagrangian and Eulerian frameworks, and an overview of the different levels of coupling between the

phases. Chapter 3 reviews the current body of literature on the areas of interest in this work, specifically PDF modelling, settling of particles under gravity, particle clustering, and simulation approaches. Chapter 4 introduces the PDF kinetic model and its use in construction of the transport equations for the particle phase of a two-fluid model, and highlights the contributions of interest in this research. Chapter 5 presents the details of the simulation approach which is taken to numerically evaluate the terms of the PDF kinetic model, and details a novel method of initialising the particle velocities such that the particle phase statistics conform to their steady-state levels. Chapter 6 is focused upon the settling of inertial particles which are subject to a gravitational body force, and highlights the ability of the PDF kinetic model to describe the increase in particle settling velocity which is exhibited as a result of particle interaction with the turbulent structures in the fluid velocity field. Additionally, a symmetry analysis is conducted that shows which components of variables associated with the particle phase are non-zero, and a closure model is developed that is able to account for the increase in particle settling velocity. Chapter 7 considers the use of a particle velocity field for capturing the increase in particle settling velocity, and in particular the numerical treatment of the quantities that arise within this formulation. Chapter 8 deals with particle-pair models, and how through the construction of an appropriate inhomogeneous velocity field the PDF kinetic model is able to capture the additional convective flux terms which arise in this configuration, with the focus being upon how these contributions act to affect particle clustering. Chapter 9 summarises the findings of this research, and details further avenues of investigation.

Chapter 2

Fundamentals of Disperse Particle Transport

The objective of this research is to develop improved mathematical models for predicting the behaviour of inertial particles within different turbulent flow configurations. In order to achieve this, a thorough understanding of the fundamental physical processes which take place within these flows is required. An overview of the different types of flow regimes that exist is provided, followed by the governing equations used for describing turbulent flows. The approaches of particle tracking and two-fluid models are introduced and then compared, and the different levels of coupling that can be included between the two phases is detailed.

2.1 Classification of Multi-Phase Flow Regimes

Multi-phase transport encompasses many different types of flow, the classification of which is determined by factors including the separation between phases, Reynolds number and thermophysical particle properties [36]. Such flows can take on many forms with the separate phases being any of solid, liquid, gas, or even plasma [36], and are accordingly classified depending upon the form that the different phases take. If both phases are continuous and therefore separated by a line of contact, the flow is termed as a *separated* flow, an example of which is a stratified flow in which such separation occurs due to variation in density between the two phases. In contrast, if one phase consists of discrete elements that are not connected such as a collection of individual bubbles, droplets, or particles, this is referred to as a *dispersed* phase flow. It

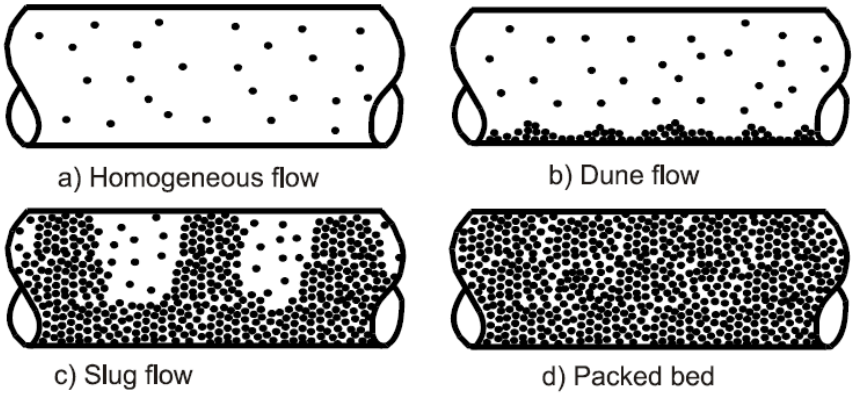

Figure 2.1: Different types of fluid-particle flow regimes, taken from [37]

is the latter type of flow which is the focus of this work, and in order to preserve clarity whilst keeping the phase mediums as arbitrary, the *continuous* phase is hereafter used to refer to the carrier flow of liquid or gas in which the dispersed phase elements are immersed.

Within the realm of dispersed phase flows, further general classification can be made depending upon the large-scale collective behaviour that is exhibited by bubbles, droplets, or particles, and this is most easily done within the context of pipe flow as illustrated in Figure 2.1 [37]. The simplest regime is a homogeneous particle flow (Figure 2.1(a)), in which the continuous phase velocity is high enough that the particles maintain an almost uniform distribution as a result of turbulent mixing. This sort of flow is termed as *dilute-phase transport*, and is characterised by the inter-particle spacing being relatively large, the energy expended by the fluid in moving the particles being very small, and the effect of collisions between particles considered as negligible. A lower fluid velocity in the case of pipe flow can result in some particles collecting on the pipe surface, with this being referred to as *dune* flow (Figure 2.1(b)). With decreasing fluid velocity or an increased particle loading, the particles building up on the side of the pipe fill more of the pipe surface area, and the next distinct classification is made where alternate regions exist in which some particles have deposited whilst other particles are still in suspension within the fluid, which is known as *slug* flow (Figure 2.1(c)). The final phenomenon of note is the case in which particles almost completely fill the pipe, and is known as a *packed bed* (Figure 2.1(d)). The latter two cases represent examples of *dense-phase transport*, where the inter-particle spacing is very low, a large proportion of energy is used by the fluid in moving particles, and the effect of collisions between particles is significant.

The classifications in Figure 2.1 serve to highlight the strong dependence of the dispersed phase on the concentration of bubbles, droplets or particles within the flow, and pertaining to that a key metric for differentiating between these different types of flow regime is the *volume fraction* of the dispersed phase, defined as [37, p. 18]

$$\alpha_d = \lim_{\delta V \to \delta V^0} \frac{\delta V_d}{\delta V} \tag{2.1}$$

where δV_d is the volume of the dispersed phase within the volume δV, and the volume δV^0 is the limiting volume which ensures a stationary average. In practice, dilute-phase transport is considered to be flows with a volume fraction of $\alpha_d < 10^{-3}$, whilst dense-phase transport is a volume fraction of $\alpha_d > 10^{-3}$. For a more detailed classification of particle-laden turbulent flows in terms of the volume fraction see section 2.4.

2.2 Description of the Continuous Phase

2.2.1 Governing Equations

For a complete description of the continuous phase, by considering the full dynamics of the carrier flow it is possible to derive a set of governing equations that determine the evolution of this phase. Such a procedure yields the continuity and momentum conservation equations of a fluid, for which different representations are available in both conservation and non-conservation forms depending on whether they are derived in a fixed Eulerian framework or moving along a fluid streamline in a Lagrangian sense [2]. In this instance the continuous phase is considered in an Eulerian framework, and further restricting to the case of an incompressible medium, this approach gives the equations for conservation of mass and momentum for a fluid of constant density as

$$\nabla \cdot \mathbf{u} = 0 \tag{2.2}$$

$$\frac{\partial \mathbf{u}}{\partial t} + (\mathbf{u} \cdot \nabla)\,\mathbf{u} = \frac{1}{\rho_f} \nabla \cdot \boldsymbol{\sigma} + \mathbf{g} \tag{2.3}$$

where $\mathbf{u}(\mathbf{x}, t)$ is the continuous phase velocity, ρ_f is the continuous phase density (constant), $\boldsymbol{\sigma}(\mathbf{x}, t)$ is the continuous phase stress tensor describing the surface forces of the fluid, and $\mathbf{g}$ is the gravitational acceleration. If other body forces such as electric or magnetic fields act upon the continuous phase, then appropriate source terms can

be added onto the momentum equation in a similar manner to gravitational acceleration. Furthermore, the effect that the dispersed phase has on the continuous phase can also be treated in this manner, with the effective point force of each particle on the fluid being incorporated as an additional source term within the momentum equation (see section 2.4). The stress tensor $\boldsymbol{\sigma}$ can be decomposed into pressure and viscous contributions [120]

$$\boldsymbol{\sigma} = -P\mathbf{I} + \boldsymbol{\tau} \tag{2.4}$$

where P is the continuous phase pressure, and $\boldsymbol{\tau}$ is the continuous phase viscous stress tensor. For an incompressible and isothermal Newtonian fluid the latter is defined as [167]

$$\boldsymbol{\tau} = \mu\left(\nabla\mathbf{u} + \nabla\mathbf{u}^{\top}\right) \tag{2.5}$$

where μ is the dynamic viscosity of the continuous phase. This results in the momentum equation (2.3) taking the form

$$\frac{\partial\mathbf{u}}{\partial t} + (\mathbf{u}\cdot\nabla)\,\mathbf{u} = -\frac{1}{\rho_f}\nabla P + \frac{\mu}{\rho_f}\nabla^2\mathbf{u} + \mathbf{g} \tag{2.6}$$

Equation (2.2) represents the volume continuity condition of an incompressible flow, whilst equation (2.6) is the Navier-Stokes equation governing the momentum of the flow. The solutions of these equations determine the underlying behaviour of the continuous phase within a multiphase flow, however analytical solutions can only be obtained for relatively simple flows such as a laminar regime, where no turbulent structures exist within the flow [167]. Proof of the existence and uniqueness of general solutions to the Navier-Stokes equations is a long standing unsolved problem of mathematical analysis, although it is widely accepted in the scientific and engineering communities that these equations are universally applicable to describing the behaviour of all fluid flows. In the case of turbulent flows the Navier-Stokes equations do not admit closed-form solutions, meaning that the alternative approach of numerical simulation must be taken to obtain an approximation for the continuous phase.

Non-dimensional Form

For clarity of working, equations (2.2) and (2.6) can be put into non-dimensional form with respect to appropriate reference values. The form adopted here uses a reference lengthscale l_{ref} and velocity u_{ref}, leading to the following definitions for the non-dimensional variables

$$\hat{\mathbf{x}} = \frac{\mathbf{x}}{l_{\text{ref}}} \quad , \quad \hat{\mathbf{u}} = \frac{\mathbf{u}}{u_{\text{ref}}} \quad , \quad \hat{t} = \frac{t\, u_{\text{ref}}}{l_{\text{ref}}} \quad , \quad \hat{P} = \frac{P}{\rho_f\, u_{\text{ref}}^2} \quad , \quad \hat{\mathbf{g}} = \frac{\mathbf{g}}{|\mathbf{g}|} \tag{2.7}$$

Application of the above transforms the governing equations for the continuous phase into the following non-dimensional form

$$\hat{\nabla} \cdot \hat{\mathbf{u}} = 0 \tag{2.8}$$

$$\frac{\partial \hat{\mathbf{u}}}{\partial \hat{t}} + \left(\hat{\mathbf{u}} \cdot \hat{\nabla}\right) \hat{\mathbf{u}} = -\hat{\nabla}\hat{P} + \frac{1}{Re}\hat{\nabla}^2\hat{\mathbf{u}} + \frac{\hat{\mathbf{g}}}{Fr^2} \tag{2.9}$$

where Re is the continuous phase *Reynolds number*, defined as

$$Re = \frac{\rho_f\, u_{\text{ref}}\, l_{\text{ref}}}{\mu} \tag{2.10}$$

which is a dimensionless quantity representing the ratio of inertial to viscous forces within the continuous phase, and is of importance as it quantifies the intensity of turbulence. The quantity Fr is the *Froude number*, defined as

$$Fr = \frac{u_{\text{ref}}}{\sqrt{|\mathbf{g}|\, l_{\text{ref}}}} \tag{2.11}$$

which is a dimensionless quantity defined as the ratio of inertial forces within the continuous phase to the magnitude of the gravitational body force.

2.2.2 Overview of Simulation Methods

Although the Navier-Stokes equations (2.2) and (2.6) fully describe the dynamics of an incompressible isothermal Newtonian fluid flow, the absence of analytical solutions for an arbitrary flow necessitates the use of approximations, and in the case of turbulent flows numerical solution has become the only viable method of treatment. In order to numerically prescribe the fluid flow field there are a range of alternative approaches which can be used, and these differ in the degree of physical refinement of the flow, leading to various levels of complexity and computational requirements. Due to the omission of a certain level of detail that characterises some approaches, the resulting governing equations are unclosed and require modelling in order to be fully specified,

which is often intricately involved with the details of solving the continuous phase numerically.

The distinction between the various methods of simulation for the Navier-Stokes equation is the level to which the scales that are inherent within the flow are resolved. This is more precisely expressed in terms of the turbulent kinetic energy spectrum $E(k)$ and the range of the wavenumber magnitude k which is taken into account, with higher wavenumbers corresponding to smaller physical lengthscales of the flow. By sampling only a certain range of the larger wavenumbers, large-scale motions are accounted for whilst the detail at smaller scales is not directly represented and must be otherwise accounted for by modelling, reducing the computational requirements accordingly. The key simulation types are described in order of decreasing level of resolution within the flow, with reference to Figure 2.2 [3].

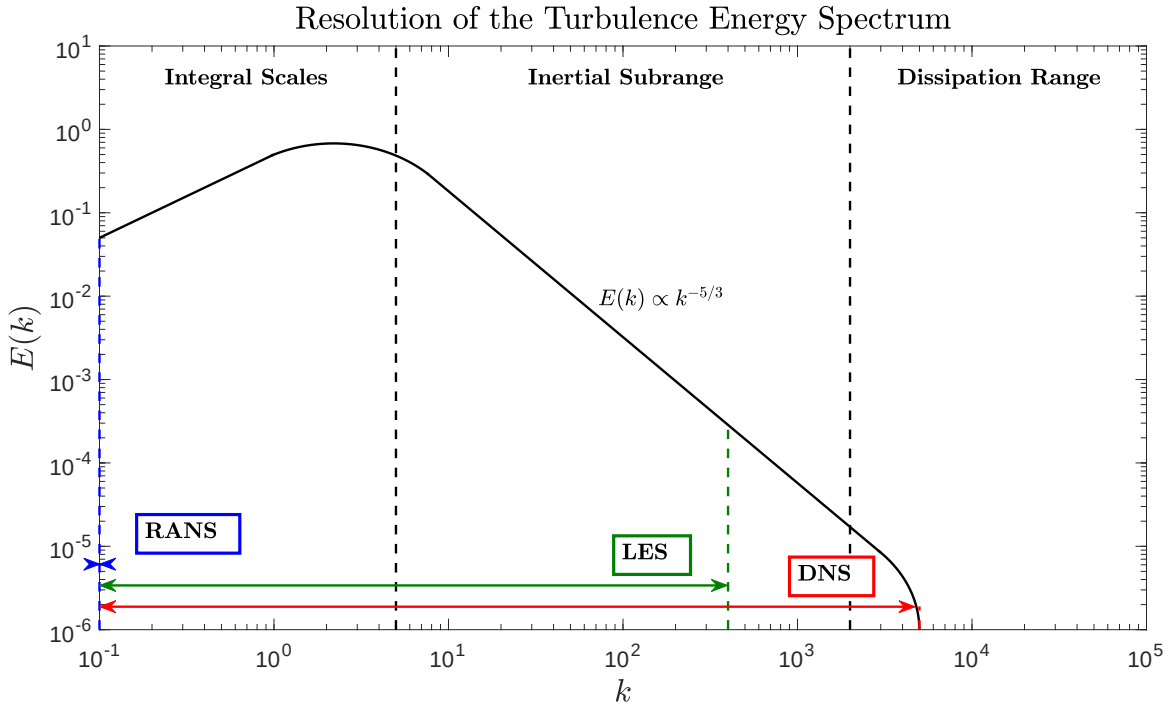

Figure 2.2: The level of detail in the turbulence energy spectrum to which different simulation approaches can resolve [3]

Direct Numerical Simulation (DNS)

Initial work involving the simulation of turbulence was instigated by Orszag [109, 110], who considered the numerical solution of the full conservation equations for mass (2.2)

and momentum (2.6) for the fluid phase in a coupled manner without assumption, an approach which is referred to as *direct numerical simulation* (DNS). This provides a complete description of the turbulent velocity field by including the behaviour at all scales that are present within the flow down to the smallest structures, which are characterised by the Kolmogorov lengthscale η. By numerically solving the governing equations without making any physical assumptions there is no requirement for any form of turbulence modelling, however due to the subsequent need to resolve down to the Kolmogorov lengthscale in order to include a sufficiently wide range of scales within the inertial subrange, DNS is by far the most computationally expensive method of simulation. As a result it is currently unfeasible for application in full-scale industrial problems, instead being mainly used to generate data in support of model development for accurately describing isolated physical effects.

Within the context of dispersed particle flow, DNS has proven an invaluable tool for gaining further insight into the behaviour of particles in various flow configurations. The governing equations for the dispersed phase (see section 2.3) are solved in conjunction with those for the continuous phase, and particle-fluid interaction (see section 2.4) is further taken into account by using a level of momentum coupling appropriate for the particle mass loading within the system. This enables a full physical description of configurations to be considered, and consequently is of great importance when it comes to understanding the mechanisms that are responsible for the phenomenological behaviour exhibited by particles.

Large-Eddy Simulation (LES)

To avoid the prohibitive computational expense of DNS, a compromise is made with *large-eddy simulation* (LES) which directly represents the large scales of turbulent motion but uses a model to account for the influence of the smallest scales. The rationale for this is that many flows of practical relevance have significant large-scale unsteadiness which requires explicit description, however the small scales are more universal in character and thus better suited to being modelled. This is achieved by spatial filtering of the Navier-Stokes equations to obtain a modified velocity field containing the large scale dynamics, however this produces unclosed terms that are associated with the sweeping of scales by the energy cascade in turbulence [118]. Consequently a sub-grid scale model is required to include this information, the pioneering of which was undertaken by Smagorinsky [145] through use of the equilibrium hypothesis, which implies that energy cascaded down from larger scales is dissipated instantaneously by

the small scales. Depending upon the degree of coarseness used to filter the velocity field, LES typically resolves scales down to within the inertial subrange of the turbulent kinetic energy spectrum, with the detail at the microscales being lost.

Due to many instances of particle-laden flows being strongly affected by turbulent structures at the large scales of motion and less so at the microscales, LES has proven to be of some use for studying disperse systems. In particular, development of turbulence models for LES of particle-laden flows has highlighted that LES is suitable for predicting temporal statistics, however the relative dispersion of particle pairs for separation distances less than the smallest resolvable scale is significantly underestimated by the sub-grid scale models [67], demonstrating that LES is not applicable for investigation into all aspects of particle behaviour.

Reynolds-averaged Navier-Stokes (RANS) Models

In order to address the need for a low-cost computational approach for approximating turbulent flows, *Reynolds-averaged Navier-Stokes* (RANS) models were pioneered as a statistical framework for estimating key flow quantities by Jones, Launder, and Spalding [80, 86]. This involves using a Reynolds decomposition on the Navier-Stokes equations to obtain the Reynolds equations, the solution of which yields the mean velocity field of the flow. As the Reynolds equations contain the unclosed Reynolds stress term, a turbulent viscosity model must be used as an approximation [152], such as that provided by the well-known k–ε model [86]. This results in loss of physical resolution of the turbulence fluctuations, meaning that RANS models can only resolve the turbulence down to the scale of the largest eddy structures in the flow field at the longitudinal integral lengthscale L_{11}, with all detail of the turbulence in the inertial subrange and dissipation range being neglected. RANS models are commonly employed for industrial purposes due to their relatively low computational cost, however this is offset by it also being the least accurate approach compared to DNS and LES.

As RANS models of the carrier flow do not include any information about the instantaneous turbulence fluctuations which are often the most salient influence on the behaviour of disperse particle transport, they have limited applicability for such purposes. Existing models tend to be highly specialised towards a specific flow configuration or set of parameters, and consequently are not relevant in more general contexts [90, 154].

Kinematic Simulation (KS)

Whilst DNS, LES, and RANS are all based on methods originating from the physical description of a carrier flow provided by the Navier-Stokes equations, an alternative class of stochastic models exist which are widely used to generate velocity fields that exhibit the key characteristics of turbulence. One such approach is that of *kinematic simulation* (KS) as developed by Kraichnan [84], in which a synthetic velocity field is generated by the linear superposition of random Fourier modes, producing a flow-field which is correlated in both space and time such that it conforms to standard energy spectra. The main advantage of KS is that it can be used to create flow fields with prescribed decorrelation rates by specification of the fluid velocity as a coloured Gaussian process, making it a more realistic means of investigation than if a simple white-noise process was used. Additionally, the fluid velocity field can be constructed such that a constant level of kinetic energy is maintained, thus avoiding the complication of a forcing mechanism in order to keep the flow statistically stationary. Conversely, KS does not capture all of the physics present in a true turbulent flow, and in particular does not contain the energy cascade effect of sweeping of the small scales by the larger scales, meaning that KS is inadequate for investigation into the behaviour of single-phase flows.

Notwithstanding this, KS does have scope as a useful means of investigation for studying dispersed multiphase flows, as it can generate a velocity field which includes large scale structures that are able to reproduce aspects of particle behaviour that are observed in true turbulent flows. Furthermore, since the fluid velocities are generated at the particle locations as needed at a given time, no interpolation from a fixed grid of fluid velocities is required, avoiding the error which arises from this procedure in highly intermittent flows [78].

2.3 Description of the Dispersed Phase

Considering the contrast in physical behaviour between the various types of multiphase flow regimes, it is clear that different strategies are required to accurately describe the dispersed phase for each classification of flow, and in the case of dilute-phase transport the approaches fall into two distinct categories [90]. *Particle tracking* models each particle as an individual entity, with the local fluid behaviour being used to determine the trajectory of each particle by solving an equation of motion in the Lagrangian

frame of reference, and together with the continuous phase constitutes a Lagrangian-Eulerian description. This has the advantage of a conceptually simple formulation even when complex forces such as lift and rotational effects on the particles have to be taken into account, however the computational expense of simulating many such particles individually can require a large amount of both processing power and time, and means that simulations representing real-world applications are often unfeasible at the desired level of detail. In contrast, *two-fluid models* represent the particle phase as a continuum in a fixed Eulerian frame of reference, with the average properties of the particles governed by a set of transport equations which can be constructed in a similar manner to those of the continuous phase, together constituting an Eulerian-Eulerian formulation. The statistical nature of such treatment means that solutions can be obtained much more quickly than particle tracking, however dealing with complex particle forces is considerably more difficult, and furthermore some detail of the particle behaviour is necessarily omitted due to the averaging procedures used. Nonetheless, research into two-fluid models is useful for a variety of applications, and the issues presented by the approach are steadily being addressed.

2.3.1 Particle Tracking

Fully Resolved Simulations

For dealing with the dispersed phase, the starting point is an equation of motion which determines the evolution of particle trajectories within a flow field. From first principles, such an equation is derived by considering the momentum transfer between the fluid and the particle. This results in the force exerted on the particle being equal to the sum of body forces on the particle (only gravitational acceleration is taken into account in this case) and the total hydrodynamic force exerted by the fluid on a particle [120]

$$m_p \frac{d\boldsymbol{v}_p}{dt} = m_p \mathbf{g} + \oint_S \boldsymbol{\sigma} \cdot \mathbf{n} \, dS \tag{2.12}$$

where m_p is the mass of an individual particle, $\boldsymbol{v}_p(t)$ is the particle velocity, $\boldsymbol{\sigma}$ is the fluid stress tensor defined in (2.4), and $\mathbf{n}$ is the outward unit normal on the surface S of the particle. The integral in (2.12) is over the entire surface of the particle, and as such this representation takes into account all physical effects of the continuous phase upon particles. In principle, it is possible to solve equation (2.12) numerically within a

particle tracking simulation, and this is referred to as a fully resolved simulation (FRS), since all the fluid stresses acting on the particle surface are captured. Unfortunately the computational expense of FRS is so high for even simple turbulent flow configurations that it is impractical for any simulations of relevance in engineering applications [120].

Basset-Boussinesq-Oseen Equation

In order to obtain a model equation of motion which captures the necessary particle dynamics at an acceptable computational cost, the integral of the fluid stress tensor in (2.12) can be simplified by modelling particles as points. This is achieved by assuming that their mass acts only at their centre of mass, and therefore negates the need to integrate the fluid stress tensor over the entire particle surface. In practice the *point particle approximation* applies when particles are small compared to the smallest scales over which the continuous phase velocity field varies (i.e. the Kolmogorov lengthscale η). Further assuming that particles are rigid and spherical, a general equation of motion can be derived which takes into account all the important forces acting upon the particle such as weight, buoyancy, drag, and lift, so that a high degree of physical realism is maintained. Many different forms of such an equation of motion exist, however the benchmark form is considered to be given by the Basset-Boussinesq-Oseen (BBO) equation of motion [37], also referred to as the Maxey-Riley-Gatignol equation [93, 58]

$$
\begin{aligned}
m_p \frac{d\boldsymbol{v}_p}{dt} = {} & \underbrace{\frac{1}{2}\rho_f C_D A_p |\mathbf{u}_p - \boldsymbol{v}_p| \left(\mathbf{u}_p - \boldsymbol{v}_p\right)}_{\text{steady-state drag}} + \underbrace{m_p \mathbf{g}}_{\text{gravitational force}} \\
& - \underbrace{V_p \nabla P_p}_{\text{buoyancy}} + \underbrace{V_p \nabla \boldsymbol{\tau}_p}_{\text{shear stress}} + \underbrace{\frac{\rho_f V_p}{2}\left[\frac{\partial \mathbf{u}_p}{\partial t} + \left(\mathbf{u}_p \cdot \nabla\right)\mathbf{u}_p - \frac{\partial \boldsymbol{v}_p}{\partial t}\right]}_{\text{added mass}} \\
& + \underbrace{\frac{3}{2} d_p^2 \sqrt{\pi \rho_f \mu}\left[\int_0^t \frac{\frac{\partial \mathbf{u}_p'}{\partial t'} + \left(\mathbf{u}_p' \cdot \nabla\right)\mathbf{u}_p' - \frac{\partial \boldsymbol{v}_p'}{\partial t'}}{\sqrt{t - t'}}\, dt' + \frac{\left(\mathbf{u}_p - \boldsymbol{v}_p\right)_0}{\sqrt{t}}\right]}_{\text{Basset history}}
\end{aligned}
\tag{2.13}
$$

where V_p is the particle volume, C_D is the corrective drag coefficient, A_p is the projected cross sectional area of the particle in the direction of the relative velocity $|\mathbf{u}_p - \boldsymbol{v}_p|$, d_p is

the particle diameter, and $(\mathbf{u}_p - \boldsymbol{v}_p)_0$ is the initial velocity difference between the particle and the continuous phase. The subscript p denotes that quantities are evaluated at the particle position $\boldsymbol{x}_p$ as a consequence of the point particle approximation being used, and furthermore the prime denotes that the temporal argument of the associated quantity within the Basset history term is t', i.e. $\boldsymbol{v}'_p = \boldsymbol{v}_p(t')$. The various forces each describe the effect of different physical phenomena acting upon the particle, and may be more or less important depending upon the specific flow configuration. These are [37]:

- Steady-state drag: the force acting upon a particle in a uniform pressure field when there is no acceleration of the relative velocity between the particle and continuous phase
- Gravitational force: the body force acting upon the particle as a result of acceleration due to gravity (similar terms are included in the presence of other body forces, e.g. electric or magnetic fields)
- Buoyancy: the effective buoyancy force is the difference between the particle weight and buoyancy force acting upon the particle
- Shear stress: arises from the viscous stresses and pressure gradients within the continuous phase
- Added mass: of use when the particle density is comparable to or less than the continuous phase density, and balances the work done in accelerating the fluid surrounding a particle
- Basset history: addresses the temporal delay in boundary layer development as the relative velocity between the local fluid and particle changes with time

The formulation of the BBO equation (2.13) uses only the drag forces affecting the particle momentum, and still omits some forces that could be included. These are pressure distributions induced by a velocity gradient (Saffman lift), rotation of a particle (Magnus lift), and the Faxén contribution to the drag force due to non-uniformity of the continuous phase [37]. For the conditions under which the point-particle approximation is valid these contributions are generally negligible compared to the drag forces, and as a result are not considered further in this work.

Steady-state Drag Models

The momentum conservation equation for the continuous phase given by (2.3) along with the definition of the stress tensor $\boldsymbol{\sigma}$ in (2.4) can be used to replace the buoyancy and shear stress terms in the BBO equation (2.13) with the material fluid acceleration and gravitational body force. The limitation of this substitution is that the BBO equation can then only be used for the motion of particles within a dilute suspension, since the effect of local fluid disturbance from one particle on the motion of a different particle (i.e. three-way coupling - see section 2.4) can no longer be included. Using this substitution and rearranging transforms (2.13) into the following equation of motion

$$\left(1+\frac{1}{2}\frac{\rho_f}{\rho_p}\right)\frac{d\boldsymbol{v}_p}{dt} = \frac{\rho_f d_p}{24\mu}C_D\frac{1}{\tau_p}|\mathbf{u}_p-\boldsymbol{v}_p|\left(\mathbf{u}_p-\boldsymbol{v}_p\right)+\left(1-\frac{\rho_f}{\rho_p}\right)\mathbf{g}+\frac{3}{2}\frac{\rho_f}{\rho_p}\left[\frac{\partial \mathbf{u}_p}{\partial t}+\left(\mathbf{u}_p\cdot\nabla\right)\mathbf{u}_p\right] + \sqrt{\frac{9}{2\pi}}\left(\frac{\rho_f}{\rho_p}\right)^{\frac{1}{2}}\frac{1}{\sqrt{\tau_p}}\left[\int_0^t \frac{\frac{\partial \mathbf{u}_p'}{\partial t'}+\left(\mathbf{u}_p'\cdot\nabla\right)\mathbf{u}_p'-\frac{\partial \boldsymbol{v}_p'}{\partial t'}}{\sqrt{t-t'}}\,dt'+\frac{\left(\mathbf{u}_p-\boldsymbol{v}_p\right)_0}{\sqrt{t}}\right] \tag{2.14}$$

where ρ_p is the density of the particle phase, and τ_p is a characteristic response time of the particle to changes in the local fluid velocity as a result of its inertia, which is defined as

$$\tau_p = \frac{\rho_p d_p^2}{18\mu} \tag{2.15}$$

From (2.14) it is seen that the expression $\frac{\rho_f}{\rho_p}$ giving the ratio of continuous phase density to particle density appears in several terms. For situations where the particle density is much larger than the continuous phase density this ratio becomes very small, which is typical of a gas-particle or gas-droplet flow. When sufficiently small, and specifically satisfying the condition

$$\frac{\rho_f}{\rho_p} < 10^{-3} \tag{2.16}$$

this ratio can justifiably be approximated as being equal to zero [37], simplifying (2.14) to just the contribution of the steady-state drag force and gravitational acceleration

$$\frac{d\boldsymbol{v}_p}{dt} = \frac{\rho_f d_p}{24\mu}C_D\frac{1}{\tau_p}|\mathbf{u}_p-\boldsymbol{v}_p|\left(\mathbf{u}_p-\boldsymbol{v}_p\right)+\mathbf{g} \tag{2.17}$$

It is useful to define the particle Reynolds number Re_p by taking the reference length-scale as the particle diameter d_p and reference velocity as the relative velocity of the particle compared to the local fluid velocity $|\mathbf{u} - \boldsymbol{v}_p|$

$$Re_p = \frac{\rho_f d_p |\mathbf{u}_p - \boldsymbol{v}_p|}{\mu} \tag{2.18}$$

Using this definition, the particle equation of motion (2.17) becomes

$$\frac{d\boldsymbol{v}_p}{dt} = \frac{Re_p}{24} C_D \frac{1}{\tau_p} (\mathbf{u}_p - \boldsymbol{v}_p) + \mathbf{g} \tag{2.19}$$

Despite the level of detail that it contains, the BBO equation still has limitations. It does not directly account for some effects that are of importance in physical applications, such as variation in local Reynolds number, the influence of neighbouring particles, and turbulence effects. This is addressed by use of the corrective drag coefficient C_D, which is incorporated into the particle equation of motion in order to capture the dependencies on particle shape, orientation, local turbulence intensity, and particle Reynolds number [37]. Several correlations are available for C_D as a function of Re_p, with one such often used correlation having been developed by Schiller & Neumann [33, 120, 38], which is given by

$$C_D = \frac{24}{Re_p} \left(1 + \frac{1}{6} Re_p^{\frac{2}{3}} \right) \tag{2.20}$$

The form of drag coefficient in (2.20) is used to account for the effect of turbulence on particles, and is valid for $Re_p < 1000$ meaning that although the turbulence will not be fully developed, this form of drag coefficient is valid for all values of Re_p that can feasibly be simulated computationally.

Linear Drag Models

A simpler model for C_D known as the Stokes drag coefficient is defined by [37]

$$C_D = \frac{24}{Re_p} \tag{2.21}$$

This is applicable in the low particle Reynolds number regime ($Re_p < 1$) [37], and transforms the particle equation of motion (2.19) into a simple linear drag law

$$\frac{d\boldsymbol{v}_p}{dt} = \frac{1}{\tau_p}\left(\mathbf{u}_p - \boldsymbol{v}_p\right) + \mathbf{g} \tag{2.22}$$

This is referred to as Stokes drag model for the particle equation of motion. In order for (2.22) to be valid, the condition (2.16) must be strictly observed, as if the density of the dispersed phase is comparable to or less than that of the continuous phase, the complete BBO equation is required so that the added mass and Basset history forces are taken into account. Nonetheless, within the field of particle dispersion a large body of work is still undertaken utilising a Stokes drag model in order to keep subsequent analysis tractable, and as such it is the predominant form of the particle equation of motion used throughout this work.

To summarise, the assumptions invoked in order for a Stokes drag model to be valid are:

- Point particle approximation: $d_p \ll \eta$
- Particles modelled as rigid spheres
- Dilute particle loading within the flow field: $\alpha_d < 10^{-6}$
- Continuous phase density is much less than that of the particle phase: $\rho_f/\rho_p < 10^{-3}$ (restricts model applicability to gas-particle or gas-droplet flows)
- Small particle Reynolds number: $Re_p < 1$

Non-dimensional Form

The Stokes drag model (2.22) can be non-dimensionalised in terms of the reference lengthscale l_{ref} and velocity scale u_{ref} by using the non-dimensional quantities defined in (2.7), resulting in

$$\frac{d\hat{\boldsymbol{v}}_p}{dt} = \frac{1}{St}\left(\hat{\mathbf{u}}_p - \hat{\boldsymbol{v}}_p\right) + \frac{\hat{\mathbf{g}}}{Fr^2} \tag{2.23}$$

where St is the *Stokes number* defined as

$$St = \frac{\tau_p}{\tau_f} \tag{2.24}$$

and in which τ_f is some characteristic response time of the continuous phase, defined from the reference lengthscale l_{ref} and velocity u_{ref}

$$\tau_f = \frac{l_{\text{ref}}}{u_{\text{ref}}} \tag{2.25}$$

The Stokes number is a non-dimensional quantity representing the ratio of response timescales between the particles and continuous phase, and is a key parameter in the study of particle transport. The behaviour of particles is strongly dependent on the Stokes number, and observation of different phenomenon across a range of St is a hallmark feature of parametric simulation studies focusing upon particle transport in turbulence. Large values of St imply that particle inertia is the dominant influence in the dispersion process with particles acting in a ballistic manner, whereas small values of St infer that the turbulence is a more important factor and the particles behave almost like fluid elements.

It is possible to define various Stokes numbers depending on the specific flow configuration under investigation, and the length and velocity scales associated with it that determine the corresponding fluid timescale τ_f. For instance, a fluid timescale representative of the large scales of motion within the continuous phase is obtained by taking $l_{\text{ref}} = L_{11}$ (longitudinal integral lengthscale) and $u_{\text{ref}} = u'$ (continuous phase root mean square (RMS) velocity fluctuation), giving the eddy turnover time $\tau_{\text{eddy}} = L_{11}/u'$. Similarly, a fluid timescale typical of the smallest microscales is obtained by taking $l_{\text{ref}} = \eta$ (Kolmogorov lengthscale) and $u_{\text{ref}} = u_\eta$ (Kolmogorov velocity scale), resulting in the Kolmogorov timescale $\tau_\eta = \eta/u_\eta$.

Gravitational Effects on Particles

The collective behaviour of particles which are subject to gravity is an area with incomplete understanding, with the research interest into this topic originating from the study of atmospheric pollution problems [36]. In this context, a further quantity for evaluating the significance of the gravitational body force $\mathbf{g}$ on particle dispersion is the magnitude of terminal velocity due to gravity in still fluid, defined by

$$V_g = |\mathbf{V}_g| = \tau_p \, \mathbf{g} \tag{2.26}$$

which is also referred to as the *Stokes settling velocity*, and is obtained as the averaged steady-state solution of the Stokes drag model (2.22). When dealing when this quantity, rather than classification in terms of the Froude number Fr, a more suitable non-dimensional parameter for determining the effect of gravity within particle-laden flows is the *Rouse number*

$$Ro = \frac{V_g}{u_{\text{ref}}} \tag{2.27}$$

which is simply the ratio of the Stokes settling velocity experienced by the particles to the continuous phase reference velocity. Large values of Ro indicate that the gravitational body force dominates the dispersion process, whereas in small Ro systems the turbulence is the main influence on particle motion.

Consideration of Light Particles

In situations when the dispersed phase medium has a density that is either roughly comparable to or less than that of the continuous phase medium, the heavy particle condition of $\rho_f/\rho_p < 10^{-3}$ has to be relaxed in order to keep the physical description of the dispersed phase suitably accurate. This is extremely important in the case of bubble flow, in which the particles have a very low density and added mass effects are now the dominant force acting upon particles, meaning that the linear drag law (2.22) is an inadequate representation. The added mass contribution and buoyancy terms in (2.14) can be included as additional terms in the linear drag law, which extends the range of flow regimes that can be addressed using a simplified particle equation of motion without having to account for the Basset history force, which requires substantially more computation.

2.3.2 Two-Fluid Models

Despite the relative simplicity and numerical accuracy of particle tracking, in reality simulations using this approach for even simple applications can require a large amount of computation, and furthermore do not necessarily provide insight into the behaviour that particles exhibit. More complex phenomenon resembling those seen in industrial or environmental processes are computationally unfeasible to model at this level of detail, and therefore an alternative approach is needed. Often the quantities of interest

in such processes are average statistics of the particle phase rather than the extreme values of individual particle motion, and this motivates a different framework for modelling multiphase flows in which only these average quantities are computed. Such an averaged approach is considered in an Eulerian sense, and is known as two-fluid modelling [49].

A description of this manner for the dispersed phase requires a careful set of assumptions to be made, and the following considerations constitute the most basic form of two-fluid model [49]:

1. The dispersed phase behaves only macroscopically as a continuum, with microscopic behaviour not being represented in a two-fluid model
2. The dispersed phase contains particles which are uniform in size and spherical
3. The dispersed phase volume fraction is sufficiently small to ensure that particle collisions do not need to be accounted for ($\alpha_d < 10^{-3}$ - see section 2.4)
4. Neither the continuous nor dispersed phase undergoes any phase changes

Subject to these conditions, the particle phase can be interpreted as if it were itself a continuum, with the most straightforward approach to this being the deterministic construction of transport equations for the key particle statistics. Specifically, continuity and momentum equations for the particle concentration ρ and average particle velocity $\overline{\mathbf{v}}$ respectively are given by [48]

$$\frac{\partial \rho}{\partial t} + \nabla \cdot (\rho \overline{\mathbf{v}}) = 0 \tag{2.28}$$

$$\frac{\partial}{\partial t}(\rho \overline{\mathbf{v}}) + \nabla \cdot (\rho \, \overline{\mathbf{v}} \, \overline{\mathbf{v}}) = \nabla \cdot (\alpha_d \boldsymbol{\sigma}_d) + \rho \mathbf{g} \tag{2.29}$$

where $\boldsymbol{\sigma}_d$ is the stress tensor for the dispersed phase. Equations (2.28) and (2.29) are obtained for a single realisation of the flow field by averaging over a control volume that is much larger than single particles, and it is emphasised that in the two-fluid framework the quantities ρ, $\overline{\mathbf{v}}$, and $\boldsymbol{\sigma}_d$ represent the values for a cloud of particles within this control volume, and not individual particles. In the general form above the momentum equation (2.29) is unclosed, with the dispersed phase stress tensor $\boldsymbol{\sigma}_d$ remaining to be modelled.

It is instructive to compare the form of (2.28) and (2.29) with the corresponding equations for the continuous phase given by (2.2) and (2.3). The difference in the dispersed phase continuity equation arises due to incompressibility no longer being invoked; indeed the finite compressibility of the dispersed phase is a fundamental feature of multiphase flows which gives rise to many of the phenomena that are of interest in such systems (see Chapter 3). The momentum equation for the dispersed phase is seen to be essentially identical to that of the continuous phase, however it is again the compressibility of the dispersed phase that leads to the momentum equation differing for the two phases. In particular, the dispersed phase stress tensor $\boldsymbol{\sigma}_d$ can be decomposed into pressure and viscous contributions analogous to that for the continuous phase in (2.4), i.e. $\boldsymbol{\sigma}_d = -P_d\mathbf{I} + \boldsymbol{\tau}_d$ with P_d being the dispersed phase pressure and $\boldsymbol{\tau}_d$ the dispersed phase viscous stress tensor, however the form of $\boldsymbol{\tau}_d$ will differ. Obtaining an exact expression for $\boldsymbol{\tau}_d$ constitutes the *closure problem* of two-fluid modelling, with this being considerably more complicated than in single-phase flows in the sense that ideas such as Prandtl's mixing length hypothesis give useful results in turbulence modelling, whereas the availability of such ideas in multiphase flow is much more limited and the performance of them often even more so [120]. The simplest case of using a Boussinesq approximation for $\boldsymbol{\tau}_d$, in which variation in properties other than ρ is ignored and the viscous stresses are modelled as proportional to the rate of strain [36], results in

$$\boldsymbol{\tau}_d = \mu_d \left(\nabla\mathbf{u} + \nabla\mathbf{u}^\top\right) - \frac{2}{3}\mu_d \left(\nabla\cdot\mathbf{u}\right)\mathbf{I} \tag{2.30}$$

where μ_d is the dispersed phase dynamic viscosity. This can be considered as the compressible analogue to the continuous phase viscous stress tensor $\boldsymbol{\tau}$ given in (2.5), however even this basic model presents problems, with the question arising of how to suitably define a global value for μ_d. This parameter encompasses much of the behaviour of the dispersed phase in the model (2.30), with μ_d being related to the particle velocity fluctuations which are themselves dependent on both the local turbulence and particle history [36]. Subsequent choice of a constant value for μ_d is paramount to neglecting these effects upon which much particle behaviour of interest is dependent, producing a model for the dispersed phase which does not capture anything other than large scale average behaviour. On the other hand, introducing a variable value of μ_d as a function of St is possible [32], however this involves producing a suitable fit for such a function which is a non-trivial task. Furthermore, encompassing a range of effects all within the single parameter μ_d does not shed any physical insight into the individual factors which are responsible for given behaviour of the dispersed phase, demonstrating

the need for a specification of $\boldsymbol{\tau}_d$ which is less empirical in nature. However, formulating a closure which captures the relevant physics in the dispersed phase is often non-trivial, and remains the most challenging aspect of utilising two-fluid models.

As an alternative to the aforementioned method of obtaining a set of governing equations which describe the behaviour of the dispersed phase, a separate statistical framework exists which involves the construction of such equations through the use of probability density functions, and this is detailed separately in Chapter 4. Such a formulation provides a higher level of detail in the associated transport equations, meaning that the closures which are required can be made at a more basic level, and consequently are more likely to produce an accurate model.

2.4 Inter-phase Coupling

The description of the continuous phase in section 2.2 only contains information about the carrier flow as an individual entity, whilst that of the dispersed phase in section 2.3 is influenced by only the local properties of the continuous phase. In reality a given flow regime will contain a certain level of interaction between the two phases which is dependent upon the physical characteristics of the system in question; notably the volume fraction α_d and Stokes number St. Dilute and dense-phase transport thus each require different levels of particle-fluid interaction to be taken into account, and an overview of these different instances of phase-coupling is therefore detailed in the following [36].

The starting point is one-way coupling, in which there is no feedback from the dispersed phase to the continuous phase, and further the motion of individual particles is independent of each other. To create a better model, the effect of particles on the surrounding fluid should also be taken into account, and in conjunction with the one-way coupling mechanism this is termed as two-way coupling. In the case of dilute phase flows, the large inter-particle separation distance means that particle-particle interaction can be assumed to be negligible, and thus two-way coupling is a valid model. However for dispersed flows which have a higher volume fraction and therefore smaller inter-particle separation distance, the particles will begin to have an effect upon each other. Three-way coupling accounts for this by including the effect of local fluid disturbance from one particle on the motion of another particle, whilst the highest level of accuracy is achieved by four-way coupling which takes particle collisions into account. Once the volume fraction is increased to a certain level, the problem is classed

as dense-phase flow, in which the particle-particle interactions become the dominant contribution to the coupling mechanism, meaning that four-way coupling is absolutely necessary in this situation.

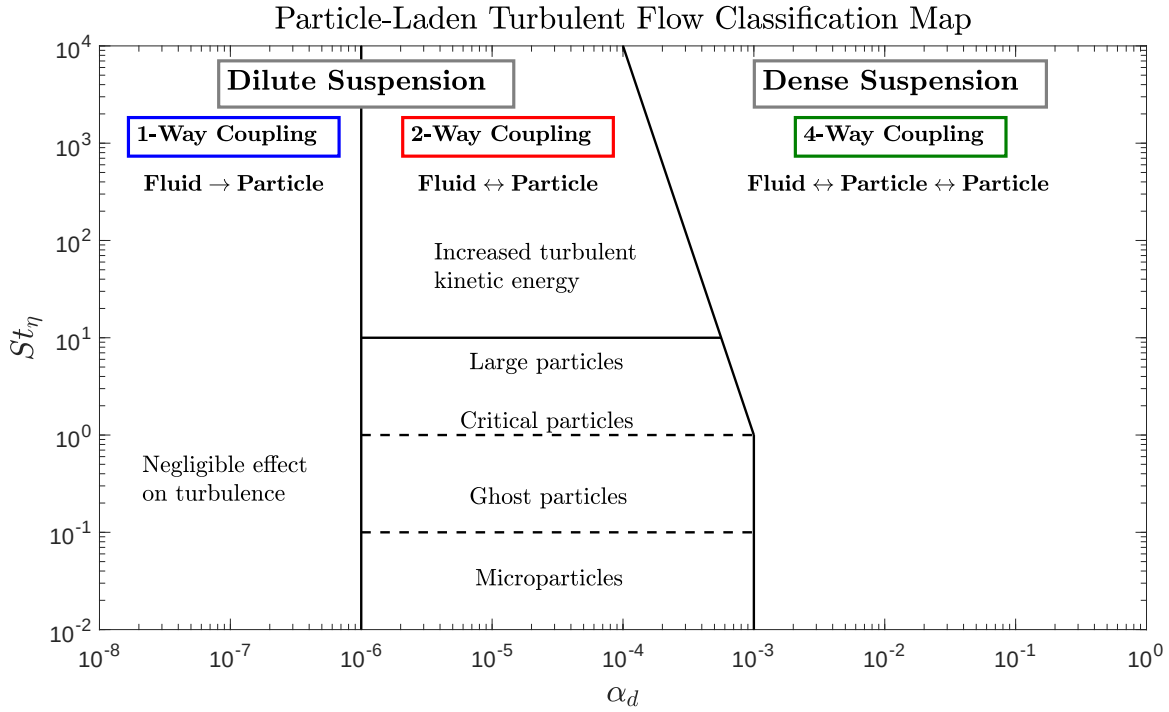

Figure 2.3: Classification map of dispersed two-phase turbulent flows [48]

Classification of two-phase flows in terms of the degree of coupling required can be made for different volume fractions and Stokes numbers, and depicted as a regime diagram as shown in Figure 2.3 [48]. For $\alpha_d < 10^{-6}$ the particles have negligible effect on the turbulence meaning that two-way coupling does not need to be accounted for, and one-way coupling is sufficient for accurately capturing the particle behaviour. For the range $10^{-6} < \alpha_d < 10^{-3}$ however, the effect of the particles on the turbulence is great enough to alter the structure of the turbulence, and therefore needs to be accounted for through use of two-way coupling. Within this range the effect of different Stokes numbers on this coupling mechanism gives rise to different degrees of *turbulence modulation*, with the Stokes number here being defined in terms of the Kolmogorov timescale $St_\eta = \tau_p/\tau_\eta$. Systems that fall within this range of volume fraction have particles classified as [36]:

- *Microparticles* ($St_\eta \ll 1$): particles behave almost like fluid elements due to their response time τ_p being much less than the Kolmogorov timescale τ_η, however both

turbulent kinetic energy and dissipation rate are increased compared to single-phase flow

- *Ghost particles* ($St_\eta \sim 0.25$): the energy spectrum is modified in such a way that the **turbulent kinetic energy is identical to that of single-phase flow**, whilst the dissipation rate is increased

- *Critical particles* ($St_\eta \sim 1$): maximum preferential accumulation is observed as a result of interaction with the structures of the turbulence, with the energy spectrum being modified such that the turbulent kinetic energy is decreased, whilst the **dissipation rate is identical to that of single-phase flow**

- *Large particles* ($1 \lesssim St_\eta \lesssim 10$): particles behave more ballistically due to their response time τ_p being greater than the Kolmogorov timescale τ_η, and both **turbulent kinetic energy and dissipation rate are decreased** compared to single-phase flow

When particles become sufficiently large ($St_\eta \gtrsim 10$) within the two-way coupling range, their motion becomes fully ballistic and they are classified differently to large particles. This is due to the very high inertia meaning that the particle Reynolds number is now large enough to cause vortex shedding, which in turn results in enhanced production within the energy spectrum. Therefore in contrast to large particles which cause the turbulent kinetic energy to decrease, for ($St_\eta \gtrsim 10$) an increase in turbulent kinetic energy is instead observed. In the case of $\alpha_d > 10^{-3}$ the particle loading is now a dense suspension and inter-particle collisions become important, necessitating the use of four-way coupling. At higher values of St_η the tendency of particles to collide is increased, with this behaviour making a non-negligible contribution even for $\alpha_d < 10^{-3}$, and this is why the separation between two-way coupling and four-way coupling varies with α_d in Figure 2.3. For dense suspensions the effects of particles on the turbulence are varied, classification of which is a subject of ongoing research [36].

Chapter 3

Literature Review

Although the fundamentals of particle transport are well-established, modelling the behaviour of multiphase flows and a true understanding of the physical mechanisms that underlie various phenomena remains an active research topic. As such, a large body of literature addressing these issues exists, from which the relevant advances are detailed in the subsequent sections.

3.1 PDF Modelling

The PDF approach (see Chapter 4) is a methodology for representing both single-phase fluid flows and disperse particle flows, with the objective being to develop mathematical models that can accurately describe the behaviour exhibited in various flow configurations. Considerable focus has been given to using the PDF approach in single-phase flows as a method of constructing closures to the Reynolds averaged Navier-Stokes (RANS) equations [118] (see section 2.2.2), through use of stochastic Lagrangian methods such as the generalised Langevin model [117]. Such approaches consider the PDF of the fluid velocity at a given position and time in a Lagrangian sense, leading to closures for various moments of the fluid velocity along the trajectory of a fluid element.

In the case of disperse particle flows, two different forms of PDF equation have been introduced and studied. One choice of variables for analysis of particle dispersion is the particle position and velocity at a given time, and this formulation is known as the kinetic model (KM). The associated PDF transport equation is referred to as the kinetic equation, and is derived from the particle equation of motion itself. In contrast, the local fluid velocity at the particle position can also be included within the PDF in

addition to the particle position and velocity, with this approach being referred to as the generalised Langevin model (GLM). The name arises from the need for an additional equation of motion for the fluid velocity along the particle trajectory in the modelling procedure, with the standard model for this purpose being a simple derivative of the Langevin equation [117]. In principle both approaches can arrive at the same results, however this requires that the closures made are exact in either PDF equation, and that the statistics of the process are the same in both cases [127]. It is important to note that the PDF equation in both of these general forms remains unclosed, with the methods used to derive them reducing the closure problem from that of the phase-space diffusion current to correlations of the phase-space variables of the PDF.

3.1.1 Kinetic Models

The KM approach was pioneered by Buyevich [23] in the early 1970's, with the first derivation of the kinetic equation obtained via the classical Fokker-Planck equation using a simple decomposition of the particle and fluid velocities into mean and fluctuating components. This form of the kinetic equation is however only valid when the random particle motion is described by a Markov process [124], which restricts usage to when the particle timescale τ_p is much greater than that of the turbulence in the continuous phase τ_f, a restriction which is known as the white noise approximation. The specification of the continuum equations from the kinetic equation was also first performed in the work by Buyevich, in the standard manner of Chapman & Cowling [28]. Buyevich followed this with further work on closure of the kinetic equation using the Chapman-Enskog method [24], and application of the KM to homogeneous suspensions in pseudo-turbulence [25].

A number of other workers have since developed the KM approach. Reeks [122, 124] obtained a kinetic equation by modelling the particle motion as a Langevin equation (i.e. the fluctuating continuous phase driving force is prescribed along a particle trajectory) and performing a cumulant expansion to close the phase-space diffusion current arising from the Liouville equation for the PDF. In order to circumvent the implied restriction on the particle timescale of $\tau_p \gg \tau_f$ that is implicit in the kinetic equation of Buyevich, the Lagrangian History Direct Interaction (LHDI) approximation of Kraichnan [83] was used to preserve the invariance under random Galilean transformations (RGT). This involves consideration of an added random translational velocity which is uniform in space and time invariant to each realisation of the continuous phase flow, and Kraichnan [85] took the distribution of these translational velocities to be

Gaussian. Along with the LHDI approximation Reeks supposed that the fluctuating component of the continuous phase driving force along particle trajectories was also Gaussian, resulting in every term within the cumulant expansion apart from the first becoming zero, and thus producing a kinetic equation no longer constrained to the random particle motion being Markov. The resultant dependence of the PDF upon the history of particle trajectories is encapsulated in the kinetic equation within the so-called *dispersion tensors*, which in turn contain a two-point two-time correlation tensor of the fluctuating continuous phase driving force and a particle *response tensor* in the form of a functional derivative with respect to the fluctuating continuous phase driving force. In addition, Reeks [125] formally demonstrated that a well-posed set of continuum equations for the particle phase could be derived using this approach.

Obtaining a kinetic equation directly from the particle equation of motion without recourse to RGT invariance has also been carried out. Swailes & Darbyshire [150] used the correlation splitting result of Furutsu and Novikov (FN) [56, 107] for functionals to produce an expansion of the phase-space diffusion current, which truncates to just the first cumulant by modelling the Eulerian continuous phase fluctuating velocity as Gaussian. This produces a similar form of kinetic equation to that of Reeks [124], with the distinction that the fluctuating continuous phase driving force is interpreted in an Eulerian sense in this case rather than along a trajectory. Indeed, since the starting point in this formulation is the true particle equation of motion, the closure is exact up to the point of using the Gaussian assumption, resulting in a theoretically sound kinetic equation. In the same manner as Reeks, this approach also leads to continuum equations for the particle phase [151].

The FN correlation splitting approach has been used by other workers to close the phase-space diffusion current, notably Hyland *et al.* [71], and Derevich & Zaichik [44]. Both of these derivations arrive at a kinetic equation different from that of Swailes & Darbyshire due to varying treatment of the functional derivatives involved. Hyland *et al.* assume that the probability of transition for a particle along a trajectory is independent of the fluctuating continuous phase driving force, by invoking Corrsin's hypothesis [35] on the grounds of the driving force being small enough compared to a characteristic speed that is determined by an explicit condition on the turbulence spectrum [168], and also numerical accuracy [122]. This addresses the implied timescale restriction of the classical Fokker-Planck equation in an equivalent manner to the LHDI approximation, and consequently results in a kinetic equation identical to that of Reeks [124]. In contrast, Derevich & Zaichik assume that the infinitesimal change in fluid velocity is delta-correlated in both space and time, resulting in the functional derivative

losing its dependence on the particle trajectory and becoming a deterministic function of the particle phase variables. This leads to a form of the kinetic equation which is also fully deterministic, with the only unclosed quantity being the Reynold's stresses.

A further derivation of the kinetic equation was performed by Pozorski & Minier [119], and makes use of the cumulant expansion method proposed by Van Kampen [162] for the solution of linear stochastic differential equations, by modelling the particle equation of motion as such a process. This features both deterministic and random components as linear operators, however a restriction on the timescale and fluctuation intensity of the random component is inherent within application of the cumulant expansion [160, 161]. Assuming that the random component of the stochastic differential equation has a zero-mean Gaussian distribution results in a kinetic equation of the same form as that obtained by Reeks [124] using the LHDI procedure, however the fluctuating continuous phase driving force is only a function of phase-space variables [90]. Consequently the unclosed terms in this formulation of the kinetic equation do not involve non-local correlations along particle trajectories, meaning that it differs from the approaches using LHDI and FN.

The closures provided for the phase-space diffusion current by LHDI, FN, and Van Kampen's method all result in PDF kinetic equations which are fundamentally different [12], and any reconciliation between the various approaches in their general forms remains unestablished. Consideration of this is an unresolved issue within the area of PDF modelling, and demonstrating correspondence between the different assumptions used in the various closures would be a result of significant interest.

3.1.2 Generalised Langevin Models

The GLM approach was first proposed by Simonin *et al.* [141] by using an equation of motion to model the continuous phase velocity along particle trajectories. This equation was developed from the Langevin equation used as an analogue of the Navier-Stokes equation for fluid point motion by Pope & Haworth [66]. The higher-dimensional PDF of the particle location, velocity, and local fluid velocity is then considered in order to derive expressions for the fluid/particle turbulent moments. Since all the necessary variables are specified within the phase-space vector of the PDF, the only unknown term within the PDF transport equation is the fluid acceleration. As this is defined by the Langevin equation, the PDF transport equation in a GLM model is in fact already closed, with the assumption of modelling the fluid velocity along a particle trajectory

as a stochastic process providing all the information that is required to fully determine the associated PDF [98]. Thus the problem reduces to specification of an appropriate form of Langevin model that captures the necessary features of the flow field.

3.1.3 Stochastic Models

A more general approach of modelling the behaviour of an arbitrary stochastic process rather than the specific case of particle motion was taken by Hänggi [64], in which a FN closure was applied via use of the characteristic functional. This procedure yields a recursive relationship between the n-point correlation function and cumulants of the process in question. This work considers processes governed by a GLM, and derives a master equation for the PDF of the process by using the cumulants of the fluctuating part of the process to characterise its stochastic properties. Assuming that the random force is a coloured Gaussian noise, the subsequent master equation takes a closed linear form, for which the solution can be written in terms of a Green's function.

This work was followed up by Hänggi [65] with the development of an approximate non-linear Fokker-Planck type equation for modelling the long-time dynamics of a general stochastic system. This equation is written in terms of dispersion tensors of a similar form to those that appear within the various forms of kinetic model. The two-point two-time correlation tensor is treated simply using an exponential decay model due to a Langevin process being assumed for the stochastic system, whilst the response tensor is written in an iterated integral form to which a decoupling approximation is applied in order to neglect correlations among components of the response tensor. This still retains some of the important long-time information about the underlying stochastic process, producing an improved model compared to the earlier work of Hänggi [64]. This work does however assume that the response tensor and PDF itself are independent. Further work [54] on this approach involved extending the decoupling approximation applied to the response tensor by using projector-operator techniques on the GLM process.

A more recent investigation [6] into systems of stochastic differential equations with coloured noise as the driving force uses a modified large-eddy diffusivity (LED) method to make a closure of the associated PDF model. The stochastic flux appearing in this closure is shown to be equivalent to the second-order cumulant expansion of van Kampen [160, 161], and a local linearisation is used to obtain a PDF transport equation. This is found to be accurate when the decorrelation time of the coloured noise is

much different from the relaxation time involved in the system in question, i.e. in the case of disperse particle transport the PDF model is only valid for $St \neq 1$. It was noted that the accuracy of the PDF decreases with increased standard deviation of the coloured noise, indicating that the long-time history effects of the process are responsible. Notwithstanding this, the PDF model in [6] for processes involving noise with finite decorrelation times is still an improvement over white noise models which do not capture any history effects, and the subsequent non-local nature of the PDF equation reflects the non-Markovian behaviour of the process. The closure for the stochastic flux is written in terms of dispersion tensors that take a similar form to the kinetic model, however instead of a response tensor (see section 4.1.4), the Jacobian tensor representing the elemental deformation of a fluid element along a particle trajectory (see section 3.3.1) appears. This presents the interesting possibility of whether reconciliation between these two different classes of model is possible. In [6] further evaluation of the dispersion tensors is carried out by linearising the response tensor, which effectively loses the detail of the relationship between the response and correlation tensor, and leads to a fully localised quasi-Fokker-Planck transport equation for the PDF. When applied to a set of coupled Kramer's equations, there is no general solution to the PDF transport equation, however approximate analytical solutions can be derived. These capture the stochastic resonance behaviour which is present in the system, thereby offering an improvement over classical LED closures which are inaccurate in such systems due to neglection of this behaviour.

3.1.4 Spurious Drift

For investigation into the various stochastic fluxes that arise within the different forms of PDF models it is essential that the drift contribution can be accurately quantified, and that so-called spurious drift does not make a contribution [98]. This applies in the limit of particle inertia becoming negligible, in which case particles effectively become fluid tracers and move along streamlines of the flow field. When dealing with incompressible flows, mass continuity implies that given an initially uniform distribution of particles, the concentration must remain uniform. Models which do not respect this constraint are said to exhibit spurious drift, and this constitutes a serious shortcoming of that model.

In terms of PDF models, an important contribution was made by Bragg *et al.* [12] by showing that of all the forms of kinetic equation outlined in section 3.1.1, only the Furutsu-Novikov closure of Swailes & Darbyshire [150] respects this condition for

general flow configurations, with the LHDI procedure of Reeks [124] only doing so for homogeneous flows, and application of Van Kampen's method by Pozorski & Minier [119] only doing so by neglecting an important scalar flux contribution associated with non-uniform flows. On the other hand, the form of the stochastic model used for the continuous phase in the GLM approach determines whether spurious drift is present, meaning that appropriate specification of this stochastic model ensures that the constraint is automatically respected [98]. This limits the choice of PDF models which are appropriate for studying drift enhancement, but still allows for either the KM or GLM to be used depending upon preferences.

3.1.5 Current Developments

The foundations of the work on kinetic models has recently been brought into question by Minier & Profeta [99, 97], with claims that the kinetic equation is ill-posed and therefore invalid as a PDF description of dispersed two-phase flows. The assertion made is that the kinetic equation has the properties of a backward heat equation and therefore its solution exhibits singularities within a finite time, which is justified by arguing that the phase space diffusion tensor possesses both positive and negative eigenvalues. The validity of this argument was addressed by Reeks *et al.* [128] by noting that the drift coefficient in the kinetic equation contains both convective and diffusive contributions in a transformed phase space due to the coupling of phase space variables, i.e. particle position and velocity are not independent. This implies that the drift contribution is not purely a convection term within the kinetic equation, but has a specific form consisting of both convective and diffusive parts, since it is a functional of the solution to the kinetic equation. It is formally demonstrated that the diffusive contribution offsets the convective contribution to the negative eigenvalue of the phase space diffusion tensor for the entire range of values in the particle parameter space, meaning that the kinetic model is in fact well-posed.

Furthermore, it was noted in [128] that the claim of ill-posedness of the kinetic equation contradicts the well-posedness of the PDF equation for the GLM, with some further contrasts between these two different classes of PDF model also considered. Firstly, the GLM cannot capture the influence of spatio-temporal structures within the flow on particle behaviour, as the Langevin model is used to prescribe the flow. This effect is very important for describing the spatial distribution of particles, which the kinetic model captures through the two-point two-time correlation tensor. Secondly, the GLM fails to preserve the RGT invariance which is a cornerstone of the LHDI procedure.

This is due to the fluctuating stochastic acceleration field described by the Fokker-Planck equation, and causes the GLM to predict short term dispersion of $\mathcal{O}(t)$ rather than $\mathcal{O}(t^2)$ as the kinetic model predicts. The difference lies within the assumptions made on the history of particle trajectories, for which the dispersion tensors of the kinetic model cannot be considered time-independent in analysis due to non-zero time correlations of the flow field, i.e. the system is inherently non-Markovian. These factors result in the GLM and kinetic model producing different quantitative behaviour over a vast range of flow configurations, with agreement only being observed in the case of a simple shear flow in which statistics of fluid velocity along particle trajectories are assumed to be Gaussian.

3.2 Drift Enhancement under Gravitational Settling

The study of particle dispersion subject to an applied body force is most easily realised by considering the case of gravity, due to the additional force acting in only one direction, and therefore if the underlying flow field is isotropic the inclusion of gravity results in a reduction in the symmetry of the particle phase in just the gravitational direction. The interest in this configuration is due to the tendency of the average settling velocity of particles within a turbulent flow to be be modified compared to the settling velocity within a still fluid V_g, and this has been the subject of a number of investigations into the physical mechanisms responsible. A large body of work has focused upon using a linear drag law for the particle equation of motion, and from equations (2.23) and (2.9) it can be seen that particle behaviour involving a gravitational body force can be viewed as a function of Stokes number St, Froude number Fr (or Rouse number Ro), and flow Reynolds number Re. Furthermore, if the particle equation of motion is relaxed to a steady-state drag law as in equation (2.19) then behaviour also becomes a function of the particle Reynolds number Re_p. Despite this dependence on as few as three parameters, the modification in settling velocity is still not well understood, and precisely attributing these effects to individual factors remains a focus of ongoing research.

3.2.1 Crossing Trajectories Effect

The *effect of crossing trajectories* was first highlighted by Yudine [174], and arises due to the influence of an external body force causing inertial particle trajectories to cross

those of fluid elements. The consecutive interaction with many separate fluid elements results in a different velocity for the inertial particles than the corresponding fluid elements, and this causes particles to move from one region in which the flow is correlated to another. Since the fluid element neighbourhood of particles is continuously changing, the particle velocity correlation decorrelates more rapidly with time than that of fluid elements [39]. The crossing trajectories effect has been recognised as being of great practical importance in relation to the diffusion rate of inertial particles, with the rate of dispersion decreasing as the effect becomes more pronounced [169]. Further, it is observed that crossing trajectory effects are negligible when the drift velocity of the particles produced by the associated body force is less than the RMS fluid velocity [169]. Nonetheless, crossing trajectory effects are central to modification of the average settling velocity of particles, in addition to being responsible for a number of other mechanisms that contribute to particles moving between different regions in which the flow is correlated.

3.2.2 Preferential Concentration and Sweeping

The effect of an unsteady flow on particle settling was first studied by Maxey & Corrsin [92] in cellular flow fields, who observed that inertial particles subject to a Stokes drag force reached an equilibrium settling velocity that is greater than the Stokes settling velocity V_g. Furthermore, the tendency of particles with a small inertia that are subject to a small gravitational acceleration to collect along isolated paths was observed. Following on from this work, Maxey [91] conducted an investigation into the physical mechanisms behind the observed behaviour by using a more rigorous study of inertial particles in a Gaussian random velocity field. By performing an asymptotic analysis for small particle inertia and defining a particle velocity field, Maxey showed that the divergence of this velocity field is positive in regions of high vorticity and low strain rate, and negative in regions of high strain rate. This results in an inertial bias on the particles causing them to accumulate in regions of high strain rate and low vorticity, thus leading to a locally non-uniform particle concentration, referred to as *preferential concentration*. Note that this is defined distinctly as a special case of particle *clustering*, which is non-uniformity of the particle spatial distribution irrespective of any correlation this has with the fluid flow field. In contrast, preferential concentration is where the particle spatial distribution is not only non-uniform, but is also correlated with local properties the flow [155].

Further work was undertaken by Wang & Maxey [163] using full direct numerical sim-

ulations to capture the effect of the flow dynamics at small scales on the increase in settling velocity. In contrast to the Gaussian random velocity field where the increase in settling rate was found to be up to 10% of the terminal velocity in still fluid, inclusion of the full flow dynamics increased the settling rate as much as 50%, with the peak increase being when the particle timescale and gravitational settling velocity are comparable to the respective Kolmogorov microscales of the flow. This was justified by previous work [139] which demonstrated that intense vortical regions are a feature of the small scale dissipation range flow dynamics, with the higher intensity at these scales serving to accentuate the effect of inertial bias on particles. This is in contrast to particle dispersion, which is dominated by the bulk stirring of the large scale eddies. Furthermore, in [163] an additional mechanism contributing towards the increase in settling velocity was identified as the tendency of particles to collect in the downflow side of local fluid structures with respect to the direction in which the gravitational body force is acting, a phenomenon known as *preferential sweeping*. The proposal of such a mechanism followed from the observation that regions of higher particle concentration tend to appear as long connected patches that are aligned in the gravitational direction, with these patches being located precisely in the downflow regions in the velocity field which form between neighbouring regions of vorticity. Thus [163] concludes that the faster settling rate of particles is due to both preferential concentration and preferential sweeping.

The observation of Wang & Maxey [163] that regions of higher particle concentration are characterised by long connected patches of particles in the gravitational direction has attracted attention to classification of these patches and the dependence of such clustering due to gravity on physical parameters. By considering clustering only within the inertial range where forcing and dissipation are not relevant, different defined spatial clustering patterns referred to as *attractors* have been observed [51, 105], with the different forms of attractor dependent upon St and Fr. Clustering patterns are found to exist as 1D, 2D and 3D attractors, and exhibit different concentration gradients dependent upon the dimensionality of the attractor which is formed in a given case. However, it is noted that across most cases of St and Fr the particle distribution did not form defined patterns, and dispersed throughout the domain. Further to this, depending upon the value of St, gravity can either reduce or enhance the degree to which clustering occurs. In particular, one-dimensional clustering patterns move from the horizontal direction to the vertical direction with increasing Fr, and for low values of Fr, two-dimensional clustering patterns are recovered due to the gravity preventing uniform settling of particles.

3.2.3 Loitering

Wang & Maxey [163] also examined the particle settling rate in the case of a nonlinear drag law, and in doing so produced the first simulations which identified a net decrease in the particle settling velocity in turbulent flows, referred to as the *loitering* of particles. This phenomenon was previously observed by Tunstall & Houghton [156] and Hwang [70] for simple oscillatory flows, and Mei [94] for random flow fields, with Wang & Maxey's contribution confirming that the effect also exists in flows governed with a full physical description. This study only observed a decrease in the particle settling velocity in the case of both St and V_g being large, and this effect is attributed to the fluctuating slip velocity between particles and the surrounding fluid within a turbulent flow, which is opposite in sense to the effect of preferential sweeping, and exists even when the inertial bias is not present. The overall effect of nonlinear drag is a slight decrease in the average particle settling rate compared to a linear drag law at the same St and V_g.

Another early investigation into whether the average settling velocity of inertial particles in homogeneous stationary turbulence differs from that in still fluid was carried out by Fung [55], with the influence of turbulent structures on this behaviour specifically being focused upon. This study also used a Gaussian random velocity field rather than true turbulence, however in contrast to the initial work of Maxey [91], preferential concentration is observed in eddy regions for small gravitational settling velocities, resulting in a decreased average settling velocity compared to still fluid. Crucially, this study used a square drag law within the particle equation of motion, consistent with the hypothesis of decreases in the average particle settling velocity being attributable to nonlinear drag effects.

A theoretical investigation considering particle settling velocity in the asymptotic limit of negligible particle inertia for a vortex flow was performed by Davila & Hunt [41] using a particle equation of motion that takes added mass effects into account. A Rankine vortex of radius R_v and circulation Γ is used to define the flow field, resulting in a completely deterministic configuration. The simulation characteristics are determined by two parameters: the dimensionless ratio $V_T = V_g R_v/\Gamma$ and the ratio between the particle timescale and the characteristic time for a particle to move around a vortex $F_p = \tau_p V_T^2/\Gamma$. By calculating the differential settling distance of inertial particles, an expression for the average settling velocity is obtained. This is predicted to be up to 80% greater than in still fluid for $V_g < u'$, but also up to 20% less for $V_g > u'$, providing the first theoretical justification for the loitering of particles. The increase in average

settling velocity further becomes negligible for $V_g/u' > 4$. The analysis also proceeds to define a particle velocity field as an asymptotic expansion for small F_p, with the resultant expression for the divergence of this particle velocity field being equal to that obtained by Maxey [91], demonstrating the equivalence of these two approaches. Additionally, despite added mass effects being included, the particle equation of motion used in [41] contains a linear drag law, bringing into question whether nonlinear drag effects are solely responsible for the phenomenon of loitering.

3.2.4 Experimental Studies

Although the initial work into modification of the average particle settling velocity was carried out using a combination of numerical simulation and theoretical analysis, more recent studies have made an important contribution by undertaking experimental investigations into the phenomenon in order to validate the existing research. The first such work was by Aliseda *et al.* [1] and confirmed that the highly non-uniform spatial distribution of particles is due to interaction with the underlying turbulence resulting in preferential concentration within certain regions of the flow, and that the crossing trajectories effect causes particles to experience preferential sweeping which results in the mean effect of the turbulence on particles being a net force that results in a downwards acceleration. As with simulation studies, particle settling velocity enhancement due to turbulence was found to depend primarily on the two non-dimensional parameters St_η and the Rouse number defined using the Kolmogorov velocity scale $Ro_\eta = V_g/u_\eta$, with the maximum settling increase observed at $St_\eta \sim 1$ and $Ro_\eta \sim 1$. However, enhancement of the average particle settling velocity was also found to be highly dependent on the particle mass loading in the flow, where a monotonic increase in the average particle settling velocity with the local concentration was reported. This means that preferential sweeping cannot be the only mechanism responsible for settling enhancement, otherwise the effect would be independent of the number of particles in the flow. Consequently an additional mechanism for clustering due to particle loading results from regions of high particle concentration behaving like large pseudo-particles (clusters) which have their own settling velocity, and adding this onto the settling velocity of the individual particles contained within the cluster produces an increase in the overall particle settling velocity.

More recent experimental investigations have confirmed that in a linear velocity field heavy particles preferentially accumulate in strain-dominated regions of the flow [59], and further considered the contribution of preferential sweeping, loitering, and nonlin-

ear drag towards the variation (enhancement or reduction) in drift velocity by isolating these distinct mechanisms [61]. The latter study reported that a reduction in the average particle settling velocity is only observed at large Stokes numbers (for which a point-particle approximation is made) when one-way coupling is used with nonlinear drag corrections, and this behaviour is attributed to the increase in drag coefficient with slip velocity introducing a bias towards upward flowing regions. Reduced settling speeds are only observed with a linear drag model in the case of artificial flows that eliminate preferential sweeping by the eddies, and this demonstrated by considering particle motion which is constrained to vertical paths, removing the preferential sweeping effect and thereby reproducing loitering. For linear drag forces and unconstrained particle motion, preferential sweeping dominates any loitering effects, meaning that enhancements to the settling velocity are observed across the whole range of parameter values. It is also observed that particles respond more to fluid fluctuations in the vertical (gravitational) direction than in the horizontal direction(s), due to vertical fluctuations being correlated over longer distances than horizontal fluctuations, in agreement with Wang & Stock [165].

A very recent study [69] has further investigated experimentally the role of particle loading on the settling velocity of inertial particles in homogeneous isotropic turbulence (HIT), with behaviour characterised in terms of the local particle volume fraction. For $\alpha_d < 10^{-6}$, corresponding to the one-way coupling regime, particles respond only to the background flow and there are no collective effects amongst particles. However for $\alpha_d \sim 4.5 \times 10^{-5}$, corresponding to the two-way coupling regime, particles are subject to a rapid settling velocity enhancement which is proportional to the turbulence fluctuations. Finally for $\alpha_d > 10^{-3}$, corresponding to the four-way coupling regime, particles experience no further increase in settling velocity as volume fraction is increased, and the enhancement typically remains at $60-100\%$ of that seen by particles in the one-way coupling regime.

3.2.5 Effect of Settling Velocity Modification on Particle Dynamics

Recent simulation studies have attempted to quantify and understand the interaction between particles and the turbulent carrier phase in a higher level of detail, focusing upon the physical mechanisms responsible for altering the average settling rate of particles as a result of the flow dynamics. In particular, the effect of different mass

loadings on average settling velocity has been considered by varying the particle volume fraction, with such investigations using fully-resolved simulations in order to capture all the physical forces acting on particles and accurately quantify the effect of different particle mass loadings. In a study [182] focusing upon dense particle suspensions, for low volume fraction ($\alpha_d < 0.01$) and high Reynolds number flows ($Re \geq 175$) particles are observed to cluster in high strain regions, while for high volume fraction flows ($\alpha_d > 0.03$) a reduced averaged particle settling velocity is observed across all values of Re. In contrast, another numerical study [52] found that a volume fraction in the range $0.005 - 0.01$ decreased the average particle settling velocity by $12 - 14\%$, with the mechanisms responsible being the unsteady drag effects and non-stationary effects related to vortex shedding. In particular, the main contribution to the overall drag force is the steady part, however the reduction in average settling velocity is almost entirely due to the unsteady effects. Additionally, gravity has been found to play an important role in particle acceleration statistics by disrupting the near equilibrium behaviour of particle response to local turbulent motion and also amplifying extreme acceleration events in all directions, thereby reducing the inertial filtering mechanism [114].

A DNS investigation [43] using one-way coupling into the effect of settling enhancement as a result of preferential concentration found that in addition to the preferential sweeping of particles by the fluid velocity on the downward side of flow structures, a similar mechanism exists due to the fluid acceleration on the downward side of flow structures. However, the magnitude of the effect is reported to be marginal, and it could not be detected from statistical analysis of the particle concentration. This study further observed that in the case of one-way coupling the maximum enhancement of settling velocity is of order of $0.1u'$, and the average particle settling velocity monotonically increases with local particle concentration.

As a follow-up to [43], the effect of different levels of inter-phase coupling at a given mass loading has also been addressed in a further DNS study [102], in which analysis of gravitational settling with two-way coupling effects included was carried out in order to obtain insights into the interplay between local preferential concentration and turbulence. In this work particle settling is parametrised by the Rouse number $Ro = V_g/u'$, and the particle concentration is determined by Voronoï analysis, in which clustering is classified using connected components of Voronoï cells whose individual volume is below a given threshold [100]. It was found that the particle settling velocity increases up to $Ro \sim 0.4$ and then decreases for $Ro > 0.4$, although the influence of gravity upon particle settling rate is weaker than that of the Stokes number. Further, the maximum

increase in settling velocity is reported at $St_\eta \sim 1.5$, however the maximum increase in preferential concentration is observed at $St_\eta \sim 2$. The study confirms that including momentum exchange by use of two-way coupling increases the settling rate in areas of high particle concentration compared to one-way coupling, in agreement with the experimental work of Aliseda *et al.* [1]. In particular, the mean increase in particle settling velocity was attributed to the local mean contribution of the fluid velocity, of which the dominant part comes from the main mechanism in two-way coupling.

Investigation into the various forces other than drag which act upon a particle has been the focus of a number of studies, as for $\rho_p/\rho_f < 10^2$ the pressure gradient, added mass, and Basset history forces are all non-negligible and must be taken into account. One such study [159] concluded that the pressure gradient force results in a decreased settling velocity in HIT by preventing preferential sweeping, as it forces particles towards the centre of vortices, ensuring that they are kept there for a longer period of time. In this work, the effect of the Basset history force is found to be Stokes number dependent, increasing the settling velocity for large St and decreasing the settling velocity for small St accordingly. Further to this, a nonlinear drag law significantly changes the settling velocity, however the enhancement in settling velocity is small. Another investigation [53] focused upon the case of finite-size particles with a density being roughly comparable to that of the fluid, establishing that the average settling velocity is reduced by between $6 - 60\%$ compared to the still fluid settling velocity, dependent upon the value of V_g/u'. Additionally, as the ratio ρ_p/ρ_f is reduced, it was observed that the average settling speed reduces correspondingly due to increased vertical drag induced by the fluid-particle relative velocity. Furthermore, expanding upon earlier work [52], the contribution of unsteady effects to the mean overall drag force is quantified as only about $6 - 10\%$.

The effect of gravity on particle dynamics in isotropic turbulence has been investigated by Ireland *et al.* [76], however firstly the particle dynamics without gravity were analysed in order to both understand the underlying behaviour and also enable the effect of gravity to be isolated once introduced. This entailed classification of the flow field by regions in terms of the strain and rotation rate tensors, with high strain and high rotation areas termed as *vortex sheets*, high strain and low rotation areas termed as *irrotational dissipation regions*, and low strain and low rotation areas termed as *vortex tubes*. It was found that low St_η particles are ejected from both vortex tubes and vortex sheets, but preferentially accumulate in irrotational dissipation regions. Within these regions, the rotation rate timescale is much more sensitive to changes in St_η than the strain rate timescale, which suggests that the dominant effect of inertia is to cause

particles to spend less time in strongly rotating regions. Preferential sampling effects are determined to be important for $St_\eta < 0.1$, whilst the path history and non-local effects become important for $St_\eta > 0.2$, and as St_η increases the timescale over which particles retain a memory of their interactions with turbulence also increases. The dependence on the turbulence intensity was also considered, and it was found that for low Taylor Reynolds number Re_λ (defined by taking $l_{\text{ref}} = \lambda$, the Taylor microscale) flows the response time of the largest particles exceeds the timescales of many large-scale flow features, whilst for higher Re_λ flows more flow features are present with timescales that exceed the particle response time.

The introduction of gravity in the follow up work of Ireland *et al.* [77] causes particles to preferentially sample certain regions of the flow as expected. The resultant reduction in symmetry for the particle field causes particles to sample flow more uniformly, and reduces the time that particles can spend interacting with the underlying turbulence. The particle accelerations tend to be increased, whilst the particle relative velocities decrease, reducing both the degree of preferential sampling and the importance of path-history interactions. As a result gravity causes reduced clustering at low St_η, and increased clustering at high St_η. Classification of the average increase in settling velocity is made as $\langle \Delta \boldsymbol{v}_p \rangle > 0$ corresponding with the preferential sweeping of particles noted by Wang & Maxey [163], and $\langle \Delta \boldsymbol{v}_p \rangle < 0$ representing the loitering of particles. The average settling velocity is found to be independent of Re_λ for $St_\eta \leq 0.1$, suggesting that the average settling velocity is determined entirely by the small scale turbulence. In contrast, at higher St_η settling speeds are stronger functions of Re_λ. Gravity was also shown to reduce the Lagrangian timescales of both the strain and rotation rates along particle trajectories. Analysis of the mechanisms reveals that preferential sweeping cannot fully explain the trends in acceleration variances with gravity. Particles are shown to experience vertical fluid velocities that are more strongly correlated over a particle timescale than the horizontal fluid velocities, meaning that the horizontal fluid velocities sampled by the particle change more rapidly, leading to larger particle accelerations in these directions. This is responsible for the clustering on the downward side of turbulent eddies that induces the drift enhancement due to gravity.

An independent study [134] into the settling velocity of non-interacting small heavy particles pursued a similar line of investigation, and concluded that the dominant effect on the increase in settling velocity is preferential sweeping. However, a reduction of settling velocity in HIT without large scale vortical structures is only found to emerge if particle horizontal motions are artificially blocked (in the direction perpendicular to gravity). The tendency of particles to be swept preferentially by the downward flow

regions is subsequently prevented, thereby causing a reduction in settling velocity.

3.2.6 Influence of Flow Scales

Work into the feasibility of using different methods of numerical simulation to study enhancement of particle settling was undertaken by Yang & Lei [173], with the focus upon Large-Eddy Simulation. It is argued that preferential concentration in low vorticity regions is controlled by small scales at a wavenumber which corresponds to the maximum in the dissipation spectrum, but the smaller (by an order of magnitude) Kolmogorov scales have no contribution to the increase in average settling velocity, and thus small eddies also have negligible effect. However, the increase in average settling velocity also depends on particle drag, as controlled by the large scale eddies. Therefore the mechanisms responsible for the increase in settling velocity operate entirely above a certain cutoff lengthscale, meaning that Large-Eddy Simulation is therefore adequate for studying the increase in settling velocity behaviour if this cutoff lengthscale is used for the filtering of the fluid velocity field. Yang & Lei also noted the dependence of the increase in average particle settling velocity on the RMS of the velocity field, finding that the increase is of order $u'/10$ for $St_\eta \sim 1$. Furthermore, for these simulations it is observed that the behaviour of the average settling velocity in decaying turbulence is qualitatively similar to stationary turbulence.

A very recent investigation by Tom & Bragg [155] has developed a new theoretical result to address the effect which different flow scales have on settling velocity enhancement by revealing the multiscale nature of the physical mechanisms which are responsible. Noting that the asymptotic result obtained by Maxey [91] breaks down for $St \gg 1$ due to the formation of caustics (see section 3.4.1) in the particle velocity distribution [170], it follows that this result can be extended to arbitrary St by construction of an appropriate particle velocity field. The formal solution to the particle velocity field may then be written by integrating the particle equation of motion, and this shows that non-local contributions to the particle velocity field exist from the history of fluid velocities along the particle trajectories. Further, the particle density conservation equation has a solution in terms of the divergence of the particle velocity field, from which it is apparent that the clustering related to the divergence of the particle velocity field must be correlated with the underlying fluid velocity for settling enhancement to occur. The influence of different flow scales is considered in [155] by decomposing the particle velocity field into coarse and subgrid parts, from which it is argued that there is no contribution to the increase in settling velocity from the coarse part. This is

because the divergence of the particle velocity field only significantly deviates from zero at scales less than the coarse-graining length scale, and is therefore uncorrelated with the coarse-grained fluid velocity field. As a result, it is concluded in [155] that settling enhancement occurs due to inertial particles being preferentially swept by eddies which are smaller than the coarse-graining length scale, but also that there is no single turbulent velocity scale that characterises the enhanced settling rate. For example, as the still fluid settling velocity of particles is increased, the flow scales of the turbulence which cause the enhancement in particle settling velocity become larger. Similarly, as St is increased the dominant contribution to the preferential sweeping mechanism comes from progressively larger flow scales of the turbulence. Furthermore, preferential sampling of the fluid velocity gradient at scales outside of the dissipation range occurs for rapidly settling particles [77].

Comparing the work of Yang & Lei [173] with Tom & Bragg [155], the main issue arising is that the former proposes that the mechanisms leading to enhancement of the particle settling velocity operate at flow scales *above* a certain lengthscale, while the latter argue that such mechanisms only occur at flow scales *below* a certain lengthscale. Notwithstanding the fact that these two lengthscales are not necessarily the same, the differing conclusions of the two investigations highlights the need for a more complete understanding of particle settling behaviour.

3.2.7 Applications of Drift Enhancement

The salient applications of gravitational settling enhancement have been highlighted by Wang & Maxey [163] as being the growth rate of water droplets in clouds and the residence time of dust or aerosols in the atmosphere. This is due to these processes being strongly influenced by changes in the settling rate, as in atmospheric turbulence where the flow scales are widely separated, the average settling rate of small particles would only be affected by a limited range of flow scales near the dissipation range, thereby resulting in an increase in settling velocity which is comparable to the peak increase observed at Kolmogorov scaling. Furthermore, in [77] it has been noted that in warm cumulus clouds the gravitational settling velocity of droplets has been observed as up to an order of magnitude larger than the Kolmogorov velocity scale of the local atmosphere, thus the droplets have a substantially modified response to the underlying flow, demonstrating the potential implications of an improved understanding of settling velocity enhancement.

3.3 Particle Velocity Field Formulation

The initial work of Maxey [91] in defining a particle velocity field (PVF) in the limit of small particle inertia was central to the emergence of preferential concentration as a dominant mechanism responsible for the enhancement of the average settling velocity of particles subject to gravity. In particular, Maxey showed that it is the compressibility of the particle velocity field that is responsible for this effect. Davila & Hunt [41] also arrived at the same result for the divergence of the particle velocity field, however as with Maxey's approach the analysis is only valid for $St \ll 1$, limiting the scope of this particle velocity field to identify all the physical mechanisms that contribute to the settling enhancement. This motivated the consideration of a more generally defined particle velocity field that is valid for arbitrary St, and capable of accounting for the different physical mechanisms which act across the entire range of values of particle inertia.

3.3.1 Full Lagrangian Methods

Investigation into the formal development for the particle phase of a two-fluid model by using the particle velocity field approach has been pioneered by Reeks [129], and entails the construction of the PDF equation that is associated with a stochastic process that consists of both the particle velocity and its divergence. Of particular note is that the divergence of the particle velocity field can be computed by making use of the derivative of the particle position along a trajectory with respect to an initial fixed position, which represents the particle phase deformation tensor, and can also be interpreted as the Jacobian $\boldsymbol{\mathcal{J}}(\mathbf{x}^0, t)$ of the Eulerian-Lagrangian transformation. The determinant of the Jacobian tensor $J(\mathbf{x}^0, t) = \det\left[\boldsymbol{\mathcal{J}}(\mathbf{x}^0, t)\right]$ then provides the elemental volume deformation along a particle trajectory, which is directly related to the compressibility of the particle phase. This Jacobian tensor is therefore central to analysing the particle velocity field, and was first introduced by Osiptsov [111] for determining the particle concentration along a trajectory. Further work [112] culminated with the development of a class of models that completely describe the particle phase known as *full Lagrangian methods* (FLM), which originate from the Lagrangian form of the particle continuity equation. These methods have since been used for investigating preferential accumulation of particles within a number of contexts, including in boundary layers [116] and flow near a stagnation point [68]. This subsequent work has highlighted the efficacy of Osiptsov's method due to its ability to handle singu-

larities appearing in the particle phase, i.e. where the particle concentration becomes mathematically infinite, although it should be noted that in practice this would never occur due to the effect of finite particle size and particle collisions. The behaviour of the evolution of the Jacobian has also been further analysed [68], with two important outcomes being that the Jacobian changes sign if particle trajectories cross, and that correct specification of initial conditions for the Jacobian $\boldsymbol{\mathcal{J}}(\mathbf{x}^0, t_0)$ and its derivative $\dot{\boldsymbol{\mathcal{J}}}(\mathbf{x}^0, t_0)$ is of paramount importance.

The latter issue has since been addressed in a series of studies [130] which apply Osiptsov's method to Stokes drag model, producing a governing equation for the Jacobian that is identical in form to the particle equation of motion. In particular, the initial condition for the Jacobian itself naturally emerges as $\boldsymbol{\mathcal{J}}(\mathbf{x}^0, t_0) = \mathbf{I}$, whilst the Jacobian derivative $\dot{\boldsymbol{\mathcal{J}}}(\mathbf{x}^0, t_0)$ represents deformation in velocity space, which poses the question as to what value this should physically take. In [130] $\dot{\boldsymbol{\mathcal{J}}}(\mathbf{x}^0, t_0)$ is defined using the fluid strain rate S and particle timescale τ_p so that only diagonal components are nonzero, specifically $\dot{\mathcal{J}}_{ij}(\mathbf{x}^0, t_0) = (-1)^{i+1}\,\tau_p^{-1}\,S\,\delta_{ij}$. Whilst this choice of initial condition respects incompressibility, it is somewhat artificial, and was revised in later work [72] to the more general condition of simply imposing the initial fluid velocity gradient field, i.e. $\dot{\mathcal{J}}_{ij}(\mathbf{x}^0, t_0) = \partial \mathrm{u}_i(\mathbf{x}^0, t_0)/\partial \mathrm{x}_j$. This arises from the choice of initial particle velocity, which in this case is set equal to the fluid velocity at the particle position, and then the above condition follows from the definition of $\dot{\boldsymbol{\mathcal{J}}}(\mathbf{x}^0, t)$.

This particular series of work [130, 72] has focused on evaluating the preferential concentration associated with nonzero compressibility of the particle velocity field, as for finite St an analytical expression for the divergence of the particle velocity field is not available and must be determined numerically. This is done with both the FLM using Osiptsov's method and also the mesoscopic Eulerian formalism (MEF), which is in essence a box counting method (BCM) requiring a large number of particles to achieve meaningful particle concentration statistics. The methodology of the FLM here involves calculating the determinant of the Jacobian tensor to obtain the size of an infinitesimally small volume occupied by a group of particles along the trajectory of one single particle. This then yields the particle concentration along the trajectory, as this corresponds to the inverse of the volume occupied by a fixed number of particles. It is reported [72] that FLM can be used to compute local concentration gradients more accurately and at less computational expense than the MEF which is based on a difference equation, demonstrating the advantage of the two-fluid approach over a purely computational method. Further, if the particle velocity field is written as an expansion in St then truncation to the leading order retrieves the approximation pro-

posed by Maxey [91], reconciliating the more general theory of the FLM [72, 73] with this established result.

Additional insight from the use of a particle velocity field can be made in the case of a straining region, in which the particle equation of motion can be simplified, leading to a linearised equation for the deformation tensor and thus an analytical solution [73]. Statistics of the average divergence of the particle velocity field are examined, for which extreme values are related to events when the deformation along a trajectory passes through zero, and a negative value represents the accumulation of particles. The averaged compressibility of particle phase is shown to approach a constant value in the long time limit, and the PDF of the divergence of the PVF is reported to be highly asymmetric with intermittent tails. Despite this insight, straining flows only have limited applicability in reality, and utilisation of the PVF approach in a synthetic random velocity field is also considered in [73]. It was found that the divergence of the PVF is proportional to St^2 in the limit of small St, in agreement with previous work in periodic flow fields [10] and direct numerical simulation of HIT [31]. Furthermore, the distribution in time of particle compressibility was shown to be non-Gaussian beyond the third and fourth moments [95]. Additional work [95] involved a DNS study in order to capture the full effect of flow dynamics on the compressibility of the particle phase using FLM, with the outcome that the wider distribution of scales in DNS did not significantly alter the results for the deformation along a trajectory. It was also noted in this work that preferential sweeping from high vorticity to high strain regions of flow may only be appropriate for small St, with other mechanisms that rely on the history of the particle trajectory contributing at larger St, a premise which has since been expanded upon in work [19] focusing on particle clustering (see section 3.4.3).

3.4 Particle Clustering

The clustering of particles within various turbulent flow configurations is a striking feature of disperse particle transport, and has been subject to extensive investigation since the 1960s [5]. Despite this, a complete classification of the extent of this phenomenon is still not available, with many questions yet to be answered. Identification of the key physical mechanisms responsible for this effect is a focus of current research, and requires analysis of the structures and dynamics of the dispersed phase in order to quantify these. In particular, an early observation by Reeks [123] noted the tendency for particles to migrate in the direction of decreasing turbulence level, a phenomenon

that has been termed *turbophoresis*. This arises from a force balance between the net drag force and the gradient of the kinetic stresses acting on the particles due to the turbulence, leading to a build-up of concentration near the wall in boundary layers, and subsequently an enhanced rate of particle deposition.

The enhanced settling velocity of particles subject to gravity within turbulence observed by Maxey [92, 91] resulted from the preferential concentration of particles due to interaction with the structures of the flow field. This was some of the first work done using numerical simulations on the clustering of particles, and these early findings set the scene for more detailed investigations into the mechanisms responsible. The first direct numerical simulation studies focusing upon this phenomenon were undertaken by Squires & Eaton [146], in which parametric simulations were performed in order to gauge the conditions under which preferential concentration was most pronounced. In this study it was also noted that the observed clustering behaviour implied that under certain conditions the turbulence could actually inhibit rather than enhance the mixing of particles, going against the conventional views that consider particle mixing as a homogeneous process resulting in uniform dispersion. In terms of the effect of flow scales on particle clustering, experimental investigation [172] across different Stokes numbers in HIT has validated the Kolmogorov timescale as being the most appropriate fluid timescale for measuring preferential concentration with respect to.

3.4.1 Caustics

Aside from the preferential concentration in areas of high strain and low vorticity [91] and preferential sweeping which causes particles to collect on the downward side of eddies [163] when subject to a gravitational body force, other physical mechanisms involving the turbulence-particle interactions and which contribute to particle clustering have come to light in subsequent work. A somewhat artificial process is the development of *caustics* [170], defined as the occurrence of multiple particles occupying the same point in physical space but with differing velocities, and therefore purely a modelling artefact of point-particle treatment in dispersed systems where inter-particle collisions are not accounted for. Clustering of inertial particles is found to occur on a network of caustic lines, with the caustics themselves providing one mechanism which is responsible for the clustering. This is due to the formation of caustics resulting in particles passing through areas of greatly increased particle density, thereby affecting the rates of collision and coagulation which holds particular relevance for explaining the rapid onset of rainfall from convective clouds [171]. Clustering as a result of caus-

tics is thus a more general theory than that of the preferential concentration seen in low vorticity high strain regions, yet within computational studies it still provides a mechanism for which the clustering effect has to be accounted for.

More recently, the influence of particle relative velocities on spatial distribution and collision rates has been investigated [62, 16, 115, 11]. It is known that the collision rate is affected by both the radial distribution function (see section 3.4.5) and the mean radial relative velocities [166], and it is reported [115] that the dependence of the latter on Stokes number is attributable to the formation of caustics. Additionally, the joint PDF of relative velocities at small separations is computed and compared to a model which matches the asymptotic limits of the distribution [62], dominated by pair diffusion (characterised by highly correlated motion between particles) and caustics (characterised by large velocity differences between particles at small separations) respectively. It is concluded [115] that this model is accurate up to a separation distance of 0.1 of the Kolmogorov lengthscale for any Stokes number, subject to enough caustics being present to allow large velocity differences at small separations, and also a sufficiently large separation in scales existing between τ_p and the integral timescale of the system to ensure that particle dynamics are not influenced by the system driving force. Furthermore, a recent DNS investigation [11] into the joint PDF of relative separation and radial velocity of inertial particle pairs in HIT concluded that the PDF is scale invariant at small scales. This was reasoned to be a consequence of two distinct clustering mechanisms at work, namely interaction with fluid structures causing the separation between particle pairs to become small for an extended period of time, and caustics respectively.

3.4.2 Sweep-Stick Mechanism

Another phenomenon that has been observed is referred to as the *sweep-stick mechanism* [30, 34], and follows the observation that clustering of particles in HIT coincides with acceleration stagnation points of the carrier fluid. This is explained by these regions of zero-acceleration in the fluid being swept together with inertial particles by the large scale motions of the fluid, however when a particle arrives at an acceleration stagnation point it moves with the fluid velocity for a longer period of time than would be otherwise expected, constituting the stick part of the mechanism. This is applicable to particles with a small inertia, and is dependent upon the dynamic sweeping of small scales by the larger scales within a flow field [101]. The result is clustering in the spatial distribution of particles over multiple different scales, with this sweep-stick mechanism

reported to be dominant over the preferential concentration arising from centrifuging out of high vorticity regions [34].

A subsequent experimental investigation [108] into the effect of Re_λ and St_η on clustering focused on the centrifugal effects and sweep-stick mechanisms at work, with the setup consisting of grid generated HIT in a wind tunnel. Clusters are identified using Voronoï analysis by locating cells with areas below a critical threshold [100], and from this it is concluded that the dominant clustering mechanism is the sweep-stick effect of heavy particles preferentially sticking to zero-acceleration points for the parameter space in this study of $Re_\lambda \in [200\text{–}400]$ and $St_\eta \in [2\text{–}10]$. Additionally, it is implied that the resultant increase in local particle concentration from the sweep-stick mechanism could further be responsible for enhancement in the settling velocity under gravity [1]. Another experimental study [148] considering the clustering of small heavy polydisperse particles in HIT examined the dependence on $Re_\lambda \in [170\text{–}450]$, $St_\eta \in [0.1\text{–}5]$, and the volume fraction $\alpha_d \in [2\times10^{-6}\text{–}2\times10^{-5}]$. In [148] clustering was found to be strongly enhanced by increased Re_λ and noticeably enhanced by increased α_d, however a lack of sensitivity in clustering due to variation of St_η is also apparent, which supports the sweep-stick effect as the main physical mechanism responsible for the clustering. Furthermore, a DNS study [157] of finite-size particles ($\rho_p/\rho_f = 1.5$) observed that clustering tendency increases as particle diameter is increased. No significant statistical correlation is reported between particle location and the intense vortical structures within the flow, however preferential concentration of particles is correlated statistically significantly with zero acceleration points of the carrier flow.

3.4.3 Non-Local Path History Effects

On the basis of existing work [178, 15] highlighting the importance to clustering of the history of the velocity gradient tensor sampled by particles, Bragg *et al.* [18] undertook a detailed analysis of the mechanisms responsible for particle clustering in the inertial range of isotropic turbulence in order to determine their relative contribution to the net drift. It is concluded that for $St_\eta \ll 1$, clustering is due to preferential sampling of the coarse-grained fluid velocity gradient tensor resulting in the centrifuge mechanism of Maxey [91], whilst for $St_\eta > 1$ a clustering mechanism involving the sampling of larger fluid velocity differences along the *non-local path history* is responsible. Additionally, if the Taylor Reynolds number Re_λ is sufficiently large, particles may also cluster due to mechanisms which act in the inertial range of turbulence, with such mechanisms being analogous to those in the dissipation range. In this work it is also noted that the

sweep-stick mechanism idea that particles stick to particular acceleration stagnation points and are swept along is probably not valid, however particles may be swept by clusters of stagnation points. Nonetheless, it is found that the sweep-stick mechanism breaks down at $St_\eta \sim \mathcal{O}(10)$ as it is a local mechanism, and for $St_\eta \ll 1$ is the same as the preferential sampling of strain over rotation.

Further investigation into the relationship between the non-local path history and preferential concentration mechanisms was undertaken by Bragg *et al.* [19]. Despite the dominant clustering mechanism changing from centrifuging for $St_\eta \ll 1$ to the symmetry breaking effects of non-local path history for $St_\eta > 1$, the particle positions continue to correlate with high strain, low rotation regions of turbulence in both cases. This is due to the non-local path history effects being influenced by the preferential sampling of the fluid velocity gradient tensor along the particle trajectories in such a way as to generate a bias for clustering in high strain regions of the turbulence. The strength of the resulting inward drift in the dissipation range is influenced by the way particles have interacted with the strain and rotation tensors along their path history. For $St_\eta = \mathcal{O}(1)$, the centrifuge mechanism is not the primary cause of clustering, but influences it through the way it causes particles to preferentially sample the fluid velocity gradient tensor along their path histories. Clustering is possible at this Stokes number even if the centrifuge mechanism does not operate, causing preferential concentration to disappear. From simulations it was seen that over the timescale for which particles retain memory of their path history, the strain and rotation fields remain significantly correlated along the particle trajectory, with the preferential sampling affecting the non-local contributions to the drift velocity, which subsequently generates the clustering. It was also noted that for particles settling under gravity, the centrifuge mechanism no longer operates and preferential concentration vanishes, however clustering still exists due to the non-local path history symmetry breaking mechanism.

A separate line of enquiry [40] analysed the effect of the often neglected Basset history force on particle statistics including preferential concentration. This was shown to be significant, with a reduction observed in all of preferential concentration, particle slip velocity, acceleration of particles relative to the fluid, and collision rate, which were attributed to the history force causing inertial particles to stay closer to the flow and behave more like fluid elements.

3.4.4 Further Developments

The effect of clustering mechanisms in a synthetic velocity field has been the focus of one investigation [106] on the premise that the correlation of particle concentration and local fluid properties cannot be accurately predicted unless at least convection is included, and thus in general synthetic flow fields will result in less clustering and enhanced settling than fully developed turbulence. As the centrifuge effect requires finite-time decorrelation of vortex structures, clustering in velocity fields which are delta-correlated in time therefore cannot occur from centrifuging as the dominant mechanism, with this instead being attributed to a *sling effect*. This involves the presence of fluid structures that result in regions of increased particle concentration being significantly removed in both time and space from where the effect is observed. Clustering is found to be generally stronger for non-Gaussian velocity fields with a finite-time decorrelation, in which case a significant widening of the tails for the PDF of the second invariant of the fluid velocity gradient tensor occurs, meaning that large values of strain and rotation are more likely and causing centrifuging to be the main mechanism responsible for clustering in this case. Additionally, for high St it is observed that particles in non-Gaussian turbulence preferentially sample regions of low kinetic energy, whereas particles in Gaussian turbulence preferentially sample regions of high kinetic energy, leading to different contributions towards overall clustering from centrifuging effects in these two distinct cases.

An investigation [147] into the spatial patterns that are formed due to particle clustering as St is varied involved computation of the finite-time Lyapunov exponent field for the full BBO equation in order to characterise the clustering, with the main result being that inertial particles are attracted to or repelled from zones of high concentration depending on whether the particles are aerosol (high density) or bubbles (low density). In the case of true turbulence, a DNS study [4] of particles in HIT using one-way coupling with a linear drag law has confirmed that the average particle concentration is strongly dependent on Stokes number, but also observed that individual clusters of particles display strongly multi-scale behaviour (in agreement with recent work [155] on preferential concentration arising due to gravity), and that clusters are aligned with the local vorticity vector. Particles within coherent clusters are found to display a much stronger tendency to sample high-strain low-vorticity regions, and this is demonstrated to be true for both St_η significantly larger than unity as well as small St_η. In terms of settling speed due to a gravitational body force, particles inside coherent clusters oversample downward flow regions, leading to an average settling velocity of almost

double that of the still-fluid terminal velocity. Further to this occurrence of preferential sweeping, clustering is stronger in the presence of gravitational settling, a finding which is at odds with the centrifuging mechanism, since settling is expected to decorrelate particles from the turbulent structures within the flow field.

3.4.5 Particle Pair Modelling

One approach to analysing the clustering of particles is by using so-called particle-pair models, in which the separation between particles is studied. Of the work done in this area, the radial distribution function (RDF) has provided a key measure of particle clustering [46]. Defined by Reade & Collins [121], the RDF has the physical interpretation of the number of particle centres located in a spherical shell about a central particle divided by the expected number of particles given a uniformly distributed particle field. The first analytical model for the RDF was obtained by Zaichik [177], by treating the clustering phenomenon in homogeneous turbulence as a result of a particle migration drift in the separation direction due to the gradient of the radial relative fluctuating velocity, and therefore interpreting the drift as an additional attractive velocity. This work involved the development of a kinetic equation for the joint pair PDF of separation and relative velocity. The Furutsu-Novikov closure is applied to the phase-space diffusion current, and the functional derivatives are approximated by assuming that the infinitesimal change in fluid velocity is delta-correlated in both space and time, meaning that the unclosed expressions within the resultant kinetic equation reduce to Lagrangian correlations and structure functions of the fluid velocity. From the kinetic equation a set of continuum equations for the particle pair density, mean relative velocity, and second-order two-point Lagrangian velocity structure functions are derived. Closure of these is performed by modelling the fluid velocity structure functions over the viscous and inertial subranges using an interpolation of Taylor expansions and Kolmogorov's similarity hypothesis. The RDF is interpreted as a renormalisation of the particle pair density, leading to a power law behaviour with an exponent that is proportional to St^2 for small St, and providing a benchmark for quantifying particle clustering.

Further work by Zaichik [178] refined this approach using improved closure methodologies. The approach taken to modelling the second-order two-point Lagrangian fluid velocity structure functions in the previous work [177] assumed that the timescales of the two-point strain and rotation correlations are equal, however Brunk *et al.* [21] observed through use of the DNS data of Girimaji & Pope [60] that these timescales

can differ significantly over small separations. By modelling the structure functions in terms of the strain and rotation rate tensors, the different timescales introduced by these components ensures the turbulence-particle interaction mechanism that contributes to the preferential clustering is captured to a greater extent. This is done by means of constructing a transport equation for the strain and rotation tensors, which are closed using a quasi-Gaussian approximation for the third-order moments. At small separations the clustering effect is found to increase with the ratio between the timescales of the rotation and strain rate correlations, however this result is only valid in the viscous subrange. Extension of the applicability of this work from zero-size to finite-size particles was also considered by Zaichik [179] by applying boundary conditions to the continuum equations at a separation equal to the particle diameter, along with further minor refinement of approximating the second-order two-point Lagrangian fluid velocity structure functions. Additionally, the timescales of the strain and rotation rate correlations were expressed in terms of the Kolmogorov timescale as $\tau_\Sigma = 2.3\tau_\eta$ and $\tau_\Omega = 7.2\tau_\eta$ following on from previous work [21, 60].

In some other pioneering work, Chun *et al.* [31] developed an analytical theory for predicting the the RDF in turbulent flows for small particles, by supposing that the preferential concentration of particles at lengthscales smaller than the Kolmogorov scale can be attributed to a radial inward drift of inertial particles in a locally linear flow field. This was performed within a particle pair framework by analysis of particle equations of motion written in terms of the particle separation and relative velocity. Noting that the definition of drift can be obtained by performing a perturbation expansion in Stokes numbers on these equations, averaging to obtain expressions for the drift velocity, and making closures using the rate of strain and rotation tensors, a model for the relative particle separation and velocity is obtained. A PDF equation in terms of the relative particle separation and velocity is developed using the method of characteristics, with the distinction that the joint PDF is not used, but rather a separate PDF for each phase-space variable. Closure is made using the previously derived models, and the RDF is related to the average of the PDF by a simple normalisation procedure. Solution for the RDF leads to the expected power law behaviour with an exponent that is proportional to St_η^2 in agreement with Zaichik [177], and testing against both a stochastic model and DNS data confirms good agreement between the model and simulations. Due to the perturbation expansion used this result is only valid for small Stokes numbers (i.e. at Kolmogorov scaling $St_\eta = \tau_p/\tau_\eta$), whereas Zaichik [177, 178, 179] also investigated the preferential concentration at intermediate St (i.e. the integral scales $St_E = \tau_p/\tau_E$).

Building upon this work, further analysis of the approaches by Chun *et al.* [31] and

Zaichik [178] was undertaken by Bragg & Collins [15] in order to compare the two theoretical models and gauge their applicability. It is observed that the model proposed by Chun *et al.* neglects the effect of the path history contribution due to truncation of the perturbation expansion used, with the physical explanation of the drift coming purely from the centrifuge mechanism of oversampling strain over rotation. Additionally, the effect of caustics is not taken into account. In contrast, the Zaichik model captures the path history contribution, whilst also including the effect of caustics. Despite this, the Zaichik model observes a quantitative discrepancy in the power law exponent of the RDF, which could be attributable to a number of reasons. Chief among these is the local closure used on the functional derivative within the kinetic equation, with the omission of non-local effects possibly accounting for this discrepancy. Subject to the restriction of $St \ll 1$ for which the Chun *et al.* model is valid, it does capture the leading order effects of the clustering mechanism behaviour in the Zaichik model, whilst the non-local contribution to the mechanism significantly enhances the inward drift. However the Chun *et al.* model incorrectly assumes that the PDF of relative velocity is incompressible, meaning that the non-centrifuge mechanism proposed by Ijzermans *et al.* [73] involving evolution of the deformation tensor along a trajectory is not accounted for. In the second part of this study Bragg & Collins [16] analysed the relative velocity distribution of particles using the same models in order to determine whether the influence of non-local dynamics on the formation of caustics is captured. It was observed that particle pairs originating from larger separations have experienced on average more energetic turbulence than pairs that have come from smaller separations in their path history, with this creating a net inward drift and therefore clustering.

Additionally it is noted by Bragg & Collins [16] that an error arises in the non-local drift contribution as the forward-in-time (FIT) separation is used whereas for consideration of particles at a previous time it is actually the backward-in-time (BIT) separation that is required. Since the dynamics of particle separation are not invariant under time reversal, the resultant contributions from using the forward-in-time separation to represent the path history are technically incorrect, forming the basis of an ongoing line of investigation by Bragg [20, 14]. The research in this vein to date has reported that for a critical Stokes number St_c, in two-dimensional turbulence FIT dispersion is faster than BIT dispersion for $St < St_c$, but for $St > St_c$ BIT dispersion is faster than FIT dispersion [17]. This behaviour was attributed to two distinct irreversibility mechanisms competing against each other, which are specified as the local energy flux in the turbulent field and non-local path history effect that also serves to induce clustering respectively. In three-dimensional turbulence, both mechanisms act together so that

BIT dispersion is faster than FIT dispersion across all St, however in two-dimensional turbulence, the two mechanisms have opposite effects due to the energy flux from small to large scales which exists. Further to this, investigation [45] into the moments of separation between two fluid particles for separations within the dissipation range has found that these moments grow first as power law at small times, followed by exponential growth for $t > 200\tau_\eta$. This long time exponential behaviour is due to fluctuations of the strain rate along particle trajectories, and results in the difference between the rate of particle separation FIT and BIT growing exponentially at long times, for which the implications on clustering are a present research interest.

3.5 Methods of Simulation

Although the main focus of investigation into multiphase flow systems is to develop better understanding of the physical behaviour in various flow regimes and applied contexts, focus purely upon how such situations are treated numerically is also an area of research in its own right. The salient approaches are DNS and KS, with each having their own distinct advantages for use, and some of the current developments regarding these methods are outlined in this section.

3.5.1 Direct Numerical Simulation

In the context of dispersed particle transport DNS is an eminently suitable means of investigation, as the mechanisms responsible for particle behaviour can occur over a wide range of lengthscales, and therefore a full physical description of the carrier flow is necessary in order to gain an accurate understanding of phenomenological observations. One requirement in the study of particle behaviour is for the continuous phase to ideally be statistically stationary, and this constitutes an added consideration within DNS, as the turbulent kinetic energy (TKE) naturally decays when the simulation is advanced in time. To address this, a range of turbulence forcing mechanisms have been developed that maintain a constant TKE, with the original focus being on schemes implemented in spectral space [50]. This is the obvious starting point conceptually, since injection of energy at the lowest wavenumber modes allows for the energy cascade to naturally pass this energy down to the high wavenumber modes, without altering the turbulence energy spectrum in the process. However, the disadvantage to forcing in spectral space is that many DNS codes run in physical space, making forcing in this way impractical

due to the high computational overhead of using the inverse Fast Fourier Transform (FFT) to convert the forcing contribution to a physical velocity field at every timestep. As a result attention has more recently been devoted to developing forcing mechanisms in physical space, with the simplest proposal being that of linear forcing [87], and subsequent refinements introducing control mechanisms that tightly regulate the TKE to the desired level [26, 89]. Despite this, direct forcing of the velocity field in such a manner distributes the injected energy over all wavenumber modes in spectral space, and as a consequence artificially modifies the turbulence energy spectrum from its natural form. This has the drawback of altering the longitudinal integral lengthscale L_{11} of the turbulence so that it converges to a constant fraction of the simulation domain size independent of the initial conditions, and cannot be changed as a variable parameter in parametric studies, thereby limiting the applicability of linear forcing [135]. More recent work [81, 113] has addressed this shortcoming by use of a low-pass filter on the forcing contribution to the velocity field to ensure that energy is only injected into the largest scales of turbulent motion, thus allowing the energy cascade to evolve naturally, and regaining control of the longitudinal integral lengthscale L_{11} as a simulation parameter.

3.5.2 Kinematic Simulation

The application of KS to disperse particle transport research has been widespread due to its relatively low computational expense, and has produced insights into phenomena not previously observed [92, 91, 72, 73], with this work often being the precursor to further studies using DNS [163, 95]. A particularly helpful feature of KS is to control structures within the flow [73], so that the influence of such structures on particle behaviour can be accurately quantified. Furthermore, KS can be used to construct non-Gaussian flow fields which take into account physics such as convection [106], leading to local flow structures being transported with the particles. Other variants include target Lagrangian KS [104], in which the Lagrangian integral timescale is enforced rather than Eulerian integral timescale, on the premise that to ensure recovery of the expected Lagrangian behaviour the realism of the Eulerian behaviour can be sacrificed. The expected behaviour of inertial particles is recovered using this approach, including the crossing trajectories effect, and the Lagrangian statistics are effectively captured. Additionally, the ability to vary the energy spectrum in KS has been used to investigate the effect on the clustering of inertial particles subject to gravity [105], by quantifying the different spectral power laws on the form of attractor

to which the particles equilibrate. It is found that variation of the spectral law can have a significant effect on the attractor shape, and notably in two-dimensional simulations that the attractor is only affected by a changed spectrum power in the presence of gravity.

The suitability of KS for reproducing particle statistics is an often raised point, and work [103] addressing this has concluded that KS qualitatively reproduces the continuity effect, clustering of particles, and pairwise dispersion of particles, but not to the same extent as DNS owing to the behaviour at the microscales being omitted. However, Lagrangian correlations along particle trajectories are overpredicted by KS compared to DNS, but do compare better in the case when gravity is included. Focusing upon the structures within the velocity field, KS has been found [55] to be deficient compared to DNS chiefly because vortical regions are not sufficiently elongated, and higher-order statistics are too closely Gaussian. This stems directly from the fact that KS does not represent the dynamical processes in turbulence which are responsible for vortex stretching and turbulence intermittency, and this in turn affects higher-order statistics. However, this work does observe that generation of random displacements of fluid elements and a flow field which has a time dependent structure is sufficient to capture the effect of the evolution of fluid structures upon particles. Further to this, KS has been used to investigate the separation of particle pairs [153], finding that the mean-square separation of particle pairs in the inertial subrange grows like t^6 in the presence of a strong mean velocity and as $t^{9/2}$ in the case of no mean flow. This compares with a growth in separation like t^3 in both flow configurations for true turbulence, and raises questions about the applicability of KS to simulate particle pair separation in real turbulent flows.

3.6 Research Aims of the Current Work

The scope of this research falls under the application of PDF modelling to disperse particle transport, with specific attention on the class of kinetic models [44, 124, 71], and notably that developed by Swailes & Darbyshire [150, 151] using the Furutsu-Novikov closure. As the focus is upon dilute-phase transport, the effects of inter-particle collisions and local fluid disturbances generated as a result of particle motion can be taken to be negligible, and consequently three and four-way coupling mechanisms do not need to be accounted for in this work. Additionally, when dealing with the closure of two-fluid models it is advantageous to restrict attention to the case of just one-way

coupling in order to keep the description of the problem more tractable, meaning that the condition of $\alpha_d < 10^{-6}$ must be observed. Furthermore, the particles are taken to have a density much greater than that of the fluid so that a linear drag law can be used for the equation of motion as is typical in gas-solid flows.

The aim of this work is firstly to use data from particle tracking simulations within various flow configurations to demonstrate that the PDF kinetic model is a suitable means of assessing the contributions arising from the particle mass flux which act as additional drift terms, and thereby lead to subtle modification in the particle behaviour. The use of certain flow configurations enables these contributions to the particle mass flux to be manipulated and therefore analysed in isolation, meaning that the physical mechanisms responsible can be investigated using such an approach. Evaluation of existing local [151, 127] and non-local [142, 13] models are addressed, in order to demonstrate the inadequacy of these closures for describing particle behaviour in the specific flow configurations which are considered. The secondary focus is then the development of closure models which are able to account for the additional drift terms that arise, by relating them to the underlying physical mechanisms outlined in the literature which are responsible for the existence of these contributions.

The first flow configuration of interest is that of a homogeneous isotropic fluid velocity field subject to gravity. The presence of a physical body force results in identification of a contribution to the particle mass flux from the PDF kinetic model that acts as an additional body force, and is equal to the increase in settling rate compared to a quiescent flow. This term, which is critical in the formulation of two-fluid models, requires closure. Existing closures are shown to be inadequate for capturing the enhancement in settling rate, meaning that an improved methodology is required which accounts for the physical mechanisms behind the observed behaviour. As the PDF kinetic model is exact when the continuous phase is Gaussian, all the necessary physics leading to the observed settling enhancement is contained within the unclosed terms, leaving the challenge of capturing the non-local path history effects and subsequent inertial bias experienced by particles as a result of preferential sampling of strain over rotation within a closure model.

The relative distribution of particle-pair models can also be studied within the alternative configuration of an appropriate inhomogeneous flow field using the PDF kinetic model, with analysis of the corresponding RDF being carried out in order to investigate particle clustering. In this case the PDF approach identifies two key contributions within the convective-diffusive representation of the particle mass flux, the balance of

which governs the associated net drift and thereby preferential concentration of particles. These emerge from a density weighted body force term associated with the statistical inhomogeneities of the turbulence, and a term contributing to the particle phase stress tensor, which both require closure. As in the case of gravitational settling, it is seen that simple local closures which neglect the non-local path history of particles cause both contributions to the particle mass flux to vanish, and thereby do not capture the observed clustering behaviour within the description provided by the PDF kinetic model. However, it can be demonstrated that the non-local drift term is not identically zero for low inertia particles, and is in fact a significant flux contribution for $St \ll 1$.

Chapter 4

PDF Modelling of Disperse Particle Transport

Two-fluid modelling has distinct advantages in several respects when compared to particle tracking, notably that the statistical nature which is intrinsic to the modelling means that it is less computationally demanding and therefore much quicker to obtain solutions for, and also that it can provide some insight into the underlying physics of the average behaviours observed in particle dispersion. On the other hand, the averaged nature of two-fluid models introduces a number of difficulties, namely including the more complex forces which act upon a particle such as lift and history terms, incorporating physically relevant boundary conditions within the dispersed phase transport equations, and also causing the loss of some level of detail due to this statistical means of description [36]. Treatment of these issues using the heuristic means of construction for the dispersed phase transport equations outlined in section 2.3.2 is reliant upon closures of an empirical nature which are made at a high level of physics, and consequently have a more limited chance of resulting in a sufficiently accurate description for a given flow configuration. This heuristic approach is not however the only method of construction for the dispersed phase transport equations of two-fluid models, with an alternative statistical formulation existing in terms of the probability density function (PDF), which exists as a class of models in its own right for describing the behaviour of particles within a turbulent velocity field [48].

The PDF approach presents a rational framework for the development of two-fluid models, as the starting point is from the underlying particle equation of motion used for particle tracking. A master transport equation governing the evolution of the PDF itself can formally be derived in particle phase space, which contains unclosed terms

involving the particle-fluid interactions. The dispersed phase continuum equations for the corresponding two-fluid model can then be derived directly from the PDF transport equation, however the unclosed terms also emerge in the two-fluid model as part of the dispersed phase stress tensor $\boldsymbol{\sigma}_d$, and therefore once the PDF itself is known then specification of the associated two-fluid model automatically follows without need for any further closures. This is advantageous, as the PDF transport equation in phase space can be closed at a more basic level of dynamics than the two-fluid model. Thus a given closure is more likely to be sufficiently accurate for describing the required particle behaviour than a similar strategy applied directly to the two-fluid model, which is more dependent on intuition and empiricism. For instance, making simple Boussinesq approximations at phase-space level does not necessarily mean that the corresponding closures within the two-fluid model will also be in the form of Boussinesq approximations. Furthermore, correct specification of boundary conditions for near-wall behaviour can be encapsulated within the general form of the PDF framework, since these involve knowledge of the particle velocity distribution at the walls [48].

4.1 Derivation of The Kinetic Equation

Within the framework of the PDF approach the research in this thesis uses the kinetic model, for which the PDF is associated with the joint probability distribution of a particle in phase-space having position $\mathbf{x}$ and velocity $\mathbf{v}$ at time t, and is characterised by the average probability density function given by $p(\mathbf{x}, \mathbf{v}, t)$. In order to derive a transport equation that defines $p(\mathbf{x}, \mathbf{v}, t)$, it is natural to consider the construction of a PDF equation that corresponds to a general system of stochastic ordinary differential equations.

4.1.1 Phase-Space Representation

For modelling purposes it is convenient to write the particle equation of motion in the general form

$$\begin{aligned} \frac{d\boldsymbol{x}_p}{dt} &= \boldsymbol{v}_p \qquad\qquad\qquad , \quad \boldsymbol{x}_p(t_0) = \mathbf{x}^0 \\ \frac{d\boldsymbol{v}_p}{dt} &= \mathbf{F}(\boldsymbol{x}_p, \boldsymbol{v}_p, t) + \mathbf{f}(\boldsymbol{x}_p, t) \quad , \quad \boldsymbol{v}_p(t_0) = \mathbf{v}^0 \end{aligned} \tag{4.1}$$

where $\mathbf{F}(\mathbf{x}, \mathbf{v}, t)$ defines the mean continuous phase force per unit mass acting on particles with position $\mathbf{x}$ and velocity $\mathbf{v}$ at time t, and $\mathbf{f}(\mathbf{x}, t)$ is a zero-mean stochastic field modelling the fluctuating acceleration experienced by a particle with position $\mathbf{x}$ at time t. It is important at this stage to distinguish between $(\mathbf{x}, \mathbf{v})$ denoting coordinates in phase space, and $(\boldsymbol{x}_p, \boldsymbol{v}_p)$ denoting the particle position and velocity along an individual trajectory at time t. Then by introducing the Reynolds decomposition $\mathbf{u} = \langle \mathbf{u} \rangle + \mathbf{u}'$ of the continuous phase velocity $\mathbf{u}$ into components for the mean flow $\langle \mathbf{u} \rangle$ and fluctuating flow $\mathbf{u}'$, the decomposition for the particle equation of motion (4.1) in the case of the Stokes drag model (2.22) corresponds to

$$\mathbf{F}(\mathbf{x}, \mathbf{v}, t) = \beta \left(\left\langle \mathbf{u}(\mathbf{x}, t) \right\rangle - \mathbf{v} \right) + \mathbf{g} \tag{4.2}$$

$$\mathbf{f}(\mathbf{x}, t) = \beta \mathbf{u}'(\mathbf{x}, t) \tag{4.3}$$

where $\beta = \tau_p^{-1}$ is the particle inertia parameter. For further ease of working, it is helpful to recast the problem into phase-space, which not only permits a more concise formulation but also provides a generic framework in which the PDF of other systems can be analysed. This is achieved by converting the particle equation of motion into system form through introduction of the phase-space coordinate vector $\boldsymbol{\xi} = (\mathbf{x}, \mathbf{v})$, and in the same manner denoting a trajectory within phase-space as $\boldsymbol{z}(t) = (\boldsymbol{x}_p(t), \boldsymbol{v}_p(t))$. The particle equation of motion (4.1) can then be described by the general phase-space form

$$\dot{\boldsymbol{z}}(t) = \mathbf{a}(\boldsymbol{z}(t), t) + \mathbf{b}(\boldsymbol{z}(t), t) \quad , \quad \boldsymbol{z}(t_0) = \boldsymbol{\xi}^0 \tag{4.4}$$

with $\mathbf{a}(\boldsymbol{\xi}, t) = (\mathbf{v}, \mathbf{F}(\mathbf{x}, \mathbf{v}, t))$ being a deterministic function and $\mathbf{b}(\boldsymbol{\xi}, t) = (\mathbf{0}, \mathbf{f}(\mathbf{x}, t))$ being a zero-mean stochastic field.

4.1.2 The Fine-Grained PDF and Liouville Equation

Formally, the average PDF $p(\mathbf{x}, \mathbf{v}, t)$ defining the distribution of the stochastic process $\boldsymbol{z}(t)$ can be expressed as

$$p(\boldsymbol{\xi}, t) = \left\langle \delta(\boldsymbol{z}(t) - \boldsymbol{\xi}) \right\rangle \tag{4.5}$$

where $\langle\cdot\rangle$ denotes an ensemble average taken over all realisations of $\boldsymbol{z}(t)$, and $\delta(\cdot)$ is the Dirac delta function. The PDF interpretation (4.5) can be viewed as the mathematical idealisation of a box counting method, in which the proportion of trajectories $\boldsymbol{z}(t)$ that pass through an elemental phase-space volume that is centred on $\boldsymbol{\xi}$ is computed. Following from this, the instantaneous PDF $\mathcal{P}(\boldsymbol{\xi}, t)$ for a particle with position $\mathbf{x}$ and velocity $\mathbf{v}$ at time t is defined as the *fine-grained* version of $p(\boldsymbol{\xi}, t)$ [150, 71]

$$\mathcal{P}(\boldsymbol{\xi}, t) = \delta(\boldsymbol{z}(t) - \boldsymbol{\xi}) \tag{4.6}$$

Thus the relationship between the average and fine-grained PDFs is $p(\boldsymbol{\xi}, t) = \langle \mathcal{P}(\boldsymbol{\xi}, t) \rangle$. A transport equation for the PDF $p(\boldsymbol{\xi}, t)$ is obtained by taking the derivative of (4.5) with respect to time, from which it follows that [44, 71]

$$\frac{\partial}{\partial t} p(\boldsymbol{\xi}, t) = -\frac{\partial}{\partial \boldsymbol{\xi}} \cdot \left[\mathbf{a}(\boldsymbol{\xi}, t)\, p(\boldsymbol{\xi}, t) + \left\langle \mathbf{b}(\boldsymbol{z}(t), t)\, \mathcal{P}(\boldsymbol{\xi}, t) \right\rangle \right] \tag{4.7}$$

This is the Liouville equation for $p(\boldsymbol{\xi}, t)$, in which the ensemble average on the right-hand side of is referred to as the *phase-space diffusion current*, with specification of this expression representing the closure problem in the PDF kinetic framework.

4.1.3 Correlation Splitting

Various methods of closing the phase-space diffusion current have been used (see section 3.1.1), with one such approach being through the use of correlation splitting techniques. To proceed with closure in this manner, firstly note that due to the filtering property of the fine-grained PDF $\mathcal{P}(\boldsymbol{\xi}, t)$ only realisations of $\boldsymbol{z}$ for which $\boldsymbol{z} = \boldsymbol{\xi}$ contribute to the ensemble average, and therefore

$$\left\langle \mathbf{b}(\boldsymbol{z}(t), t)\, \mathcal{P}(\boldsymbol{\xi}, t) \right\rangle = \left\langle \mathbf{b}(\boldsymbol{\xi}, t)\, \mathcal{P}(\boldsymbol{\xi}, t) \right\rangle \tag{4.8}$$

Furthermore, $\mathcal{P}(\boldsymbol{\xi}, t)$ is a function of $\boldsymbol{z}(t)$, which has a functional dependence on the process $\mathbf{b}(\boldsymbol{z}(t), t)$ through the phase-space equation of motion (4.4), meaning that the fine-grained PDF can be denoted as $\mathcal{P}(\mathbf{b}; \boldsymbol{\xi}, t)$. The subsequent form of the phase-space diffusion current then enables a result from stochastic analysis to be used which provides an expansion in terms of the cumulants $\mathbf{K}$ of $\mathbf{b}$, specifically written in multi-index notation as [56, 107]

$$\left\langle \mathrm{b}_i\left(\boldsymbol{\xi},t\right)\mathcal{P}\left(\mathbf{b};\boldsymbol{\xi},t\right)\right\rangle = \sum_{k=1}^{\infty}\frac{1}{k!}\sum_{\mathbf{j}^k}\int_{t_1=t_0}^{t}\int_{\boldsymbol{\xi}_1}\cdots\int_{t_k=t_0}^{t}\int_{\boldsymbol{\xi}_k}\mathrm{K}_{i,\mathbf{j}^k}^{k+1}(\boldsymbol{\xi},t;\boldsymbol{\xi}_1,t_1\cdots;\boldsymbol{\xi}_k,t_k) \cdot\left\langle\frac{\delta^k}{\delta\mathrm{b}_{j_1}(\boldsymbol{\xi}_1,t_1)\cdots\delta\mathrm{b}_{j_k}(\boldsymbol{\xi}_k,t_k)}\mathcal{P}\left(\mathbf{b};\boldsymbol{\xi},t\right)\right\rangle d\boldsymbol{\xi}_k\,dt_k\cdots d\boldsymbol{\xi}_1\,dt_1 \tag{4.9}$$

where $\sum_{\mathbf{j}^k}$ indicates a sum over all components of the k-tuple $\mathbf{j}^k=(j_1,...,j_k)$, and $\mathbf{K}^{k+1}$ is the $(k+1)^{th}$ cumulant of the stochastic field $\mathbf{b}\left(\boldsymbol{\xi},t\right)$. The formula (4.9) thus represents the correlation between $\mathbf{b}$ and $\mathcal{P}$ in terms of the cumulants of $\mathbf{b}$ and the functional derivative of $\mathcal{P}$, and contains an infinite number of terms without the use of a specific choice of probably distribution for $\mathbf{b}$. In order to make the use of (4.9) more tractable, it is advantageous to select a distribution of $\mathbf{b}$ which avoids the appearance of the higher-order cumulants; in particular all the cumulants $\mathbf{K}^n$ of a Gaussian distribution for $n>2$ are zero, and it is the only distribution with this property [132]. Therefore assuming that $\mathbf{b}$ is a Gaussian field reduces the correlation splitting result to the exact representation known as the Furutsu–Novikov formula [82]

$$\left\langle \mathrm{b}_i\left(\boldsymbol{\xi},t\right)\mathcal{P}\left(\mathbf{b};\boldsymbol{\xi},t\right)\right\rangle = \int_{t_0}^{t}\int_{\boldsymbol{\xi}'}\mathrm{K}_{ij}^{2}(\boldsymbol{\xi},t;\boldsymbol{\xi}',t')\left\langle\frac{\delta}{\delta\mathrm{b}_j(\boldsymbol{\xi}',t')}\mathcal{P}\left(\mathbf{b};\boldsymbol{\xi},t\right)\right\rangle d\boldsymbol{\xi}'\,dt' \tag{4.10}$$

in which summation over the index j is now assumed implicitly. From (4.10) the closure problem reduces to evaluation of the functional derivative of $\mathcal{P}$, for which correct treatment is essential in order to include the full effect of the field $\mathbf{b}$ on the evolution of $\mathcal{P}$. Specifically, the chain rule for functional differentiation is used since the functional dependence of $\mathcal{P}$ on $\mathbf{b}$ is through the phase-space trajectory $\boldsymbol{z}(t)$, following which making use of the filtering property of the δ-function results in [44, 71, 150]

$$\frac{\delta}{\delta\mathrm{b}_j(\boldsymbol{\xi}',t')}\mathcal{P}\left(\mathbf{b};\boldsymbol{\xi},t\right) = -\frac{\delta z_k(t)}{\delta\mathrm{b}_j(\boldsymbol{z}(t'),t')}\frac{\partial\mathcal{P}}{\partial\xi_k}\left(\boldsymbol{\xi},t\right)\,\delta(\boldsymbol{\xi}'-\boldsymbol{z}(t')) \tag{4.11}$$

in which summation over the dummy index k is implied, and the functional dependence of $\mathcal{P}$ on $\mathbf{b}$ is no longer stated explicitly. Noting that in (4.10) the operations of ensemble averaging and integration commute, substitution of (4.11) and evaluation of the integral over the phase-space coordinate $\boldsymbol{\xi}'$ yields

$$\left\langle \mathrm{b}_i\left(\boldsymbol{\xi},t\right)\mathcal{P}\left(\mathbf{b};\boldsymbol{\xi},t\right)\right\rangle = -\int_{t_0}^{t}\left\langle \mathrm{K}_{ij}^{2}(\boldsymbol{\xi},t;\boldsymbol{z}(t'),t')\,\frac{\delta z_k(t)}{\delta \mathrm{b}_j(\boldsymbol{z}(t'),t')}\,\frac{\partial\mathcal{P}}{\partial\xi_k}\left(\boldsymbol{\xi},t\right)\right\rangle dt' \tag{4.12}$$

in which it is emphasised that the expression $\mathbf{K}^2(\boldsymbol{\xi},t;\boldsymbol{z}(t'),t')$ denotes that the Eulerian form of the cumulant $\mathbf{K}^2(\boldsymbol{\xi},t;\boldsymbol{\xi}',t')$ is taken and then subsequently evaluated along the phase-space trajectory $\boldsymbol{\xi}'=\boldsymbol{z}(t')$. The key outcome of this treatment is that $\mathbf{K}^2(\boldsymbol{\xi},t;\boldsymbol{z}(t'),t')$ is a stochastic quantity, and hence must appear within the ensemble average in (4.12). Then since the cumulant $\mathbf{K}^2$ has a dependence on the phase-space coordinate $\boldsymbol{\xi}$ but the functional derivative that appears within (4.12) does not, manipulation of the partial derivative $\partial/\partial\boldsymbol{\xi}$ leads to

$$\begin{aligned}\left\langle \mathrm{b}_i\left(\boldsymbol{\xi},t\right)\mathcal{P}\left(\mathbf{b};\boldsymbol{\xi},t\right)\right\rangle = &\int_{t_0}^{t}\left\langle \frac{\partial}{\partial\xi_k}\mathrm{K}_{ij}^{2}(\boldsymbol{\xi},t;\boldsymbol{z}(t'),t')\,\frac{\delta z_k(t)}{\delta \mathrm{b}_j(\boldsymbol{z}(t'),t')}\,\mathcal{P}\left(\boldsymbol{\xi},t\right)\right\rangle dt' \\ &-\frac{\partial}{\partial\xi_k}\int_{t_0}^{t}\left\langle \mathrm{K}_{ij}^{2}(\boldsymbol{\xi},t;\boldsymbol{z}(t'),t')\,\frac{\delta z_k(t)}{\delta \mathrm{b}_j(\boldsymbol{z}(t'),t')}\,\mathcal{P}\left(\boldsymbol{\xi},t\right)\right\rangle dt'\end{aligned} \tag{4.13}$$

Finally, the fine-grained PDF $\mathcal{P}\left(\boldsymbol{\xi},t\right)$ can be extracted from the ensemble average to give an expression in terms of the average PDF $p\left(\boldsymbol{\xi},t\right)$

$$\begin{aligned}\left\langle \mathrm{b}_i\left(\boldsymbol{\xi},t\right)\mathcal{P}\left(\mathbf{b};\boldsymbol{\xi},t\right)\right\rangle = &\int_{t_0}^{t}\left\langle \frac{\partial}{\partial\xi_k}\mathrm{K}_{ij}^{2}(\boldsymbol{\xi},t;\boldsymbol{z}(t'),t')\,\frac{\delta z_k(t)}{\delta \mathrm{b}_j(\boldsymbol{z}(t'),t')}\right\rangle_{\boldsymbol{z}=\boldsymbol{\xi}} dt'\,p\left(\boldsymbol{\xi},t\right) \\ &-\frac{\partial}{\partial\xi_k}\left[\int_{t_0}^{t}\left\langle \mathrm{K}_{ij}^{2}(\boldsymbol{\xi},t;\boldsymbol{z}(t'),t')\,\frac{\delta z_k(t)}{\delta \mathrm{b}_j(\boldsymbol{z}(t'),t')}\right\rangle_{\boldsymbol{z}=\boldsymbol{\xi}} dt'\,p\left(\boldsymbol{\xi},t\right)\right]\end{aligned} \tag{4.14}$$

where $\langle\cdot\rangle_{\boldsymbol{z}=\boldsymbol{\xi}}$ denotes a conditional ensemble average based on the subset of realisations for which $\boldsymbol{z}(t)=\boldsymbol{\xi}$. Furthermore, since $\mathbf{K}^2$ is the second cumulant of the zero-mean field $\mathbf{b}$, it can simply be written as the covariance of $\mathbf{b}$

$$\mathrm{K}_{ij}^{2}\left(\boldsymbol{\xi},t;\boldsymbol{\xi}',t'\right)=\left\langle \mathrm{b}_i\left(\boldsymbol{\xi},t\right)\mathrm{b}_j\left(\boldsymbol{\xi}',t'\right)\right\rangle \tag{4.15}$$

Then noting that $\mathrm{K}_{ij}^{2}\left(\boldsymbol{\xi},t;\boldsymbol{\xi}',t'\right)=\mathrm{K}_{ji}^{2}\left(\boldsymbol{\xi}',t';\boldsymbol{\xi},t\right)$, the final correlation splitting result can be written explicitly in terms of the stochastic field $\mathbf{b}$ as

$$\left\langle \mathrm{b}_i\left(\boldsymbol{\xi},t\right)\mathcal{P}\left(\mathbf{b};\boldsymbol{\xi},t\right)\right\rangle = \int_{t_0}^{t}\left\langle \frac{\delta z_k(t)}{\delta \mathrm{b}_j(\boldsymbol{z}(t'),t')}\frac{\partial}{\partial \xi_k}\left\langle \mathrm{b}_j\left(\boldsymbol{\xi}',t'\right)\mathrm{b}_i\left(\boldsymbol{\xi},t\right)\right\rangle\Big|_{\boldsymbol{\xi}'=\boldsymbol{z}(t')}\right\rangle_{\boldsymbol{z}=\boldsymbol{\xi}} dt'\, p\left(\boldsymbol{\xi},t\right) - \frac{\partial}{\partial \xi_k}\left[\int_{t_0}^{t}\left\langle \frac{\delta z_k(t)}{\delta \mathrm{b}_j(\boldsymbol{z}(t'),t')}\left\langle \mathrm{b}_j\left(\boldsymbol{\xi}',t'\right)\mathrm{b}_i\left(\boldsymbol{\xi},t\right)\right\rangle\Big|_{\boldsymbol{\xi}'=\boldsymbol{z}(t')}\right\rangle_{\boldsymbol{z}=\boldsymbol{\xi}} dt'\, p\left(\boldsymbol{\xi},t\right)\right] \tag{4.16}$$

where the inner ensemble average is taken over all realisations of the stochastic field $\mathbf{b}$, and then subsequently evaluated along the phase-space trajectory $\boldsymbol{\xi}' = \boldsymbol{z}(t')$. At this point it is appropriate to denote the functional derivative that appears by $\boldsymbol{\mathcal{G}}[t;t']$

$$\mathcal{G}_{kj}\left[t;t'\right] = \frac{\delta z_k(t)}{\delta \mathrm{b}_j\left(\boldsymbol{z}(t'),t'\right)} \tag{4.17}$$

This has the interpretation of a stochastic 1-point *response tensor* which is dependent on the sample path $\boldsymbol{z}(t)$, and physically describes the effect on the trajectory $\boldsymbol{z}$ at time t that is caused by a perturbation in the field $\mathbf{b}$ at an earlier time t' and corresponding location $\boldsymbol{z}(t')$. The behaviour of this response tensor is therefore central to that of the PDF $p\left(\boldsymbol{\xi},t\right)$, and satisfies the governing equation [150]

$$\dot{\boldsymbol{\mathcal{G}}}\left[t;t'\right] = \left[\frac{\delta \mathbf{a}}{\delta \boldsymbol{\xi}}(\boldsymbol{z}(t),t) + \frac{\delta \mathbf{b}}{\delta \boldsymbol{\xi}}(\boldsymbol{z}(t),t)\right]^{\top}\cdot\boldsymbol{\mathcal{G}}\left[t;t'\right] \quad , \quad \boldsymbol{\mathcal{G}}\left[t';t'\right] = \tilde{\mathbf{I}} = \begin{bmatrix}\mathbf{0} & \mathbf{0}\\ \mathbf{0} & \mathbf{I}\end{bmatrix} \tag{4.18}$$

in which the time derivative is with respect to t rather than t'. Then using the definitions of $\mathbf{K}^2$ in (4.15) and $\boldsymbol{\mathcal{G}}[t;t']$ in (4.17) enables (4.16) to be expressed in the more compact form

$$\left\langle \mathbf{b}\left(\boldsymbol{\xi},t\right)\mathcal{P}\left(\mathbf{b};\boldsymbol{\xi},t\right)\right\rangle = \mathbf{d}\left(\boldsymbol{\xi},t\right)p\left(\boldsymbol{\xi},t\right) - \frac{\partial}{\partial \boldsymbol{\xi}}\cdot\left[\mathbf{D}\left(\boldsymbol{\xi},t\right)p\left(\boldsymbol{\xi},t\right)\right] \tag{4.19}$$

in which $\mathbf{d}\left(\boldsymbol{\xi},t\right)$ is a *drift tensor* with the interpretation of a convective flux and $\mathbf{D}\left(\boldsymbol{\xi},t\right)$ is a *diffusion tensor* representing a diffusive flux, which are defined respectively as

$$\mathbf{d}\left(\boldsymbol{\xi},t\right) = \int_{t_0}^{t}\left\langle \boldsymbol{\mathcal{G}}^{\top}\left[t;t'\right] : \frac{\partial}{\partial \boldsymbol{\xi}}\mathbf{K}^2\left(\boldsymbol{z}',t';\boldsymbol{\xi},t\right)\right\rangle_{\boldsymbol{z}=\boldsymbol{\xi}} dt' \tag{4.20}$$

$$\mathbf{D}\left(\boldsymbol{\xi},t\right) = \int_{t_0}^{t}\left\langle \boldsymbol{\mathcal{G}}\left[t;t'\right]\cdot\mathbf{K}^2\left(\boldsymbol{z}',t';\boldsymbol{\xi},t\right)\right\rangle_{\boldsymbol{z}=\boldsymbol{\xi}} dt' \tag{4.21}$$

where $\boldsymbol{z}' = \boldsymbol{z}(t')$. Using the closure (4.19) in the Liouville equation (4.7) for $p(\boldsymbol{\xi}, t)$ then yields the phase-space form of the PDF *kinetic equation* for the case in which the stochastic field $\mathbf{b}$ has a Gaussian distribution [150]

$$\frac{\partial}{\partial t} p(\boldsymbol{\xi}, t) = -\frac{\partial}{\partial \boldsymbol{\xi}} \cdot \left[\Big(\mathbf{a}(\boldsymbol{\xi}, t) + \mathbf{d}(\boldsymbol{\xi}, t) \Big) p(\boldsymbol{\xi}, t) \right] + \frac{\partial}{\partial \boldsymbol{\xi}} \cdot \frac{\partial}{\partial \boldsymbol{\xi}} \cdot \left[\mathbf{D}(\boldsymbol{\xi}, t)\, p(\boldsymbol{\xi}, t) \right] \tag{4.22}$$

For instances in which important contributions to the particle behaviour are dependent upon non-Gaussian aspects of the stochastic field $\mathbf{b}$, the expansion (4.9) can be extended to include higher-order terms. This results in the kinetic equation (4.22) containing additional drift and diffusion tensors, which in turn consist of the higher-order cumulants $\mathbf{K}^n$ of $\mathbf{b}$ and (n-1)-point response tensors with respect to $\mathbf{b}$ [150].

4.1.4 Physical Space Interpretation

The corresponding interpretation of the PDF kinetic equation in physical space $(\mathbf{x}, \mathbf{v})$ is recovered by recalling the phase-space coordinate definitions

$$\begin{aligned} \boldsymbol{\xi} &= (\mathbf{x}, \mathbf{v}) & \mathbf{a}(\boldsymbol{\xi}, t) &= (\mathbf{v}, \mathbf{F}(\mathbf{x}, \mathbf{v}, t)) \\ \boldsymbol{z}(t) &= (\boldsymbol{x}_p(t), \boldsymbol{v}_p(t)) & \mathbf{b}(\boldsymbol{\xi}, t) &= (\mathbf{0}, \mathbf{f}(\mathbf{x}, t)) \end{aligned} \tag{4.23}$$

This produces

$$\mathbf{K}^2(\boldsymbol{\xi}', t'; \boldsymbol{\xi}, t) = \begin{bmatrix} \mathbf{0} & \mathbf{0} \\ \mathbf{0} & \mathbf{R}(\mathbf{x}', t'; \mathbf{x}, t) \end{bmatrix} \tag{4.24}$$

in which $\mathbf{R}(\mathbf{x}', t'; \mathbf{x}, t)$ is the Eulerian two-point two-time correlation tensor of the fluctuating particle acceleration $\mathbf{f}(\mathbf{x}, t)$

$$\mathrm{R}_{ji}(\mathbf{x}', t'; \mathbf{x}, t) = \Big\langle \mathrm{f}_j(\mathbf{x}', t')\, \mathrm{f}_i(\mathbf{x}, t) \Big\rangle \tag{4.25}$$

and

$$\boldsymbol{\mathcal{G}}[t; t'] = \begin{bmatrix} \mathbf{0} & \boldsymbol{\mathcal{H}}[t; t'] \\ \mathbf{0} & \dot{\boldsymbol{\mathcal{H}}}[t; t'] \end{bmatrix} \tag{4.26}$$

in which $\boldsymbol{\mathcal{H}}[t; t']$ and $\dot{\boldsymbol{\mathcal{H}}}[t; t']$ are respectively the particle response in position $\boldsymbol{x}_p(t)$ and

velocity $\boldsymbol{v}_p(t)$ with respect to the fluctuating particle acceleration along a trajectory $\mathbf{f}(\boldsymbol{x}_p(t'), t')$

$$\mathcal{H}_{ij}\left[t;t'\right] = \frac{\delta x_{p_i}(t)}{\delta \mathrm{f}_j\left(\boldsymbol{x}_p(t'), t'\right)} \quad , \quad \dot{\mathcal{H}}_{ij}\left[t;t'\right] = \frac{\delta v_{p_i}(t)}{\delta \mathrm{f}_j\left(\boldsymbol{x}_p(t'), t'\right)} \tag{4.27}$$

The governing equation for the phase-space response tensor $\boldsymbol{\mathcal{G}}\left[t;t'\right]$ in (4.18) then becomes [151]

$$\ddot{\boldsymbol{\mathcal{H}}}\left[t;t'\right] = \left[\frac{\partial \mathbf{F}}{\partial \mathbf{v}}\right]_p^\top \cdot \dot{\boldsymbol{\mathcal{H}}}\left[t;t'\right] + \left[\frac{\partial \mathbf{F}}{\partial \mathbf{x}} + \frac{\partial \mathbf{f}}{\partial \mathbf{x}}\right]_p^\top \cdot \boldsymbol{\mathcal{H}}\left[t;t'\right] \quad , \quad \begin{matrix} \boldsymbol{\mathcal{H}}\left[t';t'\right] = \mathbf{0} \\ \dot{\boldsymbol{\mathcal{H}}}\left[t';t'\right] = \mathbf{I} \end{matrix} \tag{4.28}$$

where $[\cdot]_p$ denotes that the derivatives of $\mathbf{F}\left(\mathbf{x}, \mathbf{v}, t\right)$ and $\mathbf{f}\left(\mathbf{x}, t\right)$ are quantities which are evaluated along the particle trajectory $(\boldsymbol{x}_p(t), \boldsymbol{v}_p(t))$. The corresponding forms for the drift and diffusion tensors in physical space are [151]

$$\mathbf{d}\left(\boldsymbol{\xi}, t\right) = \left(\mathbf{0}, \boldsymbol{\kappa}\left(\mathbf{x}, \mathbf{v}, t\right)\right) \quad , \quad \mathbf{D}\left(\boldsymbol{\xi}, t\right) = \begin{bmatrix} \mathbf{0} & \boldsymbol{\lambda}\left(\mathbf{x}, \mathbf{v}, t\right) \\ \mathbf{0} & \boldsymbol{\mu}\left(\mathbf{x}, \mathbf{v}, t\right) \end{bmatrix} \tag{4.29}$$

in which the *dispersion tensors* $\boldsymbol{\kappa}\left(\mathbf{x}, \mathbf{v}, t\right)$, $\boldsymbol{\lambda}\left(\mathbf{x}, \mathbf{v}, t\right)$, and $\boldsymbol{\mu}\left(\mathbf{x}, \mathbf{v}, t\right)$ are given by

$$\boldsymbol{\kappa}\left(\mathbf{x}, \mathbf{v}, t\right) = \int_{t_0}^{t} \left\langle \boldsymbol{\mathcal{H}}^\top\left[t;t'\right] : \frac{\partial}{\partial \mathbf{x}} \mathbf{R}\left(\boldsymbol{x}_p', t'; \mathbf{x}, t\right) \right\rangle_{\mathbf{x},\mathbf{v}} dt' \tag{4.30}$$

$$\boldsymbol{\lambda}\left(\mathbf{x}, \mathbf{v}, t\right) = \int_{t_0}^{t} \left\langle \boldsymbol{\mathcal{H}}\left[t;t'\right] \cdot \mathbf{R}\left(\boldsymbol{x}_p', t'; \mathbf{x}, t\right) \right\rangle_{\mathbf{x},\mathbf{v}} dt' \tag{4.31}$$

$$\boldsymbol{\mu}\left(\mathbf{x}, \mathbf{v}, t\right) = \int_{t_0}^{t} \left\langle \dot{\boldsymbol{\mathcal{H}}}\left[t;t'\right] \cdot \mathbf{R}\left(\boldsymbol{x}_p', t'; \mathbf{x}, t\right) \right\rangle_{\mathbf{x},\mathbf{v}} dt' \tag{4.32}$$

where $\boldsymbol{x}_p' = \boldsymbol{x}_p(t')$. The PDF kinetic equation (4.22) can then be re-written in terms of the dispersion tensors (4.30 - 4.32) and the physical space variables $\mathbf{x}$ and $\mathbf{v}$ for when the fluctuating particle acceleration $\mathbf{f}(\mathbf{x}, t)$ has a Gaussian distribution as [150, 124, 71]

$$\frac{\partial p}{\partial t} = -\frac{\partial}{\partial \mathbf{x}} \cdot \left[\mathbf{v} p\right] - \frac{\partial}{\partial \mathbf{v}} \cdot \left[\left(\mathbf{F} + \boldsymbol{\kappa}\right) p\right] + \frac{\partial}{\partial \mathbf{v}} \cdot \left[\frac{\partial}{\partial \mathbf{x}} \cdot \left[\boldsymbol{\lambda} p\right] + \frac{\partial}{\partial \mathbf{v}} \cdot \left[\boldsymbol{\mu} p\right]\right] \tag{4.33}$$

in which the arguments are omitted for clarity. The evolution of the PDF $p\left(\mathbf{x}, \mathbf{v}, t\right)$ is thus governed by the particle dispersion tensors $\boldsymbol{\kappa}\left(\mathbf{x}, \mathbf{v}, t\right)$, $\boldsymbol{\lambda}\left(\mathbf{x}, \mathbf{v}, t\right)$, and $\boldsymbol{\mu}\left(\mathbf{x}, \mathbf{v}, t\right)$,

which can be interpreted as memory integrals that capture the influence of the flow field on particle trajectories through the action of the response tensor $\boldsymbol{\mathcal{H}}\left[t;t'\right]$. More specifically, $\boldsymbol{\kappa}\left(\mathbf{x},\mathbf{v},t\right)$ describes spatial convection of particles and behaves as a momentum source, $\boldsymbol{\lambda}\left(\mathbf{x},\mathbf{v},t\right)$ represents spatial diffusion of particles, and $\boldsymbol{\mu}\left(\mathbf{x},\mathbf{v},t\right)$ accounts for velocity diffusion of particles and acts as a stress source [143]. These dispersion tensors are unknown quantities, with the conditional averages that constitute the integrands requiring a further level of closure in order to completely specify the PDF $p\left(\mathbf{x},\mathbf{v},t\right)$. Within these conditional averages, it is therefore the response tensor $\boldsymbol{\mathcal{H}}\left[t;t'\right]$ and correlation tensor $\mathbf{R}\left(\mathbf{x}',t';\mathbf{x},t\right)$ evaluated along the particle trajectory $\mathbf{x}'=\boldsymbol{x}_p'$ that need modelling in order to make such a closure.

4.2 Application to Two-Fluid Models

4.2.1 Particle Mean-Field Variables

The PDF kinetic model detailed in section 4.1 can provide much insight into particle behaviour as a stand-alone framework, however it also provides a rigorous method for deriving the transport equations that constitute the dispersed phase of a two-fluid model. The starting point for this procedure lies in consideration of the average, or mean-field properties of particles at a macroscopic level, which can be defined by generating different sets of trajectories $\boldsymbol{x}_p(t)$ and velocities $\boldsymbol{v}_p(t)$ for each realisation of the stochastic field $\mathbf{f}\left(\boldsymbol{x}_p(t),t\right)$ and collectively averaging over these. Specifically, and assuming that the PDF $p\left(\mathbf{x},\mathbf{v},t\right)$ vanishes in the limit $\mathbf{v}\rightarrow\pm\boldsymbol{\infty}$, the particle number density $\rho\left(\mathbf{x},t\right)$ is defined as the average PDF of just spatial position $\mathbf{x}$ [149]

$$\rho\left(\mathbf{x},t\right)=\left\langle \delta\left(\boldsymbol{x}_p(t)-\mathbf{x}\right)\right\rangle \tag{4.34}$$

Alternatively, the particle mean-field variables can be obtained by extracting the moments of $p\left(\mathbf{x},\mathbf{v},t\right)$, with the *number density* $\rho\left(\mathbf{x},t\right)$ determined as the zeroth moment

$$\rho\left(\mathbf{x},t\right)=\int_{\mathbf{v}}p\left(\mathbf{x},\mathbf{v},t\right)\,d\mathbf{v} \tag{4.35}$$

A related quantity is the *fine-grained number density* $\varrho\left(\mathbf{x},t\right)$, which is simply the instantaneous realisation of the number density

$$\varrho\left(\mathbf{x},t\right)=\delta\left(\boldsymbol{x}_p(t)-\mathbf{x}\right) \tag{4.36}$$

It follows that the relationship between the number density and fine-grained number density is $\rho\left(\mathbf{x},t\right)=\left\langle \varrho\left(\mathbf{x},t\right)\right\rangle$. The *mean particle velocity* $\overline{\mathbf{v}}\left(\mathbf{x},t\right)$ is defined in a similar manner as

$$\overline{\mathbf{v}}\left(\mathbf{x},t\right)=\Big\langle \boldsymbol{v}_p(t)\Big\rangle_{\boldsymbol{x}_p(t)=\mathbf{x}}=\frac{1}{\rho\left(\mathbf{x},t\right)}\Big\langle \boldsymbol{v}_p(t)\delta\left(\boldsymbol{x}_p(t)-\mathbf{x}\right)\Big\rangle \tag{4.37}$$

The mean particle velocity can also be interpreted as the first moment of the PDF $p\left(\mathbf{x},\mathbf{v},t\right)$

$$\overline{\mathbf{v}}\left(\mathbf{x},t\right)=\frac{1}{\rho\left(\mathbf{x},t\right)}\int_{\mathbf{v}}\mathbf{v}p\left(\mathbf{x},\mathbf{v},t\right)\,d\mathbf{v} \tag{4.38}$$

Defining the particle fluctuating velocity as $\boldsymbol{c}(t)=\boldsymbol{v}_p(t)-\overline{\mathbf{v}}\left(\boldsymbol{x}_p(t),t\right)$, the particle *kinetic stresses* $\overline{\mathbf{cc}}\left(\mathbf{x},t\right)$ are given in the same manner by

$$\overline{\mathbf{cc}}\left(\mathbf{x},t\right)=\Big\langle \boldsymbol{c}(t)\boldsymbol{c}(t)\Big\rangle_{\boldsymbol{x}_p(t)=\mathbf{x}}=\frac{1}{\rho\left(\mathbf{x},t\right)}\Big\langle \boldsymbol{c}(t)\boldsymbol{c}(t)\delta\left(\boldsymbol{x}_p(t)-\mathbf{x}\right)\Big\rangle \tag{4.39}$$

The kinetic stresses are analogous to the Reynold's stresses $\overline{\mathbf{u}'\mathbf{u}'}$ for the continuous phase, and can also be represented as the second moment of the PDF $p\left(\mathbf{x},\mathbf{v},t\right)$

$$\overline{\mathbf{cc}}\left(\mathbf{x},t\right)=\frac{1}{\rho\left(\mathbf{x},t\right)}\int_{\mathbf{v}}\left(\mathbf{v}-\overline{\mathbf{v}}\right)\left(\mathbf{v}-\overline{\mathbf{v}}\right)p\left(\mathbf{x},\mathbf{v},t\right)\,d\mathbf{v} \tag{4.40}$$

4.2.2 Particle Phase Continuum Equations

The particle mean-field variables $\rho\left(\mathbf{x},t\right)$, $\overline{\mathbf{v}}\left(\mathbf{x},t\right)$, and $\overline{\mathbf{cc}}\left(\mathbf{x},t\right)$ can be used to interpret the particle phase as if it were itself a continuum, by construction of subsidiary transport equations directly from the underlying PDF kinetic equation (4.33). In particular, by integrating (4.33) over the phase-space velocity $\mathbf{v}$, the particle phase continuity equation is given as [149]

$$\frac{\partial\rho}{\partial t}+\nabla\cdot\left(\rho\overline{\mathbf{v}}\right)=0 \tag{4.41}$$

Similarly, multiplying the PDF equation (4.33) by $\mathbf{v}$ and then integrating over $\mathbf{v}$ leads to the particle phase momentum equation [149]

$$\frac{\partial}{\partial t}\left(\rho\overline{\mathbf{v}}\right)+\nabla\cdot\left(\rho\,\overline{\mathbf{v}}\,\overline{\mathbf{v}}\right)=-\nabla\cdot\left[\rho\left(\overline{\mathbf{cc}}+\overline{\boldsymbol{\lambda}}\right)\right]+\rho\left(\overline{\mathbf{F}}+\overline{\boldsymbol{\kappa}}\right) \tag{4.42}$$

in which overbars denote the velocity averaged form of the dispersion tensors given by

$$\overline{\mathbf{F}}=\frac{1}{\rho}\int_{\mathbf{v}}p\mathbf{F}\,d\mathbf{v}\quad,\quad\overline{\boldsymbol{\kappa}}=\frac{1}{\rho}\int_{\mathbf{v}}p\boldsymbol{\kappa}\,d\mathbf{v}\quad,\quad\overline{\boldsymbol{\lambda}}=\frac{1}{\rho}\int_{\mathbf{v}}p\boldsymbol{\lambda}\,d\mathbf{v}\quad,\quad\overline{\boldsymbol{\mu}}=\frac{1}{\rho}\int_{\mathbf{v}}p\boldsymbol{\mu}\,d\mathbf{v} \tag{4.43}$$

Furthermore, multiplying the PDF equation (4.33) by $\mathbf{vv}$ and then integrating over $\mathbf{v}$ leads to the kinetic stress transport equation [149]

$$\rho\frac{D}{Dt}\overline{\mathbf{cc}}=-\nabla\cdot\left(\rho\,\overline{\mathbf{ccc}}\right)+\rho\left(\boldsymbol{\Psi}+\boldsymbol{\Psi}^{\top}\right) \tag{4.44}$$

where D/Dt is the material derivative operator given by

$$\frac{D}{Dt}\equiv\frac{\partial}{\partial t}+\overline{\mathbf{v}}\cdot\nabla \tag{4.45}$$

the particle kinetic stress flux $\overline{\mathbf{ccc}}\left(\mathbf{x},t\right)$ is defined as the third moment of the PDF $p\left(\mathbf{x},\mathbf{v},t\right)$

$$\overline{\mathbf{ccc}}\left(\mathbf{x},t\right)=\frac{1}{\rho\left(\mathbf{x},t\right)}\int_{\mathbf{v}}\left(\mathbf{v}-\overline{\mathbf{v}}\right)\left(\mathbf{v}-\overline{\mathbf{v}}\right)\left(\mathbf{v}-\overline{\mathbf{v}}\right)p\left(\mathbf{x},\mathbf{v},t\right)\,d\mathbf{v} \tag{4.46}$$

and

$$\boldsymbol{\Psi}=-\frac{1}{\rho}\nabla\cdot\left(\rho\overline{\boldsymbol{\lambda}\mathbf{c}}\right)-\left(\overline{\mathbf{cc}}+\overline{\boldsymbol{\lambda}}^{\top}\right)\cdot\nabla\overline{\mathbf{v}}+\overline{\boldsymbol{\mu}}+\overline{\mathbf{c}\left(\mathbf{F}+\boldsymbol{\kappa}\right)} \tag{4.47}$$

Equations (4.41), (4.42), and (4.44) then constitute the dispersed phase of a two-fluid model, and it is insightful to compare the particle phase continuity and momentum equations retrieved from the PDF approach to those from the heuristic two-fluid framework outlined in section 2.3.2 as given by (2.28) and (2.29) respectively. Specifically,

the continuity equation is identical, however the particle phase stress tensor $\boldsymbol{\sigma}_d$ appearing in the momentum equation for the heuristic two-fluid model has been replaced with terms that originate from the PDF transport equation (4.33). The additional detail provided by the form of these terms reduces the problem from developing a closure for $\boldsymbol{\sigma}_d$ at a macroscopic level of physical description to that of the unknown quantities in the momentum equation at a more fundamental level, namely the velocity averaged dispersion tensors $\overline{\boldsymbol{\kappa}}(\mathbf{x},t)$ and $\overline{\boldsymbol{\lambda}}(\mathbf{x},t)$, and the kinetic stresses $\overline{\mathbf{cc}}(\mathbf{x},t)$.

As detailed in section 4.1.4, closure of $\overline{\boldsymbol{\kappa}}(\mathbf{x},t)$ and $\overline{\boldsymbol{\lambda}}(\mathbf{x},t)$ is dependent on modelling of the response tensor $\boldsymbol{\mathcal{H}}[t;t']$ and correlation tensor $\mathbf{R}(\mathbf{x}',t';\mathbf{x},t)$ evaluated along a particle trajectory, however treatment of the kinetic stresses $\overline{\mathbf{cc}}(\mathbf{x},t)$ is restricted to the continuum equations, and can be specified by closing the kinetic stress transport equation (4.44). This in turn necessitates closure of the unknown kinetic stress flux $\overline{\mathbf{ccc}}(\mathbf{x},t)$, modelling of which requires supplementary information, with the Chapman-Enskog methodology providing an often used approach [149]. In conjunction, closure of these quantities then fully specifies the particle phase continuum equations, whilst also determining the PDF $p(\mathbf{x},\mathbf{v},t)$.

4.2.3 Particle Mass Flux Representation

Further to highlighting the differences between the heuristic and statistical formulations of two-fluid models in terms of the additional detail provided by extracting the particle phase continuum equations directly from the PDF transport equation, it is helpful to interpret these additions in terms of the underlying physics involved. This is possible by considering the relative significance of the terms which emerge in the particle phase momentum equation (4.42) as derived using the PDF approach. For the particular case of the Stokes drag model, in which the mean continuous phase driving force per unit mass $\mathbf{F}(\mathbf{x},\mathbf{v},t)$ that acts on particles is linear in $\mathbf{v}$ as in (4.2), then rearrangement of the particle phase momentum equation produces an expression for the *particle mass flux* $\rho\overline{\mathbf{v}}$

$$\rho\overline{\mathbf{v}} = \underbrace{\rho\left[\langle\mathbf{u}\rangle + \mathbf{V}_g + \tau_p\left\{\underbrace{\left[\overline{\boldsymbol{\kappa}} - \nabla\cdot\overline{\boldsymbol{\lambda}}\right]}_{\boxed{1}} - \underbrace{\nabla\cdot\overline{\mathbf{cc}}}_{\boxed{2}} - \underbrace{\frac{D}{Dt}\overline{\mathbf{v}}}_{\boxed{3}}\right\}\right]}_{\text{convective flux}} \underbrace{- \tau_p\left(\overline{\mathbf{cc}} + \overline{\boldsymbol{\lambda}}^{\top}\right)\cdot\nabla\rho}_{\boxed{4}\ \text{diffusive flux}} \tag{4.48}$$

The importance of the contributions that the terms $\boxed{1} - \boxed{4}$ make to this flux is of interest within the context of various flow configurations, with a broad split into the balance of convective and diffusive flux terms. The diffusive flux in $\boxed{4}$ is a relatively known entity, and the inertial term $\boxed{3}$ vanishes when the behaviour under consideration is steady-state, however it is the remaining contributions to the convective flux which are noteworthy. In the case of the non-local drift flux $\boxed{1}$, previous modelling approaches have often neglected one or both of these terms, with assumptions that $\overline{\boldsymbol{\kappa}} = 0$ in homogeneous flows of all configurations [125, 48], $\overline{\boldsymbol{\kappa}} - \nabla \cdot \overline{\boldsymbol{\lambda}} \equiv \mathbf{0}$ across all values of St [178], and representations which do not explicitly take into account these terms [31]. It has been formally demonstrated that $\overline{\boldsymbol{\kappa}} - \nabla \cdot \overline{\boldsymbol{\lambda}}$ is only equal to zero in the case of fluid elements with no inertia, a result known as the *fully mixed condition* [12]. The gradient of the kinetic stresses in $\boxed{2}$ is the turbophoretic contribution, and acts in the opposite sense to $\boxed{1}$. Although turbophoresis has been accounted for in some work [178], the balance between $\boxed{1}$ and $\boxed{2}$ can become a non-negligible contribution in some flow configurations, and warrants further research. Indeed, as will been seen in Chapters 6 and 8, the particle mass flux expression (4.48) is central to the work in this thesis due to the role it plays in quantifying the various flux contributions that arise in different flow configurations.

4.3 Benchmarking the Dispersion Tensors in Homogeneous Flow

For the purpose of evaluating the contributions of interest in the particle mass flux and developing closure models, calculation of the dispersion tensors $\boldsymbol{\kappa}(\mathbf{x}, \mathbf{v}, t)$, $\boldsymbol{\lambda}(\mathbf{x}, \mathbf{v}, t)$, and $\boldsymbol{\mu}(\mathbf{x}, \mathbf{v}, t)$ in the PDF framework as defined by (4.30 - 4.32) is somewhat involved, requiring solution for the particle response tensor $\boldsymbol{\mathcal{H}}[t; t']$. Even in the simple case of a homogeneous flow, the presence of turbulence means that an analytical solution to the response tensor governing equation (4.28) becomes intractable for modelling purposes (see Appendix A), and thus it is necessary to seek a numerical solution. For such an approach it is useful to have an alternative measure against which to assess the accuracy of these evaluations, and that is thus able to provide validation of the procedure used.

This is possible in the case of homogeneous systems by considering the physical interpretation of the dispersion tensors $\boldsymbol{\lambda}(\mathbf{x}, \mathbf{v}, t)$ and $\boldsymbol{\mu}(\mathbf{x}, \mathbf{v}, t)$ as measures of spatial diffusion and velocity diffusion respectively. Since the dispersion tensors are dependent

on the history of fluid-particle interaction along trajectories, this poses the question as to how they are related to the quantities $\left\langle \boldsymbol{x}_p(t)\mathbf{f}(\boldsymbol{x}_p(t),t)\right\rangle$ and $\left\langle \boldsymbol{v}_p(t)\mathbf{f}(\boldsymbol{x}_p(t),t)\right\rangle$, i.e. the correlation between each of the particle location and velocity respectively with the fluctuating component of the flow field. A convenient way of investigating these correlations is to use the phase-space interpretations $\boldsymbol{z}(t) = (\boldsymbol{x}_p(t), \boldsymbol{v}_p(t))$ and $\mathbf{b}\left(\boldsymbol{\xi},t\right) = (\mathbf{0}, \mathbf{f}\left(\mathbf{x},t\right))$ from (4.23), leading to representation of both quantities within the expression $\left\langle \boldsymbol{z}(t)\mathbf{b}\left(\boldsymbol{z}(t),t\right)\right\rangle$. Then the fine-grained PDF $\mathcal{P}$ as defined in (4.6) enables $\mathbf{b}\left(\boldsymbol{z}(t),t\right)$ to be written in terms of the phase space variable $\boldsymbol{\xi}$ by making use of the filtering property of the δ-function, and by the same reasoning only points where $\boldsymbol{z} = \boldsymbol{\xi}$ then contribute to the ensemble average, meaning that it is possible to write

$$\left\langle \boldsymbol{z}(t)\mathbf{b}\left(\boldsymbol{z}(t),t\right)\right\rangle = \left\langle \boldsymbol{z}(t)\int_{\boldsymbol{\xi}}\mathbf{b}\left(\boldsymbol{\xi},t\right)\mathcal{P}\left(\boldsymbol{\xi},t\right)d\boldsymbol{\xi}\right\rangle = \int_{\boldsymbol{\xi}}\boldsymbol{\xi}\left\langle \mathbf{b}\left(\boldsymbol{\xi},t\right)\mathcal{P}\left(\boldsymbol{\xi},t\right)\right\rangle d\boldsymbol{\xi} \tag{4.49}$$

Thus the problem reduces to the closure of the phase-space diffusion current $\left\langle \mathbf{b}\left(\boldsymbol{\xi},t\right)\mathcal{P}\left(\boldsymbol{\xi},t\right)\right\rangle$ identified in the Liouville equation (4.7), and therefore the FN correlation splitting technique result in (4.19) can be applied, resulting in

$$\left\langle \boldsymbol{z}(t)\mathbf{b}\left(\boldsymbol{z}(t),t\right)\right\rangle = \int_{\boldsymbol{\xi}}\boldsymbol{\xi}\left(\mathbf{d}\left(\boldsymbol{\xi},t\right)p\left(\boldsymbol{\xi},t\right) - \frac{\partial}{\partial\boldsymbol{\xi}}\cdot\left[\mathbf{D}\left(\boldsymbol{\xi},t\right)p\left(\boldsymbol{\xi},t\right)\right]\right)d\boldsymbol{\xi} \tag{4.50}$$

Performing the integration then yields

$$\left\langle \boldsymbol{z}(t)\mathbf{b}\left(\boldsymbol{z}(t),t\right)\right\rangle = \left\langle \boldsymbol{z}(t)\mathbf{d}\left(\boldsymbol{z}(t),t\right)\right\rangle + \left\langle \mathbf{D}\left(\boldsymbol{z}(t),t\right)\right\rangle \tag{4.51}$$

Re-introducing the physical space interpretations (4.23) along with those for the drift and diffusion tensors in terms of the dispersion tensors (4.29) enables the closure to be decoupled into the original correlations

$$\left\langle \boldsymbol{x}_p(t)\mathbf{f}(\boldsymbol{x}_p(t),t)\right\rangle = \left\langle \boldsymbol{x}_p(t)\boldsymbol{\kappa}\big(\boldsymbol{x}_p(t),\boldsymbol{v}_p(t),t\big) + \boldsymbol{\lambda}\big(\boldsymbol{x}_p(t),\boldsymbol{v}_p(t),t\big)\right\rangle \tag{4.52}$$

$$\left\langle \boldsymbol{v}_p(t)\mathbf{f}(\boldsymbol{x}_p(t),t)\right\rangle = \left\langle \boldsymbol{v}_p(t)\boldsymbol{\kappa}\big(\boldsymbol{x}_p(t),\boldsymbol{v}_p(t),t\big) + \boldsymbol{\mu}\big(\boldsymbol{x}_p(t),\boldsymbol{v}_p(t),t\big)\right\rangle \tag{4.53}$$

Considering the first equation (4.52), the term $\left\langle \boldsymbol{x}_p(t)\boldsymbol{\kappa}\big(\boldsymbol{x}_p(t),\boldsymbol{v}_p(t),t\big)\right\rangle$ can be written

$$\left\langle \boldsymbol{x}_p(t)\boldsymbol{\kappa}\big(\boldsymbol{x}_p(t),\boldsymbol{v}_p(t),t\big)\right\rangle = \int_{\mathbf{v}}\int_{\mathbf{x}} \mathbf{x}\,\boldsymbol{\kappa}\left(\mathbf{x},\mathbf{v},t\right)\,p\left(\mathbf{x},\mathbf{v},t\right)\,d\mathbf{x}\,d\mathbf{v} = \int_{\mathbf{x}} \mathbf{x}\,\rho\left(\mathbf{x},t\right)\overline{\boldsymbol{\kappa}}\left(\mathbf{x},t\right)\,d\mathbf{x} \tag{4.54}$$

Now in homogeneous statistically stationary systems with no external body forces, it is evident that $\overline{\mathbf{v}} = 0$, and all spatial or temporal gradients of averaged quantities are zero. Applying these criterion reduces the particle phase momentum equation (4.42) in form to

$$0 = \overline{\mathbf{F}} + \overline{\boldsymbol{\kappa}} \tag{4.55}$$

For the case of a linear drag law the mean continuous phase force per unit mass is $\mathbf{F}\left(\mathbf{x},\mathbf{v},t\right) = \beta\left(\left\langle\mathbf{u}(\mathbf{x},t)\right\rangle - \mathbf{v}\right)$, as given by (4.2) with $\mathbf{g} = \mathbf{0}$. However for homogeneous turbulence it is also true that $\langle\mathbf{u}(\mathbf{x},t)\rangle = 0$, producing the velocity averaged form

$$\overline{\mathbf{F}} = -\beta\overline{\mathbf{v}} \tag{4.56}$$

Therefore as $\overline{\mathbf{v}} = 0$ it follows that $\overline{\mathbf{F}} = 0$, and thus from (4.55) then $\overline{\boldsymbol{\kappa}} = 0$ (although note that this does not imply that $\boldsymbol{\kappa} = 0$, as even in homogeneous systems, $\boldsymbol{\kappa} = \boldsymbol{\kappa}\left(\mathbf{v},t\right)$). From (4.54) it is then seen that $\left\langle \boldsymbol{x}_p(t)\boldsymbol{\kappa}\big(\boldsymbol{x}_p(t),\boldsymbol{v}_p(t),t\big)\right\rangle = 0$, subsequently reducing (4.52) to

$$\left\langle \boldsymbol{x}_p(t)\mathbf{f}(\boldsymbol{x}_p(t),t)\right\rangle = \left\langle \boldsymbol{\lambda}\big(\boldsymbol{x}_p(t),\boldsymbol{v}_p(t),t\big)\right\rangle \tag{4.57}$$

Further to this, properties of the PDF $p\left(\mathbf{x},\mathbf{v},t\right)$ can be used to write

$$\left\langle \boldsymbol{\lambda}\big(\boldsymbol{x}_p(t),\boldsymbol{v}_p(t),t\big)\right\rangle = \int_{\mathbf{v}}\int_{\mathbf{x}} \boldsymbol{\lambda}\left(\mathbf{x},\mathbf{v},t\right)\,p\left(\mathbf{x},\mathbf{v},t\right)\,d\mathbf{x}\,d\mathbf{v} = \int_{\mathbf{x}} \rho\left(\mathbf{x},t\right)\overline{\boldsymbol{\lambda}}\left(\mathbf{x},t\right)\,d\mathbf{x} = \overline{\boldsymbol{\lambda}}\left(\mathbf{x},t\right)$$

giving the final expression as [150, 151]

$$\left\langle \boldsymbol{x}_p(t)\mathbf{f}(\boldsymbol{x}_p(t),t)\right\rangle = \overline{\boldsymbol{\lambda}}\left(\mathbf{x},t\right) \tag{4.58}$$

For the case of equation (4.53), it can similarly be written that

$$\begin{aligned}\left\langle \boldsymbol{v}_p(t)\boldsymbol{\kappa}\big(\boldsymbol{x}_p(t),\boldsymbol{v}_p(t),t\big)\right\rangle &= \int_{\mathbf{x}}\int_{\mathbf{v}} \mathbf{v}\,\boldsymbol{\kappa}\left(\mathbf{x},\mathbf{v},t\right)\,p\left(\mathbf{x},\mathbf{v},t\right)\,d\mathbf{v}\,d\mathbf{x}\\ &= \int_{\mathbf{x}} \rho\left(\mathbf{x},t\right)\overline{\mathbf{c}\boldsymbol{\kappa}}\left(\mathbf{x},t\right)\,d\mathbf{x}\\ &= \overline{\mathbf{c}\boldsymbol{\kappa}}\left(\mathbf{x},t\right)\end{aligned} \tag{4.59}$$

This expression cannot be simplified any further in the case of a homogeneous statistically stationary flow, however it is generally modelled as being negligible. Additionally, in the same vein as for $\boldsymbol{\lambda}\left(\mathbf{x},\mathbf{v},t\right)$ the properties of the PDF $p\left(\mathbf{x},\mathbf{v},t\right)$ give

$$\left\langle \boldsymbol{\mu}\big(\boldsymbol{x}_p(t),\boldsymbol{v}_p(t),t\big)\right\rangle = \int_{\mathbf{x}}\int_{\mathbf{v}} \boldsymbol{\mu}\left(\mathbf{x},\mathbf{v},t\right)\,p\left(\mathbf{x},\mathbf{v},t\right)\,d\mathbf{v}\,d\mathbf{x} = \int_{\mathbf{x}} \rho\left(\mathbf{x},t\right)\overline{\boldsymbol{\mu}}\left(\mathbf{x},t\right)\,d\mathbf{x} = \overline{\boldsymbol{\mu}}\left(\mathbf{x},t\right)$$

meaning that with the approximation $\overline{\mathbf{c}\boldsymbol{\kappa}}\left(\mathbf{x},t\right) \approx \mathbf{0}$ in (4.59) then (4.53) can be written in the form

$$\left\langle \boldsymbol{v}_p(t)\mathbf{f}(\boldsymbol{x}_p(t),t)\right\rangle \approx \overline{\boldsymbol{\mu}}\left(\mathbf{x},t\right) \tag{4.60}$$

Thus for homogeneous statistically stationary flows, equations (4.58) and (4.60) give expressions for which the left-hand sides can be evaluated using particle tracking simulations, thereby providing a benchmark for testing $\overline{\boldsymbol{\lambda}}\left(\mathbf{x},t\right)$ and $\overline{\boldsymbol{\mu}}\left(\mathbf{x},t\right)$ as obtained from direct computation of (4.31) and (4.32) against.

4.4 Local Closure Models

In general there are two ways of approaching the closure problem for unknown quantities; either developing an algebraic closure or modelling each unclosed term using an additional transport equation. Within the context of PDF models, the continuum equations constitute such a hierarchy of transport equations, however whether closure is made at this level or directly in the PDF kinetic equation, modelling of the dispersion tensors $\boldsymbol{\kappa}\left(\mathbf{x},\mathbf{v},t\right)$, $\boldsymbol{\lambda}\left(\mathbf{x},\mathbf{v},t\right)$, and $\boldsymbol{\mu}\left(\mathbf{x},\mathbf{v},t\right)$ given by (4.30 - 4.32) is a requirement. These dispersion tensors are intrinsically non-local in nature, with their values at $(\mathbf{x},t)$ depending upon the particle trajectories $\boldsymbol{x}_p(t')$ for times $0 \leq t' \leq t$, however the extent

to which this non-locality is captured in closure models is highly variable, and is the subject of ongoing research.

4.4.1 Local Homogeneous Approximations

The starting point for modelling $\boldsymbol{\kappa}(\mathbf{x},\mathbf{v},t)$, $\boldsymbol{\lambda}(\mathbf{x},\mathbf{v},t)$, and $\boldsymbol{\mu}(\mathbf{x},\mathbf{v},t)$ is by constructing simple approximations that are local to the point in physical space $\mathbf{x}$ at which the dispersions tensor describe the particle behaviour, and consequently ignore the history effect of previous particle-fluid interactions that are of importance in certain flow configurations. Further assuming a homogeneous flow, such a model is referred to as a *local homogeneous approximation* (LHA).

These various assumptions are applied to the response and correlation tensors that constitute the unclosed conditional average within the dispersion tensors. In the case of the two-point two-time correlation tensor evaluated along a particle trajectory $\mathbf{R}\left(\boldsymbol{x}_p',t';\mathbf{x},t\right)$ defined by (4.25), a locality assumption can be made by supposing that $\boldsymbol{x}_p(t') \approx \mathbf{x}$, thereby reducing the correlation required in space to a single point. Additionally, a model $E(t-t';\mathbf{x})$ can be introduced for the temporal decorrelation of the random field $\mathbf{f}(\mathbf{x},t)$ along trajectories that satisfy $\boldsymbol{x}_p(t) = \mathbf{x}$, which further reduces the correlation to the one-point one-time form $\mathbf{R}(\mathbf{x},t;\mathbf{x},t)$. Thus the LHA for $\mathbf{R}\left(\boldsymbol{x}_p',t';\mathbf{x},t\right)$ takes the form [151]

$$\mathbf{R}\left(\boldsymbol{x}_p',t';\mathbf{x},t\right) \approx \mathbf{R}(\mathbf{x},t;\mathbf{x},t)\; E(t-t';\mathbf{x}) \tag{4.61}$$

The further assumption of a homogeneous flow removes the spatial dependence in the one-point one-time correlations, and if the flow is also isotropic this results in $\mathbf{R}(\mathbf{x},t;\mathbf{x},t) = \beta^2 u'^2\mathbf{I}$ for the case of a linear drag law where the fluctuating particle acceleration is given by (4.3). For the time component $E(t-t';\mathbf{x})$, an appropriate model is an exponential decorrelation specified by

$$E(t-t';\mathbf{x}) = \exp\left[-\frac{1}{\tau_{Lp}(\mathbf{x})}(t-t')\right] \tag{4.62}$$

where τ_{Lp} is the Lagrangian fluid integral timescale for the random field $\mathbf{f}(\mathbf{x},t)$ evaluated along inertial particle trajectories. Following Wang & Stock [165], a suitable model for τ_{Lp} in a homogeneous flow as obtained from curve fitting of DNS data is

$$\tau_{Lp} = \tau_E - \frac{\tau_E - \tau_L}{(1 + St_E)^{-0.4(1+0.01\,St_E)}} \tag{4.63}$$

where τ_E is the Eulerian fluid integral timescale, τ_L is the Lagrangian fluid integral timescale along fluid element trajectories, and St_E is the Stokes number defined in terms of the Eulerian integral timescale $St_E = \tau_p/\tau_E$. The model (4.63) is valid for the case in which τ_E is equal to the eddy turnover time τ_{eddy} of the flow field, and satisfies the limiting cases of $\tau_{Lp} \to \tau_L$ as $\tau_p \to 0$ and $\tau_{Lp} \to \tau_E$ as $\tau_p \to \infty$, with $\tau_L \leq \tau_{Lp} \leq \tau_E$ applying in the general case of inertial particles. Accordingly, the approximation to $\mathbf{R}\left(\boldsymbol{x}'_p, t'; \mathbf{x}, t\right)$ in (4.61) becomes

$$\mathbf{R}\left(\boldsymbol{x}'_p, t'; \mathbf{x}, t\right) \approx \beta^2 u'^2 \exp\left[-\frac{1}{\tau_{Lp}}(t - t')\right]\mathbf{I} \tag{4.64}$$

Therefore this approximation captures the expected spatial and temporal decorrelation behaviour using the single quantity τ_{Lp} to account for the effects of particle inertia. In terms of the particle response tensor $\boldsymbol{\mathcal{H}}[t; t']$, for the linear drag law specified in (4.2 - 4.3) the contribution from $\partial\mathbf{F}/\partial\mathbf{x}$ in the governing equation (4.28) is zero, and further neglecting contribution from $\partial\mathbf{f}/\partial\mathbf{x}$ makes $\boldsymbol{\mathcal{H}}[t; t']$ trajectory independent. Since the particle history is not taken into account as a result, this is equivalent to the locality assumption made for the correlation tensor $\mathbf{R}\left(\boldsymbol{x}'_p, t'; \mathbf{x}, t\right)$, and the resulting simplified governing equation can be solved to produce an approximation for $\boldsymbol{\mathcal{H}}[t; t']$ known as the *Green's tensor* [151]

$$\mathbf{H}\,[t; t'] = \frac{1}{\beta}\Big[1 - \exp\big[-\beta\,(t - t')\big]\Big]\mathbf{I} \tag{4.65}$$

The name arises from the fact that the scalar part of (4.65) is also the Green's function of the particle equation of motion (2.22) in the case of a linear drag law, which further implies that this approximation is consistent with the interpretation of $\boldsymbol{\mathcal{H}}[t; t']$ as the particle response to a perturbation. The approximations for $\mathbf{R}\left(\boldsymbol{x}'_p, t'; \mathbf{x}, t\right)$ (4.64) and $\boldsymbol{\mathcal{H}}[t; t']$ (4.65) are then both deterministic quantities, meaning that evaluation of the dispersion tensors $\overline{\boldsymbol{\kappa}}\,(\mathbf{x}, t)$, $\overline{\boldsymbol{\lambda}}\,(\mathbf{x}, t)$, and $\overline{\boldsymbol{\mu}}\,(\mathbf{x}, t)$ (4.30 - 4.32) using these expressions causes the conditional averages to drop out, thus solving the closure problem. Subsequent evaluation of the integrals and taking the limit $t \to \infty$ yields the steady-state LHA for the dispersion tensors

$$\begin{aligned}
\overline{\boldsymbol{\lambda}}^{\mathrm{LHA}} &= u'^2 \frac{1}{St_{Lp}\left(1+St_{Lp}\right)}\mathbf{I} \\
\overline{\boldsymbol{\mu}}^{\mathrm{LHA}} &= u'^2 \frac{\beta}{1+St_{Lp}}\mathbf{I} \qquad\qquad = \frac{1}{\tau_{Lp}}\overline{\boldsymbol{\lambda}}^{\mathrm{LHA}} \\
\overline{\boldsymbol{\kappa}}^{\mathrm{LHA}} &= \mathbf{0}
\end{aligned} \tag{4.66}$$

where St_{Lp} is the Stokes number defined by $St_{Lp} = \tau_p/\tau_{Lp}$. The constant approximations in (4.66) are the simplest closure for the dispersion tensors in an isotropic flow, and constitute the benchmark form of model which is assessed against data from particle tracking simulations.

In the event that the LHA does not adequately describe the particle behaviour within more complex flow configurations, it nevertheless provides a starting point for developing improved closure methodologies. An appropriate example to illustrate this is when added mass effects are accounted for within the PDF modelling framework so that the behaviour of arbitrary density particles can be described. Although the forces acting upon particles are more complex, the PDF kinetic modelling procedure in section 4.1 can still be applied by decomposing the particle equation of motion into mean $\mathbf{F}(\mathbf{x},\mathbf{v},t)$ and fluctuating $\mathbf{f}(\mathbf{x},t)$ components. The closures required in such a model remain those of two-point two-time correlation tensors for both fluid velocity and acceleration, and response tensors with respect to perturbations in both the fluid velocity and acceleration fields. Research in this area has used the locality assumption (4.61) as a standard model for the correlation tensors, whilst treatment of the response tensors has varied, with both the usual LHA of neglecting the contribution $\partial\mathbf{f}/\partial\mathbf{x}$ to keep the treatment deterministic [144], but also inclusion of further detail that accounts for the path history of particles and therefore makes the response tensors trajectory dependent [180].

4.4.2 Uniform Shear Flow

If the restriction of an isotropic flow is relaxed to that of a uniform shear flow in which a non-zero mean fluid velocity $\langle\mathbf{u}\rangle(\mathbf{x})$ exists in one direction, the geometry of the flow makes it convenient to consider this configuration in two-dimensional form. Then the mean flow rate is given by $\langle\mathbf{u}\rangle(\mathbf{x}) = (\langle \mathrm{u}_1\rangle(\mathrm{x}_2), 0)$, where x_1 varies in the streamwise direction and x_2 varies normally to the mean flow, and is characterised by the constant shear rate [151]

$$\mathbf{S} = \begin{bmatrix} 0 & \gamma \\ 0 & 0 \end{bmatrix} \tag{4.67}$$

where $\gamma = \partial\langle \mathrm{u}_1 \rangle / \partial \mathrm{x}_2$. In this configuration the one-point one-time correlations in the model (4.61) for $\mathbf{R}\left(\boldsymbol{x}_p', t'; \mathbf{x}, t\right)$ can still be taken to be spatially independent since the fluctuating part of the flow field $\mathbf{u}'$ is homogeneous, however each component now has a distinct value as isotropy is no longer satisfied. Notwithstanding this, the local approximation (4.61) can still be utilised for the linear drag law with fluctuating particle acceleration $\mathbf{f}\left(\mathbf{x}, t\right)$ given by (4.3), resulting in

$$\mathbf{R}\left(\boldsymbol{x}_p', t'; \mathbf{x}, t\right) \approx \beta^2 \left\langle \mathbf{u}'\mathbf{u}' \right\rangle \exp\left[-\frac{1}{\tau_{Lp}} (t - t') \right] \tag{4.68}$$

The particle response tensor $\boldsymbol{\mathcal{H}}[t; t']$ can be treated in the same manner as in the LHA by neglecting the contribution from $\partial \mathbf{f} / \partial \mathbf{x}$ in the governing equation (4.28), however the presence of a mean flow implies that the contribution from $\partial \mathbf{F} / \partial \mathbf{x} \neq \mathbf{0}$ in this context, resulting in an approximation for $\boldsymbol{\mathcal{H}}[t; t']$ that is anisotropic [126, 127, 13]

$$\mathbf{H}\left[s\right] = \begin{bmatrix} \frac{1}{\beta}\left[1 - \exp\left[-\beta s\right]\right] & \frac{\gamma}{\beta^2}\left[\beta s - 2 + (2 + \beta s)\exp\left[-\beta s\right]\right] \\ 0 & \frac{1}{\beta}\left[1 - \exp\left[-\beta s\right]\right] \end{bmatrix} \tag{4.69}$$

where $s = t - t'$. Crucially, both the models (4.68) for $\mathbf{R}\left(\boldsymbol{x}_p', t'; \mathbf{x}, t\right)$ and (4.69) for $\boldsymbol{\mathcal{H}}[t; t']$ in the case of uniform shear flow remain trajectory independent, meaning that in the same manner as the LHA the conditional average within the dispersion tensors is automatically closed without further assumption. This yields corresponding long-time values for the approximations $\overline{\boldsymbol{\kappa}}^{\mathrm{LHA}}$, $\overline{\boldsymbol{\lambda}}^{\mathrm{LHA}}$, and $\overline{\boldsymbol{\mu}}^{\mathrm{LHA}}$ [126, 127, 142], presentation of which is omitted here for clarity, however it is noted that $\overline{\boldsymbol{\kappa}}^{\mathrm{LHA}} = \mathbf{0}$ in this configuration since the models for $\mathbf{R}\left(\boldsymbol{x}_p', t'; \mathbf{x}, t\right)$ and $\boldsymbol{\mathcal{H}}[t; t']$ contain no spatial dependence.

4.5 Non-local Closure Models

The impact of non-local effects on inertial particles is of relevance for inhomogeneous flows, when the LHA cannot be reasonably expected to capture all the relevant fluid-particle interactions that influence particle behaviour. Evaluation of the particle dispersion tensors in the case of an inhomogeneous flow was first considered by Skartlien [142] within the context of one-dimensional stratified turbulent channel flow with a

non-linear mean shear rate, and requires numerical computation of the instantaneous response tensor $\boldsymbol{\mathcal{H}}[t;t']$ and evaluation of $\mathbf{R}\left(\boldsymbol{x}_p', t'; \mathbf{x}, t\right)$ along individual trajectories using particle tracking simulations. This work demonstrated that $\overline{\boldsymbol{\lambda}}\left(\mathbf{x}, t\right)$ deviates significantly from the LHA, in contrast to $\overline{\boldsymbol{\mu}}\left(\mathbf{x}, t\right)$ which is actually well approximated by the LHA across the width of the channel, and this difference in sensitivity to inhomogeneities within the flow is attributed to the weightings of the particle response tensor $\boldsymbol{\mathcal{H}}[t;t']$ within each dispersion tensor. This arises due to the respective timescales associated with each of $\boldsymbol{\mathcal{H}}[t;t']$ and $\mathbf{R}\left(\boldsymbol{x}_p', t'; \mathbf{x}, t\right)$; from the Green's tensor (4.65) it can be seen that τ_p is representative of $\boldsymbol{\mathcal{H}}[t;t']$, whilst the locality assumption (4.61) can be used to associate τ_{Lp} with $\mathbf{R}\left(\boldsymbol{x}_p', t'; \mathbf{x}, t\right)$. It is then the weightings of $\boldsymbol{\mathcal{H}}[t;t']$ and $\mathbf{R}\left(\boldsymbol{x}_p', t'; \mathbf{x}, t\right)$ within the integrands for $\overline{\boldsymbol{\lambda}}\left(\mathbf{x}, t\right)$ and $\overline{\boldsymbol{\mu}}\left(\mathbf{x}, t\right)$ as evaluated using (4.31) and (4.32) respectively that determine the sensitivity of the dispersion tensors [142]. For $\overline{\boldsymbol{\lambda}}\left(\mathbf{x}, t\right)$, the displacement response $\boldsymbol{\mathcal{H}}[t;t']$ is shown not to reduce to zero with increasing time separation $s = t - t'$, meaning that the dominant decorrelation timescale is τ_{Lp}, and $\overline{\boldsymbol{\lambda}}\left(\mathbf{x}, t\right)$ is therefore more dependent on the particle path history and consequently relatively sensitive to changes in the flow. In contrast, for $\overline{\boldsymbol{\mu}}\left(\mathbf{x}, t\right)$ the velocity response $\dot{\boldsymbol{\mathcal{H}}}[t;t']$ does decrease to zero with increasing time separation, and because in general $\tau_p \ll \tau_{Lp}$ for small particles, the dominant decorrelation timescale is therefore τ_p. This results in $\overline{\boldsymbol{\mu}}\left(\mathbf{x}, t\right)$ sampling much less of the particle path history, meaning that it is subsequently less sensitive to changes in the flow, and that the trajectory independent LHA is a better model in this case. This work clearly highlighted the scope for including the not insignificant non-local path history effects within a closure model for $\overline{\boldsymbol{\lambda}}\left(\mathbf{x}, t\right)$ in particular, which is otherwise only obtainable to a sufficient level of accuracy in inhomogeneous flows by using particle tracking simulations.

4.5.1 Passive Scalar Approximation

The concept of the *passive scalar approximation* (PSA) was introduced by Skartlien [142] in order to satisfy the requirement of fully mixed particles in the limit of zero particle inertia (i.e. fluid elements), and ensure that the particle phase momentum equation is correct. For the PDF kinetic framework this is stated in terms of the dispersion tensors as

$$\overline{\boldsymbol{\kappa}}\left(\mathbf{x}, t\right) = \nabla \cdot \overline{\boldsymbol{\lambda}}\left(\mathbf{x}, t\right) \tag{4.70}$$

This approximation can then reasonably be applied for $St \ll 1$, and includes a higher

level of detail than the LHA as the gradient in turbulence intensity is not neglected [142], with $\overline{\boldsymbol{\kappa}}(\mathbf{x},t) \neq \mathbf{0}$ and $\nabla \cdot \overline{\boldsymbol{\lambda}}(\mathbf{x},t) \neq \mathbf{0}$ in general for a inhomogeneous flow. Use of the LHA would approximate both of these quantities as zero, thereby trivially satisfying (4.70), however development of a non-local closure for $\overline{\boldsymbol{\lambda}}(\mathbf{x},t)$ with subsequent use of (4.70) to obtain $\overline{\boldsymbol{\kappa}}(\mathbf{x},t)$ includes this higher level of detail, and is therefore a more appropriate closure.

4.5.2 Modelling the Conditional PDF of Particle Trajectories

It was highlighted by Swailes & Darbyshire [151] that even in flow configurations where the response tensor $\boldsymbol{\mathcal{H}}[t;t']$ can be specified deterministically, the standard closure approximation on the two-point two-time correlation tensor $\mathbf{R}\left(\boldsymbol{x}_p', t'; \mathbf{x}, t\right)$ still utilises the locality assumption, namely

$$\left\langle \mathbf{R}\left(\boldsymbol{x}_p', t'; \mathbf{x}, t\right) \right\rangle_{\mathbf{x},\mathbf{v}} \approx \mathbf{R}\left(\mathbf{x}, t'; \mathbf{x}, t\right) \tag{4.71}$$

Consequently any particle-fluid interactions along the history of the particle trajectory are not taken into account, and this presents the major shortcoming of such an approximation, with improved closures being the subject of subsequent work. Such closures are largely based on the more fundamental approach of considering the joint distribution ϕ of $\boldsymbol{x}_p(t')$ and $\boldsymbol{v}_p(t')$ conditional on $\boldsymbol{x}_p(t) = \mathbf{x}$ and $\boldsymbol{v}_p(t) = \mathbf{v}$, from which stems the identity [151]

$$\left\langle \mathbf{R}\left(\boldsymbol{x}_p', t'; \mathbf{x}, t\right) \right\rangle_{\mathbf{x},\mathbf{v}} = \int_{\mathbf{x}'} \int_{\mathbf{v}'} \mathbf{R}\left(\mathbf{x}', t'; \mathbf{x}, t\right) \phi\left(\mathbf{x}', \mathbf{v}', t' \mid \mathbf{x}, \mathbf{v}, t\right) \, d\mathbf{v}' \, d\mathbf{x}' \tag{4.72}$$

where $\phi\left(\mathbf{x}', \mathbf{v}', t' \mid \mathbf{x}, \mathbf{v}, t\right)$ is the conditional PDF for particle trajectories $(\mathbf{x}', \mathbf{v}')$ at time t' which satisfy $(\mathbf{x}, \mathbf{v})$ at a later time t. The non-local effects can therefore be included within a closure by specification of $\phi\left(\mathbf{x}', \mathbf{v}', t' \mid \mathbf{x}, \mathbf{v}, t\right)$, and in the absence of a suitable closed form, this is most easily realised through supposition of a certain distribution and construction of the necessary moments. In particular, for the choice of a Gaussian approximation the closure problem reduces to determination of the mean $\mathbf{m}' = \mathbf{m}(t' \mid t) = (\langle \mathbf{x}' \rangle, \langle \mathbf{v}' \rangle)$ and covariance $\boldsymbol{\Theta}' = \boldsymbol{\Theta}(t' \mid t) = \left\langle \left(\mathbf{x}' - \langle \mathbf{x}' \rangle\right)\left(\mathbf{v}' - \langle \mathbf{v}' \rangle\right) \right\rangle$ of ϕ. The intricacy of such a procedure is that the distribution of particle trajectories at $(\mathbf{x}', \mathbf{v}')$ conditional on the later position $(\mathbf{x}, \mathbf{v})$ can be treated by taking this final position as a fixed initial condition and considering trajectories described by the time-

reversed particle equation of motion [151]. Closure is made in the corresponding time-reversed PDF transport equation for ϕ by assuming a Gaussian form and utilising the locality assumption (4.71) at this level within the associated expressions for $\mathbf{m}'$ and $\boldsymbol{\Theta}'$. Specification of these moments then fully determines ϕ, meaning that the identity (4.72) can be evaluated and in turn used for deducing closed expressions for the dispersion tensors $\overline{\boldsymbol{\kappa}}(\mathbf{x},t)$, $\overline{\boldsymbol{\lambda}}(\mathbf{x},t)$, and $\overline{\boldsymbol{\mu}}(\mathbf{x},t)$ at the top level of the problem.

This approach was first applied to the case of fluid element transport (the limiting case of $\tau_p \to 0$) in an incompressible isotropic flow [151], for which the simplified equation of motion means that $\boldsymbol{\mu}(\mathbf{x},t)$ does not appear within the corresponding transport equation for the PDF $\phi(\mathbf{x}',t' \mid \mathbf{x},t)$ and $\boldsymbol{\kappa}(\mathbf{x},t) = \mathbf{0}$, thereby restricting attention to the spatial diffusion $\boldsymbol{\lambda}(\mathbf{x},t)$. This system admits analytical solutions with $\mathbf{m}' = \mathbf{0}$ and $\boldsymbol{\Theta}'$ reducing to a function of time separation s, resulting in an improved approximation for $\boldsymbol{\lambda}(\mathbf{x},t)$ which is able to capture non-local path history effects of fluid elements within the dispersion process.

4.5.3 Application to Inertial Particles

Application of the non-local closure methodology in section 4.5.2 to capturing the behaviour of inertial particles in inhomogeneous flows was undertaken by Bragg *et al.* [13] within the context of a turbulent boundary layer. This is specified as a statistically stationary non-uniform shear flow, in which the mean flow $\langle\mathbf{u}\rangle(\mathbf{x})$ is taken to be locally linear, modifying the shear rate defined in (4.67) to the location-dependent form $\gamma(\mathrm{x}_2) = \partial\langle\mathrm{u}_1\rangle/\partial\mathrm{x}_2$. In the same manner as for a uniform shear flow, using the LHA on the response tensor $\boldsymbol{\mathcal{H}}[t;t']$ by neglecting the contribution from $\partial\mathbf{f}/\partial\mathbf{x}$ in the governing equation (4.28) produces the approximation given in (4.69), with the distinction that in this case $\gamma(\mathrm{x}_2)$ and therefore also $\mathcal{H}_{12}[t;t';\mathrm{x}_2]$ are both location dependent in the wall-normal direction x_2. This allows for deterministic treatment of $\boldsymbol{\mathcal{H}}[t;t']$ since it is trajectory independent, meaning that it can be extracted from the conditional averages within the dispersion tensors (4.30 - 4.32), which reduce to averages of only the two-point two-time correlation tensor $\mathbf{R}\left(\boldsymbol{x}_p',t';\mathbf{x},t\right)$. Further, since it is the particle spatial distribution which is of interest in boundary layers, the velocity averaged form of the dispersion tensors can be used, and then for the purposes of developing a non-local closure the identity (4.72) simplifies to

$$\left\langle \mathbf{R}\left(\boldsymbol{x}_p',t';\mathbf{x},t\right)\right\rangle_{\mathbf{x}} = \int_{\mathbf{x}'} \mathbf{R}(\mathbf{x}',t';\mathbf{x},t)\,\phi(\mathbf{x}',t' \mid \mathbf{x},t)\,d\mathbf{x}' \tag{4.73}$$

In this work, construction of the moments $\mathbf{m}'$ and $\boldsymbol{\Theta}'$ for the assumed Gaussian conditional PDF for particle trajectories $\phi\left(\mathbf{x}', t' \mid \mathbf{x}, t\right)$ was carried out by expressing the time-reversed particle equation of motion in integral form, which is admissible for a linear drag law. This modelling procedure then reduces the required closures to the averages of fluid velocity along trajectories $\left\langle \mathbf{u}(\boldsymbol{x}_p(t), t) \right\rangle$ and particle velocity $\left\langle \boldsymbol{v}_p(t) \right\rangle$, the particle kinetic stresses $\overline{\mathbf{cc}}\left(\mathbf{x}, t\right)$, and the covariances of fluid velocities $\left\langle \mathbf{u}'(\boldsymbol{x}_p(t_1), t_1)\mathbf{u}'(\boldsymbol{x}_p(t_2), t_2) \right\rangle$ and particle-fluid velocities $\left\langle \boldsymbol{v}_p'(t_1)\mathbf{u}'(\boldsymbol{x}_p(t_2), t_2) \right\rangle$ along trajectories. By utilising the particle-phase momentum and kinetic stress equations (4.42) and (4.44), closure is made at this level with the LHA forms of the dispersion tensors $\overline{\boldsymbol{\kappa}}^{\mathrm{LHA}}\left(\mathbf{x}, t\right)$, $\overline{\boldsymbol{\lambda}}^{\mathrm{LHA}}\left(\mathbf{x}, t\right)$, and $\overline{\boldsymbol{\mu}}^{\mathrm{LHA}}\left(\mathbf{x}, t\right)$. For a turbulent boundary layer these approximations generalise the form of $\mathbf{R}\left(\boldsymbol{x}_p', t'; \mathbf{x}, t\right)$ in the homogeneous shear flow model (4.68), with the distinction that both the one-point one-time correlations $\mathbf{R}\left(\mathbf{x}, t; \mathbf{x}, t\right)$ and the fluid decorrelation timescale along particle trajectories $\tau_{Lp}(\mathbf{x})$ should be modelled as a function of the wall-normal position x_2, resulting in

$$\mathbf{R}\left(\mathbf{x}', t'; \mathbf{x}, t\right) \approx \beta^2 \left\langle \mathbf{u}'\left(\mathrm{x}_2\right) \mathbf{u}'\left(\mathrm{x}_2\right) \right\rangle \exp\left[-\frac{1}{\tau_{Lp}(\mathrm{x}_2)} (t - t') \right] \tag{4.74}$$

This procedure determines the moments $\mathbf{m}'$ and $\boldsymbol{\Theta}'$ analytically, however the subsequent evaluation at the top level of closure in (4.73) and thereafter for the dispersion tensors $\overline{\boldsymbol{\kappa}}\left(\mathbf{x}, t\right)$, $\overline{\boldsymbol{\lambda}}\left(\mathbf{x}, t\right)$, and $\overline{\boldsymbol{\mu}}\left(\mathbf{x}, t\right)$ is necessarily undertaken numerically due to the level of detail included in the modelling process. Nonetheless it is demonstrated that this approach accounts very well for the non-local effects that are characteristic of a turbulent boundary layer, with all three of the dispersion tensors in close agreement with particle tracking simulation results. As with the work of Skartlien [142], the LHA is shown to be less accurate for $\overline{\boldsymbol{\lambda}}\left(\mathbf{x}, t\right)$ than $\overline{\boldsymbol{\mu}}\left(\mathbf{x}, t\right)$ compared to simulation data, however the non-local closure model successfully captures the correct behaviour. Additionally, it is shown that in general the PSA (4.70) does not hold across a range of particle inertias, with the non-local closure model offering a significant improvement in $\overline{\boldsymbol{\kappa}}\left(\mathbf{x}, t\right)$. Due to the modelling framework being self-contained, no additional input data is required in the procedure, meaning that the closure model can be evaluated a-priori of the particle tracking simulations. This attributes the accuracy of the closure model solely to the non-local treatment of $\left\langle \mathbf{R}\left(\boldsymbol{x}_p', t'; \mathbf{x}, t\right) \right\rangle_{\mathbf{x}}$, and highlights the potential of such a methodology for producing accurate closures in other flow configurations or for a more general particle model than that of gas-solid flows.

4.6 Appraisal of Existing Closure Models

Previous work has almost without exception approximated the particle response tensor $\boldsymbol{\mathcal{H}}[t;t']$ with a deterministic expression, thereby taking into account only the mean behaviour of $\boldsymbol{\mathcal{H}}[t;t']$. This approach has yielded appropriate closure models for both uniform shear flow (section 4.4.2) and a turbulent boundary layer (section 4.5.3) when the two-point two-time correlation tensor $\mathbf{R}(\mathbf{x}',t';\mathbf{x},t)$ is modelled using local and non-local approximations respectively, however in all cases the underlying flow field in which particles are immersed has a non-zero mean flow.

The work presented in this thesis is concerned with analysing the importance of certain contributions that arise within the particle mass flux representation of the PDF kinetic model given by equation (4.48). In order to better understand these contributions, it is desirable to consider flow configurations that limit the confounding effects of multiple such terms by isolating individual contributions. This is achieved in the present work using both a homogeneous isotropic flow in which particles are subject to a gravitational body force in one direction (Chapter 6), and also a specially constructed inhomogeneous flow field with no external body forces (Chapter 8). In both of these configurations the fluid velocity field is statistically stationary, and is further characterised by a zero-mean flow, meaning that the LHA for $\boldsymbol{\mathcal{H}}[t;t']$ takes the isotropic form given by (4.65). An immediate consequence of this is that within the integrand of the dispersion tensor $\overline{\boldsymbol{\kappa}}(\mathbf{x},t)$ as given by (4.30), the expression $\frac{\partial}{\partial \mathbf{x}}\mathbf{R}(\mathbf{x}',t';\mathbf{x},t)$ contracts to $\frac{\partial}{\partial \mathbf{x}}\cdot\mathbf{R}(\mathbf{x}',t';\mathbf{x},t)$, which is identically zero due to the incompressibility of the flow field regardless of the modelling approach taken for $\mathbf{R}(\mathbf{x}',t';\mathbf{x},t)$. Therefore configurations with a zero-mean flow automatically yield $\overline{\boldsymbol{\kappa}}^{\mathrm{LHA}}(\mathbf{x},t)=\mathbf{0}$, meaning that the effect of this important contribution to the particle mass flux is lost in all such flows by using the simplified description of $\boldsymbol{\mathcal{H}}[t;t']$ given in (4.65). The challenge then is to develop a model that is able to capture in particular the non-zero behaviour of $\overline{\boldsymbol{\kappa}}(\mathbf{x},t)$ in these flow configurations, by specifically including a fuller description of the particle response tensor $\boldsymbol{\mathcal{H}}[t;t']$.

Chapter 5

Numerical Methodology

For the development of closure models using the PDF framework to be objective, assessment of proposed models against some form of data is essential in order to evaluate the accuracy of the closures. As alluded to in Chapter 1, the alternative options of experimental and computational approaches are available for such purposes, with each having their own distinct merits. The present research takes the computational point of view, chiefly due to the relative ease with which the required statistics can be extracted from a numerical simulation as opposed to an experiment, but also due to the versatility of the methods available. In this work computational fluid dynamics is used as a means for running particle tracking simulations in the Lagrangian frame of reference, with this approach being particularly applicable to the PDF kinetic model since the framework is developed from the underlying particle equation of motion. Specifically, particle trajectories governed by the linear drag law in equation (2.22) are computed in flow fields constructed using kinematic simulation (KS), the details of which are outlined in section 5.1. Furthermore, it is useful to initialise particle velocities in a way that reflects emergent correlations between particle and fluid velocities, and the approach used to achieve this is discussed in section 5.3, with the effect on the initial transience of the PDF kinetic model dispersion tensors $\overline{\boldsymbol{\kappa}}(\mathbf{x},t)$, $\overline{\boldsymbol{\lambda}}(\mathbf{x},t)$, and $\overline{\boldsymbol{\mu}}(\mathbf{x},t)$ detailed in section 5.4.

5.1 Kinematic Simulation

The suitability of KS as a means for making inferences about the physical mechanisms that are responsible for particle behaviour in a given flow configuration is detailed in

section 3.5.2, with the consensus being that it provides a sufficiently detailed input to the particle equation of motion for behaviour to be attributable to structures within the flow field, whilst not including the effect of dissipation and full description of the microscales that vastly amplify the computational cost of such a simulation. The main advantage of KS within the context of the PDF kinetic model is that it can be used to create flow fields with prescribed decorrelation rates, thereby providing a closed form of the Eulerian two-point two-time correlation tensor $\mathbf{R}(\mathbf{x}', t'; \mathbf{x}, t)$ given by (4.25) that is easily evaluated, and thus avoiding the otherwise non-trivial evaluation of this from simulation data. A direct comparison of closure models and particle tracking simulation results is then possible without any further modelling required, meaning that any discrepancy can be attributed solely to inadequacies of the closure for the particular flow field being considered. Additionally, the fluid velocities $\mathbf{u}(\mathbf{x}, t)$ can be generated to conform to a specific probability distribution. For the PDF kinetic model it is therefore particularly helpful to choose this to be a Gaussian, since then the higher order terms in the cumulant expansion (4.9) of the phase-space diffusion current $\left\langle \mathbf{b}(\boldsymbol{\xi}, t)\, \mathcal{P}(\mathbf{b}; \boldsymbol{\xi}, t) \right\rangle$ are all identically zero, meaning that the Furutsu-Novikov formula (4.10) can be used to give an exact closure. A true turbulent velocity field on the other hand is not Gaussian [118], and the higher-order moments cause the tails to deviate significantly from those of a normal distribution. Subsequent inclusion of the higher-order terms in the cumulant expansion (4.9) may be necessary to maintain the accuracy of this closure, thereby considerably complicating the form of the PDF kinetic model for dynamic turbulent flow. Another salient advantage of a synthetic flow field is that the fluid velocity can then be specified explicitly and calculated as needed within the simulation domain, thereby avoiding the need for interpolation from a fixed grid of points as required for the numerical treatment of the Navier-Stokes equations, and the associated truncation error which comes with this.

5.1.1 Specification and Generation of the Velocity Field

The aim is to construct an incompressible flow field that is also homogeneous, isotropic, and statistically stationary for a rectangular domain of side length $2\mathcal{L}$ with periodic boundary conditions. Specifically, suppose that the zero-mean velocity field $\mathbf{U}(\mathbf{x}, t)$ is defined on the uniform 'box' $\boldsymbol{\mathcal{B}} = [-\mathcal{L}, +\mathcal{L}]^d$ where $d \in \{2, 3\}$ is the number of physical spatial dimensions. Therefore due to periodicity

$$\mathbf{U}(\mathbf{x}, t)\big|_{\mathrm{x}_j = -\mathcal{L}} = \mathbf{U}(\mathbf{x}, t)\big|_{\mathrm{x}_j = +\mathcal{L}} \qquad \forall j \in \{1, \ldots, d\} \tag{5.1}$$

Then $\mathbf{U}(\mathbf{x}, t)$ and its periodic extension to all $\mathbf{x}$ can be expressed in terms of its Fourier series representation as

$$\mathbf{U}(\mathbf{x}, t) \;=\; \sum_{\mathbf{k}} \mathbf{c}_{\mathbf{k}}(t) \exp\left[i\,\mathbf{k}\cdot\mathbf{x}\right] \tag{5.2}$$

where $\mathbf{k} = \Delta k\,\mathbf{n}$ are the Fourier space modes, $\Delta k = 2\pi/\mathcal{L}$ is the spacing between Fourier modes, $\mathbf{n} \in \mathbb{Z}^d$ is the number of modes included in the summation (5.2) in each direction, and the complex Fourier coefficients $\mathbf{c}_{\mathbf{k}}(t)$ are defined as

$$\mathbf{c}_{\mathbf{k}}(t) = \frac{1}{(2\mathcal{L})^d} \int_{\mathcal{B}} \mathbf{U}(\mathbf{x}, t) \exp\left[-i\,\mathbf{k}\cdot\mathbf{x}\right] d\mathbf{x} \tag{5.3}$$

To ensure that $\mathbf{U}(\mathbf{x}, t)$ is real-valued, the complex Fourier coefficients $\mathbf{c}_{\mathbf{k}}(t)$ are subject to the relation

$$\mathbf{c}_{-\mathbf{k}}(t) = \overline{\mathbf{c}}_{\mathbf{k}}(t) \tag{5.4}$$

Furthermore, taking the divergence of the velocity field definition (5.2) results in

$$\nabla\cdot\mathbf{U}(\mathbf{x}, t) \;=\; \sum_{\mathbf{k}} i\,\mathbf{c}_{\mathbf{k}}(t)\cdot\mathbf{k} \exp\left[i\,\mathbf{k}\cdot\mathbf{x}\right] \tag{5.5}$$

meaning that for the velocity field to be incompressible and satisfy $\nabla\cdot\mathbf{U} = 0$, the equivalent condition in Fourier space is $\mathbf{c}_{\mathbf{k}}\cdot\mathbf{k} = 0$. In order to respect these constraints, generation of the complex Fourier coefficients $\mathbf{c}_{\mathbf{k}}(t)$ is motivated by previous approaches to KS [84, 151], and are taken to be independent random variables such that

$$\mathbf{c}_{\mathbf{k}}(t) = \mathbf{z}_{\mathbf{k}} \times \mathbf{k} \exp\left[i\,\omega_{\mathbf{k}} t\right] \tag{5.6}$$

where the complex vectors $\mathbf{z}_{\mathbf{k}}$ are in turn specified by

$$\mathbf{z}_{\mathbf{k}} = \frac{1}{2}\alpha_{\mathbf{k}}\left(\boldsymbol{\zeta}_{\mathbf{k}} - i\,\boldsymbol{\xi}_{\mathbf{k}}\right) \tag{5.7}$$

in which $\alpha_{\mathbf{k}}$ is a scaling coefficient satisfying $\alpha_{-\mathbf{k}} = \alpha_{\mathbf{k}}$ to be chosen such that the desired form of energy spectrum can be recovered from the velocity field, and the random velocities $\boldsymbol{\zeta}_{\mathbf{k}}$, $\boldsymbol{\xi}_{\mathbf{k}}$ and frequencies $\omega_{\mathbf{k}}$ are subject to the constraints $\boldsymbol{\zeta}_{-\mathbf{k}} = -\boldsymbol{\zeta}_{\mathbf{k}}$,

$\boldsymbol{\xi}_{-\mathbf{k}} = \boldsymbol{\xi}_{\mathbf{k}}$ and $\omega_{-\mathbf{k}} = -\omega_{\mathbf{k}}$ as a consequence of (5.4). This is realised by generating $\boldsymbol{\zeta}_{\mathbf{k}}$, $\boldsymbol{\xi}_{\mathbf{k}}$ and $\omega_{\mathbf{k}}$ as zero-mean Gaussian random numbers according to

$$\begin{aligned} \zeta_{\mathbf{k}}^{j}, \xi_{\mathbf{k}}^{j} &\sim \mathrm{N}\left(0, \sigma_z^2\right) \\ \omega_{\mathbf{k}} &\sim \mathrm{N}\left(0, \sigma_\omega^2\right) \end{aligned} \tag{5.8}$$

where σ_z and σ_ω are the standard deviations of the respective velocity and frequency distributions. Furthermore, the velocity field $\mathbf{U}(\mathbf{x}, t)$ defined in (5.2) can be reduced to a two-dimensional form $\mathbf{U} = (U_1, U_2, 0)$ by taking

$$\begin{aligned} \mathbf{z}_{\mathbf{k}} &= (0, 0, z_{\mathbf{k}}) \\ \mathbf{k} &= (\mathrm{k}_1, \mathrm{k}_2, 0) = \Delta k \, (\mathrm{n}_1, \mathrm{n}_2, 0) \end{aligned} \tag{5.9}$$

Then specification of the Fourier coefficients by (5.6) produces $\mathbf{c}_{\mathbf{k}} = \left(\mathrm{c}_{\mathbf{k}}^1, \mathrm{c}_{\mathbf{k}}^2, 0\right)$ as required.

5.1.2 Reconciliation of KS with the Velocity Spectrum Tensor

The parameters $\alpha_{\mathbf{k}}$, σ_z and σ_ω are chosen to recover a prescribed form of the two-point two-time fluid velocity correlations $\left\langle \mathbf{U}(\mathbf{x}_1, t_1)\mathbf{U}(\mathbf{x}_2, t_2) \right\rangle$ consistent with a homogeneous isotropic flow field. For this velocity field it is desired for convenience to specify the spatial and temporal correlations as independent decorrelation functions such that

$$\left\langle \mathbf{U}(\mathbf{x}_1, t_1)\mathbf{U}(\mathbf{x}_1 + \mathbf{r}, t_2) \right\rangle = \mathbf{Q}(\mathbf{r})\mathrm{E}_\omega(s) \tag{5.10}$$

where $\mathbf{Q}(\mathbf{r})$ is the two-point one-time fluid velocity correlation tensor $\mathbf{Q}(\mathbf{r}) = \left\langle \mathbf{U}(\mathbf{x}, t)\mathbf{U}(\mathbf{x}+\mathbf{r}, t) \right\rangle$, $\mathbf{r}$ is the spatial separation vector defined as $\mathbf{r} = \mathbf{x}_2 - \mathbf{x}_1$, s is the time separation given by $s = t_2 - t_1$, and $\mathrm{E}_\omega(s)$ is the Eulerian temporal decorrelation function for the velocity field that satisfies $\mathrm{E}_\omega(s) \to 0$ as $|s| \to \infty$.

Since the KS flow field properties are specified in terms of the Fourier coefficients $\mathbf{c}_{\mathbf{k}}(t)$, it is most natural to determine the parameter values needed to retrieve a given form of $\mathbf{Q}(\mathbf{r})$ in terms of the Fourier modes. From the definition of $\mathbf{c}_{\mathbf{k}}(t)$ in (5.3), it can be shown that

$$\big\langle \mathbf{c}_{-\mathbf{k}}(t_1)\mathbf{c}_{\mathbf{k}}(t_2)\big\rangle = \frac{1}{(2\mathcal{L})^d}\int_{\boldsymbol{\mathcal{B}}} \big\langle \mathbf{U}(\mathbf{x}_1,t_1)\mathbf{U}(\mathbf{x}_1+\mathbf{r},t_2)\big\rangle \exp\big[-i\,\mathbf{k}\cdot\mathbf{r}\big]\,d\mathbf{r} \tag{5.11}$$

Then making use of the assumed independence of spatial and temporal decorrelation functions as given in (5.10) and the relation $\Delta k = 2\pi/\mathcal{L}$ produces

$$\big\langle \mathbf{c}_{-\mathbf{k}}(t_1)\mathbf{c}_{\mathbf{k}}(t_2)\big\rangle = (2\pi)^{-d}\,(\Delta k)^d \int_{\boldsymbol{\mathcal{B}}} \mathbf{Q}(\mathbf{r}) \exp\big[-i\,\mathbf{k}\cdot\mathbf{r}\big]\,d\mathbf{r}\,\mathrm{E}_\omega(s) \tag{5.12}$$

If the domain $\boldsymbol{\mathcal{B}} = [-\mathcal{L},+\mathcal{L}]^d$ is considered to be sufficiently large relative to the lengthscales implicit in the correlation tensor $\mathbf{Q}(\mathbf{r})$, then the integral over $\boldsymbol{\mathcal{B}}$ can be approximated as the standard Fourier transform of $\mathbf{Q}(\mathbf{r})$, enabling (5.12) to be written in terms of the velocity spectrum tensor $\boldsymbol{\Phi}(\mathbf{k})$ [9]

$$\big\langle \mathbf{c}_{-\mathbf{k}}(t_1)\mathbf{c}_{\mathbf{k}}(t_2)\big\rangle \approx (2\pi)^{-\frac{d}{2}}\,(\Delta k)^d\,\boldsymbol{\Phi}(\mathbf{k})\mathrm{E}_\omega(s) \tag{5.13}$$

On the other hand, taking the chosen method for generation of the Fourier coefficients $\mathbf{c}_{\mathbf{k}}(t)$ for the KS flow field defined by (5.6) with the distribution of random velocities $\zeta^j_{\mathbf{k}}\,,\xi^j_{\mathbf{k}} \sim \mathrm{N}\big(0,\sigma_{\mathrm{z}}^2\big)$ as in (5.8), it follows that

$$\big\langle \mathbf{c}_{-\mathbf{k}}(t_1)\mathbf{c}_{\mathbf{k}}(t_2)\big\rangle_{ij} = \frac{1}{2}\sigma_z^2\left(k^2\delta_{ij} - \mathrm{k}_i\mathrm{k}_j\right)\big\langle \exp\left[i\,\omega_{\mathbf{k}}s\right]\big\rangle \tag{5.14}$$

where $k = |\mathbf{k}|$ is the magnitude of the Fourier mode $\mathbf{k}$. Then with $\omega_{\mathbf{k}} \sim \mathrm{N}\big(0,\sigma_\omega^2\big)$ as specified in (5.8), the characteristic function of $\omega_{\mathbf{k}}$ yields a Gaussian decorrelation in time

$$\mathrm{E}_\omega(s) = \big\langle \exp\left[i\,\omega_{\mathbf{k}}s\right]\big\rangle = \exp\left[-\frac{1}{2}\sigma_\omega^2 s^2\right] \tag{5.15}$$

in which σ_ω can be interpreted as a measure of the velocity field temporal correlations. Comparison between the different forms of Fourier coefficient correlation arising from the flow field definition (5.13) and chosen method of generation for KS (5.14) then shows that the velocity spectrum tensor $\boldsymbol{\Phi}(\mathbf{k})$ is determined as

$$\Phi_{ij}(\mathbf{k}) \approx \frac{1}{2}\sigma_z^2\alpha_{\mathbf{k}}^2\,(2\pi)^{\frac{d}{2}}\,(\Delta k)^{-d}\left(k^2\delta_{ij} - \mathrm{k}_i\mathrm{k}_j\right) \tag{5.16}$$

From this the constant multiplier $\frac{1}{2}\sigma_z^2$ can be interpreted as a characteristic velocity of the flow field, whilst the scaling coefficient $\alpha_{\mathbf{k}}^2$ is taken as a Fourier mode dependent expression to be chosen such that the desired form of $\mathbf{\Phi}(\mathbf{k})$ is recovered.

5.1.3 Imposition of an Isotropic Two-Point Correlation Tensor

Determination of the parameters σ_z and $\alpha_{\mathbf{k}}$ requires explicit specification of $\mathbf{Q}(\mathbf{r})$, which is done for this velocity field by appealing to isotropy [9, 118]

$$\mathrm{Q}_{ij}(\mathbf{r}) = u'^2 \left[g(\mathrm{r})\delta_{ij} + \big(f(\mathrm{r}) - g(\mathrm{r})\big)\frac{\mathrm{r}_i \mathrm{r}_j}{\mathrm{r}^2} \right] \tag{5.17}$$

where $\mathrm{r} = |\mathbf{r}|$, and $f(\mathrm{r})$ and $g(\mathrm{r})$ are the normalised longitudinal and lateral correlation coefficients of the underlying velocity field respectively. For an incompressible velocity field the correlation functions $f(\mathrm{r})$ and $g(\mathrm{r})$ are related by [9]

$$g(\mathrm{r}) = f(\mathrm{r}) + \frac{1}{d-1}\mathrm{r}\frac{d}{d\mathrm{r}}f(\mathrm{r}) \tag{5.18}$$

Thus the characteristics of $\mathbf{Q}(\mathbf{r})$ for an isotropic flow field are dependent solely on the longitudinal correlation function $f(\mathrm{r})$. For dynamical turbulence $f(\mathrm{r})$ is governed by the Kármán–Howarth equation [42] and cannot be uniquely determined without further physical assumption about the flow field, however self-similar approximations emerge for a decaying flow after a sufficiently long period of time has elapsed [8]. When dealing with numerical simulations the long-established practice is to use the corresponding form of the turbulent kinetic energy spectrum $E(k)$ to inform the choice of $f(\mathrm{r})$, and specifically the requirement that $E(k)$ decreases sufficiently fast over the range of Fourier modes $\mathbf{k}$ used in the simulation [137]. One such appropriate form of $E(k)$ is the Batchelor-Townsend energy spectrum [8], which corresponds to a Gaussian form of $f(\mathrm{r})$ [84, 137, 122, 91, 164]. In this work the following form of $f(\mathrm{r})$ is therefore adopted

$$f(\mathrm{r}) = \exp\left[-\frac{1}{2}\sigma_k^2 \mathrm{r}^2 \right] \tag{5.19}$$

where σ_k is the magnitude of the Fourier modes corresponding to the peak of the energy spectrum $E(k)$, and therefore acts as a measure of the velocity field spatial correlations

characteristic of the larger energetic eddies. With this form of $f(\mathrm{r})$ in $\mathbf{Q}(\mathbf{r})$ as specified in (5.17), taking the Fourier transform then yields the velocity spectrum tensor $\mathbf{\Phi}(\mathbf{k})$ as

$$\Phi_{ij}(\mathbf{k}) = \frac{1}{d-1} u'^2 \left(k^2 \delta_{ij} - \mathrm{k}_i \mathrm{k}_j\right) \frac{1}{\sigma_k^{d+2}} \exp\left[-\frac{1}{2}\frac{k^2}{\sigma_k^2}\right] \tag{5.20}$$

Comparison with the approximation of $\mathbf{\Phi}(\mathbf{k})$ used for generating the KS flow field in (5.16) directly reveals expressions for the parameters σ_z and $\alpha_{\mathbf{k}}$

$$\sigma_z^2 = \frac{2}{d-1} u'^2 \tag{5.21}$$

$$\alpha_{\mathbf{k}}^2 = (2\pi)^{-\frac{d}{2}} (\Delta k)^d \frac{1}{\sigma_k^{d+2}} \exp\left[-\frac{1}{2}\frac{k^2}{\sigma_k^2}\right] \tag{5.22}$$

where it is now noted that the explicit condition for the approximation (5.16) to be valid is $\mathcal{L}\sigma_k \gg 1$. This fully specifies the KS flow field for the selected form of $f(\mathrm{r})$ in (5.19), and leaves the free parameters u', σ_k, and σ_ω to be chosen as appropriate within each simulation.

5.1.4 Recovering the Form of the Kinetic Energy Spectrum

For an isotropic velocity field the kinetic energy spectrum $E(k)$ is uniquely determined by the longitudinal correlation coefficient $f(\mathrm{r})$, and is also related to the velocity spectrum tensor $\mathbf{\Phi}(\mathbf{k})$ by [9]

$$\Phi_{ij}(\mathbf{k}) = \frac{E(k)}{k^2 A_d(k)} \left(k^2 \delta_{ij} - \mathrm{k}_i \mathrm{k}_j\right) \quad , \quad A_d(k) = \begin{cases} 2\pi k & , \quad d = 2 \\ 4\pi k^2 & , \quad d = 3 \end{cases} \tag{5.23}$$

where $A_d(k)$ is the area of bounding surface of the Fourier modes which form a shell at magnitude k in d dimensions. From this $E(k)$ can therefore be recovered by comparing $\mathbf{\Phi}(\mathbf{k})$ as given by (5.20) for the chosen case of $f(\mathrm{r})$ with (5.23), which results in a form consistent with the Batchelor-Townsend spectrum as desired

$$E(k) = \frac{1}{d-1} u'^2 k^2 A_d(k) \frac{1}{\sigma_k^{d+2}} \exp\left[-\frac{1}{2}\frac{k^2}{\sigma_k^2}\right] \tag{5.24}$$

This can be generalised for an arbitrary kinetic energy spectrum $E(k)$ by comparing the relation (5.23) with the approximation (5.16) for $\mathbf{\Phi}(\mathbf{k})$ arising from the chosen method of generation for the KS flow field, from which in turn emerges

$$E(k) = \underbrace{\frac{1}{2}\sigma_z^2}_{\text{Multiplier}} \; k^2 A_d(k) \; \underbrace{(2\pi)^{\frac{d}{2}} (\Delta k)^{-d} \, \alpha_{\mathbf{k}}^2}_{\text{Fourier mode dependent tail}} \tag{5.25}$$

Thus, of the parameters emerging from the method of generation for the KS flow field in (5.6), for an arbitrary kinetic energy spectrum, σ_z acts as a multiplier, whilst $\alpha_{\mathbf{k}}$ contains information about the roll off at high Fourier modes within a suitably defined spectrum tail.

5.1.5 Velocity Field Statistics

Specification of the KS velocity field in the manner outlined uses an explicit form (5.19) of the longitudinal correlation coefficient $f(\mathrm{r})$, and produces the Gaussian form (5.15) for the Eulerian temporal decorrelation function $\mathrm{E}_\omega(s)$ when the rate parameter σ_ω is normally distributed. From these key quantities the longitudinal integral lengthscale L_{11} and Eulerian integral timescale τ_E of the velocity field directly follow, given as [118]

$$L_{11} = \int_0^\infty f(\mathrm{r}) \, d\mathrm{r} = \sqrt{\frac{\pi}{2}} \frac{1}{\sigma_k} \tag{5.26}$$

$$\tau_E = \int_0^\infty \mathrm{E}_\omega(s) \, ds = \sqrt{\frac{\pi}{2}} \frac{1}{\sigma_\omega} \tag{5.27}$$

The parameters σ_k and σ_ω are therefore used to determine the associated values of L_{11} and τ_E, and are interpreted as an inverse lengthscale and timescale respectively. Further statistics do not emerge automatically as a result of the velocity field specification, but are considered from a computational viewpoint.

5.2 Computational Implementation

The KS velocity field for the continuous phase constructed in section 5.1 was implemented in MATLAB® for $d = \{2, 3\}$, employing the Parallel Computing Toolbox in

order to keep the physical program runtime tractable. Simulations have been carried out using the Newcastle University Rocket HPC service, and to ensure sufficiently smooth statistics for the dispersed phase the required ensemble size used is 10^6 particles. The ability to directly generate fluid velocities using the flow field definition (5.2) makes it feasible for each particle to be tracked in a separate realisation of the velocity field, further reducing the variability of subsequent statistics. The parallelisation procedure can be considerably simplified in the case of one-way coupling by sending each particle to a separate processor, meaning that there is then no need for communication between processors during the simulation itself, and thus resulting in an embarrassingly parallel implementation. This has the advantage of being free from parallel slowdown, with a near linear speed-up in program efficiency compared to a serial version, thereby facilitating the extraction of results which are sufficiently smooth. Further details concerning the numerical treatment for aspects of particle tracking are outlined as follows.

5.2.1 Time Advancement

For the purposes of evaluating the dispersion tensors $\overline{\boldsymbol{\kappa}}(\mathbf{x},t)$, $\overline{\boldsymbol{\lambda}}(\mathbf{x},t)$, and $\overline{\boldsymbol{\mu}}(\mathbf{x},t)$ within a particle tracking simulation, both the particle equation of motion (4.1) and governing equation (4.28) for the particle response tensor $\boldsymbol{\mathcal{H}}[t;t']$ must be solved numerically. To enable the use of standard numerical methods, $\boldsymbol{\mathcal{H}}[t;t']$ is recast as a first-order system of the form $\dot{\mathbf{y}} = \mathbf{f}(t,\mathbf{y})$ in the same manner as the particle equation of motion, as given by the phase-space response tensor $\boldsymbol{\mathcal{G}}[t;t']$ with the corresponding equation of evolution (4.18). For marching these equations forward in time, the standard Adams fourth-order predictor-corrector method is utilised [22]. This consists of two substeps; firstly a prediction step that approximates updated values using the four-step explicit Adams-Bashforth method (AB4)

$$\mathbf{y}^*_{i+1} = \mathbf{y}_i + \frac{\Delta t}{24}\Big[55\mathbf{f}(t_i,\mathbf{y}_i) - 59\mathbf{f}(t_{i-1},\mathbf{y}_{i-1}) + 37\mathbf{f}(t_{i-2},\mathbf{y}_{i-2}) - 9\mathbf{f}(t_{i-3},\mathbf{y}_{i-3})\Big] \quad (5.28)$$

where $\mathbf{y}^*_{i+1}$ is the approximation for the predictor step to the solution $\mathbf{y}_{i+1}$, and Δt is the computational timestep. This is followed by a corrector step that improves the approximated values using the three-step implicit Adams-Moulton method (AM3)

$$\mathbf{y}_{i+1} = \mathbf{y}_i + \frac{\Delta t}{24}\left[9\mathbf{f}(t_{i+1}, \mathbf{y}^*_{i+1}) + 19\mathbf{f}(t_i, \mathbf{y}_i) - 5\mathbf{f}(t_{i-1}, \mathbf{y}_{i-1}) + \mathbf{f}(t_{i-2}, \mathbf{y}_{i-2})\right] \tag{5.29}$$

Inclusion of this corrector step achieves a noticeable improvement in accuracy compared to just the explicit AB4 predictor step done alone, due to the greater stability and smaller round-off errors inherent in the implicit AM3 method. Furthermore, the corrector step only requires one further functional evaluation of $\mathbf{f}(t_{i+1}, \mathbf{y}^*_{i+1})$, as all other values of $\mathbf{f}$ have been previously computed for use in the predictor step. In theory, the corrector step could be iterated to within a convergence criterion, however this would converge on the approximation given by AM3 rather than the true solution $\mathbf{y}_{i+1}$, and in practice just one iteration is found to offer a sufficient improvement in accuracy within the context of tracking both particles and the response tensor. Additionally, the starting values required for these multistep methods are computed using the fourth-order Runge-Kutta method (RK4) in order to maintain an accuracy of $\mathcal{O}\left[(\Delta t)^4\right]$ [22].

5.2.2 Numerical Treatment of the Particle Response Tensor

To compute the dispersion tensors $\overline{\boldsymbol{\kappa}}(\mathbf{x}, t)$, $\overline{\boldsymbol{\lambda}}(\mathbf{x}, t)$ and $\overline{\boldsymbol{\mu}}(\mathbf{x}, t)$ using the definitions (4.30 - 4.32), evaluation of the path-history integrals requires knowledge of the particle response tensor $\boldsymbol{\mathcal{H}}[t; t']$ at time t for perturbations in the velocity field at all previous times t' throughout the sampling period $t_0 \leq t' \leq t$. Since the response tensor is unique to each individual particle trajectory, when the simulation runtime t is advanced to $t + \Delta t$ the value of $\boldsymbol{\mathcal{H}}[t; t']$ corresponding to each trajectory must then be advanced to $\boldsymbol{\mathcal{H}}[t + \Delta t; t']$ for all discrete time points t'. This is illustrated in Figure 5.1, and demonstrates that the different instances of $\boldsymbol{\mathcal{H}}[t; t']$ needed to evaluate the dispersion tensors at a fixed time point t require indexing in terms of only the reference time t', with all such instances then being updated accordingly when the simulation runtime t is advanced. As a point of computational efficiency this means that at a given time t in the simulation, only the current values of $\boldsymbol{\mathcal{H}}[t; t']$ for all instances of the reference time t' are needed, and therefore it is unnecessary to store the history of the response tensor in the computer memory as the simulation is advanced in time. This is in contrast to the particle trajectory, where for the two-point two-time correlation tensor $\mathbf{R}\left(\boldsymbol{x}'_p, t'; \mathbf{x}, t\right)$ to be evaluated over all values of t' requires storage of the complete particle trajectory for the duration of the sampling period $t_0 \leq t' \leq t$ until the simulation is complete.

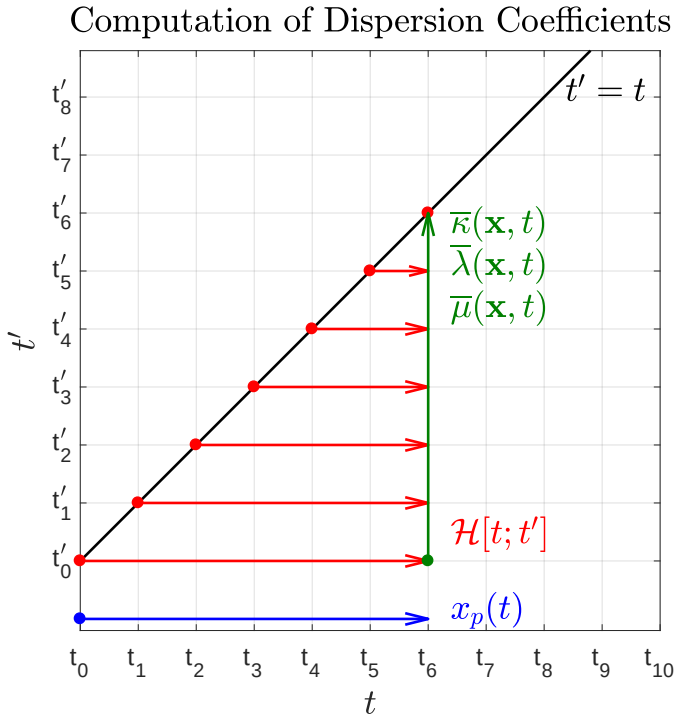

Figure 5.1: Schematic representation outlining the computation procedure of the particle trajectory $\boldsymbol{x}_p(t)$, particle response tensor $\boldsymbol{\mathcal{H}}[t; t']$, and dispersion tensors $\overline{\boldsymbol{\kappa}}(\mathbf{x}, t)$, $\overline{\boldsymbol{\lambda}}(\mathbf{x}, t)$ and $\overline{\boldsymbol{\mu}}(\mathbf{x}, t)$ at a given time point t in the simulation

5.2.3 Non-dimensionalisation and Parameter Independence

To keep non-dimensional quantities consistent across simulations, it is convenient to use the free parameters arising from the KS velocity field formulation as the reference scales for non-dimensionalisation denoted in equation (2.7). Specifically, taking $l_{\text{ref}} = \sigma_k^{-1}$ and $t_{\text{ref}} = \sigma_\omega^{-1}$ produces the reference velocity $u_{\text{ref}} = \sigma_k^{-1}\sigma_\omega$, and further setting these reference scales as $\sigma_k = 1$ and $\sigma_\omega = 1$ has the effect of fixing both the longitudinal integral lengthscale L_{11} and Eulerian integral timescale τ_E. As a point of convenience, this also results in the non-dimensional form of the governing equations for both the continuous phase as specified by the KS flow field (5.2) and particle phase as given by the equation of motion (4.1) being the same as their original dimensional forms, meaning that no further treatment is required in their implementation. Therefore all variables referred to forthwith are taken to be in non-dimensional form, even though this is not denoted explicitly for notational clarity. Additionally, fixing both σ_k and σ_ω in this manner leaves the only free parameters for the fluid velocity field as the RMS u' and domain size $2\mathcal{L}$, which in conjunction with τ_p and $\mathrm{g} = |\mathbf{g}|$ then constitute the

free parameters for these simulations.

Further, since the gravitational settling velocity V_g and Stokes number St are both defined in terms of the particle timescale τ_p, it is helpful to be able to vary these independently as the primary parameters of interest in disperse particle transport, and thereby isolate the effects of gravity and particle inertia in different simulations. As τ_E is fixed from non-dimensionalisation, St_E is naturally controlled through variation of τ_p, and for a fixed value of the gravitational acceleration g this variation would consequently also affect V_g. It is therefore judicious to choose V_g as a fixed input parameter to the simulation, and then variation of τ_p instead changes the effective value of g, which is inconsequential as all subsequent computation and post-processing for particle phase involving gravity uses V_g. Thus the coupling between V_g and St is not an issue with this approach, meaning that they can be treated as independent parameters.

5.2.4 Specification of Simulation Parameters

Domain Size

For running particle tracking simulations, the remaining free parameters must be specified a-priori. Firstly, fixing $\sigma_k = 1$ as part of the non-dimensionalisation procedure simplifies the requirement on the domain size to $\mathcal{L} \gg 1$, and since the reference lengthscale σ_k^{-1} uniquely determines the integral lengthscale $L_{11} = \sqrt{\frac{\pi}{2}} \approx 1.25$, the constraint on domain size can be expressed in terms of the ratio of these two quantities

$$\frac{\mathcal{L}}{L_{11}} \gg 1 \tag{5.30}$$

This can be simply be interpreted as the requirement that there must be many eddies at the largest scales of motion within the periodic simulation domain, and in order to satisfy the requirement $\mathcal{L}$ is set such that the simulation domain contains either 6 or 8 eddies in each direction for the present work, which is consistent with resolution recommendations for turbulent flows [118].

Computational Timestep

The computational timestep is determined from a stability analysis of the explicit AB4 method (5.28) used for time advancement which is relevant to the phase-space

response tensor $\boldsymbol{\mathcal{G}}\left[t;t'\right]$. Specifically, for the linear drag law in (2.22) that corresponds to $\mathbf{F}\left(\mathbf{x},\mathbf{v},t\right)=\beta\left(\left\langle\mathbf{u}(\mathbf{x},t)\right\rangle-\mathbf{v}\right)+\mathbf{g}$ and $\mathbf{f}\left(\mathbf{x},t\right)=\beta\mathbf{u}'(\mathbf{x},t)$, the governing equation for $\boldsymbol{\mathcal{G}}\left[t;t'\right]$ given in (4.18) explicitly becomes

$$\dot{\boldsymbol{\mathcal{G}}}\left[t;t'\right]=\begin{bmatrix}\mathbf{0} & \mathbf{I}\\ \beta\boldsymbol{\nabla}\mathbf{u}^{\top}(\boldsymbol{x}_p(t),t) & -\beta\mathbf{I}\end{bmatrix}\cdot\boldsymbol{\mathcal{G}}\left[t;t'\right]\quad,\quad\boldsymbol{\mathcal{G}}\left[t';t'\right]=\tilde{\mathbf{I}}=\begin{bmatrix}\mathbf{0} & \mathbf{0}\\ \mathbf{0} & \mathbf{I}\end{bmatrix}\tag{5.31}$$

Since $\boldsymbol{\mathcal{G}}\left[t;t'\right]$ is dependent upon the fluid velocity gradient $\boldsymbol{\nabla}\mathbf{u}^{\top}$, in contrast to the particle trajectories which depend on the fluid velocity $\mathbf{u}$, the larger fluctuations exhibited by the fluid velocity gradient relative to the fluid velocity implies that constructing a timestep criterion for numerical solution of $\boldsymbol{\mathcal{G}}\left[t;t'\right]$ will then also be a sufficient criterion for the particle trajectories. Furthermore, since the implicit AM3 method has greater stability than the explicit AB4 method at the same order of accuracy [22], such a criterion will also be applicable to both substeps of the predictor-corrector method. Then proceeding with a stability analysis of the linear system (5.31) for the explicit AB4 method as detailed in Appendix E yields the timestep criterion given in (E.11) as

$$\Delta t\ll\frac{3}{10\max\left(\beta,\beta|\boldsymbol{\nabla}\mathbf{u}^{\top}(\boldsymbol{x}_p(t),t)|\right)}\tag{5.32}$$

for which the dependencies in the denominator arise from the coefficient matrix in (5.31). This is interpreted as the requirement for the timestep to be defined using whichever of the particles or fluid velocity gradient has a smaller timescale for a given value of β, and this is taken into account by using an order of magnitude approximation for $|\boldsymbol{\nabla}\mathbf{u}^{\top}|$. The simple estimate for the RMS fluid velocity gradient of u'/L_{11} is used for this purpose, and following that the assumption that $\boldsymbol{\nabla}\mathbf{u}^{\top}(\boldsymbol{x}_p(t),t)$ can be approximated as normally distributed produces the condition $|\boldsymbol{\nabla}\mathbf{u}^{\top}(\boldsymbol{x}_p(t),t)|<4u'/L_{11}$. Further introducing a contingency factor of 1.2 for β to ensure that (5.32) remains strictly satisfied and guarantee numerical stability for all aspects of the simulation gives the final timestep criterion as

$$\Delta t\ll\frac{3}{10\max\left(1.2\beta,4u'/L_{11}\right)}\tag{5.33}$$

Fluid-Particle Timescale

To utilise the Wang & Stock [165] model of the fluid timescale along particle trajectories τ_{Lp} given in (4.63) and as used in the LHA, a suitable value of the fluid Lagrangian integral timescale τ_L is required. In the absence of an analytical result a suitable approximation of τ_L must therefore be made, and this is considered in terms of the *turbulence structure parameter* m, defined as [165]

$$m = \frac{\tau_E u'}{L_{11}} \tag{5.34}$$

which is the ratio of the fluid Eulerian integral timescale τ_E to the one-point eddy turnover time τ_{eddy}. The approximation of $\tau_L/\tau_E = 0.356$ is then provided by Wang & Stock [165] as a model from simulation data, however it is conditional on m having a value of unity. For the current KS flow field, the non-dimensionalisation procedure in section 5.2.3 fixes the values $\tau_E = \sqrt{\pi/2}$ and $L_{11} = \sqrt{\pi/2}$, and consequently the constraint $m = 1$ therefore imposes that $u' = 1$ in this case. The validity of the Wang & Stock approximation for the KS flow field is straightforward to check by tracking fluid elements as governed by the equation of motion

$$\dot{\boldsymbol{x}}_f = \mathbf{u}\left(\boldsymbol{x}_f(t), t\right) \tag{5.35}$$

where $\boldsymbol{x}_f$ is the trajectory of a fluid element as it travels through the velocity field. Then τ_L can be computed directly for an isotropic velocity field by [118]

$$\tau_L = \int_0^\infty \frac{\left\langle \mathbf{u}'\left(\boldsymbol{x}_f(t), t\right) \cdot \mathbf{u}'\left(\boldsymbol{x}_f(t+s), t+s\right) \right\rangle}{\left\langle \mathbf{u}'\left(\boldsymbol{x}_f(t), t\right) \cdot \mathbf{u}'\left(\boldsymbol{x}_f(t), t\right) \right\rangle} \, ds \tag{5.36}$$

For the KS flow field specified in section 5.1.1 it is found that $\tau_L/\tau_E = 0.465$, with the appreciable difference from the Wang & Stock value of 0.356 making it appropriate to use this more representative figure. For a given Stokes number St, it is also possible to confirm the suitability of the value of τ_{Lp} obtained from the model (4.63) by comparison with direct computation of τ_{Lp} from simulation data as the integral timescale (5.36), in which the fluid velocity is instead evaluated along inertial particle trajectories $\boldsymbol{x}_p(t)$ rather than fluid element trajectories $\boldsymbol{x}_f(t)$.

Simulation Runtime

During the initial part of the simulation, particles are required to reach steady-state behaviour such that the concentration profile and average particle velocity both equilibrate, in order for statistics that can be considered statistically stationary to subsequently be extracted. As with the computational timestep, the length of time taken to achieve equilibrium values is dependent upon the relative response times of the particles and fluid velocity, and for this flow field it is found that a suitable period across a range of values for the particle inertia is $3\tau_p + 3\tau_E$. Following this, the sampling period for computation of particle statistics also needs to be specified, for which the required duration hinges on how long it takes for the two-point two-time correlation tensor $\mathbf{R}\left(\boldsymbol{x}_p', t'; \mathbf{x}, t\right)$ to decorrelate. The length of the sampling period is therefore heavily dependent on the fluid-particle interaction, and as a result is most appropriately expressed in terms of the fluid timescale along a particle trajectory τ_{Lp}. For the cases run the duration of sampling was set to $4\tau_{Lp}$, which was found to be adequate for the particle dispersion tensors $\overline{\boldsymbol{\kappa}}\left(\mathbf{x}, t\right)$, $\overline{\boldsymbol{\lambda}}\left(\mathbf{x}, t\right)$ and $\overline{\boldsymbol{\mu}}\left(\mathbf{x}, t\right)$ to reach their steady-state values across a range of particle inertias.

5.2.5 Periodicity Considerations

Since the flow field defined using KS in section 5.1.1 is periodic in space, this results in a discontinuity whenever the particle location is used directly in evaluation of an expression. In particular, this occurs during the evaluation of the two-point two-time correlation tensor $\mathbf{R}\left(\boldsymbol{x}_p', t'; \mathbf{x}, t\right)$ within the dispersion tensors, and also the homogeneous benchmark value for $\overline{\boldsymbol{\lambda}}\left(\mathbf{x}, t\right)$ given by $\left\langle \boldsymbol{x}_p(t)\mathbf{f}(\boldsymbol{x}_p(t), t)\right\rangle$ in section 4.3, each of which require different treatment.

For the case of evaluating $\mathbf{R}\left(\boldsymbol{x}_p', t'; \mathbf{x}, t\right)$ within an isotropic flow field, the dependence on particle location is through the separation vector $\boldsymbol{r}_p(t)$. Due to the periodicity of the flow field, the spatial part of the correlation tensor $\mathbf{Q}(\mathbf{r})$ given in (5.17) will also be periodic with period $2\mathcal{L}$ for the separation in each direction r_j. This means that whenever a particle passes through a boundary and re-enters the domain on the opposite side, the separation vector $\boldsymbol{r}_p(t)$ will automatically shift accordingly so that it remains within the domain, thereby creating a discontinuity in the time series of the magnitude $r_p = |\boldsymbol{r}_p|$. This can be remedied by keeping track of the history of boundary crossings for each particle, meaning that the true non-periodic trajectory can be constructed, and the resultant continuous separation vector $\boldsymbol{r}_p(t)$ correctly computed.

When considering the quantity $\left\langle \boldsymbol{x}_p(t)\mathbf{f}(\boldsymbol{x}_p(t),t)\right\rangle$, it is clear that the explicit dependence on $\boldsymbol{x}_p(t)$ will cause the correlation to be heavily affected by the manner in which the periodicity is handled. In fact, periodic treatment of $\boldsymbol{x}_p(t)$ produces the result $\left\langle \boldsymbol{x}_p(t)\mathbf{f}(\boldsymbol{x}_p(t),t)\right\rangle \equiv \mathbf{0}$, since every time a particle passes through a domain boundary its location in that direction changes from $\pm\mathcal{L}$ to $\mp\mathcal{L}$, and the net effect of negating the particle location over the entire ensemble of particles averages out at zero correlation with the fluctuating particle acceleration $\mathbf{f}(\boldsymbol{x}_p(t),t)$. On the other hand, non-periodic handling of $\boldsymbol{x}_p(t)$ in the same manner as for $\mathbf{R}\left(\boldsymbol{x}_p',t';\mathbf{x},t\right)$ means that on average $\boldsymbol{x}_p(t)$ experiences unbounded growth when all particles are initially placed within the box $\boldsymbol{\mathcal{B}} = [-\mathcal{L},+\mathcal{L}]^d$. This is inherently also manifest in the correlation $\left\langle \boldsymbol{x}_p(t)\mathbf{f}(\boldsymbol{x}_p(t),t)\right\rangle$ as a consequence, which instead of reaching an equilibrium value continues to grow in size throughout the sampling period, highlighting the need for an alternative method for handling the periodicity of $\boldsymbol{x}_p(t)$. To achieve this it is necessary to make use of the ability to track each particle within its own realisation of the KS flow field, and then by initialising all particles at the centre of the domain, they will on average uniformly disperse across the ensemble of separate realisations without crossing any boundaries for a certain period of time. The sampling of particle trajectories within this period can then be done without needing to account for periodicity, providing a means of calculating $\left\langle \boldsymbol{x}_p(t)\mathbf{f}(\boldsymbol{x}_p(t),t)\right\rangle$ for comparing against $\overline{\boldsymbol{\lambda}}\left(\mathbf{x},t\right)$ as directly computed from (4.31).

5.3 Particle Velocity Initialisation

The manner in which the velocity of particles is initialised within a particle tracking simulation can have a strong impact on the time taken for the particle statistics to equilibrate, and in particular the asymptotic ($t \to \infty$) forms of the dispersion tensors $\overline{\boldsymbol{\kappa}}\left(\mathbf{x},t\right)$, $\overline{\boldsymbol{\lambda}}\left(\mathbf{x},t\right)$, and $\overline{\boldsymbol{\mu}}\left(\mathbf{x},t\right)$ given by (4.30 - 4.32). It is therefore a point of computational importance as to how the particle velocity $\mathbf{v}^0$ can be specified in such a manner as to minimise initial transience of the particle statistics, with the objective then being to find a method of initialising the particle velocities at the desired equilibrium level. An intuitive approach to this problem is to determine the required distribution of particle velocities using knowledge of the flow field at the particle position, which is given by the PDF of particle velocity conditional on the local fluid velocity $\phi(\mathbf{v} \mid \mathbf{u})$. In order to generate $\mathbf{v}^0$ such that the particle-fluid velocity correlations $\left\langle \mathbf{v}^0\,\mathbf{u}(\mathbf{x}^0,t_0)\right\rangle$ conform to the equilibrium statistics, knowledge of the joint particle-fluid velocity PDF $\phi(\mathbf{u},\mathbf{v})$

is also required. Since the relationship between the conditional PDF and joint PDF is given by [57]

$$\phi(\mathbf{v} \mid \mathbf{u}) = \frac{\phi(\mathbf{u}, \mathbf{v})}{\phi(\mathbf{u})} \tag{5.37}$$

the problem reduces to finding the joint PDF $\phi(\mathbf{u}, \mathbf{v})$ in the limit $t \to \infty$. From this the marginal PDF $\phi(\mathbf{u})$ can be extracted, thereby providing a means of calculating $\phi(\mathbf{v} \mid \mathbf{u})$.

5.3.1 Modelling the Fluid Acceleration along Inertial Particle Trajectories

To go about finding the joint PDF $\phi(\mathbf{u}, \mathbf{v})$, it is instructive to start by considering the higher-dimensional framework utilised by the generalised Langevin model as outlined in section 3.1.2, in which an equation governing the evolution of the fluid velocity along an inertial particle trajectory $\boldsymbol{u}_p$ is specified in addition to those for particle position $\boldsymbol{x}_p$ and velocity $\boldsymbol{v}_p$ [98]

$$\begin{aligned} \dot{\boldsymbol{x}_p} &= \boldsymbol{v}_p \\ \dot{\boldsymbol{v}_p} &= \mathbf{F}\left(\boldsymbol{x}_p, \boldsymbol{v}_p, \boldsymbol{u}_p, t\right) + \mathbf{f}\left(\boldsymbol{x}_p, t\right) \\ \dot{\boldsymbol{u}_p} &= \mathbf{G}\left(\boldsymbol{x}_p, \boldsymbol{v}_p, \boldsymbol{u}_p, t\right) \end{aligned} \tag{5.38}$$

The form of the model $\mathbf{G}\left(\boldsymbol{x}_p, \boldsymbol{v}_p, \boldsymbol{u}_p, t\right)$ for the fluid acceleration is informed by interpreting the process $\boldsymbol{u}_p(t)$ as $\boldsymbol{u}_p(t) \equiv \mathbf{U}(\boldsymbol{x}_p(t), t)$. Then it follows that along a particle trajectory $\boldsymbol{v}_p(t)$ [141]

$$\dot{\boldsymbol{u}_p}(t) = \frac{d}{dt}\mathbf{U}(\boldsymbol{x}_p(t), t) = \frac{D\mathbf{U}}{Dt}(\boldsymbol{x}_p(t), t) - \big(\boldsymbol{u}_p(t) - \boldsymbol{v}_p(t)\big) \cdot \frac{\partial}{\partial \mathbf{x}}\mathbf{U}(\boldsymbol{x}_p(t), t) \tag{5.39}$$

The phase-space model for the fluid acceleration along particle trajectories is thus given by

$$\mathbf{G}\left(\mathbf{x}, \mathbf{v}, \mathbf{u}, t; \mathbf{U}(\mathbf{x}, t)\right) = \frac{D\mathbf{U}}{Dt}(\mathbf{x}, t) - \big(\mathbf{u} - \mathbf{v}\big) \cdot \frac{\partial}{\partial \mathbf{x}}\mathbf{U}(\mathbf{x}, t) \tag{5.40}$$

Decomposing the fluid velocity and acceleration into mean and fluctuating parts $\mathbf{U} = \langle\mathbf{U}\rangle + \mathbf{U}'$ and $\frac{D\mathbf{U}}{Dt} = \left\langle\frac{D\mathbf{U}}{Dt}\right\rangle + \left(\frac{D\mathbf{U}}{Dt}\right)'$ respectively leads to an expression for the fluctuating model fluid acceleration along a particle trajectory $\mathbf{G}' = \mathbf{G} - \langle\mathbf{G}\rangle$. Furthermore, for a statistically stationary and homogeneous flow field, the average parts $\langle\mathbf{U}\rangle$ and $\left\langle\frac{D\mathbf{U}}{Dt}\right\rangle$ are zero, meaning that $\langle\mathbf{G}\rangle = \mathbf{0}$ and therefore [141]

$$\mathbf{G}\left(\mathbf{x}, \mathbf{v}, \mathbf{u}, t; \mathbf{U}(\mathbf{x}, t)\right) = \left(\frac{D\mathbf{U}}{Dt}\right)'(\mathbf{x}, t) - \left(\mathbf{u} - \mathbf{v}\right) \cdot \frac{\partial}{\partial \mathbf{x}}\mathbf{U}'(\mathbf{x}, t) \tag{5.41}$$

An appropriate model for the fluctuating fluid acceleration along a fluid element trajectory is that of Haworth and Pope [66, 117]

$$\left(\frac{D}{Dt}\mathbf{U}(\mathbf{x}, t)\right)' = -\boldsymbol{\alpha}(\mathbf{x}) \cdot \mathbf{U}'(\mathbf{x}, t) + \mathbf{w}(\mathbf{x}, t) \tag{5.42}$$

where $\boldsymbol{\alpha}$ is a rate scale representing the decorrelation timescales for the normalised fluctuating fluid velocity along particle trajectories, and $\mathbf{w}(\mathbf{x}, t)$ is the Wiener process used to describe Brownian motion [118]. Then since $\mathbf{U}'(\mathbf{x}, t) = \mathbf{U}(\mathbf{x}, t)$ for homogeneous flows, along with the further simplification $\mathbf{U}'(\mathbf{x}, t) \approx \langle\mathbf{U}'(\mathbf{x}, t)\rangle$ causing the last term of (5.41) to vanish, the final model emerges as

$$\mathbf{G}\left(\mathbf{x}, \mathbf{v}, \mathbf{u}, t; \mathbf{U}(\mathbf{x}, t)\right) \approx -\boldsymbol{\alpha}(\mathbf{x}) \cdot \mathbf{U}(\mathbf{x}, t) + \mathbf{w}(\mathbf{x}, t) \tag{5.43}$$

The rate scale tensor $\boldsymbol{\alpha}(\mathbf{x})$ is taken in the form $\boldsymbol{\alpha}(\mathbf{x}) = \mathrm{diag}\left(\tau_i^{-1}(\mathbf{x})\right)$, where $\tau_i^{-1}(\mathbf{x})$ are the decorrelation timescales for components of normalised fluctuating fluid velocity along particle trajectories [158], and in isotropic turbulence this becomes $\boldsymbol{\alpha}(\mathbf{x}) = \tau^{-1}(\mathbf{x})\,\mathbf{I}$. Further assuming a homogeneous flow field means that the Wang & Stock [165] model $\tau = \tau_{Lp}$ as defined in (4.63) is a suitable representation for the rate scale, resulting in

$$\boldsymbol{\alpha} = \tau_{Lp}^{-1}\,\mathbf{I} \tag{5.44}$$

Modelling of the Wiener process $\mathbf{w}(\mathbf{x}, t)$ involves decomposition into separate spatial and temporal components such that $\mathbf{w}(\mathbf{x}, t) = \mathbf{B}(\mathbf{x}) \cdot \boldsymbol{\Gamma}(t)$, where $\boldsymbol{\Gamma}(t)$ is the standard Gaussian white-noise process. Following the work of Iliopoulos & Hanratty [74, 75], the spatial covariance of $\mathbf{B}(\mathbf{x})$ is specified as

$$\mathbf{B}\cdot\mathbf{B}^{\top} = \langle\mathbf{U}\rangle\cdot\nabla\langle\mathbf{U}'\mathbf{U}'\rangle + \nabla\cdot\langle\mathbf{U}'\mathbf{U}'\mathbf{U}'\rangle + \boldsymbol{\alpha}\cdot\langle\mathbf{U}'\mathbf{U}'\rangle + \langle\mathbf{U}'\mathbf{U}'\rangle\cdot\boldsymbol{\alpha}^{\top} \tag{5.45}$$

For the case of a homogeneous flow field, the spatial gradients of averaged quantities are zero, and further assuming isotropy enables use of the model (5.44) for $\boldsymbol{\alpha}$, reducing (5.45) to

$$\mathbf{B}^2(\mathbf{x}) = 2\tau_{Lp}^{-1}\langle\mathbf{U}'(\mathbf{x})\mathbf{U}'(\mathbf{x})\rangle \tag{5.46}$$

For the assumed homogeneous isotropic flow the Reynolds stresses are given by $\langle\mathbf{U}'\mathbf{U}'\rangle = u'^2\,\mathbf{I}$, and this then fully specifies the parameters of the model for fluid acceleration along particle trajectories.

5.3.2 Calculation of the Joint Particle-Fluid PDF

Taking the GLM system (5.38), assuming the linear drag law for $\boldsymbol{v}_p$ in (4.2 - 4.3) together with the acceleration model along particle trajectories for $\boldsymbol{u}_p$ (5.43), and also omitting the first equation along with all dependence on particle position $\boldsymbol{x}_p$ reduces the system for the simple homogeneous case to

$$\begin{aligned}\dot{\boldsymbol{v}}_p &= \beta\,(\boldsymbol{u}_p - \mathbf{v}_p) + \mathbf{g}\\ \dot{\boldsymbol{u}}_p &= -\alpha\boldsymbol{u}_p + \mathbf{B}\cdot\boldsymbol{\Gamma}\end{aligned} \tag{5.47}$$

Note that neglecting the dependence on $\boldsymbol{x}_p$ implies that this framework is only strictly valid for modelling the fluid velocity along particle trajectories $\boldsymbol{u}_p$ as a process, which is of importance when it comes to applying this formulation to the dispersion tensors in the PDF kinetic model. This also formally restricts the spatial coefficient $\mathbf{B}$ of the Wiener process to being a constant, although this is already the case for the assumed homogeneous isotropic flow. Interpreting the phase-space coordinate and trajectory vectors as $\boldsymbol{\xi} = (\mathbf{u}, \mathbf{v})$ and $\boldsymbol{z} = (\boldsymbol{u}_p, \boldsymbol{v}_p)$ respectively converts (5.47) to the system form

$$\dot{\boldsymbol{z}} = \mathbf{A}\cdot\boldsymbol{z} + \mathbf{b} + \mathbf{k} \tag{5.48}$$

where

$$\mathbf{A} = \begin{bmatrix} -\alpha\mathbf{I} & \mathbf{0} \\ \beta\mathbf{I} & -\beta\mathbf{I} \end{bmatrix} \quad , \quad \mathbf{b} = \begin{bmatrix} \mathbf{B}\cdot\boldsymbol{\Gamma} \\ \mathbf{0} \end{bmatrix} \quad , \quad \mathbf{k} = \begin{bmatrix} \mathbf{0} \\ \mathbf{g} \end{bmatrix} \tag{5.49}$$

This enables the joint PDF $\phi(\mathbf{u}, \mathbf{v}, t)$ for $\boldsymbol{z}$ to be reconciled with the phase-space framework of the PDF kinetic model outlined in section 4.1, the distinctions in this case being that the deterministic part is now linear in the phase-space trajectory $\boldsymbol{z}$ and the random field $\mathbf{b}(\mathbf{x}, t)$ is now a random process $\mathbf{b}(t)$. In particular, the removal of dependence on $\boldsymbol{\xi}$ in $\mathbf{b}(t)$ causes the drift tensor $\mathbf{d}(\boldsymbol{\xi}, t)$ in (4.20) to vanish, reducing the kinetic equation (4.22) to the Fokker-Planck equation [150]

$$\frac{\partial}{\partial t}\phi\left(\boldsymbol{\xi}, t\right) = -\frac{\partial}{\partial \boldsymbol{\xi}} \cdot \Big[\big(\mathbf{A}\cdot\boldsymbol{\xi} + \mathbf{k}\big)\phi\left(\boldsymbol{\xi}, t\right)\Big] + \frac{\partial}{\partial \boldsymbol{\xi}} \cdot \frac{\partial}{\partial \boldsymbol{\xi}} \cdot \Big[\mathbf{D}\left(t\right)\phi\left(\boldsymbol{\xi}, t\right)\Big] \tag{5.50}$$

in which $\mathbf{D}\left(t\right)$ is the diffusion tensor as specified in (4.21) without dependence on $\boldsymbol{\xi}$. In this case, since the white-noise process $\boldsymbol{\Gamma}(t)$ is delta-correlated in time, the integral along the path history can be evaluated directly, reducing $\mathbf{D}\left(t\right)$ to the simple constant form.

$$\mathbf{D} = \begin{bmatrix} \frac{1}{2}\mathbf{B}\cdot\mathbf{B}^{\top} & \mathbf{0} \\ \mathbf{0} & \mathbf{0} \end{bmatrix} = \begin{bmatrix} \tau_{Lp}^{-1}\, u'^{2}\,\mathbf{I} & \mathbf{0} \\ \mathbf{0} & \mathbf{0} \end{bmatrix} \tag{5.51}$$

where the final step utilises the model (5.46) for the case of a homogeneous and isotropic flow field. For the linear system in (5.48), the Fokker-Planck equation admits analytical solutions for the PDF $\phi\left(\boldsymbol{\xi}, t\right)$ in the form of a multivariate Gaussian distribution [150]

$$\phi\left(\boldsymbol{\xi}, t\right) = (2\pi)^{-\frac{d}{2}} \det\left[\boldsymbol{\Theta}\right]^{-\frac{1}{2}} \exp\left[-\frac{1}{2}\left(\boldsymbol{\xi} - \mathbf{m}\right)\cdot\boldsymbol{\Theta}^{-1}\cdot\left(\boldsymbol{\xi} - \mathbf{m}\right)\right] \tag{5.52}$$

where the time dependent mean $\mathbf{m} = \langle \boldsymbol{z} \rangle$ and covariance matrix $\boldsymbol{\Theta} = \langle (\boldsymbol{z} - \mathbf{m})\,(\boldsymbol{z} - \mathbf{m}) \rangle$ satisfy

$$\dot{\mathbf{m}} = \mathbf{A}\cdot\mathbf{m} + \mathbf{k} \quad , \quad \mathbf{m}(t_0) = \boldsymbol{\xi}^0 \tag{5.53}$$

$$\dot{\boldsymbol{\Theta}} = (\mathbf{A}\cdot\boldsymbol{\Theta} + \mathbf{D}) + (\mathbf{A}\cdot\boldsymbol{\Theta} + \mathbf{D})^{\top} \quad , \quad \boldsymbol{\Theta}(t_0) = \mathbf{0} \tag{5.54}$$

As it is the asymptotic PDF $\phi\left(\boldsymbol{\xi}\right)$ for $t \to \infty$ which is sought, the mean and covariance matrix in (5.52) are no longer time dependent, meaning that $\dot{\mathbf{m}} = \mathbf{0}$ and $\dot{\boldsymbol{\Theta}} = \mathbf{0}$. This

reduces (5.53) and (5.54) to steady-state systems of algebraic equations for $\mathbf{m} = (\hat{\mathbf{u}}, \hat{\mathbf{v}})$ and $\boldsymbol{\Theta}$, and subject to $\det(\mathbf{A}) \neq 0$ it then follows with reference to $\mathbf{k}$ and $\mathbf{A}$ from (5.49), $\mathbf{D}$ from (5.51), and the model for α from (5.44) that

$$\mathbf{m} = \begin{bmatrix} \mathbf{0} \\ \mathbf{V}_g \end{bmatrix} \quad , \quad \boldsymbol{\Theta} = u'^2 \begin{bmatrix} \mathbf{I} & \frac{1}{1+St_{Lp}}\mathbf{I} \\ \frac{1}{1+St_{Lp}}\mathbf{I} & \frac{1}{1+St_{Lp}}\mathbf{I} \end{bmatrix} \tag{5.55}$$

Specification of $\mathbf{m}$ and $\boldsymbol{\Theta}$ then fully determines $\phi(\mathbf{u}, \mathbf{v})$ as given by (5.52), and since the PDF is a multivariate Gaussian, the moments of the conditional PDF $\phi(\mathbf{v} \mid \mathbf{u})$ can be expressed directly in terms of $\mathbf{m}$ and $\boldsymbol{\Theta}$. Specifically, $\phi(\mathbf{v} \mid \mathbf{u})$ also takes the form of a multivariate Gaussian distribution with the mean $\mathbf{q}(\mathbf{u})$ and covariance matrix $\mathbf{Q}$ given by the standard results [150]

$$\mathbf{q}(\mathbf{u}) = \hat{\mathbf{v}} + \boldsymbol{\Theta}_{21} \cdot \boldsymbol{\Theta}_{21}^{-1} \cdot (\mathbf{u} - \hat{\mathbf{u}}) \tag{5.56}$$

$$\mathbf{Q} = \boldsymbol{\Theta}_{22} - \boldsymbol{\Theta}_{21} \cdot \boldsymbol{\Theta}_{11}^{-1} \cdot \boldsymbol{\Theta}_{12} \tag{5.57}$$

Thus with $\mathbf{m}$ and $\boldsymbol{\Theta}$ as calculated in (5.55) the resultant expressions for $\mathbf{q}(\mathbf{u})$ and $\mathbf{Q}$ are

$$\mathbf{q}(\mathbf{u}) = \frac{1}{1 + St_{Lp}}\mathbf{u} + \mathbf{V}_g \quad , \quad \mathbf{Q} = \frac{St_{Lp}}{(1 + St_{Lp})^2} u'^2 \mathbf{I} \tag{5.58}$$

These parameters then determine the required conditional distribution $\phi(\mathbf{v} \mid \mathbf{u})$ such that $\mathbf{v} \sim \mathrm{N}\big(\mathbf{q}(\mathbf{u}), \mathbf{Q}\big)$, from which the initial particle velocities can be generated within a particle tracking simulation such that they conform to the equilibrium statistics given by (5.55). The behaviour of $\phi(\mathbf{v} \mid \mathbf{u})$ in the limit of small and large particle inertia is as physically expected, with

$$St_{Lp} \to 0 \;\; : \;\; \mathbf{q} \to \mathbf{u} \quad , \quad \mathbf{Q} \to \mathbf{0} \qquad \Rightarrow \phi(\mathbf{v} \mid \mathbf{u}) \to \delta(\mathbf{v} - \mathbf{u}) \tag{5.59}$$

$$St_{Lp} \to \infty \;\; : \;\; \mathbf{q} \to \boldsymbol{\infty} \quad , \quad \mathbf{Q} \to \mathbf{0} \qquad \Rightarrow \phi(\mathbf{v} \mid \mathbf{u}) \to \delta(\mathbf{v}) \tag{5.60}$$

This demonstrates that the distribution reduces to a zero-variance δ-function in both limits, retrieving the expected behaviour of fluid elements and ballistic particles respectively when subject to a gravitational body force.

5.4 Initial Condition Dependent Formulation of the Dispersion Tensors

In a homogeneous statistically stationary flow field, representations of the velocity-averaged particle dispersion tensors $\overline{\boldsymbol{\lambda}}(\mathbf{x},t)$ and $\overline{\boldsymbol{\mu}}(\mathbf{x},t)$ are given by expressions (4.58) and (4.60) respectively as

$$\begin{aligned}\overline{\boldsymbol{\lambda}}(\mathbf{x},t) &= \left\langle \boldsymbol{x}_p(t)\mathbf{f}(\boldsymbol{x}_p(t),t)\right\rangle \\ \overline{\boldsymbol{\mu}}(\mathbf{x},t) &\approx \left\langle \boldsymbol{v}_p(t)\mathbf{f}(\boldsymbol{x}_p(t),t)\right\rangle\end{aligned} \tag{5.61}$$

It follows that the initial value $\overline{\boldsymbol{\lambda}}(\mathbf{x},t_0)$ is determined by the correlation between the initial particle positions $\boldsymbol{x}_p(t_0)$ and fluctuating continuous phase driving force $\mathbf{f}(\boldsymbol{x}_p(t_0),t_0)$, and similarly the initial value $\overline{\boldsymbol{\mu}}(\mathbf{x},t_0)$ is determined by the correlation between the initial particle velocities $\boldsymbol{v}_p(t_0)$ and $\mathbf{f}(\boldsymbol{x}_p(t_0),t_0)$. These correlations then automatically account for any interaction between the particle trajectories $(\boldsymbol{x}_p(t_0),\boldsymbol{v}_p(t_0))$ and flow field evaluated along a trajectory $\mathbf{f}(\boldsymbol{x}_p(t_0),t_0)$ at the initial time t_0. However when $\overline{\boldsymbol{\lambda}}(\mathbf{x},t)$ and $\overline{\boldsymbol{\mu}}(\mathbf{x},t)$ are explicitly calculated using the definitions (4.31) and (4.32), information about initial particle-fluid interaction is embedded within the particle response tensor $\boldsymbol{\mathcal{H}}[t;t']$ defined in (4.27), and since the response tensor is subject to the causality condition $\boldsymbol{\mathcal{H}}[t;t']=\mathbf{0}$ for $t_0\leq t<t'$ such interaction is not taken into account when initial conditions are imposed at $t=t'$ as in (4.28) [150]. This therefore highlights a disparity between the evolution of the two sides of equations (5.61), and shows the need for incorporating the effect of initial particle-fluid interaction into $\boldsymbol{\mathcal{H}}[t;t']$.

5.4.1 Dependence of Initial Conditions on the Continuous Phase

In order to determine the effect of a modification to $\boldsymbol{\mathcal{H}}[t;t']$ on all of $\overline{\boldsymbol{\kappa}}(\mathbf{x},t)$, $\overline{\boldsymbol{\lambda}}(\mathbf{x},t)$ and $\overline{\boldsymbol{\mu}}(\mathbf{x},t)$, it is convenient to use the phase-space representation of the response tensor $\boldsymbol{\mathcal{G}}[t;t']$ defined in (4.17). The evolution of $\boldsymbol{\mathcal{G}}[t;t']$ is governed by (4.18), the derivation of which is based upon the condition that the initial particle trajectories $\boldsymbol{z}(t_0)=\boldsymbol{\xi}^0$ are independent of the stochastic field $\mathbf{b}(\boldsymbol{\xi}^0,t_0)$. However, for the joint particle-fluid PDF derived in section 5.3.2, the covariance matrix $\boldsymbol{\Theta}$ specifies non-zero equilibrium values of the particle-fluid velocity correlations $\left\langle \mathbf{u}'\mathbf{v}'\right\rangle$, given in (5.55) by

$$\boldsymbol{\Theta}_{12} = \boldsymbol{\Theta}_{21} = \frac{1}{1 + St_{Lp}} u'^2 \mathbf{I} \tag{5.62}$$

Consequently, initialising the particle trajectories using the conditional distribution $\phi(\mathbf{v} \mid \mathbf{u})$ requires that this correlation is taken into account in the PDF kinetic model by assuming that the initial conditions $\boldsymbol{\xi}^0$ are dependent on $\mathbf{b}(\boldsymbol{\xi}^0, t_0)$, and therefore satisfy

$$\boldsymbol{\xi}^0 = \boldsymbol{\Xi}\left(\mathbf{b}\left(\boldsymbol{\xi}^0, t_0\right)\right) \tag{5.63}$$

where $\boldsymbol{\Xi}(\mathbf{b}(\boldsymbol{\xi}^0, t_0))$ is an operator that defines the initial distribution $\boldsymbol{\xi}^0 = (\mathbf{x}^0, \mathbf{v}^0)$. Initial particle positions $\mathbf{x}^0$ which are uniformly distributed in each direction are specified by

$$\mathbf{x}^0 = \left(\boldsymbol{\psi} - \frac{\mathbf{1}}{\mathbf{2}}\right) \mathcal{L} \tag{5.64}$$

where $\boldsymbol{\psi} \sim \mathrm{U}[\mathbf{0}, \mathbf{1}]$ is a uniformly distributed parameter. Additionally, to generate initial particle velocities $\mathbf{v}^0$ that conform to the conditional distribution $\phi(\mathbf{v} \mid \mathbf{u}) \sim \mathrm{N}\big(\mathbf{q}(\mathbf{u}), \mathbf{Q}\big)$ as given by (5.58), the standard normal deviate $\mathbf{Z} \sim \mathrm{N}[\mathbf{0}, \mathbf{1}]$ is related to the uniformly distributed parameter $\boldsymbol{\psi}$ by $\mathbf{Z} = \sqrt{2}\,\mathrm{erf}^{-1}(2\boldsymbol{\psi} - \mathbf{1})$, resulting in the explicit formula for $\mathbf{v}^0$ of

$$\mathbf{v}^0 = \frac{1}{1 + St_{Lp}} \left[\sqrt{2St_{Lp}}\, u'\, \mathrm{erf}^{-1}(2\boldsymbol{\psi} - \mathbf{1}) + \mathbf{u}_p(t_0)\right] + \mathbf{V}_g \tag{5.65}$$

where the fluid velocity along particle trajectories is given formally by $\mathbf{u}_p(t_0) = \mathbf{u}(\mathbf{x}^0, t_0)$. Then in physical space the initial distribution operator $\boldsymbol{\Xi}(\mathbf{f}(\mathbf{x}^0, t_0))$ is given for the assumed homogeneous and statistically stationary flow by

$$\boldsymbol{\Xi}\left(\mathbf{f}\left(\mathbf{x}^0, t_0\right)\right) = \begin{bmatrix} \left(\boldsymbol{\psi} - \frac{\mathbf{1}}{\mathbf{2}}\right) \mathcal{L} \\ \frac{1}{1+St_{Lp}} \left[\sqrt{2St_{Lp}}\, u'\, \mathrm{erf}^{-1}(2\boldsymbol{\psi} - \mathbf{1}) + \mathbf{u}_p(t_0)\right] + \mathbf{V}_g \end{bmatrix} \tag{5.66}$$

5.4.2 Modification of the Particle Response Tensor

The dependence of the initial conditions $\boldsymbol{\xi}^0$ on the stochastic field $\mathbf{b}(\boldsymbol{\xi}^0, t_0)$ through the operator $\boldsymbol{\Xi}(\mathbf{b}(\boldsymbol{\xi}^0, t_0))$ defined in (5.66) can be accounted for within the phase-space

response tensor $\boldsymbol{\mathcal{G}}\left[t;t'\right]$ by using the notion of 'extending' a differential operator [133, pp. 159–163]. Such an approach leads to modification of the governing equation (4.18) for $\boldsymbol{\mathcal{G}}\left[t;t'\right]$, resulting in [71]

$$\dot{\boldsymbol{\mathcal{G}}}\left[t;t'\right]=\left[\frac{\delta\mathbf{a}}{\delta\boldsymbol{\xi}}(\boldsymbol{z}(t),t)+\frac{\delta\mathbf{b}}{\delta\boldsymbol{\xi}}(\boldsymbol{z}(t),t)\right]^{\top}\cdot\boldsymbol{\mathcal{G}}\left[t;t'\right]+\delta\left(t-t'\right)\mathbf{I}+\delta\left(t-t_0\right)\left[\frac{\delta\boldsymbol{\xi}^0}{\delta\mathbf{b}(\boldsymbol{z}(t'),t')}\right]^{\top} \tag{5.67}$$

where the initial condition on $\boldsymbol{\mathcal{G}}\left[t;t'\right]$ at time $t=t'$ in (4.18) has been incorporated as a source term, and the effect of $\mathbf{b}\left(\boldsymbol{\xi}^0,t_0\right)$ on the initial values of the trajectories $\boldsymbol{\xi}^0$ at time $t=t_0$ appears as a further source term. Note that in (5.67) $\boldsymbol{\mathcal{G}}\left[t;t'\right]$ now also depends on the value of t_0, and this is denoted as $\boldsymbol{\mathcal{G}}=\boldsymbol{\mathcal{G}}\left[t;t',t_0\right]$ with the understanding that $t_0\leq t'\leq t$. Further treatment involves splitting $\boldsymbol{\mathcal{G}}\left[t;t',t_0\right]$ into two components denoted as $\boldsymbol{\mathcal{G}}^{(1)}\left[t;t'\right]$ and $\boldsymbol{\mathcal{G}}^{(2)}\left[t;t',t_0\right]$ upon which the initial conditions are imposed separately at $t=t'$ and $t=t_0$ respectively, and which therefore satisfy [133]

$$\dot{\boldsymbol{\mathcal{G}}}^{(1)}\left[t;t'\right]=\left[\frac{\delta\mathbf{a}}{\delta\boldsymbol{\xi}}(\boldsymbol{z}(t),t)+\frac{\delta\mathbf{b}}{\delta\boldsymbol{\xi}}(\boldsymbol{z}(t),t)\right]^{\top}\cdot\boldsymbol{\mathcal{G}}^{(1)}\left[t;t'\right]+\delta\left(t-t'\right)\mathbf{I} \tag{5.68}$$

$$\dot{\boldsymbol{\mathcal{G}}}^{(2)}\left[t;t',t_0\right]=\left[\frac{\delta\mathbf{a}}{\delta\boldsymbol{\xi}}(\boldsymbol{z}(t),t)+\frac{\delta\mathbf{b}}{\delta\boldsymbol{\xi}}(\boldsymbol{z}(t),t)\right]^{\top}\cdot\boldsymbol{\mathcal{G}}^{(2)}\left[t;t',t_0\right]+\delta\left(t-t_0\right)\left[\frac{\delta\boldsymbol{\xi}^0}{\delta\mathbf{b}(\boldsymbol{z}(t'),t')}\right]^{\top} \tag{5.69}$$

The sum of these two components $\boldsymbol{\mathcal{G}}\left[t;t',t_0\right]=\boldsymbol{\mathcal{G}}^{(1)}\left[t;t'\right]+\boldsymbol{\mathcal{G}}^{(2)}\left[t;t',t_0\right]$ then satisfies the modified governing equation (5.67), for which insight can be sought through consideration of the separate components. The equation (5.68) for $\boldsymbol{\mathcal{G}}^{(1)}\left[t;t'\right]$ is identical to the case when the initial conditions $\boldsymbol{\xi}^0$ are independent of the stochastic field $\mathbf{b}\left(\boldsymbol{\xi}^0,t_0\right)$, and thus $\boldsymbol{\mathcal{G}}^{(1)}\left[t;t'\right]$ can be obtained in the standard numerical fashion. To construct $\boldsymbol{\mathcal{G}}^{(2)}\left[t;t',t_0\right]$, consider the equation (5.68) for $\boldsymbol{\mathcal{G}}^{(1)}\left[t;t'\right]$ evaluated at $t'=t_0$ and right-multiplied by $\left[\frac{\delta\boldsymbol{\xi}^0}{\delta\mathbf{b}(\boldsymbol{z}(t'),t')}\right]^{\top}$, then comparing to the equation (5.69) for $\boldsymbol{\mathcal{G}}^{(2)}$ yields [71]

$$\boldsymbol{\mathcal{G}}^{(2)}\left[t;t',t_0\right]=\boldsymbol{\mathcal{G}}^{(1)}\left[t;t_0\right]\cdot\left[\frac{\delta\boldsymbol{\xi}^0}{\delta\mathbf{b}(\boldsymbol{z}(t'),t')}\right]^{\top} \tag{5.70}$$

Therefore once $\boldsymbol{\mathcal{G}}^{(1)}\left[t;t'\right]$ is known it can be used to obtain $\boldsymbol{\mathcal{G}}^{(2)}\left[t;t',t_0\right]$, and hence the solution for $\boldsymbol{\mathcal{G}}\left[t;t',t_0\right]$ that satisfies the modified governing equation (5.67) is given by

$$\boldsymbol{\mathcal{G}}\left[t;t',t_0\right]=\boldsymbol{\mathcal{G}}^{(1)}\left[t;t'\right]+\boldsymbol{\mathcal{G}}^{(1)}\left[t;t_0\right]\cdot\left[\frac{\delta\boldsymbol{\xi}^0}{\delta\mathbf{b}(\boldsymbol{z}(t'),t')}\right]^{\top} \tag{5.71}$$

In order to calculate the modified response tensor $\boldsymbol{\mathcal{G}}\left[t;t',t_0\right]$ using (5.71), it remains to find an expression for the initial condition dependency on the continuous phase at time t_0 given by the functional derivative in the final term. Then for the relationship $\boldsymbol{\xi}^0=\boldsymbol{\Xi}\left(\mathbf{b}\left(\boldsymbol{\xi}^0,t_0\right)\right)$ defined in (5.63), using the chain rule for functional differentiation formally gives

$$\frac{\delta\boldsymbol{\xi}^0}{\delta\mathbf{b}(\boldsymbol{z}(t'),t')}=\left[\frac{\delta\boldsymbol{\xi}^0}{\delta\mathbf{b}(\boldsymbol{z}(t'),t')}\cdot\frac{\partial\mathbf{b}}{\partial\boldsymbol{\xi}}(\boldsymbol{\xi}^0,t_0)+\delta\left(t'-t_0\right)\mathbf{I}\right]\cdot\frac{\partial\boldsymbol{\Xi}}{\partial\mathbf{b}}\left(\mathbf{b}\left(\boldsymbol{\xi}^0,t_0\right)\right) \tag{5.72}$$

Now, in order to obtain the conditional distribution $\phi\left(\mathbf{v}\mid\mathbf{u}\right)$ used to specify the initial particle velocity $\mathbf{v}^0$ as an *analytical* solution to the PDF equation for the underlying GLM in section 5.3.1, the necessary assumption of modelling $\boldsymbol{u}_p(t)$ as a process rather than a spatially dependent field has been made. In keeping with this, the phase-space zero-mean stochastic field $\mathbf{b}\left(\boldsymbol{\xi},t\right)$ should also be interpreted as a process $\mathbf{b}\left(t\right)$, and thereby treated as independent of the phase-space coordinate $\boldsymbol{\xi}$. In this context it is therefore true that

$$\frac{\partial\mathbf{b}}{\partial\boldsymbol{\xi}}(\boldsymbol{\xi}^0,t_0)=\frac{\partial\mathbf{b}}{\partial\boldsymbol{\xi}}(t_0)=\mathbf{0} \tag{5.73}$$

Additionally, using the physical space interpretation $\mathbf{b}=(\mathbf{0},\mathbf{f})$, the derivative of the initial distribution operator $(\mathbf{x}^0,\mathbf{v}^0)=\boldsymbol{\Xi}\left(\mathbf{f}\left(\mathbf{x}^0,t_0\right)\right)$ as specified in (5.66) is

$$\frac{\partial\boldsymbol{\Xi}}{\partial\mathbf{b}}\left(\mathbf{b}\left(\boldsymbol{\xi}^0,t_0\right)\right)=\begin{bmatrix}\mathbf{0} & \mathbf{0}\\ \frac{\partial\mathbf{x}^0}{\partial\mathbf{f}} & \frac{\partial\mathbf{v}^0}{\partial\mathbf{f}}\end{bmatrix}=\begin{bmatrix}\mathbf{0} & \mathbf{0}\\ \mathbf{0} & \frac{1}{\beta\left(1+St_{Lp}\right)}\mathbf{I}\end{bmatrix} \tag{5.74}$$

Then using the results (5.73), (5.74), and the expression for the initial condition dependency on the continuous phase at time t_0 in (5.72), the modified response tensor $\boldsymbol{\mathcal{G}}\left[t;t',t_0\right]$ given by (5.71) for the set of initial conditions specified by $\boldsymbol{\Xi}\left(\mathbf{b}\left(\boldsymbol{\xi}^0,t_0\right)\right)$ takes the form

$$\boldsymbol{\mathcal{G}}\left[t;t',t_0\right]=\boldsymbol{\mathcal{G}}^{(1)}\left[t;t'\right]+\boldsymbol{\mathcal{G}}^{(1)}\left[t;t_0\right]\cdot\begin{bmatrix}\mathbf{0} & \mathbf{0}\\ \mathbf{0} & \frac{1}{\beta\left(1+St_{Lp}\right)}\mathbf{I}\end{bmatrix}\delta\left(t'-t_0\right) \tag{5.75}$$

Therefore $\boldsymbol{\mathcal{G}}\left[t;t',t_0\right]$ is given by the original response tensor $\boldsymbol{\mathcal{G}}^{(1)}\left[t;t'\right]$ with the addition of a source term that only acts at the initial time of sampling t_0 and is proportional to the dependence of the initial conditions $\boldsymbol{\Xi}\left(\mathbf{b}\left(\boldsymbol{\xi}^0,t_0\right)\right)$ on the continuous phase. Re-interpreting in terms of the particle response tensor $\boldsymbol{\mathcal{H}}\left[t;t'\right]$ in physical space through use of (4.26), the corresponding modified expressions for $\boldsymbol{\mathcal{H}}\left[t;t',t_0\right]$ and $\dot{\boldsymbol{\mathcal{H}}}\left[t;t',t_0\right]$ are

$$\boldsymbol{\mathcal{H}}\left[t;t',t_0\right]=\boldsymbol{\mathcal{H}}^{(1)}\left[t;t'\right]+\delta\left(t'-t_0\right)\frac{1}{\beta\left(1+St_{Lp}\right)}\boldsymbol{\mathcal{H}}^{(1)}\left[t;t_0\right] \tag{5.76}$$

$$\dot{\boldsymbol{\mathcal{H}}}\left[t;t',t_0\right]=\dot{\boldsymbol{\mathcal{H}}}^{(1)}\left[t;t'\right]+\delta\left(t'-t_0\right)\frac{1}{\beta\left(1+St_{Lp}\right)}\dot{\boldsymbol{\mathcal{H}}}^{(1)}\left[t;t_0\right] \tag{5.77}$$

Application of expressions (5.76) and (5.77) to the velocity averaged form of the dispersion tensors $\overline{\boldsymbol{\kappa}}\left(\mathbf{x},t\right)$, $\overline{\boldsymbol{\lambda}}\left(\mathbf{x},t\right)$, and $\overline{\boldsymbol{\mu}}\left(\mathbf{x},t\right)$ defined in (4.30 - 4.32) finally results in

$$\begin{aligned}\overline{\boldsymbol{\kappa}}\left(\mathbf{x},t\right)=&\int_{t_0}^{t}\left\langle\boldsymbol{\mathcal{H}}^{(1)^{\top}}\left[t;t'\right]:\frac{\partial}{\partial\mathbf{x}}\mathbf{R}\left(\boldsymbol{x}_p',t';\mathbf{x},t\right)\right\rangle_{\mathbf{x}}dt'\\&+\frac{1}{\beta\left(1+St_{Lp}\right)}\left\langle\boldsymbol{\mathcal{H}}^{(1)^{\top}}\left[t;t_0\right]:\frac{\partial}{\partial\mathbf{x}}\mathbf{R}\left(\mathbf{x}^0,t_0;\mathbf{x},t\right)\right\rangle_{\mathbf{x}}\end{aligned} \tag{5.78}$$

$$\begin{aligned}\overline{\boldsymbol{\lambda}}\left(\mathbf{x},t\right)=&\int_{t_0}^{t}\left\langle\boldsymbol{\mathcal{H}}^{(1)}\left[t;t'\right]\cdot\mathbf{R}\left(\boldsymbol{x}_p',t';\mathbf{x},t\right)\right\rangle_{\mathbf{x}}dt'\\&+\frac{1}{\beta\left(1+St_{Lp}\right)}\left\langle\boldsymbol{\mathcal{H}}^{(1)}\left[t;t_0\right]\cdot\mathbf{R}\left(\mathbf{x}^0,t_0;\mathbf{x},t\right)\right\rangle_{\mathbf{x}}\end{aligned} \tag{5.79}$$

$$\begin{aligned}\overline{\boldsymbol{\mu}}\left(\mathbf{x},t\right)=&\int_{t_0}^{t}\left\langle\dot{\boldsymbol{\mathcal{H}}}^{(1)}\left[t;t'\right]\cdot\mathbf{R}\left(\boldsymbol{x}_p',t';\mathbf{x},t\right)\right\rangle_{\mathbf{x}}dt'\\&+\frac{1}{\beta\left(1+St_{Lp}\right)}\left\langle\dot{\boldsymbol{\mathcal{H}}}^{(1)}\left[t;t_0\right]\cdot\mathbf{R}\left(\mathbf{x}^0,t_0;\mathbf{x},t\right)\right\rangle_{\mathbf{x}}\end{aligned} \tag{5.80}$$

The expressions (5.78 - 5.80) are equal to the original forms of the dispersion tensors $\overline{\boldsymbol{\kappa}}\left(\mathbf{x},t\right)$, $\overline{\boldsymbol{\lambda}}\left(\mathbf{x},t\right)$, and $\overline{\boldsymbol{\mu}}\left(\mathbf{x},t\right)$ with an additional source term accounting for the initial particle-fluid velocity correlations at the initial time of sampling t_0. The conditional averages within these source terms are simply the integrands from the corresponding standard forms of $\overline{\boldsymbol{\kappa}}\left(\mathbf{x},t\right)$, $\overline{\boldsymbol{\lambda}}\left(\mathbf{x},t\right)$, and $\overline{\boldsymbol{\mu}}\left(\mathbf{x},t\right)$ evaluated at $t'=t_0$, and can therefore easily be computed within a simulation at relatively little extra expense. This enables the dispersion tensors to reach their steady-state values in a shorter period of time, meaning that sampling of statistics can be started sooner, and consequently placing less demand on the computational resources needed.

5.5 Verification of Flow Field Statistics

The KS flow field defined in section 5.1.1 was constructed with the aim of being able to retrieve a given form of the two-point two-time correlation tensor $\langle \mathbf{U}(\mathbf{x}_1, t_1)\mathbf{U}(\mathbf{x}_2, t_2)\rangle$; specifically where the spatial correlations $\mathbf{Q}(\mathbf{r})$ satisfy isotropy as given by (5.17). The validity of this form is subject to the constraint (5.30) of $\mathcal{L}/L_{11} \gg 1$, and therefore it remains to verify that the chosen value of $\mathcal{L}$ is sufficient to retrieve the desired form of $\mathbf{Q}(\mathbf{r})$. It is also instructive to similarly check the components of $\nabla\mathbf{Q}(\mathbf{r})$ as required for evaluation of the dispersion tensor $\overline{\boldsymbol{\kappa}}\,(\mathbf{x}, t)$ using (4.30), due to the larger gradients that are involved in these expressions, for which the expected profile is given in Appendix C by (C.16). Demonstration that $\mathbf{Q}(\mathbf{r})$ and $\nabla\mathbf{Q}(\mathbf{r})$ are successfully recovered from the flow field is shown in Figures 5.2 and 5.3, for which $\mathcal{L}/L_{11} = 4$ is used (meaning that there are 8 eddies in the domain of side length $2\mathcal{L}$). The resulting profiles for $f(\mathrm{r})$ and $g(\mathrm{r})$ are necessarily in accordance with (5.19) and (5.18) respectively in order for $\mathbf{Q}(\mathbf{r})$ to assume the correct form, and $\mathrm{E}_\omega(s)$ automatically satisfies the temporal decorrelation function profile (5.15) by virtue of $\omega_{\mathbf{k}} \sim \mathrm{N}\big(0, \sigma_\omega^2\big)$. It is seen that the profiles for $\mathbf{Q}(\mathbf{r})$ and $\nabla\mathbf{Q}(\mathbf{r})$ are zero to within statistical variation for $\mathrm{r}_1/L_{11} \gtrsim 3$, meaning that as long as the side length of the domain is greater than 6 eddies, the full decorrelation behaviour of the flow is captured by the simulation. Further, visualisation of the velocity field reveals that the evolution of the large-scale structures within the flow exhibits the expected effect of influencing particle trajectories, as displayed in Figure 5.4. This confirms that the KS velocity field is suitable for the simulation of inertial particles within a statistically stationary homogeneous isotropic flow, and therefore also an appropriate means for numerically evaluating the dispersion tensors $\overline{\boldsymbol{\kappa}}\,(\mathbf{x}, t)$, $\overline{\boldsymbol{\lambda}}\,(\mathbf{x}, t)$ and $\overline{\boldsymbol{\mu}}\,(\mathbf{x}, t)$ in this flow configuration.

5.6 Validation of the Dispersion Tensors in Homogeneous Flow

A suitable means of validating the procedure for computing the dispersion tensors $\overline{\boldsymbol{\kappa}}\,(\mathbf{x}, t)$, $\overline{\boldsymbol{\lambda}}\,(\mathbf{x}, t)$ and $\overline{\boldsymbol{\mu}}\,(\mathbf{x}, t)$ in homogeneous flow is available using the benchmark values from section 4.3, specifically equations (4.58) and (4.60), which are repeated below for ease of reference

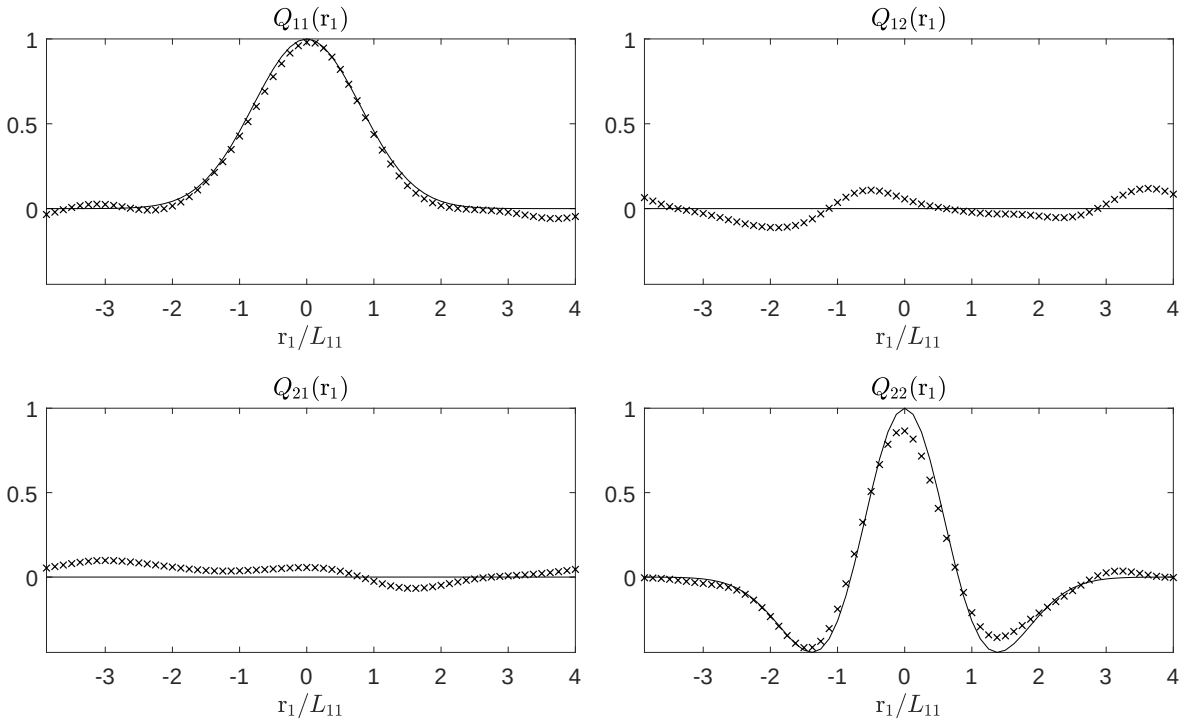

Figure 5.2: Recovery of the components of $\mathbf{Q}(\mathbf{r})$ in a two-dimensional KS velocity field for which $\mathcal{L}/L_{11} = 4$ and with spatial separation r_1 varied in the x_1 direction: —— expected profile given by (5.17); $\times$ simulation values

$$\overline{\boldsymbol{\lambda}}\,(\mathbf{x},t) = \Big\langle \boldsymbol{x}_p(t)\mathbf{f}(\boldsymbol{x}_p(t),t) \Big\rangle$$
$$\overline{\boldsymbol{\mu}}\,(\mathbf{x},t) \approx \Big\langle \boldsymbol{v}_p(t)\mathbf{f}(\boldsymbol{x}_p(t),t) \Big\rangle$$

where also $\overline{\boldsymbol{\kappa}}\,(\mathbf{x},t) = \mathbf{0}$ for a homogeneous flow with no external body forces. The above expressions have the advantage of being able to quantify not only the steady-state values of $\overline{\boldsymbol{\lambda}}\,(\mathbf{x},t)$ and $\overline{\boldsymbol{\mu}}\,(\mathbf{x},t)$, but also the evolution of these quantities from their initial conditions, meaning that the benchmark expressions are suitable for assessing the amendment to the dispersion tensors developed in section 5.4. This is realised by computing $\overline{\boldsymbol{\lambda}}\,(\mathbf{x},t)$ and $\overline{\boldsymbol{\mu}}\,(\mathbf{x},t)$ as they evolve in the KS velocity field specified in section 5.1.1, along with evaluation of $\langle \boldsymbol{x}_p\mathbf{f}_p \rangle$ and $\langle \boldsymbol{v}_p\mathbf{f}_p \rangle$ along the same ensemble of particle trajectories.

In the first instance, Figure 5.5 displays the case where the initial correlation between particle and fluid velocities is not included in the evaluation of the dispersion tensors

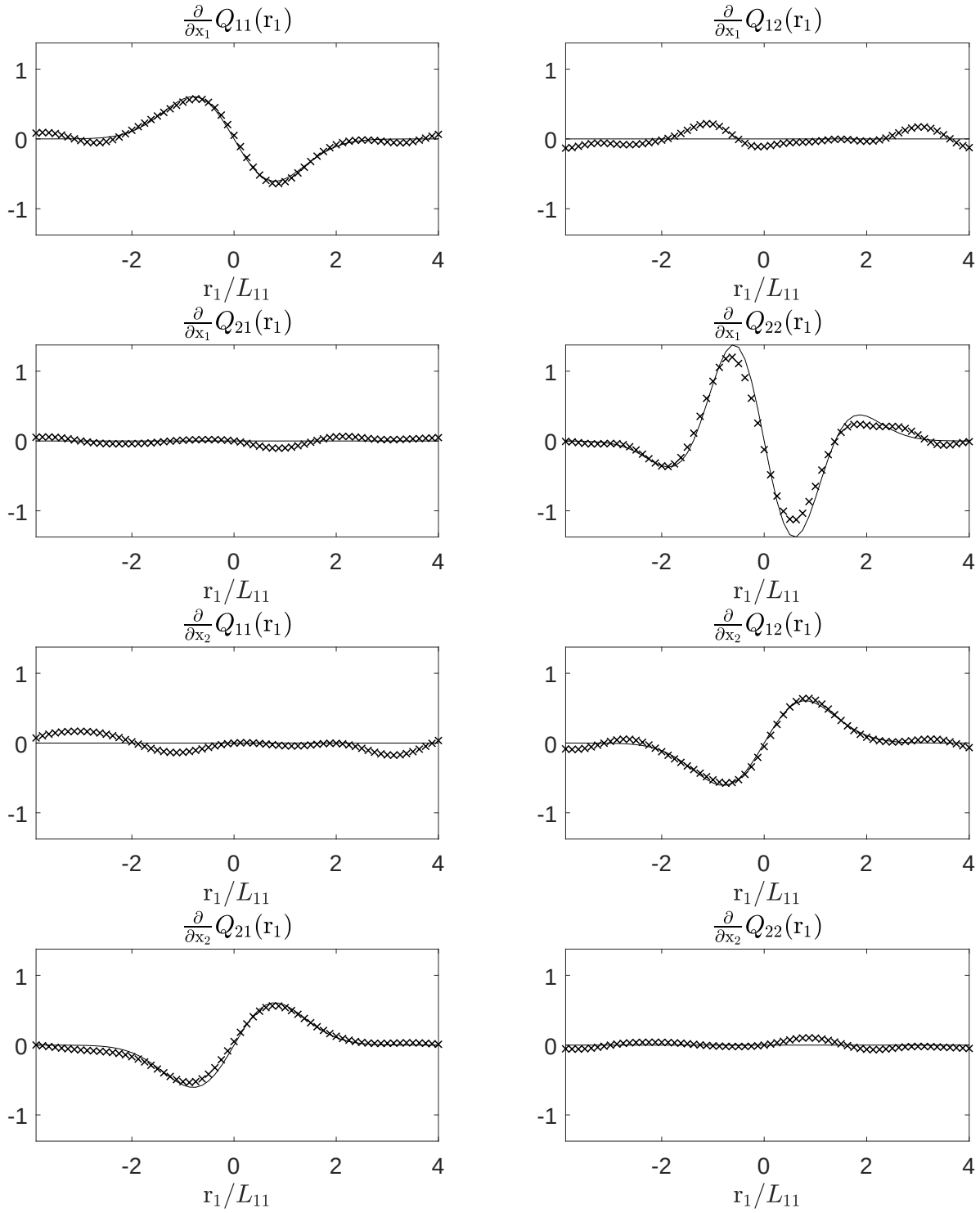

Figure 5.3: Recovery of the components of $\nabla\mathbf{Q}(\mathbf{r})$ in a two-dimensional KS velocity field for which $\mathcal{L}/L_{11} = 4$ and with spatial separation r_1 varied in the x_1 direction: —— expected profile given by (C.16); $\times$ simulation values

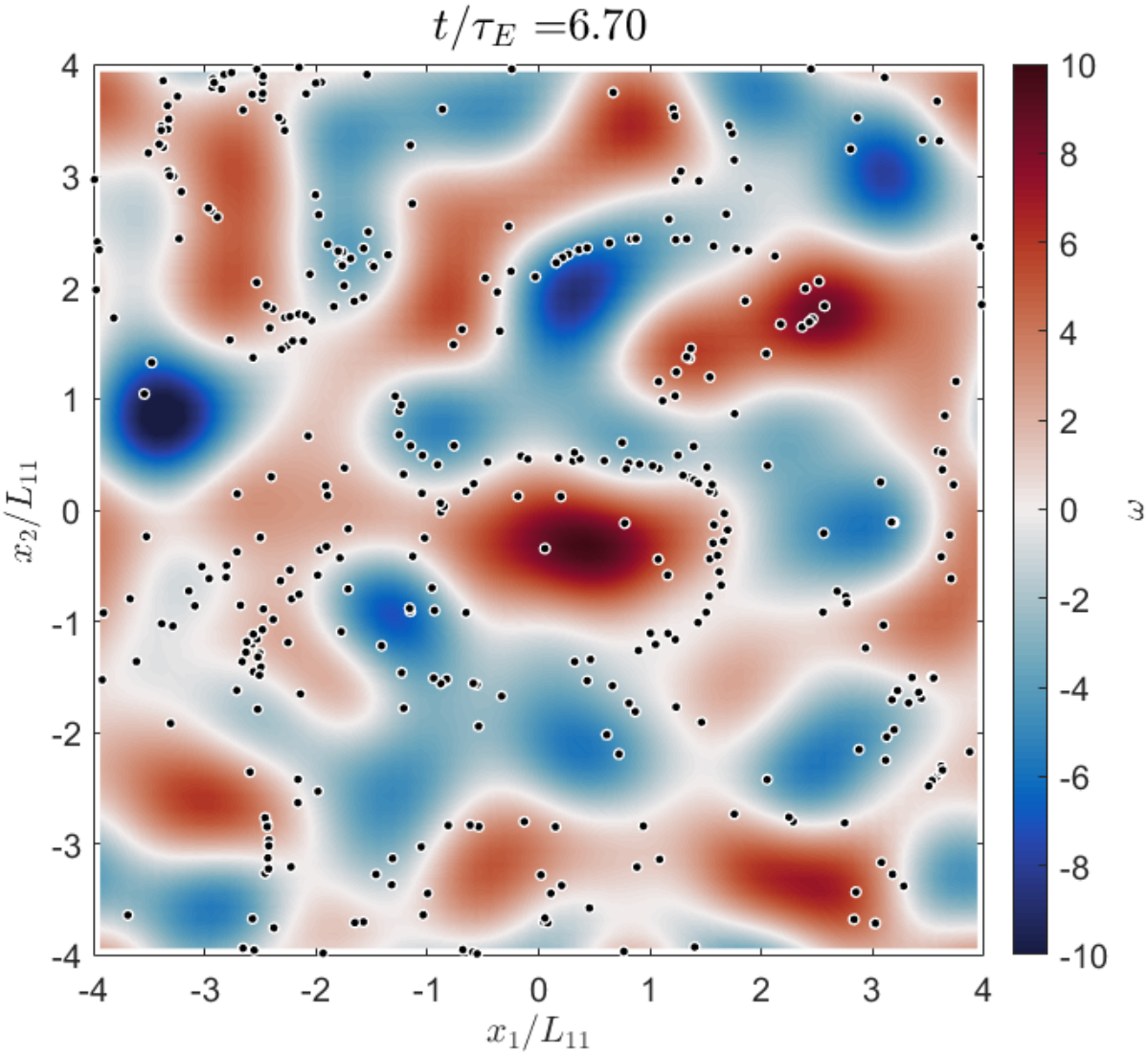

Figure 5.4: Visualisation of the KS velocity field with the continuous phase coloured by vorticity ω, demonstrating the influence of large-scale flow structures on particle behaviour for the case $St_E = 0.1$ and $V_g/u' = 1.0$

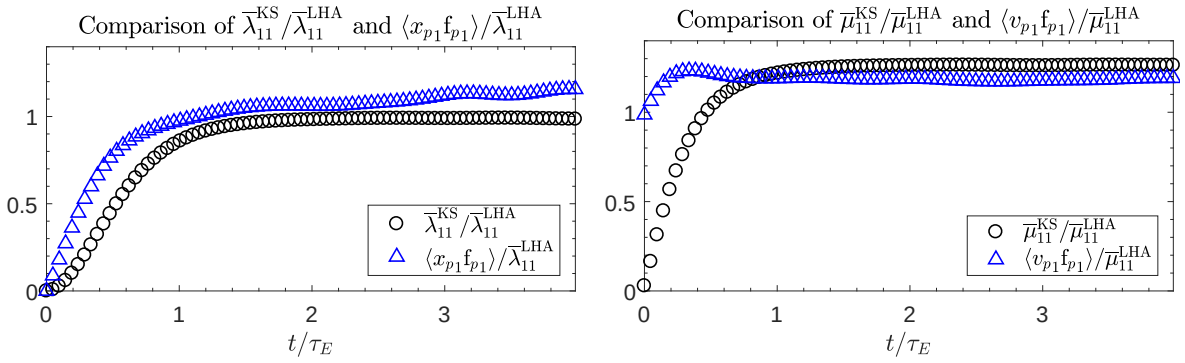

Figure 5.5: Evolution of the PDF dispersion tensors in a homogeneous KS velocity field with $St_E = 1$ not including initial correlation amendments, normalised with respect to $\overline{\lambda}_{11}^{\mathrm{LHA}}$ and $\overline{\mu}_{11}^{\mathrm{LHA}}$: ◯ $\overline{\lambda}_{11}^{\mathrm{KS}}/\overline{\lambda}_{11}^{\mathrm{LHA}}$, $\overline{\mu}_{11}^{\mathrm{KS}}/\overline{\mu}_{11}^{\mathrm{LHA}}$; △ $\langle x_{p_1}\mathrm{f}_{p_1}\rangle/\overline{\lambda}_{11}^{\mathrm{LHA}}$, $\langle v_{p_1}\mathrm{f}_{p_1}\rangle/\overline{\mu}_{11}^{\mathrm{LHA}}$

when $St_E = 1$. The expressions $\langle x_{p_1}\mathrm{f}_{p_1}\rangle$ and $\langle v_{p_1}\mathrm{f}_{p_1}\rangle$ are seen to account for existing initial correlations, with no interdependence between the particle position x_{p_1} and fluctuating continuous phase driving force along a particle trajectory $\mathrm{f}_{p_1} = \mathrm{f}_1(\boldsymbol{x}_p(t), t)$ at the start of the simulation, and an initial correlation between the particle velocity v_{p_1} and f_{p_1} that is equal to the LHA value $\overline{\mu}_{11}^{\mathrm{LHA}}$. By contrast, the evolution of $\overline{\lambda}_{11}$ and $\overline{\mu}_{11}$ both begin from zero when no initial amendment is made, highlighting the discrepancy between $\overline{\mu}_{11}$ which has an initial value of zero and the benchmark $\langle v_{p_1}\mathrm{f}_{p_1}\rangle = \overline{\mu}_{11}^{\mathrm{LHA}}$. Further to this, even though the initial values of $\overline{\lambda}_{11}$ and $\langle x_{p_1}\mathrm{f}_{p_1}\rangle$ are the same, the rate of evolution differs, with $\langle x_{p_1}\mathrm{f}_{p_1}\rangle$ reaching the equilibrium value of $\overline{\lambda}_{11}^{\mathrm{LHA}}$ more quickly. This shows that knowledge of the initial correlations not only affects the dispersion tensors at the initial time t_0, but also the length of time taken to reach their respective steady-state values.

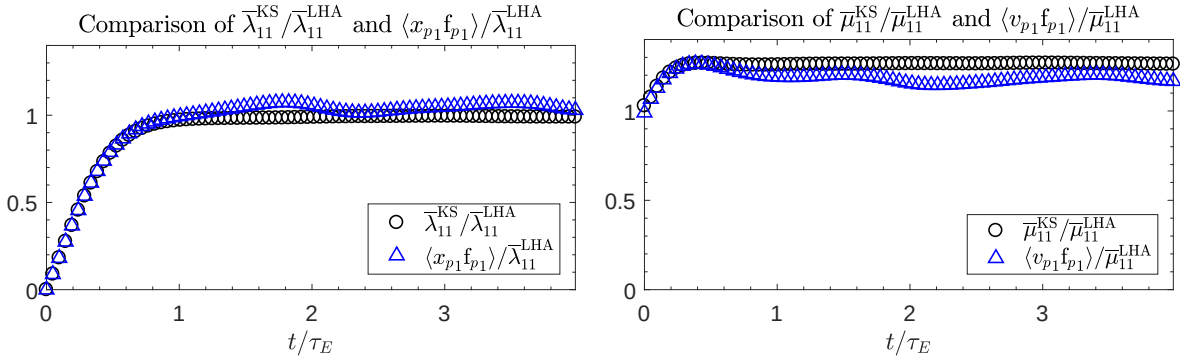

Figure 5.6: Evolution of the PDF dispersion tensors in a homogeneous KS velocity field with $St_E = 1$ including initial correlation amendments, normalised with respect to $\overline{\lambda}_{11}^{\mathrm{LHA}}$ and $\overline{\mu}_{11}^{\mathrm{LHA}}$: ◯ $\overline{\lambda}_{11}^{\mathrm{KS}}/\overline{\lambda}_{11}^{\mathrm{LHA}}$, $\overline{\mu}_{11}^{\mathrm{KS}}/\overline{\mu}_{11}^{\mathrm{LHA}}$; △ $\langle x_{p_1}\mathrm{f}_{p_1}\rangle/\overline{\lambda}_{11}^{\mathrm{LHA}}$, $\langle v_{p_1}\mathrm{f}_{p_1}\rangle/\overline{\mu}_{11}^{\mathrm{LHA}}$

With the initial condition dependent formulations of the dispersion tensors $\overline{\lambda}_{11}$ and $\overline{\mu}_{11}$ given by equations (5.79) and (5.80) incorporated into the KS computation, the behaviour in Figure 5.6 is observed for the case $St_E = 1$. It is observed that both $\overline{\lambda}_{11}$ and $\overline{\mu}_{11}$ show close agreement with the respective benchmarks $\langle x_{p_1} \mathrm{f}_{p_1} \rangle$ and $\langle v_{p_1} \mathrm{f}_{p_1} \rangle$ at the start of the simulation and during the initial transience. Furthermore, this method of initialization captures the equilibrium behaviour of the dispersion tensors fairly well, with the steady-state values achieved more quickly than the corresponding cases in Figure 5.5. The extent of this speed-up can be seen to be not insignificant, with a time of $t \approx \tau_E$ required for $\overline{\lambda}_{11}$ and $\overline{\mu}_{11}$ to reach a statistically stationary state compared to that of $t \approx 2\tau_E$ when the initial fluid-particle correlations are not taken into account. Knowledge of this initial interdependence consequently enables the sampling period to be shortened by τ_E, providing a saving in the computational cost of the simulation.

Further to this, both Figures 5.5 and 5.6 can be used to make inferences about various aspects of the dispersion tensor behaviour in homogeneous flow. Firstly, it is seen that the asymptotic value of $\overline{\mu}_{11}$ closely matches that of $\langle v_{p_1} \mathrm{f}_{p_1} \rangle$. From this, since the exact relationship between these quantities from section 4.3 is $\left\langle \boldsymbol{v}_p \mathbf{f}_p \right\rangle = \overline{\mathbf{c}\boldsymbol{\kappa}} + \overline{\boldsymbol{\mu}}$, this naturally supports the conclusion that $\overline{\mathbf{c}\boldsymbol{\kappa}} = \mathbf{0}$ in homogeneous flows. Secondly, it is observed that once the dispersion tensors reach their steady state values, the correlation $\langle x_{p_1} \mathrm{f}_{p_1} \rangle$ exhibits somewhat intermittent behaviour, which can be attributed to the treatment of the particle position $\boldsymbol{x}_p$ within the periodic domain as outlined in section 5.2.5. In this case $\boldsymbol{x}_p$ has been handled as a non-periodic position which results in the correlation $\langle x_{p_1} \mathrm{f}_{p_1} \rangle$ progressively increasing after a certain amount of time, and it is the effect of this which is evident in Figures 5.5 and 5.6. Finally, these results are normalised with respect to the long-time local homogeneous approximation values for the dispersion tensors presented in equation (4.66), with the variation from unity in Figures 5.5 and 5.6 demonstrating that a margin of error is inherent in the LHA values even in homogeneous flows.

Overall, these results serve to validate the procedure for evaluating the dispersion tensors $\overline{\boldsymbol{\lambda}}(\mathbf{x}, t)$ and $\overline{\boldsymbol{\mu}}(\mathbf{x}, t)$ within the particle tracking simulations for the simple case of a homogeneous flow, and complete the groundwork required for investigation of particle behaviour in more complex flow configurations.

Chapter 6

Drift Enhancement in Gravitational Settling

6.1 Motivation

Despite the numerous studies outlined in section 3.2 that have focused upon developing a more complete understanding of the physical mechanisms responsible for the modification in settling rate of inertial particles in turbulent flows, no single mechanism has been identified as being the dominant causal factor of this behaviour. The various numerical and experimental approaches that have been used to study the response of particles across the range of parameters have provided significant insight into the nature of individual physical mechanisms, yet unification of these isolated explanations remains out of reach. As a result, it is prudent to both analyse this phenomenon in more detail so that the consequences of the reduction in symmetry on particle behaviour can be determined, and also consider the application of mathematical modelling to see if further information can be extracted from such techniques.

The PDF kinetic model framework detailed in Chapter 4 is a suitable means for investigating the phenomenon of enhanced settling rate, since it contains a complete physical description within the dispersion tensors $\overline{\boldsymbol{\kappa}}(\mathbf{x},t)$, $\overline{\boldsymbol{\lambda}}(\mathbf{x},t)$, and $\overline{\boldsymbol{\mu}}(\mathbf{x},t)$ of the behaviour associated with the underlying particle equation of motion. As noted, the exactness of this approach applies only when the zero-mean random fluctuating particle acceleration $\mathbf{f}(\mathbf{x},t)$ has a Gaussian distribution. This is a strong assumption for true turbulence, as the energy cascade explicitly depends upon non-Gaussian aspects of the velocity field [118], however the KS flow field constructed in Chapter 5 to generate

fluid velocities which conform to a Gaussian distribution is ideally suited for use with the PDF kinetic model. Then using this methodology, the focus falls upon closure of the dispersion tensors in order to make inferences about the particle behaviour. To begin with however, the form of the PDF kinetic model in the case of a homogeneous isotropic flow subject to the influence of a gravitational body force in one direction is considered.

6.2 The PDF Kinetic Model Applied to Gravitational Settling

As set out in section 3.2, the range of experimental and numerical research into modification of the average particle settling velocity $\overline{\mathbf{v}}$ compared to the Stokes settling velocity $\mathbf{V}_g$ has shown that the level of physical detail taken into account can result not only in enhancement of $\overline{\mathbf{v}}$, but also loitering. Specifically, loitering is found only to occur in the cases when a nonlinear drag law is used, or in cases of high particle mass loading that fall within the two-way coupling regime. With regard to this, the remit of the present work is consideration of the PDF kinetic model applied to the linear drag law (2.22), meaning that this investigation is limited to the enhancement of $\overline{\mathbf{v}}$ since nonlinear drag corrections are not included and one-way coupling is used.

6.2.1 Particle Mass Flux Interpretation

To apply the PDF kinetic model to the phenomenon of particle settling rate enhancement, it is helpful to begin by considering the particle mass flux representation in the case of a Stokes drag model as detailed in section 4.2.3, and specifically the rearrangement (4.48) of the particle-phase momentum equation, repeated here for reference

$$\rho\overline{\mathbf{v}} = \rho\left[\langle\mathbf{u}\rangle + \mathbf{V}_g + \tau_p\left\{\left[\overline{\boldsymbol{\kappa}} - \nabla\cdot\overline{\boldsymbol{\lambda}}\right] - \nabla\cdot\overline{\mathbf{cc}} - \frac{D}{Dt}\overline{\mathbf{v}}\right\}\right] - \tau_p\left(\overline{\mathbf{cc}} + \overline{\boldsymbol{\lambda}}^{\top}\right)\cdot\nabla\rho \quad (6.1)$$

Since there is no mean flow the Eulerian average $\langle\mathbf{u}(\mathbf{x},t)\rangle$ is equal to zero, and as the constant gravitational acceleration $\mathbf{g}$ acts uniformly across the domain the behaviour of the particle phase is therefore homogeneous, meaning that it is permissible to neglect all spatial gradients. Additionally, because it is the steady-state behaviour that is of

interest the inertial term $D\overline{\mathbf{v}}/Dt$ can also be neglected, and then equation (6.1) is considerably simplified to the form

$$\overline{\boldsymbol{\kappa}} = \beta(\overline{\mathbf{v}} - \mathbf{V}_g) \tag{6.2}$$

Thus the drift enhancement responsible for the increase in average particle settling velocity $\overline{\mathbf{v}} - \mathbf{V}_g$ is solely quantified by the dispersion tensor $\overline{\boldsymbol{\kappa}}$ in the PDF kinetic model, consistent with the interpretation of $\overline{\boldsymbol{\kappa}}$ as an additional drift contribution. Consequently, quantification of this enhanced settling rate using the PDF kinetic model therefore reduces the focus to closure of $\overline{\boldsymbol{\kappa}}$.

6.2.2 Correlation Splitting Interpretation

In addition to the result (6.2) emanating from the particle mass flux balance, it is possible to obtain a further expression for increase in average particle settling velocity $\overline{\mathbf{v}} - \mathbf{V}_g$ by consideration of the particle equation of motion. Taking the average of the Stokes drag model (2.22) yields

$$\frac{d\overline{\mathbf{v}}}{dt} = \beta\Big[\big\langle \mathbf{u}\left(\boldsymbol{x}_p(t), t\right)\big\rangle_{\mathbf{x}} - \overline{\mathbf{v}} + \mathbf{V}_g\Big] \tag{6.3}$$

For the steady-state behaviour, neglecting the inertial term $d\overline{\mathbf{v}}/dt$ as before produces the relation

$$\overline{\mathbf{v}} - \mathbf{V}_g = \big\langle \mathbf{u}\left(\boldsymbol{x}_p(t), t\right)\big\rangle_{\mathbf{x}} \tag{6.4}$$

Therefore the increase in average particle settling velocity can also be interpreted as the average of the fluid velocity sampled along inertial particle trajectories $\big\langle \mathbf{u}\left(\mathbf{x}_p(t), t\right)\big\rangle_{\mathbf{x}}$ [91]. It is subsequently instructive to investigate the significance of this quantity, which can be realised by utilising the filtering property of the fine-grained particle number density $\varrho\left(\mathbf{x}, t\right)$ to write the conditional form of the average as

$$\big\langle \mathbf{u}\left(\boldsymbol{x}_p(t), t\right)\big\rangle_{\mathbf{x}} = \frac{1}{\rho\left(\mathbf{x}, t\right)}\big\langle \mathbf{u}\left(\mathbf{x}, t\right)\varrho\left(\mathbf{x}, t\right)\big\rangle \tag{6.5}$$

Then decomposing the Eulerian fluid velocity into its mean and fluctuating parts gives $\mathbf{u}\left(\mathbf{x}, t\right) = \mathbf{u}'\left(\mathbf{x}, t\right)$ since $\langle \mathbf{u}\left(\mathbf{x}, t\right)\rangle = \mathbf{0}$ in this configuration, resulting in

$$\big\langle \mathbf{u}\left(\boldsymbol{x}_p(t), t\right)\big\rangle_{\mathbf{x}}\,\rho\left(\mathbf{x}, t\right) = \big\langle \mathbf{u}'\left(\mathbf{x}, t\right)\varrho\left(\mathbf{x}, t\right)\big\rangle \tag{6.6}$$

This form permits the use of correlation splitting techniques to further describe the interaction between $\mathbf{u}'(\mathbf{x},t)$ and $\varrho(\mathbf{x},t)$, and in keeping with the PDF kinetic model $\mathbf{u}'(\mathbf{x},t)$ is taken to be Gaussian. Then using the interpretations of the phase space variables directly in terms of the configuration coordinates $\boldsymbol{\xi}=\mathbf{x}$ and $\mathbf{b}(\boldsymbol{\xi},t)=\mathbf{f}(\mathbf{x},t)$ results in equation (4.16) taking the form

$$\begin{aligned}\Big\langle \mathrm{f}_i(\mathbf{x},t)\,\varrho(\mathbf{f};\mathbf{x},t)\Big\rangle = &\int_{t_0}^{t}\left\langle \frac{\delta x_{p_k}(t)}{\delta \mathrm{f}_j(\boldsymbol{x}_p(t'),t')}\frac{\partial}{\partial \mathrm{x}_k}\Big\langle \mathrm{f}_j(\mathbf{x}',t')\,\mathrm{f}_i(\mathbf{x},t)\Big\rangle\Big|_{\mathbf{x}'=\boldsymbol{x}_p(t')}\right\rangle_{\mathbf{x}} dt'\,\rho(\mathbf{x},t)\\ &-\frac{\partial}{\partial \mathrm{x}_k}\left[\int_{t_0}^{t}\left\langle \frac{\delta x_{p_k}(t)}{\delta \mathrm{f}_j(\boldsymbol{x}_p(t'),t')}\Big\langle \mathrm{f}_j(\mathbf{x}',t')\,\mathrm{f}_i(\mathbf{x},t)\Big\rangle\Big|_{\mathbf{x}'=\boldsymbol{x}_p(t')}\right\rangle_{\mathbf{x}} dt'\,\rho(\mathbf{x},t)\right]\end{aligned} \tag{6.7}$$

In this the familiar interpretations $\mathrm{R}_{ji}\left(\boldsymbol{x}_p',t';\mathbf{x},t\right)=\big\langle \mathrm{f}_j(\mathbf{x}',t')\,\mathrm{f}_i(\mathbf{x},t)\big\rangle\big|_{\mathbf{x}'=\boldsymbol{x}_p(t')}$ from (4.25) and $\mathcal{H}_{kj}[t;t']=\delta x_{p_k}(t)/\delta \mathrm{f}_j(\boldsymbol{x}_p(t'),t')$ from (4.27) can be reintroduced, following which the definitions of the velocity averaged dispersion tensors $\overline{\boldsymbol{\kappa}}(\mathbf{x},t)$, $\overline{\boldsymbol{\lambda}}(\mathbf{x},t)$ emerge, and further consistent with the specification of $\mathbf{f}(\mathbf{x},t)=\beta\mathbf{u}'(\mathbf{x},t)$ for the Stokes drag model in (4.3) and use of (6.6) produces the general result

$$\beta\big\langle \mathbf{u}'(\boldsymbol{x}_p(t),t)\big\rangle_{\mathbf{x}}\rho(\mathbf{x},t)=\overline{\boldsymbol{\kappa}}(\mathbf{x},t)\,\rho(\mathbf{x},t)-\frac{\partial}{\partial\mathbf{x}}\cdot\Big[\overline{\boldsymbol{\lambda}}(\mathbf{x},t)\,\rho(\mathbf{x},t)\Big] \tag{6.8}$$

For the homogeneous configuration under consideration the spatial gradient can be neglected, and the conditional average reduces to an ensemble average, finally yielding

$$\overline{\boldsymbol{\kappa}}(t)=\beta\big\langle \mathbf{u}'(\boldsymbol{x}_p(t),t)\big\rangle \tag{6.9}$$

It can be seen that equating (6.9) with the result (6.2) from the particle mass flux interpretation reproduces the expression (6.4) from the equilibrium form of the averaged Stokes drag model, demonstrating the robustness of these two representations. Furthermore, because the interpretation of $\overline{\boldsymbol{\kappa}}/\beta$ is known to be identical to the increase in average particle settling velocity from section 6.2.1, the result (6.9) implies that the average fluctuating fluid velocity along particle trajectories can also be interpreted as this enhancement in settling velocity. There are therefore a number of ways to determine the settling velocity enhancement experienced by inertial particles, which provide useful benchmarks against which both the validity of numerical simulations and the accuracy of closures for the PDF kinetic model can be assessed.

6.3 Validation of the PDF Kinetic Model using KS

With appropriate means in place for verifying the level of description provided by the PDF kinetic model in the context of particle settling subject to gravity, numerical simulation is the natural way of making this assessment. To that end, the KS velocity field outlined in Chapter 5 has been used to run parametric simulations across a range of Stokes numbers $0.05 < St_E < 5$ and gravitational settling velocities $0.05 < V_g < 2$ in order to quantify the increase in settling velocity under different conditions. The exact version of $\overline{\boldsymbol{\kappa}}$ is evaluated directly using (4.30), whilst also storing values of $\langle \mathbf{u}' (\boldsymbol{x}_p(t), t) \rangle$ from the simulation so that (6.9) can be used to judge the efficacy of $\overline{\boldsymbol{\kappa}}$. To assist with both the computational expense and subsequent modelling process, it is helpful to consider the restricted case of a two-dimensional domain so that the analysis is somewhat simplified. Then for $\mathbf{g} = (0, -\mathrm{g})$, it is expected that only $\overline{\kappa}_2$ will yield a non-zero result, due to there being no body force on particles in the x_1 direction.

The results for the asymptotic values of the component in the gravitational direction are shown in Figure 6.1 for a selection of different values of V_g, in which data points coloured in black represent normalised values of $\overline{\kappa}_2$ and data points coloured in blue represent normalised values of $\langle \mathrm{u}'_{p_2} \rangle = \langle \mathrm{u}'_2 (\boldsymbol{x}_p) \rangle$. All values are normalised with respect to the fluid RMS velocity u' in order to provide a consistent scaling for the different values of St_E and V_g used, and error bars represent the standard deviation from time averaging once $\overline{\kappa}_2$ has reached an equilibrium in the sampling period. It is seen that the expected modification in settling rate emerges, and is further only positive as anticipated, with the omission of nonlinear drag effects precluding the occurrence of loitering. The resultant enhancement in average particle settling velocity tails off to zero as $St_E \to \infty$, and would also decrease to zero in the limit $St_E \to 0$, however the lowest Stokes number in the simulations of $St_E = 0.05$ still shows a non-zero enhancement. Notably a pronounced peak in the settling velocity enhancement is observed at $St_E \approx 0.1$ and $V_g \approx 1$ of around a 7% increase. This is in line with previous studies using KS [91], and notably does not match the increase of up to 50% as seen in DNS [163], highlighting the effect of neglecting the physical detail of the flow at the microscales. Nonetheless, it can be seen that the reference values of $\langle \mathrm{u}'_{p_2} \rangle$ are closely matched by those of $\overline{\kappa}_2$ across the entire range of St_E and V_g. This demonstrates that the PDF kinetic model captures the physical mechanisms responsible for the increase in average particle settling velocity within a Gaussian flow field, and is therefore a suitable framework for model development of this phenomenon. Furthermore, although not shown here for brevity, the expected result of $\overline{\kappa}_1 = 0$ is also retrieved from the

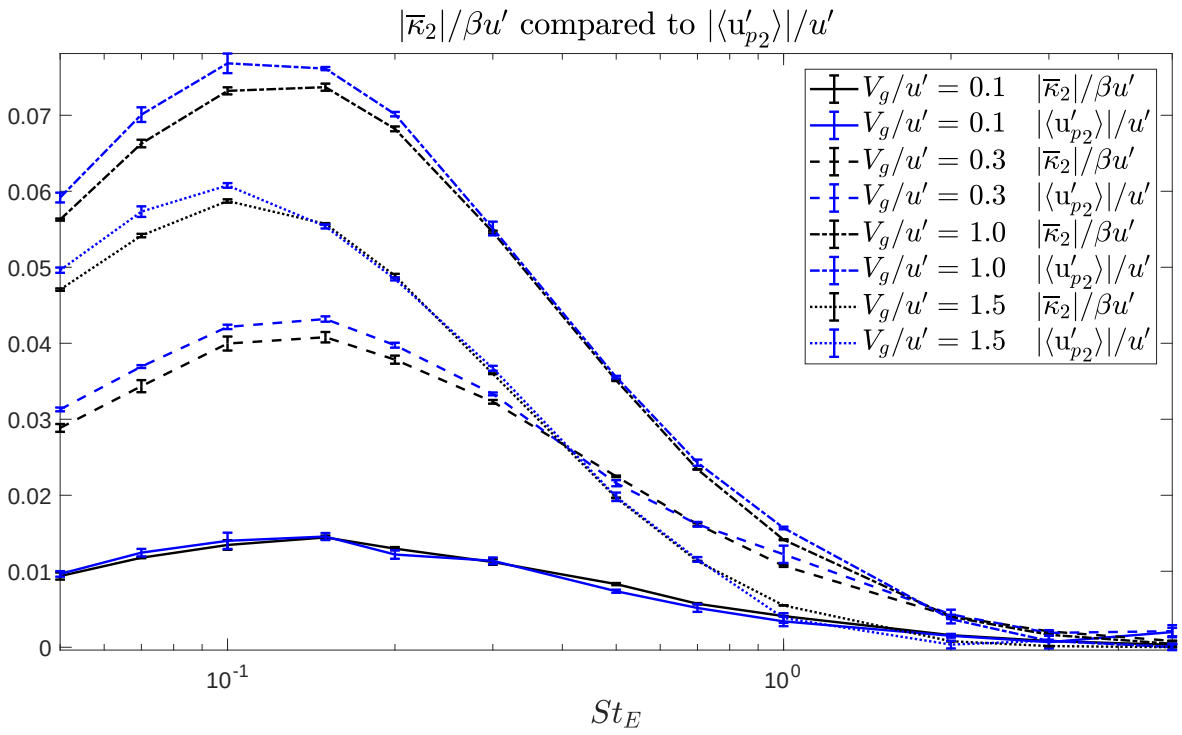

Figure 6.1: Variation of —o— $|\overline{\kappa}_2|/\beta u'$ and —o— $|\langle \mathrm{u}'_{p_2}\rangle|/u'$ with St_E and V_g/u' in a two-dimensional fluid velocity field. Error bars represent the standard deviation from time averaging. ——— $V_g/u' = 0.1$; - - - $V_g/u' = 0.3$; — · — · —· $V_g/u' = 1.0$; · · · · · $V_g/u' = 1.5$

simulations, verifying that this form of the PDF kinetic model does not introduce any spurious drift into the results. Finally, it is worth noting that although the use of a KS flow field to evaluate the increase in particle settling velocity means that only mechanisms associated with the large-scale flow structures are captured in this case, the PDF kinetic approach can in principle be extended to include the mechanisms which arise from the small-scale features that are characteristic of true turbulence. This is achieved by the inclusion of higher-order terms in the expansion (4.9) from which the PDF kinetic framework is formulated, and verification that the drift tensors which emerge from this approach are able to account for the finer level of detail is then possible through numerical evaluation using data obtained from a full DNS flow field.

6.4 Understanding the PDF Dispersion Tensors in an Isotropic Flow Field

In order to use the PDF kinetic framework for the development of closure models that attempt to capture the effect of particle settling rate enhancement, it is first instructive

to analyse the conditional average appearing within the dispersion tensor $\overline{\boldsymbol{\kappa}}$ given in (4.30). To proceed with such an analysis, it is appropriate to express $\overline{\boldsymbol{\kappa}}$ in component form

$$\overline{\kappa}_i\left(\mathbf{x},t\right)=\int_{t_0}^{t}\left\langle \mathcal{H}_{kj}\left[t;t'\right]\frac{\partial}{\partial \mathrm{x}_k}\mathrm{R}_{ji}\left(\boldsymbol{x}_p',t';\mathbf{x},t\right)\right\rangle_{\mathbf{x}}dt' \tag{6.10}$$

Consideration of this expression raises the question of how the particle response tensor $\boldsymbol{\mathcal{H}}\left[t;t'\right]$ influences drift enhancement, and specifically its interaction with $\nabla\mathbf{R}\left(\boldsymbol{x}_p',t';\mathbf{x},t\right)$. For an isotropic flow field, the form of the spatial derivative $\nabla\mathbf{R}\left(\mathbf{x}',t';\mathbf{x},t\right)$ expressed explicitly in terms of the separation vector $\mathbf{r}=\mathbf{x}-\mathbf{x}'$ is calculated in Appendix C for the choice of longitudinal decorrelation function $f(\mathrm{r})$ specified in (5.19). The result is given by combining equations (C.10) and (C.16), and for $d=2$ this results in $\frac{\partial}{\partial \mathrm{x}_k}\mathrm{R}_{ji}$ taking the form

$$\frac{\partial}{\partial \mathrm{x}_k}\mathrm{R}_{ji}(\mathbf{r},s)=\beta^2u^2\sigma_k^2f(\mathrm{r})\Big[\left(\sigma_k^2\mathrm{r}^2-3\right)\mathrm{r}_k\delta_{ij}-\sigma_k^2\mathrm{r}_k\mathrm{r}_j\mathrm{r}_i+\mathrm{r}_i\delta_{jk}+\mathrm{r}_j\delta_{ik}\Big]\mathrm{E}_\omega(s) \tag{6.11}$$

where $\mathrm{r}=|\mathbf{r}|$. Substitution of the isotropic tensor (6.11) into the integrand for $\overline{\boldsymbol{\kappa}}$ in (6.10), performing the contraction between $\mathcal{H}_{kj}$ and $\frac{\partial}{\partial \mathrm{x}_k}\mathrm{R}_{ji}$, and evaluating for $i=2$ since the drift enhancement is only expected to occur in the gravitational direction gives an expression for $\overline{\kappa}_2$ in a two-dimensional isotropic flow field

$$\begin{aligned}\overline{\kappa}_2\left(\mathbf{x},t\right)=\beta^2u^2\sigma_k^2\int_{t_0}^{t}\Big(&\left\langle \mathcal{H}_{11}f(r_p)\left[1-\sigma_k^2{r_{p1}}^2\right]r_{p2}\right\rangle_{\mathbf{x}}+\left\langle \mathcal{H}_{12}f(r_p)\left[\sigma_k^2{r_{p1}}^2-3\right]r_{p1}\right\rangle_{\mathbf{x}}\\&+\left\langle \mathcal{H}_{21}f(r_p)\left[1-\sigma_k^2{r_{p2}}^2\right]r_{p1}\right\rangle_{\mathbf{x}}+\left\langle \mathcal{H}_{22}f(r_p)\left[\sigma_k^2{r_{p1}}^2-1\right]r_{p2}\right\rangle_{\mathbf{x}}\Big)\mathrm{E}_\omega(t-t')\,dt'\end{aligned} \tag{6.12}$$

where $\boldsymbol{r}_p\left(t';t\right)=\mathbf{x}-\boldsymbol{x}_p\left(t'\right)$ is the separation along particle trajectories, $r_p=|\boldsymbol{r}_p|$, and $r_{p_i}=(\boldsymbol{r_p})_i$. It is seen that the enhancement in the average particle drift velocity is therefore a consequence of the interaction that exists between $\boldsymbol{r}_p\left(t';t\right)$ and $\boldsymbol{\mathcal{H}}\left[t;t'\right]$.

Further insight into this dependence can be obtained from simulation, and this is illustrated in Figure 6.2 in terms of the correlation of r_{p_1} and $\boldsymbol{\mathcal{H}}$ as computed using KS data. It can be observed that the correlation of r_{p_1} with the diagonal components of $\boldsymbol{\mathcal{H}}$ is negligible, with product-moment correlation coefficients ρ that are zero to within noise. In contrast, correlation of r_{p_1} with the non-diagonal components of $\boldsymbol{\mathcal{H}}$ is marked, demonstrated by the distinctly non-zero values of the product-moment correlation coefficient (0.2441 and -0.1308) and the skewness of the distribution in the

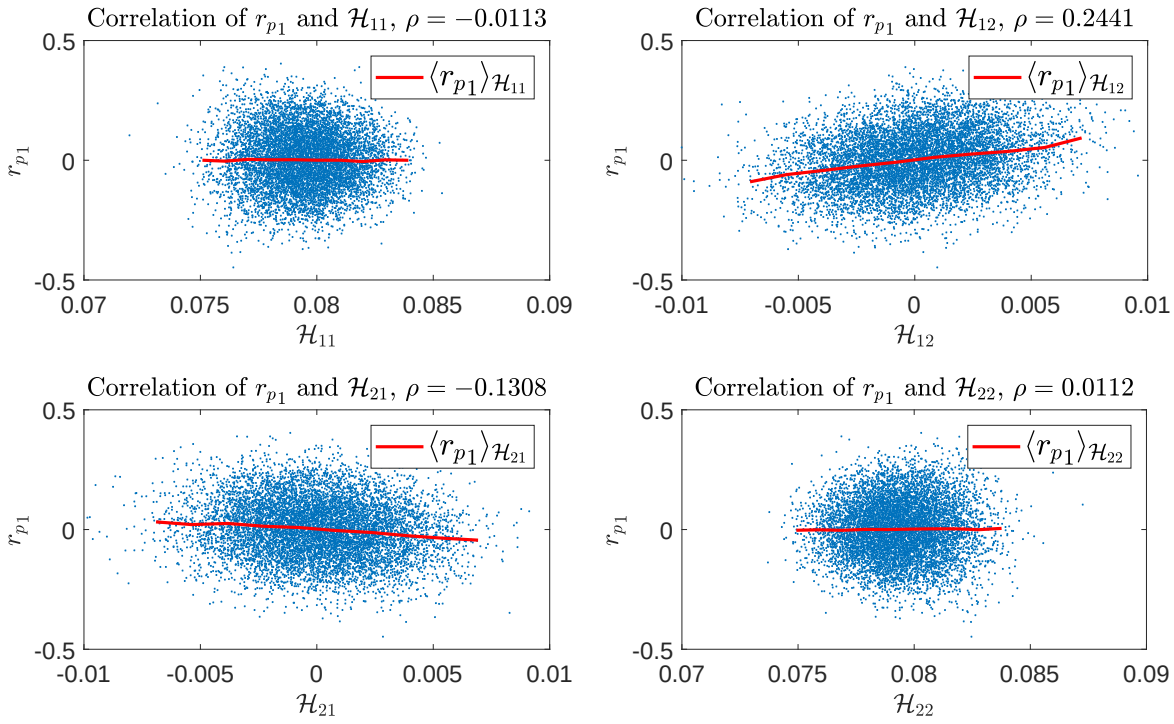

Figure 6.2: Correlation of $r_{p_1}(t';t)$ and $\boldsymbol{\mathcal{H}}[t;t']$ for $St_E = 0.1$ and $V_g/u' = 1.0$ in a two-dimensional fluid velocity field, with product-moment correlation coefficients ρ: —— Average of $r_{p_1}(t';t)$ conditional on $\boldsymbol{\mathcal{H}}[t;t']$

scatter plots for these two components. Another way of visualising this is to consider the average of r_{p_1} conditional on $\boldsymbol{\mathcal{H}}$, denoted by $\langle r_{p_1} \rangle_{\boldsymbol{\mathcal{H}}}$. If r_{p_1} and $\boldsymbol{\mathcal{H}}$ were uncorrelated this conditional average would be constant across different values of all components in $\boldsymbol{\mathcal{H}}$, however in Figure 6.2 it is seen that for the non-diagonal components of $\boldsymbol{\mathcal{H}}$ the conditional average $\langle r_{p_1} \rangle_{\boldsymbol{\mathcal{H}}}$ does in fact vary, providing a graphical interpretation of the product-moment correlation coefficient for these components. In contrast, the value of $\langle r_{p_1} \rangle_{\boldsymbol{\mathcal{H}}}$ does not vary with the diagonal components of $\boldsymbol{\mathcal{H}}$, in agreement with the product-moment correlation coefficient vanishing. The outcome of this is that the correlations between $\boldsymbol{r}_p(t';t)$ and $\boldsymbol{\mathcal{H}}[t;t']$ require modelling in order to explain the physical mechanisms responsible for the observed drift enhancement, and this is then the fundamental requirement of any proposed closure strategy.

6.5 Symmetry Considerations

As a further precursor to the development of closures using the PDF kinetic model, it is also helpful to consider the reduction of symmetry that is inherent to the particle phase

in this configuration. Specifically, the isotropic nature of the flow field with an external body force acting in only one direction means that the particle behaviour can be likened to an axisymmetric configuration, in which symmetry arguments hold in every direction except that in which gravity acts. For the more general three-dimensional domain with $\mathbf{g} = (0, 0, -\mathrm{g})$, the aim is then to use such arguments to show that $\overline{\kappa}_1 = \overline{\kappa}_2 = 0$, and simplify the model development required for quantification of $\overline{\kappa}_3$.

6.5.1 Characterisation of Rotations and Reflections

Intuitively, the PDF $\phi(\mathbf{r})$ is even in r_1 and r_2 since there is no direction bias in the x_1 and x_2 directions. That is, $\phi(-\mathrm{r}_1, -\mathrm{r}_2, \mathrm{r}_3) = \phi(+\mathrm{r}_1, +\mathrm{r}_2, \mathrm{r}_3)$, and hence $\langle r_{p_1} \rangle \equiv \langle r_{p_2} \rangle \equiv 0$. In the light of the interaction between the separation along particle trajectories $\boldsymbol{r}_p(t'; t)$ and the particle response tensor $\boldsymbol{\mathcal{H}}[t; t']$ in section 6.4, extension of this reasoning to the joint distribution of $\boldsymbol{r}_p$ and $\boldsymbol{\mathcal{H}}$ is required.

Formalisation of this is possible by considering the invariance of the system for defining $\overline{\boldsymbol{\kappa}}$ under a number of co-ordinate transforms which correspond to certain rotations and reflections of axes. In particular, with a co-ordinate axis system x_i, the following transformations $\mathrm{x}_i \rightarrow \widetilde{\mathrm{x}}_i$ concerning all permutations of sign changes in x_1 and x_2 are of interest

$$(\mathrm{x}_1, \mathrm{x}_2, \mathrm{x}_3) \rightarrow (\widetilde{\mathrm{x}}_1, \widetilde{\mathrm{x}}_2, \widetilde{\mathrm{x}}_3) = \begin{cases} (-\mathrm{x}_1, -\mathrm{x}_2, \mathrm{x}_3) & ① \\ (-\mathrm{x}_1, +\mathrm{x}_2, \mathrm{x}_3) & ② \\ (+\mathrm{x}_1, -\mathrm{x}_2, \mathrm{x}_3) & ③ \\ (+\mathrm{x}_2, +\mathrm{x}_1, \mathrm{x}_3) & ④ \\ (+\mathrm{x}_2, -\mathrm{x}_1, \mathrm{x}_3) & ⑤ \\ (-\mathrm{x}_2, +\mathrm{x}_1, \mathrm{x}_3) & ⑥ \end{cases} \tag{6.13}$$

These transformations can all be defined in the form $\widetilde{\mathbf{x}} = \mathbf{P} \cdot \mathbf{x}$, where the transformation matrix $\mathbf{P}$ is a signed permutation matrix of the form

$$\mathbf{P} = \left[\begin{array}{cc|c} & \mathbf{A} & \begin{matrix} 0 \\ 0 \end{matrix} \\ \hline 0 & 0 & 1 \end{array}\right] \tag{6.14}$$

in which $\det(\mathbf{A}) = \pm 1$ and $\mathbf{P}^{-1} = \mathbf{P}^{\top}$.

6.5.2 Invariance of the System Governing Equations

The usefulness of the type of coordinate transformations described by $\mathbf{P}$ emerges by considering their application to the evolution of $\boldsymbol{r}_p(t';t)$ and $\boldsymbol{\mathcal{H}}[t;t']$, which are each governed by an equation of motion. In the case of $\boldsymbol{r}_p$, the governing equation for the particle position $\boldsymbol{x}_p(t)$ is the Stokes drag model 2.22 written in the form

$$\frac{d^2\boldsymbol{x}_p}{dt^2} = \beta\left[\mathbf{u}\left(\boldsymbol{x}_p(t),t\right) - \frac{d\boldsymbol{x}_p}{dt}\right] + \mathbf{g} \quad , \quad \begin{matrix}\boldsymbol{x}_p(t') = \mathbf{X}' \\ \frac{d\boldsymbol{x}_p}{dt}(t') = \mathbf{V}'\end{matrix} \tag{6.15}$$

in which $\mathbf{X}'$ and $\mathbf{V}'$ are the initial conditions for the trajectory. Then for the separation along particle trajectories $\boldsymbol{r}_p(t';t) = \mathbf{x} - \boldsymbol{x}_p(t')$, the corresponding equation of motion is given by

$$\frac{d^2\boldsymbol{r}_p}{dt'^2} = \beta\left[\mathbf{u}\left(\boldsymbol{r}_p(t') + \mathbf{x}, t'\right) - \frac{d\boldsymbol{r}_p}{dt'}\right] + \mathbf{g} \quad , \quad \begin{matrix}\boldsymbol{r}_p(t;t) = \mathbf{0} \\ \frac{d\boldsymbol{r}_p}{dt}(t;t) = \mathbf{V}\end{matrix} \tag{6.16}$$

where $\mathbf{0}$ and $\mathbf{V}$ are now interpreted as final conditions for the trajectory. Then in terms of the signed permutation matrix $\mathbf{P}$, the first-order tensors are transformed to the coordinate system $\widetilde{\mathbf{x}}$ by means of the relations

$$\widetilde{\mathbf{x}} = \mathbf{P}\cdot\mathbf{x}, \quad \widetilde{\mathbf{u}}\left(\widetilde{\mathbf{x}},t\right) = \mathbf{P}\cdot\mathbf{u}\left(\mathbf{x},t\right), \quad \widetilde{\boldsymbol{r}}_p\left(t';t\right) = \mathbf{P}\cdot\boldsymbol{r}_p\left(t';t\right), \quad \widetilde{\mathbf{V}} = \mathbf{P}\cdot\mathbf{V}, \quad \widetilde{\mathbf{g}} = \mathbf{P}\cdot\mathbf{g} = \mathbf{g} \tag{6.17}$$

where the invariance of $\mathbf{g}$ in the final relation is due to the form of $\mathbf{P}$ specified in (6.14). Then applying the transformations in (6.17) to the governing equation for the separation $\boldsymbol{r}_p(t';t)$ (6.16) results in

$$\frac{d^2\widetilde{\boldsymbol{r}}_p}{dt'^2} = \beta\left[\widetilde{\mathbf{u}}\left(\widetilde{\boldsymbol{r}}_p(t') + \widetilde{\mathbf{x}}, t'\right) - \frac{d\widetilde{\boldsymbol{r}}_p}{dt'}\right] + \mathbf{g} \quad , \quad \begin{matrix}\widetilde{\boldsymbol{r}}_p(t;t) = \mathbf{0} \\ \frac{d\widetilde{\boldsymbol{r}}_p}{dt}(t;t) = \widetilde{\mathbf{V}}\end{matrix} \tag{6.18}$$

Comparison of (6.16) and (6.18) therefore reveals that the equation of motion for $\boldsymbol{r}_p(t';t)$ remains unchanged under the type of transformation described by $\mathbf{P}$. In terms of the the particle response tensor $\boldsymbol{\mathcal{H}}[t;t']$, the governing equation given in (4.28) evaluated for the Stokes drag model with mean continuous phase driving force $\mathbf{F}(\mathbf{x},\mathbf{v},t)$ and fluctuating particle acceleration $\mathbf{f}(\mathbf{x},t)$ as given by equations (4.2) and (4.3) is

$$\ddot{\boldsymbol{\mathcal{H}}}\left[t;t'\right]=-\beta\dot{\boldsymbol{\mathcal{H}}}\left[t;t'\right]+\beta\nabla\mathbf{u}^{\top}(\boldsymbol{x}_p(t),t)\cdot\boldsymbol{\mathcal{H}}\left[t;t'\right]\quad,\quad\begin{matrix}\boldsymbol{\mathcal{H}}\left[t';t'\right]=\mathbf{0}\\ \dot{\boldsymbol{\mathcal{H}}}\left[t';t'\right]=\mathbf{I}\end{matrix}\tag{6.19}$$

Since $\boldsymbol{\mathcal{H}}\left[t;t'\right]$ is a second-order tensor, the appropriate transformation to the frame of reference $\widetilde{\mathbf{x}}$ is given by

$$\widetilde{\boldsymbol{\mathcal{H}}}\left[t;t'\right]=\mathbf{P}\cdot\boldsymbol{\mathcal{H}}\left[t;t'\right]\cdot\mathbf{P}^{\top}\tag{6.20}$$

Furthermore, using the first and second relations in (6.17) for $\widetilde{\mathbf{x}}$ and $\widetilde{\mathbf{u}}$ respectively it can be shown that for the specific transformations given by $\mathbf{P}$ such that $\mathbf{P}^{-1}=\mathbf{P}^{\top}$, the fluid velocity gradient along particle trajectories $\nabla\mathbf{u}^{\top}(\boldsymbol{x}_p(t),t)$ transforms in the same manner

$$\widetilde{\nabla}\widetilde{\mathbf{u}}^{\top}(\widetilde{\boldsymbol{x}}_p(t),t)=\mathbf{P}\cdot\nabla\mathbf{u}^{\top}(\boldsymbol{x}_p(t),t)\cdot\mathbf{P}^{\top}\tag{6.21}$$

Applying the transformations in the definition (6.20) and result (6.21) to the governing equation for the particle response tensor $\boldsymbol{\mathcal{H}}\left[t;t'\right]$ (6.19) then yields

$$\ddot{\widetilde{\boldsymbol{\mathcal{H}}}}\left[t;t'\right]=-\beta\dot{\widetilde{\boldsymbol{\mathcal{H}}}}\left[t;t'\right]+\beta\widetilde{\nabla}\widetilde{\mathbf{u}}^{\top}(\widetilde{\boldsymbol{x}}_p(t),t)\cdot\widetilde{\boldsymbol{\mathcal{H}}}\left[t;t'\right]\quad,\quad\begin{matrix}\widetilde{\boldsymbol{\mathcal{H}}}\left[t';t'\right]=\mathbf{0}\\ \dot{\widetilde{\boldsymbol{\mathcal{H}}}}\left[t';t'\right]=\mathbf{I}\end{matrix}\tag{6.22}$$

Comparing (6.22) and (6.19) shows that the governing equation for $\boldsymbol{\mathcal{H}}\left[t;t'\right]$ also remains unchanged in the coordinate system $\widetilde{\mathbf{x}}$. The evolution equations (6.18) and (6.22) demonstrate that $\widetilde{\boldsymbol{r}}_p$ and $\widetilde{\boldsymbol{\mathcal{H}}}$ can be considered realisations of the system associated with the corresponding realisation $\widetilde{\mathbf{u}}$ of the fluid velocity field. Since the averaged particle concentration field remains spatially uniform, the distribution of $\boldsymbol{r}_p$ and $\boldsymbol{\mathcal{H}}$ will be independent of $\mathbf{x}$, and as the governing equations for both $\widetilde{\boldsymbol{r}}_p$ and $\widetilde{\boldsymbol{\mathcal{H}}}$ remain unchanged it then follows that the system is statistically invariant under transformations with $\mathbf{P}$ as defined in (6.14). Then denoting the phase-space vector of the system as $\boldsymbol{z}=(\boldsymbol{r}_p,\boldsymbol{\mathcal{H}})$, it follows that

$$\widetilde{\boldsymbol{z}}=\left(\widetilde{\boldsymbol{r}}_p,\widetilde{\boldsymbol{\mathcal{H}}}\right)=\left(\mathbf{P}\cdot\boldsymbol{r}_p,\mathbf{P}\cdot\boldsymbol{\mathcal{H}}\cdot\mathbf{P}^{\top}\right):=\mathbb{P}(\boldsymbol{z})\tag{6.23}$$

where $\det(\mathbb{P})=\pm1$. The foregoing discussion shows that the distribution of $\widetilde{\boldsymbol{z}}$ is the same as that of $\boldsymbol{z}$, and this property can be used to make inferences about the symmetries inherent in $\boldsymbol{z}$.

6.5.3 Deductions Regarding the System Symmetry

For the different transformations listed in equation (6.14), the signed permutation matrix $\mathbf{P}$ and relations between the components of $\widetilde{\boldsymbol{r}}_p$ and $\widetilde{\boldsymbol{\mathcal{H}}}$ with those of $\boldsymbol{r}_p$ and $\boldsymbol{\mathcal{H}}$ respectively are given by

Case	$\mathbf{P}$	$\widetilde{\boldsymbol{r}}_p$	$\widetilde{\boldsymbol{\mathcal{H}}}$
①	$\begin{bmatrix} -1 & 0 & 0 \\ 0 & -1 & 0 \\ 0 & 0 & +1 \end{bmatrix}$	$(-r_{p_1}, -r_{p_2}, +r_{p_3})$	$\begin{bmatrix} +\mathcal{H}_{11} & +\mathcal{H}_{12} & -\mathcal{H}_{13} \\ +\mathcal{H}_{21} & +\mathcal{H}_{22} & -\mathcal{H}_{23} \\ -\mathcal{H}_{31} & -\mathcal{H}_{32} & +\mathcal{H}_{33} \end{bmatrix}$
②	$\begin{bmatrix} -1 & 0 & 0 \\ 0 & +1 & 0 \\ 0 & 0 & +1 \end{bmatrix}$	$(-r_{p_1}, +r_{p_2}, +r_{p_3})$	$\begin{bmatrix} +\mathcal{H}_{11} & -\mathcal{H}_{12} & -\mathcal{H}_{13} \\ -\mathcal{H}_{21} & +\mathcal{H}_{22} & +\mathcal{H}_{23} \\ -\mathcal{H}_{31} & +\mathcal{H}_{32} & +\mathcal{H}_{33} \end{bmatrix}$
③	$\begin{bmatrix} +1 & 0 & 0 \\ 0 & -1 & 0 \\ 0 & 0 & +1 \end{bmatrix}$	$(+r_{p_1}, -r_{p_2}, +r_{p_3})$	$\begin{bmatrix} +\mathcal{H}_{11} & -\mathcal{H}_{12} & +\mathcal{H}_{13} \\ -\mathcal{H}_{21} & +\mathcal{H}_{22} & -\mathcal{H}_{23} \\ +\mathcal{H}_{31} & -\mathcal{H}_{32} & +\mathcal{H}_{33} \end{bmatrix}$
④	$\begin{bmatrix} 0 & +1 & 0 \\ +1 & 0 & 0 \\ 0 & 0 & +1 \end{bmatrix}$	$(+r_{p_2}, +r_{p_1}, +r_{p_3})$	$\begin{bmatrix} +\mathcal{H}_{22} & +\mathcal{H}_{21} & +\mathcal{H}_{23} \\ +\mathcal{H}_{12} & +\mathcal{H}_{11} & +\mathcal{H}_{13} \\ +\mathcal{H}_{32} & +\mathcal{H}_{31} & +\mathcal{H}_{33} \end{bmatrix}$
⑤	$\begin{bmatrix} 0 & +1 & 0 \\ -1 & 0 & 0 \\ 0 & 0 & +1 \end{bmatrix}$	$(+r_{p_2}, -r_{p_1}, +r_{p_3})$	$\begin{bmatrix} +\mathcal{H}_{22} & -\mathcal{H}_{21} & +\mathcal{H}_{23} \\ -\mathcal{H}_{12} & +\mathcal{H}_{11} & -\mathcal{H}_{13} \\ +\mathcal{H}_{32} & -\mathcal{H}_{31} & +\mathcal{H}_{33} \end{bmatrix}$
⑥	$\begin{bmatrix} 0 & -1 & 0 \\ +1 & 0 & 0 \\ 0 & 0 & +1 \end{bmatrix}$	$(-r_{p_2}, +r_{p_1}, +r_{p_3})$	$\begin{bmatrix} +\mathcal{H}_{22} & -\mathcal{H}_{21} & -\mathcal{H}_{23} \\ -\mathcal{H}_{12} & +\mathcal{H}_{11} & +\mathcal{H}_{13} \\ -\mathcal{H}_{32} & +\mathcal{H}_{31} & +\mathcal{H}_{33} \end{bmatrix}$

Table 6.1: The different cases of coordinate system transformations which are invariant in the configuration of particle settling under gravity in an isotropic flow field

Since all the cases of transformation listed in Table 6.1 are invariant in this system, direct comparison of the components of $\widetilde{\boldsymbol{r}}_p$ and $\widetilde{\boldsymbol{\mathcal{H}}}$ with the corresponding components of $\boldsymbol{r}_p$ and $\boldsymbol{\mathcal{H}}$ reveals which components exhibit symmetric behaviour. It then follows directly from ① and ② that the following components have even distributions, and therefore zero means

$$r_{p_1},\ r_{p_2},\ \mathcal{H}_{12},\ \mathcal{H}_{13},\ \mathcal{H}_{21},\ \mathcal{H}_{23},\ \mathcal{H}_{31},\ \mathcal{H}_{32} \tag{6.24}$$

Moreover, ④ is simply the case where the indices 1 and 2 are interchanged, and can be used to identify components with the same distribution, namely

$$r_{p_1} \sim r_{p_2},\ \mathcal{H}_{11} \sim \mathcal{H}_{22},\ \mathcal{H}_{12} \sim \mathcal{H}_{21},\ \mathcal{H}_{13},\ \mathcal{H}_{23} \tag{6.25}$$

Considering the components of $\widetilde{\mathbf{u}}$ and $\widetilde{\nabla}\widetilde{\mathbf{u}}^{\top}(\widetilde{\boldsymbol{x}}_p(t), t)$ in the same manner produces corresponding relations which are equivalent, specifically that the following components have even distributions and therefore zero means

$$\mathrm{u}_1,\ \mathrm{u}_2,\ \nabla_1\mathrm{u}_2,\ \nabla_1\mathrm{u}_3,\ \nabla_2\mathrm{u}_1,\ \nabla_2\mathrm{u}_3,\ \nabla_3\mathrm{u}_1,\ \nabla_3\mathrm{u}_2 \tag{6.26}$$

whilst the components with the same distribution are

$$\mathrm{u}_1 \sim \mathrm{u}_2,\ \nabla_1\mathrm{u}_1 \sim \nabla_2\mathrm{u}_2,\ \nabla_1\mathrm{u}_2 \sim \nabla_2\mathrm{u}_1,\ \nabla_1\mathrm{u}_3 \sim \nabla_2\mathrm{u}_3 \tag{6.27}$$

An immediate consequence of this is that all the non-diagonal components of $\nabla\mathbf{u}^{\top}(\boldsymbol{x}_p(t), t)$ have zero means, implying that the antisymmetric contribution from the fluid velocity gradient sampled by particles is on average zero. This is more concisely expressed in terms of the fluid rotation rate $\boldsymbol{\Omega}(\boldsymbol{x}_p(t), t)$ as

$$\left\langle \boldsymbol{\Omega}(\boldsymbol{x}_p(t), t) \right\rangle = \mathbf{0} \tag{6.28}$$

This makes sense intuitively, as when particles settle in the gravitational direction x_3, they would not be expected to be biased in either of the x_1 or x_2 directions as they alter their trajectory to pass around regions of high rotation. Consequently, sampling of the fluid rotation rate by particles would be expected to be evenly distributed in both the x_1 and x_2 directions. The implication of this is that the contribution to $\left\langle \nabla\mathbf{u}^{\top}(\boldsymbol{x}_p(t), t) \right\rangle$ emerges entirely from sampling of the average fluid strain rate along particle trajectories $\left\langle \boldsymbol{\Sigma}(\boldsymbol{x}_p(t), t) \right\rangle$.

6.5.4 Implications on the PDF Dispersion Tensors

Application of this analysis to the PDF dispersion tensor $\overline{\boldsymbol{\kappa}}(t)$ given in (6.10) requires use of the joint distribution of $\boldsymbol{r}_p$ and $\boldsymbol{\mathcal{H}}$, denoted $\phi(\boldsymbol{r}_p, \boldsymbol{\mathcal{H}}) = \phi(\boldsymbol{z})$. The transformation of this PDF into the frame of reference $\widetilde{\mathbf{x}}$ can then be realised using results from

probability theory. Specifically, for the arbitrary random variables $\boldsymbol{x}$ and $\boldsymbol{y}$ related to each other by $\boldsymbol{y} = \mathbb{F}(\boldsymbol{x})$, the transformation between the associated PDFs $\phi_X(\boldsymbol{x})$ and $\phi_Y(\boldsymbol{y})$ is given by [140]

$$\phi_Y(\boldsymbol{y}) = \phi_X(\boldsymbol{x}) \left| \det\left(\frac{\partial \mathbb{F}}{\partial \boldsymbol{x}} \right) \right|^{-1} \tag{6.29}$$

In terms of the distributions under consideration, taking $\boldsymbol{x} = \boldsymbol{z}$, $\boldsymbol{y} = \widetilde{\boldsymbol{z}}$, the Jacobian of the transformation as $\partial \mathbb{F}/\partial \boldsymbol{x} = \mathbb{P}$, the relation $\widetilde{\boldsymbol{z}} = \mathbb{P} \cdot \boldsymbol{z}$ shown to hold in (6.23), and further that $\phi_{\widetilde{\mathbf{Z}}} = \phi_{\mathbf{Z}}$ since it was demonstrated that the distribution of $\widetilde{\boldsymbol{z}}$ is the same as that of $\boldsymbol{z}$ then extracts from (6.29) the relation

$$\phi_{\mathbf{Z}}(\mathbb{P} \cdot \boldsymbol{z}) = \phi_{\mathbf{Z}}(\boldsymbol{z}) \tag{6.30}$$

It follows from the definition of expectation that for any function $\mathrm{F}(\boldsymbol{\zeta})$

$$\big\langle \mathrm{F}(\boldsymbol{z}) \big\rangle = \big\langle \mathrm{F}(\mathbb{P} \cdot \boldsymbol{z}) \big\rangle \tag{6.31}$$

In the context of the PDF kinetic framework, using the interpretation $\boldsymbol{z} = (\boldsymbol{r}_p, \boldsymbol{\mathcal{H}})$ it is necessary to consider sets of functions $\mathrm{F}_{\mathbf{n}}(\boldsymbol{\zeta})$ indexed by $\mathbf{n} \in \mathrm{S}^3$, $\mathrm{S} = \{1, 2, 3\}$ in order to understand the symmetries that are inherent within $\overline{\boldsymbol{\kappa}}(\mathbf{x}, t)$. The specific cases of interest are sets of functions such that

1. $\mathrm{F}_{\mathbf{n}}(\mathbb{P} \cdot \boldsymbol{\zeta}) = -\mathrm{F}_{\mathbf{n}}(\boldsymbol{\zeta}) \quad$ giving $\quad \langle \mathrm{F}_{\mathbf{n}}(\boldsymbol{z}) \rangle = -\langle \mathrm{F}_{\mathbf{n}}(\boldsymbol{z}) \rangle = 0$
2. $\mathrm{F}_{\mathbf{n}}(\mathbb{P} \cdot \boldsymbol{\zeta}) = \pm \mathrm{F}_{\mathbf{m}}(\boldsymbol{\zeta}) \quad$ giving $\quad \langle \mathrm{F}_{\mathbf{n}}(\boldsymbol{z}) \rangle = \pm \langle \mathrm{F}_{\mathbf{m}}(\boldsymbol{z}) \rangle$

Considering the integrand of $\overline{\boldsymbol{\kappa}}(t)$ in (6.10), denote the expression within the conditional average as

$$\mathrm{F}_{kji}(\boldsymbol{z}; t, t') = \mathcal{H}_{kj}[t; t'] \frac{\partial}{\partial \mathrm{x}_k} \mathrm{R}_{ji}(\boldsymbol{r}_p(t'; t), t - t') \tag{6.32}$$

The two-point two time correlation tensor $\mathbf{R}(\boldsymbol{r}_p(t'; t), t - t')$ and spatial gradient operator $\partial/\partial \mathbf{x}$ are further defined in the transformed coordinate system $\widetilde{\mathbf{x}}$ by

$$\widetilde{\mathbf{R}}(\widetilde{\boldsymbol{r}}_p(t'; t), t - t') = \mathbf{P} \cdot \mathbf{R}(\boldsymbol{r}_p(t'; t), t - t') \cdot \mathbf{P}^{\top} \quad , \quad \frac{\partial}{\partial \widetilde{\mathbf{x}}} = \mathbf{P} \cdot \frac{\partial}{\partial \mathbf{x}} \tag{6.33}$$

Then, omitting explicit reference to the time dependencies in F_{kji}, it follows that representation of F_{kji} in the frame of reference $\widetilde{\mathbf{x}}$ is given by the direct transformation

$$\mathrm{F}_{kji}\left(\widetilde{\boldsymbol{z}}\right) \;=\; \mathrm{F}_{kji}\left(\mathbb{P}\cdot\boldsymbol{z}\right) \;=\; \widetilde{\mathcal{H}}_{kj}\left[t;t'\right]\frac{\partial}{\partial\widetilde{\mathrm{x}}_k}\widetilde{\mathrm{R}}_{ji}\left(\widetilde{\boldsymbol{r}}_p\left(t';t\right),t-t'\right) \tag{6.34}$$

As a first-order tensor, $\partial/\partial\widetilde{\mathbf{x}}$ is transformed for a given instance of $\mathbf{P}$ in the same manner as $\widetilde{\boldsymbol{r}}_p$, whilst as a second-order tensor $\widetilde{\mathbf{R}}$ transforms in the same manner as $\widetilde{\boldsymbol{\mathcal{H}}}$, as both set out in Table 6.1. The conditional average of equation (6.34) is equal to the integrand of the dispersion tensor $\widetilde{\overline{\kappa}}_i\left(t\right)$ in the coordinate system $\widetilde{\mathbf{x}}$, meaning that the different cases of $\mathbf{P}$ given by ① - ⑥ can be used to infer which components of F_{kji} are symmetric, and thereby which components of $\overline{\kappa}_i\left(t\right)$ are non-zero. For instance, taking $\mathbf{P}=\mathbf{P}_1$ corresponding to the transform ①, by Table 6.1 it can be seen that

$$\mathrm{F}_{111}\left(\widetilde{\boldsymbol{z}}\right) \;=\; \widetilde{\mathcal{H}}_{11}\frac{\partial}{\partial\widetilde{\mathrm{x}}_1}\widetilde{\mathrm{R}}_{11} \;=\; \left(+\mathcal{H}_{11}\right)\left(-\frac{\partial}{\partial\mathrm{x}_1}\right)\left(+\mathrm{R}_{11}\right) \;=\; -\mathrm{F}_{111}\left(\boldsymbol{z}\right) \tag{6.35}$$

This component satisfies instance 1 of the sets of functions that are of interest in this system, and therefore $\mathrm{F}_{111}\left(\boldsymbol{z}\right)$ is an even function, and it follows that

$$\left\langle\,\mathrm{F}_{111}\left(\boldsymbol{z}\right)\,\right\rangle \;=\; \left\langle\,\mathcal{H}_{11}\frac{\partial}{\partial\mathrm{x}_1}\mathrm{R}_{11}\,\right\rangle \;=\; 0 \tag{6.36}$$

In the same fashion, using the transforms ①, ②, and ③, it is established for all values of k and j with $i=1,2$ that

$$\left\langle\,\mathrm{F}_{kji}\left(\boldsymbol{z}\right)\,\right\rangle \;=\; \left\langle\,\mathcal{H}_{kj}\frac{\partial}{\partial\mathrm{x}_k}\mathrm{R}_{ji}\,\right\rangle \;=\; 0 \quad,\quad \forall k,j\in\mathrm{S}\,,\; i\in\{1,2\} \tag{6.37}$$

Since (6.37) constitutes the integrand of $\overline{\kappa}_i\left(t\right)$ as given in (6.10), then by contraction of k and j for a given value of i, it immediately follows that $\overline{\kappa}_1\left(t\right)\equiv\overline{\kappa}_2\left(t\right)\equiv 0$. Thus the symmetries inherent in the system imply that there is no drift enhancement in the non-gravitational direction as required, however the transforms ①, ②, and ③ provide no information about $\overline{\kappa}_3\left(t\right)$, simply stating that $\mathrm{F}_{kj3}\left(\widetilde{\boldsymbol{z}}\right)=\mathrm{F}_{kj3}\left(\boldsymbol{z}\right)\;\forall k,j\in\mathrm{S}$. Simplification of $\overline{\kappa}_3\left(t\right)$ is achieved using $\mathbf{P}=\mathbf{P}_4$ corresponding to the transform ④, then use of Table 6.1 results in, for example,

$$\mathrm{F}_{113}\left(\widetilde{\boldsymbol{z}}\right) \;=\; \widetilde{\mathcal{H}}_{11}\frac{\partial}{\partial\widetilde{\mathrm{x}}_1}\widetilde{\mathrm{R}}_{13} \;=\; \left(+\mathcal{H}_{22}\right)\left(+\frac{\partial}{\partial\mathrm{x}_2}\right)\left(+\mathrm{R}_{23}\right) \;=\; \mathrm{F}_{223}\left(\boldsymbol{z}\right) \tag{6.38}$$

From this the equivalence of these two components of $\langle \mathrm{F}_{kj3}(\boldsymbol{z}) \rangle$ follows

$$\langle \mathrm{F}_{113}(\boldsymbol{z}) \rangle = \left\langle \mathcal{H}_{11} \frac{\partial}{\partial \mathrm{x}_1} \mathrm{R}_{13} \right\rangle = \left\langle \mathcal{H}_{22} \frac{\partial}{\partial \mathrm{x}_2} \mathrm{R}_{23} \right\rangle = \langle \mathrm{F}_{223}(\boldsymbol{z}) \rangle \tag{6.39}$$

Likewise, using the transform ④ to interchange the subscripts 1 and 2 also produces

$$\begin{aligned} \left\langle \mathcal{H}_{12} \frac{\partial}{\partial \mathrm{x}_1} \mathrm{R}_{23} \right\rangle &= \left\langle \mathcal{H}_{21} \frac{\partial}{\partial \mathrm{x}_2} \mathrm{R}_{13} \right\rangle \\ \left\langle \mathcal{H}_{13} \frac{\partial}{\partial \mathrm{x}_1} \mathrm{R}_{33} \right\rangle &= \left\langle \mathcal{H}_{23} \frac{\partial}{\partial \mathrm{x}_2} \mathrm{R}_{33} \right\rangle \\ \left\langle \mathcal{H}_{31} \frac{\partial}{\partial \mathrm{x}_3} \mathrm{R}_{13} \right\rangle &= \left\langle \mathcal{H}_{32} \frac{\partial}{\partial \mathrm{x}_3} \mathrm{R}_{23} \right\rangle \end{aligned} \tag{6.40}$$

Contraction of k and j in the expression $\mathcal{H}_{kj} \frac{\partial}{\partial \mathrm{x}_k} \mathrm{R}_{ji}$ along with use of the results (6.39) and (6.40) means that the number of terms appearing in the explicit expression for $\overline{\kappa}_3(t)$ can be reduced to

$$\begin{aligned} \overline{\kappa}_3(t) = \int_{t_0}^{t} \Bigg[2 \Bigg\{ \left\langle \mathcal{H}_{11} \frac{\partial}{\partial \mathrm{x}_1} \mathrm{R}_{13} \right\rangle + \left\langle \mathcal{H}_{12} \frac{\partial}{\partial \mathrm{x}_1} \mathrm{R}_{23} \right\rangle + \left\langle \mathcal{H}_{13} \frac{\partial}{\partial \mathrm{x}_1} \mathrm{R}_{33} \right\rangle \\ + \left\langle \mathcal{H}_{31} \frac{\partial}{\partial \mathrm{x}_3} \mathrm{R}_{13} \right\rangle \Bigg\} + \left\langle \mathcal{H}_{33} \frac{\partial}{\partial \mathrm{x}_3} \mathrm{R}_{33} \right\rangle \Bigg] \, dt' \end{aligned} \tag{6.41}$$

Making use of the fluid incompressibility expressed in the form $\frac{\partial}{\partial \mathbf{x}} \cdot \mathbf{R} = \mathbf{0}$ yields the alternative expression

$$\begin{aligned} \overline{\kappa}_3(t) = \int_{t_0}^{t} \Bigg[2 \Bigg\{ \left\langle \mathcal{H}_{12} \frac{\partial}{\partial \mathrm{x}_1} \mathrm{R}_{23} \right\rangle + \left\langle \mathcal{H}_{13} \frac{\partial}{\partial \mathrm{x}_1} \mathrm{R}_{33} \right\rangle + \left\langle \mathcal{H}_{31} \frac{\partial}{\partial \mathrm{x}_3} \mathrm{R}_{13} \right\rangle \Bigg\} \\ + \left\langle (\mathcal{H}_{33} - \mathcal{H}_{11}) \frac{\partial}{\partial \mathrm{x}_3} \mathrm{R}_{33} \right\rangle \Bigg] \, dt' \end{aligned} \tag{6.42}$$

In a two-dimensional system with $\mathbf{g} = (0, -\mathrm{g})$, this formula simplifies to

$$\overline{\kappa}_2(t) = \int_{t_0}^{t} \left[\left\langle \mathcal{H}_{12} \frac{\partial}{\partial \mathrm{x}_1} \mathrm{R}_{22} \right\rangle + \left\langle \mathcal{H}_{21} \frac{\partial}{\partial \mathrm{x}_2} \mathrm{R}_{12} \right\rangle + \left\langle (\mathcal{H}_{22} - \mathcal{H}_{11}) \frac{\partial}{\partial \mathrm{x}_2} \mathrm{R}_{22} \right\rangle \right] dt' \tag{6.43}$$

In conclusion, the preceding symmetry analysis has demonstrated that the components of $\overline{\boldsymbol{\kappa}}(t)$ are zero for directions which gravity does not act in, and further reduces the number of individual terms which require modelling for $\overline{\kappa}_d(t)$, where $d = \{2, 3\}$. Notwithstanding this, the terms in equations (6.42) and (6.43) are all of the same form, meaning that it is still appropriate to use a general modelling approach for the average $\left\langle \mathcal{H}_{kj} \frac{\partial}{\partial \mathrm{x}_k} \mathrm{R}_{ji} \right\rangle$ rather than model different components separately. Furthermore, the symmetry considerations do not provide any insight into the subsequent modelling process except that models should be compatible with these results, meaning that a more specific focus on the roles played by the separation along a particle trajectory $\boldsymbol{r}_p(t'; t)$ and the particle response tensor $\boldsymbol{\mathcal{H}}[t; t']$ is required.

6.6 Model Development in the PDF Kinetic Framework

In contrast to a homogeneous flow with no external body forces in which $\overline{\boldsymbol{\kappa}}(t) = 0$, the symmetry analysis of section 6.5 reveals that the addition of a gravitational body force means that the general form of $\overline{\boldsymbol{\kappa}}(t)$ becomes non-zero in the gravitational direction, however no information regarding the quantification of this value is provided. This naturally poses the question as to whether this phenomenon can be effectively modelled, however the majority of existing work on particle settling rate enhancement has focused upon furthering the understanding of the physical mechanisms involved rather than developing a simplified description of the behaviour. In terms of modelling this drift enhancement using the PDF kinetic framework, it is consequently prudent to start by examining the ability of existing closures developed for other flow configurations to capture this effect.

6.6.1 Use of Existing Closure Models

The existing closure strategies for the PDF dispersion tensors outlined in sections 4.4 and 4.5 make varying levels of approximation to the two-point two-time correlation tensor $\mathbf{R}\left(\boldsymbol{x}'_p, t'; \mathbf{x}, t\right)$, dependent on whether local or non-local effects are included within the modelling procedure. However, all previous work has approximated the particle response tensor $\boldsymbol{\mathcal{H}}[t; t']$ by using the Green's function approximation of neglecting the fluid velocity gradients in the governing equation (6.19), leading to the deterministic model given by (4.65). As discussed in section 4.6, attempting to use this manner of

closure for $\boldsymbol{\mathcal{H}}[t;t']$ in a configuration with a zero-mean flow results in $\overline{\boldsymbol{\kappa}}^{\mathrm{LHA}}(t)$ becoming identically zero, thus in the present context failing to capture any of the expected increase in particle settling velocity. In light of section 6.4 this is unsurprising, since the non-zero drift velocity observed by particles settling under gravity is seen to be a result of the hydrodynamic interaction between the separation along particle trajectories $\boldsymbol{r}_p(t';t)$ and $\boldsymbol{\mathcal{H}}[t;t']$ within the conditional average in the expression (6.10) for $\overline{\boldsymbol{\kappa}}(t)$. Because the LHA completely neglects the stochasticity of $\boldsymbol{\mathcal{H}}[t;t']$, the effect of any interaction with $\boldsymbol{r}_p(t';t)$ is therefore lost using this simple level of approximation, necessitating the need for a model which provides a more complete description of $\boldsymbol{\mathcal{H}}[t;t']$. This presents the challenge which is inherent in capturing the increase in particle settling velocity, and thereby highlights the need for an improved closure methodology for $\overline{\boldsymbol{\kappa}}(t)$ in this context.

6.6.2 Cumulant Expansion of the Conditional Average

From the isotropic representation of $\overline{\boldsymbol{\kappa}}(t)$ in the expression (6.12) it is explicit that the stochastic quantities within the conditional average that determine the drift enhancement are $\boldsymbol{r}_p(t';t)$ and $\boldsymbol{\mathcal{H}}[t;t']$. In order to include the full physical description of these quantities within the representation of $\overline{\boldsymbol{\kappa}}(t)$ given by (6.10), it is noted that the stochasticity which is intrinsic within the expression $\frac{\partial}{\partial \mathbf{x}}\mathbf{R}\left(\boldsymbol{x}_p', t';\mathbf{x},t\right)$ is solely characterised by $\boldsymbol{r}_p(t';t)$ in an isotropic flow field. The conditional average that requires closure can then expressed as a function of just $\boldsymbol{r}_p(t';t)$ and $\boldsymbol{\mathcal{H}}[t;t']$, and further since the distribution of these two quantities is independent of $\mathbf{x}$ in this configuration, the conditional average can be written simply as the ensemble average

$$\left\langle \mathcal{H}_{kj}\frac{\partial}{\partial \mathrm{x}_k}\mathrm{R}_{ji}\left(\boldsymbol{r}_p\right)\right\rangle \tag{6.44}$$

where all time dependencies are omitted for notational clarity. Considering $\boldsymbol{r}_p$ and $\boldsymbol{\mathcal{H}}$ as random variables, it is possible to formally express this ensemble average in terms of the joint PDF $\phi(\boldsymbol{r}_p, \boldsymbol{\mathcal{H}})$ of $\boldsymbol{r}_p$ and $\boldsymbol{\mathcal{H}}$ using the definition of expectation

$$\left\langle \mathcal{H}_{kj}\frac{\partial}{\partial \mathrm{x}_k}\mathrm{R}_{ji}\left(\boldsymbol{r}_p\right)\right\rangle = \int_{\boldsymbol{\mathcal{H}}}\int_{\boldsymbol{r}_p} \mathcal{H}_{kj}\frac{\partial}{\partial \mathrm{x}_k}\mathrm{R}_{ji}\left(\boldsymbol{r}_p\right)\phi\left(\boldsymbol{r}_p,\boldsymbol{\mathcal{H}}\right)\, d\boldsymbol{r}_p\, d\boldsymbol{\mathcal{H}} \tag{6.45}$$

Thus in order to close the ensemble average using this means, the distribution $\phi(\boldsymbol{r}_p, \boldsymbol{\mathcal{H}})$ needs to be known, requiring that a suitable model is proposed. In section 6.4 it was

noted that it is the variation in the distribution of $\boldsymbol{r}_p$ conditional on $\boldsymbol{\mathcal{H}}$ which results in the increased settling velocity of particles, however a probability distribution including such information would be non-trivial to model. An alternative method of expressing the ensemble average (6.44) more directly in terms of the stochastic quantities $\boldsymbol{r}_p$ and $\boldsymbol{\mathcal{H}}$ rather than the full PDF would provide a more tractable modelling framework, and therefore an appropriate way of examining the intrinsic behaviour of the system before introducing any approximations. In particular, since a PDF is fully determined by its moments, a means of expressing (6.44) in terms of the moments of $\phi\left(\boldsymbol{r}_p, \boldsymbol{\mathcal{H}}\right)$ would retain all the information embedded within the distribution whilst leading to a simplified description. Accordingly, a cumulant expansion of the average (6.44) in terms of $\boldsymbol{r}_p$ and $\boldsymbol{\mathcal{H}}$ is performed in Appendix B, with the result for the first four cumulants given by (B.11) as

$$\begin{aligned}\left\langle \mathcal{H}_{kj}\frac{\partial}{\partial \mathrm{x}_k}\mathrm{R}_{ji}(\boldsymbol{r}_p)\right\rangle \approx{}& \underbrace{\left\langle \mathcal{H}_{kj}\right\rangle \left\langle \frac{\partial}{\partial \mathrm{x}_k}\mathrm{R}_{ji}(\boldsymbol{r}_p)\right\rangle}_{\boxed{1}} + \underbrace{\left\langle \mathcal{H}'_{kj}r'_{p_m}\right\rangle \left\langle \frac{\partial}{\partial \mathrm{r}_m}\frac{\partial}{\partial \mathrm{x}_k}\mathrm{R}_{ji}(\boldsymbol{r}_p)\right\rangle}_{\boxed{2}} \\ &+ \underbrace{\frac{1}{2}\left\langle \mathcal{H}'_{kj}r'_{p_m}r'_{p_n}\right\rangle \left\langle \frac{\partial}{\partial \mathrm{r}_m}\frac{\partial}{\partial \mathrm{r}_n}\frac{\partial}{\partial \mathrm{x}_k}\mathrm{R}_{ji}(\boldsymbol{r}_p)\right\rangle}_{\boxed{3}} \\ &+ \underbrace{\frac{1}{6}\Big[\left\langle \mathcal{H}'_{kj}r'_{p_m}r'_{p_n}r'_{p_q}\right\rangle - \left\langle \mathcal{H}'_{kj}r'_{p_m}\right\rangle\left\langle r'_{p_n}r'_{p_q}\right\rangle - \left\langle \mathcal{H}'_{kj}r'_{p_n}\right\rangle\left\langle r'_{p_m}r'_{p_q}\right\rangle \\ &\quad - \left\langle \mathcal{H}'_{kj}r'_{p_q}\right\rangle\left\langle r'_{p_m}r'_{p_n}\right\rangle\Big]\left\langle \frac{\partial}{\partial \mathrm{r}_m}\frac{\partial}{\partial \mathrm{r}_n}\frac{\partial}{\partial \mathrm{r}_q}\frac{\partial}{\partial \mathrm{x}_k}\mathrm{R}_{ji}(\boldsymbol{r}_p)\right\rangle}_{\boxed{4}}\end{aligned} \tag{6.46}$$

This expression then describes the interaction between $\boldsymbol{r}_p$ and $\boldsymbol{\mathcal{H}}$ in the ensemble average (6.44) without any inferences made upon the form of the joint distribution $\phi\left(\boldsymbol{r}_p, \boldsymbol{\mathcal{H}}\right)$, and indeed the only approximation involved is truncation after the first four cumulants. To determine the relative contribution of each cumulant to the expansion (6.46), and in particular ascertain the significance of the higher-order cumulants on the mechanism of drift enhancement, the terms $\boxed{1} - \boxed{4}$ can be evaluated using numerical simulation. Additionally, the expansion (6.46) provides a framework for modelling the physical behaviour inherent in the ensemble average (6.44) at a more basic level, thus reducing the generality of the closure problem to a more specific set of unknown expres-

sions, which can be approached in a more straightforward manner from a modelling perspective.

6.6.3 Implications of the Cumulant Expansion on Existing Closures

The Green's function approximation for the particle response tensor $\boldsymbol{\mathcal{H}}\left[t;t'\right]$ is effectively a model for the average $\left\langle \boldsymbol{\mathcal{H}}\left[t;t'\right]\right\rangle$, meaning that the decoupling between $\left\langle \boldsymbol{\mathcal{H}}\right\rangle$ and $\left\langle \frac{\partial}{\partial \mathbf{x}}\mathbf{R}(\boldsymbol{r}_p)\right\rangle$ in the first term $\boxed{1}$ of the expansion (6.46) is an automatic consequence of using such an approximation, and as a result the Green's function approximation only has the capacity to include information contained within the first cumulant $\mathbf{K}^1 = \left\langle \boldsymbol{\mathcal{H}}\right\rangle$ of $\phi\left(\boldsymbol{r}_p, \boldsymbol{\mathcal{H}}\right)$. However, in the context of gravitational setting in a homogeneous flow, use of the Green's function approximation in the expression for $\overline{\boldsymbol{\kappa}}\left(t\right)$ produces a result of zero. Consequently the true contribution from the first term $\boxed{1}$ of the expansion can be assumed to be negligible, and therefore the dominant contribution towards the increase in particle settling velocity is likely to come from the second term $\boxed{2}$ in (6.46). The second cumulant $\mathbf{K}^2 = \left\langle \boldsymbol{\mathcal{H}}'\boldsymbol{r}_p'\right\rangle$ is the cross-correlation of the fluctuating quantities $\boldsymbol{r}_p'$ and $\boldsymbol{\mathcal{H}}'$, and due to the Green's function approximation being a deterministic quantity it only describes average behaviour, and therefore cannot contain any of the information within $\mathbf{K}^2$. On the other hand, the form of $\mathbf{K}^2$ explicitly accounts for the interaction between $\boldsymbol{r}_p'$ and $\boldsymbol{\mathcal{H}}'$ that was observed in section 6.4, and thus it is foreseen that the second term $\boxed{2}$ in (6.46) will be fundamental to the modelling process for capturing the increase in particle settling velocity in this context. Furthermore, there are no reasonable grounds on which to assume that the contributions from the third and fourth cumulants $\mathbf{K}^3$ and $\mathbf{K}^4$ can be neglected at this stage, which would be equivalent to assuming $\boldsymbol{r}_p'$ and $\boldsymbol{\mathcal{H}}'$ have a joint Gaussian distribution.

It is also worthwhile to note that all existing closures for the PDF kinetic model only include information about $\phi\left(\boldsymbol{r}_p, \boldsymbol{\mathcal{H}}\right)$ contained within the first cumulant $\mathbf{K}^1 = \left\langle \boldsymbol{\mathcal{H}}\right\rangle$ as a direct result of the average treatment of $\boldsymbol{\mathcal{H}}\left[t;t'\right]$. The reason that such an approach is able to produce accurate models is due to the behaviour of the ensemble average (6.44) being dominated by the effect of a non-zero mean flow on $\left\langle \boldsymbol{\mathcal{H}}\left[t;t'\right]\right\rangle$ over the interactions between $\boldsymbol{r}_p'$ and $\boldsymbol{\mathcal{H}}'$, meaning that the the second cumulant $\mathbf{K}^2$ is relatively insignificant in such flow configurations. On the other hand, for a configuration with a zero-mean flow, the contribution of $\left\langle \boldsymbol{\mathcal{H}}\left[t;t'\right]\right\rangle$ to the first cumulant $\mathbf{K}^1$ is negligible compared to the interactions between $\boldsymbol{r}_p'$ and $\boldsymbol{\mathcal{H}}'$, inferring that the second cumulant $\mathbf{K}^2$

encompasses the dominant contribution to the behaviour of the ensemble average (6.44) in these cases. Consequently, the effect of this higher-order behaviour will be smaller in magnitude than that of systems in which the first cumulant $\mathbf{K}^1$ is dominant, and furthermore the modelling process required to capture such higher-order behaviour is expected to be more intricate, with additional detail being needed in order to construct an accurate closure.

6.7 Closure of the Cumulant Expansion

To utilise the cumulant expansion (6.46) for modelling purposes, closure of the averages within the expansion still remains; specifically for the cumulants themselves as specified in terms of certain moments of $\phi\left(\boldsymbol{r}_p, \boldsymbol{\mathcal{H}}\right)$ in (B.7), and the average of derivatives of the two-point two-time correlation tensor $\mathbf{R}\left(\mathbf{x}', t'; \mathbf{x}, t\right)$ evaluated along particle trajectories $\boldsymbol{r}_p\left(t'; t\right)$. Both of these averages depend upon the stochastic particle behaviour through the particle response tensor $\boldsymbol{\mathcal{H}}\left[t; t'\right]$ and separation along a particle trajectory $\boldsymbol{r}_p\left(t'; t\right)$, and a closure methodology will require models for these two quantities. To that end, the evolution of both $\boldsymbol{\mathcal{H}}\left[t; t'\right]$ and particle trajectories $\boldsymbol{x}_p\left(t'\right)$ is governed by associated equations of motion which can be used for modelling purposes.

6.7.1 Representation of Separation along Particle Trajectories

Considering the particle trajectory $\boldsymbol{x}_p\left(t'\right)$, in the case of Stokes drag model (6.15) the solution can be represented directly since the equation of motion is linear. Subject to arbitrary initial conditions at time t' of $\boldsymbol{x}_p(t')$ and $\dot{\boldsymbol{x}}_p(t')$ and the assumption that $\mathbf{u}_p(s) = \mathbf{u}(\boldsymbol{x}_p(s), s)$ is considered to be a process along the particle trajectory, the solution is given by the integral form of a trajectory

$$\boldsymbol{x}_p(t) = \boldsymbol{x}_p(t') + \mathbf{V}_g(t - t') + h\left(t, t'\right)\left[\dot{\boldsymbol{x}}_p(t') - \mathbf{V}_g\right] + \beta \int_{t'}^{t} h\left(t, s\right) \mathbf{u}_p(s)\, ds \tag{6.47}$$

in which the kernel of the integral $h(t, t')$ is the Green's function of the Stokes drag model (6.15), given by

$$h\left(t, t'\right) = \frac{1}{\beta}\Big[1 - \exp\big[-\beta(t - t')\big]\Big] \tag{6.48}$$

The form of particle trajectory described by (6.47) is for a particle moving away from fixed initial conditions (FIT dispersion), and indeed this is reflected by the causality condition inherent in $h(t,t')$, with the Green's function growing exponentially for times $t < t'$. This poses a problem, as the particle trajectory $\boldsymbol{x}_p(t')$ which emerges in the dispersion tensors of the PDF kinetic model evolves through time towards final conditions $\boldsymbol{x}_p(t) = \mathbf{X}$ and $\dot{\boldsymbol{x}}_p(t) = \mathbf{V}$ (BIT dispersion), as stipulated by the conditional average within the dispersion tensors [13]. The correct physical description of such motion is given by the time-reversed particle equation of motion, however this is formally unstable, since the input from the fluid velocity $\mathbf{u}(\mathbf{x},t)$ then acts in the same direction as the particle velocity $\boldsymbol{v}_p(t)$. Consequently the transformed contribution $\big(\mathbf{u}(\mathbf{x},t)+\boldsymbol{v}_p(t)\big)$ that characterises the drag force within the time-reversed particle equation of motion is no longer physically representative of a slip velocity, and this causes numerical solutions to grow exponentially in time [63]. This is consistent with the causality condition in $h(t,t')$, and therefore explicit treatment of the time-reversed particle trajectories is not advisable.

As it is the spatial distribution of particles that are of interest in this work and not that of particle velocities, it is sufficient to consider the velocity averaged form of the PDF dispersion tensors throughout the present work. This only requires that the particle trajectory satisfies $\boldsymbol{x}_p(t) = \mathbf{X}$ at a later time t, with no need for trajectories to also satisfy $\dot{\boldsymbol{x}}_p(t) = \mathbf{V}$ as part of the conditional averaging involved. Thus to obtain an expression for $\boldsymbol{x}_p(t')$ as it moves along a trajectory towards a fixed endpoint, it is permissible to rearrange (6.47) for $\boldsymbol{x}_p(t')$ and apply the fixed final condition on particle location of $\boldsymbol{x}_p(t) = \mathbf{X}$ and arbitrary initial condition on particle velocity of $\dot{\boldsymbol{x}}_p(t') = \boldsymbol{v}^0$ [20]. This then yields an expression for the particle position at time t' given these conditions

$$\boldsymbol{x}_p(t') = \mathbf{X} - \mathbf{V}_g(t-t') - h(t,t')\left[\boldsymbol{v}^0 - \mathbf{V}_g\right] - \beta\int_{t'}^{t} h(t,s)\,\mathbf{u}_p(s)\,ds \tag{6.49}$$

As a result, (6.49) is formally a boundary value problem, subject to an initial velocity $\boldsymbol{v}^0$ and final position $\mathbf{X}$. Then taking the separation along a particle trajectory $\boldsymbol{r}_p(t';t)$ to be given by the endpoint of that trajectory $\mathbf{X}$ relative to the particle position $\boldsymbol{x}_p(t')$, i.e. $\boldsymbol{r}_p(t';t) = \mathbf{X} - \boldsymbol{x}_p(t')$, use of (6.49) produces

$$\boldsymbol{r}_p(t';t) = \mathbf{V}_g(t-t') + h(t,t')\left[\boldsymbol{v}^0 - \mathbf{V}_g\right] + \beta\int_{t'}^{t} h(t,s)\,\mathbf{u}_p(s)\,ds \tag{6.50}$$

This then provides a full description of the separation of a particle $\boldsymbol{x}_p(t')$ from the fixed trajectory endpoint $\mathbf{X}$ as the particle moves along its trajectory towards this endpoint. Furthermore, the spatial independence of $\boldsymbol{r}_p(t';t)$ emerges as expected through this manner of description, which is consistent with equation (6.50) only being of relevance in an isotropic velocity field. This is also accordant with the conditioning on the trajectory endpoint $\mathbf{X}$ not being necessary in homogeneous systems, in which case all trajectories then contribute to the ensemble average (6.44). Consequently, use of the time-reversed particle equation of motion to adequately capture the BIT dispersion that is intrinsic in the conditioning on particle trajectories is not required in homogeneous systems, with FIT dispersion providing an appropriate description of the particle evolution. This is reflected in the form of the separation along particle trajectories $\boldsymbol{r}_p(t';t)$ given in (6.50), with this expression being identical to the FIT description of a particle trajectory $\boldsymbol{x}_p(t)$ in (6.47) save for the initial position term. Nonetheless, for general inhomogeneous systems the conditioning on the trajectory endpoint $\mathbf{X}$ must be taken into account by considering the BIT dispersion of particles.

6.7.2 Representation of the Particle Response Tensor

Considering the particle response tensor $\boldsymbol{\mathcal{H}}[t;t']$, in the case of a Stokes drag model the fluid velocity gradient along particle trajectories $\nabla\mathbf{u}^\top(\boldsymbol{x}_p(t),t)$ appears as a multiplicative coefficient to $\boldsymbol{\mathcal{H}}[t;t']$ in the final term of the governing equation (6.19), meaning that a direct integral solution of this equation cannot be obtained in the same manner as for the particle equation of motion. Indeed, the analytical solution of (6.19) for $\boldsymbol{\mathcal{H}}[t;t']$ can be shown to be an infinite series involving time-ordered products of $\nabla\mathbf{u}_p^\top(t)$ (see Appendix A), the involvement of which makes it unsuitable for modelling purposes. Notwithstanding this, a simpler explicit representation of $\boldsymbol{\mathcal{H}}[t;t']$ can be obtained by starting from the more basic level of the particle equation of motion. Using the integral form of the Stokes drag model given in (6.47), and taking the functional derivative with respect to the fluid velocity along a particle trajectory at an earlier time t' yields

$$\frac{\delta\boldsymbol{x}_p(t)}{\delta\mathbf{u}(\boldsymbol{x}_p(t'),t')} = \frac{\delta\boldsymbol{x}_p(t')}{\delta\mathbf{u}(\boldsymbol{x}_p(t'),t')} + h(t,t')\frac{\delta\dot{\boldsymbol{x}}_p(t')}{\delta\mathbf{u}(\boldsymbol{x}_p(t'),t')} + \beta\int_{t'}^{t} h(t,s)\left[\frac{\partial\mathbf{u}_p(s)}{\partial\mathbf{x}}\right]^\top\cdot\frac{\delta\boldsymbol{x}_p(s)}{\delta\mathbf{u}(\boldsymbol{x}_p(t'),t')}\,ds$$

where the chain rule for functional differentiation has been applied to the final term. Making the interpretation $\boldsymbol{\mathcal{H}}[t;t'] = \delta\boldsymbol{x}_p(t)/\delta\mathbf{u}(\boldsymbol{x}_p(t'),t')$ as valid for a zero-mean flow

and consistent with the definition of the particle response tensor in (4.27), and also further subject to the appropriate initial conditions in (6.19), it is seen that $\boldsymbol{\mathcal{H}}\left[t;t'\right]$ therefore satisfies the integral equation

$$\boldsymbol{\mathcal{H}}\left[t;t'\right] = h(t,t')\mathbf{I} + \beta\int_{t'}^{t} h(t,s)\nabla\mathbf{u}_p^{\top}(s)\cdot\boldsymbol{\mathcal{H}}\left[s;t'\right]\,ds \tag{6.51}$$

Note that (6.51) expresses $\boldsymbol{\mathcal{H}}\left[t;t'\right]$ as the sum of an average particle response $h\left(t,t'\right)\mathbf{I}$ and a fluctuating response given by the integral term, in which $\nabla\mathbf{u}^{\top}(\boldsymbol{x}_p(t),t)$ is intrinsic. In particular, the first term of (6.51) is precisely the Green's function approximation for $\boldsymbol{\mathcal{H}}\left[t;t'\right]$ given in (4.65), meaning that in order to include sufficient information for describing the increase in particle settling velocity, at least some detail from the second term in (6.51) must be included within a representation for $\boldsymbol{\mathcal{H}}\left[t;t'\right]$. This highlights the dependence of $\boldsymbol{\mathcal{H}}\left[t;t'\right]$ on $\nabla\mathbf{u}^{\top}(\boldsymbol{x}_p(t),t)$, with the implication that the true solution of $\boldsymbol{\mathcal{H}}\left[t;t'\right]$ is inherently trajectory dependent. In principle (6.51) can be used recursively to include further detail within an explicit representation for $\boldsymbol{\mathcal{H}}\left[t;t'\right]$ [175, 176], and using this procedure once results in

$$\begin{aligned}\boldsymbol{\mathcal{H}}\left[t;t'\right] = h(t,t')\mathbf{I} &+ \beta\int_{t'}^{t} h(t,s)\nabla\mathbf{u}_p^{\top}(s)h(s,t')\,ds \\ &+ \beta^2\int_{t'}^{t}\int_{t'}^{t} h(t,s)h(t,s_1)\nabla\mathbf{u}_p^{\top}(s)\cdot\nabla\mathbf{u}_p^{\top}(s_1)\cdot\boldsymbol{\mathcal{H}}\left[s_1;t'\right]\,ds\,ds_1\end{aligned} \tag{6.52}$$

Continued use of such recursion results in higher-order terms which converge to zero due to the increased appearances of $h\left(t;t'\right)$ with differing time arguments, and the exponential form of $h\left(t;t'\right)$ in (6.48) then guaranteeing that the higher-order contributions have successively decreasing importance. It is therefore acceptable to truncate the expression (6.52) for $\boldsymbol{\mathcal{H}}\left[t;t'\right]$ by simply neglecting these higher-order contributions, and in this case taking just the first two terms leaves the approximation

$$\boldsymbol{\mathcal{H}}\left[t;t'\right] \approx h(t,t')\mathbf{I} + \beta\int_{t'}^{t} h(t,s)\nabla\mathbf{u}_p^{\top}(s)\,h(s,t')\,ds \tag{6.53}$$

This expression is equivalent to simply substituting the Green's function approximation (4.65) for $\boldsymbol{\mathcal{H}}\left[t;t'\right]$ into the final term of the exact integral equation (6.51), and results in an explicit integral representation for $\boldsymbol{\mathcal{H}}\left[t;t'\right]$ which can be used for modelling purposes. The approximation (6.53) can be considered the logical approach to including the next level of detail in an expression for $\boldsymbol{\mathcal{H}}\left[t;t'\right]$ within the framework of the recursion

(6.52). This is since the LHA constitutes the zeroth-order contribution to $\boldsymbol{\mathcal{H}}\left[t;t'\right]$, which is insufficient by itself for describing the increase in particle settling velocity, and therefore including the first-order contribution from (6.52) will incorporate the detail necessary for representing this effect. Note that the Green's function of the particle response tensor governing equation (6.19) is the same as that of Stokes drag model (6.15), resulting in the appearance of $h(t,t')$ as both the kernel of the integral term and also as the approximation to the response tensor within this term in (6.53), with differing time arguments for each. Crucially, this expression also retains information about the fluid velocity gradient along the particle trajectories, which is important in accounting for the history of fluid-particle interaction as this can have a substantial effect upon particle dispersion statistics. However, it should be noted that the coupling between components of $\nabla\mathbf{u}^{\top}(\boldsymbol{x}_p(t),t)$ and $\boldsymbol{\mathcal{H}}\left[t;t'\right]$ that is inherent in (6.51) is lost in (6.53), which may be significant in some flow configurations. In order to account for this coupling within an explicit representation for $\boldsymbol{\mathcal{H}}\left[t;t'\right]$, at least the second-order contribution from the recursion (6.52) would need to be included.

6.7.3 Decomposition into Mean and Fluctuating Contributions

For the purposes of model development using the cumulant expansion (6.46), the mean and fluctuating parts of the integral representations for $\boldsymbol{r}_p(t';t)$ and $\boldsymbol{\mathcal{H}}$ given by (6.50) and (6.53) respectively are also needed. The corresponding mean parts are given by

$$\left\langle \boldsymbol{r}_p(t';t)\right\rangle = \mathbf{V}_g(t-t') + h(t,t')\left[\left\langle \boldsymbol{v}^0\right\rangle - \mathbf{V}_g\right] + \beta\int_{t'}^{t} h(t,s)\left\langle \mathbf{u}_p(s)\right\rangle ds \tag{6.54}$$

$$\left\langle \boldsymbol{\mathcal{H}}\left[t;t'\right]\right\rangle \approx h(t,t')\mathbf{I} + \beta\int_{t'}^{t} h(t,s)\left\langle \nabla\mathbf{u}_p^{\top}(s)\right\rangle h(s,t')\,ds \tag{6.55}$$

whilst the associated fluctuating contributions, defined in the usual manner as $\boldsymbol{r}'_p(t';t) = \boldsymbol{r}_p(t';t) - \left\langle \boldsymbol{r}_p(t';t)\right\rangle$ and $\boldsymbol{\mathcal{H}}'\left[t;t'\right] = \boldsymbol{\mathcal{H}}\left[t;t'\right] - \left\langle \boldsymbol{\mathcal{H}}\left[t;t'\right]\right\rangle$ respectively, are then

$$\boldsymbol{r}'_p(t';t) = h(t,t')\boldsymbol{v}^{0\prime} + \beta\int_{t'}^{t} h(t,s)\mathbf{u}'_p(s)\,ds \tag{6.56}$$

$$\boldsymbol{\mathcal{H}}'\left[t;t'\right] \approx \beta\int_{t'}^{t} h(t,s)\nabla\mathbf{u}_p^{\top\prime}(s)\,h(s,t')\,ds \tag{6.57}$$

This provides expressions for evaluating the cumulants $\mathbf{K}^n$ of the expansion (6.46), which has the effect of reducing the required closures from the level of $\boldsymbol{r}_p(t';t)$ and $\boldsymbol{\mathcal{H}}[t;t']$ to the more fundamental processes $\mathbf{u}_p(s)$ and $\nabla\mathbf{u}_p^\top(s)$. The modelling of these closures is now considered.

6.7.4 Simple Approximations for the Mean Contributions

In the same vein as the LHA, the simplest possible model for stochastic quantities involves approximating them by their mean part. However for the mean contributions to $\boldsymbol{r}_p(t';t)$ and $\boldsymbol{\mathcal{H}}[t;t']$ given in (6.54) and (6.55) respectively, it is observed that in order to close these expressions there are three averages that require specification. Specifically, following the results in sections 6.2.1 and 6.2.2, use of both the particle mass flux representation and correlation splitting show that within the context of gravitational settling the averages $\langle\boldsymbol{v}^0\rangle$ and $\langle\mathbf{u}_p(s)\rangle$ are both directly proportional to $\overline{\boldsymbol{\kappa}}(t)$ in equations (6.2) and (6.9) respectively. Thus closure of the averages $\langle\boldsymbol{v}^0\rangle$ and $\langle\mathbf{u}_p(s)\rangle$ is equivalent to developing an approximation for $\overline{\boldsymbol{\kappa}}(t)$ at the top level of the problem under consideration. Without developing a recursive approach to the closure of $\overline{\boldsymbol{\kappa}}(t)$ which would considerably complicate the modelling process, this leaves the only reasonable approximation as using the existing LHA for these expressions. In the case of $\langle\mathbf{u}_p(s)\rangle$, using (6.9) with $\overline{\boldsymbol{\kappa}}^{\mathrm{LHA}} = \mathbf{0}$ simply yields

$$\langle\mathbf{u}_p(s)\rangle \approx \mathbf{0} \tag{6.58}$$

Use of (6.58) in the averaged equilibrium form of the Stokes drag model (6.4) then leads to approximation of $\langle\boldsymbol{v}^0\rangle$ as the Stokes settling velocity $\mathbf{V}_g$

$$\langle\boldsymbol{v}^0\rangle \approx \mathbf{V}_g \tag{6.59}$$

For the average $\langle\nabla\mathbf{u}_p^\top(s)\rangle$, it is possible to develop a closure by application of correlation splitting in the same manner as for $\langle\mathbf{u}_p(s)\rangle$ in section 6.2.2. The result for $\langle\nabla\mathbf{u}_p^\top(s)\rangle$ is derived in Appendix D.1, and consistent with the approximations for $\langle\mathbf{u}_p(s)\rangle$ and $\langle\boldsymbol{v}^0\rangle$, using the Green's function approximation in equation D.16 leads to

$$\langle\nabla\mathbf{u}_p^\top(s)\rangle \approx \mathbf{0} \tag{6.60}$$

Substituting the three approximations (6.58) - (6.60) into the expressions for the mean parts of $\boldsymbol{r}_p(t';t)$ and $\boldsymbol{\mathcal{H}}[t;t']$ given by (6.54) and (6.55) respectively then yields

$$\left\langle \boldsymbol{r}_p(t';t) \right\rangle \approx \mathbf{V}_g(t-t') \tag{6.61}$$

$$\left\langle \boldsymbol{\mathcal{H}}[t;t'] \right\rangle \approx h(t,t')\mathbf{I} \tag{6.62}$$

Thus (6.61) approximates $\left\langle \boldsymbol{r}_p(t';t) \right\rangle$ as the average rate of particle settling due to gravity, whilst (6.62) simply retrieves the existing Green's function approximation (4.65) for $\left\langle \boldsymbol{\mathcal{H}}[t;t'] \right\rangle$. As a consequence of the basic estimates (6.58) - (6.60) neglecting all fluctuations which occur in $\boldsymbol{r}_p(t';t)$ and $\boldsymbol{\mathcal{H}}[t;t']$ due to the stochastic nature of the underlying flow field, the drift enhancement that the modelling process is attempting to capture is also neglected in the approximations (6.61) and (6.62). Whilst this is a major shortcoming of these simple models, no alternative exists without analysing the processes $\boldsymbol{r}_p(t';t)$ and $\boldsymbol{\mathcal{H}}[t;t']$ in a higher level of detail.

6.7.5 Modelling the Spatial Derivatives of the Two-Point Two-Time Correlation Tensor along Particle Trajectories

Within the cumulant expansion (6.46), the terms $\boxed{1}$ - $\boxed{4}$ all contain spatial derivatives of the two-point two-time correlation tensor $\mathbf{R}(\boldsymbol{r}_p)$. In order to specify these derivatives, the spatial component of $\mathbf{R}$ is represented by appealing to isotropy as in (5.17). This enables an explicit representation for the spatial derivatives of $\mathbf{R}$ to be calculated for an isotropic flow, the detail of which is outlined in Appendix C. A natural approach to evaluating these derivatives along the particle trajectories $\boldsymbol{r}_p(t';t)$ is then to continue considering $\boldsymbol{r}_p$ as a random variable, and perform further expansions in terms of the cumulants of the distribution $\phi(\boldsymbol{r}_p)$. Whilst this approach clearly has the scope to include all the physical effects that are manifest in $\boldsymbol{r}_p$, it is appropriate to make simpler approximations at this stage since the spatial derivatives of $\mathbf{R}(\boldsymbol{r}_p)$ are expressed in terms of just $\boldsymbol{r}_p$, and no longer dependent on the particle response tensor $\boldsymbol{\mathcal{H}}$. Specifically, the model $\mathbf{r}_0(t';t)$ is introduced as the mean separation along a particle trajectory given in (6.61)

$$\mathbf{r}_0(t';t) = \left\langle \boldsymbol{r}_p(t';t) \right\rangle \approx \mathbf{V}_g(t-t') \tag{6.63}$$

This approximation removes the stochastic element of $\boldsymbol{r}_p(t';t)$, and therefore produces closures for the desired expressions

$$\left\langle \frac{\partial}{\partial \mathrm{x}_k} \mathrm{R}_{ji}(\boldsymbol{r}_p) \right\rangle \approx \frac{\partial}{\partial \mathrm{x}_k} \mathrm{R}_{ji}\big(\mathbf{r}_0(t';t)\big) \tag{6.64}$$

$$\left\langle \frac{\partial}{\partial \mathrm{r}_m} \frac{\partial}{\partial \mathrm{x}_k} \mathrm{R}_{ji}(\boldsymbol{r}_p) \right\rangle \approx \frac{\partial}{\partial \mathrm{r}_m} \frac{\partial}{\partial \mathrm{x}_k} \mathrm{R}_{ji}\big(\mathbf{r}_0(t';t)\big) \tag{6.65}$$

$$\left\langle \frac{\partial}{\partial \mathrm{r}_m} \frac{\partial}{\partial \mathrm{r}_n} \frac{\partial}{\partial \mathrm{x}_k} \mathrm{R}_{ji}(\boldsymbol{r}_p) \right\rangle \approx \frac{\partial}{\partial \mathrm{r}_m} \frac{\partial}{\partial \mathrm{r}_n} \frac{\partial}{\partial \mathrm{x}_k} \mathrm{R}_{ji}\big(\mathbf{r}_0(t';t)\big) \tag{6.66}$$

$$\left\langle \frac{\partial}{\partial \mathrm{r}_m} \frac{\partial}{\partial \mathrm{r}_n} \frac{\partial}{\partial \mathrm{r}_q} \frac{\partial}{\partial \mathrm{x}_k} \mathrm{R}_{ji}(\boldsymbol{r}_p) \right\rangle \approx \frac{\partial}{\partial \mathrm{r}_m} \frac{\partial}{\partial \mathrm{r}_n} \frac{\partial}{\partial \mathrm{r}_q} \frac{\partial}{\partial \mathrm{x}_k} \mathrm{R}_{ji}\big(\mathbf{r}_0(t';t)\big) \tag{6.67}$$

The models (6.64) - (6.67) can then be expressed explicitly in terms of $\mathbf{r}_0$ using the isotropic form of the spatial derivatives of $\mathbf{R}$ as given by (C.16), (C.20), (C.23), and (C.26) respectively. To further account for the fact that the correlations are along particle trajectories, the fluid Eulerian integral timescale τ_E associated with the temporal decorrelation $\mathrm{E}_\omega(t-t')$ can be replaced with an appropriate Lagrangian timescale. Specifically, using τ_E as given in (5.27) for the KS velocity field in conjunction with the definition of $\mathrm{E}_\omega(t-t')$ in (5.15) and substituting the fluid timescale along a particle trajectory τ_{Lp} for τ_E results in the modified temporal decorrelation

$$\mathrm{E}_{\tau_{Lp}}(t-t') = \exp\left[-\frac{1}{2}\frac{\pi}{2\tau_{Lp}^2}(t-t')^2\right] \tag{6.68}$$

Use of this decorrelation within the models (6.64) - (6.67) then completes the closure of the spatial derivatives of $\mathbf{R}$ along particle trajectories, leaving just modelling of the cumulants (B.7) themselves remaining to be specified within the expansion (6.46).

6.7.6 Inefficacy of the Green's Function Approximation

Although the focus is on developing an accurate model which captures the effect of the drift enhancement and is able to relate this to the underlying fluid-particle interaction mechanisms, it is worth considering application of the Green's function approximation to the cumulant expansion (6.46) to determine if a simple model for the drift enhancement can be produced from existing approximations. This would attribute

any improvement in accuracy to the closure strategy of utilising a cumulant expansion, rather than alternative physical assumptions or additional input from simulation data.

The higher-order cumulants $\boxed{3}$ and $\boxed{4}$ in (6.46) will contribute less to the drift enhancement than the first two, and therefore attention is restricted to $\boxed{1}$ and $\boxed{2}$

$$\left\langle \mathcal{H}_{kj} \frac{\partial}{\partial \mathrm{x}_k} \mathrm{R}_{ji}(\boldsymbol{r}_p) \right\rangle \approx \underbrace{\left\langle \mathcal{H}_{kj} \right\rangle \left\langle \frac{\partial}{\partial \mathrm{x}_k} \mathrm{R}_{ji}(\boldsymbol{r}_p) \right\rangle}_{\boxed{1}} + \underbrace{\left\langle \mathcal{H}'_{kj} r'_{p_m} \right\rangle \left\langle \frac{\partial}{\partial \mathrm{r}_m} \frac{\partial}{\partial \mathrm{x}_k} \mathrm{R}_{ji}(\boldsymbol{r}_p) \right\rangle}_{\boxed{2}} \tag{6.69}$$

Within these terms, it is the cumulants $\mathbf{K}^1$ and $\mathbf{K}^2$ themselves which require approximating. In $\boxed{1}$, this entails modelling of $\langle\, \boldsymbol{\mathcal{H}}\,[t;t']\,\rangle$, for which the Green's function approximation (6.62) can be used directly. The consequence of this is that the isotropic form of (6.62) immediately results in the contraction $\frac{\partial}{\partial \mathrm{x}_j}\mathrm{R}_{ji}(\boldsymbol{r}_p)$, producing a result of zero due to incompressibility of the flow field, meaning that there is no contribution from the first cumulant.

$$\left\langle \mathcal{H}_{kj} \right\rangle \left\langle \frac{\partial}{\partial \mathrm{x}_k} \mathrm{R}_{ji}(\boldsymbol{r}) \right\rangle \approx h(t,t') \left\langle \frac{\partial}{\partial \mathrm{x}_j} \mathrm{R}_{ji}(\boldsymbol{r}) \right\rangle \equiv 0 \tag{6.70}$$

This leaves the remaining term $\boxed{2}$, in which the second cumulant $\langle \boldsymbol{\mathcal{H}}' \boldsymbol{r}'_p \rangle$ requires modelling, necessitating the use of expressions for the fluctuating quantities $\boldsymbol{\mathcal{H}}'$ and $\boldsymbol{r}'_p$. However, the Green's function approximation only describes average behaviour, and therefore consistent with (6.61) and (6.62) approximations for the fluctuations are given by

$$\boldsymbol{r}'_p(t';t) \approx \mathbf{0} \tag{6.71}$$

$$\boldsymbol{\mathcal{H}}'[t;t'] \approx \mathbf{0} \tag{6.72}$$

Thus the second cumulant $\mathbf{K}^2$ is simply approximated as

$$\left\langle \mathcal{H}'_{kj} r'_{p_m} \right\rangle \approx 0 \tag{6.73}$$

Therefore in keeping with direct use in the dispersion tensor $\overline{\boldsymbol{\kappa}}(t)$, use of the Green's function approximation in the cumulant expansion (6.69) also produces a trivial ap-

proximation which does not capture any of the observed drift enhancement. This is also consistent with the discussion in section 6.6.3 that the Green's function approximation is only capable of retrieving behaviour contained within the first cumulant $\mathbf{K}^1$ of the distribution $\phi\left(\boldsymbol{r}_p, \boldsymbol{\mathcal{H}}\right)$, highlighting the need for more detailed modelling of the cumulants themselves that is able to include the higher-order behaviour.

6.7.7 Modelling of the Second Cumulant

Focusing attention upon the second term $\boxed{2}$ in the expansion (6.69), it is evident that the Local Homogeneous Approximation breaks down in (6.73) due to inadequate representations of the fluctuating quantities $\boldsymbol{\mathcal{H}}'$ and $\boldsymbol{r}_p'$. In order to develop a model which includes sufficient information about these processes, the integral forms presented in (6.56) and (6.57) are utilised; note that at this level the expression for $\boldsymbol{r}_p'$ is exact, whilst that for $\boldsymbol{\mathcal{H}}'$ is an approximation due to the truncation of the recursive expression (6.52). This produces an associated integral expression for the second cumulant

$$\begin{aligned}\left\langle \mathcal{H}_{kj}'[t,t']\, r_{p_m}'(t';t)\right\rangle \approx \beta h(t,t') \int_{t'}^{t} h(t,s)\left\langle \nabla_j \mathrm{u}_{p_k}{}'(s) v_m^{0}{}'(t')\right\rangle h(s,t')\, ds \\ + \beta^2 \int_{t'}^{t}\int_{t'}^{t} h(t,s_1)h(t,s_2)\left\langle \nabla_j \mathrm{u}_{p_k}'(s_1)\mathrm{u}_{p_m}'(s_2)\right\rangle h(s_1,t')\, ds_1 ds_2\end{aligned} \tag{6.74}$$

It is seen that the stochastic behaviour in this expression is contained within the cross-correlations of the fluctuating fluid velocity gradient along particle trajectories $\nabla \mathbf{u}_p^{\top\prime}(s_1)$ with the fluctuating fluid velocity along particle trajectories $\mathbf{u}_p'(s_2)$ and initial fluctuating particle velocity $\boldsymbol{v}^{0\prime}(t')$. To develop a closure model for the second cumulant of the expansion, these correlations require specification.

To begin with, the correlation $\left\langle \nabla \mathbf{u}_p^{\top\prime}(s_1)\mathbf{u}_p'(s_2)\right\rangle$ in the second term of (6.74) is focused upon. Writing the fluctuating components in terms of their original full and averaged variables gives

$$\left\langle \nabla_j \mathrm{u}_{p_k}'(s_1)\mathrm{u}_{p_m}'(s_2)\right\rangle = \left\langle \nabla_j \mathrm{u}_{p_k}(s_1)\mathrm{u}_{p_m}(s_2)\right\rangle - \left\langle \nabla_j \mathrm{u}_{p_k}(s_1)\right\rangle\left\langle \mathrm{u}_{p_m}(s_2)\right\rangle \tag{6.75}$$

In the second term of (6.75), closure of the averages $\left\langle \nabla \mathbf{u}_p^{\top}(s_1)\right\rangle$ and $\left\langle \mathbf{u}_p(s_2)\right\rangle$ is equivalent to modelling of the drift enhancement effect at the top level, and therefore as

before these averages are simply approximated as zero in (6.58) and (6.60). This leaves the cross-correlation in the first term of (6.75) remaining. For a standard correlation of fluid velocities along a particle trajectory, the usual modelling approach consists of using a temporal decorrelation function $\psi(s_1 - s_2)$ characterised by an appropriate timescale τ_{Lp} along particle trajectories, with the one-point one-time RMS fluid velocity u' as a multiplier. However, since the cross-correlation of the Lagrangian fluid velocity and fluid velocity gradients are being dealt with in this case, the approach of assuming a simple decorrelation function cannot be applied. The current literature does not address the direct modelling of the cross-correlation (6.75), with the most appropriate work being an examination into the structure of the velocity-vorticity correlations [29], which provided insight into the form of these correlations using DNS but did not attempt modelling of the behaviour.

The form of the correlation (6.75) is expected to be inherently anisotropic, due to the Lagrangian nature of the quantities $\nabla \mathbf{u}_p^{\top\prime}(s_1)$ and $\mathbf{u}_p'(s_2)$ and the reduction in symmetry of the particle phase within this configuration. Nonetheless, to proceed from here the lack of a suitable model necessitates a simplified approach, and to that end it is noted that the spatial derivative of the *Eulerian* two-point two-time correlation tensor $\mathbf{R}(\mathbf{x}', t'; \mathbf{x}, t)$ can be expressed for a zero-mean flow field as

$$\frac{1}{\beta^2}\frac{\partial}{\partial \mathrm{x}_k}\mathrm{R}_{ji}(\mathbf{x}', t'; \mathbf{x}, t) \equiv \Big\langle \mathrm{u}_j(\mathbf{x}', t')\nabla_k \mathrm{u}_i(\mathbf{x}, t)\Big\rangle \tag{6.76}$$

Since $\frac{\partial}{\partial \mathrm{x}_k}\mathrm{R}_{ji}(\mathbf{r})$ is a third-order tensor isotropic tensor, it is an odd function of the spatial separation $\mathbf{r} = \mathbf{x} - \mathbf{x}'$ (as seen upon examination of (C.16)). This implies that for $\mathbf{r} = \mathbf{0}$ the one-point cross-correlation in the Eulerian sense is equal to zero, demonstrating that the behaviour of this cross-correlation is not that of a simple decorrelation function. In order to model the correlation of the Lagrangian quantities $\nabla \mathbf{u}_p^{\top\prime}(s_1)$ and $\mathbf{u}_p'(s_2)$ along particle trajectories consistently with the forms that arise in equation (6.74), the descriptions must be restricted to time-dependent processes rather than a location and time dependent fields. To that end, the spatial dependence within $\frac{\partial}{\partial \mathrm{x}_k}\mathrm{R}_{ji}(\mathbf{r})$ is manifest within the separation vector $\mathbf{r}$, meaning that a suitable model is required that represents this separation in terms of time. Since the correlation in question (6.75) is for quantities that are evaluated along particle trajectories, it is appropriate to also use a model for $\boldsymbol{r}_p(t'; t)$ to account for this, and specifically the simple approximation of using the average particle separation $\mathbf{r}_0(t'; t) \approx \mathbf{V}_g(t - t')$ in (6.63) is invoked. The cross-correlation (6.75) along particle trajectories is then approximated by the isotropic model

$$\left\langle \nabla_j \mathrm{u}_{p_k}(t) \mathrm{u}_{p_m}(t') \right\rangle \approx \frac{1}{\beta^2} \frac{\partial}{\partial \mathrm{x}_j} \mathrm{R}_{mk}\big(\mathbf{r}_0(t';t)\big) \tag{6.77}$$

Some detail of the true structure of these cross-correlations is unavoidably lost by using an isotropic model, however (6.77) is still expected to capture the leading-order behaviour of this interaction. Evaluating the right hand side of (6.77) through use of the expression for $\frac{\partial}{\partial \mathrm{x}_j}\mathrm{R}_{mk}(\mathbf{r})$ given in (C.16), approximation for separation along particle trajectories $\mathbf{r}_0(t';t)$ in (6.63), and the model for the temporal decorrelation function along particle trajectories in (6.68) produces the explicit form

$$\begin{aligned}\left\langle \nabla_j \mathrm{u}_{p_k}(t) \mathrm{u}_{p_m}(t') \right\rangle \approx \frac{1}{d-1} u'^2 \sigma_k^2 \Big[\Big(\sigma_k^2 V_g^2 (t-t')^2 - (d+1) \Big) V_{g_j} \delta_{km}(t-t') \\ - \sigma_k^2 V_{g_j} V_{g_m} V_{g_k} (t-t')^3 + V_{g_m} \delta_{jk}(t-t') + V_{g_k} \delta_{mj}(t-t') \Big] \\ \cdot \exp\left[-\frac{1}{2} \left\{ \sigma_k^2 V_g^2 + \frac{\pi}{2\tau_{Lp}^2} \right\} (t-t')^2 \right]\end{aligned} \tag{6.78}$$

Within this isotropic expression three terms are of leading order in $(t-t')$, whilst two third-order terms appear. To simplify the modelling procedure it is chosen to neglect the third-order terms, both because their contribution is negligible compared to terms which are linear in time separation, but also since $V_{g_i} = 0$ for $i \neq d$ the second third-order term is non-zero for just one component of the tensor. The final model for the cross-correlation of the fluctuating Lagrangian fluid velocity gradient and fluid velocity in (6.75) is then

$$\begin{aligned}\left\langle \nabla_j \mathrm{u}'_{p_k}(t) \mathrm{u}'_{p_m}(t') \right\rangle \approx \frac{1}{d-1} u'^2 \sigma_k^2 \Big[V_{g_m} \delta_{jk} + V_{g_k} \delta_{mj} - (d+1) V_{g_j} \delta_{km} \Big] \\ \cdot (t-t') \exp\left[-\frac{1}{2} \left\{ \sigma_k^2 V_g^2 + \frac{\pi}{2\tau_{Lp}^2} \right\} (t-t')^2 \right]\end{aligned} \tag{6.79}$$

The first term of (6.74) contains the correlation $\left\langle \nabla \mathbf{u}_p^{\top\prime}(s) \boldsymbol{v}^{0\prime}(t') \right\rangle$, and in the same manner as before this can be expressed using the decomposition

$$\left\langle \nabla_j \mathrm{u}'_{p_k}(s) v_m^{0\,\prime}(t') \right\rangle = \left\langle \nabla_j \mathrm{u}_{p_k}(s) v_m^0(t') \right\rangle - \left\langle \nabla_j \mathrm{u}_{p_k}(s) \right\rangle \left\langle v_m^0(t') \right\rangle \tag{6.80}$$

Making the approximation $\left\langle \nabla \mathbf{u}_p^\top(s) \right\rangle = \mathbf{0}$ as before leaves just the first term remaining, for which there is no obvious method of evaluation. In the absence of an established model for such a correlation, in this case explicit approximation of the particle velocity $\boldsymbol{v}^0(t')$ is considered. In particular, using the equilibrium form of the *instantaneous* Stokes drag model (6.15) as an approximation yields the simple substitution $\boldsymbol{v}^0(t') \approx \mathbf{u}_p(t') + \mathbf{V}_g$, resulting in (6.80) becoming

$$\left\langle \nabla_j \mathrm{u}_{p_k}(s) v_m^0(t') \right\rangle \approx \left\langle \nabla_j \mathrm{u}_{p_k}(s) \mathrm{u}_{p_m}(t') \right\rangle + \left\langle \nabla_j \mathrm{u}_{p_k}(s) \right\rangle V_{g_m} \tag{6.81}$$

This a strong approximation, and neglects the true behaviour of the fluid velocity gradient - particle velocity interactions. In principle, it is possible to include some of this behaviour by constructing a model for the one-point one-time correlations $\left\langle \nabla \mathbf{u}_p^\top(t) \boldsymbol{v}^0(t) \right\rangle$ as outlined in Appendix D.2, however this approach is not considered in the present modelling procedure. Using the simple model in (6.81), the second term vanishes due to the existing approximation of $\left\langle \nabla \mathbf{u}_p^\top(s) \right\rangle = \mathbf{0}$, whilst the first term is now equal to the first term of (6.75), and can thus also be modelled using (6.79). This therefore leads to the same model as before for (6.80)

$$\begin{aligned} \left\langle \nabla_j \mathrm{u}'_{p_k}(t) v_m^{0\,\prime}(t') \right\rangle \approx \frac{1}{d-1} u'^2 \sigma_k^2 \Big[V_{g_m}\delta_{jk} + V_{g_k}\delta_{mj} - (d+1) V_{g_j}\delta_{km} \Big] \\ \cdot (t-t') \exp\left[-\frac{1}{2} \left\{ \sigma_k^2 V_g^2 + \frac{\pi}{2\tau_{Lp}^2} \right\} (t-t')^2 \right] \end{aligned} \tag{6.82}$$

Specification of (6.79) and (6.82) completes the closure of the expression for the second cumulant $\left\langle \boldsymbol{\mathcal{H}}'[t,t']\, \boldsymbol{r}'_p(t';t) \right\rangle$ in (6.74), resulting in the explicit model

$$\begin{aligned} \left\langle \mathcal{H}'_{kj}[t;t'] r'_{p_m}(t';t) \right\rangle \approx \frac{1}{d-1} \beta u'^2 \sigma_k^2 \Big[V_{g_k}\delta_{mj} + V_{g_m}\delta_{jk} - (d+1) V_{g_j}\delta_{km} \Big] h(t,t') \\ \cdot \int_{t'}^{t} (s-t') h(t,s) h(s,t') \exp\left[-\frac{1}{2} \left\{ \sigma_k^2 V_g^2 + \frac{\pi}{2\tau_{Lp}^2} \right\} (s-t')^2 \right] ds \\ + \frac{1}{d-1} \beta^2 u'^2 \sigma_k^2 \Big[V_{g_k}\delta_{mj} + V_{g_m}\delta_{jk} - (d+1) V_{g_j}\delta_{km} \Big] \int_{t'}^{t} \int_{t'}^{t} (s_1 - s_2) \\ \cdot h(t,s_1) h(t,s_2) h(s_1,t') \exp\left[-\frac{1}{2} \left\{ \sigma_k^2 V_g^2 + \frac{\pi}{2\tau_{Lp}^2} \right\} (s_1-s_2)^2 \right] ds_1 ds_2 \end{aligned} \tag{6.83}$$

Denoting the decorrelation parameter by

$$A = \frac{1}{2}\left\{\sigma_k^2 V_g^2 + \frac{\pi}{2\tau_{Lp}^2}\right\} \tag{6.84}$$

along with the two integrals which appear as

$$\mathcal{M}_{\text{int}}(t;t') = \beta h(t,t') \int_{t'}^{t} (s-t') h(t,s) h(s,t') \exp\left(-A(s-t')^2\right)\, ds \tag{6.85}$$

$$\mathcal{N}_{\text{int}}(t;t') = \beta^2 \int_{t'}^{t}\int_{t'}^{t} (s_1-s_2) h(t,s_1) h(t,s_2) h(s_1,t') \exp\left(-A(s_1-s_2)^2\right)\, ds_1 ds_2 \tag{6.86}$$

leads to the more compact form

$$\left\langle \mathcal{H}'_{kj}[t;t'] r'_{p_m}(t';t)\right\rangle \approx \frac{1}{d-1} u'^2 \sigma_k^2 \Big[V_{g_k}\delta_{mj} + V_{g_m}\delta_{jk} - (d+1) V_{g_j}\delta_{km}\Big]\Big(\mathcal{M}_{\text{int}}(t;t') + \mathcal{N}_{\text{int}}(t;t')\Big) \tag{6.87}$$

To complete the modelling of the second term $\boxed{2}$ in the expansion (6.69), the cumulant $\left\langle \boldsymbol{\mathcal{H}}' \boldsymbol{r}'_p\right\rangle$ is contracted with the second derivative of the correlation tensor evaluated along particle trajectories $\left\langle \frac{\partial}{\partial \mathrm{r}_m}\frac{\partial}{\partial \mathrm{x}_k}\mathrm{R}_{ji}\big(\mathbf{r}_0(t';t)\big)\right\rangle$, as given in (6.65). The explicit expression for the latter model in d-dimensional physical space is

$$\begin{aligned}
\frac{\partial}{\partial \mathrm{r}_m}\frac{\partial}{\partial \mathrm{x}_k}\mathrm{R}_{ji}\big(\mathbf{r}_0(t';t)\big) = \frac{1}{d-1}\beta^2 u'^2 \sigma_k^2 \Big\{ & \sigma_k^4 V_{g_m} V_{g_k} V_{g_j} V_{g_i} (t-t')^4 \\
& + \sigma_k^2 \left[(d+3) - \sigma_k^2 V_g^2 (t-t')^2\right] V_{g_m} V_{g_k} \delta_{ji} (t-t')^2 - \sigma_k^2 \Big[V_{g_j} V_{g_i}\delta_{mk} \\
& + V_{g_k} V_{g_i}\delta_{mj} + V_{g_k} V_{g_j}\delta_{mi} + V_{g_m} V_{g_j}\delta_{ki} + V_{g_m} V_{g_i}\delta_{kj}\Big] (t-t')^2 \\
& + \left[\sigma_k^2 V_g^2 (t-t')^2 - (d+1)\right]\delta_{mk}\delta_{ji} + \delta_{mj}\delta_{ik} + \delta_{mi}\delta_{jk}\Big\} \\
& \cdot \exp\left[-A(t-t')^2\right]
\end{aligned} \tag{6.88}$$

in which the decorrelation parameter A defined in (6.84) is again used. Then contraction of $\left\langle \boldsymbol{\mathcal{H}}' \boldsymbol{r}'_p\right\rangle$ given by (6.87) with (6.88) presents the final expression for the second term $\boxed{2}$ of (6.69) as

$$\left\langle \mathcal{H}'_{kj}[t;t']r'_{p_m}(t';t)\right\rangle \left\langle \frac{\partial}{\partial \mathrm{r}_m}\frac{\partial}{\partial \mathrm{x}_k}\mathrm{R}_{ji}(\boldsymbol{r}_p)\right\rangle$$
$$\approx -\frac{d+1}{d-1}\beta^2 u'^4\sigma_k^4 V_{g_i}\left[\sigma_k^2 V_g^2\left(t-t'\right)^2-(d+2)\right]\exp\left[-A\left(t-t'\right)^2\right]\left(\mathcal{M}_{\mathrm{int}}(t;t')+\mathcal{N}_{\mathrm{int}}(t;t')\right) \tag{6.89}$$

From the appearance of V_{g_i} within this expression it directly follows that this cumulant only makes a contribution in the direction which gravity acts in, consistent with the symmetry arguments in section 6.5. In principle the two integrals given by $\mathcal{M}_{\mathrm{int}}(t;t')$ and $\mathcal{N}_{\mathrm{int}}(t;t')$ in (6.85) and (6.86) respectively can be evaluated analytically, however the number of terms quickly becomes excessive due to $h(t;t')$ containing two terms and the complexities involved in integrating the error function, meaning that such an approach would produce expressions which are unsuitable for modelling purposes. This is compounded in the case of $\mathcal{N}_{\mathrm{int}}(t;t')$ as it is a double integral. Yet further time integration would then be required to evaluate the drift enhancement directly by calculating $\overline{\boldsymbol{\kappa}}(t)$ from the resultant expressions within the cumulant expansion (6.46). This final step of integration contains terms which cannot be evaluated using standard analytical techniques, and therefore it is most appropriate to evaluate the closure model for the second cumulant $\left\langle \boldsymbol{\mathcal{H}}'\boldsymbol{r}'_p\right\rangle$ numerically over an appropriate time interval. Alternative analytical approaches are to consider the asymptotic behaviour of the closure under certain limiting constraints, e.g. small St, large V_g, or small $\boldsymbol{r}_p$, or linearisation of certain parts of the integrands for $\mathcal{M}_{\mathrm{int}}(t;t')$ and $\mathcal{N}_{\mathrm{int}}(t;t')$, however these avenues of investigation are not pursued here.

6.7.8 Modelling of the First Cumulant

Now considering the first term $\boxed{1}$ in the cumulant expansion (6.69), it is clear that the LHA gives a net zero result in (6.70) due to inadequate representation of the mean of the response tensor $\left\langle \boldsymbol{\mathcal{H}}[t;t']\right\rangle$ using (6.62). To include a fuller description of $\left\langle \boldsymbol{\mathcal{H}}[t;t']\right\rangle$, it is appropriate to use the integral representation for the average of $\left\langle \boldsymbol{\mathcal{H}}[t;t']\right\rangle$ as given in (6.55), namely

$$\left\langle \boldsymbol{\mathcal{H}}\left[t;t'\right]\right\rangle \approx h(t,t')\mathbf{I}+\beta\int_{t'}^{t}h(t,s)\left\langle \nabla\mathbf{u}_p^{\top}(s)\right\rangle h(s,t')\,ds \tag{6.90}$$

Therefore the problem at this point is focused upon closure of the average fluid velocity gradient along a particle trajectory $\left\langle \nabla\mathbf{u}_p^{\top}(s)\right\rangle$. In the same manner as for the fluid

velocity along a particle trajectory $\langle \mathbf{u}_p(s) \rangle$ in section 6.2.2, it is possible to use correlation splitting on this expression, the detail of which is contained within Appendix D.1. In the case of a homogeneous Gaussian fluid velocity field, the result is given by D.16 as the dispersion tensor

$$\langle \nabla_l \mathrm{u}_{p_i}(t) \rangle = \frac{1}{\beta} \int_{t_0}^{t} \left\langle \mathcal{H}_{kj}[t;t'] \frac{\partial}{\partial \mathrm{x}_l} \frac{\partial}{\partial \mathrm{x}_k} \mathrm{R}_{ji}(\boldsymbol{x}'_p, t'; \mathbf{x}, t) \right\rangle dt' \tag{6.91}$$

In order to capture the behaviour of $\langle \nabla \mathbf{u}_p^\top(t) \rangle$ adequately, the integrand in (6.91) requires closure in the same manner as that of $\overline{\boldsymbol{\kappa}}(t)$ (compare to equation (6.10)). To that end, the cumulant expansion for an arbitrary phase-space variable $\boldsymbol{z}$ as given in (B.8) is applied to the integrand of (6.91) with the interpretations $\boldsymbol{z} = (\boldsymbol{r}_p, \boldsymbol{\mathcal{H}})$, and $f(\boldsymbol{z}) = \frac{\partial}{\partial \mathrm{x}_l} \frac{\partial}{\partial \mathrm{x}_k} \mathrm{R}_{ji}(\boldsymbol{z})$. Since the random variable $\boldsymbol{z}$ is the same as in section 6.6.2, the cumulants themselves are still given by equation (B.7), with the distinct interpretation of $f(\boldsymbol{z})$ in this case then resulting in the expansion

$$\left\langle \mathcal{H}_{kj} \frac{\partial}{\partial \mathrm{x}_l} \frac{\partial}{\partial \mathrm{x}_k} \mathrm{R}_{ji}(\boldsymbol{r}_p) \right\rangle \approx \underbrace{\langle \mathcal{H}_{kj} \rangle \left\langle \frac{\partial}{\partial \mathrm{x}_l} \frac{\partial}{\partial \mathrm{x}_k} \mathrm{R}_{ji}(\boldsymbol{r}_p) \right\rangle}_{\boxed{\mathrm{I}}} + \underbrace{\langle \mathcal{H}'_{kj} r'_{p_m} \rangle \left\langle \frac{\partial}{\partial \mathrm{r}_m} \frac{\partial}{\partial \mathrm{x}_l} \frac{\partial}{\partial \mathrm{x}_k} \mathrm{R}_{ji}(\boldsymbol{r}_p) \right\rangle}_{\boxed{\mathrm{II}}} \tag{6.92}$$

in which only the contributions from the first two cumulants are taken into account. Considering the first cumulant $\boxed{\mathrm{I}}$ of this expansion, the problem of closure here also reduces to specification of $\langle \boldsymbol{\mathcal{H}}[t;t'] \rangle$. At this point, the problem is the same as that encountered in the modelling of the first cumulant $\boxed{1}$ of the original expansion, and becomes circular. Thus at this level it is prudent to assume the LHA for $\langle \boldsymbol{\mathcal{H}}[t;t'] \rangle$ as given by (6.62), which once again causes contraction of $\boxed{\mathrm{I}}$ to zero due to incompressibility of the flow field

$$\langle \mathcal{H}_{kj} \rangle \left\langle \frac{\partial}{\partial \mathrm{x}_l} \frac{\partial}{\partial \mathrm{x}_k} \mathrm{R}_{ji}(\boldsymbol{r}_p) \right\rangle \approx h(t,t') \left\langle \frac{\partial}{\partial \mathrm{x}_l} \frac{\partial}{\partial \mathrm{x}_j} \mathrm{R}_{ji}(\boldsymbol{r}_p) \right\rangle \equiv 0 \tag{6.93}$$

Therefore attention can be restricted to the second cumulant $\boxed{\mathrm{II}}$ of (6.92). Closure of both of the necessary quantities in this expression has already been undertaken within the scope of the second term $\boxed{2}$ of the original expansion in section 6.7.7, with the model for $\langle \boldsymbol{\mathcal{H}}' \boldsymbol{r}'_p \rangle$ given in (6.87) and the model for $\left\langle \frac{\partial}{\partial \mathrm{r}_m} \frac{\partial}{\partial \mathrm{x}_l} \frac{\partial}{\partial \mathrm{x}_k} \mathrm{R}_{ji}(\boldsymbol{r}_p) \right\rangle$ given in (6.66). The explicit expression for the latter model in d-dimensional physical space is

$$\begin{aligned}\frac{\partial}{\partial \mathrm{r}_m}\frac{\partial}{\partial \mathrm{x}_l}\frac{\partial}{\partial \mathrm{x}_k}\mathrm{R}_{ji}\big(\mathbf{r}_0(t';t)\big) = \frac{1}{d-1}\beta^2 u'^2\sigma_k^4\Big\{&\sigma_k^2\Big[V_{g_k}V_{g_j}V_{g_i}\delta_{ml}+V_{g_l}V_{g_j}V_{g_i}\delta_{mk}\\&+V_{g_l}V_{g_k}V_{g_i}\delta_{mj}+V_{g_l}V_{g_k}V_{g_j}\delta_{mi}+V_{g_m}V_{g_j}V_{g_i}\delta_{lk}+V_{g_m}V_{g_k}V_{g_i}\delta_{lj}\\&+V_{g_m}V_{g_k}V_{g_j}\delta_{li}+V_{g_m}V_{g_l}V_{g_j}\delta_{ik}+V_{g_m}V_{g_l}V_{g_i}\delta_{jk}\Big](t-t')^3\\&-\sigma_k^4V_{g_m}V_{g_l}V_{g_k}V_{g_j}V_{g_i}(t-t')^5+\Big[(d+3)-\sigma_k^2V_g^2(t-t')^2\Big]\\&\cdot\Big[V_{g_k}\delta_{lm}\delta_{ij}+V_{g_l}\delta_{km}\delta_{ij}+V_{g_m}\delta_{lk}\delta_{ij}\Big](t-t')\\&-\sigma_k^2\Big[(d+5)-\sigma_k^2V_g^2(t-t')^2\Big]V_{g_m}V_{g_l}V_{g_k}\delta_{ji}(t-t')^3\\&-\Big[V_{g_m}\delta_{lj}\delta_{mk}+V_{g_m}\delta_{li}\delta_{jk}+V_{g_i}\delta_{jm}\delta_{kl}+V_{g_j}\delta_{im}\delta_{kl}+V_{g_k}\delta_{im}\delta_{lj}\\&+V_{g_i}\delta_{km}\delta_{lj}+V_{g_k}\delta_{jm}\delta_{li}+V_{g_j}\delta_{km}\delta_{li}+V_{g_l}\delta_{jm}\delta_{ik}+V_{g_j}\delta_{lm}\delta_{ik}\\&+V_{g_l}\delta_{im}\delta_{jk}+V_{g_i}\delta_{lm}\delta_{jk}\Big](t-t')\Big\}\exp\Big[-A(t-t')^2\Big]\end{aligned}\tag{6.94}$$

Contraction of $\langle\boldsymbol{\mathcal{H}}'\boldsymbol{r}'_p\rangle$ as given in (6.87) with (6.94) then produces the final result for the second term $\boxed{\text{II}}$ in the expansion (6.92) of

$$\begin{aligned}&\Big\langle\mathcal{H}'_{kj}[t;t']r'_{p_m}(t';t)\Big\rangle\Big\langle\frac{\partial}{\partial \mathrm{r}_m}\frac{\partial}{\partial \mathrm{x}_l}\frac{\partial}{\partial \mathrm{x}_k}\mathrm{R}_{ji}(\boldsymbol{r}_p)\Big\rangle\\&\approx-\frac{d+1}{(d-1)^2}\beta^2u'^4\sigma_k^6\Big(dV_{g_l}V_{g_i}-V_g^2\delta_{li}\Big)\Big[(d+4)-\sigma_k^2V_g^2(t-t')^2\Big](t-t')\\&\cdot\exp\Big[-A(t-t')^2\Big]\Big(\mathcal{M}_{\mathrm{int}}(t;t')+\mathcal{N}_{\mathrm{int}}(t;t')\Big)\end{aligned}\tag{6.95}$$

Due to $\mathbf{V}_g$ being nonzero only in the gravitational direction, the tensorial component $\big(dV_{g_l}V_{g_i}-V_g^2\delta_{li}\big)$ within (6.95) implies that the expression is zero for $i\neq l$, and for the case of $d=2$ the components $i=l$ are of equal and opposite values. Then since the components of (6.95) transfer directly to those of $\langle\nabla\mathbf{u}_p^\top(t)\rangle$ in (6.91), the mean fluid velocity gradient along particle trajectories is also nonzero only for $i=l$, with the condition of equal and opposite values for these two cases demonstrating that incompressibility is satisfied by this modelling procedure.

Owing to the appearance of the integrals $\mathcal{M}_{\mathrm{int}}(t;t')$ and $\mathcal{N}_{\mathrm{int}}(t;t')$ within (6.95), a compact analytical representation explicitly in terms of times t and t' is not available, meaning that it must be evaluated numerically in the same vein as the second term $\boxed{2}$ of the original expansion. This then completes the closure of the cumulant expansion

(6.92) for the integrand of the dispersion tensor $\left\langle \nabla \mathbf{u}_p^{\top}(t) \right\rangle$, which can subsequently be evaluated numerically through use of (6.91). Specification of $\left\langle \nabla \mathbf{u}_p^{\top}(t) \right\rangle$ in turn allows numerical evaluation of the mean particle response tensor $\left\langle \boldsymbol{\mathcal{H}}[t;t'] \right\rangle$ using (6.90). As a consequence of $\left\langle \boldsymbol{\mathcal{H}}[t;t'] \right\rangle$ being a linear function of $\left\langle \nabla \mathbf{u}_p^{\top}(t) \right\rangle$, it follows that $\left\langle \mathcal{H}_{kj}[t;t'] \right\rangle = 0$ for $k \neq j$, and has non-zero and differing values for the two cases in which $k = j$. This contrasts with the LHA (6.62), in which the non-zero values of the components given by $k = j$ are equal. This qualitative difference in the resulting model for $\left\langle \boldsymbol{\mathcal{H}}[t;t'] \right\rangle$ reflects the effect of the drift enhancement that is present in the system, and therefore constitutes an improvement that adequately captures the form of the required behaviour within the first cumulant $\boxed{1}$ of the original expansion.

Since $\left\langle \boldsymbol{\mathcal{H}}[t;t'] \right\rangle$ must be evaluated numerically, explicit representation of its time dependence within the first cumulant $\boxed{1}$ in (6.69) is not tractable. However, the expression for the derivative of the correlation tensor evaluated along particle trajectories $\left\langle \frac{\partial}{\partial \mathrm{x}_k} \mathrm{R}_{ji}(\boldsymbol{r}_p) \right\rangle$ as given in (6.64) is known, which has the form

$$\begin{aligned} \frac{\partial}{\partial \mathrm{x}_k} \mathrm{R}_{ji}\big(\mathbf{r}_0(t';t)\big) = \frac{1}{d-1} \beta^2 u'^2 \sigma_k^2 \Big\{ & \left[\sigma_k^2 V_g^2 \left(t-t'\right)^2 - (d+1) \right] V_{g_k} \delta_{ji} \left(t-t'\right) \\ & - \sigma_k^2 V_{g_k} V_{g_j} V_{g_i} \left(t-t'\right)^3 + V_{g_j} \delta_{ik} \left(t-t'\right) + V_{g_i} \delta_{jk} \left(t-t'\right) \Big\} \\ & \cdot \exp\left[-A \left(t-t'\right)^2 \right] \end{aligned} \tag{6.96}$$

Contraction of $\left\langle \boldsymbol{\mathcal{H}}[t;t'] \right\rangle$ with (6.96) then produces an expression for the first term $\boxed{1}$ of the original cumulant expansion

$$\begin{aligned} & \left\langle \mathcal{H}_{kj}[t;t'] \right\rangle \left\langle \frac{\partial}{\partial \mathrm{x}_k} \mathrm{R}_{ji}(\boldsymbol{r}_p) \right\rangle \\ \approx & \frac{1}{d-1} \beta^2 u'^2 \sigma_k^2 \Big\{ \left[\sigma_k^2 V_g^2 \left(t-t'\right)^2 - (d+1) \right] \left\langle \mathcal{H}_{di}[t;t'] \right\rangle V_g \left(t-t'\right) + \left\langle \mathcal{H}_{id}[t;t'] \right\rangle V_g \left(t-t'\right) \\ & - \sigma_k^2 \left\langle \mathcal{H}_{dd}[t;t'] \right\rangle V_g^2 V_{g_i} \left(t-t'\right)^3 + \left\langle \mathcal{H}_{jj}[t;t'] \right\rangle V_{g_i} \left(t-t'\right) \Big\} \exp\left[-A \left(t-t'\right)^2 \right] \end{aligned} \tag{6.97}$$

in which d is the index associated with the direction x_d that the gravitational body force acts in, with *no summation implied*, and j is a standard dummy variable over which summation is implied. In particular, as the index i corresponds to the component $\overline{\kappa}_i$ then taking $i \neq d$ (in the non-gravitational direction(s)) in (6.97) reduces the result to

zero (since $\langle \mathcal{H}_{kj}[t;t'] \rangle = 0$ for $k \neq j$), consistent with the fact that there is no drift enhancement for $i \neq d$. On the other hand, taking $i = d$ in (6.97) results in

$$\begin{aligned} &\langle \mathcal{H}_{kj}[t;t'] \rangle \left\langle \frac{\partial}{\partial \mathrm{x}_k} \mathrm{R}_{jd}(\boldsymbol{r}_p) \right\rangle \\ &\approx \frac{1}{d-1} \beta^2 u'^2 \sigma_k^2 \Big\{ \langle \mathcal{H}_{jj}[t;t'] \rangle - d \langle \mathcal{H}_{dd}[t;t'] \rangle \Big\} V_g(t-t') \exp\left[-A(t-t')^2 \right] \end{aligned} \tag{6.98}$$

This demonstrates that the existence of the first term $\boxed{1}$ within the cumulant expansion (6.69) is dependent on $\langle \mathcal{H}_{jj}[t;t'] \rangle$ and $d \langle \mathcal{H}_{dd}[t;t'] \rangle$ having different values in the modelling approach which is used, which is only satisfied in the event that $\langle \boldsymbol{\mathcal{H}}[t;t'] \rangle$ is not isotropic. This is in agreement with the LHA (6.62) resulting in no contribution from (6.98), whereas taking the mean fluid velocity gradient along particle trajectories into account through use of (6.90) is sufficient to include this anisotropy, and thereby the effect of drift enhancement within $\langle \boldsymbol{\mathcal{H}}[t;t'] \rangle$. The form of the model (6.98) is also consistent with the results from the symmetry analysis for $d = 2, 3$ given in (6.43) and (6.42) respectively, clarifying that the reduction in symmetry which is inherent to the flow configuration is respected by this modelling procedure. In particular, the assumption of modelling the Lagrangian correlations $\langle \nabla \mathbf{u}_p^{\top\prime}(s_1) \mathbf{u}_p'(s_2) \rangle$ and $\langle \nabla \mathbf{u}_p^{\top\prime}(s) \boldsymbol{v}^{0\prime}(t') \rangle$ as isotropic tensors does not introduce a spurious drift in the non-gravitational direction(s), meaning that even though such models do not constitute a full physical description of the behaviour intrinsic to these correlations, they do adhere to the system configuration.

6.7.9 Higher Order Cumulants

Specification of terms $\boxed{1}$ and $\boxed{2}$ by (6.89) and (6.97) respectively is sufficient to close the truncated cumulant expansion (6.69) in which only the first two cumulants $\mathbf{K}^1$ and $\mathbf{K}^2$ are included. Furthermore, if the assumption is made that the random variables $\boldsymbol{r}_p$ and $\boldsymbol{\mathcal{H}}$ have a joint Gaussian distribution, then the approximation (6.69) becomes exact. However, in the context of particle settling velocity enhancement this is not an obvious assumption to make as alluded to in section 6.6.3, even in the case of the underlying flow field $\mathbf{u}(\mathbf{x}, t)$ being Gaussian. This naturally leads to consideration of the higher order contributions $\boxed{3}$ and $\boxed{4}$ in (6.46). Within these expressions, the average of the derivatives of $\mathbf{R}$ evaluated along particle trajectories have already been modelled in (6.66) and (6.67), leaving just the third and fourth cumulants $\mathbf{K}^3$ and $\mathbf{K}^4$ themselves which require modelling, given by

$$\mathrm{K}^3_{kjmn} = \frac{1}{2}\langle \mathcal{H}'_{kj} r_{p_m}{}' r_{p_n}{}' \rangle \tag{6.99}$$

$$\mathrm{K}^4_{kjmnq} = \frac{1}{6}\Big[\langle \mathcal{H}'_{kj} r_{p_m}{}' r_{p_n}{}' r_{p_q}{}' \rangle - \langle \mathcal{H}'_{kj} r_{p_m}{}' \rangle \langle r_{p_n}{}' r_{p_q}{}' \rangle - \langle \mathcal{H}'_{kj} r_{p_n}{}' \rangle \langle r_{p_m}{}' r_{p_q}{}' \rangle - \langle \mathcal{H}'_{kj} r_{p_q}{}' \rangle \langle r_{p_m}{}' r_{p_n}{}' \rangle \Big] \tag{6.100}$$

For these the same approach as the second cumulant can be taken, with the integral representations of $\boldsymbol{r}'_p$ and $\boldsymbol{\mathcal{H}}'$ given by (6.56) and (6.57) utilised to express the cumulants in terms of correlations of the underlying processes $\boldsymbol{v}^{0\prime}(t')$, $\mathbf{u}'_p(s)$ and $\nabla \mathbf{u}_p^{\top\prime}(s)$. However at this level the resultant expressions for $\mathbf{K}^3$ and $\mathbf{K}^4$ are somewhat involved, and in particular the quantities which require closure are three-time and four-time correlations of $\boldsymbol{v}^{0\prime}(t')$, $\mathbf{u}'_p(s)$ and $\nabla \mathbf{u}_p^{\top\prime}(s)$. Even with the assumption of isotropy, there is no analytical expression available in the current body of literature that can represent such quantities. Additionally, attempting to use correlation splitting on the terms in (6.99) and (6.100) is of no further avail, since the quantities involved are the random variables $\boldsymbol{r}'_p$ and $\boldsymbol{\mathcal{H}}'$ themselves. As such, the modelling of $\mathbf{K}^3$ and $\mathbf{K}^4$ is not tractable at this level, and is not considered further in this work.

6.8 Numerical Evaluation of the Cumulant Expansions

Before assessing the model developed in section 6.7, it is first prudent to evaluate the true contribution of the separate terms $\boxed{1}$ - $\boxed{4}$ in the cumulant expansion (6.46) to the average $\left\langle \mathcal{H}_{kj} \frac{\partial}{\partial \mathrm{x}_k} \mathrm{R}_{ji}(\boldsymbol{r}_p) \right\rangle$ that arises within $\overline{\boldsymbol{\kappa}}$, and also the terms $\boxed{\mathrm{I}}$ - $\boxed{\mathrm{II}}$ for the corresponding expansion (6.92) for the average $\left\langle \mathcal{H}_{kj} \frac{\partial}{\partial \mathrm{x}_l} \frac{\partial}{\partial \mathrm{x}_k} \mathrm{R}_{ji}(\boldsymbol{r}_p) \right\rangle$ that emerges within the dispersion tensor description of $\langle \nabla \mathbf{u}_p^{\top}(t) \rangle$. This is performed using KS simulation data, with the cumulants $\mathbf{K}^n$ being directly computed, and the various spatial derivatives of $\mathbf{R}(\mathbf{r})$ expressed using the formulae (C.16), (C.20), (C.23), and (C.26), and evaluated along particle trajectories $\boldsymbol{r}_p$.

6.8.1 Numerical Evaluation of (6.46)

Considering the average $\left\langle \mathcal{H}_{kj} \frac{\partial}{\partial \mathrm{x}_k} \mathrm{R}_{ji}(\boldsymbol{r}_p) \right\rangle$ for just the gravitational direction $i = 2$, the contributions arising from the terms $\boxed{1}$ - $\boxed{4}$ in (6.46) are displayed in Figure 6.3. It is

immediately seen that the dominant contribution comes from the second cumulant $\mathbf{K}^2$ of the expansion, as reasoned in section 6.6.3. Of the remaining cumulants, $\mathbf{K}^1$ offers the most significant contribution by a small margin, although its effect is somewhat less than $\mathbf{K}^2$. The relatively small magnitude of $\mathbf{K}^1$ is consistent with the LHA for $\overline{\boldsymbol{\kappa}}$ being zero, as making such an approximation for just $\mathbf{K}^1$ only neglects a small part of the true value of $\left\langle \mathcal{H}_{kj} \frac{\partial}{\partial x_k} \mathrm{R}_{j2}(\boldsymbol{r}_p) \right\rangle$, and then the averaged nature of the LHA is unable to retrieve any information about the higher-order cumulants due to their dependence on the fluctuating quantities $\boldsymbol{r}'_p$ and $\boldsymbol{\mathcal{H}}'$. The cumulant $\mathbf{K}^3$ offers an almost negligible contribution, whilst $\mathbf{K}^4$ is slightly more distinct, and becomes of more importance at larger time separations $t - t'$. This confirms that the distribution $\phi\left(\boldsymbol{r}_p, \boldsymbol{\mathcal{H}}\right)$ is not Gaussian, demonstrating that the inertia of particles affects the distribution of the variables $\boldsymbol{r}_p$ and $\boldsymbol{\mathcal{H}}$ so that they differ from that of the underlying fluid velocity field $\mathbf{u}\left(\mathbf{x}, t\right)$, which is Gaussian in this case.

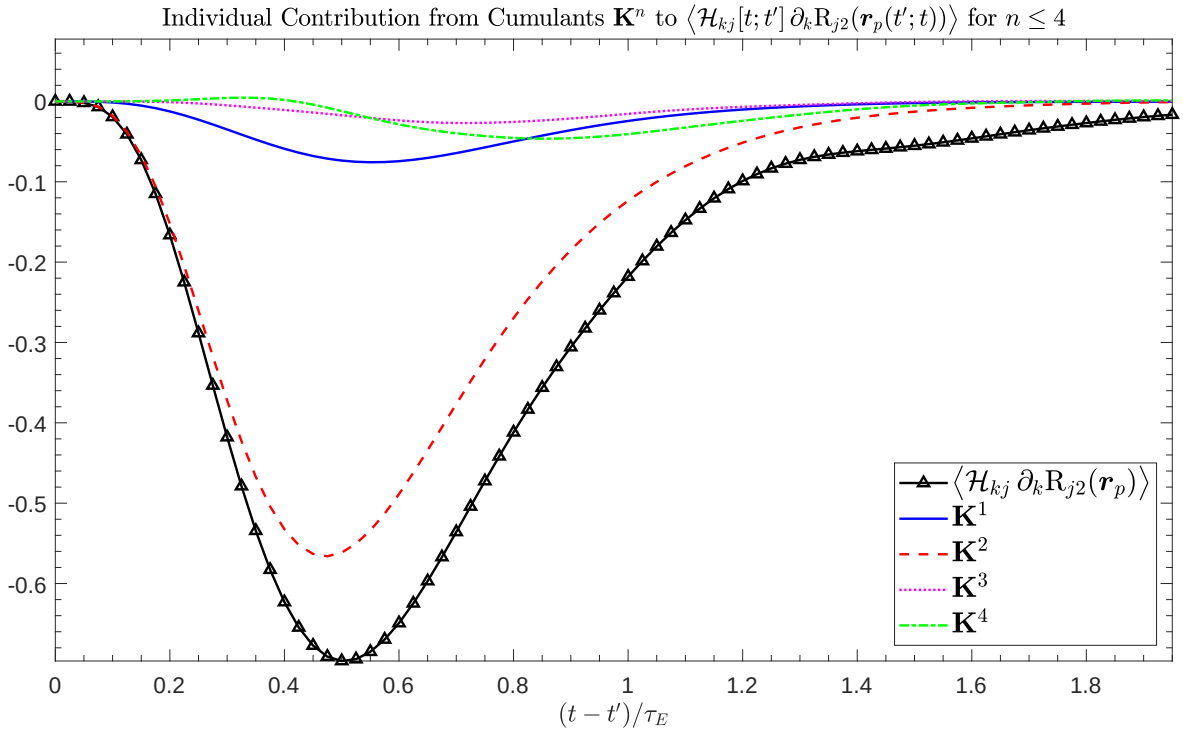

Figure 6.3: Contribution of individual cumulants $\mathbf{K}^n$ to the average $\left\langle \mathcal{H}_{kj}[t;t']\,\partial_k \mathrm{R}_{j2}(\boldsymbol{r}_p(t';t)) \right\rangle$ for $n \leq 4$, obtained from KS evaluation for $St_E = 0.1$ and $V_g/u' = 1.0$ in a two-dimensional fluid velocity field: —△— $\left\langle \mathcal{H}_{kj}\,\partial_k \mathrm{R}_{j2}(\boldsymbol{r}_p) \right\rangle$; —— $\mathbf{K}^1$; - - - - $\mathbf{K}^2$; ····· $\mathbf{K}^3$; — · — · — $\mathbf{K}^4$

In terms of the combined effect of the individual terms [1] - [4], Figure 6.4 shows the sum of the first n cumulants for $n \leq 4$. As discussed, the first cumulant $\mathbf{K}^1$ is relatively small in magnitude, and by itself cannot be considered as a meaningful

descriptor of the average $\left\langle \mathcal{H}_{kj} \frac{\partial}{\partial \mathrm{x}_k} \mathrm{R}_{j2}(\boldsymbol{r}_p) \right\rangle$. However, due to the dominant contribution of $\mathbf{K}^2$, the sum of $\mathbf{K}^1$ and $\mathbf{K}^2$ is seen to account for the majority of the effect that is present in the true value $\left\langle \mathcal{H}_{kj} \frac{\partial}{\partial \mathrm{x}_k} \mathrm{R}_{j2}(\boldsymbol{r}_p) \right\rangle$, representing $\sim 80\%$ of the full behaviour. The addition of the third cumulant $\mathbf{K}^3$ includes only marginally more detail, whilst inclusion of $\mathbf{K}^4$ brings the cumulant expansion up to accounting for $\sim 90\%$ of the true value, with the remaining deficiency concentrated around the peak in amplitude of $\left\langle \mathcal{H}_{kj} \frac{\partial}{\partial \mathrm{x}_k} \mathrm{R}_{j2}(\boldsymbol{r}_p) \right\rangle$ and at larger time separations $t - t'$. This also demonstrates that the effect of the cumulants $\mathbf{K}^5$ and $\mathbf{K}^6$ of $\phi(\boldsymbol{r}_p, \boldsymbol{\mathcal{H}})$ will barely be discernible relative to the full behaviour of the average, justifying their omission. The outcome then is that the information contained within $\mathbf{K}^1$ and $\mathbf{K}^2$ is certainly an adequate enough contribution to be used for making inferences about the physical mechanisms responsible for the increase in particle settling velocity, with the inclusion of this level of detail corresponding to the closure model developed in section 6.7.

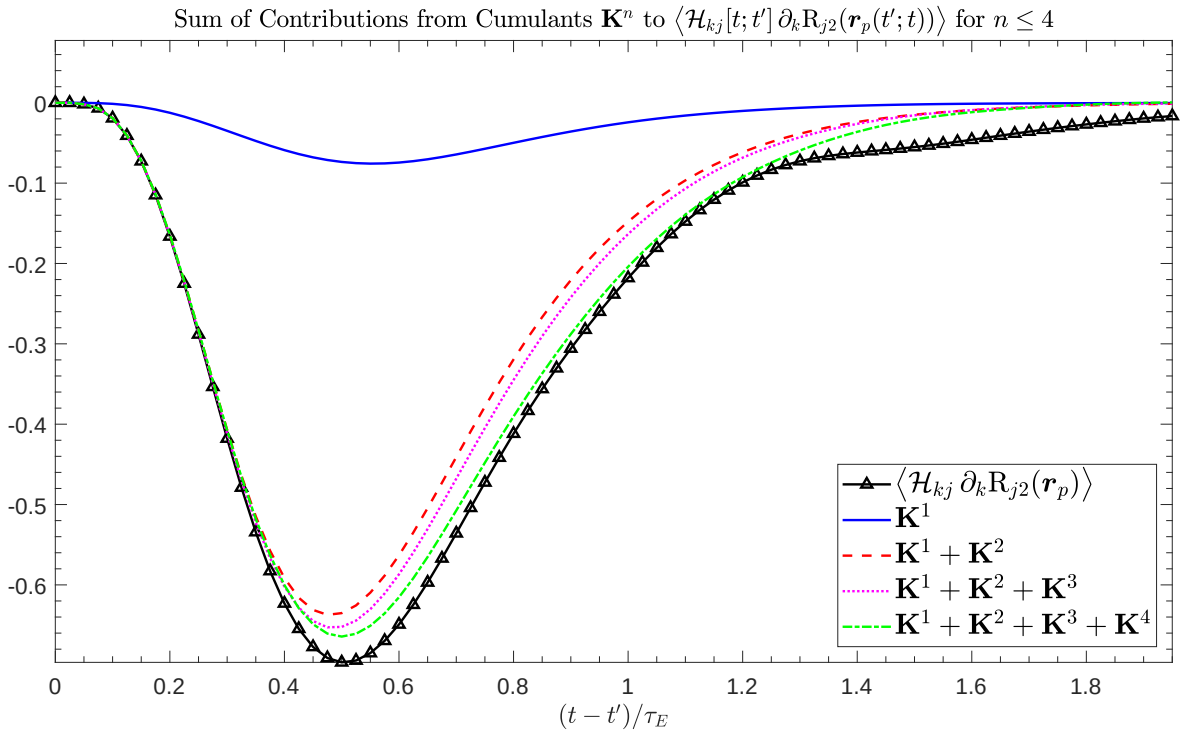

Figure 6.4: Sum of contributions from cumulants $\mathbf{K}^n$ compared to the average $\langle \mathcal{H}_{kj}[t;t']\,\partial_k \mathrm{R}_{j2}(\boldsymbol{r}_p(t';t))\rangle$ for $n \leq 4$, obtained from KS evaluation for $St_E = 0.1$ and $V_g/u' = 1.0$ in a two-dimensional fluid velocity field: —△— $\langle \mathcal{H}_{kj}\,\partial_k \mathrm{R}_{j2}(\boldsymbol{r}_p)\rangle$; —— $\mathbf{K}^1$; - - - - $\mathbf{K}^1 + \mathbf{K}^2$; ····· $\mathbf{K}^1 + \mathbf{K}^2 + \mathbf{K}^3$; — · — · — · $\mathbf{K}^1 + \mathbf{K}^2 + \mathbf{K}^3 + \mathbf{K}^4$

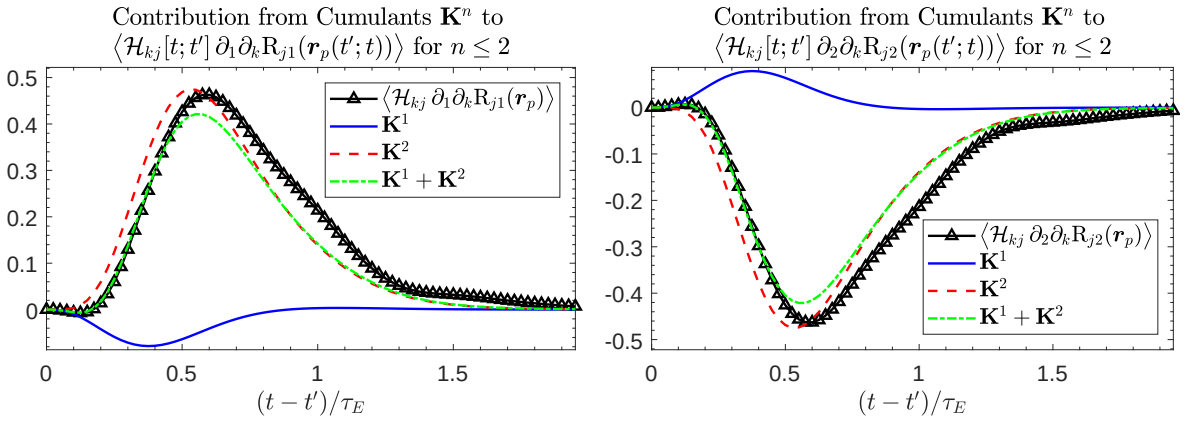

Figure 6.5: Contributions from cumulants $\mathbf{K}^n$ to the average $\langle \mathcal{H}_{kj}\,\partial_l\partial_k \mathrm{R}_{ji}(\boldsymbol{r}_p)\rangle$ for $n \leq 2$, obtained from KS evaluation for $St_E = 0.1$ and $V_g/u' = 1.0$ in a two-dimensional fluid velocity field: —△— $\langle \mathcal{H}_{kj}\,\partial_k \mathrm{R}_{j2}(\boldsymbol{r}_p)\rangle$; ——— $\mathbf{K}^1$; - - - - $\mathbf{K}^2$; — · — · — $\mathbf{K}^1 + \mathbf{K}^2$

6.8.2 Numerical Evaluation of (6.92)

Now focusing upon the average $\left\langle \mathcal{H}_{kj}\frac{\partial}{\partial \mathrm{x}_l}\frac{\partial}{\partial \mathrm{x}_k}\mathrm{R}_{ji}(\boldsymbol{r}_p)\right\rangle$ for just the non-zero components $i = l$, the contributions arising from the terms I - II in (6.92) are shown in Figure 6.5. It is seen that the two components for $i = l = 1$ and $i = l = 2$ are of equal and opposite magnitude as a consequence of the incompressibility of the fluid velocity field in the two-dimensional configuration, and as with the average $\left\langle \mathcal{H}_{kj}\frac{\partial}{\partial \mathrm{x}_k}\mathrm{R}_{j2}(\boldsymbol{r}_p)\right\rangle$, the dominant contribution again comes from the second cumulant $\mathbf{K}^2$. The input from the first cumulant $\mathbf{K}^1$ is again relatively unimportant, however in this case it also acts in the opposite sense to $\mathbf{K}^2$. The upshot of this is that $\mathbf{K}^2$ is a better predictor of the true behaviour of the average $\left\langle \mathcal{H}_{kj}\frac{\partial}{\partial \mathrm{x}_l}\frac{\partial}{\partial \mathrm{x}_k}\mathrm{R}_{ji}(\boldsymbol{r}_p)\right\rangle$ than the combined sum of $\mathbf{K}^1$ and $\mathbf{K}^2$, meaning that by neglecting the contribution from $\mathbf{K}^1$, a closure model for this average will actually see an improvement in accuracy. Together with the increasingly diminishing contributions of the higher-order cumulants, this characteristic in the behaviour of $\left\langle \mathcal{H}_{kj}\frac{\partial}{\partial \mathrm{x}_l}\frac{\partial}{\partial \mathrm{x}_k}\mathrm{R}_{ji}(\boldsymbol{r}_p)\right\rangle$ means that a closure of sufficient accuracy for this average can in theory be constructed from consideration of $\mathbf{K}^2$ alone.

6.9 Model Assessment using KS

In order to construct a closure for the cumulant expansion (6.46), models for both the spatial derivatives of the correlation tensor $\mathbf{R}$ evaluated along particle trajectories and the cumulants $\mathbf{K}^1$ and $\mathbf{K}^2$ of $\phi\,(\boldsymbol{r}_p, \boldsymbol{\mathcal{H}})$ themselves were developed in section 6.7. The

assessment of both aspects of the closure is addressed in this section via the use of KS data for a two-dimensional system.

6.9.1 Average of Spatial Derivatives of the Correlation Tensor Evaluated along Particle Trajectories

In terms of the average of the spatial derivatives of the correlation tensor $\mathbf{R}(\boldsymbol{r}_p)$, the closures proposed in section 6.7.5 that are relevant to $\mathbf{K}^1$ and $\mathbf{K}^2$ are given in (6.64) and (6.65) by

$$\left\langle \frac{\partial}{\partial \mathrm{x}_k} \mathrm{R}_{ji}(\boldsymbol{r}_p) \right\rangle \approx \frac{\partial}{\partial \mathrm{x}_k} \mathrm{R}_{ji}\big(\mathbf{r}_0(t';t)\big)$$
$$\left\langle \frac{\partial}{\partial \mathrm{r}_m} \frac{\partial}{\partial \mathrm{x}_k} \mathrm{R}_{ji}(\boldsymbol{r}_p) \right\rangle \approx \frac{\partial}{\partial \mathrm{r}_m} \frac{\partial}{\partial \mathrm{x}_k} \mathrm{R}_{ji}\big(\mathbf{r}_0(t';t)\big)$$

where the model separation along particle trajectories in (6.63) is $\mathbf{r}_0(t';t) = \mathbf{V}_g(t-t')$, and the temporal decorrelation is also modified using the model $\mathrm{E}_{\tau_{Lp}}(t-t')$ in (6.68). These closures therefore completely neglect the effect of the covariance of $\boldsymbol{r}_p$ on the behaviour of the isotropic tensors $\frac{\partial}{\partial \mathrm{x}_k}\mathrm{R}_{ji}(\mathbf{r})$ and $\frac{\partial}{\partial \mathrm{r}_m}\frac{\partial}{\partial \mathrm{x}_k}\mathrm{R}_{ji}(\mathbf{r})$ when evaluated along particle trajectories, only accounting for the mean behaviour that arises due to the presence of the gravitational body force.

The performance of these models is shown in Figures 6.6 and 6.7 respectively. In the case of $\left\langle \frac{\partial}{\partial \mathrm{x}_k}\mathrm{R}_{ji}(\boldsymbol{r}_p) \right\rangle$, it is seen that half of the components are identically zero due to the isotropic form of the tensor, with this also being the case for the model $\frac{\partial}{\partial \mathrm{x}_k}\mathrm{R}_{ji}\big(\mathbf{r}_0(t';t)\big)$. For the non-zero components, since $\left\langle \frac{\partial}{\partial \mathrm{x}_k}\mathrm{R}_{ji}(\boldsymbol{r}_p) \right\rangle$ is a third-order isotropic tensor it is an odd function, and therefore will have an amplitude of zero at $t-t'=0$. This gives rise to behaviour that becomes more significant for $t-t' \lessapprox 0.3\tau_E$, before decorrelating to zero for large time separations as expected. It is seen in Figure 6.6 that despite not including any detail about the covariance of $\boldsymbol{r}_p$, both the amplitude and timescale inherent to the behaviour of this average are well approximated by the model $\frac{\partial}{\partial \mathrm{x}_k}\mathrm{R}_{ji}\big(\mathbf{r}_0(t';t)\big)$, with only small deviations noticeable around the peak in amplitude and as the function decorrelates.

For the average $\left\langle \frac{\partial}{\partial \mathrm{r}_m}\frac{\partial}{\partial \mathrm{x}_k}\mathrm{R}_{ji}(\boldsymbol{r}_p) \right\rangle$, Figure 6.7 reveals that again half the components are identically zero, however since this average is a fourth-order isotropic tensor and therefore an even function, the non-zero components will have a non-zero value at

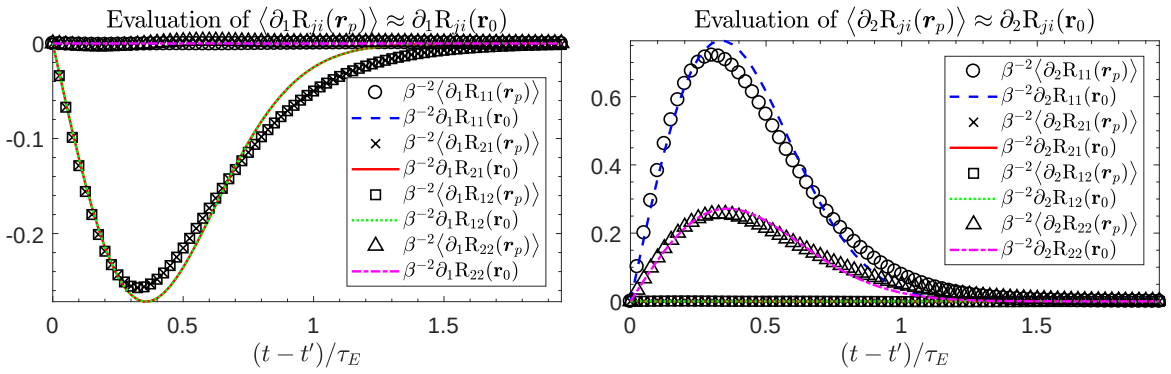

Figure 6.6: Evaluation of all components of the model $\langle \partial_k \mathrm{R}_{ji}(\boldsymbol{r}_p)\rangle \approx \partial_k \mathrm{R}_{ji}(\mathbf{r}_0)$ using KS for $St_E = 0.1$ and $V_g/u' = 1.0$ in a two-dimensional fluid velocity field: Symbols ◯ , × , □ , △ components of $\langle \partial_k \mathrm{R}_{ji}(\boldsymbol{r}_p)\rangle$; lines - - - - , ——— , ····· , — · — · — components of $\partial_k \mathrm{R}_{ji}(\mathbf{r}_0)$

$t - t' = 0$. The behaviour of the average is then that of an exponential decorrelation function, with different scalings for the various non-zero components determined by the values at zero time separation, which the isotropic form of the model $\frac{\partial}{\partial \mathrm{r}_m}\frac{\partial}{\partial \mathrm{x}_k}\mathrm{R}_{ji}\big(\mathbf{r}_0(t';t)\big)$ captures exactly. As in Figure 6.7, this model is also seen to capture the timescale associated with this decorrelation reasonably well, with only a slight over-prediction evident. Thus it is concluded that both of these models provide an acceptable level of accuracy, which can nonetheless be refined by including detail about the covariance of $\boldsymbol{r}_p$ through further use of correlation splitting on $\left\langle \frac{\partial}{\partial \mathrm{x}_k}\mathrm{R}_{ji}(\boldsymbol{r}_p)\right\rangle$.

6.9.2 Cumulants

For modelling of the cumulant $\mathbf{K}^2$, the representations of $\boldsymbol{r}_p$ and $\boldsymbol{\mathcal{H}}$ used led to the expression (6.74), in which the correlations $\langle \nabla \mathbf{u}_p^{\top\prime}(s_1)\mathbf{u}_p'(s_2)\rangle$ and $\langle \nabla \mathbf{u}_p^{\top\prime}(s)\boldsymbol{v}^{0\prime}(t')\rangle$ emerged. For $\langle \nabla \mathbf{u}_p^{\top\prime}(s_1)\mathbf{u}_p'(s_2)\rangle$, the modelling approach which was implemented used the leading order contribution to the isotropic approximation (6.77) of

$$\left\langle \nabla_j \mathrm{u}_{p_k}(t)\mathrm{u}_{p_m}(t')\right\rangle \approx \frac{1}{\beta^2}\frac{\partial}{\partial \mathrm{x}_j}\mathrm{R}_{mk}\big(\mathbf{r}_0(t';t)\big)$$

The efficacy of such a closure is shown in Figure 6.8. It is immediately apparent that in contrast to the average $\left\langle \frac{\partial}{\partial \mathrm{x}_j}\mathrm{R}_{mk}(\boldsymbol{r}_p)\right\rangle$ in section 6.9.1, the correlation $\langle \nabla \mathbf{u}_p^{\top\prime}(s_1)\mathbf{u}_p'(s_2)\rangle$ is not strictly an odd function, exhibiting non-zero values at $t - t' = 0$. The consequence of modelling such behaviour using the isotropic model $\beta^{-2}\frac{\partial}{\partial \mathrm{x}_j}\mathrm{R}_{mk}\big(\mathbf{r}_0(t';t)\big)$ is that this information is lost, which is significant for the majority of the non-zero com-

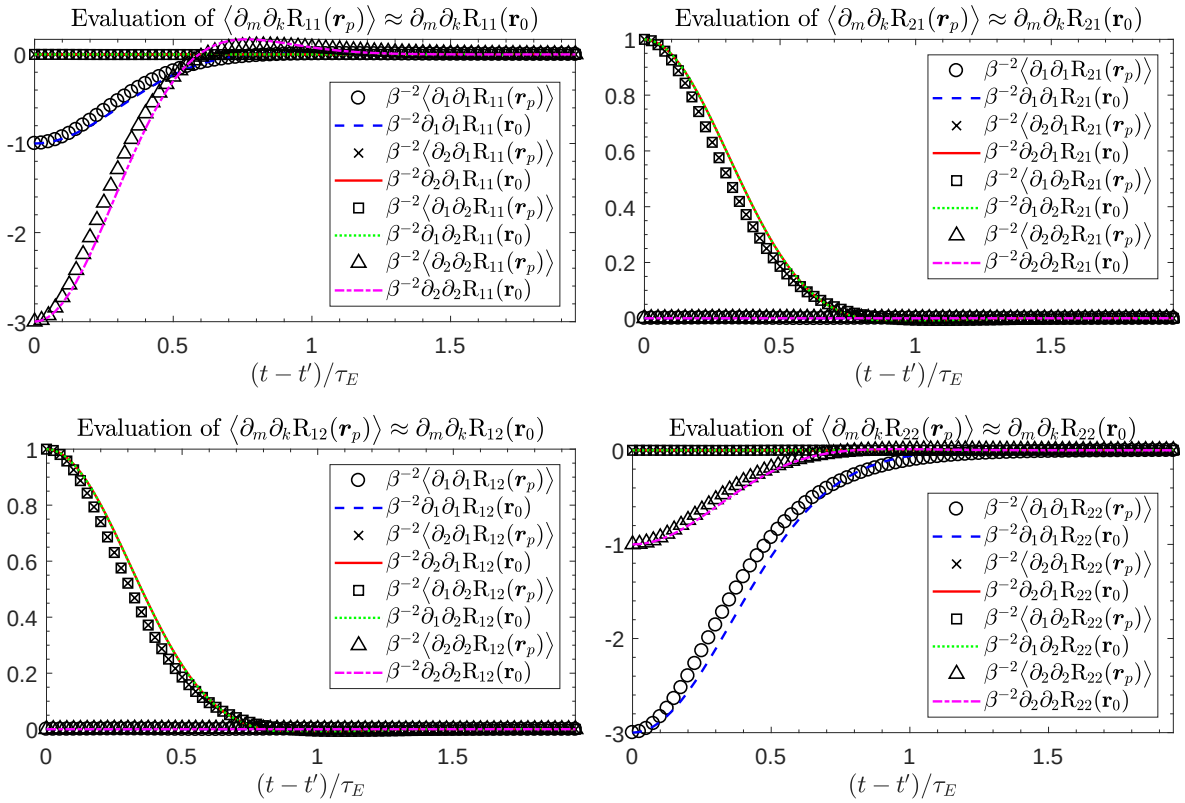

Figure 6.7: Evaluation of all components of the model $\langle \partial_m \partial_k \mathrm{R}_{ji}(\boldsymbol{r}_p) \rangle \approx \partial_m \partial_k \mathrm{R}_{ji}(\mathbf{r}_0)$ using KS for $St_E = 0.1$ and $V_g/u' = 1.0$ in a two-dimensional fluid velocity field: Symbols ◯ , × , □ , △ components of $\langle \partial_m \partial_k \mathrm{R}_{ji}(\boldsymbol{r}_p) \rangle$; lines - - - - , ——— , ····· , – · – · – components of $\partial_m \partial_k \mathrm{R}_{ji}(\mathbf{r}_0)$

ponents. Nonetheless, half of the total components of $\langle \nabla \mathbf{u}_p^{\top\prime}(s_1) \mathbf{u}_p'(s_2) \rangle$ are seen to be zero on average, which corresponds with the associated components of the isotropic model. As with the behaviour of $\left\langle \frac{\partial}{\partial \mathrm{x}_j} \mathrm{R}_{mk}(\boldsymbol{r}_p) \right\rangle$, since $\langle \nabla \mathbf{u}_p^{\top\prime}(s_1) \mathbf{u}_p'(s_2) \rangle$ is a third-order tensor there is still a peak in amplitude of the correlation at $t - t' \approx 0.3\tau_E$, with a decorrelation to zero at larger time separations. The amplitude of the behaviour is captured reasonably well by the model, however the timescale associated with the correlation is seen to differ markedly between components. This highlights the disadvantage of using an isotropic model, in which the single timescale characterised by $\mathrm{E}_{\tau_{Lp}}(t - t')$ is intrinsic to all components, with the result that the decorrelation of $\langle \nabla \mathbf{u}_p^{\top\prime}(s_1) \mathbf{u}_p'(s_2) \rangle$ is captured sufficiently for some components, but not all. In particular, the component $\langle \nabla_1 \mathrm{u}_{p_1}'(s_1) \mathrm{u}_{p_2}'(s_2) \rangle$ is seen to decorrelate in Figure 6.8 more like $\mathcal{O}(t)$ than the other non-zero components which decorrelate like $\mathcal{O}(t^2)$, with this behaviour not being captured by the $\mathcal{O}(t^2)$ decay inherent in $\mathrm{E}_{\tau_{Lp}}(t - t')$. As a result, the model $\beta^{-2} \frac{\partial}{\partial \mathrm{x}_j} \mathrm{R}_{mk}\big(\mathbf{r}_0(t'; t)\big)$ amounts to only a rudimentary approximation in this context, and leaves the question remaining as to what appropriate timescales for these

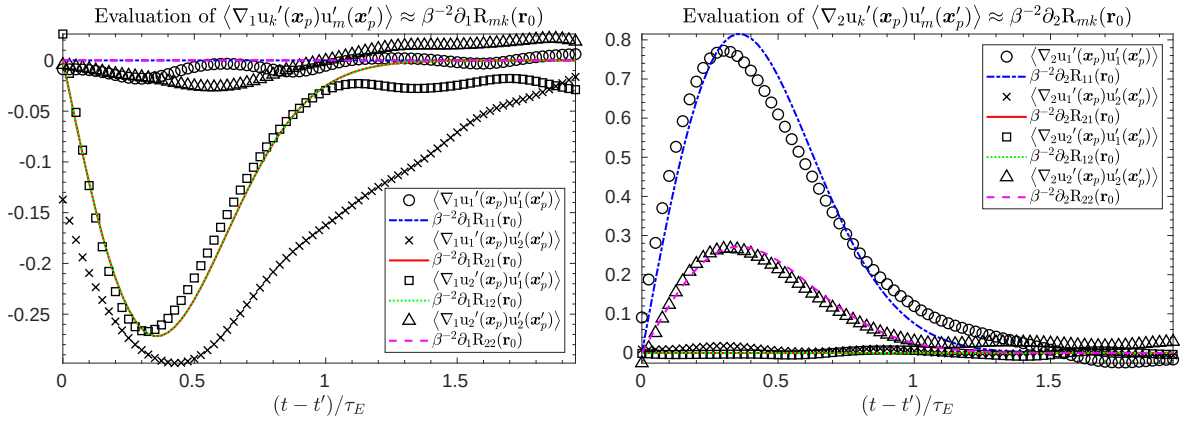

Figure 6.8: Evaluation of all components of the model $\langle \nabla_j \mathrm{u}_k'(\boldsymbol{x}_p)\mathrm{u}_m'(\boldsymbol{x}_p')\rangle \approx \beta^{-2}\partial_j \mathrm{R}_{mk}(\mathbf{r}_0)$ using KS for $St_E = 0.1$ and $V_g/u' = 1.0$ in a two-dimensional fluid velocity field: Symbols ◯, ×, □, △ components of $\langle \nabla_j \mathrm{u}_k'(\boldsymbol{x}_p)\mathrm{u}_m'(\boldsymbol{x}_p')\rangle$; lines – · – · – · , ——— , · · · · · , - - - - components of $\beta^{-2}\partial_j \mathrm{R}_{mk}(\mathbf{r}_0)$

correlations would be.

In terms of the correlation $\langle \nabla \mathbf{u}_p^{\top\prime}(s)\boldsymbol{v}^{0\prime}(t')\rangle$ the chosen modelling approach used the approximation $\boldsymbol{v}^0(t') \approx \mathbf{u}_p(t') + \mathbf{V}_g$ to yield (6.81) from which emerges the relation

$$\left\langle \nabla_j \mathrm{u}_{p_k}(s) v_m^0(t') \right\rangle \approx \left\langle \nabla_j \mathrm{u}_{p_k}(s) \mathrm{u}_{p_m}(t') \right\rangle$$

Thus the information pertaining to the particle velocity is lost in this model, and Figure 6.9 illustrates the repercussions of this. As a third-order tensor, $\langle \nabla \mathbf{u}_p^{\top\prime}(s)\boldsymbol{v}^{0\prime}(t')\rangle$ still exhibits a peak amplitude at $t - t' \approx 0.3\tau_E$, however both the value of the correlation at $t - t' = 0$ and the decorrelation rates of the components are seen to vary more than those of $\langle \nabla \mathbf{u}_p^{\top\prime}(s_1)\mathbf{u}_p'(s_2)\rangle$ displayed in Figure 6.8. Consequently, use of the leading order contribution from the model $\beta^{-2}\frac{\partial}{\partial \mathrm{x}_j}\mathrm{R}_{mk}\big(\mathbf{r}_0(t';t)\big)$ to represent $\langle \nabla \mathbf{u}_p^{\top\prime}(s)\boldsymbol{v}^{0\prime}(t')\rangle$ produces an approximation of questionable quality. The peak in amplitude is captured less accurately in this case, however the major shortcomings are the omission of the behaviour for the non-zero components at $t - t' = 0$, which is distinctly non-zero, and the decorrelation rate of the different components. Although the latter is adequately addressed by the model for some components, again the behaviour of one specific component $\langle \nabla_1 \mathrm{u}_{p_1}'(s_1) v_2^{0\prime}(t')\rangle$ is more characteristic of decay like $\mathcal{O}(t)$ than $\mathcal{O}(t^2)$, with the single timescale of the isotropic model encapsulated in $\mathrm{E}_{\tau_{Lp}}(t - t')$ failing to capture this. Therefore in addition to refinement of appropriate timescales for the various components of $\langle \nabla \mathbf{u}_p^{\top\prime}(s)\boldsymbol{v}^{0\prime}(t')\rangle$, the values of the one-time correlation $\langle \nabla \mathbf{u}_p^{\top\prime}(t')\boldsymbol{v}^{0\prime}(t')\rangle$ also ideally need to be accounted for, with the use of correlation

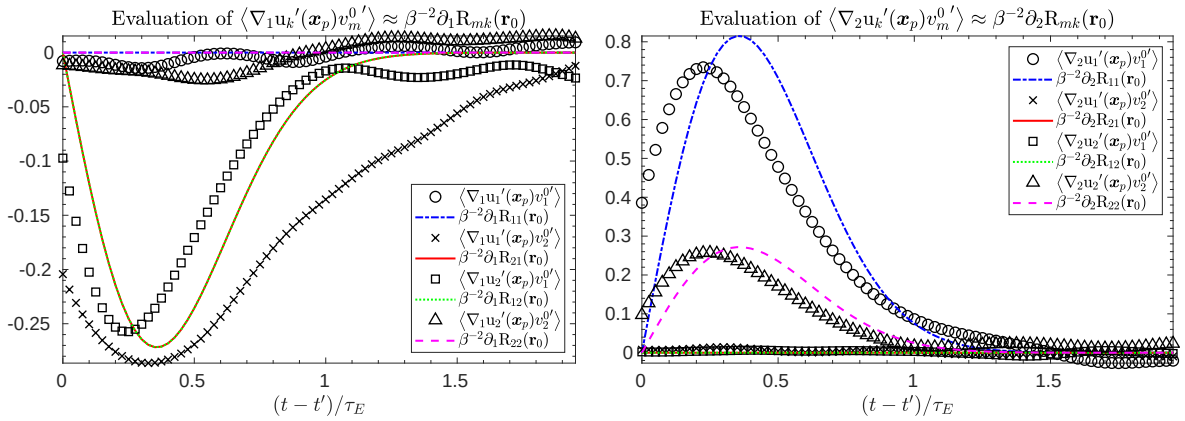

Figure 6.9: Evaluation of all components of the model $\langle \nabla_j \mathrm{u}_k'(\boldsymbol{x}_p) v_m^{0\prime} \rangle \approx \beta^{-2} \partial_j \mathrm{R}_{mk}(\mathbf{r}_0)$ using KS for $St_E = 0.1$ and $V_g/u' = 1.0$ in a two-dimensional fluid velocity field: Symbols ◯, ×, □, △ components of $\langle \nabla_j \mathrm{u}_k'(\boldsymbol{x}_p) v_m^{0\prime} \rangle$; lines – · – · –, ——, · · · · · ·, - - - - components of $\beta^{-2} \partial_j \mathrm{R}_{mk}(\mathbf{r}_0)$

splitting on this average detailed in Appendix D.2.

On balance, the models for $\langle \nabla \mathbf{u}_p^{\top\prime}(s_1) \mathbf{u}_p'(s_2) \rangle$ and $\langle \nabla \mathbf{u}_p^{\top\prime}(s) \boldsymbol{v}^{0\prime}(t') \rangle$ both capture the essential behaviour of each component, and therefore constitute a starting point for representing these correlations. However, important aspects of the detail inherent in both correlations are lost through using an isotropic model, which naturally leads to consideration of how best to represent these interactions given the reduction in symmetry of the particle phase in this flow configuration. Furthermore, the models for both $\langle \nabla \mathbf{u}_p^{\top\prime}(s_1) \mathbf{u}_p'(s_2) \rangle$ and $\langle \nabla \mathbf{u}_p^{\top\prime}(s) \boldsymbol{v}^{0\prime}(t') \rangle$ are also used in closure of the first cumulant $\mathbf{K}^1$ in section 6.7.8, meaning that the accuracy of these models affects that of the model forms for both $\mathbf{K}^1$ and $\mathbf{K}^2$.

6.9.3 Capturing the Increase in Particle Settling Velocity

The models developed for the spatial derivatives of the correlation tensor $\mathbf{R}(\boldsymbol{r}_p)$ and the cumulants $\mathbf{K}^1$ and $\mathbf{K}^2$ of $\phi(\boldsymbol{r}_p, \boldsymbol{\mathcal{H}})$ together determine the accuracy of the dispersion tensor $\overline{\boldsymbol{\kappa}}(t)$ at the top level of the problem. Verification of the model performance in this aspect must be undertaken numerically, since the time integrals $\mathcal{M}_{\mathrm{int}}(t;t')$ and $\mathcal{N}_{\mathrm{int}}(t;t')$ that arise in the modelling process in (6.85) and (6.86) are too complicated to admit tractable analytical expressions. This process is however computationally undemanding, with three nested integrations being required in total to evaluate $\overline{\boldsymbol{\kappa}}(t)$.

To begin with, the average $\left\langle \mathcal{H}_{kj} \frac{\partial}{\partial \mathrm{x}_l} \frac{\partial}{\partial \mathrm{x}_k} \mathrm{R}_{ji}(\boldsymbol{r}_p) \right\rangle$ is evaluated for just the non-zero components $i = l$, the outcome of which is shown in Figure 6.10. As noted in section

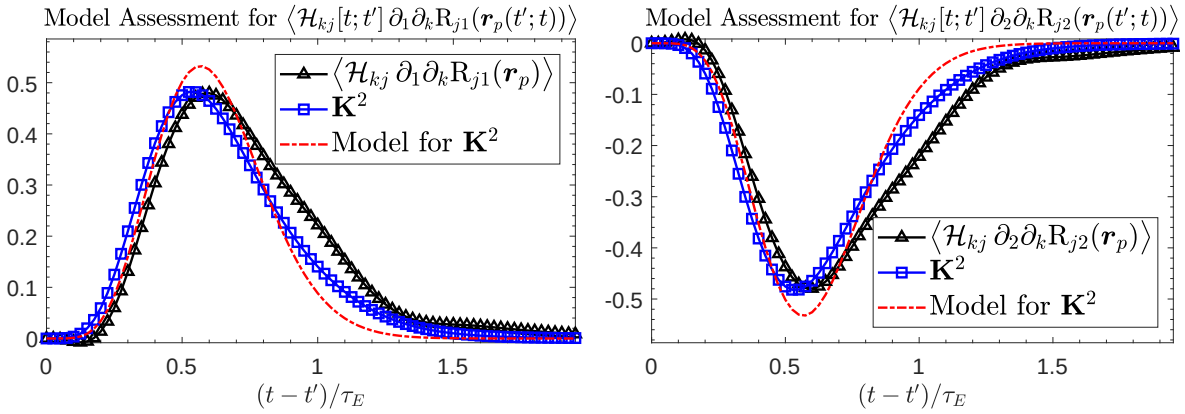

Figure 6.10: Model assessment for the average $\langle \mathcal{H}_{kj}[t;t']\,\partial_l\partial_k \mathrm{R}_{ji}(\boldsymbol{r}_p(t';t))\rangle$, obtained from KS evaluation for $St_E = 0.1$ and $V_g/u' = 1.0$ in a two-dimensional fluid velocity field: —△— $\langle \mathcal{H}_{kj}\,\partial_k \mathrm{R}_{j2}(\boldsymbol{r}_p)\rangle$; ——True contribution from $\mathbf{K}^2$; - - - - Model for $\mathbf{K}^2$

6.8.2, omission of the first cumulant $\mathbf{K}^1$ actually improves the model for this average since it acts in the opposite sense to $\mathbf{K}^2$, and following this it is seen that the model for $\mathbf{K}^2$ is a good approximation to $\left\langle \mathcal{H}_{kj}\frac{\partial}{\partial \mathrm{x}_l}\frac{\partial}{\partial \mathrm{x}_k}\mathrm{R}_{ji}(\boldsymbol{r}_p)\right\rangle$. The peak in amplitude is slightly overpredicted, whilst the decorrelation rate is also marginally too large, but the model otherwise describes the behaviour well. The reason that the model manages to overpredict these characteristics is due both to the adequacy of the models for $\left\langle \frac{\partial}{\partial \mathrm{r}_m}\frac{\partial}{\partial \mathrm{x}_k}\mathrm{R}_{ji}(\boldsymbol{r}_p)\right\rangle$, $\langle \nabla \mathbf{u}_p^{\top\prime}(s_1)\mathbf{u}_p'(s_2)\rangle$ and $\langle \nabla \mathbf{u}_p^{\top\prime}(s)\boldsymbol{v}^{0\prime}(t')\rangle$, but also due to the filtering effect arising from multiple appearances of the particle Green's function $h(t;t')$ that is embedded within the time integrals $\mathcal{M}_{\mathrm{int}}(t;t')$ and $\mathcal{N}_{\mathrm{int}}(t;t')$. In particular, specification of the temporal decorrelation function along particle trajectories $\mathrm{E}_{\tau_{Lp}}(t-t')$, and notably the selection of model for τ_{Lp}, will have a significant influence on the timescale associated with the overall model for $\mathbf{K}^2$ within this average.

For the average $\left\langle \mathcal{H}_{kj}\frac{\partial}{\partial \mathrm{x}_k}\mathrm{R}_{ji}(\boldsymbol{r}_p)\right\rangle$ models for both $\mathbf{K}^1$ and $\mathbf{K}^2$ are needed, with the model for $\mathbf{K}^1$ being directly dependent on $\left\langle \mathcal{H}_{kj}\frac{\partial}{\partial \mathrm{x}_l}\frac{\partial}{\partial \mathrm{x}_k}\mathrm{R}_{ji}(\boldsymbol{r}_p)\right\rangle$ by virtue of (6.90) and (6.91). Accordingly, the relative accuracy of the model for this average observed in Figure 6.10 is transferred to the model for $\mathbf{K}^1$, which is seen from Figure 6.11 to capture most of the behaviour associated with this cumulant. Notwithstanding this, the relative contribution of $\mathbf{K}^1$ is small compared to that of $\mathbf{K}^2$, which is where the real shortcomings of the modelling procedure become apparent. It is seen that the model for $\mathbf{K}^2$ is a reasonable descriptor of the behaviour, however it underpredicts the peak in amplitude by a small margin, whilst in common with $\mathbf{K}^1$ overpredicts the decorrelation timescale. As for the average $\left\langle \mathcal{H}_{kj}\frac{\partial}{\partial \mathrm{x}_l}\frac{\partial}{\partial \mathrm{x}_k}\mathrm{R}_{ji}(\boldsymbol{r}_p)\right\rangle$, this variation from the true behaviour is attributable both to the suitability of the various models used and

the filtering effect of $h(t;t')$ in $\mathcal{M}_{\text{int}}(t;t')$ and $\mathcal{N}_{\text{int}}(t;t')$, with the choice of τ_{Lp} being a key factor in determining the effective decorrelation timescale of the overall model. Consequently, the model for $\mathbf{K}^2$ is seen to retrieve most, but not all, of the contribution that this cumulant makes in reality. This then compounds the issue that $\mathbf{K}^1$ and $\mathbf{K}^2$ only account for $\sim 80\%$ of the full behaviour in the average $\left\langle \mathcal{H}_{kj} \frac{\partial}{\partial \mathrm{x}_k} \mathrm{R}_{ji}(\boldsymbol{r}_p) \right\rangle$, with the model further representing only $\sim 80\%$ of the contribution that $\mathbf{K}^1$ and $\mathbf{K}^2$ make. The resultant final model therefore omits a not-insignificant portion of the detail contained within this average, although this is somewhat mitigated by the fact that only $\mathbf{K}^1$ and $\mathbf{K}^2$ are accounted for in the modelling procedure.

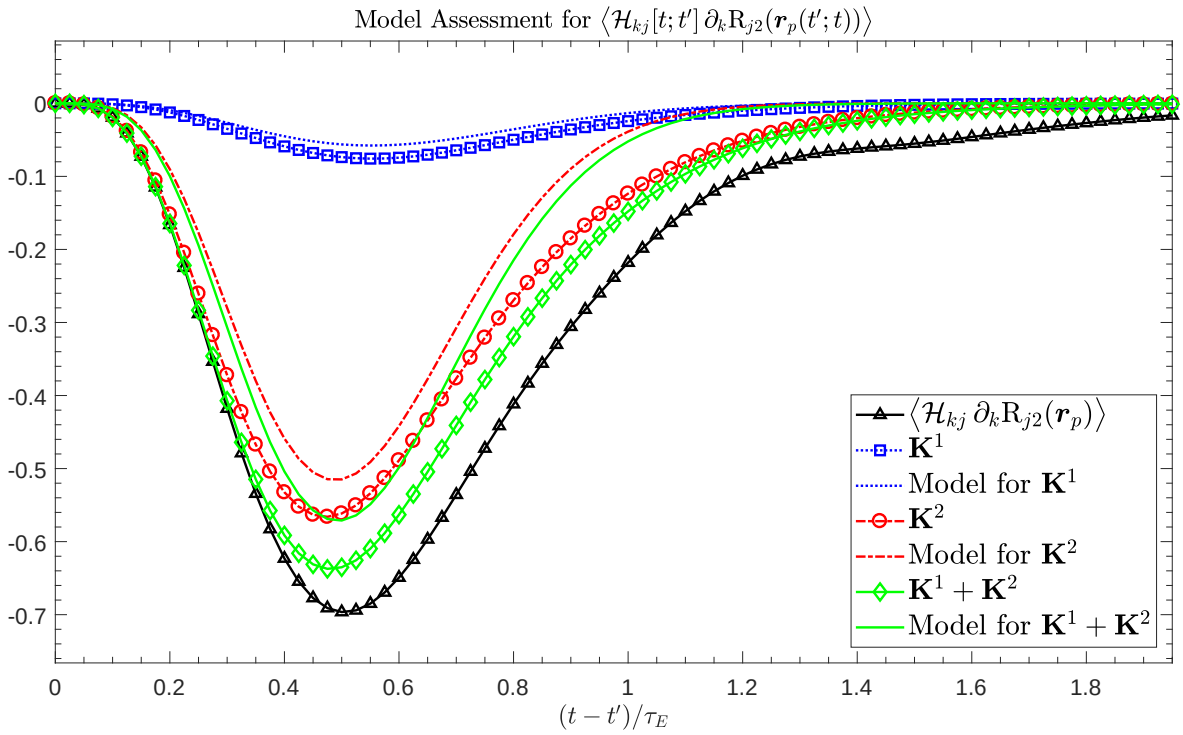

Figure 6.11: Model assessment for the average $\left\langle \mathcal{H}_{kj}[t;t']\,\partial_k \mathrm{R}_{j2}(\boldsymbol{r}_p(t';t)) \right\rangle$, obtained from KS evaluation for $St_E = 0.1$ and $V_g/u' = 1.0$ in a two-dimensional fluid velocity field: —△— $\langle \mathcal{H}_{kj}\,\partial_k \mathrm{R}_{j2}(\boldsymbol{r}_p)\rangle$; ···□··· $\mathbf{K}^1$; ····· Model for $\mathbf{K}^1$; –·◯–· $\mathbf{K}^2$; – · – · – Model for $\mathbf{K}^2$; —◇— $\mathbf{K}^1+\mathbf{K}^2$; —— Model for $\mathbf{K}^1+\mathbf{K}^2$

Evaluation of the evolution for $\overline{\kappa}_2(t)$ as predicted by this modelling procedure is carried out by a simple numerical integration of the closure for $\left\langle \mathcal{H}_{kj} \frac{\partial}{\partial \mathrm{x}_k} \mathrm{R}_{j2}(\boldsymbol{r}_p) \right\rangle$ over the sampling period. This is illustrated in Figure 6.12, with the true behaviour of $\mathbf{K}^1$ and $\mathbf{K}^2$ falling $\sim 20\%$ short of that of $\overline{\kappa}_2(t)$, and the model further underpredicting by another $\sim 20\%$. Thus overall the model is able to retrieve $\sim 65\%$ of the true increase in particle settling velocity, and therefore whilst the full effect is not captured, it is useful in the context of making inferences about the mechanisms that are responsible

for this behaviour. Indeed, on the basis that the starting point for this modelling procedure is the LHA prediction of $\overline{\kappa}_2^{\mathrm{LHA}} = 0$, the model constitutes an improvement in the sense that it is able to capture an increase in particle settling velocity as a direct consequence of accounting for the interactions between $\boldsymbol{r}_p$ and $\boldsymbol{\mathcal{H}}$. Nonetheless, in order to accurately represent this effect requires further refinement to the physical assumptions made within the modelling process, which from section 6.9.2 is seen to apply principally to the representations of $\left\langle \nabla \mathbf{u}_p^{\top\prime}(s_1)\mathbf{u}_p'(s_2)\right\rangle$ and $\left\langle \nabla \mathbf{u}_p^{\top\prime}(s)\boldsymbol{v}^{0\prime}(t')\right\rangle$ that are used.

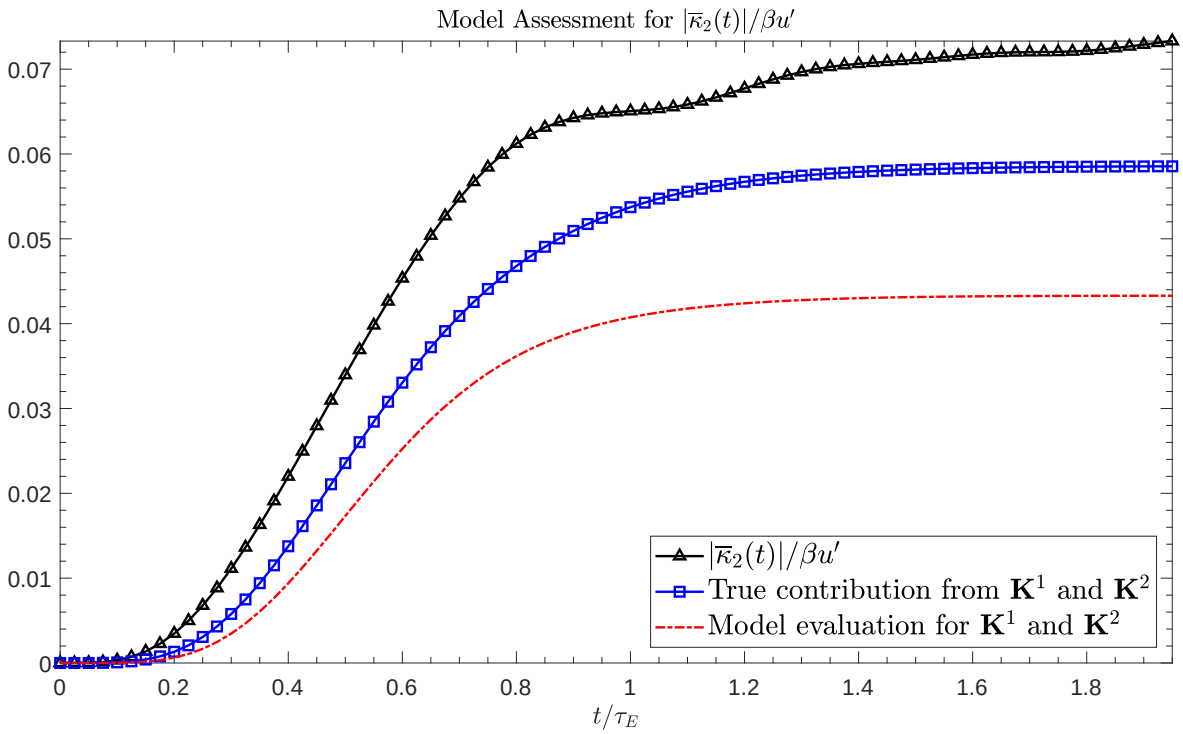

Figure 6.12: Model assessment for $|\overline{\kappa}_2(t)|/\beta u'$, obtained from KS evaluation for $St_E = 0.1$ and $V_g/u' = 1.0$ in a two-dimensional fluid velocity field: —△— $|\overline{\kappa}_2(t)|/\beta u'$; —□— True contribution from $\mathbf{K}^1$ and $\mathbf{K}^2$; – · – · – Model evaluation for $\mathbf{K}^1$ and $\mathbf{K}^2$

6.10 Consideration of the Fluid Strain and Rotation Rates

As it stands, the model descriptions for both $\left\langle \nabla \mathbf{u}_p^{\top\prime}(s_1)\mathbf{u}_p'(s_2)\right\rangle$ and $\left\langle \nabla \mathbf{u}_p^{\top\prime}(s)\boldsymbol{v}^{0\prime}(t')\right\rangle$ present the sticking point to ultimately developing a more accurate representation of the increase in particle settling velocity. It is therefore of interest to consider how these

correlations can be represented in order to include more of the underlying physical behaviour that is intrinsic to these quantities. One such approach is to decompose the fluid velocity gradient tensor $\nabla\mathbf{u}$ into its symmetric and antisymmetric parts as given by the fluid strain $\boldsymbol{\Sigma}$ and rotation $\boldsymbol{\Omega}$ [118]

$$\Sigma_{jk}(\mathbf{x},t) = \frac{1}{2}\Big[\nabla_k \mathrm{u}_j(\mathbf{x},t) + \nabla_j \mathrm{u}_k(\mathbf{x},t)\Big] \tag{6.101}$$

$$\Omega_{jk}(\mathbf{x},t) = \frac{1}{2}\Big[\nabla_k \mathrm{u}_j(\mathbf{x},t) - \nabla_j \mathrm{u}_k(\mathbf{x},t)\Big] \tag{6.102}$$

This is consistent with the work of Maxey [91] and Wang & Maxey [163], in which the primary physical mechanism attributed to causing the increase in particle settling velocity was identified as the interaction of particles with the structures in the underlying flow field, in particular the regions of strain and rotation. Therefore inclusion of such information is a natural way of refining the closure model in section 6.7, and accordingly the correlation $\big\langle \nabla\mathbf{u}_p^{\top\prime}(t)\mathbf{u}_p'(t')\big\rangle$ becomes

$$\Big\langle \nabla_j \mathrm{u}_{p_k}'(t)\mathrm{u}_{p_m}'(t')\Big\rangle = \Big\langle \Sigma_{p_{jk}}'(t)\mathrm{u}_{p_m}'(t')\Big\rangle - \Big\langle \Omega_{p_{jk}}'(t)\mathrm{u}_{p_m}'(t')\Big\rangle \tag{6.103}$$

Use of the leading order contribution from the isotropic model for $\big\langle \nabla\mathbf{u}_p^{\top\prime}(t)\mathbf{u}_p'(t')\big\rangle$ in (6.77) can then be used to gain insight into the ramifications of using such a modelling procedure on the separate correlations $\big\langle \boldsymbol{\Sigma}_p{}'(t)\mathbf{u}_p'(t')\big\rangle$ and $\big\langle \boldsymbol{\Omega}_p{}'(t)\mathbf{u}_p'(t')\big\rangle$. Making such an assumption, it follows from (6.101) and (6.102) that the associated models are given by

$$\Big\langle \Sigma_{p_{jk}}'(t)\mathrm{u}_{p_m}'(t')\Big\rangle \approx \frac{1}{2\beta^2}\left[\frac{\partial}{\partial \mathrm{x}_k}\mathrm{R}_{ji}\big(\mathbf{r}_0(t';t)\big) + \frac{\partial}{\partial \mathrm{x}_j}\mathrm{R}_{ki}\big(\mathbf{r}_0(t';t)\big)\right] \tag{6.104}$$

$$\Big\langle \Omega_{p_{jk}}'(t)\mathrm{u}_{p_m}'(t')\Big\rangle \approx \frac{1}{2\beta^2}\left[\frac{\partial}{\partial \mathrm{x}_k}\mathrm{R}_{ji}\big(\mathbf{r}_0(t';t)\big) - \frac{\partial}{\partial \mathrm{x}_j}\mathrm{R}_{ki}\big(\mathbf{r}_0(t';t)\big)\right] \tag{6.105}$$

The assessment of these models in the two-dimensional KS velocity field is shown in Figures 6.13 and 6.14 respectively. It is observed that the behaviour of the symmetric part of the correlation $\big\langle \boldsymbol{\Sigma}_p{}'(t)\mathbf{u}_p'(t')\big\rangle$ in Figure 6.13 is represented fairly well by the model, with a very good fit seen for some components, however the peak amplitude of the remaining components is slightly overpredicted. Notwithstanding this, the timescales of all components decay at very similar rates, and all like $\mathcal{O}(t^2)$. Additionally, the correlation is well approximated at small time separations, and although

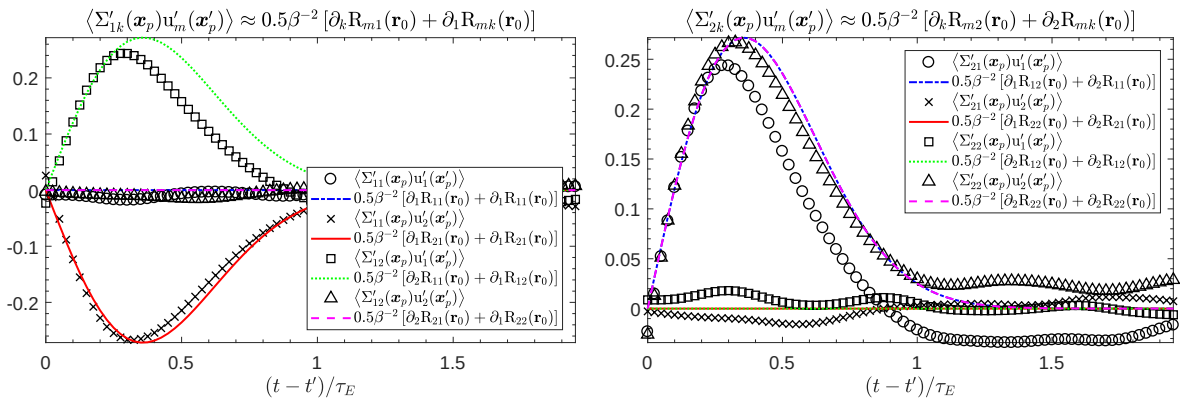

Figure 6.13: Evaluation of all components of the model $\left\langle \Sigma'_{jk}(\boldsymbol{x}_p)\mathrm{u}'_m(\boldsymbol{x}'_p)\right\rangle \approx 0.5\beta^{-2}\left[\partial_k \mathrm{R}_{mj}(\mathbf{r}_0) + \partial_j \mathrm{R}_{mk}(\mathbf{r}_0)\right]$ using KS for $St_E = 0.1$ and $V_g/u' = 1.0$ in a two-dimensional fluid velocity field: Symbols ◯, ×, □, △ components of $\left\langle \Sigma'_{jk}(\boldsymbol{x}_p)\mathrm{u}'_m(\boldsymbol{x}'_p)\right\rangle$; lines – · – · –, ——, · · · · · ·, - - - - components of $0.5\beta^{-2}\left[\partial_k \mathrm{R}_{mj}(\mathbf{r}_0) + \partial_j \mathrm{R}_{mk}(\mathbf{r}_0)\right]$

it does not pass exactly through zero at $t - t' = 0$, it is not considerably different. On the other hand, the antisymmetric part of the correlation $\left\langle \boldsymbol{\Omega}_p{}'(t)\mathbf{u}'_p(t')\right\rangle$ in Figure 6.14 is seen to behave in a markedly different manner, and although the peak amplitude is well approximated by the model, the subsequent temporal decorrelation rate is overpredicted. Notably, the true decorrelation in this case behaves more like $\mathcal{O}(t)$ rather than $\mathcal{O}(t^2)$, and this highlights the difference in timescales associated with the fluid strain and rotation rates respectively. Furthermore, at $t - t' = 0$ the correlation $\left\langle \boldsymbol{\Omega}_p{}'(t)\mathbf{u}'_p(t')\right\rangle$ is distinctly non-zero, implying that this hallmark of $\left\langle \nabla\mathbf{u}_p^{\top\prime}(t)\mathbf{u}'_p(t')\right\rangle$ arises chiefly from its antisymmetric part. As a result, $\left\langle \boldsymbol{\Sigma}_p{}'(t)\mathbf{u}'_p(t')\right\rangle$ can be fairly well described by an isotropic model, whilst the anisotropy that arises in the particle phase due to the reduction in symmetry in this flow configuration is intrinsic to $\left\langle \boldsymbol{\Omega}_p{}'(t)\mathbf{u}'_p(t')\right\rangle$, and should ideally be accounted for in an improved model.

This evaluation in terms of the symmetric and antisymmetric parts of $\left\langle \nabla\mathbf{u}_p^{\top\prime}(t)\mathbf{u}'_p(t')\right\rangle$ includes no new assumptions in the modelling procedure and therefore results in the same closure model as before, however it does highlight the fundamental role that the fluid strain and rotation tensors play in causing particles to experience an increase in settling velocity. In particular, the values of the different timescales for $\boldsymbol{\Sigma}$ and $\boldsymbol{\Omega}$ along particle trajectories is seen to play a key role in the ability of the closure model to accurately capture this behaviour, and as such this constitutes the starting point for further refinement to the existing model. As noted in section 3.4.5, the different timescales associated with $\boldsymbol{\Sigma}$ and $\boldsymbol{\Omega}$ have been modelled in an Eulerian sense [21, 60], however a general form of Lagrangian model for these timescales does not currently

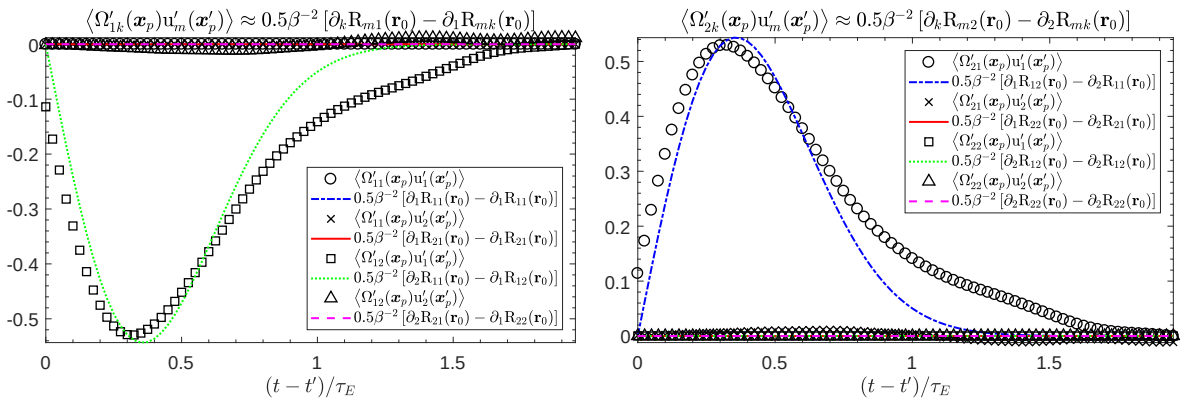

Figure 6.14: Evaluation of all components of the model $\langle \Omega'_{jk}(\boldsymbol{x}_p)\mathrm{u}'_m(\boldsymbol{x}'_p)\rangle \approx 0.5\beta^{-2}\left[\partial_k \mathrm{R}_{mj}(\mathbf{r}_0) - \partial_j \mathrm{R}_{mk}(\mathbf{r}_0)\right]$ using KS for $St_E = 0.1$ and $V_g/u' = 1.0$ in a two-dimensional fluid velocity field: Symbols ◯, ×, □, △ components of $\langle \Omega'_{jk}(\boldsymbol{x}_p)\mathrm{u}'_m(\boldsymbol{x}'_p)\rangle$; lines – · – · –, ——, · · · · · ·, - - - - components of $0.5\beta^{-2}\left[\partial_k \mathrm{R}_{mj}(\mathbf{r}_0) - \partial_j \mathrm{R}_{mk}(\mathbf{r}_0)\right]$

exist in the literature. This then requires that an approximation for these timescales is developed using a physically valid means as an additional precursor to being able to account for the full detail of the observed increase in particle settling velocity.

6.11 Concluding Comments

The foregoing research has shown that the increase in inertial particle settling velocity when subject to a gravitational body force in a zero-mean homogeneous flow is a second-order effect that arises mainly due to interaction of particles with the fluid velocity field, and is not determined solely by mean statistics of the particle phase. Notably, by use of a symmetry analysis the preferential sampling of the average fluid strain rate along particle trajectories is seen to characterise this behaviour entirely, whereas in contrast the average fluid rotation rate experienced by particles is unbiased. Furthermore, it has been demonstrated that it is possible to capture the higher-order phenomenological behaviour inherent in this configuration within a model description, and in particular that the approach of using a cumulant expansion within the PDF kinetic framework is able to account for part of the increase in particle settling velocity. As a result, this modelling procedure has a clear scope for describing particle behaviour that arises due to interaction with turbulent structures in other flow configurations, although it is noted that such models would necessarily need evaluating numerically due to the level of detail contained.

Chapter 7

Analysis of the Particle Velocity Field

7.1 Background

One approach of analysing the various flux contributions arising from particle-fluid interactions is that of a particle velocity field, as discussed in section 3.3. First introduced by Maxey [91], the idea stems from the treatment of the particles as a continuous medium, with the divergence of such a particle velocity field then being a measure of the local compressibility of the particle phase. Maxey applied this idea in the limit of small particle inertia, and was able to derive an expression for the increase in average settling velocity of inertial particles relative to their terminal velocity $\mathbf{V}_g$ for the case of a linear drag law. Specifically, by neglecting terms above $\mathcal{O}(St)$ and obtaining an alternative particle equation of motion for small St, a particular form of a particle velocity field $\boldsymbol{\mathcal{V}}(\mathbf{x}, t)$ emerged, namely [91]

$$\frac{d\boldsymbol{x}_p}{dt} = \boldsymbol{\mathcal{V}}(\boldsymbol{x}_p(t), t) \tag{7.1}$$

$$\boldsymbol{\mathcal{V}}(\mathbf{x}, t) = \mathbf{u}(\mathbf{x}, t) + \mathbf{V}_g + \frac{1}{\beta}\left[\frac{\partial \mathbf{u}}{\partial t} + \mathbf{u}\cdot\nabla\mathbf{u} + \mathbf{V}_g\cdot\nabla\mathbf{u}\right] \tag{7.2}$$

Consequently, the divergence of particle velocity field for $St \ll 1$ is given by [91]

$$\nabla\cdot\boldsymbol{\mathcal{V}}(\mathbf{x}, t) = -\frac{1}{\beta}\frac{\partial \mathrm{u}_i}{\partial \mathrm{x}_j}\frac{\partial \mathrm{u}_j}{\partial \mathrm{x}_i} \tag{7.3}$$

which can be written in terms of the fluid rate of strain $\boldsymbol{\Sigma}(\mathbf{x},t)$ and rotation $\boldsymbol{\Omega}(\mathbf{x},t)$ tensors, thereby implicating these quantities as key determinants of the compressibility of the particle phase. The resultant expression derived for the increase in average settling velocity in a zero-mean homogeneous flow, valid for $St \ll 1$, is [91]

$$\overline{\boldsymbol{\mathcal{V}}}(\mathbf{x},t) = \mathbf{V}_g + \frac{1}{\beta}\int_{t_0}^{t} \left\langle \mathbf{u}(\mathbf{x},t)\, \frac{\partial \mathbf{u}}{\partial \mathbf{x}}\big(\boldsymbol{x}_p(t'),t'\big) : \frac{\partial \mathbf{u}}{\partial \mathbf{x}}\big(\boldsymbol{x}_p(t'),t'\big) \right\rangle dt' \tag{7.4}$$

A more general construction of the particle velocity field framework is provided by Reeks [129], in which an arbitrary particle velocity field $\boldsymbol{\mathcal{V}}(\mathbf{x},t)$ is defined without restricting to the case of small particle inertia. An expression for the particle drift velocity is obtained in this case in terms of the underlying process

$$\big[\boldsymbol{\mathcal{V}}(t'), \nabla\cdot\boldsymbol{\mathcal{V}}(t')\big] \tag{7.5}$$

where formally the process $\boldsymbol{\mathcal{V}}(t')$ represents the field $\boldsymbol{\mathcal{V}}(\boldsymbol{x}_p(t'),t')$, and $\boldsymbol{x}_p(t') = \boldsymbol{x}_p(t' \mid \mathbf{x},t)$ denotes a trajectory passing through $(\mathbf{x},t)$ for a given realisation of the process (7.5) for $t_0 < t' < t$. It is implicit here that the divergence operator is applied to the spatial components of the particle velocity field $\boldsymbol{\mathcal{V}}(\mathbf{x},t)$, and does not operate on $\mathbf{x}$ in the expression $\boldsymbol{x}_p(t' \mid \mathbf{x},t)$. Assuming a Gaussian distribution of this process gives an expression for the average increase in particle settling velocity in a zero-mean homogeneous flow as [129]

$$\overline{\boldsymbol{\mathcal{V}}}(\mathbf{x},t) = \mathbf{V}_g - \int_{t_0}^{t} \Big\langle \boldsymbol{\mathcal{V}}'(\mathbf{x},t)\, \nabla\cdot\boldsymbol{\mathcal{V}}(t' \mid \mathbf{x},t) \Big\rangle\, dt' \tag{7.6}$$

where $\boldsymbol{\mathcal{V}}'(\mathbf{x},t)$ is the fluctuating part of $\boldsymbol{\mathcal{V}}(\mathbf{x},t)$ relative to its mean, and the shorthand notation $\nabla\cdot\boldsymbol{\mathcal{V}}(t' \mid \mathbf{x},t) \equiv \nabla\cdot\boldsymbol{\mathcal{V}}(\boldsymbol{x}_p(t' \mid \mathbf{x},t),t')$ is used for the explicit values of the divergence of particle velocity along particle trajectories that pass through $(\mathbf{x},t)$. It can be seen that the expression (7.4) derived by Maxey is a special case of (7.6) specific to the particle velocity field pertaining to a linear drag model and for $St \ll 1$. The point of interest then is to assess the ability of the general particle velocity field formulation to capture the increase in particle settling velocity by numerical evaluation of (7.6).

7.2 Computing the Divergence of the Particle Velocity Field

In order to determine the particle velocity field $\boldsymbol{\mathcal{V}}(t \mid \mathbf{x}^0, t_0)$ needed to evaluate the expression (7.6), the Jacobian of the Eulerian-Lagrangian transformation is utilised. This is denoted by the deformation tensor with respect to the initial position $\mathbf{x}^0$ outlined in section 3.3.1, defined as

$$\boldsymbol{\mathcal{J}}(\mathbf{x}^0, t) = \frac{\partial \boldsymbol{x}_p(t)}{\partial \mathbf{x}^0} \tag{7.7}$$

Therefore taking the derivative of the equation of evolution (7.1) for $\boldsymbol{\mathcal{V}}(t \mid \mathbf{x}^0, t_0)$ with respect to the position $\mathbf{x}^0$ yields [129]

$$\frac{\partial \dot{\boldsymbol{x}}_p(t)}{\partial \mathbf{x}^0} = \left[\frac{\partial \boldsymbol{\mathcal{V}}(t \mid \mathbf{x}^0, t_0)}{\partial \mathbf{x}}\right]^\top \cdot \frac{\partial \boldsymbol{x}_p(t)}{\partial \mathbf{x}^0}$$

Then interpretation in terms of the Jacobian (7.7) produces the governing equation for $\boldsymbol{\mathcal{J}}(\mathbf{x}^0, t)$

$$\dot{\boldsymbol{\mathcal{J}}}(\mathbf{x}^0, t) = \nabla \boldsymbol{\mathcal{V}}^\top(t \mid \mathbf{x}^0, t_0) \cdot \boldsymbol{\mathcal{J}}(\mathbf{x}^0, t) \quad , \quad \boldsymbol{\mathcal{J}}(\mathbf{x}^0, t_0) = \mathbf{I} \tag{7.8}$$

with the value for the initial condition of $\boldsymbol{\mathcal{J}}(\mathbf{x}^0, t)$ being clear from (7.7). The formal solution is subsequently given by the matrix exponential for the integral of $\nabla \boldsymbol{\mathcal{V}}^\top(t \mid \mathbf{x}^0, t_0)$ along a trajectory [12, 129]

$$\boldsymbol{\mathcal{J}}(\mathbf{x}^0, t) = \exp\left[\int_{t_0}^{t} \nabla \boldsymbol{\mathcal{V}}^\top(t' \mid \mathbf{x}^0, t_0)\, dt'\right] \tag{7.9}$$

The compressibility of the particle phase is related to the Jacobian $\boldsymbol{\mathcal{J}}(\mathbf{x}^0, t)$ through the elemental deformation $J(\mathbf{x}^0, t) = \det\left[\boldsymbol{\mathcal{J}}(\mathbf{x}^0, t)\right]$, which represents the fractional change in an elemental volume at time t along an inertial particle trajectory relative to the position $\mathbf{x}^0$. Therefore it is also instructive to consider the evolution of $J(\mathbf{x}^0, t)$ through the expression

$$\dot{J}(\mathbf{x}^0, t) = \frac{d}{dt}\left[\det\left(\frac{\partial \boldsymbol{x}_p(t)}{\partial \mathbf{x}^0}\right)\right] \tag{7.10}$$

To proceed, Jacobi's formula from linear algebra can be employed. This states that for an invertible matrix $\mathbf{A}$

$$\frac{d}{dt}\Big[\det(\mathbf{A})\Big] = \det(\mathbf{A})\,\mathrm{tr}\left[\mathbf{A}^{-1}\cdot\frac{d\mathbf{A}}{dt}\right] \tag{7.11}$$

Making use of (7.11) and assuming that the deformation tensor $\boldsymbol{\mathcal{J}}(\mathbf{x}^0,t)$ is invertible results in

$$\frac{d}{dt}\left[\det\left(\frac{\partial \boldsymbol{x}_p(t)}{\partial \mathbf{x}^0}\right)\right] = \det\left(\frac{\partial \boldsymbol{x}_p(t)}{\partial \mathbf{x}^0}\right)\,\mathrm{tr}\left[\left(\frac{\partial \boldsymbol{x}_p(t)}{\partial \mathbf{x}^0}\right)^{-1}\cdot\left(\frac{\partial \dot{\boldsymbol{x}}_p(t)}{\partial \mathbf{x}^0}\right)\right] \tag{7.12}$$

Then consistent with the definitions of $\boldsymbol{\mathcal{J}}(\mathbf{x}^0,t)$ and $J(\mathbf{x}^0,t)$ this yields

$$\dot{J}(\mathbf{x}^0,t) = J(\mathbf{x}^0,t)\,\mathrm{tr}\left[\boldsymbol{\mathcal{J}}^{-1}(\mathbf{x}^0,t)\cdot\dot{\boldsymbol{\mathcal{J}}}(\mathbf{x}^0,t)\right] \tag{7.13}$$

Evaluation for the specific particle velocity field $\boldsymbol{\mathcal{V}}(t\mid\mathbf{x}^0,t_0)$ in (7.1) is then possible using the governing equation (7.8) for $\boldsymbol{\mathcal{J}}(\mathbf{x}^0,t)$, which simplifies (7.13) to

$$\dot{J}(\mathbf{x}^0,t) = J(\mathbf{x}^0,t)\nabla\cdot\boldsymbol{\mathcal{V}}(t\mid\mathbf{x}^0,t_0) \qquad , \qquad J(\mathbf{x}^0,t_0)=1 \tag{7.14}$$

This then constitutes the equation of evolution for $J(\mathbf{x}^0,t)$, with the initial condition arising directly from that in (7.8). It is seen from (7.14) that the divergence of the particle velocity field is thus uniquely determined from the elemental deformation $J(\mathbf{x}^0,t)$. The solution then follows in the same manner as for (7.9) [129]

$$J(\mathbf{x}^0,t) = \exp\left[\int_{t_0}^{t}\nabla\cdot\boldsymbol{\mathcal{V}}(t'\mid\mathbf{x}^0,t_0)\,dt'\right] \tag{7.15}$$

Previous work [129, 130, 73] has arrived at the solution (7.15) by means of the concentration equation for particle number density $\phi\,(\mathbf{x},t)$, however the approach outlined here uses only the equation (7.1) that describes particle motion within a velocity field, which is of consequence when it comes to the numerical computation of $\nabla\cdot\boldsymbol{\mathcal{V}}(t'\mid\mathbf{x}^0,t_0)$. The usual procedure for this involves rearrangement of (7.14) to directly yield

$$\nabla\cdot\boldsymbol{\mathcal{V}}(t\mid\mathbf{x}^0,t_0) = \frac{1}{J(\mathbf{x}^0,t)}\dot{J}(\mathbf{x}^0,t) \tag{7.16}$$

Knowledge of the Jacobian $\boldsymbol{\mathcal{J}}(\mathbf{x}^0, t)$ can be used to directly compute the elemental deformation $J(\mathbf{x}^0, t)$, and from this a numerical procedure used to calculate the derivative $\dot{J}(\mathbf{x}^0, t)$. From (7.16) it is also explicit that if the elemental deformation $J(\mathbf{x}^0, t) = 0$ at any point along a particle trajectory, then the divergence of the particle velocity field $\boldsymbol{\mathcal{V}}(t \mid \mathbf{x}^0, t_0)$ will be infinite, which represents either a zero or infinite concentration of particles depending upon the sign of $\nabla \cdot \boldsymbol{\mathcal{V}}(t \mid \mathbf{x}^0, t_0)$ [91]. On the other hand, substitution of the general expression (7.13) into (7.16) determines the divergence of the particle velocity field solely in terms of the Jacobian inverse and its derivative

$$\nabla \cdot \boldsymbol{\mathcal{V}}(t \mid \mathbf{x}^0, t_0) = \mathrm{tr}\left[\boldsymbol{\mathcal{J}}^{-1}(\mathbf{x}^0, t) \cdot \dot{\boldsymbol{\mathcal{J}}}(\mathbf{x}^0, t)\right] \tag{7.17}$$

The key assumption in determining $\nabla \cdot \boldsymbol{\mathcal{V}}(t \mid \mathbf{x}^0, t_0)$ using (7.17) is that the Jacobian $\boldsymbol{\mathcal{J}}(\mathbf{x}^0, t)$ is invertible and therefore non-singular in order for the specification of $\nabla \cdot \boldsymbol{\mathcal{V}}(t \mid \mathbf{x}^0, t_0)$ to be well-posed, which is equivalent to the condition $J(\mathbf{x}^0, t) \neq 0$ inherent in (7.16). However, the advantage of (7.17) is that $\nabla \cdot \boldsymbol{\mathcal{V}}(t \mid \mathbf{x}^0, t_0)$ can then be calculated directly from the more basic quantity of $\boldsymbol{\mathcal{J}}(\mathbf{x}^0, t)$ rather than its determinant, since for a given particle equation of motion, both $\boldsymbol{\mathcal{J}}(\mathbf{x}^0, t)$ and $\dot{\boldsymbol{\mathcal{J}}}(\mathbf{x}^0, t)$ are necessarily known at any given point in time. The exact operations of computing the inverse $\boldsymbol{\mathcal{J}}^{-1}(\mathbf{x}^0, t)$ and taking the trace then require no numerical approximation, meaning that any error introduced from the numerical treatment of $\dot{J}(\mathbf{x}^0, t)$ in (7.16) is avoided, and thereby yielding a less involved means of evaluating $\nabla \cdot \boldsymbol{\mathcal{V}}(t \mid \mathbf{x}^0, t_0)$.

In terms of the particle velocity field itself, from a computational viewpoint it is only reasonable to define $\boldsymbol{\mathcal{V}}(t \mid \mathbf{x}^0, t_0)$ using the individual velocities of an ensemble of particles. Together with (7.17) the process $\left[\boldsymbol{\mathcal{V}}(t'), \nabla \cdot \boldsymbol{\mathcal{V}}(t')\right]$ involved in the formulation is then fully specified, from which the increase in particle settling velocity can be determined using (7.6).

7.3 Interpretation in terms of a Linear Drag Law

Within a simulation study, the statistics of the process (7.5) are required to determine the evolution of the particle velocity field $\boldsymbol{\mathcal{V}}(t \mid \mathbf{x}^0, t_0)$ in time, however this reasoning is somewhat circular since $\boldsymbol{\mathcal{V}}(t \mid \mathbf{x}^0, t_0)$ itself constitutes part of (7.5). Such statistics would in practice be computed by solving the particle equation of motion backwards (7.1) in time along trajectories, which in turn requires the prescription of a particle velocity field $\boldsymbol{\mathcal{V}}(t \mid \mathbf{x}^0, t_0)$. To circumvent this, the required statistics can be computed

directly using data from individual trajectories in a particle tracking simulation by employing the Jacobian $\boldsymbol{\mathcal{J}}(\mathbf{x}^0, t)$. This requires that the governing equation for $\boldsymbol{\mathcal{J}}(\mathbf{x}^0, t)$ is determined for a specific particle equation of motion, and using the standard Stokes drag model (6.15) and taking the derivative with respect to $\mathbf{x}^0$ results in

$$\frac{\partial \ddot{\boldsymbol{x}}_p(t)}{\partial \mathbf{x}^0} = \beta \left[\frac{\partial \mathbf{u}(\boldsymbol{x}_p, t)}{\partial \mathbf{x}}\right]^\top \cdot \frac{\partial \boldsymbol{x}_p(t)}{\partial \mathbf{x}^0} - \beta \frac{\partial \dot{\boldsymbol{x}}_p(t)}{\partial \mathbf{x}^0}$$

Making the interpretation (7.7) then yields the equation of evolution for $\boldsymbol{\mathcal{J}}(\mathbf{x}^0, t)$ specific to the Stokes drag model as

$$\ddot{\boldsymbol{\mathcal{J}}}(\mathbf{x}^0, t) = -\beta \dot{\boldsymbol{\mathcal{J}}}(\mathbf{x}^0, t) + \beta \nabla \mathbf{u}^\top(\boldsymbol{x}_p(t), t) \cdot \boldsymbol{\mathcal{J}}(\mathbf{x}^0, t) \tag{7.18}$$

Upon examination it is noticed that this is identical to the governing equation (6.19) of the particle response tensor $\boldsymbol{\mathcal{H}}[t; t']$ which appears in the dispersion tensors of the PDF kinetic model for the case of Stokes drag model. However, the distinction between the evolution of $\boldsymbol{\mathcal{J}}(\mathbf{x}^0, t)$ and $\boldsymbol{\mathcal{H}}[t; t']$ lies within the initial conditions. From (7.7) it is clear that $\boldsymbol{\mathcal{J}}(\mathbf{x}^0, t_0) = \mathbf{I}$ is the first initial condition as in (7.8), however since (7.8) is a first-order system it contains no information about the initial specification of $\dot{\boldsymbol{\mathcal{J}}}(\mathbf{x}^0, t)$. By definition this represents the Jacobian of the particle velocity along its trajectory with respect to its starting location

$$\dot{\boldsymbol{\mathcal{J}}}(\mathbf{x}^0, t) = \frac{\partial \boldsymbol{v}_p(t)}{\partial \mathbf{x}^0} \tag{7.19}$$

Therefore the initial condition on $\dot{\boldsymbol{\mathcal{J}}}(\mathbf{x}^0, t)$ depends on the initial distribution $\mathbf{v}^0$ of particle velocities at time t_0. In existing work [130, 72] it has been recognised that this second initial condition is unconstrained by the physical evolution of the deformation tensor, and that a careful choice is therefore required. The simplest approach is to take $\mathbf{v}^0$ as being equal to the fluid velocity at the particle position, specifically $\mathbf{v}^0 = \mathbf{u}^0 = \mathbf{u}(\boldsymbol{x}_p(t_0), t_0)$. This implies that in this case the initial condition on $\dot{\boldsymbol{\mathcal{J}}}(\mathbf{x}^0, t)$ is equal to

$$\dot{\boldsymbol{\mathcal{J}}}(\mathbf{x}^0, t_0) = \frac{\partial \mathbf{u}^0}{\partial \mathbf{x}^0} \tag{7.20}$$

Using the same principle for any choice of initial particle velocity $\mathbf{v}^0$ enables an appropriate initial condition to be imposed on $\dot{\boldsymbol{\mathcal{J}}}(\mathbf{x}^0, t)$. In particular, if the particle velocities are initialised in the manner outlined in section 5.3 using the conditional

Gaussian distribution $\phi(\mathbf{v} \mid \mathbf{u})$ as given by (5.58), then the specification of $\mathbf{v}^0$ is as in equation (5.65)

$$\mathbf{v}^0 = \frac{1}{1+St_{Lp}}\left[\sqrt{2St_{Lp}}\,u'\,\mathrm{erf}^{-1}(2\boldsymbol{\psi}-\mathbf{1}) + \mathbf{u}_p(t_0)\right] + \mathbf{V}_g$$

where $\boldsymbol{\psi} \sim \mathrm{U}[\mathbf{0},\mathbf{1}]$ is a uniformly distributed parameter. Thus by (7.19) the initial condition for $\dot{\boldsymbol{\mathcal{J}}}(\mathbf{x}^0,t)$ in this case is given by

$$\dot{\boldsymbol{\mathcal{J}}}(\mathbf{x}^0,t_0) = \frac{1}{1+St_{Lp}}\frac{\partial \mathbf{u}^0}{\partial \mathbf{x}^0} \tag{7.21}$$

This completes the specification of the evolution of $\boldsymbol{\mathcal{J}}(\mathbf{x}^0,t)$, which can then be determined from a simulation by numerically solving the governing equation (7.18) along particle trajectories with the initial conditions $\boldsymbol{\mathcal{J}}(\mathbf{x}^0,t_0) = \mathbf{I}$ and (7.21).

7.4 Comparison with the PDF Kinetic Model

For the time arguments that emerge from the derivation of the particle velocity field drift tensor (7.6), the value for the divergence of the particle velocity field which is required is given by $\nabla \cdot \boldsymbol{\mathcal{V}}(t' \mid \mathbf{x},t)$. Using the appropriate arguments in (7.17) yields

$$\nabla \cdot \boldsymbol{\mathcal{V}}(t' \mid \mathbf{x},t) = \mathrm{tr}\left[\boldsymbol{\mathcal{J}}^{-1}(\mathbf{x},t') \cdot \dot{\boldsymbol{\mathcal{J}}}(\mathbf{x},t')\right] \tag{7.22}$$

Thus in order to correctly compute the increase in settling velocity that particles experience when subject to a gravitational body force, it is the Jacobian $\boldsymbol{\mathcal{J}}(\mathbf{x},t')$ which is required, or in other words the particle deformation tensor at time t' with respect to the trajectory endpoint $\mathbf{x}$. Thus in this problem the initial conditions $\boldsymbol{\mathcal{J}}(\mathbf{x}^0,t_0) = \mathbf{I}$ and (7.21) become the equivalent final conditions, meaning that the governing equation (7.18) for $\boldsymbol{\mathcal{J}}(\mathbf{x},t')$ formally requires solution backwards in time to produce the correct interpretation of $\boldsymbol{\mathcal{J}}(\mathbf{x},t')$. This presents a problem however, as numerical solution of (7.18) for times before the initial condition results in a solution which grows exponentially, in the same manner as for the particle equation of motion outlined in section 6.7.1.

This highlights the difference between the particle velocity field approach and the PDF kinetic model; the particle response tensor $\boldsymbol{\mathcal{H}}[t;t']$ which emerges in the dispersion tensor $\overline{\boldsymbol{\kappa}}(t)$ is evaluated forwards in time, however the particle Jacobian $\boldsymbol{\mathcal{J}}(\mathbf{x},t')$ requires

evaluation backwards in time. The inherent difference between the FIT and BIT forms of the governing equation (7.18) therefore means that using the FIT form to compute $\boldsymbol{\mathcal{J}}(\mathbf{x}^0, t')$ with standard numerical methods will provide incorrect behaviour for $\nabla \cdot \boldsymbol{\mathcal{V}}(t' \mid \mathbf{x}, t)$. Thus despite $\boldsymbol{\mathcal{H}}[t; t']$ and $\boldsymbol{\mathcal{J}}(\mathbf{x}, t')$ sharing a governing equation, it is the respective imposition of conditions at the initial and final points on the trajectory which distinguishes the behaviour of these quantities, and ultimately determines the tractability of the approaches they correspond to. Nonetheless, in the absence of a suitable procedure for computing the BIT Jacobian $\boldsymbol{\mathcal{J}}(\mathbf{x}, t')$, the FIT form $\boldsymbol{\mathcal{J}}(\mathbf{x}^0, t')$ is instead used in this work. This still permits a meaningful analysis of the evolution of $\boldsymbol{\mathcal{J}}(\mathbf{x}^0, t')$ and $J(\mathbf{x}^0, t)$, however evaluation of (7.6) may not be exact.

7.5 Numerical Assessment of the Particle Velocity Field Approach

To test the efficacy of particle velocity field formulation at capturing the increase in particle settling velocity, the KS velocity field specified in Chapter 5 is utilised. The numerical treatment is identical to that outlined in section 5.2, with fact that the governing equation (7.18) of the Jacobian $\boldsymbol{\mathcal{J}}(\mathbf{x}^0, t)$ is the same as that of the particle response tensor $\boldsymbol{\mathcal{H}}[t; t']$ meaning that the procedure for computation in section 5.2.2 and timestep criterion (5.33) remain the same.

To demonstrate the intricacies involved in computing $\nabla \cdot \boldsymbol{\mathcal{V}}(t \mid \mathbf{x}^0, t_0)$, it is appropriate to consider the evolution of the elemental deformation $J(\mathbf{x}^0, t)$ along a single trajectory, in view of the condition $J(\mathbf{x}^0, t') \neq 0$ needed to ensure the well-posedness of $\nabla \cdot \boldsymbol{\mathcal{V}}(t \mid \mathbf{x}^0, t_0)$. Such a realisation is seen in Figure 7.1, which shows that $J(\mathbf{x}^0, t)$ evolves from its initial condition $J(\mathbf{x}^0, t_0) = 1$ but experiences a rapid decrease along this particular trajectory such that it passes through zero at $t \approx \tau_E$. The implication of this is that the reciprocal $1/J(\mathbf{x}^0, t)$ naturally experiences a singularity where the magnitude not only becomes infinite, but a sign change also occurs. Evaluation of $\nabla \cdot \boldsymbol{\mathcal{V}}(t \mid \mathbf{x}^0, t_0)$ using (7.16) will therefore explicitly include this singularity, meaning that any average statistics calculated using the contribution form this trajectory will be biased.

This is mostly easily seen through consideration of the average $\langle \nabla \cdot \boldsymbol{\mathcal{V}}(t \mid \mathbf{x}^0, t_0) \rangle$, as shown in Figure 7.2. Use of (7.16) and the elemental deformation $J(\mathbf{x}^0, t)$ results in $\langle \nabla \cdot \boldsymbol{\mathcal{V}}(t \mid \mathbf{x}^0, t_0) \rangle$ decreasing smoothly from zero to a minimum at $t \approx 0.25\tau_E$, however the average becomes increasingly noisy as it increases to an equilibrium value due to

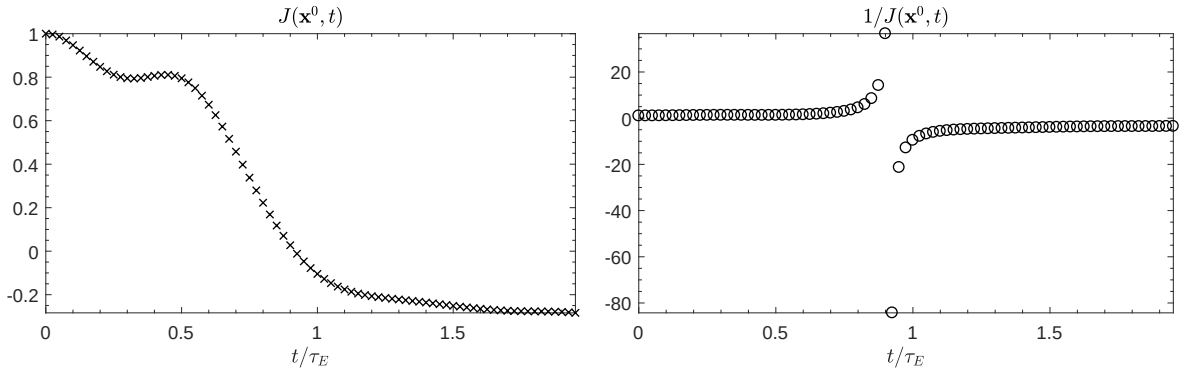

Figure 7.1: A single realisation of the evolution of $J(\mathbf{x}^0,t)$ along a particle trajectory obtained using KS for $St_E = 0.1$ and $V_g/u' = 1.0$ in a two-dimensional fluid velocity field: $\times$ $J(\mathbf{x}^0,t)$; $\bigcirc$ $1/J(\mathbf{x}^0,t)$

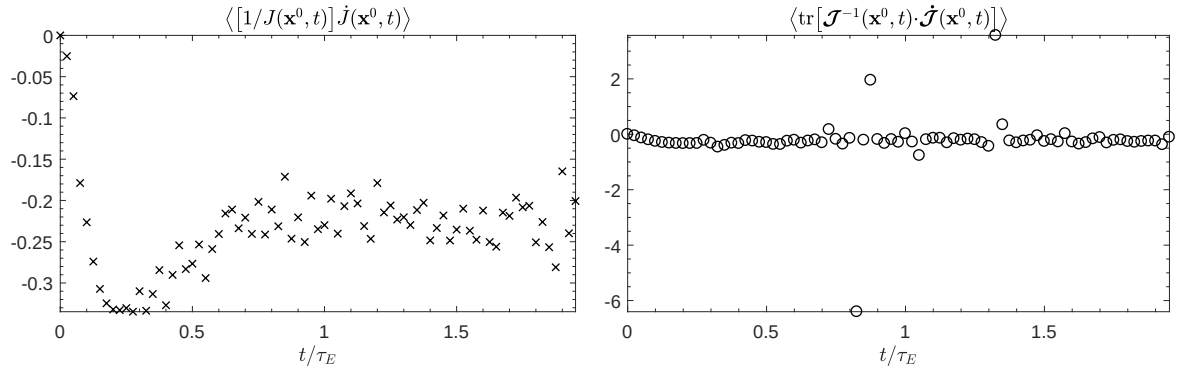

Figure 7.2: Comparison of evolution of the average $\langle \nabla\cdot\boldsymbol{\mathcal{V}}(t \mid \mathbf{x}^0,t_0)\rangle$ evaluated from both (7.16) and (7.17), obtained using KS for $St_E = 0.1$ and $V_g/u' = 1.0$ in a two-dimensional fluid velocity field: $\times$ $\langle [1/J(\mathbf{x}^0,t)]\,\dot{J}(\mathbf{x}^0,t)\rangle$; $\bigcirc$ $\langle \mathrm{tr}[\boldsymbol{\mathcal{J}}^{-1}(\mathbf{x}^0,t)\cdot\dot{\boldsymbol{\mathcal{J}}}(\mathbf{x}^0,t)]\rangle$

the presence of singularities in $1/J(\mathbf{x}^0,t)$. On the other hand, using (7.17) and the Jacobian $\boldsymbol{\mathcal{J}}(\mathbf{x}^0,t)$ actually amplifies the effect that $\boldsymbol{\mathcal{J}}(\mathbf{x}^0,t)$ being almost singular has on $\langle \nabla\cdot\boldsymbol{\mathcal{V}}(t \mid \mathbf{x}^0,t_0)\rangle$, to the extent that it cannot be considered a meaningful average. In this case then, using the expression $\langle [1/J(\mathbf{x}^0,t)]\,\dot{J}(\mathbf{x}^0,t)\rangle$ provides a more useful means of evaluating $\nabla\cdot\boldsymbol{\mathcal{V}}(t \mid \mathbf{x}^0,t_0)$ and statistics arising from it.

This naturally begs the question as to whether specific treatment of either $J(\mathbf{x}^0,t)$ or $\boldsymbol{\mathcal{J}}(\mathbf{x}^0,t)$ can provide an expression for $\nabla\cdot\boldsymbol{\mathcal{V}}(t \mid \mathbf{x}^0,t_0)$ which is relatively free of the effect from singularities. In particular, setting a limit on the degree of singularity that $\boldsymbol{\mathcal{J}}(\mathbf{x}^0,t)$ can possess in order to contribute to average statistics is an elementary method of filtering out the confounding effect of singularities, with the practical use of such a limit requiring fine tuning to exclude only the extreme values of $\nabla\cdot\boldsymbol{\mathcal{V}}(t \mid \mathbf{x}^0,t_0)$. This is considered in further detail here, with only the realisations in which $\boldsymbol{\mathcal{J}}(\mathbf{x}^0,t)$

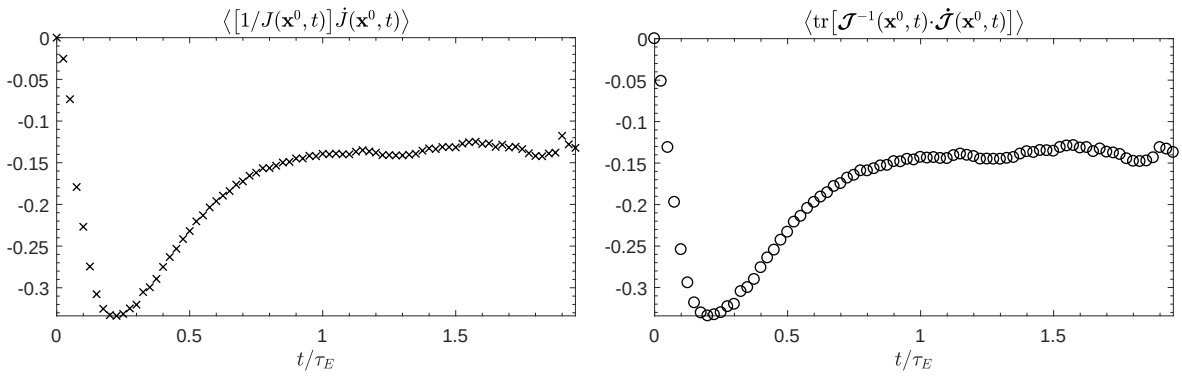

Figure 7.3: Comparison of evolution of the average $\langle \nabla \cdot \boldsymbol{\mathcal{V}}(t \mid \mathbf{x}^0, t_0)\rangle$ evaluated from both (7.16) and (7.17) by setting a limit on the degree of singularity that $\boldsymbol{\mathcal{J}}(\mathbf{x}^0,t)$ can instantaneously experience in order to be included in the average, obtained using KS for $St_E = 0.1$ and $V_g/u' = 1.0$ in a two-dimensional fluid velocity field: $\times$ $\langle\,[1/J(\mathbf{x}^0,t)]\,\dot{J}(\mathbf{x}^0,t)\rangle$; $\bigcirc$ $\langle \mathrm{tr}\big[\boldsymbol{\mathcal{J}}^{-1}(\mathbf{x}^0,t)\cdot\dot{\boldsymbol{\mathcal{J}}}(\mathbf{x}^0,t)\big]\rangle$

is almost singular being removed from the average $\langle \nabla \cdot \boldsymbol{\mathcal{V}}(t \mid \mathbf{x}^0, t_0)\rangle$. The outcome of this procedure is shown in Figure 7.3, from which it is seen that the filtering of singularities has a substantial smoothing effect on the value of $\langle \nabla \cdot \boldsymbol{\mathcal{V}}(t \mid \mathbf{x}^0, t_0)\rangle$ as it equilibrates. Furthermore, the separate evaluations of $\langle\,[1/J(\mathbf{x}^0,t)]\,\dot{J}(\mathbf{x}^0,t)\rangle$ and $\langle \mathrm{tr}\big[\boldsymbol{\mathcal{J}}^{-1}(\mathbf{x}^0,t)\cdot\dot{\boldsymbol{\mathcal{J}}}(\mathbf{x}^0,t)\big]\rangle$ are now in agreement as expected, demonstrating the ability of such a filtering procedure to produce consistent results from distinct expressions which each require different numerical treatment. It is worth noting however that this procedure results in $\langle \nabla \cdot \boldsymbol{\mathcal{V}}(t \mid \mathbf{x}^0, t_0)\rangle$ equilibrating at a higher value than that of the average asymptotic value of $\langle\,[1/J(\mathbf{x}^0,t)]\,\dot{J}(\mathbf{x}^0,t)\rangle$ in Figure 7.2, implying that such a filtering procedure may produce a bias if there are more near singularities in $\boldsymbol{\mathcal{J}}(\mathbf{x}^0,t)$ which are negative than positive. Additionally, by the end of the sampling period $\sim 25\%$ of trajectories failed to satisfy the limit set on the singularity of $\boldsymbol{\mathcal{J}}(\mathbf{x}^0,t)$, with the occurrence of singularities appearing to increase as time progresses.

With this restriction on $\boldsymbol{\mathcal{J}}(\mathbf{x}^0,t)$ being non-singular, it is now meaningful to use $\nabla\cdot\boldsymbol{\mathcal{V}}(t \mid \mathbf{x}^0, t_0)$ for the evaluation of other statistics, and specifically the drift tensor in (7.6) which is used to determine the increase in particle settling velocity. The outcome of this is shown in Figure 7.4, and it is seen that the particle velocity field $|\overline{\mathcal{V}}_2(t) - V_g|/u'$ correctly retrieves an increase in the average settling velocity, however the magnitude of this effect does not reach the full extent of the observed value $|\overline{\mathrm{v}}_2(t) - V_g|/u'$, falling $\sim 30\%$ short. At least some of this discrepancy can be attributed to the filtering procedure used for ensuring that $\boldsymbol{\mathcal{J}}(\mathbf{x}^0,t)$ remains non-singular, however this does not explain other features of the qualitative behaviour of $|\overline{\mathcal{V}}_2(t) - V_g|/u'$. In particular, the

PDF dispersion tensor $|\overline{\kappa}_2(t)|/\beta u'$ increases monotonically from zero to its asymptotic value after $\sim 1.5\tau_E$, in contrast with $|\overline{\mathcal{V}}_2(t) - V_g|/u'$ which first decreases to a negative value. Furthermore, $|\overline{\mathcal{V}}_2(t) - V_g|/u'$ also only reaches its asymptotic value after $\sim 2\tau_E$, with a slower convergence rate than $|\overline{\kappa}_2(t)|/\beta u'$. These aspects are likely to be affected by the fact that $\boldsymbol{\mathcal{J}}(\mathbf{x}^0, t)$ is being computed FIT in this work rather than the correct BIT from that is required for the drift tensor (7.6) as indicated in section 7.4, however a thorough appraisal of the consequences arising from this numerical treatment of $\boldsymbol{\mathcal{J}}(\mathbf{x}^0, t)$ requires the equivalent BIT form to be known, and is therefore beyond the scope of this preliminary investigation.

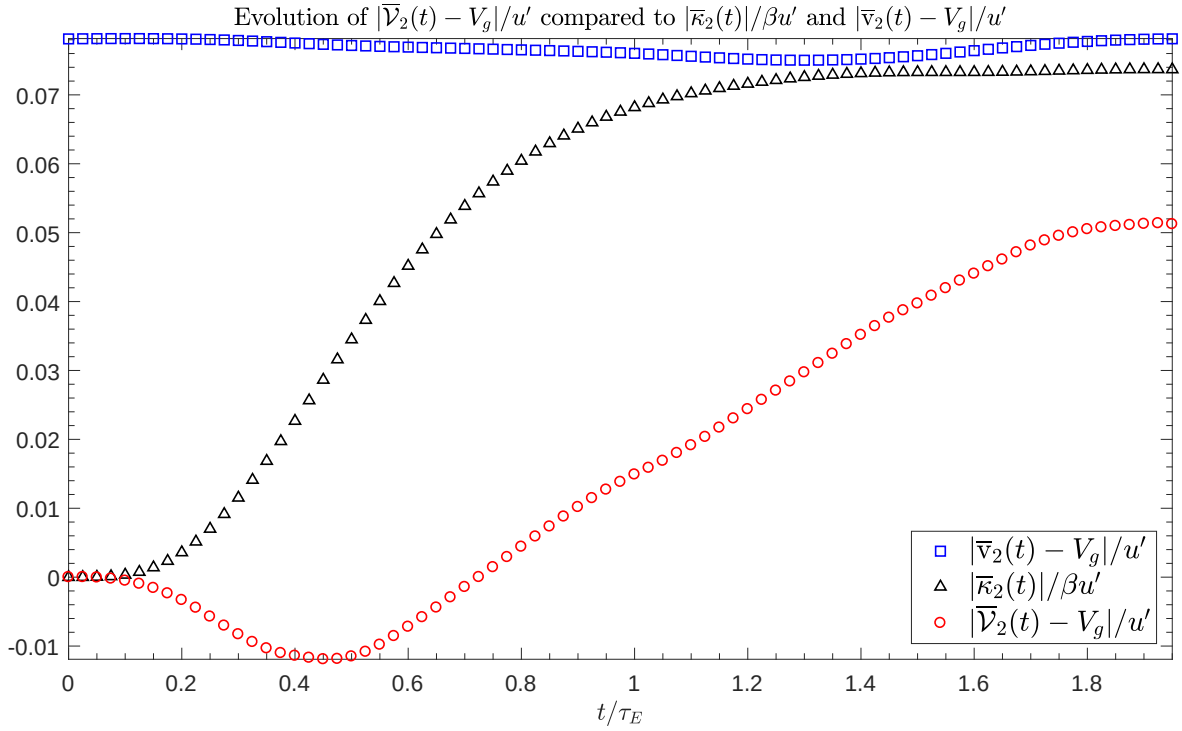

Figure 7.4: Evolution of $|\overline{\mathcal{V}}_2(t) - V_g|/u'$ compared to $|\overline{\kappa}_2(t)|/\beta u'$ and $|\overline{\mathrm{v}}_2(t) - V_g|/u'$, obtained from KS evaluation for $St_E = 0.1$ and $V_g/u' = 1.0$ in a two-dimensional fluid velocity field: —□— $|\overline{\mathcal{V}}_2(t) - V_g|/u'$; —△— $|\overline{\kappa}_2(t)|/\beta u'$; —○— $|\overline{\mathrm{v}}_2(t) - V_g|/u'$

7.6 Concluding Comments

The outcome from this analysis is that the particle velocity field formulation requires further consideration with regards to the numerical treatment of the Jacobian $\boldsymbol{\mathcal{J}}(\mathbf{x}^0, t')$, in order to provide a meaningful computational approach to evaluating inertial particle behaviour. It is worth noting that alternative specification of a compressible fluid

velocity field in which $\nabla \cdot \mathbf{u}(\mathbf{x}, t) \neq 0$ and subsequent tracking of the fluid elements along their trajectories would be another way of assessing the drift tensor (7.6). Such an approach does however raise the question of how this compressibility would be determined, and moreover how the inclusion of a gravitational body force could be accounted for, since tracking fluid elements does not allow for the inclusion of gravity.

In the case of particle settling under gravity in an incompressible velocity field, evaluation of $\nabla \cdot \boldsymbol{\mathcal{V}}(t' \mid \mathbf{x}, t)$ is able to capture some of the observed increase in settling velocity by computing $\boldsymbol{\mathcal{J}}(\mathbf{x}^0, t')$ forwards in time, however it does not retrieve the full effect as in the case of the dispersion tensor $\overline{\boldsymbol{\kappa}}(t)$ which arises from the PDF kinetic model. As discussed in section 7.4, this is because the PDF kinetic model is capable of correctly quantifying this effect through the particle response tensor $\boldsymbol{\mathcal{H}}[t; t']$ using standard numerical methods, however the particle velocity field approach formally requires backward in time evaluation of $\boldsymbol{\mathcal{J}}(\mathbf{x}, t')$, meaning that the correct behaviour cannot be obtained with the same treatment. Nonetheless, the potential of the particle velocity field approach to well describe the true particle behaviour may be possible to exploit with specific numerical treatment, and remains as an avenue of future investigation.

Chapter 8

Particle-Pair Models

8.1 Background

The phenomenon of particle clustering within turbulent flows is a subject that has attracted widespread attention, with particles not being uniformly mixed by the turbulence but instead tending to accumulate in low vorticity regions of the flow in the same manner as particles settling under gravity, as outlined in section 3.4. The majority of existing work is predominantly concerned with the clustering of small inertial particles that are governed using a simple linear drag law, with a mixture of simulation studies that seek to gain further understanding into the physical mechanisms responsible for clustering [171, 30, 18], but also the development of modelling approaches which aim to describe the behaviour in terms of a more general theoretical framework [177, 31, 15]. In particular a number of studies have investigated this effect via the application of two-particle descriptions and the analysis of corresponding radial distribution functions in homogeneous flows as discussed in section 3.4.5, which involves considering the particle concentration in terms of the separation distance between particles. In such a formulation, for two mono-dispersed particles with trajectories $\boldsymbol{x}_p^1(t)$, $\boldsymbol{x}_p^2(t)$ and velocities $\boldsymbol{v}_p^1(t)$, $\boldsymbol{v}_p^2(t)$, the inter-particle separation $\boldsymbol{r}_p(t) = \boldsymbol{x}_p^2(t) - \boldsymbol{x}_p^1(t)$ and relative velocity $\boldsymbol{w}_p(t) = \boldsymbol{v}_p^2(t) - \boldsymbol{v}_p^1(t)$ define a Lagrangian frame of reference by setting the particle $\boldsymbol{x}_p^1(t)$ as the datum point. If the particle dynamics are governed by the Stokes drag model (2.22) in a flow which is described by a velocity field $\mathbf{U}(\mathbf{x}, t)$ and subject to no external body forces, then the two-particle equation of motion is given by the difference of the respective one-particle equations of motion

$$\ddot{\boldsymbol{r}}_p(t) = \beta\Big[\mathbf{U}\left(\boldsymbol{r}_p(t) + \boldsymbol{x}_p^1(t), t\right) - \mathbf{U}\left(\boldsymbol{x}_p^1(t), t\right) - \boldsymbol{w}_p(t)\Big] \quad , \quad \begin{matrix}\boldsymbol{r}_p(t_0) = \mathbf{r}^0 \\ \boldsymbol{w}_p(t_0) = \mathbf{w}^0\end{matrix} \tag{8.1}$$

For a homogeneous flow field the notion of an effective relative velocity field $\widetilde{\mathbf{u}}(\mathbf{r}, t)$ can be introduced for small separations in space $\mathrm{r} = |\mathbf{r}|$ by using a Taylor expansion of $\mathbf{U}\left(\mathbf{x}^2, t\right)$ about $\mathbf{x}^1$, which to leading order yields the approximation [31]

$$\mathbf{U}\left(\mathbf{x}^2, t\right) - \mathbf{U}\left(\mathbf{x}^1, t\right) \approx \mathbf{r} \cdot \nabla \mathbf{U}\left(\mathbf{x}^1, t\right) \equiv \widetilde{\mathbf{u}}\left(\mathbf{r}, t\right) \tag{8.2}$$

Then the two-particle equation of motion (8.1) is statistically equivalent to

$$\ddot{\boldsymbol{r}}_p(t) = \beta\Big[\widetilde{\mathbf{u}}\left(\boldsymbol{r}_p(t), t\right) - \boldsymbol{w}_p(t)\Big] \quad , \quad \begin{matrix}\boldsymbol{r}_p(t_0) = \mathbf{r}^0 \\ \boldsymbol{w}_p(t_0) = \mathbf{w}^0\end{matrix} \tag{8.3}$$

This equation of motion takes the same form as the single particle model given by (8.1), meaning that the associated two-particle PDF $p\left(\mathbf{r}, \mathbf{w}, t\right)$ can be interpreted directly within the existing framework for the usual one-particle PDF $p\left(\mathbf{x}, \mathbf{v}, t\right)$. Of specific interest is then the expression for the particle mass flux (4.48), in this case namely

$$\rho\overline{\mathbf{w}} = \underbrace{\rho\left[\langle\widetilde{\mathbf{u}}\rangle + \tau_p\left\{\underbrace{\left[\overline{\boldsymbol{\kappa}} - \nabla\cdot\overline{\boldsymbol{\lambda}}\right]}_{\boxed{1}} - \underbrace{\nabla\cdot\overline{\mathbf{cc}}}_{\boxed{2}} - \underbrace{\frac{D}{Dt}\overline{\mathbf{w}}}_{\boxed{3}}\right\}\right]}_{\text{convective flux}} \underbrace{- \tau_p\left(\overline{\mathbf{cc}} + \overline{\boldsymbol{\lambda}}^{\top}\right)\cdot\nabla\rho}_{\substack{\boxed{4} \\ \text{diffusive flux}}} \tag{8.4}$$

Within the context of a particle-pair framework which exhibits a steady state, it is then the convective flux contributions $\boxed{1}$ and $\boxed{2}$ to $\rho\overline{\mathbf{w}}$ that determine the equilibrium distribution of $\rho(\mathbf{r}, t)$, which is also interpreted as the RDF in this case. The distinction between the two-particle and one-particle models resides in the statistical properties of $\widetilde{\mathbf{u}}\left(\mathbf{r}, t\right)$ and $\mathbf{U}\left(\mathbf{x}, t\right)$, as while $\mathbf{U}\left(\mathbf{x}, t\right)$ represents a homogeneous flow clearly $\widetilde{\mathbf{u}}\left(\mathbf{r}, t\right)$ does not, with the consequence that the frame of reference resulting from use of the separations $\boldsymbol{r}_p(t)$ and $\boldsymbol{w}_p(t)$ introduces an inhomogeneity to the model. This inhomogeneity is manifest within the contributions $\boxed{1}$ and $\boxed{2}$ to the particle mass flux, and as discussed in section 4.2.3 previous modelling approaches either do not explicitly take into account these terms [31], or assume that $\boxed{1} \equiv \mathbf{0}$ across all values of St [178].

However, the balance between $\boxed{1}$ and $\boxed{2}$ can become a non-negligible contribution in some flow configurations, the verification of which remains as an outstanding matter.

8.2 Inhomogeneous Flow Field Model

8.2.1 Specification

In order to investigate the phenomenon of particle clustering, the inhomogeneity that is intrinsic to two-particle descriptions in a homogeneous flow can be likened to that arising from one-particle behaviour within an inhomogeneous flow, thereby motivating the construction of an inhomogeneous fluid velocity field. Taking inspiration from the statistically equivalent form (8.3) of the two-particle equation of motion and following the approach implicit in the work of Zaichik [177, 178, 179, 181], an appropriate Eulerian velocity field $\mathbf{u}(\mathbf{x},t)$ can be specified by utilising the approximation for the relative fluid velocity $\widetilde{\mathbf{u}}(\mathbf{r},t)$ in (8.2), and fixing the position at which one of the fluid velocities $\mathbf{U}(\mathbf{x},t)$ acts. Specifically, making the location-independent assignment of $\mathbf{x}^1 = \mathbf{0}$ and also taking $\mathbf{x}^2 = \mathbf{x}$ in (8.2) yields the following approximation to $\widetilde{\mathbf{u}}(\mathbf{r},t)$

$$\mathbf{u}(\mathbf{x},t) = \mathbf{U}(\mathbf{x},t) - \mathbf{U}(\mathbf{0},t) \tag{8.5}$$

Thus this creates an inhomogeneity in the resultant velocity field $\mathbf{u}(\mathbf{x},t)$ from the underlying homogeneous field $\mathbf{U}(\mathbf{x},t)$, and while (8.5) does not capture the exact dynamics of particle-pair behaviour, it does offer a simple method for both evaluating the various particle mass flux contributions in (8.4) and testing closure approximations.

8.2.2 Deductive Properties

Since the form of inhomogeneous flow field $\mathbf{u}(\mathbf{x},t)$ specified in (8.5) is determined directly from the homogeneous velocity field $\mathbf{U}(\mathbf{x},t)$, relevant properties of $\mathbf{u}(\mathbf{x},t)$ can be deduced in a straightforward manner from those of $\mathbf{U}(\mathbf{x},t)$. Most notably it is clear that $\mathbf{u}(\mathbf{0},t) = \mathbf{0}$ thereby creating an artificial sink at the reference point $\mathbf{x} = \mathbf{0}$, and the various characteristics of $\mathbf{u}(\mathbf{x},t)$ that arise due to this phenomenon are detailed in the following.

Invariance of Fluid Velocity Gradient

From the definition of $\mathbf{u}(\mathbf{x},t)$ in (8.5), since the term $\mathbf{U}(\mathbf{0},t)$ contains no spatial dependence it directly follows that

$$\nabla\mathbf{u}(\mathbf{x},t) = \nabla\mathbf{U}(\mathbf{x},t) \tag{8.6}$$

Thus the fluid velocity gradient is unchanged from that of the homogeneous flow field $\mathbf{U}(\mathbf{x},t)$. An immediate consequence of this is that if $\mathbf{U}(\mathbf{x},t)$ is incompressible, then so is $\mathbf{u}(\mathbf{x},t)$.

Periodicity

If $\mathbf{U}(\mathbf{x},t)$ is taken to be periodic such that $\mathbf{U}(\mathbf{x}+\mathcal{L},t) = \mathbf{U}(\mathbf{x},t)$, then by (8.5)

$$\begin{aligned}\mathbf{u}(\mathbf{x}+\mathcal{L},t) &= \mathbf{U}(\mathbf{x}+\mathcal{L},t) - \mathbf{U}(\mathbf{0},t)\\ &= \mathbf{U}(\mathbf{x},t) - \mathbf{U}(\mathbf{0},t)\\ &= \mathbf{u}(\mathbf{x},t)\end{aligned} \tag{8.7}$$

and thus $\mathbf{u}(\mathbf{x},t)$ is also periodic.

Zero-mean Flow

Taking $\big\langle\mathbf{U}(\mathbf{x},t)\big\rangle = \mathbf{0}$ when considered as a statistically stationary flow field in the long-time limit, then using (8.5) yields

$$\big\langle\mathbf{u}(\mathbf{x},t)\big\rangle = \big\langle\mathbf{U}(\mathbf{x},t)\big\rangle - \big\langle\mathbf{U}(\mathbf{0},t)\big\rangle = \mathbf{0} \tag{8.8}$$

Therefore the steady state form of $\mathbf{u}(\mathbf{x},t)$ is also a zero-mean flow field.

8.2.3 Interpretation in terms of the KS Velocity Field

From a simulation perspective, the specific form of the inhomogeneous velocity field $\mathbf{u}(\mathbf{x},t)$ in (8.5) can be used to make further inferences about the statistical properties

of the flow as well as computational aspects. In particular, for the KS velocity field $\mathbf{U}(\mathbf{x},t)$ defined in Chapter 5 by (5.2), $\mathbf{u}(\mathbf{x},t)$ is consequently determined by

$$\mathbf{u}(\mathbf{x},t) = \sum_{\mathbf{k}} \mathbf{c}_{\mathbf{k}}(t)\Big[\exp\left[i\,\mathbf{k}\cdot\mathbf{x}\right] - 1\Big] \tag{8.9}$$

Since the only modification required is a constant shift of the spatial exponential component in the sum, (8.9) is therefore no more computationally demanding to construct than the homogeneous velocity field (5.2). Furthermore, assuming that $\mathbf{U}(\mathbf{x},t)$ conforms to a Gaussian distribution, then it follows that $\mathbf{u}(\mathbf{x},t)$ is also normally distributed. This can be seen by considering that if the form of $\mathbf{U}(\mathbf{x},t)$ as given by (5.2) is Gaussian by the central limit theorem, then the distribution of $\mathbf{u}(\mathbf{x},t)$ defined by (8.9) should be qualitatively the same as that of $\mathbf{U}(\mathbf{x},t)$, since all the random variables in the KS procedure are within the $\mathbf{c}_{\mathbf{k}}(t)$ component of (8.9) and the shift is only applied to the deterministic exponential tail of (8.9). This important fact enables use of the PDF kinetic model as an exact means of describing particle behaviour in the flow field $\mathbf{u}(\mathbf{x},t)$ without requiring the contributions from the higher-order cumulants of the expansion (4.9). The remaining implications of (8.5) are then on the fluid velocity correlations which result from using this specific form of $\mathbf{u}(\mathbf{x},t)$.

Two-point Two-time Fluid Velocity Correlation Tensor

From the definition of $\mathbf{u}(\mathbf{x},t)$ in (8.5), a direct consequence is that the two-point two-time fluid velocity correlations take the form

$$\begin{aligned}\left\langle \mathbf{u}(\mathbf{x}',t')\mathbf{u}(\mathbf{x},t)\right\rangle = \left\langle \mathbf{U}(\mathbf{x}',t')\mathbf{U}(\mathbf{x},t)\right\rangle - \left\langle \mathbf{U}(\mathbf{x}',t')\mathbf{U}(\mathbf{0},t)\right\rangle \\ - \left\langle \mathbf{U}(\mathbf{0},t')\mathbf{U}(\mathbf{x},t)\right\rangle + \left\langle \mathbf{U}(\mathbf{0},t')\mathbf{U}(\mathbf{0},t)\right\rangle\end{aligned}$$

Furthermore, the fluid velocity correlations of the zero-mean homogeneous KS velocity field constructed in Chapter 5 are decomposed into the separate spatial and temporal correlations $\mathbf{Q}(\mathbf{r})$ and $\mathrm{E}_{\omega}(s)$ respectively for $\mathbf{r} = \mathbf{x} - \mathbf{x}'$ and $s = t - t'$, as given by (5.10). Additionally, since $\mathbf{U}(\mathbf{x},t)$ is taken to be isotropic, and also denoting the two-point correlations of $\mathbf{u}(\mathbf{x},t)$ by $\widetilde{\mathbf{Q}}(\mathbf{x}';\mathbf{x}) = \left\langle \mathbf{u}(\mathbf{x}',t)\mathbf{u}(\mathbf{x},t)\right\rangle$ leads to the more compact expression

$$\widetilde{\mathbf{Q}}(\mathbf{x}';\mathbf{x})\mathrm{E}_\omega(s) = \Big[\mathbf{Q}(\mathbf{r}) - \mathbf{Q}(\mathbf{x}') - \mathbf{Q}(\mathbf{x}) + \mathbf{Q}(\mathbf{0})\Big]\mathrm{E}_\omega(s) \tag{8.10}$$

This has the implication that even though $\mathbf{u}(\mathbf{x},t)$ is inhomogeneous and anisotropic, the specific definition of the velocity field in (8.5) crucially enables the two-point correlations $\widetilde{\mathbf{Q}}(\mathbf{x}';\mathbf{x})$ to be represented as a superposition of isotropic correlation tensors. As a result $\widetilde{\mathbf{Q}}(\mathbf{x}';\mathbf{x})$ can be expressed in terms of the separation $\mathbf{r}$ and longitudinal and lateral correlation coefficients $f(\mathrm{r})$ and $g(\mathrm{r})$ of $\mathbf{U}(\mathbf{x},t)$ by means of (5.17). Since they are functions of spatial separation, the corresponding forms of $\widetilde{f}(\mathrm{r})$ and $\widetilde{g}(\mathrm{r})$ for $\mathbf{u}(\mathbf{x},t)$ can also be decomposed in the same manner as (8.10). This has the consequence that the longitudinal integral lengthscale L_{11} becomes location dependent on both the points $\mathbf{x}$ and $\mathbf{x}'$, and is therefore an intrinsically local quantity within the flow field. In contrast, the temporal decorrelation function $\mathrm{E}_\omega(s)$ remains the same as for the homogeneous velocity field $\mathbf{U}(\mathbf{x},t)$, meaning that the Eulerian integral timescale τ_E is still that given by the global value of (5.27). This will not however be the case for the model of the fluid timescale along inertial particle trajectories τ_{Lp} given in (4.63), which will be dependent on $\mathbf{x}$ in the inhomogeneous velocity field $\mathbf{u}(\mathbf{x},t)$, with this dependence manifest in the Lagrangian fluid timescale τ_L. Thus the existing model for τ_{Lp} may still be applicable within this flow field, however it would require the additional input of simulation data from $\tau_L(\mathbf{x})$. Furthermore, from (8.10), the one-point one-time correlation of $\mathbf{u}(\mathbf{x},t)$ directly emerges as

$$\big\langle \mathbf{u}(\mathbf{x},t)\mathbf{u}(\mathbf{x},t)\big\rangle = 2\Big[\mathbf{Q}(\mathbf{0}) - \mathbf{Q}(\mathbf{x})\Big] \tag{8.11}$$

This implies that the mean square fluid velocities in the flow field $\mathbf{u}(\mathbf{x},t)$ are dependent on the position $\mathbf{x}$, which is of consequence when it comes to evaluating the LHA for the PDF dispersion tensors in this configuration.

Implications on the PDF Dispersion Tensors

Following from (C.1) and (8.10), the specific form of the correlation tensor $\widetilde{\mathbf{R}}\,(\mathbf{x}',t';\mathbf{x},t)$ that emerges in the PDF kinetic model as defined in (4.25), applies in the case of Stokes drag law with the fluctuating particle acceleration $\mathbf{f}(\mathbf{x},t) = \beta\mathbf{u}'(\mathbf{x},t)$, and which is associated with the inhomogeneous velocity field $\mathbf{u}(\mathbf{x},t)$, is given by

$$\widetilde{\mathbf{R}}\,(\mathbf{x}';\mathbf{x},s) = \beta^2\Big[\mathbf{Q}(\mathbf{r}) - \mathbf{Q}(\mathbf{x}') - \mathbf{Q}(\mathbf{x}) + \mathbf{Q}(\mathbf{0})\Big]\mathrm{E}_\omega(s) \tag{8.12}$$

Additionally, the spatial gradient of $\widetilde{\mathbf{R}}\left(\mathbf{x}', t'; \mathbf{x}, t\right)$ required for evaluation of the PDF dispersion tensor $\overline{\boldsymbol{\kappa}}\left(\mathbf{x}, t\right)$ is then

$$\frac{\partial}{\partial \mathbf{x}}\widetilde{\mathbf{R}}\left(\mathbf{x}'; \mathbf{x}, s\right) = \beta^2 \left[\frac{\partial}{\partial \mathbf{x}}\mathbf{Q}(\mathbf{r}) - \frac{\partial}{\partial \mathbf{x}}\mathbf{Q}(\mathbf{x})\right] \mathrm{E}_\omega(s) \tag{8.13}$$

where the expression for $\frac{\partial}{\partial \mathbf{x}}\mathbf{Q}(\mathbf{r})$ is given in Appendix C by (C.16). One implication from (8.12) is that at $\mathbf{x} = \mathbf{0}$ it follows that $\widetilde{\mathbf{R}}\left(\mathbf{x}', t'; \mathbf{0}, t\right) = \mathbf{0}$, and therefore the dispersion tensors $\overline{\boldsymbol{\lambda}}\left(\mathbf{0}, t\right)$ and $\overline{\boldsymbol{\mu}}\left(\mathbf{0}, t\right)$ are identically zero. On the other hand, evaluation of (8.13) at $\mathbf{x} = \mathbf{0}$ yields that

$$\frac{\partial}{\partial \mathbf{x}}\widetilde{\mathbf{R}}\left(\mathbf{x}', t'; \mathbf{0}, t\right) = \beta^2 \frac{\partial}{\partial \mathbf{x}}\mathbf{Q}(-\mathbf{x}')\mathrm{E}_\omega(s)$$

which highlights that in contrast to $\overline{\boldsymbol{\lambda}}\left(\mathbf{0}, t\right)$ and $\overline{\boldsymbol{\mu}}\left(\mathbf{0}, t\right)$ the behaviour of $\overline{\boldsymbol{\kappa}}\left(\mathbf{0}, t\right)$ is highly dependent on the non-local contribution arising from $\mathbf{x}'$ in this specific inhomogeneous velocity field. On this basis alone, it is therefore appropriate to use the velocity field $\mathbf{u}(\mathbf{x}, t)$ as a means of investigating the convective flux contribution $\boxed{1}$ given by $\overline{\boldsymbol{\kappa}} - \nabla \cdot \overline{\boldsymbol{\lambda}}$ that emerges within the expression for the particle mass flux (8.4).

Periodicity Considerations

In the same manner as in section 5.2.5, the periodic treatment of the particle separation $\boldsymbol{r}_p(t) = \mathbf{x} - \boldsymbol{x}_p(t')$ along trajectories requires careful handling. Specifically, as $\boldsymbol{r}_p(t)$ is the distance between two points on a trajectory, if this quantity becomes discontinuous when it passes through a boundary this will give an incorrect result, therefore requiring that the true non-periodic trajectory is constructed in order to correctly compute $\boldsymbol{r}_p(t)$. In contrast, $\mathbf{x}$ and $\boldsymbol{x}_p(t')$ describe positions relative to the fixed origin, and as this is located at the centre of the box $\boldsymbol{\mathcal{B}} = [-\mathcal{L}, +\mathcal{L}]^d$ the correct treatment of these quantities is necessarily with the periodic values. Notwithstanding this, even though the distance of particles from the origin remains continuous when they pass through boundaries, there is a discontinuity in the value of the components of $\mathbf{x}$ itself. To rectify this discrepancy, it is therefore a necessary condition that the domain boundaries are sufficiently far from the origin in order for the fluid velocity $\mathbf{U}(\mathbf{x}, t)$ to be fully spatially decorrelated over this distance. This ensures that the change in sign to components of $\mathbf{x}$ when they pass through boundaries does not inappropriately influence the behaviour of the two-point two-time correlation tensor $\mathbf{R}\left(\mathbf{x}', t'; \mathbf{x}, t\right)$ in which all components should

behave continuously, and is equivalent to the condition of $\mathcal{L}/L_{11} \gg 1$ given in (5.30) arising from the construction of the KS velocity field. Then as long as this condition is satisfied, the evaluation of $\mathbf{R}\left(\mathbf{x}', t'; \mathbf{x}, t\right)$ for the required values of $\boldsymbol{r}_p(t)$, $\mathbf{x}$ and $\boldsymbol{x}_p(t')$ can be performed correctly.

Particle Velocity Initialisation for Inhomogeneous Flow

To initialise the particle velocities using the conditional distribution developed in section 5.3, it is necessary to replace the appearance of the mean square fluctuating fluid velocity ${u'}^2$ appropriate for a homogeneous flow with the expression for the location-dependent Reynolds stresses in (8.11) that are associated with the velocity field $\mathbf{u}(\mathbf{x}, t)$. Then taking the distribution characterised by the mean $\mathbf{q_m}(\mathbf{u})$ and covariance matrix $\mathbf{Q_\Theta}$ in (5.58) and further omitting the inclusion of gravity yields

$$\mathbf{q_m}(\mathbf{u}) = \frac{1}{1 + St_{Lp}}\mathbf{u} \quad , \quad \mathbf{Q_\Theta} = \frac{2St_{Lp}}{(1 + St_{Lp})^2}\Big[\mathbf{Q}(\mathbf{0}) - \mathbf{Q}(\mathbf{x})\Big] \tag{8.14}$$

Initialising the velocity of particles within a simulation in accordance with (8.14) will subsequently enable the steady state behaviour to be reached sooner.

8.2.4 Representation in a Radial Frame of Reference

Owing to the presence of a stagnation point in the fluid velocity field at $\mathbf{x} = \mathbf{0}$ that arises from the definition (8.5), in addition to being inhomogeneous the resultant velocity field exhibits a radial symmetry about the origin. Consequently it is instructive to consider the problem in an appropriate frame of reference, and taking $d = 2$ this determines polar coordinates as being the obvious choice.

Polar Conversion of the Dispersion Tensors

Although it is possible to formulate the PDF kinetic model in a polar frame of reference from first principles, the resulting complexity of the description that arises due to the basis vectors being non-constant complicates both the computational implementation and subsequent modelling procedure. As an alternative, it is proposed to run simulations and carry out modelling in a Cartesian frame of reference, and then transform the results to the required polar representation. Since it is the behaviour of the PDF

dispersion tensors $\overline{\boldsymbol{\kappa}}(\mathbf{x},t)$, $\overline{\boldsymbol{\lambda}}(\mathbf{x},t)$ and $\overline{\boldsymbol{\mu}}(\mathbf{x},t)$ which is of interest in this system, it is representations of these which are sought in polar form. Defining the polar coordinates by $\mathbf{q}=(\mathrm{q},\theta)$, then the standard transformations $(\mathrm{q},\theta)\leftrightarrow(\mathrm{x}_1,\mathrm{x}_2)$ given by $\mathrm{x}_1=\mathrm{q}\cos\theta$ and $\mathrm{x}_2=\mathrm{q}\sin\theta$ define the change of basis matrix

$$\mathbf{P}(\theta)=\begin{bmatrix}\cos\theta & \sin\theta\\ -\sin\theta & \cos\theta\end{bmatrix} \tag{8.15}$$

As all of $\overline{\boldsymbol{\kappa}}(\mathbf{x},t)$, $\overline{\boldsymbol{\lambda}}(\mathbf{x},t)$ and $\overline{\boldsymbol{\mu}}(\mathbf{x},t)$ describe the particle behaviour at the single point $\mathbf{x}$, it is permissible to simply use (8.15) for the polar angle θ associated with $\mathbf{x}$ to transform these tensors

$$\begin{aligned}\overline{\boldsymbol{\kappa}}(\mathbf{q},t)&=\mathbf{P}(\theta)\cdot\overline{\boldsymbol{\kappa}}(\mathbf{x},t)\\ \overline{\boldsymbol{\lambda}}(\mathbf{q},t)&=\mathbf{P}(\theta)\cdot\overline{\boldsymbol{\lambda}}(\mathbf{x},t)\cdot\mathbf{P}^{\top}(\theta)\\ \overline{\boldsymbol{\mu}}(\mathbf{q},t)&=\mathbf{P}(\theta)\cdot\overline{\boldsymbol{\mu}}(\mathbf{x},t)\cdot\mathbf{P}^{\top}(\theta)\end{aligned} \tag{8.16}$$

(8.17)

Fluid Velocity Correlation Tensor

In order to make inferences about the PDF dispersion tensors in this frame of reference, the structure of the fluid velocity correlations also needs to be considered. For the two-point correlation tensor $\mathbf{Q}(\mathbf{r})$ in the simplified case of a homogeneous isotropic flow, the difficulties arise due to the components of the separation vector $\mathbf{r}=\mathbf{x}-\mathbf{x}'$ not being expressible as a simple difference of the corresponding components for the points $\mathbf{x}$ and $\mathbf{x}'$ in polar coordinates. To illustrate this, consider the points denoted by $(\mathrm{q},\theta)\leftrightarrow(\mathrm{x}_1,\mathrm{x}_2)$ and $(\mathrm{q}',\theta')\leftrightarrow(\mathrm{x}_1',\mathrm{x}_2')$, then representation of the separation $(\mathrm{p},\varphi)\leftrightarrow(\mathrm{r}_1,\mathrm{r}_2)$ in polar coordinates is given by

$$\mathrm{p}=\sqrt{\mathrm{q}^2-2\mathrm{q}\mathrm{q}'\cos(\theta-\theta')+\mathrm{q}'^2} \tag{8.18}$$

$$\varphi=\arctan\left(\frac{\mathrm{q}\sin\theta-\mathrm{q}'\sin\theta'}{\mathrm{q}\cos\theta-\mathrm{q}'\cos\theta'}\right) \tag{8.19}$$

Thus the decoupling between the components of $\mathbf{r}$ that exists in the Cartesian frame of reference is no longer present in polar coordinates. Accordingly, the transformation of

the two point correlation tensor $\mathbf{Q}(\mathbf{x};\mathbf{x}')$ as given in (5.17) using the associated change of basis matrices $\mathbf{P}(\theta)$ and $\mathbf{P}(\theta')$ such that $\mathbf{Q}(\mathbf{q};\mathbf{q}') = \mathbf{P}(\theta') \cdot \mathbf{Q}(\mathbf{x};\mathbf{x}') \cdot \mathbf{P}^{\top}(\theta)$ yields

$$\begin{aligned}
\mathrm{Q}_{\mathrm{qq}}(\mathbf{q};\mathbf{q}') &= u'^2 \left[f(\mathrm{p})\cos(\theta-\theta') - \big[f(\mathrm{p}) - g(\mathrm{p})\big]\frac{\mathrm{qq}'}{\mathrm{p}^2}\sin^2(\theta-\theta') \right] \\
\mathrm{Q}_{\mathrm{q}\theta}(\mathbf{q};\mathbf{q}') &= -u'^2 \left[g(\mathrm{p}) + \big[f(\mathrm{p}) - g(\mathrm{p})\big]\frac{\mathrm{q}'}{\mathrm{p}^2}\big[\mathrm{q}' - \mathrm{q}\cos(\theta-\theta')\big] \right] \sin(\theta-\theta') \\
\mathrm{Q}_{\theta\mathrm{q}}(\mathbf{q};\mathbf{q}') &= u'^2 \left[g(\mathrm{p}) + \big[f(\mathrm{p}) - g(\mathrm{p})\big]\frac{\mathrm{q}}{\mathrm{p}^2}\big[\mathrm{q} - \mathrm{q}'\cos(\theta-\theta')\big] \right] \sin(\theta-\theta') \\
\mathrm{Q}_{\theta\theta}(\mathbf{q};\mathbf{q}') &= u'^2 \left[g(\mathrm{p})\cos(\theta-\theta') + \big[f(\mathrm{p}) - g(\mathrm{p})\big]\frac{\mathrm{qq}'}{\mathrm{p}^2}\sin^2(\theta-\theta') \right]
\end{aligned} \tag{8.20}$$

where the components of $\mathbf{Q}(\mathbf{q};\mathbf{q}')$ are such that $\mathrm{Q}_{\mathrm{qq}}(\mathbf{q};\mathbf{q}') = \mathrm{Q}_{\parallel}(\mathbf{q};\mathbf{q}')$, $\mathrm{Q}_{\theta\theta}(\mathbf{q};\mathbf{q}') = \mathrm{Q}_{\perp}(\mathbf{q};\mathbf{q}')$ *etc.* It is seen that the resultant correlation tensor is a function of the separation displacement p but not the angular separation φ, however an explicit dependence on both $\mathbf{q}$ and $\mathbf{q}'$ also emerges. As a result, using the general form of (8.20) for constructing closure models is too complicated to be tractable, meaning that the non-local contribution from $\mathbf{q}'$ cannot easily be accounted for with such an approach. Nonetheless, and consistent with the local homogeneous approximation, the one-point correlation at $\mathbf{q}' = \mathbf{q}$ can still be utilised as the basis of a simple model, whereby (8.20) reduces to

$$\mathbf{Q}(\mathbf{q};\mathbf{q}) = u'^2 \begin{bmatrix} f(\mathrm{q}) & 0 \\ 0 & g(\mathrm{q}) \end{bmatrix} \tag{8.21}$$

Thus the one-point correlations $\mathbf{Q}(\mathbf{q};\mathbf{q})$ depend only upon the radial displacement q from the origin, and are independent of θ. For the inhomogeneous velocity field $\mathbf{u}(\mathbf{q},t)$, this results in the Reynolds stresses given by (8.11) taking the form

$$\big\langle \mathbf{u}(\mathrm{q},t)\mathbf{u}(\mathrm{q},t) \big\rangle = 2u'^2 \begin{bmatrix} 1-f(\mathrm{q}) & 0 \\ 0 & 1-g(\mathrm{q}) \end{bmatrix} \tag{8.22}$$

For the choice of longitudinal correlation coefficient $f(\mathrm{r})$ specified in (5.19), the variation of the mean square fluid velocity profile is shown in Figure 8.1. At large radial displacements q towards the domain edges the correlation profile is uniform as in a homogeneous velocity field, however at small radial displacements the correlations decrease toward zero producing a region of marked inhomogeneity, with $\big\langle \mathrm{u}'_{\mathrm{q}}(\mathrm{q})\mathrm{u}'_{\mathrm{q}}(\mathrm{q}) \big\rangle = 0$

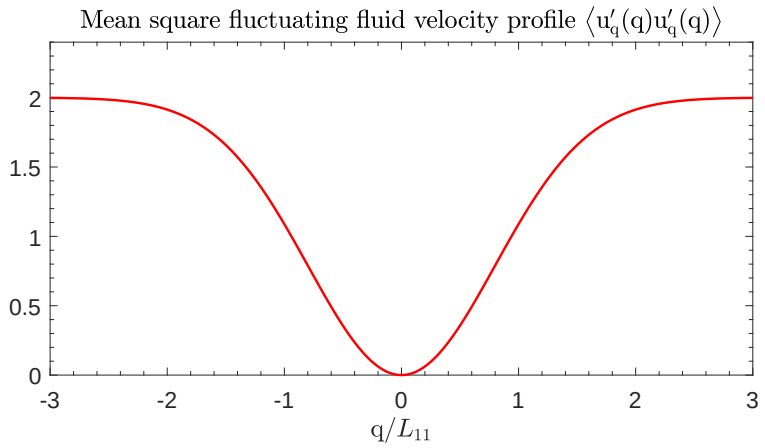

Figure 8.1: Variation of the mean square fluctuating fluid velocity correlation profile $\langle u'_q(q)u'_q(q)\rangle$ with radial displacement q for $u' = 1$

at the origin. It is the profiles of the dispersion tensors $\overline{\boldsymbol{\kappa}}(\mathbf{q},t)$, $\overline{\boldsymbol{\lambda}}(\mathbf{q},t)$ and $\overline{\boldsymbol{\mu}}(\mathbf{q},t)$ which are of interest within this region.

Local Homogeneous Approximations for the Dispersion Tensors

The steady state LHA expressions for $\overline{\boldsymbol{\kappa}}(\mathbf{q})$, $\overline{\boldsymbol{\lambda}}(\mathbf{q})$ and $\overline{\boldsymbol{\mu}}(\mathbf{q})$ which are appropriate to the inhomogeneous flow field $\mathbf{u}(\mathbf{q},t)$ in the polar frame of reference can be obtained by replacing the appearance of u'^2 in the homogeneous version of the model given by (4.66) with the Reynolds stresses associated with $\mathbf{u}(\mathbf{q},t)$ as in (8.22), leading to the expressions

$$\begin{aligned}
\overline{\boldsymbol{\lambda}}^{\mathrm{LHA}}(\mathrm{q}) &= 2u'^2 \frac{1}{St_{Lp}\left(1+St_{Lp}\right)} \begin{bmatrix} 1-f(\mathrm{q}) & 0 \\ 0 & 1-g(\mathrm{q}) \end{bmatrix} \\
\overline{\boldsymbol{\mu}}^{\mathrm{LHA}}(\mathrm{q}) &= 2u'^2 \frac{\beta}{1+St_{Lp}} \begin{bmatrix} 1-f(\mathrm{q}) & 0 \\ 0 & 1-g(\mathrm{q}) \end{bmatrix} \qquad = \frac{1}{\tau_{Lp}} \overline{\boldsymbol{\lambda}}^{\mathrm{LHA}}(\mathrm{q}) \qquad (8.23) \\
\overline{\boldsymbol{\kappa}}^{\mathrm{LHA}}(\mathrm{q}) &= \mathbf{0}
\end{aligned}$$

The approximation for $\overline{\boldsymbol{\kappa}}(\mathrm{q})$ remains zero due to the Green's function approximation $\mathbf{H}[t;t']$ in (4.65) causing $\frac{\partial}{\partial \mathbf{x}}\widetilde{\mathbf{R}}(\mathbf{x}';\mathbf{x},s)$ to contract to zero as a consequence of the incompressibility of $\mathbf{u}(\mathbf{x},t)$. Furthermore, the model for the decorrelation function $\mathrm{E}(s;\mathbf{x})$ given in (4.62) remains the same with the global form of the fluid decorrelation timescale along particle trajectories τ_{Lp} in (4.63) being used, which in the context of

an inhomogeneous flow is an approximation that is likely to cause shortcomings in the resultant models. Nonetheless, the approximations (8.23) provide a basic level of description for particle behaviour in the inhomogeneous velocity field $\mathbf{u}(\mathbf{x},t)$, as well as a benchmark against which models can be assessed.

A direct consequence of (8.23) is that $\nabla\cdot\overline{\boldsymbol{\lambda}}^{\mathrm{LHA}}(\mathrm{q})=\mathbf{0}$ due to the contraction $\frac{\partial}{\partial\mathbf{q}}\cdot\widetilde{\mathbf{R}}\,(\mathbf{q};\mathbf{q},s)=\mathbf{0}$, and as a result the LHA fails to capture any of the convective flux contribution $\overline{\boldsymbol{\kappa}}-\nabla\cdot\overline{\boldsymbol{\lambda}}$. Additionally, an estimate for the particle kinetic stresses $\overline{\mathbf{cc}}\,(\mathbf{q},t)$ can be constructed from the kinetic stress transport equation (4.44) using assumptions consistent with the LHA. Specifically, taking the steady state form of (4.44) and neglecting all spatial gradients, making the approximation $\overline{\mathbf{c}\boldsymbol{\kappa}}\,(\mathbf{q},t)\approx\mathbf{0}$ discussed in section 4.3, and from (4.56) using that $\overline{\mathbf{F}}=-\beta\overline{\mathbf{v}}$ for the Stokes drag model yields the approximation

$$\overline{\mathbf{cc}}\,(\mathbf{q},t)\approx\frac{1}{\beta}\overline{\boldsymbol{\mu}}^{\mathrm{LHA}}(\mathrm{q}) \tag{8.24}$$

with $\overline{\boldsymbol{\mu}}^{\mathrm{LHA}}(\mathrm{q})$ as given in (8.23). This then predicts that turbophoretic contribution $\boxed{2}$ arising from the expression for the particle mass flux (8.4) is $\nabla\cdot\overline{\mathbf{cc}}\,(\mathbf{q},t)\approx\mathbf{0}$ again owing to the contraction $\frac{\partial}{\partial\mathbf{q}}\cdot\widetilde{\mathbf{R}}\,(\mathbf{q};\mathbf{q},s)=\mathbf{0}$, meaning that as with $\boxed{1}$ this term is also neglected using simple local homogeneous approximations. Substitution of the appropriate approximations into (8.4) then yields for the particle number density that $\rho(\mathrm{q})=C$, with C being a constant, and therefore modelling at the level of the LHA fails to retrieve any evidence of the expected build up in particle concentration associated with particle-pair behaviour that is characterised by the RDF.

8.3 Numerical Assessment using KS

To investigate the importance of the various contributions to the particle mass flux expression (8.4) in the inhomogeneous flow field $\mathbf{u}(\mathbf{x},t)=\mathbf{U}(\mathbf{x},t)-\mathbf{U}(\mathbf{0},t)$, the KS velocity field in Chapter 5 is utilised along with the additional considerations outlined in section 8.2.3. All particle statistics including those for the PDF dispersion tensors $\overline{\boldsymbol{\kappa}}\,(\mathbf{q},t)$, $\overline{\boldsymbol{\lambda}}\,(\mathbf{q},t)$ and $\overline{\boldsymbol{\mu}}\,(\mathbf{q},t)$ are evaluated conditional on the radial coordinate q, and in particular, the steady state particle number density $\rho(\mathrm{q})$ is calculated such that

$$\rho(\mathrm{q})=\frac{N_{\mathrm{q}}}{\delta\mathcal{A}_{\mathrm{q}}} \tag{8.25}$$

where N_{q} is the number of particles at radial displacement q, and $\delta\mathcal{A}_q$ is the area of the sampling region at radial displacement q. Normalisation of $\rho(\mathrm{q})$ is then carried out using

$$\hat{\rho}(\mathrm{q}) = \frac{\rho(\mathrm{q})\mathcal{A}}{N} \tag{8.26}$$

where N is the total number of particles in the domain, and $\mathcal{A}$ is the total domain area. Therefore $\hat{\rho}(\mathrm{q})$ is equal to the RDF, and provides a measure of the concentration build-up around the origin that arises due to the form of the inhomogeneous velocity field $\mathbf{u}(\mathbf{q}, t)$. The simulations have been initialised with a uniform particle distribution, and run until a steady-state concentration $\hat{\rho}(\mathrm{q})$ is reached before the sampling of statistics is carried out. Furthermore, the spatial derivatives required for the quantities $\nabla\cdot\overline{\boldsymbol{\lambda}}(\mathrm{q})$ and $\nabla\cdot\overline{\mathbf{cc}}(\mathrm{q})$ are calculated numerically using fourth order central differencing, reducing to second-order forward and backward differencing at the boundaries. The results presented are for two different Stokes numbers, $St_E = 0.1$ and $St_E = 1.0$, across two different fluid RMS values for the velocity field $\mathbf{U}(\mathbf{x}, t)$, $u' = 1.0$ and $u' = 4.0$.

8.3.1 Particle Concentration and PDF Dispersion Tensor Behaviour

To begin with, the radial profiles of the normalised particle number density $\hat{\rho}$ and dispersion tensor components $\overline{\kappa}_{\mathrm{qq}}/\beta u'$, $\overline{\lambda}_{\mathrm{qq}}/u'^2$, and $\overline{\mu}_{\mathrm{qq}}/\beta u'^2$ are considered, with the behaviour across the respective cases being illustrated in Figures 8.2 - 8.5.

Due to the method in which the inhomogeneous flow field (8.5) is defined, a radial variation in the particle number density $\hat{\rho}(\mathrm{q})$ is observed across all cases of St_E and u'. Near the origin there is a noticeable build up of particles as $\mathbf{u}(\mathbf{x}, t)$ decreases to zero, and within the context of a particle-pair framework this is equivalent to particle clustering at small spatial separations, in agreement with previous work [31, 178]. On the other hand, a uniform concentration is observed away from the origin, which corresponds to no preferential concentration at larger separations in the particle-pair sense.

Across the different cases in Figures 8.2 - 8.5, the profile for $\hat{\rho}(\mathrm{q})$ is seen to be sensitive to changes in both St_E and u'. It is observed as expected that at the smaller Stokes number $St_E = 0.1$ there is more pronounced clustering at smaller separations, with a sharp concentration gradient being evident compared to the relatively shallow slope for $St_E = 1.0$. Notably, for the case of $St_E = 0.1$ and $u' = 1.0$ in Figure 8.2 the particle

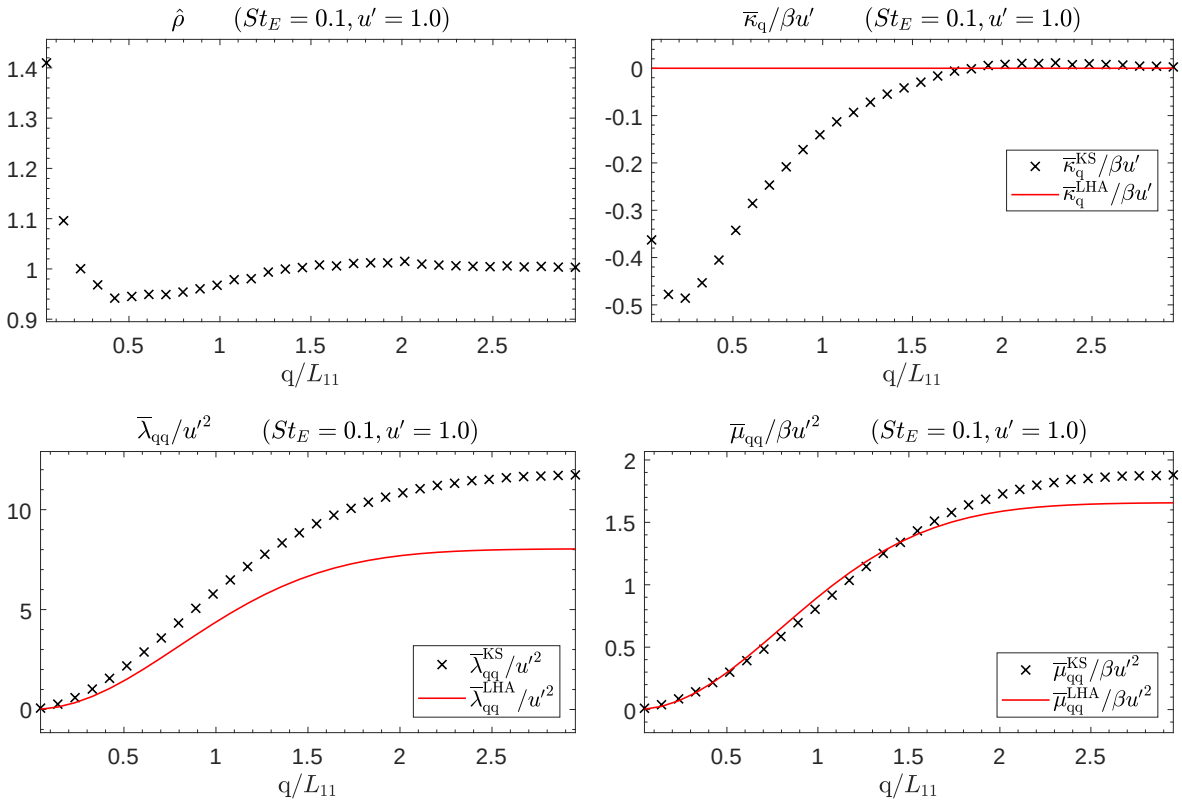

Figure 8.2: Radial profiles of the steady-state normalised particle number density $\hat{\rho}$ and dispersion tensor components $\overline{\kappa}_{\mathrm{q}}/\beta u'$, $\overline{\lambda}_{\mathrm{qq}}/u'^2$, and $\overline{\mu}_{\mathrm{qq}}/\beta u'^2$ obtained using KS for $St_E = 0.1$ and $u' = 1.0$: $\times$ $\hat{\rho}$, $\overline{\kappa}_{\mathrm{q}}^{\mathrm{KS}}/\beta u'$, $\overline{\lambda}_{\mathrm{qq}}^{\mathrm{KS}}/u'^2$, $\overline{\mu}_{\mathrm{qq}}^{\mathrm{KS}}/\beta u'^2$; —— $\overline{\kappa}_{\mathrm{q}}^{\mathrm{LHA}}/\beta u'$, $\overline{\lambda}_{\mathrm{qq}}^{\mathrm{LHA}}/u'^2$, $\overline{\mu}_{\mathrm{qq}}^{\mathrm{LHA}}/\beta u'^2$

concentration actually decreases below its uniform value as the radial separation grows before equilibrating, and in general at $St_E = 0.1$ an increase in concentration is only seen within a radial distance of L_{11} from the origin. By contrast, for $St_E = 1.0$ evidence of preferential concentration is seen up to a displacement of $1.5L_{11}$ from the origin, and this is due to the higher inertia of particles enabling them to escape further from the origin whilst the effect of the inhomogeneous flow field still makes a contribution towards the recent path-history.

The magnitude of the clustering effect at the origin is seen to be dependent on changes in both St_E and u', with the highest concentration observed as being $\sim 130\%$ greater than the uniform level for the case $St_E = 0.1$ and $u' = 4.0$ in Figure 8.4, however the lowest concentration increase of $\sim 8\%$ is also for $u' = 4.0$, this time with $St_E = 1.0$ in Figure 8.5. Consequently, the higher level of RMS fluctuation intensity does not uniformly affect the peak concentration of particles across different values of St_E. However at $u' = 1.0$, the increase in concentration at the origin of $\sim 40\%$ and $\sim 60\%$

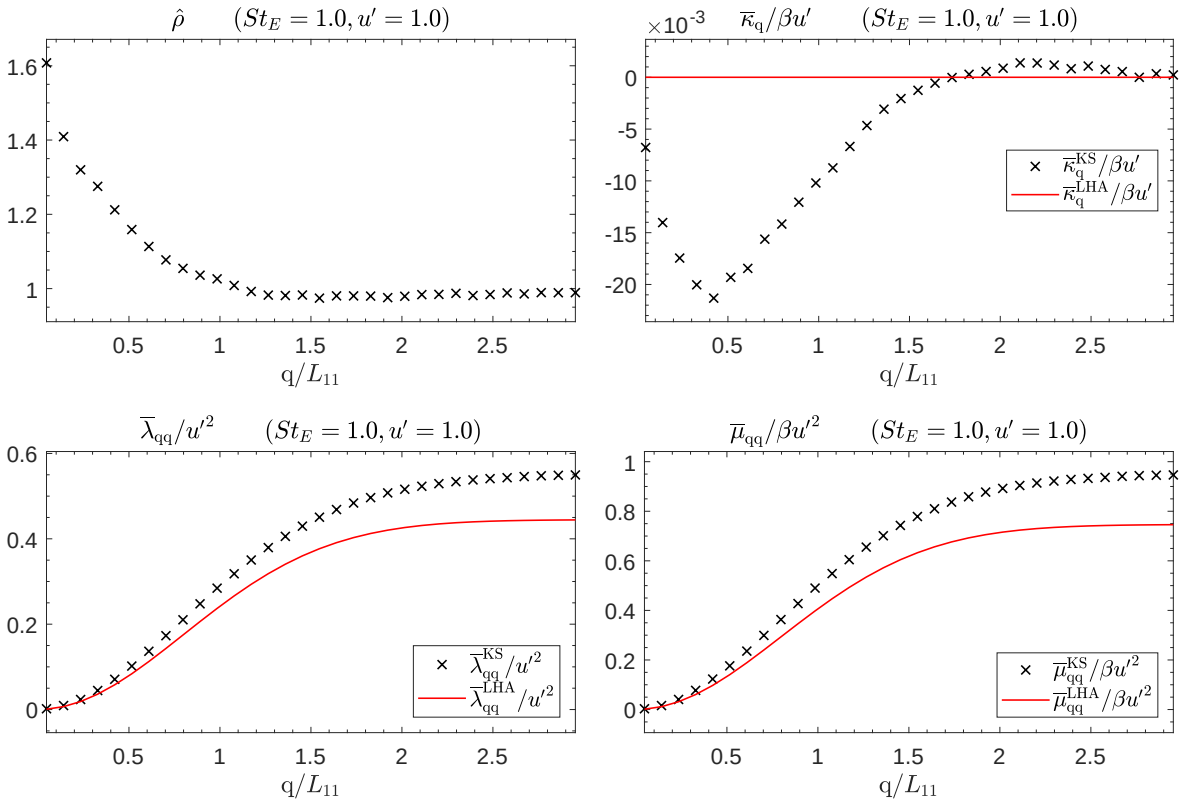

Figure 8.3: Radial profiles of the steady-state normalised particle number density $\hat{\rho}$ and dispersion tensor components $\overline{\kappa}_{\mathrm{q}}/\beta u'$, $\overline{\lambda}_{\mathrm{qq}}/u'^2$, and $\overline{\mu}_{\mathrm{qq}}/\beta u'^2$ obtained using KS for $St_E = 1.0$ and $u' = 1.0$: $\times$ $\hat{\rho}$, $\overline{\kappa}_{\mathrm{q}}^{\mathrm{KS}}/\beta u'$, $\overline{\lambda}_{\mathrm{qq}}^{\mathrm{KS}}/u'^2$, $\overline{\mu}_{\mathrm{qq}}^{\mathrm{KS}}/\beta u'^2$; —— $\overline{\kappa}_{\mathrm{q}}^{\mathrm{LHA}}/\beta u'$, $\overline{\lambda}_{\mathrm{qq}}^{\mathrm{LHA}}/u'^2$, $\overline{\mu}_{\mathrm{qq}}^{\mathrm{LHA}}/\beta u'^2$

for $St_E = 0.1$ and $St_E = 1.0$, as shown in Figures 8.2 and 8.3 respectively, demonstrates that the decreased value of u' produces a more uniform effect on the peak concentration level. Furthermore, previous work [15] has shown that peak clustering occurs at around $St_\eta = 1$, below which the preferential concentration diminishes regardless of the value of u' as the particle inertia tends to that of fluid points.

In terms of the radial component for the PDF dispersion tensors $\overline{\lambda}_{\mathrm{qq}}(\mathrm{q})$ and $\overline{\mu}_{\mathrm{qq}}(\mathrm{q})$ the expected zero behaviour at the origin is observed, away from which an increase with radial position is exhibited that levels off to a uniform value once the statistics are taken sufficiently far from the origin, where the effect of inhomogeneity in the flow field is no longer seen. This behaviour is also captured by the LHA expressions $\overline{\lambda}_{\mathrm{qq}}^{\mathrm{LHA}}(\mathrm{q})$ and $\overline{\mu}_{\mathrm{qq}}^{\mathrm{LHA}}(\mathrm{q})$ given in (8.23), although the values for the uniform region near the domain boundaries differ from those given in simulations. From (8.23), the radial dependence of these profiles is therefore determined by the parameter σ_k intrinsic to the definition (5.19) of $f(\mathrm{q})$ in this work, and since this is uniquely determined by the

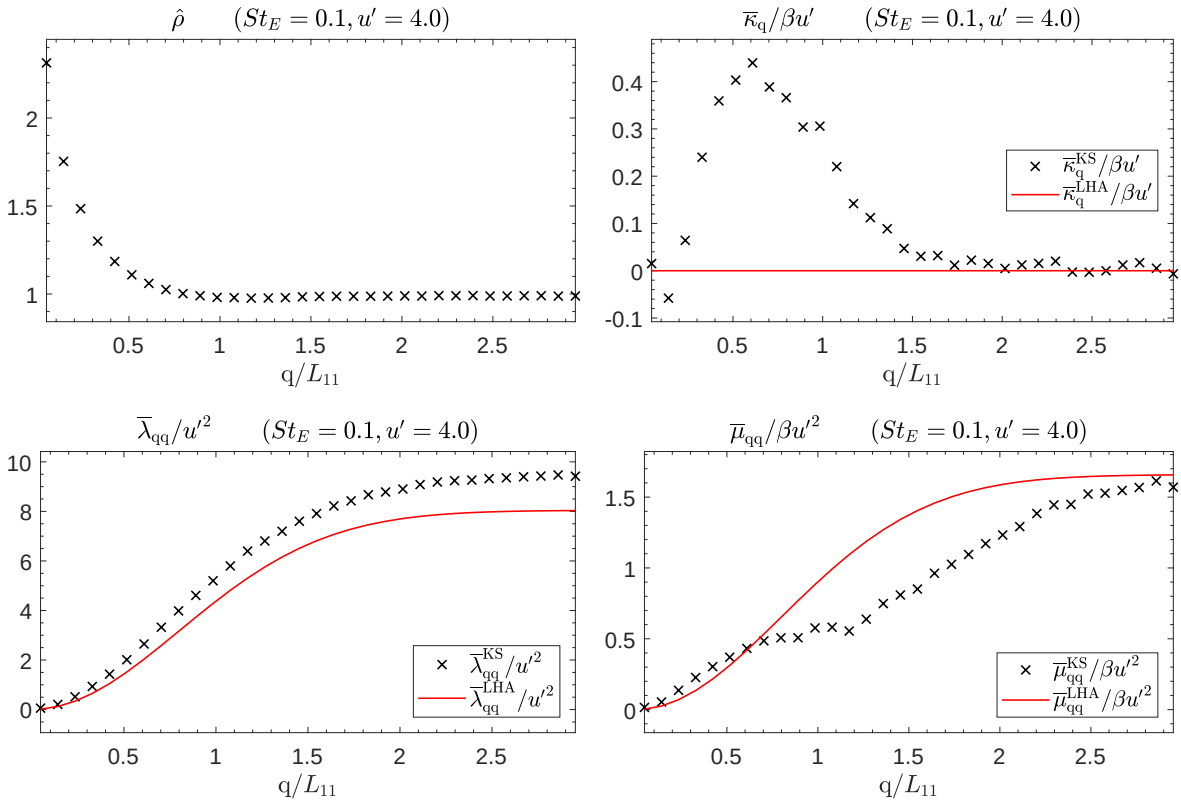

Figure 8.4: Radial profiles of the steady-state normalised particle number density $\hat{\rho}$ and dispersion tensor components $\overline{\kappa}_{\mathrm{q}}/\beta u'$, $\overline{\lambda}_{\mathrm{qq}}/u'^2$, and $\overline{\mu}_{\mathrm{qq}}/\beta u'^2$ obtained using KS for $St_E = 0.1$ and $u' = 4.0$: $\times$ $\hat{\rho}$, $\overline{\kappa}_{\mathrm{q}}^{\mathrm{KS}}/\beta u'$, $\overline{\lambda}_{\mathrm{qq}}^{\mathrm{KS}}/u'^2$, $\overline{\mu}_{\mathrm{qq}}^{\mathrm{KS}}/\beta u'^2$; —— $\overline{\kappa}_{\mathrm{q}}^{\mathrm{LHA}}/\beta u'$, $\overline{\lambda}_{\mathrm{qq}}^{\mathrm{LHA}}/u'^2$, $\overline{\mu}_{\mathrm{qq}}^{\mathrm{LHA}}/\beta u'^2$

longitudinal integral lengthscale L_{11} which is not varied in these simulations, the form of radial profile for $\overline{\lambda}_{\mathrm{qq}}(\mathrm{q})$ and $\overline{\mu}_{\mathrm{qq}}(\mathrm{q})$ is qualitatively similar across all values of St_E and u' in Figures 8.2 - 8.5. The magnitude of both $\overline{\lambda}_{\mathrm{qq}}(\mathrm{q})$ and $\overline{\mu}_{\mathrm{qq}}(\mathrm{q})$ away from the stagnation point at $\mathrm{q} = 0$ is seen to be almost independent of u', but does however vary strongly with St_E such that $\overline{\lambda}_{\mathrm{qq}}(\mathrm{q})$ is over an order of magnitude greater at $St_E = 0.1$ than $St_E = 1.0$, whilst $\overline{\mu}_{\mathrm{qq}}(\mathrm{q})$ is around twice as prominent. This is a consequence of the contribution that the particle response tensor $\boldsymbol{\mathcal{H}}[t;t']$ and its derivative $\dot{\boldsymbol{\mathcal{H}}}[t;t']$ make within the respective expressions for $\overline{\lambda}_{\mathrm{qq}}(\mathrm{q})$ and $\overline{\mu}_{\mathrm{qq}}(\mathrm{q})$, with the smaller particle inertia meaning that more of the path history interactions are accounted for by $\boldsymbol{\mathcal{H}}[t;t']$ and $\dot{\boldsymbol{\mathcal{H}}}[t;t']$ in this case, subsequently leading to the higher values of $\overline{\lambda}_{\mathrm{qq}}(\mathrm{q})$ and $\overline{\mu}_{\mathrm{qq}}(\mathrm{q})$.

The accuracy of the approximations $\overline{\lambda}_{\mathrm{qq}}^{\mathrm{LHA}}(\mathrm{q})$ and $\overline{\mu}_{\mathrm{qq}}^{\mathrm{LHA}}(\mathrm{q})$ is seen to vary across the different values of St_E and u', and despite successfully giving the zero behaviour at the origin, they fail to capture the true values of these dispersion tensors at increasing radial displacements in this inhomogeneous configuration. In the case of $St_E = 0.1$ the LHA

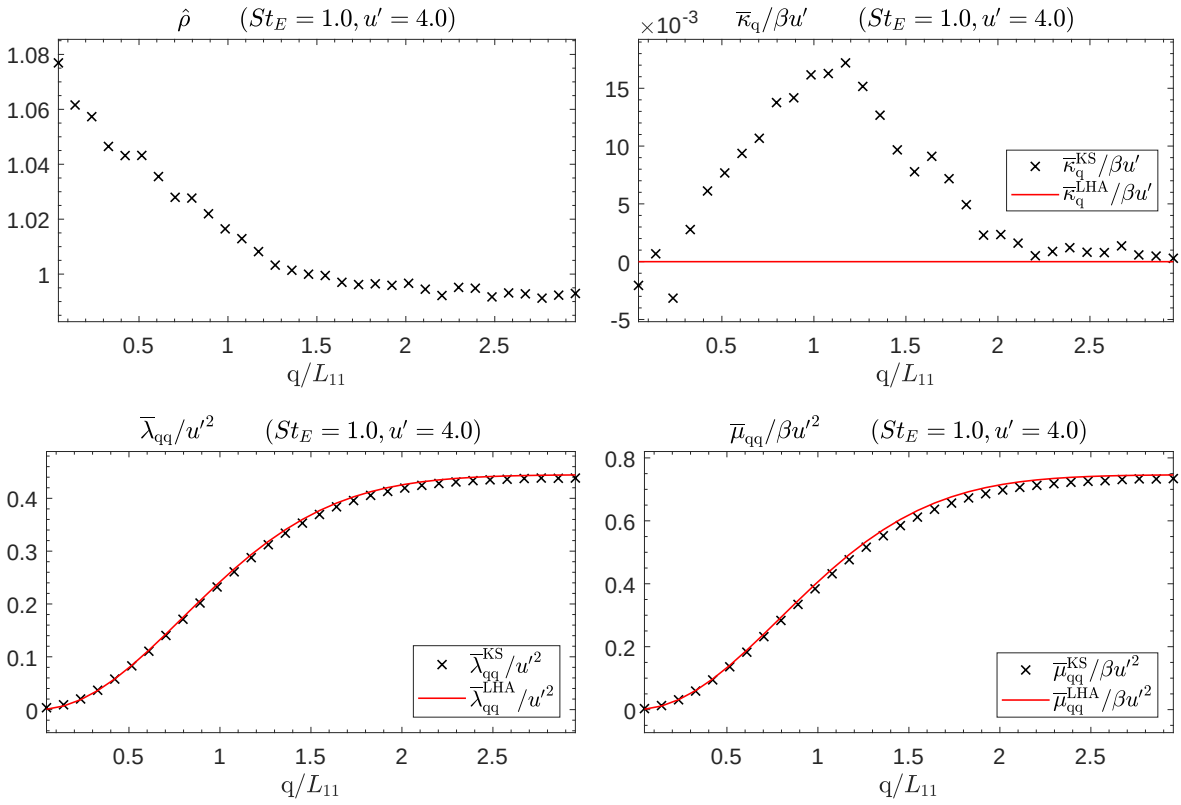

Figure 8.5: Radial profiles of the steady-state normalised particle number density $\hat{\rho}$ and dispersion tensor components $\overline{\kappa}_{\mathrm{q}}/\beta u'$, $\overline{\lambda}_{\mathrm{qq}}/u'^2$, and $\overline{\mu}_{\mathrm{qq}}/\beta u'^2$ obtained using KS for $St_E = 1.0$ and $u' = 4.0$: $\times$ $\hat{\rho}$, $\overline{\kappa}_{\mathrm{q}}^{\mathrm{KS}}/\beta u'$, $\overline{\lambda}_{\mathrm{qq}}^{\mathrm{KS}}/u'^2$, $\overline{\mu}_{\mathrm{qq}}^{\mathrm{KS}}/\beta u'^2$; —— $\overline{\kappa}_{\mathrm{q}}^{\mathrm{LHA}}/\beta u'$, $\overline{\lambda}_{\mathrm{qq}}^{\mathrm{LHA}}/u'^2$, $\overline{\mu}_{\mathrm{qq}}^{\mathrm{LHA}}/\beta u'^2$

for $\overline{\mu}_{\mathrm{qq}}(\mathrm{q})$ captures the true behaviour better than that for $\overline{\lambda}_{\mathrm{qq}}(\mathrm{q})$, and as discussed in section 4.5 previous work has shown that this is due to $\overline{\mu}_{\mathrm{qq}}(\mathrm{q})$ sampling less of the non-local particle path history than $\overline{\lambda}_{\mathrm{qq}}(\mathrm{q})$, meaning that $\overline{\mu}_{\mathrm{qq}}^{\mathrm{LHA}}(\mathrm{q})$ is able to account for a greater proportion of the true behaviour than $\overline{\lambda}_{\mathrm{qq}}^{\mathrm{LHA}}(\mathrm{q})$. Nonetheless, for the particular values of $St_E = 0.1$ and $u' = 4.0$ in Figure 8.4, the behaviour of $\overline{\mu}_{\mathrm{qq}}(\mathrm{q})$ observed from the simulation is seen to depart from the expected profile whereas that for $\overline{\lambda}_{\mathrm{qq}}(\mathrm{q})$ does not, demonstrating that $\overline{\mu}_{\mathrm{qq}}^{\mathrm{LHA}}(\mathrm{q})$ is not uniformly a better approximation than $\overline{\lambda}_{\mathrm{qq}}^{\mathrm{LHA}}(\mathrm{q})$ across the entire parameter space $\{St_E, u'\}$.

Furthermore, for the case $St_E = 1.0$ and $u' = 4.0$ in Figure 8.5, the LHA values are seen to be closely aligned with the correct behaviour of $\overline{\lambda}_{\mathrm{qq}}(\mathrm{q})$ and $\overline{\mu}_{\mathrm{qq}}(\mathrm{q})$, and indeed are actually a slight over-approximation. This can only occur if the model for the fluid timescale along particle trajectories τ_{Lp} provides an overestimation, and for the particular case of the Wang & Stock [165] model utilised here, reference to the turbulence structure parameter m in (5.34) shows why this is the case. Since the Wang

& Stock model was proposed using simulation data in which $m = 1$, this necessarily implies that for fixed L_{11} and τ_E the condition $u' = 1.0$ must be met in this KS velocity field in order for τ_{Lp} to be a valid model. Consequently, for the case in question with $u' = 4.0$, a more appropriate model for τ_{Lp} is needed to provide a realistic assessment of the LHA. Nonetheless, use of the existing model for τ_{Lp} still captures the qualitative characteristics of $\overline{\lambda}_{\mathrm{qq}}(\mathrm{q})$ and $\overline{\mu}_{\mathrm{qq}}(\mathrm{q})$ for $u' = 4.0$, and produces a first approximation to the correct behaviour.

For the dispersion tensor $\overline{\kappa}_{\mathrm{q}}(\mathrm{q})$, the LHA from (8.23) is identically zero irrespective of the values of St_E and u', however in all of Figures 8.2 - 8.5 the simulation results demonstrate that $\overline{\kappa}_{\mathrm{q}}(\mathrm{q})$ is distinctly non-zero. As with $\overline{\lambda}_{\mathrm{qq}}(\mathrm{q})$ and $\overline{\mu}_{\mathrm{qq}}(\mathrm{q})$, $\overline{\kappa}_{\mathrm{q}}(\mathrm{q})$ exhibits uniform behaviour when far from the origin, and in this region of the domain is equal to zero in agreement with $\overline{\kappa}_{\mathrm{q}}^{\mathrm{LHA}}(\mathrm{q})$. However as the origin is approached at decreasing radial displacements, $\overline{\kappa}_{\mathrm{q}}(\mathrm{q})$ becomes markedly variable, reaching a peak in magnitude before reducing to varying values at $\mathrm{q} = 0$. The normalised value of this peak is seen to exhibit a strong dependence on the Stokes number, being two orders of magnitude greater at $St_E = 0.1$ than $St_E = 1.0$. In contrast, for a given value of St_E the different cases of u' do not see much variation in this magnitude, however crucially the sense in which $\overline{\kappa}_{\mathrm{q}}(\mathrm{q})$ acts is reversed, with the net result being negative for both cases in which $u' = 1.0$ but positive for the cases with $u' = 4.0$. Furthermore, the radial displacement at which the peak magnitude of $\overline{\kappa}_{\mathrm{q}}(\mathrm{q})$ is observed increases as a function of both increasing St_E and increasing u', whilst the value of $\overline{\kappa}_{\mathrm{q}}(\mathrm{q})$ at $\mathrm{q} = 0$ is seen to increase when both St_E and u' are decreased. This clearly demonstrates the requirement for an improved description of this behaviour over the trivial approximation $\overline{\kappa}_{\mathrm{q}}^{\mathrm{LHA}}(\mathrm{q}) = 0$, and warrants further investigation into the relative contributions of the particle mass flux terms.

8.3.2 Diffusive and Convective Flux Contributions

Evaluation of the various contributions arising in the expression for the particle mass flux (8.4) using KS data is now considered across the same values of $St_E = \{0.1, 1.0\}$ and $u' = \{1.0, 4.0\}$, with the results given in Figures 8.6 - 8.9. Specifically, the ratio of the diffusive flux contributions given by $\overline{\lambda}_{\mathrm{qq}}^{\mathrm{KS}}/\overline{c_{\mathrm{q}}c_{\mathrm{q}}}^{\mathrm{KS}}$ and the individual effect of the normalised convective flux contributions $(\overline{\boldsymbol{\kappa}} - \nabla \cdot \overline{\boldsymbol{\lambda}})_{\mathrm{q}}^{\mathrm{KS}}/\beta u'$ and $(\nabla \cdot \overline{\mathbf{cc}})_{\mathrm{q}}^{\mathrm{KS}}/\beta u'$ is analysed.

In terms of the dispersion tensor $\overline{\lambda}_{\mathrm{qq}}(\mathrm{q})$, the efficacy of the LHA for retrieving the correct behaviour at different radial displacements q can be seen by analysing the ratio

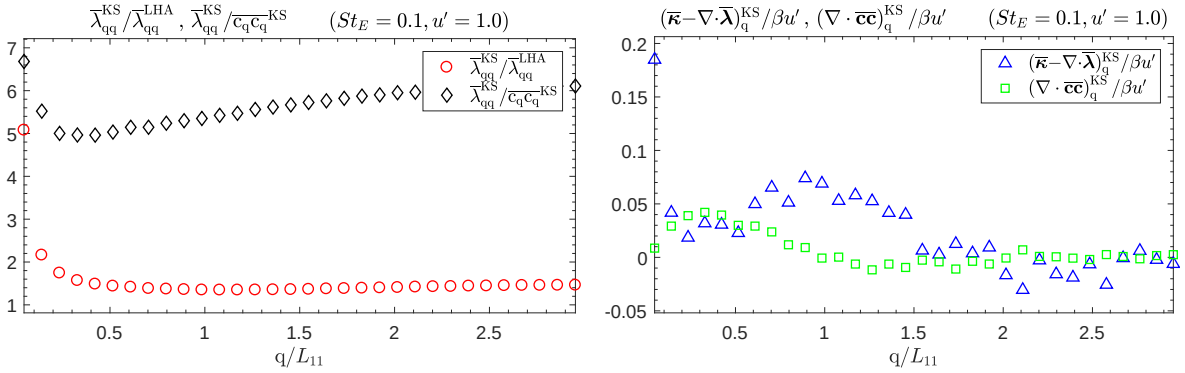

Figure 8.6: Evaluation of the relative contributions of the radial mass flux terms using KS for $St_E = 0.1$ and $u' = 1.0$. Left: ○ assessment of the LHA using $\overline{\lambda}^{KS}_{qq}/\overline{\lambda}^{LHA}_{qq}$; ◇ ratio of the diffusive flux contributions $\overline{\lambda}^{KS}_{qq}/\overline{c_q c_q}^{KS}$. Right: △ normalised convective drift flux contribution $(\overline{\boldsymbol{\kappa}}-\nabla\cdot\overline{\boldsymbol{\lambda}})^{KS}_{q}/\beta u'$; □ normalised turbophoretic flux contribution $(\nabla\cdot\overline{\mathbf{cc}})^{KS}_{q}/\beta u'$

$\overline{\lambda}_{qq}/\overline{\lambda}^{LHA}_{qq}$. Due to the fact that both of these quantities reduce to zero at the origin, even though the absolute difference between them is small their ratio is not, enabling the relative sizes of $\overline{\lambda}_{qq}$ and $\overline{\lambda}^{LHA}_{qq}$ to be discerned. From this it is clear that only at the grid point closest to the origin does the true value of $\overline{\lambda}_{qq}$ differ significantly from that of $\overline{\lambda}^{LHA}_{qq}$, with this simply representing the numerical error involved in the calculation of $\overline{\lambda}_{qq}(0)$ from an ensemble of particles, which by contrast $\overline{\lambda}^{LHA}_{qq}(0) = 0$ does not exhibit. Aside from this, the ratio $\overline{\lambda}_{qq}/\overline{\lambda}^{LHA}_{qq}$ takes on a near unity value away from the fluid stagnation point at the origin in all cases of St_E and u', showing that the dominant contribution to $\overline{\lambda}_{qq}(q)$ is retrieved by $\overline{\lambda}^{LHA}_{qq}(q)$, and that the non-local effects omitted from $\overline{\lambda}^{LHA}_{qq}(q)$ are less important in this inhomogeneous configuration.

Such an approach can also be utilised for analysing the relative importance of the diffusive flux contributions $\overline{\lambda}_{qq}(q)$ and $\overline{c_q c_q}(q)$ from the term $\boxed{4}$ in the particle mass flux expression (8.4). The ratio $\overline{\lambda}_{qq}/\overline{c_q c_q}$ is seen to varying significantly across the different cases of St_E and u' shown in Figures 8.6 - 8.9, with a strong dependence on Stokes number observed. Notably, away from the stagnation point at q = 0 the diffusive contribution from $\overline{\lambda}_{qq}(q)$ is seen to be ~ 5 times greater than that from $\overline{c_q c_q}(q)$ in the cases for $St_E = 0.1$, however for $St_E = 1.0$ the kinetic stresses $\overline{c_q c_q}(q)$ are around twice the magnitude of $\overline{\lambda}_{qq}(q)$. This is chiefly because the value of $\overline{\lambda}_{qq}(q)$ for $St_E = 0.1$ is seen to be a full order of magnitude greater than at $St_E = 1.0$ as seen in Figures 8.2 - 8.5, whereas the kinetic stresses do not exhibit such a marked change with variation of St_E. In contrast, almost no change in the ratio $\overline{\lambda}_{qq}/\overline{c_q c_q}$ is observed away from the stagnation point at the origin for the different cases of u' at a given St_E, however the

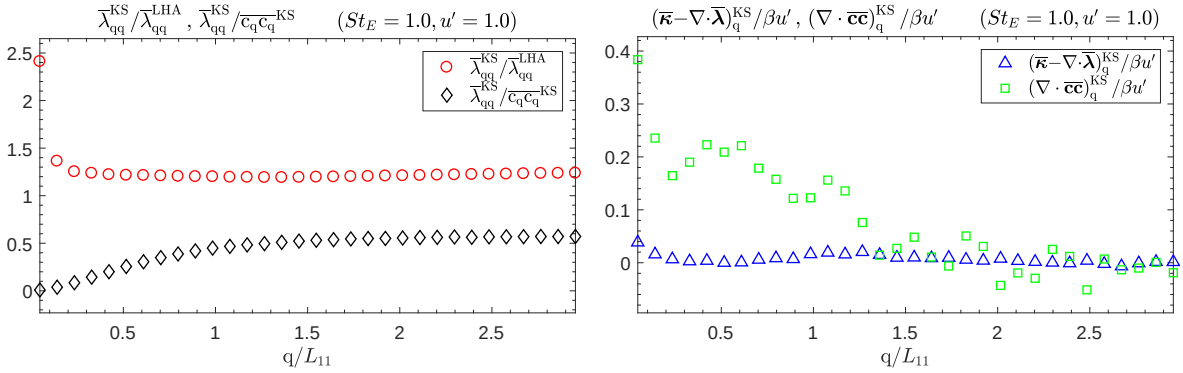

Figure 8.7: Evaluation of the relative contributions of the radial mass flux terms using KS for $St_E = 1.0$ and $u' = 1.0$. Left: ○ assessment of the LHA using $\overline{\lambda}^{KS}_{qq}/\overline{\lambda}^{LHA}_{qq}$; ◊ ratio of the diffusive flux contributions $\overline{\lambda}^{KS}_{qq}/\overline{c_q c_q}^{KS}$. Right: △ normalised convective drift flux contribution $(\overline{\boldsymbol{\kappa}}-\nabla\cdot\overline{\boldsymbol{\lambda}})^{KS}_{q}/\beta u'$; □ normalised turbophoretic flux contribution $(\nabla\cdot\overline{\mathbf{cc}})^{KS}_{q}/\beta u'$

relative importance of $\overline{\lambda}_{qq}(q)$ and $\overline{c_q c_q}(q)$ does change in the region of q = 0 for the different values of u' at $St_E = 0.1$. Specifically, for $u' = 1.0$ it is $\overline{\lambda}_{qq}(q)$ which becomes the dominant contribution in the limit $q \to 0$, whereas for $u' = 4.0$ the kinetic stresses $\overline{c_q c_q}(q)$ are dominant in this limit. On the other hand, when $St_E = 1.0$ it is $\overline{c_q c_q}(q)$ which is dominant in the limit $q \to 0$ for both values of u'. Thus overall the relative contributions of $\overline{\lambda}_{qq}(q)$ and $\overline{c_q c_q}(q)$ to the diffusive flux are strongly dependent on only the Stokes number away from the stagnation point at q = 0.

For the drift flux contributions $(\overline{\boldsymbol{\kappa}} - \nabla\cdot\overline{\boldsymbol{\lambda}})_q$ and $(\nabla\cdot\overline{\mathbf{cc}})_q$ that constitute the respective terms $\boxed{1}$ and $\boxed{2}$ in the particle mass flux expression (8.4), it is more appropriate to analyse these two quantities directly due to the near-zero values they take on away from the effect of inhomogeneity in the fluid velocity field. These two quantities do display non-zero behaviour in the region near the stagnation point q = 0 however, as evidenced in Figures 8.6 - 8.9, with the relative importance of each being determined by both the values of St_E and u', and also the radial displacement q. For $St_E = 0.1$ the dominant contribution is found to be from the non-local drift $(\overline{\boldsymbol{\kappa}} - \nabla\cdot\overline{\boldsymbol{\lambda}})_q$, however it acts in different directions depending on the value of u', being positive for $u' = 1.0$ in Figure 8.6, but negative for $u' = 4.0$ in Figure 8.8. Furthermore, in Figure 8.6 it is seen that $(\overline{\boldsymbol{\kappa}} - \nabla\cdot\overline{\boldsymbol{\lambda}})_q$ is only dominant over the turbophoretic contribution $(\nabla\cdot\overline{\mathbf{cc}})_q$ in the region $0.5L_{11} < q < 1.5L_{11}$, being of the same magnitude in the region near to q = 0. In comparison, $(\nabla\cdot\overline{\mathbf{cc}})_q$ is seen to be dominant for $St_E = 1.0$, notably becoming an order of magnitude greater than $(\overline{\boldsymbol{\kappa}} - \nabla\cdot\overline{\boldsymbol{\lambda}})_q$ at q = 0 for $u' = 1.0$ in Figure 8.7, and further this expression always acts in a positive sense.

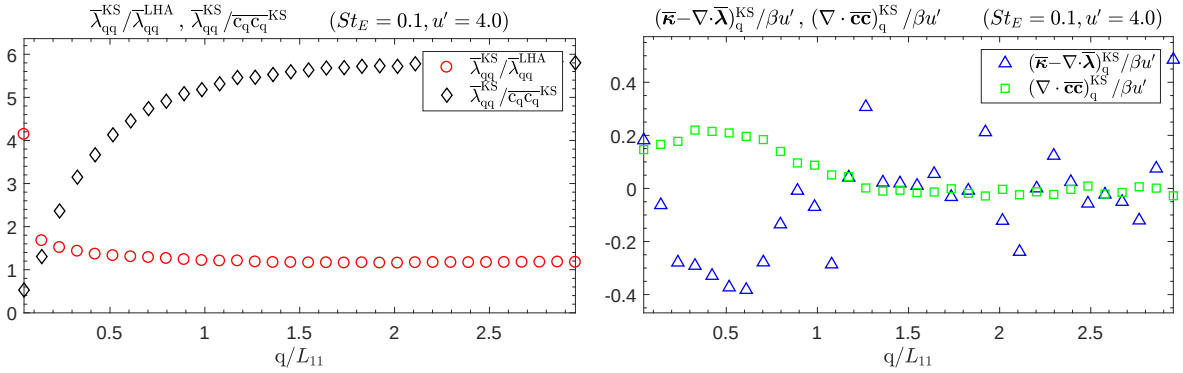

Figure 8.8: Evaluation of the relative contributions of the radial mass flux terms using KS for $St_E = 0.1$ and $u' = 4.0$. Left: ○ assessment of the LHA using $\overline{\lambda}^{KS}_{qq}/\overline{\lambda}^{LHA}_{qq}$; ◊ ratio of the diffusive flux contributions $\overline{\lambda}^{KS}_{qq}/\overline{c_q c_q}^{KS}$. Right: △ normalised convective drift flux contribution $(\overline{\boldsymbol{\kappa}}-\nabla\cdot\overline{\boldsymbol{\lambda}})^{KS}_{q}/\beta u'$; □ normalised turbophoretic flux contribution $(\nabla\cdot\overline{\mathbf{cc}})^{KS}_{q}/\beta u'$

From the particle mass flux expression (8.4) the net drift flux in a steady-state system is seen to be the difference between the terms 1 and 2, and in light of the foregoing discussion will therefore be larger when these contributions are of opposite signs and compound each other, which only happens in the case of low particle inertia and high fluid RMS velocity fluctuation intensity in Figure 8.8 which corresponds to $St_E = 0.1$ and $u' = 4.0$. Then since it is the convective flux contribution which determines the particle concentration profile, this is consistent with the case for $St_E = 0.1$ and $u' = 4.0$ displaying the highest preferential particle concentration observed in Figure 8.4. As a result, since the expression $(\overline{\boldsymbol{\kappa}} - \nabla\cdot\overline{\boldsymbol{\lambda}})_q$ is the dominant contribution to the drift flux, it is therefore this quantity which is chiefly responsible for the pronounced build-up of particle concentration at q = 0 in this instance. Additionally, it is noted that the particle concentration increase for $St_E = 1.0$ and $u' = 1.0$ is attributable to the turbophoretic contribution which is dominant in this case, with $(\overline{\boldsymbol{\kappa}}-\nabla\cdot\overline{\boldsymbol{\lambda}})_q$ being much smaller in comparison. This still causes an increase in particle concentration as $(\nabla\cdot\overline{\mathbf{cc}})_q$ is always positive, but acts inward radially in the particle mass flux expression, thereby inducing a drift flux towards the stagnation point at q = 0. In contrast, $(\overline{\boldsymbol{\kappa}} - \nabla\cdot\overline{\boldsymbol{\lambda}})_q$ acts outward radially in the particle mass flux expression, and therefore it is only when this contribution becomes negative that it acts to enhance the clustering of particles in the region of q = 0. Thus this identifies two separate mechanisms which are capable of inducing a drift flux that results in an increased preferential particle concentration occurring, and which further can act together or against each other depending upon the values of St_E and u'.

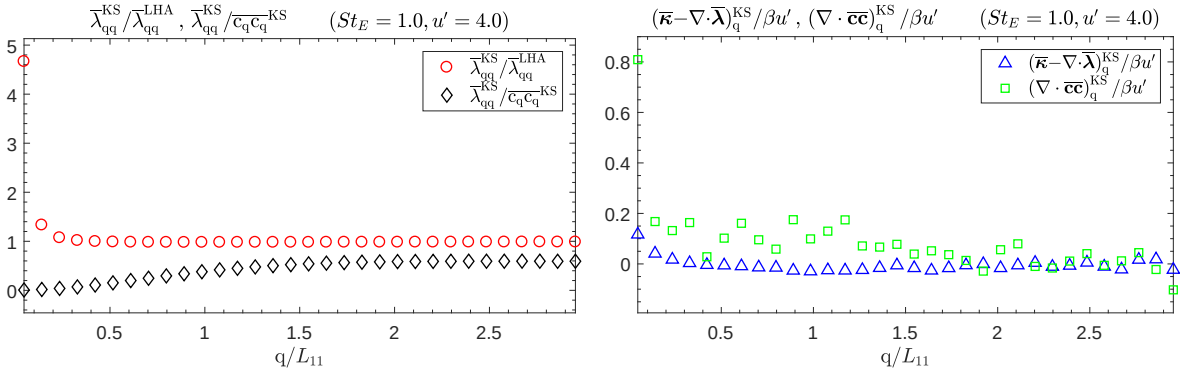

Figure 8.9: Evaluation of the relative contributions of the radial mass flux terms using KS for $St_E = 1.0$ and $u' = 4.0$. Left: ○ assessment of the LHA using $\overline{\lambda}^{KS}_{qq}/\overline{\lambda}^{LHA}_{qq}$; ◊ ratio of the diffusive flux contributions $\overline{\lambda}^{KS}_{qq}/\overline{c_q c_q}^{KS}$. Right: △ normalised convective drift flux contribution $(\overline{\boldsymbol{\kappa}}-\nabla\cdot\overline{\boldsymbol{\lambda}})^{KS}_{q}/\beta u'$; □ normalised turbophoretic flux contribution $(\nabla\cdot\overline{\mathbf{cc}})^{KS}_{q}/\beta u'$

8.4 Concluding Comments

Numerical assessment of the different terms within the particle mass flux expression using the specifically constructed KS velocity field $\mathbf{u}(\mathbf{x},t) = \mathbf{U}(\mathbf{x},t) - \mathbf{U}(\mathbf{0},t)$ has shown that the dominant contribution to both the diffusive and convective fluxes is determined principally by the value of St_E, with u' playing a lesser role and only affecting the magnitude of the resultant fluxes. For the diffusive fluxes, the dispersion tensor $\overline{\lambda}_{qq}(q)$ is dominant for small St_E, whereas the kinetic stresses $\overline{c_q c}_q(q)$ dominate for large St_E. In terms of the convective fluxes, $(\overline{\boldsymbol{\kappa}} - \nabla\cdot\overline{\boldsymbol{\lambda}})_q$ is the dominant contribution for small St_E, whilst the turbophoretic term $(\nabla\cdot\overline{\mathbf{cc}})_q$ dominates for large St_E. Furthermore, the direction in which $(\overline{\boldsymbol{\kappa}} - \nabla\cdot\overline{\boldsymbol{\lambda}})_q$ acts varies depending upon u', becoming negative for large u'. Since the two contributions to the net convective flux act opposite to each other within the expression for the particle mass flux, the highest build up of particle concentration is accordingly seen for small St_E and large u' for which $(\overline{\boldsymbol{\kappa}} - \nabla\cdot\overline{\boldsymbol{\lambda}})_q$ becomes negative, as the individual contributions that $(\overline{\boldsymbol{\kappa}} - \nabla\cdot\overline{\boldsymbol{\lambda}})_q$ and $(\nabla\cdot\overline{\mathbf{cc}})_q$ make to the particle mass flux are then in the same direction. This is notable in the context of developing closure models, as the approximation $\overline{\boldsymbol{\kappa}} - \nabla\cdot\overline{\boldsymbol{\lambda}} = \mathbf{0}$ has been used as the basis for forming closures in previous work on the premise that this expression only makes a negligible contribution to the convective flux. However, the findings presented here indicate that there are no solid grounds for making such an approximation uniformly across all cases of St_E and u', thereby providing the motive for developing improved closures for the expression $\overline{\boldsymbol{\kappa}} - \nabla\cdot\overline{\boldsymbol{\lambda}}$ in future work.

Chapter 9

Conclusions and Future Work

The research presented in this thesis has focused upon using the PDF kinetic model as a means of describing the behaviour of dispersed inertial particles in a zero-mean Gaussian fluid velocity field, with the efficacy of this framework at capturing the phenomenological behaviour in different flow configurations being numerically assessed through the use of a flow field constructed via kinematic simulation. The formulation of a new closure model appropriate to these specific flow configurations has been carried out, and it has been demonstrated that the proposed model captures the leading order effects of the particle behaviour which is exhibited in these configurations. Furthermore, the ability of the particle velocity field description to capture this behaviour has also been assessed. The following summary appraises the contributions made by this research in more detail, and outlines the subsequent avenues of investigation which naturally follow on from the work undertaken.

9.1 Distribution for Particle Velocity Initialisation

Although mainly a point of computational interest, a probability distribution of the particle velocity conditional on the fluid velocity has been constructed in section 5.3 as a means of initialising particle velocities within a simulation so that the steady-state statistics of the particle phase are conformed to. This distribution has been shown to noticeably reduce the initial transience which occurs, and consequently decreases the time needed for simulations to reach a steady-state. As further demonstrated in section 8.2.3, this distribution can be adapted to cater for inhomogeneous flows by replacement of the mean-square fluctuating fluid velocities u'^2 with the Reynolds

stresses $\langle \mathbf{u}(\mathbf{x})\mathbf{u}(\mathbf{x}) \rangle$ which are appropriate to the specific flow configuration that is under consideration. In the context of particle tracking simulations that require a large number of particles to be included within the ensemble in order for sufficiently noise-free averaged statistics to be obtained, this represents a noteworthy saving in the overall computational expense of a simulation, and as such may be of interest to other researchers working with simulations of disperse particle transport.

9.2 Drift Enhancement in Gravitational Settling

9.2.1 Conclusions

Analysis has been carried out on the enhancement in settling rate experienced by inertial particles under the influence of a gravitational body force in a zero-mean homogeneous flow, and this has shown that the reduction in symmetry which is intrinsic to this configuration can be used to determine which components of quantities associated with the particle phase will be non-zero. It is shown that the dispersion tensor $\overline{\boldsymbol{\kappa}}$ that emerges within the PDF kinetic model [44, 124, 150, 71] is an exact representation of the modification in particle settling velocity, and furthermore this is also demonstrated numerically for the case of a linear drag law through the use of kinematic simulation in which the Eulerian fluid velocity has a Gaussian distribution. Additionally, by using a cumulant expansion on the unclosed average within $\overline{\boldsymbol{\kappa}}$, it is demonstrated that the dominant contribution to the increase in particle settling velocity is a second-order effect that arises due to interaction of particles with the structures of the fluid velocity field. In contrast, the leading-order contribution that arises from the mean behaviour of particles only plays a minor role in causing the increase in particle settling velocity, to the extent where it can realistically be neglected in a closure model. A closure model accounting for the particle-fluid interactions that result in the settling enhancement has further been developed, and is found to retrieve a significant portion of the drift enhancement exhibited by particles. Notwithstanding this, the full effect of the behaviour is not captured by the modelling procedure used, with the attributable factors for this being the use of isotropic tensors for particle phase statistics, and a timescale model for τ_{Lp} which does not account for the presence of a gravitational body force.

9.2.2 Future Work

Owing to the deficiencies which are present in the current closure model arising mainly from the use of isotropic tensors to model correlations taken along particle trajectories, an appropriate starting point for an improved model would be to use axisymmetric tensors for these quantities, an assumption which is consistent with the reduced symmetry that is intrinsic to the particle phase in this configuration. Such an approach would utilise the theories of axisymmetric turbulence developed by Batchelor [7] and Chandrasekhar [27], which develop expressions for axisymmetric tensors from the starting point of assuming that they are invariant by an arbitrary rotation of the axes of reference about a given direction. Choosing this direction to be given by the normalised gravitational acceleration $\hat{\mathbf{g}}$, determination of the various coefficients in terms of the longitudinal and lateral fluid velocity correlation coefficients $f(\mathrm{r})$ and $g(\mathrm{r})$ would then provide a model which would be expected to constitute an improvement over the isotropic form.

The secondary consideration for improving the existing model is to split the correlations which require modelling into symmetric and antisymmetric parts, as discussed in section 6.10. This follows on from existing work [91, 163] having established the importance of the distinct mechanisms of fluid strain and rotation at inducing the observed modification in settling velocity, and therefore undertaking the modelling explicitly in terms of these mechanisms would be a natural way of incorporating this information into the closure model that is developed in this work. In particular, modelling of the separate timescales for the fluid strain and rotation rates along inertial particle trajectories would be needed in such an approach, and in the absence of any existing models in the literature these would have to be developed as a further precursor to such work.

The simple approximation of $\left\langle \nabla_j \mathrm{u}_{p_k}(s) v^0_m(t') \right\rangle \approx \left\langle \nabla_j \mathrm{u}_{p_k}(s) \mathrm{u}_{p_m}(t') \right\rangle$ was utilised in this work, however it was noted that in Figure 6.9 the one-time correlations $\left\langle \nabla_j \mathrm{u}_{p_k}(t) v^0_m(t) \right\rangle$ are not equal to zero. This is not accounted for by the current model, and therefore development of an expression for this quantity using correlation splitting is a natural improvement. Such a procedure is undertaken in Appendix D.2, however application of this to a closure model remains to be done. Furthermore, this would also require the specification of a suitable decorrelation function, which could be constructed as an axisymmetric tensor in the fashion outlined above.

It should be noted that the level of detail involved in any of these improvements would necessarily mean that the resultant closure model has to be evaluated numerically if it is developed for arbitrary St and V_g. This naturally brings about the question as to

whether it is possible to derive a useful analytical result for the modification in gravitational settling velocity using the cumulant expansion approach in this work. Possible avenues of investigation along these lines could include a perturbation expansion of the particle equation of motion in either of the limits $St \to 0$ or $V_g \to \infty$, and application of the resultant asymptotic form in the cumulant expansion. Furthermore, it may be worth investigating the modification in particle settling velocity in the limit of small separations $\boldsymbol{r}_p$, which could be accomplished using a Taylor expansion of the isotropic two-point two-time correlation tensor $\mathbf{R}(\boldsymbol{x}'_p, t'; \mathbf{x}, t)$. The other possibility for extracting an analytical result is an appropriate linearisation of the second cumulant $\left\langle \boldsymbol{\mathcal{H}}' \boldsymbol{r}'_p \right\rangle$ of the expansion, which could be done by linearising the Green's function $h(t; t')$ that makes multiple appearances within the resultant time integrals.

9.3 Analysis of the Particle Velocity Field

9.3.1 Conclusions

The form of particle velocity field proposed by Reeks [129] has been numerically evaluated using kinematic simulation to compute the particle Jacobian $\boldsymbol{\mathcal{J}}(\mathbf{x}^0, t)$ as it evolves along trajectories. Distinction is made between two expressions that can be used for evaluating the divergence of the particle velocity field $\nabla \cdot \boldsymbol{\mathcal{V}}(t' \mid \mathbf{x}, t)$, which use $\boldsymbol{\mathcal{J}}(\mathbf{x}^0, t)$ and the elemental deformation $J(\mathbf{x}^0, t)$ respectively, and the performance of these expressions is assessed numerically. It is found that due to the occurrence of $\boldsymbol{\mathcal{J}}(\mathbf{x}^0, t)$ becoming singular along some trajectories, evaluation of $\nabla \cdot \boldsymbol{\mathcal{V}}(t \mid \mathbf{x}^0, t_0)$ using either expression is affected to the extent that the average $\left\langle \nabla \cdot \boldsymbol{\mathcal{V}}(t \mid \mathbf{x}^0, t_0) \right\rangle$ cannot be considered meaningful. A simple filtering procedure on the conditionality of $\boldsymbol{\mathcal{J}}(\mathbf{x}^0, t)$ is tested to see whether valid results for $\nabla \cdot \boldsymbol{\mathcal{V}}(t \mid \mathbf{x}^0, t_0)$ can be obtained, and in this case the average $\left\langle \nabla \cdot \boldsymbol{\mathcal{V}}(t \mid \mathbf{x}^0, t_0) \right\rangle$ is found to be consistent when calculated using both $\boldsymbol{\mathcal{J}}(\mathbf{x}^0, t)$ and $J(\mathbf{x}^0, t)$. Subsequent evaluation of the drift tensor associated with the particle velocity field formulation in the case of particles settling under gravity reveals that this framework is able to retrieve some but not all of the increase in settling enhancement, and this highlights that the correct interpretation of $\boldsymbol{\mathcal{J}}(\mathbf{x}, t')$ needed to calculate $\nabla \cdot \boldsymbol{\mathcal{V}}(t' \mid \mathbf{x}, t)$ as used within this drift tensor is only obtainable when computed backwards-in-time.

9.3.2 Future Work

The work carried out on numerical solution for the divergence of the particle velocity field raises two main issues which need to be addressed for this to be viable method of accurately analysing particle behaviour. Firstly, computation of the Jacobian $\mathcal{J}(\mathbf{x}, t')$ that is needed for evaluation of $\nabla \cdot \boldsymbol{\mathcal{V}}(t' \mid \mathbf{x}, t)$ requires special numerical treatment, since calculation of the deformation at time t', with respect to the trajectory endpoint $\mathbf{x}$ at a later time t at which the initial conditions are imposed, necessary implies that the solution is sought at earlier times. For the particular second-order equation (7.18) in the case of a linear drag law, although the backwards-in-time solution is technically well-posed it is also numerically unstable, meaning that standard numerical methods will produce a solution which grows exponentially with reversed time. This issue has been addressed in the case of determining inertial particle trajectories at times earlier than the initial conditions through the use of dynamical systems theory, which entails construction of an attracting slow manifold that governs the asymptotic behaviour of particles [63], thereby avoiding the instability that is inherent in the backward-in-time particle equation of motion. Due to the similarity of the particle equation of motion in the case of a linear drag law with the governing equation for $\mathcal{J}(\mathbf{x}, t')$, it is reasoned that such an approach would also be applicable to determining $\mathcal{J}(\mathbf{x}, t')$ at times earlier than the initial conditions are applied, thus providing the correct interpretation of $\mathcal{J}(\mathbf{x}, t')$ for use in evaluation of $\nabla \cdot \boldsymbol{\mathcal{V}}(t' \mid \mathbf{x}, t)$.

Additionally, the issue of $\mathcal{J}(\mathbf{x}^0, t)$ becoming singular along some trajectories requires further treatment to ensure that the numerical values for $\nabla \cdot \boldsymbol{\mathcal{V}}(t' \mid \mathbf{x}, t)$ can be deemed as physically representative of the true compressibility along these trajectories. The approach taken in this work of using a simple filter on the conditionality of $\mathcal{J}(\mathbf{x}^0, t)$ has no rational grounds for being used, and the development of a method for dealing with these singularities which has a more justifiable physical basis is therefore an obvious extension of the current research.

9.4 Particle-Pair Models

9.4.1 Conclusions

Within the context of particle-pair models, the various terms that emerge in the expression for the particle mass flux have been assessed numerically using an inhomogeneous

velocity field with a stagnation point at $\mathbf{x} = 0$ which is specifically constructed using kinematic simulation. It is found that the dominant contribution to both the diffusive and convective fluxes is determined principally by the Stokes number St_E, with RMS fluid velocity fluctuation intensity u' not being as important a factor. The role of the expression $(\overline{\boldsymbol{\kappa}}-\nabla\cdot\overline{\boldsymbol{\lambda}})_{\mathrm{q}}$ in determining the net convective flux is analysed, and it is found that this contribution can be both positive and negative depending upon the value of u', becoming negative when u' is large. Furthermore, $(\overline{\boldsymbol{\kappa}} - \nabla \cdot \overline{\boldsymbol{\lambda}})_{\mathrm{q}}$ is the dominant contribution to the net convective flux for small St_E, whereas the turbophoretic term $(\nabla\cdot\overline{\mathbf{cc}})_{\mathrm{q}}$ is more important at large St_E. As the net convective flux is determined by the difference between $(\overline{\boldsymbol{\kappa}} - \nabla \cdot \overline{\boldsymbol{\lambda}})_{\mathrm{q}}$ and $(\nabla \cdot \overline{\mathbf{cc}})_{\mathrm{q}}$, it accordingly becomes most pronounced for the case of small St_E and large u' in which case $(\overline{\boldsymbol{\kappa}} - \nabla \cdot \overline{\boldsymbol{\lambda}})_{\mathrm{q}}$ is negative, and this corresponds to the highest value of particle concentration observed at the stagnation point $\mathbf{x} = 0$. Furthermore, the turbophoretic flux $(\nabla \cdot \overline{\mathbf{cc}})_{\mathrm{q}}$ is seen to be positive for all values of St_E and u', and therefore always contributes towards an increase in preferential concentration of particles, in contrast to $(\overline{\boldsymbol{\kappa}} - \nabla \cdot \overline{\boldsymbol{\lambda}})_{\mathrm{q}}$ which acts to decrease the preferential concentration of particles unless it is negative. This demonstrates that there are therefore two distinct mechanisms which can result in a build-up of particle concentration, and that there are no solid grounds on which to uniformly neglect the contributions associated with either of these mechanisms in closure models.

9.4.2 Future Work

Although a numerical investigation into the relative importance of the convective flux contributions of the non-local drift $(\overline{\boldsymbol{\kappa}} - \nabla \cdot \overline{\boldsymbol{\lambda}})_{\mathrm{q}}$ and turbophoresis $(\nabla \cdot \overline{\mathbf{cc}})_{\mathrm{q}}$ has been carried out, development of a closure model that can describe the observed behaviour remains to be done. The starting point for this would be application of the cumulant expansion used on the PDF dispersion tensors within the context of gravitational settling of particles in this research. In the event that this did not provide a satisfactory description of the behaviour, a closure strategy based on construction of a PDF model that represents the non-local contributions which are lost in the local homogeneous approximations would contain the required information, for which some work has already been done in the context of boundary layers [13]. A further outcome from developing an improved closure methodology would be to evaluate the profile of the associated radial distribution function $\hat{\rho}(\mathrm{q})$, and see how it compares with both the concentration profiles obtained using KS and other existing closure models [31, 178].

It is noted that the level of detail inherent in such a closure would necessarily preclude

analytical results for both the convective flux contributions $(\overline{\boldsymbol{\kappa}} - \nabla \cdot \overline{\boldsymbol{\lambda}})_{\mathrm{q}}$ and $(\nabla \cdot \overline{\mathbf{cc}})_{\mathrm{q}}$, and also the RDF $\hat{\rho}(\mathrm{q})$, which leads to consideration of whether developing a closure in a limit of particular parameters would yield such an expression. Existing work has taken the limits of both the inter-particle separation $\mathbf{r}_p \to \mathbf{0}$ and $St \to 0$ and been able to produce expressions for the RDF [177, 31], and if these limits are also applied to the PDF kinetic model framework by means of appropriate asymptotic expansions or linearisation procedures, then it may be possible to extract a corresponding form of the RDF.

9.5 General Extensions

Including the full physical description of the fluid and in particular detail of the behaviour at the microscales is of interest both in the context of gravitational settling of particles for which an increase of up to 50% has been observed using DNS [163, 69], and also particle-pair dispersion for small St which is strongly dependent on the behaviour of small scale structures within the fluid velocity field [31, 15]. Consequently, numerical assessment of the PDF kinetic model using DNS would be of great interest in both of these configurations, and further enable closure methodologies to use existing models that have been developed from the full description provided by the Navier-Stokes equation [96, 79]. This could lead to more refined closure models for both particle settling velocity modification and particle-pair dispersion, and hence also improved descriptions of particle collision and agglomeration rates. A further point of interest would be to assess the closure model developed in this work using DNS data, in order to see how well it captures the particle settling velocity enhancement that arises for the case of a linear drag law in true turbulence.

The use of the PDF kinetic model in this work has made it convenient to assume that the Eulerian fluid velocity field is normally distributed, however it is known that this is not the case for a true turbulent flow, with the higher-order moments of the PDF for fluid velocity deviating significantly from that of a Gaussian distribution [118]. Whilst this issue is avoided in the present work by using a synthetic flow field which is constructed such that the fluid velocities conform to a Gaussian distribution, it would become a consideration if the PDF kinetic model is used evaluate the behaviour of particles using DNS. This would involve including the higher-order cumulants of $\mathbf{b}(\mathbf{x}, t)$ within the expansion (4.9), in order to determine the contribution that they make to the overall behaviour for true turbulence. Notwithstanding this, as a first approximation

it is appropriate to omit the contribution from these higher-order cumulants since statistical considerations based upon the central limit theorem argue that non-extreme values of fluid velocity should be close to a normal distribution, and it is these non-extreme values which constitute the majority of the velocity field. As a consequence, the truncated form of the PDF kinetic model used in the present work would be expected to capture the leading-order behaviour of particles in a DNS fluid velocity field, especially for homogeneous flows. However, it may be found that in other flow configurations the omitted contribution is of greater importance, and would therefore have to be included in order for the PDF kinetic model to accurately capture the particle behaviour in such cases.

The other complication arising when the PDF kinetic model is used to describe particle behaviour in a DNS flow field is that the form of the two-point two-time fluid velocity correlation tensor $\mathbf{R}(\mathbf{x}', t'; \mathbf{x}, t)$ is no longer automatically specified. For the case of isotropic turbulence, this is due to the longitudinal autocorrelation function $f(\mathrm{r}, t)$ not being uniquely determined by the full Navier-Stokes equation, and therefore requiring non-trivial surface fitting using DNS data. A suitable form of such a fit would be a bivariate Gaussian of r and t, and although the integral lengthscale L_{11} and Eulerian integral timescale τ_E of the fluid would determine the marginal distributions for each of $f(\mathrm{r}, 0)$ and $f(0, t)$, these spatial and temporal decorrelations would not be independent in contrast to the KS flow field used for the present work. Thus it is the correlation coefficient between the respective spatial and temporal autocorrelation functions $f(\mathrm{r}, 0)$ and $f(0, t)$ that would need to be calculated using DNS data for the specific flow configuration which is being considered.

Whilst capturing the particle behaviour is only dealt with in this work using the PDF kinetic model, such an approach may also be tractable using the GLM to describe both particle settling velocity enhancement and particle-pair dispersion. The development of a corresponding closure model and assessment of its performance relative to that of the model constructed in the present work would therefore be of interest as a means of comparing these different PDF descriptions. Furthermore, since the PDF kinetic model is not restricted to describing the behaviour of only point particles, extension of the closure model to account for a wider range of physical particle behaviour could be carried out by considering arbitrary density particles for which added mass effects are important, such as in the case of bubble flows.

9.6 Summary

This work has shown that the PDF kinetic framework provides a fundamental means of describing the behaviour of inertial particles in Gaussian flow fields within the context of both gravitational settling and particle-pair dispersion, and is able to numerically capture the different convective contributions to the particle mass flux that emerge in each case. It has been further demonstrated that it is possible to construct closure models for this particular form of PDF framework which are capable of capturing these flux contributions, although accounting for the full effect of the higher-order physical behaviour that is observed in the specific zero-mean flow configurations which are considered is not achieved by the models in their current form. Nonetheless, the full behaviour is seen to be contained within the description provided by the unclosed form of the PDF kinetic model, which highlights the potential for improved closures to be developed using this framework in future research.

References

[1] Aliseda, A., Cartellier, A., Hainaux, F., and Lasheras, J. C. Effect of preferential concentration on the settling velocity of heavy particles in homogeneous isotropic turbulence. *Journal of Fluid Mechanics 468* (2002), 77–105.

[2] Anderson, J. D., and Wendt, J. *Computational fluid dynamics*, vol. 206. Springer, 1995.

[3] Argyropoulos, C., and Markatos, N. Recent advances on the numerical modelling of turbulent flows. *Applied Mathematical Modelling 39*, 2 (2015), 693–732.

[4] Baker, L., Frankel, A., Mani, A., and Coletti, F. Coherent clusters of inertial particles in homogeneous turbulence. *Journal of Fluid Mechanics 833* (2017), 364–398.

[5] Balachandar, S., and Eaton, J. K. Turbulent dispersed multiphase flow. *Annual Review of Fluid Mechanics 42* (2010), 111–133.

[6] Barajas-Solano, D. A., and Tartakovsky, A. M. Probabilistic density function method for nonlinear dynamical systems driven by colored noise. *Physical Review E 93*, 5 (2016), 052121.

[7] Batchelor, G. The theory of axisymmetric turbulence. *Proceedings of the Royal Society of London. Series A. Mathematical and Physical Sciences 186*, 1007 (1946), 480–502.

[8] Batchelor, G., and Townsend, A. Decay of turbulence in the final period. *Proceedings of the Royal Society of London. Series A. Mathematical and Physical Sciences 194*, 1039 (1948), 527–543.

[9] Batchelor, G. K. *The theory of homogeneous turbulence*. Cambridge University Press, 1953.

[10] Bec, J. Multifractal concentrations of inertial particles in smooth random flows. *Journal of Fluid Mechanics 528* (2005), 255–277.

[11] Bhatnagar, A., Gustavsson, K., and Mitra, D. Statistics of the relative velocity of particles in turbulent flows: Monodisperse particles. *Physical Review E 97*, 2 (2018), 023105.

[12] Bragg, A., Swailes, D., and Skartlien, R. Drift-free kinetic equations for turbulent dispersion. *Physical Review E 86*, 5 (2012), 056306.

[13] Bragg, A., Swailes, D., and Skartlien, R. Particle transport in a turbulent boundary layer: Non-local closures for particle dispersion tensors accounting for particle-wall interactions. *Physics of Fluids 24*, 10 (2012), 103304.

[14] Bragg, A. D. Analysis of the forward and backward in time pair-separation probability density functions for inertial particles in isotropic turbulence. *Journal of Fluid Mechanics 830* (2017), 63–92.

[15] Bragg, A. D., and Collins, L. R. New insights from comparing statistical theories for inertial particles in turbulence: I. Spatial distribution of particles. *New Journal of Physics 16*, 5 (2014), 055013.

[16] Bragg, A. D., and Collins, L. R. New insights from comparing statistical theories for inertial particles in turbulence: II. Relative velocities. *New Journal of Physics 16*, 5 (2014), 055014.

[17] Bragg, A. D., De Lillo, F., and Boffetta, G. Irreversibility inversions in two-dimensional turbulence. *Physical Review Fluids 3*, 2 (2018), 024302.

[18] Bragg, A. D., Ireland, P. J., and Collins, L. R. Mechanisms for the clustering of inertial particles in the inertial range of isotropic turbulence. *Physical Review E 92*, 2 (2015), 023029.

[19] Bragg, A. D., Ireland, P. J., and Collins, L. R. On the relationship between the non-local clustering mechanism and preferential concentration. *Journal of Fluid Mechanics 780* (2015), 327–343.

[20] Bragg, A. D., Ireland, P. J., and Collins, L. R. Forward and backward in time dispersion of fluid and inertial particles in isotropic turbulence. *Physics of Fluids 28*, 1 (2016), 013305.

[21] Brunk, B. K., Koch, D. L., and Lion, L. W. Turbulent coagulation of colloidal particles. *Journal of Fluid Mechanics 364* (1998), 81–113.

[22] Burden, R. L., and Faires, J. D. *Numerical analysis*. Brooks/Cole, 1997.

[23] Buyevich, Y. A. Statistical hydromechanics of disperse systems. Part 1. Physical background and general equations. *Journal of Fluid Mechanics 49*, 3 (1971), 489–507.

[24] Buyevich, Y. A. Statistical hydromechanics of disperse systems. Part 2. Solution of the kinetic equation for suspended particles. *Journal of Fluid Mechanics 52*, 2 (1972), 345–355.

[25] Buyevich, Y. A. Statistical hydromechanics of disperse systems. Part 3. Pseudo-turbulent structure of homogeneous suspensions. *Journal of Fluid Mechanics 56*, 2 (1972), 313–336.

[26] Carroll, P. L., and Blanquart, G. A proposed modification to Lundgren's physical space velocity forcing method for isotropic turbulence. *Physics of Fluids 25*, 10 (2013), 105114.

[27] Chandrasekhar, S. The theory of axisymmetric turbulence. *Philosophical Transactions of the Royal Society of London. Series A, Mathematical and Physical Sciences 242*, 855 (1950), 557–577.

[28] Chapman, S., Cowling, T. G., and Burnett, D. *The mathematical theory of non-uniform gases: an account of the kinetic theory of viscosity, thermal conduction and diffusion in gases*. Cambridge University Press, 1970.

[29] Chen, J., Hussain, F., Pei, J., and She, Z.-S. Velocity–vorticity correlation structure in turbulent channel flow. *Journal of Fluid Mechanics 742* (2014), 291–307.

[30] Chen, L., Goto, S., and Vassilicos, J. Turbulent clustering of stagnation points and inertial particles. *Journal of Fluid Mechanics 553* (2006), 143–154.

[31] Chun, J., Koch, D. L., Rani, S. L., Ahluwalia, A., and Collins, L. R. Clustering of aerosol particles in isotropic turbulence. *Journal of Fluid Mechanics 536* (2005), 219–251.

[32] Chung, M. K., Sung, H. J., and Lee, K. B. Computational study of turbulent gas-particle flow in a Venturi. *Journal of Fluids Engineering 108*, 2 (1986), 248–253.

[33] Clift, R., Grace, J. R., and Weber, M. E. *Bubbles, drops, and particles*. Courier Corporation, 2005.

[34] Coleman, S., and Vassilicos, J. A unified sweep-stick mechanism to explain particle clustering in two-and three-dimensional homogeneous, isotropic turbulence. *Physics of Fluids 21*, 11 (2009), 113301.

[35] Corrsin, S. Progress report on some turbulent diffusion research. In *Advances in Geophysics*, vol. 6. Elsevier, 1959, pp. 161–164.

[36] Crowe, C. T. *Multiphase flow handbook*. CRC Press, 2014.

[37] Crowe, C. T., Schwarzkopf, J. D., Sommerfeld, M., and Tsuji, Y. *Multiphase flows with droplets and particles*. CRC Press, 2011.

[38] Crowe, C. T., Sharma, M. P., and Stock, D. E. The particle-source-in cell (PSI-CELL) model for gas-droplet flows. *Journal of Fluids Engineering 99*, 2 (1977), 325–332.

[39] Csanady, G. Turbulent diffusion of heavy particles in the atmosphere. *Journal of the Atmospheric Sciences 20*, 3 (1963), 201–208.

[40] Daitche, A. On the role of the history force for inertial particles in turbulence. *Journal of Fluid Mechanics 782* (2015), 567–593.

[41] Davila, J., and Hunt, J. C. Settling of small particles near vortices and in turbulence. *Journal of Fluid Mechanics 440* (2001), 117–145.

[42] De Karman, T., and Howarth, L. On the statistical theory of isotropic turbulence. *Proceedings of the Royal Society of London. Series A-Mathematical and Physical Sciences 164*, 917 (1938), 192–215.

[43] Dejoan, A., and Monchaux, R. Preferential concentration and settling of heavy particles in homogeneous turbulence. *Physics of Fluids 25*, 1 (2013), 013301.

[44] Derevich, I., and Zaichik, L. Particle deposition from a turbulent flow. *Fluid Dynamics 23*, 5 (1988), 722–729.

[45] Dhariwal, R., and Bragg, A. D. Fluid particles only separate exponentially in the dissipation range of turbulence after extremely long times. *Physical Review Fluids 3*, 3 (2018), 034604.

[46] Dhariwal, R., Rani, S., and Koch, D. A stochastic model for the relative motion of high Stokes number particles in isotropic turbulence. *Bulletin of the American Physical Society 59* (2014).

[47] Domingo, P., Vervisch, L., and Réveillon, J. DNS analysis of partially premixed combustion in spray and gaseous turbulent flame-bases stabilized in hot air. *Combustion and Flame 140*, 3 (2005), 172–195.

[48] Elghobashi, S. On predicting particle-laden turbulent flows. *Applied Scientific Research 52*, 4 (1994), 309–329.

[49] Elghobashi, S., and Abou-Arab, T. A two-equation turbulence model for two-phase flows. *The Physics of Fluids 26*, 4 (1983), 931–938.

[50] Eswaran, V., and Pope, S. An examination of forcing in direct numerical simulations of turbulence. *Computers & Fluids 16*, 3 (1988), 257–278.

[51] Farhan, M., Nicolleau, F., and Nowakowski, A. Effect of gravity on clustering patterns and inertial particle attractors in kinematic simulations. *Physical Review E 91*, 4 (2015), 043021.

[52] Fornari, W., Picano, F., and Brandt, L. Sedimentation of finite-size spheres in quiescent and turbulent environments. *Journal of Fluid Mechanics 788* (2016), 640–669.

[53] Fornari, W., Picano, F., Sardina, G., and Brandt, L. Reduced particle settling speed in turbulence. *Journal of Fluid Mechanics 808* (2016), 153–167.

[54] Fronzoni, L., Grigolini, P., Hanggi, P., Moss, F., Mannella, R., and McClintock, P. Bistable oscillator dynamics driven by nonwhite noise. *Physical Review A 33*, 5 (1986), 3320.

[55] Fung, J. C. H. Gravitational settling of particles and bubbles in homogeneous turbulence. *Journal of Geophysical Research: Oceans 98*, C11 (1993), 20287–20297.

[56] Furutsu, K. On the statistical theory of electromagnetic waves in a fluctuating medium (I). *J. Res. Nat. Bur. Standards D*, 67 (1963), 303–323.

[57] Gardiner, C. W., et al. *Handbook of stochastic methods*, vol. 3. Springer Berlin, 1985.

[58] Gatignol, R. The Faxén formulas for a rigid particle in an unsteady non-uniform Stokes-flow. *Journal de Mécanique Théorique et Appliquée 2*, 2 (1983), 143–160.

[59] Gibert, M., Xu, H., and Bodenschatz, E. Where do small, weakly inertial particles go in a turbulent flow? *Journal of Fluid Mechanics 698* (2012), 160–167.

[60] Girimaji, S., and Pope, S. A diffusion model for velocity gradients in turbulence. *Physics of Fluids A: Fluid Dynamics 2*, 2 (1990), 242–256.

[61] Good, G., Ireland, P., Bewley, G., Bodenschatz, E., Collins, L., and Warhaft, Z. Settling regimes of inertial particles in isotropic turbulence. *Journal of Fluid Mechanics 759* (2014).

[62] Gustavsson, K., and Mehlig, B. Relative velocities of inertial particles in turbulent aerosols. *Journal of Turbulence 15*, 1 (2014), 34–69.

[63] Haller, G., and Sapsis, T. Where do inertial particles go in fluid flows? *Physica D: Nonlinear Phenomena 237*, 5 (2008), 573–583.

[64] Hänggi, P. Correlation functions and masterequations of generalized (non-Markovian) Langevin equations. *Zeitschrift für Physik B Condensed Matter 31*, 4 (1978), 407–416.

[65] Hänggi, P., Mroczkowski, T. J., Moss, F., and McClintock, P. V. Bistability driven by colored noise: Theory and experiment. *Physical Review A 32*, 1 (1985), 695.

[66] Haworth, D. C., and Pope, S. A generalized Langevin model for turbulent flows. *The Physics of Fluids 29*, 2 (1986), 387–405.

[67] He, G., Jin, G., and Yang, Y. Space-time correlations and dynamic coupling in turbulent flows. *Annual Review of Fluid Mechanics 49* (2017), 51–70.

[68] Healy, D., and Young, J. Full Lagrangian methods for calculating particle concentration fields in dilute gas-particle flows. *Proceedings of the Royal Society A: Mathematical, Physical and Engineering Sciences 461*, 2059 (2005), 2197–2225.

[69] Huck, P. D., Bateson, C., Volk, R., Cartellier, A., Bourgoin, M., and Aliseda, A. The role of collective effects on settling velocity enhancement for inertial particles in turbulence. *Journal of Fluid Mechanics 846* (2018), 1059–1075.

[70] Hwang, P. A. Fall velocity of particles in oscillating flow. *Journal of Hydraulic Engineering 111*, 3 (1985), 485–502.

[71] Hyland, K., McKee, S., and Reeks, M. Derivation of a pdf kinetic equation for the transport of particles in turbulent flows. *Journal of Physics A: Mathematical and General 32*, 34 (1999), 6169.

[72] Ijzermans, R., Reeks, M., Meneguz, E., Picciotto, M., and Soldati, A. Measuring segregation of inertial particles in turbulence by a full Lagrangian approach. *Physical Review E 80*, 1 (2009), 015302.

[73] Ijzermans, R. H., Meneguz, E., and Reeks, M. W. Segregation of particles in incompressible random flows: singularities, intermittency and random uncorrelated motion. *Journal of Fluid Mechanics 653* (2010), 99–136.

[74] Iliopoulos, I., and Hanratty, T. J. Turbulent dispersion in a non-homogeneous field. *Journal of Fluid Mechanics 392* (1999), 45–71.

[75] Iliopoulos, I., and Hanratty, T. J. A non-Gaussian stochastic model to describe passive tracer dispersion and its comparison to a direct numerical simulation. *Physics of Fluids 16*, 8 (2004), 3006–3030.

[76] Ireland, P. J., Bragg, A. D., and Collins, L. R. The effect of Reynolds number on inertial particle dynamics in isotropic turbulence. Part 1. Simulations without gravitational effects. *Journal of Fluid Mechanics 796* (2016), 617–658.

[77] Ireland, P. J., Bragg, A. D., and Collins, L. R. The effect of Reynolds number on inertial particle dynamics in isotropic turbulence. Part 2. Simulations with gravitational effects. *Journal of Fluid Mechanics 796* (2016), 659–711.

[78] Ireland, P. J., Vaithianathan, T., Sukheswalla, P. S., Ray, B., and Collins, L. R. Highly parallel particle-laden flow solver for turbulence research. *Computers & Fluids 76* (2013), 170–177.

[79] Johnson, P. L., and Meneveau, C. A closure for Lagrangian velocity gradient evolution in turbulence using recent-deformation mapping of initially Gaussian fields. *Journal of Fluid Mechanics 804* (2016), 387–419.

[80] Jones, W., and Launder, B. The calculation of low-Reynolds-number phenomena with a two-equation model of turbulence. *International Journal of Heat and Mass Transfer 16*, 6 (1973), 1119–1130.

[81] Klein, M., Chakraborty, N., and Ketterl, S. A comparison of strategies for direct numerical simulation of turbulence chemistry interaction in generic planar turbulent premixed flames. *Flow, Turbulence and Combustion 99*, 3-4 (2017), 955–971.

[82] Klyatskin, V. I. *Dynamics of stochastic systems*. Elsevier, 2005.

[83] Kraichnan, R. H. Lagrangian-history closure approximation for turbulence. *Physics of Fluids 8*, 4 (1965), 575–598.

[84] Kraichnan, R. H. Diffusion by a random velocity field. *Physics of Fluids 13*, 1 (1970), 22–31.

[85] Kraichnan, R. H. Eulerian and Lagrangian renormalization in turbulence theory. *Journal of Fluid Mechanics 83*, 2 (1977), 349–374.

[86] Launder, B., and Spalding, D. The numerical computation of turbulent flows. *Computer Methods in Applied Mechanics and Engineering 3*, 2 (1974), 269–289.

[87] Lundgren, T. Linearly forced isotropic turbulence. *Annual Research Briefs* (2003), 361–473.

[88] Magnus, W. On the exponential solution of differential equations for a linear operator. *Communications on Pure and Applied Mathematics 7*, 4 (1954), 649–673.

[89] Mallouppas, G., George, W., and van Wachem, B. New forcing scheme to sustain particle-laden homogeneous and isotropic turbulence. *Physics of Fluids 25*, 8 (2013), 083304.

[90] Mashayek, F., and Pandya, R. Analytical description of particle/droplet-laden turbulent flows. *Progress in Energy and Combustion Science 29*, 4 (2003), 329–378.

[91] Maxey, M. The gravitational settling of aerosol particles in homogeneous turbulence and random flow fields. *Journal of Fluid Mechanics 174* (1987), 441–465.

[92] Maxey, M., and Corrsin, S. Gravitational settling of aerosol particles in randomly oriented cellular flow fields. *Journal of the Atmospheric Sciences 43*, 11 (1986), 1112–1134.

[93] Maxey, M. R., and Riley, J. J. Equation of motion for a small rigid sphere in a nonuniform flow. *Physics of Fluids 26*, 4 (1983), 883–889.

[94] Mei, R., Adrian, R. J., and Hanratty, T. J. Particle dispersion in isotropic turbulence under Stokes drag and Basset force with gravitational settling. *Journal of Fluid Mechanics 225* (1991), 481–495.

[95] Meneguz, E., and Reeks, M. W. Statistical properties of particle segregation in homogeneous isotropic turbulence. *Journal of Fluid Mechanics 686* (2011), 338–351.

[96] Meneveau, C. Lagrangian dynamics and models of the velocity gradient tensor in turbulent flows. *Annual Review of Fluid Mechanics 43* (2011), 219–245.

[97] Minier, J.-P. Statistical descriptions of polydisperse turbulent two-phase flows. *Physics Reports 665* (2016), 1–122.

[98] Minier, J.-P., and Peirano, E. The PDF approach to turbulent polydispersed two-phase flows. *Physics Reports 352*, 1-3 (2001), 1–214.

[99] Minier, J.-P., and Profeta, C. Kinetic and dynamic probability-density-function descriptions of disperse turbulent two-phase flows. *Physical Review E 92*, 5 (2015), 053020.

[100] Monchaux, R., Bourgoin, M., and Cartellier, A. Preferential concentration of heavy particles: a Voronoï analysis. *Physics of Fluids 22*, 10 (2010), 103304.

[101] Monchaux, R., Bourgoin, M., and Cartellier, A. Analyzing preferential concentration and clustering of inertial particles in turbulence. *International Journal of Multiphase Flow 40* (2012), 1–18.

[102] Monchaux, R., and Dejoan, A. Settling velocity and preferential concentration of heavy particles under two-way coupling effects in homogeneous turbulence. *Physical Review Fluids 2*, 10 (2017), 104302.

[103] Murray, S., Lightstone, M., and Tullis, S. Single-particle Lagrangian and structure statistics in kinematically simulated particle-laden turbulent flows. *Physics of Fluids 28*, 3 (2016), 033302.

[104] Murray, S., Lightstone, M., and Tullis, S. Target Lagrangian kinematic simulation for particle-laden flows. *Physical Review E 94*, 3 (2016), 033303.

[105] Nicolleau, F., Farhan, M., and Nowakowski, A. Effect of the energy-spectrum law on clustering patterns for inertial particles subjected to gravity in kinematic simulation. *Physical Review E 94*, 4 (2016), 043109.

[106] Nilsen, C., and Andersson, H. I. Mechanisms of particle clustering in Gaussian and non-Gaussian synthetic turbulence. *Physical Review E 90*, 4 (2014), 043005.

[107] Novikov, E. Functionals and the random-force method in turbulence theory. *Sov. Phys. JETP 20*, 5 (1965), 1290–1294.

[108] Obligado, M., Teitelbaum, T., Cartellier, A., Mininni, P., and Bourgoin, M. Preferential concentration of heavy particles in turbulence. *Journal of Turbulence 15*, 5 (2014), 293–310.

[109] Orszag, S. A. Numerical methods for the simulation of turbulence. *The Physics of Fluids 12*, 12 (1969), II–250.

[110] Orszag, S. A., and Patterson Jr, G. Numerical simulation of three-dimensional homogeneous isotropic turbulence. *Physical Review Letters 28*, 2 (1972), 76.

[111] Osiptsov, A. Investigation of regions of unbounded growth of the particle concentration in disperse flows. *Fluid Dynamics 19*, 3 (1984), 378–385.

[112] Osiptsov, A. Modified Lagrangian method for calculating the particle concentration in dusty-gas flows with intersecting particle trajectories. In *Proceedings 3rd Int. Conf. on Multiphase Flow* (1998), no. 98.

[113] Palmore Jr, J. A., and Desjardins, O. Technique for forcing high Reynolds number isotropic turbulence in physical space. *Physical Review Fluids 3*, 3 (2018), 034605.

[114] Parishani, H., Ayala, O., Rosa, B., Wang, L.-P., and Grabowski, W. Effects of gravity on the acceleration and pair statistics of inertial particles in homogeneous isotropic turbulence. *Physics of Fluids 27*, 3 (2015), 033304.

[115] Perrin, V. E., and Jonker, H. J. Relative velocity distribution of inertial particles in turbulence: A numerical study. *Physical Review E 92*, 4 (2015), 043022.

[116] Picciotto, M., Marchioli, C., Reeks, M. W., and Soldati, A. Statistics of velocity and preferential accumulation of micro-particles in boundary layer turbulence. *Nuclear Engineering and Design 235*, 10-12 (2005), 1239–1249.

[117] Pope, S. Lagrangian PDF methods for turbulent flows. *Annual Review of Fluid Mechanics 26*, 1 (1994), 23–63.

[118] Pope, S. B. *Turbulent flows*. Cambridge University Press, 2000.

[119] Pozorski, J., and Minier, J.-P. Probability density function modeling of dispersed two-phase turbulent flows. *Physical Review E 59*, 1 (1999), 855.

[120] Prosperetti, A., and Tryggvason, G. *Computational methods for multiphase flow*. Cambridge University Press, 2007.

[121] Reade, W. C., and Collins, L. R. Effect of preferential concentration on turbulent collision rates. *Physics of Fluids 12*, 10 (2000), 2530–2540.

[122] Reeks, M. Eulerian direct interaction applied to the statistical motion of particles in a turbulent fluid. *Journal of Fluid Mechanics 97*, 3 (1980), 569–590.

[123] Reeks, M. The transport of discrete particles in inhomogeneous turbulence. *Journal of Aerosol Science 14*, 6 (1983), 729–739.

[124] Reeks, M. On a kinetic equation for the transport of particles in turbulent flows. *Physics of Fluids A: Fluid Dynamics 3*, 3 (1991), 446–456.

[125] Reeks, M. On the continuum equations for dispersed particles in nonuniform flows. *Physics of Fluids A: Fluid Dynamics 4*, 6 (1992), 1290–1303.

[126] Reeks, M. On the constitutive relations for dispersed particles in nonuniform flows. I: Dispersion in a simple shear flow. *Physics of Fluids A: Fluid Dynamics 5*, 3 (1993), 750–761.

[127] Reeks, M. On probability density function equations for particle dispersion in a uniform shear flow. *Journal of Fluid Mechanics 522* (2005), 263–302.

[128] Reeks, M., Swailes, D., and Bragg, A. Is the kinetic equation for turbulent gas-particle flows ill posed? *Physical Review E 97*, 2 (2018), 023104.

[129] Reeks, M. W. Particle drift in turbulent flows: the influence of local structure and inhomogeneity. In *Proceedings 4th Int. Conf. on Multiphase Flow* (2001), no. 187.

[130] Reeks, M. W. Simulation of particle diffusion, segregation, and intermittency in turbulent flows. In *IUTAM Symposium on Computational Approaches to Multiphase Flow* (2006), Springer, pp. 21–30.

[131] Rice, H. P., Fairweather, M., Hunter, T. N., Mahmoud, B., Biggs, S., and Peakall, J. Measuring particle concentration in multiphase pipe flow using acoustic backscatter: Generalization of the dual-frequency inversion method. *The Journal of the Acoustical Society of America 136*, 1 (2014), 156–169.

[132] Risken, H. *The Fokker-Planck equation*. Springer, 1996.

[133] Roach, G. F. *Green's functions*. Cambridge University Press, 1982.

[134] Rosa, B., Parishani, H., Ayala, O., and Wang, L.-P. Settling velocity of small inertial particles in homogeneous isotropic turbulence from high-resolution DNS. *International Journal of Multiphase Flow 83* (2016), 217–231.

[135] Rosales, C., and Meneveau, C. Linear forcing in numerical simulations of isotropic turbulence: Physical space implementations and convergence properties. *Physics of Fluids 17*, 9 (2005), 095106.

[136] Schreurs, P., Mewis, J., and Havens, J. Numerical aspects of a Lagrangian particle model for atmospheric dispersion of heavy gases. *Journal of Hazardous Materials 17*, 1 (1987), 61–80.

[137] Schumann, U., and Patterson, G. Numerical study of pressure and velocity fluctuations in nearly isotropic turbulence. *Journal of Fluid Mechanics 88*, 04 (1978), 685–709.

[138] Shaw, R. A. Particle-turbulence interactions in atmospheric clouds. *Annual Review of Fluid Mechanics 35*, 1 (2003), 183–227.

[139] She, Z.-S., Jackson, E., and Orszag, S. A. Intermittent vortex structures in homogeneous isotropic turbulence. *Nature 344*, 6263 (1990), 226.

[140] Sheldon, R., et al. *A first course in probability*. Pearson Education India, 2002.

[141] Simonin, O., Deutsch, E., and Minier, J. Eulerian prediction of the fluid/particle correlated motion in turbulent two-phase flows. *Applied Scientific Research: Advances In Turbulence IV 51* (1993), 275–283.

[142] Skartlien, R. Kinetic modeling of particles in stratified flow–evaluation of dispersion tensors in inhomogeneous turbulence. *International Journal of Multiphase Flow 33*, 9 (2007), 1006–1022.

[143] Skartlien, R. A droplet transport model for channel and pipe flow based on particle kinetic theory and a stress–ω turbulence model. *International Journal of Multiphase Flow 35*, 7 (2009), 603–616.

[144] Skartlien, R., Drazen, D., Swailes, D., and Jensen, A. Suspensions in turbulent liquid pipe flow: Kinetic modelling and added mass effects. *International Journal of Multiphase Flow 35*, 11 (2009), 1017–1035.

[145] Smagorinsky, J. General circulation experiments with the primitive equations: I. The basic experiment. *Monthly Weather Review 91*, 3 (1963), 99–164.

[146] Squires, K. D., and Eaton, J. K. Preferential concentration of particles by turbulence. *Physics of Fluids A: Fluid Dynamics 3*, 5 (1991), 1169–1178.

[147] Sudharsan, M., Brunton, S. L., and Riley, J. J. Lagrangian coherent structures and inertial particle dynamics. *Physical Review E 93*, 3 (2016), 033108.

[148] Sumbekova, S., Cartellier, A., Aliseda, A., and Bourgoin, M. Preferential concentration of inertial sub-Kolmogorov particles: the roles of mass loading of particles, Stokes numbers, and Reynolds numbers. *Physical Review Fluids 2*, 2 (2017), 024302.

[149] Swailes, D., Sergeev, Y., and Parker, A. Chapman–Enskog closure approximation in the kinetic theory of dilute turbulent gas-particulate suspensions. *Physica A: Statistical Mechanics and its Applications 254*, 3 (1998), 517–547.

[150] Swailes, D. C., and Darbyshire, K. F. A generalized Fokker-Planck equation for particle transport in random media. *Physica A: Statistical Mechanics and its Applications 242*, 1 (1997), 38–48.

[151] Swailes, D. C., and Darbyshire, K. F. Probabilistic models for particle and scalar transport in fluctuating flows: an evaluation of simple closure approximations. *Physica A: Statistical Mechanics and its Applications 262*, 3 (1999), 307–327.

[152] Tennekes, H., and Lumley, J. L. *A first course in turbulence*. MIT Press, 1972.

[153] Thomson, D., and Devenish, B. Particle pair separation in kinematic simulations. *Journal of Fluid Mechanics 526* (2005), 277–302.

[154] Tinoco, H., Lindqvist, H., and Frid, W. Numerical simulation of industrial flows. In *Numerical Simulations: Examples and Applications in Computational Fluid Dynamics*. InTech Croatia, 2010, pp. 231–262.

[155] Tom, J., and Bragg, A. D. Multiscale preferential sweeping of particles settling in turbulence. *Journal of Fluid Mechanics 871* (2019), 244–270.

[156] Tunstall, E., and Houghton, G. Retardation of falling spheres by hydrodynamic oscillations. *Chemical Engineering Science 23*, 9 (1968), 1067–1081.

[157] Uhlmann, M., and Chouippe, A. Clustering and preferential concentration of finite-size particles in forced homogeneous-isotropic turbulence. *Journal of Fluid Mechanics 812* (2017), 991–1023.

[158] van Dijk, P., and Swailes, D. Hermite-DG methods for pdf equations modelling particle transport and deposition in turbulent boundary layers. *Journal of Computational Physics 231*, 14 (2012), 4904–4920.

[159] van Hinsberg, M., Clercx, H., and Toschi, F. Enhanced settling of nonheavy inertial particles in homogeneous isotropic turbulence: The role of the pressure gradient and the Basset history force. *Physical Review E 95*, 2 (2017), 023106.

[160] Van Kampen, N. A cumulant expansion for stochastic linear differential equations. I. *Physica 74*, 2 (1974), 215–238.

[161] Van Kampen, N. A cumulant expansion for stochastic linear differential equations. II. *Physica 74*, 2 (1974), 239–247.

[162] Van Kampen, N. G. *Stochastic processes in physics and chemistry*, vol. 1. Elsevier, 1992.

[163] Wang, L.-P., and Maxey, M. R. Settling velocity and concentration distribution of heavy particles in homogeneous isotropic turbulence. *Journal of Fluid Mechanics 256* (1993), 27–68.

[164] Wang, L.-P., and Stock, D. Numerical simulation of heavy particle dispersion time step and nonlinear drag considerations. *Journal of Fluids Engineering 114*, 1 (1992), 100–106.

[165] Wang, L.-P., and Stock, D. E. Dispersion of heavy particles by turbulent motion. *Journal of the Atmospheric Sciences 50*, 13 (1993), 1897–1913.

[166] Wang, L.-P., Wexler, A. S., and Zhou, Y. Statistical mechanical description and modelling of turbulent collision of inertial particles. *Journal of Fluid Mechanics 415* (2000), 117–153.

[167] Warsi, Z. U. *Fluid dynamics: theoretical and computational approaches*. CRC Press, 2005.

[168] Weinstock, J. Lagrangian–Eulerian relation and the independence approximation. *The Physics of Fluids 19*, 11 (1976), 1702–1711.

[169] Wells, M., and Stock, D. The effects of crossing trajectories on the dispersion of particles in a turbulent flow. *Journal of Fluid Mechanics 136* (1983), 31–62.

[170] Wilkinson, M., and Mehlig, B. Caustics in turbulent aerosols. *Europhysics Letters 71*, 2 (2005), 186.

[171] Wilkinson, M., Mehlig, B., and Bezuglyy, V. Caustic activation of rain showers. *Physical Review Letters 97*, 4 (2006), 048501.

[172] Wood, A., Hwang, W., and Eaton, J. Preferential concentration of particles in homogeneous and isotropic turbulence. *International Journal of Multiphase Flow 31*, 10-11 (2005), 1220–1230.

[173] Yang, C., and Lei, U. The role of the turbulent scales in the settling velocity of heavy particles in homogeneous isotropic turbulence. *Journal of Fluid Mechanics 371* (1998), 179–205.

[174] Yudine, M. Physical considerations on heavy-particle diffusion. In *Advances in Geophysics*, vol. 6. Elsevier, 1959, pp. 185–191.

[175] Zaichik, L. Modelling of the motion of particles in non-uniform turbulent flow using the equation for the probability density function. *Journal of Applied Mathematics and Mechanics 61*, 1 (1997), 127–133.

[176] Zaichik, L. A statistical model of particle transport and heat transfer in turbulent shear flows. *Physics of Fluids 11*, 6 (1999), 1521–1534.

[177] Zaichik, L. I., and Alipchenkov, V. M. Pair dispersion and preferential concentration of particles in isotropic turbulence. *Physics of Fluids 15*, 6 (2003), 1776–1787.

[178] Zaichik, L. I., and Alipchenkov, V. M. Refinement of the probability density function model for preferential concentration of aerosol particles in isotropic turbulence. *Physics of Fluids 19*, 11 (2007), 113308.

[179] Zaichik, L. I., and Alipchenkov, V. M. Statistical models for predicting pair dispersion and particle clustering in isotropic turbulence and their applications. *New Journal of Physics 11*, 10 (2009), 103018.

[180] Zaichik, L. I., and Alipchenkov, V. M. Modelling of transport and dispersion of arbitrary-density particles in turbulent flows. *International Journal of Heat and Fluid Flow 31*, 5 (2010), 850–861.

[181] Zaichik, L. I., Alipchenkov, V. M., and Sinaiski, E. G. *Particles in turbulent flows*. John Wiley & Sons, 2008.

[182] Zaidi, A. A., Tsuji, T., and Tanaka, T. Direct numerical simulation of finite sized particles settling for high Reynolds number and dilute suspension. *International Journal of Heat and Fluid Flow 50* (2014), 330–341.

Appendix A

Analytical Solution for the Particle Response Tensor

The particle response tensor $\boldsymbol{\mathcal{H}}[t;t']$ plays a key role in quantifying the history of fluid-particle interaction within the PDF kinetic framework, and is accordingly highly sensitive to variations in the underlying fluid velocity field. In the case of the Stokes drag model (6.15), the equation of evolution for $\boldsymbol{\mathcal{H}}[t;t']$ takes the form

$$\ddot{\boldsymbol{\mathcal{H}}}[t;t'] = -\beta\dot{\boldsymbol{\mathcal{H}}}[t;t'] + \beta\nabla\mathbf{u}^{\top}(\boldsymbol{x}_p(t),t)\cdot\boldsymbol{\mathcal{H}}[t;t'] \quad , \quad \begin{matrix}\boldsymbol{\mathcal{H}}[t';t'] = \mathbf{0} \\ \dot{\boldsymbol{\mathcal{H}}}[t';t'] = \mathbf{I}\end{matrix} \tag{A.1}$$

The appearance of the fluid velocity gradient along particle trajectories $\nabla\mathbf{u}^{\top}(\boldsymbol{x}_p(t),t)$ as a coefficient to $\boldsymbol{\mathcal{H}}[t;t']$ in the final term of (A.1) precludes an explicit analytical solution using Green's functions in the same manner as for the Stokes drag model, requiring that a more considered approach is taken to constructing a solution. Accordingly, for ease of working it is instructive to first put (A.1) into canonical form such that the first derivative does not appear. Specifically, let

$$\boldsymbol{\mathcal{H}}[t;t'] = \phi(t;t')\,\boldsymbol{\mathcal{L}}[t;t'] \quad , \quad \begin{matrix}\boldsymbol{\mathcal{L}}[t';t'] = \mathbf{0} \\ \dot{\boldsymbol{\mathcal{L}}}[t';t'] = \mathbf{I}\end{matrix} \tag{A.2}$$

where $\boldsymbol{\mathcal{L}}[t;t']$ is the transformed version of $\boldsymbol{\mathcal{H}}[t;t']$ which satisfies the canonical form of the governing equation (A.1), and $\phi(t;t')$ is a scalar function to be determined. For convenience $\boldsymbol{\mathcal{L}}[t;t']$ is chosen to have the same initial conditions as $\boldsymbol{\mathcal{H}}[t;t']$, which then uniquely determines the initial condition on $\phi(t;t')$ as

$$\phi\left(t';t'\right)=1 \tag{A.3}$$

Substitution of (A.2) into the governing equation (A.1) results in the transformed equation

$$\phi\ddot{\boldsymbol{\mathcal{L}}}+\left[2\dot{\phi}+\beta\phi\right]\dot{\boldsymbol{\mathcal{L}}}+\left[\ddot{\phi}\mathbf{I}+\beta\dot{\phi}\mathbf{I}-\beta\nabla\mathbf{u}^{\top}\phi\right]\cdot\boldsymbol{\mathcal{L}}=\mathbf{0} \tag{A.4}$$

The canonical form of (A.4) then requires that the $\dot{\boldsymbol{\mathcal{L}}}$ term vanishes, which is satisfied when

$$2\dot{\phi}+\beta\phi=0 \tag{A.5}$$

With use of the initial condition (A.3), this admits the solution

$$\phi\left(t;t'\right)=\exp\left[-\frac{\beta}{2}(t-t')\right] \tag{A.6}$$

Evaluation of the transformed equation (A.4) using (A.6) then yields the canonical form of (A.1)

$$\ddot{\boldsymbol{\mathcal{L}}}\left[t;t'\right]=\beta\left[\frac{\beta}{4}\mathbf{I}+\nabla\mathbf{u}^{\top}(\boldsymbol{x}_p(t),t)\right]\cdot\boldsymbol{\mathcal{L}}\left[t;t'\right] \tag{A.7}$$

in which $\dot{\boldsymbol{\mathcal{L}}}$ does not feature as desired. Casting (A.7) into first-order system form results in

$$\begin{bmatrix}\dot{\boldsymbol{\mathcal{L}}}\\ \ddot{\boldsymbol{\mathcal{L}}}\end{bmatrix}=\begin{bmatrix}\mathbf{0} & \mathbf{I}\\ \beta\left[\frac{\beta}{4}\mathbf{I}+\nabla\mathbf{u}^{\top}\right] & \mathbf{0}\end{bmatrix}\cdot\begin{bmatrix}\boldsymbol{\mathcal{L}}\\ \dot{\boldsymbol{\mathcal{L}}}\end{bmatrix} \tag{A.8}$$

Then defining the following variables

$$\boldsymbol{\mathcal{Q}}=\begin{bmatrix}\boldsymbol{\mathcal{L}}\\ \dot{\boldsymbol{\mathcal{L}}}\end{bmatrix}\quad,\quad\mathbf{N}(t)=\begin{bmatrix}\mathbf{0} & \mathbf{I}\\ \mathbf{F}(t) & \mathbf{0}\end{bmatrix}\quad,\quad\mathbf{F}(t)=\beta\left[\frac{\beta}{4}\mathbf{I}+\nabla\mathbf{u}^{\top}(\boldsymbol{x}_p(t),t)\right] \tag{A.9}$$

the system (A.8) is written simply as

$$\dot{\boldsymbol{\mathcal{Q}}}\left[t;t'\right]=\mathbf{N}(t)\cdot\boldsymbol{\mathcal{Q}}\left[t;t'\right]\quad,\quad\boldsymbol{\mathcal{Q}}\left[t';t'\right]=\boldsymbol{\mathcal{Q}}^{0}=\begin{bmatrix}\mathbf{0}\\\mathbf{I}\end{bmatrix}\tag{A.10}$$

The solution to (A.10) is then given by the matrix exponential as

$$\boldsymbol{\mathcal{Q}}\left[t;t'\right]=\exp\left[\int_{t'}^{t}\mathbf{N}(s)\,ds\right]\cdot\boldsymbol{\mathcal{Q}}^{0}\tag{A.11}$$

In order to make further inferences, (A.11) can be expanded formally as a time-ordered exponential

$$\boldsymbol{\mathcal{Q}}\left[t;t'\right]=\left[\sum_{k=0}^{\infty}\frac{1}{k!}\int_{t'}^{t}\int_{t'}^{t}\cdots\int_{t'}^{t}\mathcal{T}\left[\mathbf{N}(s_1)\cdot\mathbf{N}(s_2)\cdots\mathbf{N}(s_k)\right]ds_k\cdots ds_2\,ds_1\right]\cdot\boldsymbol{\mathcal{Q}}^{0}\tag{A.12}$$

where $\mathcal{T}\left[\cdot\right]$ is the time-ordering operator which for times $s_1,s_2,\cdots,s_k$ is defined such that

$$\mathcal{T}\left[\mathbf{N}(s_1)\cdot\mathbf{N}(s_2)\cdots\mathbf{N}(s_k)\right]=\mathbf{N}(s_1)\cdot\mathbf{N}(s_2)\cdots\mathbf{N}(s_k)\iff s_k<\cdots<s_2<s_1\tag{A.13}$$

Then by respecting the time-ordering condition $s_k<s_{k-1}\,,\forall k\in\mathbb{N}$, (A.12) can be written formally as the Magnus expansion [88]

$$\boldsymbol{\mathcal{Q}}\left[t;t'\right]=\left[\sum_{k=0}^{\infty}\int_{t'}^{t}\int_{t'}^{s_1}\cdots\int_{t'}^{s_{k-1}}\mathcal{T}\left[\mathbf{N}(s_1)\cdot\mathbf{N}(s_2)\cdots\mathbf{N}(s_k)\right]ds_k\cdots ds_2\,ds_1\right]\cdot\boldsymbol{\mathcal{Q}}^{0}\tag{A.14}$$

in which the first term of the expansion for $k=0$ is $\mathbf{I}$. To extract an expression for $\boldsymbol{\mathcal{L}}\left[t;t'\right]$ from (A.14), the time-ordered product $\mathcal{T}\left[\prod_{n=1}^{k}\mathbf{N}(s_n)\right]$ needs to be calculated. Then with the definition of $\mathbf{N}(t)$ from (A.9), the first k terms in the product are found to be

$$
\begin{aligned}
\mathbf{N}(s_1) &= \begin{bmatrix} \mathbf{0} & \mathbf{I} \\ \mathbf{F}(s_1) & \mathbf{0} \end{bmatrix} \\
\mathbf{N}(s_1)\cdot\mathbf{N}(s_2) &= \begin{bmatrix} \mathbf{F}(s_2) & \mathbf{0} \\ \mathbf{0} & \mathbf{F}(s_1) \end{bmatrix} \\
\mathbf{N}(s_1)\cdot\mathbf{N}(s_2)\cdot\mathbf{N}(s_3) &= \begin{bmatrix} \mathbf{0} & \mathbf{F}(s_2) \\ \mathbf{F}(s_1)\cdot\mathbf{F}(s_3) & \mathbf{0} \end{bmatrix} \\
\mathbf{N}(s_1)\cdot\mathbf{N}(s_2)\cdot\mathbf{N}(s_3)\cdot\mathbf{N}(s_4) &= \begin{bmatrix} \mathbf{F}(s_2)\cdot\mathbf{F}(s_4) & \mathbf{0} \\ \mathbf{0} & \mathbf{F}(s_1)\cdot\mathbf{F}(s_3) \end{bmatrix} \\
\mathbf{N}(s_1)\cdot\mathbf{N}(s_2)\cdot\mathbf{N}(s_3)\cdot\mathbf{N}(s_4)\cdot\mathbf{N}(s_5) &= \begin{bmatrix} \mathbf{0} & \mathbf{F}(s_2)\cdot\mathbf{F}(s_4) \\ \mathbf{F}(s_1)\cdot\mathbf{F}(s_3)\cdot\mathbf{F}(s_5) & \mathbf{0} \end{bmatrix} \\
\mathbf{N}(s_1)\cdot\mathbf{N}(s_2)\cdot\mathbf{N}(s_3)\cdot\mathbf{N}(s_4)\cdot\mathbf{N}(s_5)\cdot\mathbf{N}(s_6) &= \begin{bmatrix} \mathbf{F}(s_2)\cdot\mathbf{F}(s_4)\cdot\mathbf{F}(s_6) & \mathbf{0} \\ \mathbf{0} & \mathbf{F}(s_1)\cdot\mathbf{F}(s_3)\cdot\mathbf{F}(s_5) \end{bmatrix}
\end{aligned}
$$

By extension, the general product is seen to be

$$
\prod_{n=1}^{k}\mathbf{N}(s_n) = \begin{cases} \begin{bmatrix} \prod_{n=1}^{\frac{k}{2}}\mathbf{F}(s_{2n}) & \mathbf{0} \\ \mathbf{0} & \prod_{n=1}^{\frac{k}{2}}\mathbf{F}(s_{2n-1}) \end{bmatrix} & k = 2m\,,\ m\in\mathbb{N} \\ \begin{bmatrix} \mathbf{0} & \prod_{n=1}^{\frac{k-1}{2}}\mathbf{F}(s_{2n}) \\ \prod_{n=1}^{\frac{k+1}{2}}\mathbf{F}(s_{2n-1}) & \mathbf{0} \end{bmatrix} & k = 2m+1\,,\ m\in\mathbb{N} \end{cases} \tag{A.15}
$$

The advantage of using canonical form is evident from this expression, with the fact that the coefficient matrix $\mathbf{N}(t)$ only has non-zero elements on the trailing diagonal blocks yielding a more tractable form of (A.15). The formal solution to $\boldsymbol{\mathcal{Q}}[t;t']$ in (A.14) can then be written

$$\boldsymbol{\mathcal{Q}}\left[t;t'\right]=\sum_{m=0}^{\infty}\Bigg\{ \int_{t'}^{t}\int_{t'}^{s_1}\cdots\int_{t'}^{s_{2m-1}}\begin{bmatrix}\mathcal{T}\left[\prod_{n=1}^{m}\mathbf{F}(s_{2n})\right] & \mathbf{0}\\ \mathbf{0} & \mathcal{T}\left[\prod_{n=1}^{m}\mathbf{F}(s_{2n-1})\right]\end{bmatrix} ds_{2m}\cdots ds_2\, ds_1 + \int_{t'}^{t}\int_{t'}^{s_1}\cdots\int_{t'}^{s_{2m}}\begin{bmatrix}\mathbf{0} & \mathcal{T}\left[\prod_{n=1}^{m}\mathbf{F}(s_{2n})\right]\\ \mathcal{T}\left[\prod_{n=1}^{m+1}\mathbf{F}(s_{2n-1})\right] & \mathbf{0}\end{bmatrix} ds_{2m+1}\cdots ds_2\, ds_1\Bigg\}\cdot\boldsymbol{\mathcal{Q}}^{0} \tag{A.16}$$

Then using the system form definitions of $\boldsymbol{\mathcal{Q}}\left[t;t'\right]$ from (A.9) and $\boldsymbol{\mathcal{Q}}^{0}$ from (A.10) results in expressions for $\boldsymbol{\mathcal{L}}\left[t;t'\right]$ and $\dot{\boldsymbol{\mathcal{L}}}\left[t;t'\right]$

$$\boldsymbol{\mathcal{L}}\left[t;t'\right]=\sum_{m=0}^{\infty}\int_{t'}^{t}\int_{t'}^{s_1}\cdots\int_{t'}^{s_{2m}}\mathcal{T}\left[\prod_{n=1}^{m}\mathbf{F}(s_{2n})\right] ds_{2m+1}\cdots ds_2\, ds_1 \tag{A.17}$$

$$\dot{\boldsymbol{\mathcal{L}}}\left[t;t'\right]=\sum_{m=0}^{\infty}\int_{t'}^{t}\int_{t'}^{s_1}\cdots\int_{t'}^{s_{2m-1}}\mathcal{T}\left[\prod_{n=1}^{m}\mathbf{F}(s_{2n-1})\right] ds_{2m}\cdots ds_2\, ds_1 \tag{A.18}$$

Therefore it is seen that only the odd terms of the expansion contribute to $\boldsymbol{\mathcal{L}}\left[t;t'\right]$, whilst only the even terms contribute to $\dot{\boldsymbol{\mathcal{L}}}\left[t;t'\right]$. Since the solution for just $\boldsymbol{\mathcal{L}}\left[t;t'\right]$ is of immediate interest, taking (A.17) and substituting back into the canonical transformation (A.2) along with the specific form of $\phi\left(t;t'\right)$ in (A.6) and $\mathbf{F}(t)$ as denoted in (A.9) yields the analytical solution for the particle response tensor $\boldsymbol{\mathcal{H}}\left[t;t'\right]$ in the case of the Stokes drag model

$$\boldsymbol{\mathcal{H}}\left[t;t'\right]=\exp\left[-\frac{\beta}{2}(t-t')\right]\cdot\sum_{m=0}^{\infty}\int_{t'}^{t}\int_{t'}^{s_1}\cdots\int_{t'}^{s_{2m}}\mathcal{T}\left[\prod_{n=1}^{m}\beta\left[\frac{\beta}{4}\mathbf{I}+\nabla\mathbf{u}^{\top}(\boldsymbol{x}_p(s_{2n}),s_{2n})\right]\right] ds_{2m+1}\cdots ds_2\, ds_1 \tag{A.19}$$

Since this expression contains an infinite number of terms, some form of approximation is required for (A.19) to be of practical use from a modelling perspective. To that end, the simplest approach of setting $\nabla\mathbf{u}^{\top}(\boldsymbol{x}_p(s_{2n}),s_{2n})=\mathbf{0}$ removes the time dependence

of the integrand, and with it the need for time-ordering

$$\begin{aligned}
\mathbf{H}\left[t;t'\right] &= \exp\left[-\frac{\beta}{2}(t-t')\right]\sum_{m=0}^{\infty}\int_{t'}^{t}\int_{t'}^{s_1}\cdots\int_{t'}^{s_{2m}}\prod_{n=1}^{m}\frac{\beta^2}{4}\mathbf{I}\,ds_{2m+1}\cdots ds_2\,ds_1 \\
&= \exp\left[-\frac{\beta}{2}(t-t')\right]\sum_{m=0}^{\infty}\left(\frac{\beta^2}{4}\right)^m\frac{1}{(2m+1)!}\left(t-t'\right)^{2m+1}\mathbf{I} \\
&= \exp\left[-\frac{\beta}{2}(t-t')\right]\frac{2}{\beta}\sinh\left(\frac{\beta}{2}\left(t-t'\right)\right)\mathbf{I} \\
&= \frac{1}{\beta}\Big[1-\exp\big[-\beta(t-t')\big]\Big]\mathbf{I}
\end{aligned}$$

Thus the full solution to $\boldsymbol{\mathcal{H}}\left[t;t'\right]$ in (A.19) is consistent with the Green's function approximation (4.65) as expected. For a more detailed approximation, taking the first few terms of (A.19) can be done to include the desired level of information about $\nabla\mathbf{u}^{\top}(\boldsymbol{x}_p(t),t)$. The same detail is also contained within the integral representation for $\boldsymbol{\mathcal{H}}\left[t;t'\right]$ given by (6.51), which can be used recursively as needed, and is ultimately a more effective means of including this information in a closure model.

Appendix B

Cumulant Expansion of the Conditional Average within the PDF Dispersion Tensors

In order to include the behaviour which is needed to describe the increase in settling velocity experienced by particles under the influence of a gravitational body force within a model that is developed using the PDF kinetic framework, it is necessary to extract higher-order information from the unclosed conditional average that constitutes the integrand of the PDF dispersion tensor $\overline{\boldsymbol{\kappa}}$, given by (6.44)

$$\left\langle \mathcal{H}_{kj} \frac{\partial}{\partial \mathrm{x}_k} \mathrm{R}_{ji}\left(\boldsymbol{r}_p\right) \right\rangle \tag{B.1}$$

One such approach to this is further use of correlation splitting, which is most easily realised by utilising the phase-space vector $\boldsymbol{z} = (\boldsymbol{r}_p, \boldsymbol{\mathcal{H}}_V)$, where $\boldsymbol{\mathcal{H}}_V\left[t;t'\right]$ is the response tensor $\boldsymbol{\mathcal{H}}\left[t;t'\right]$ reshaped into first-order tensor form. This leads to consideration of (B.1) in the higher-dimensional form given by

$$\left\langle z_l \frac{\partial}{\partial \mathrm{x}_k} \mathrm{R}_{ji}(\boldsymbol{z}) \right\rangle \tag{B.2}$$

Motivated by the potential to describe (B.2) in terms of the moments of $\phi(\boldsymbol{z})$, it is suitable to consider a series expansion of this correlation in terms of the cumulants of $\phi(\boldsymbol{z})$ by making the interpretation $f(\boldsymbol{z}) = \frac{\partial}{\partial \mathrm{x}_k}\mathrm{R}_{ji}(\boldsymbol{z})$, and then using the general result for a random variable $\boldsymbol{z}$ of [82, p. 53]

$$\Big\langle z_i f(\boldsymbol{z})\Big\rangle = \left[\sum_{k=0}^{\infty}\frac{1}{k!}\sum_{\mathbf{j}^k}\mathrm{K}^{k+1}_{i,\mathbf{j}^k}\frac{\partial^k}{\partial \mathrm{z}_{j_1}\cdots\partial \mathrm{z}_{j_k}}\right]\Big\langle f(\boldsymbol{z})\Big\rangle \tag{B.3}$$

where $\sum_{\mathbf{j}^k}$ indicates a sum over all components of the k-tuple $\mathbf{j}^k = (j_1, ..., j_k)$, and $\mathbf{K}^{k+1}$ is the $(k+1)^{th}$ cumulant of the distribution $\phi(\boldsymbol{z})$. It should be noted that it is implicit in (B.3) that the partial derivative operator $\frac{\partial^k}{\partial \mathrm{z}_{j_1}\cdots\partial \mathrm{z}_{j_k}}$ is applied to the deterministic function $f(\mathbf{z})$ before evaluation using the random variable $\boldsymbol{z}$ is made, and the ensemble average then subsequently taken. Without recourse to a specific choice of probability distribution for $\phi(\boldsymbol{z})$ (i.e. Gaussian), it is necessary to consider a sufficient number of terms in this expansion in order to account for all the physical effects that are manifest within the correlation. In practice the fifth and higher cumulants have negligible influence on the form of $\phi(\boldsymbol{z})$, and therefore only the first four cumulants are considered here, resulting in the approximation

$$\Big\langle z_i f(\boldsymbol{z})\Big\rangle \approx \mathrm{K}^1_i\Big\langle f(\boldsymbol{z})\Big\rangle + \mathrm{K}^2_{ij}\left\langle\frac{\partial}{\partial \mathrm{z}_j}f(\boldsymbol{z})\right\rangle + \frac{1}{2}\mathrm{K}^3_{ijk}\left\langle\frac{\partial}{\partial \mathrm{z}_j}\frac{\partial}{\partial \mathrm{z}_k}f(\boldsymbol{z})\right\rangle + \frac{1}{6}\mathrm{K}^4_{ijkl}\left\langle\frac{\partial}{\partial \mathrm{z}_j}\frac{\partial}{\partial \mathrm{z}_k}\frac{\partial}{\partial \mathrm{z}_l}f(\boldsymbol{z})\right\rangle \tag{B.4}$$

The task is then to express the cumulants $\mathbf{K}^n$ in terms of the more versatile moments of $\phi(\boldsymbol{z})$. To proceed, the cumulants in this expression can be written in terms of the moments for an arbitrary probability distribution as [132]

$$\begin{aligned}
\mathrm{K}^1_i &= M^1_i \\
\mathrm{K}^2_{ij} &= M^2_{ij} - M^1_i M^1_j \\
\mathrm{K}^3_{ijk} &= M^3_{ijk} - M^2_{ij}M^1_k - M^2_{ik}M^1_j - M^2_{jk}M^1_i + 2M^1_i M^1_j M^1_k \\
\mathrm{K}^4_{ijkl} &= M^4_{ijkl} - M^3_{ijk}M^1_l - M^3_{ijl}M^1_k - M^3_{ikl}M^1_j - M^3_{jkl}M^1_i - M^2_{ij}M^2_{kl} - M^2_{ik}M^2_{jl} \\
&\quad - M^2_{il}M^2_{jk} + 2M^2_{ij}M^1_k M^1_l + 2M^2_{ik}M^1_j M^1_l + 2M^2_{il}M^1_j M^1_k + 2M^2_{jk}M^1_i M^1_l \\
&\quad + 2M^2_{jl}M^1_i M^1_k + 2M^2_{kl}M^1_i M^1_j - 6M^1_i M^1_j M^1_k M^1_l
\end{aligned} \tag{B.5}$$

where $\boldsymbol{M}^n$ is the n^{th} moment of $\phi(\boldsymbol{z})$ *about the origin*. These expressions can be simplified using the *central* moments of $\phi(\boldsymbol{z})$, specifically for the fluctuating part of the phase-space variable $\boldsymbol{z}' = \boldsymbol{z} - \langle\boldsymbol{z}\rangle$ the covariance $\Theta_{ij} = \langle z'_i z'_j\rangle$, coskewness $\gamma_{ijk} = \langle z'_i z'_j z'_k\rangle$, and cokurtosis $\kappa_{ijkl} = \langle z'_i z'_j z'_k z'_l\rangle$ which are defined in terms of the moments about the origin $\boldsymbol{M}^n$ respectively by

$$
\begin{aligned}
\Theta_{ij} &= M^2_{ij} - M^1_i M^1_j \\
\gamma_{ijk} &= M^3_{ijk} - M^2_{ij} M^1_k - M^2_{ik} M^1_j - M^2_{jk} M^1_i + 2 M^1_i M^1_j M^1_k \\
\kappa_{ijkl} &= M^4_{ijkl} - M^3_{ijk} M^1_l - M^3_{ijl} M^1_k - M^3_{ikl} M^1_j - M^3_{jkl} M^1_i \\
&\quad + M^2_{ij} M^1_k M^1_l + M^2_{ik} M^1_j M^1_l + M^2_{il} M^1_j M^1_k + M^2_{jk} M^1_i M^1_l \\
&\quad + M^2_{jl} M^1_i M^1_k + M^2_{kl} M^1_i M^1_j - 3 M^1_i M^1_j M^1_k M^1_l
\end{aligned}
\tag{B.6}
$$

Along with the first moment about the origin $\boldsymbol{M}^1$ being the mean $\mathrm{m}_i = \langle z_i \rangle$, use of the relations (B.6) then enables the cumulants as expressed in (B.5) to be written in terms of the moments of $\phi(\boldsymbol{z})$ as desired

$$
\begin{aligned}
\mathrm{K}^1_i &= \mathrm{m}_i \\
\mathrm{K}^2_{ij} &= \Theta_{ij} \\
\mathrm{K}^3_{ijk} &= \gamma_{ijk} \\
\mathrm{K}^4_{ijkl} &= \kappa_{ijkl} - \Theta_{ij}\Theta_{kl} - \Theta_{ik}\Theta_{jl} - \Theta_{il}\Theta_{jk}
\end{aligned}
\tag{B.7}
$$

Then the cumulant expansion (B.4) explicitly expressed in terms of the moments of $\phi(\boldsymbol{z})$ is given by

$$
\begin{aligned}
\Big\langle z_i f(\boldsymbol{z}) \Big\rangle &= \mathrm{m}_i \Big\langle f(\boldsymbol{z}) \Big\rangle + \Theta_{ij} \left\langle \frac{\partial}{\partial \mathrm{z}_j} f(\boldsymbol{z}) \right\rangle + \frac{1}{2} \gamma_{ijk} \left\langle \frac{\partial}{\partial \mathrm{z}_j} \frac{\partial}{\partial \mathrm{z}_k} f(\boldsymbol{z}) \right\rangle \\
&\quad + \frac{1}{6} \Big[\kappa_{ijkl} - \Theta_{ij}\Theta_{kl} - \Theta_{ik}\Theta_{jl} - \Theta_{il}\Theta_{jk} \Big] \left\langle \frac{\partial}{\partial \mathrm{z}_j} \frac{\partial}{\partial \mathrm{z}_k} \frac{\partial}{\partial \mathrm{z}_l} f(\boldsymbol{z}) \right\rangle
\end{aligned}
\tag{B.8}
$$

The components of this higher-dimensional correlation which are of interest in the context of the interpretation $f(\boldsymbol{z}) = \frac{\partial}{\partial \mathrm{x}_k} \mathrm{R}_{ji}(\boldsymbol{z})$ in (B.2) can be considered by expressing the moments of $\phi(\boldsymbol{z})$ in terms of the phase-space variable $\boldsymbol{z}$ as follows

$$\begin{aligned}\left\langle z_l \frac{\partial}{\partial \mathrm{x}_k}\mathrm{R}_{ji}(\boldsymbol{z})\right\rangle \approx \left\langle z_l\right\rangle \left\langle \frac{\partial}{\partial \mathrm{x}_k}\mathrm{R}_{ji}(\boldsymbol{z})\right\rangle + \left\langle z'_l z'_m\right\rangle \left\langle \frac{\partial}{\partial \mathrm{z}_m}\frac{\partial}{\partial \mathrm{x}_k}\mathrm{R}_{ji}(\boldsymbol{z})\right\rangle \\ + \frac{1}{2}\left\langle z'_l z'_m z'_n\right\rangle \left\langle \frac{\partial}{\partial \mathrm{z}_m}\frac{\partial}{\partial \mathrm{z}_n}\frac{\partial}{\partial \mathrm{x}_k}\mathrm{R}_{ji}(\boldsymbol{z})\right\rangle \\ + \frac{1}{6}\Big[\left\langle z'_l z'_m z'_n z'_q\right\rangle - \left\langle z'_l z'_m\right\rangle\left\langle z'_n z'_q\right\rangle - \left\langle z'_l z'_n\right\rangle\left\langle z'_m z'_q\right\rangle \\ - \left\langle z'_l z'_q\right\rangle\left\langle z'_m z'_n\right\rangle\Big] \left\langle \frac{\partial}{\partial \mathrm{z}_m}\frac{\partial}{\partial \mathrm{z}_n}\frac{\partial}{\partial \mathrm{z}_q}\frac{\partial}{\partial \mathrm{x}_k}\mathrm{R}_{ji}(\boldsymbol{z})\right\rangle \end{aligned} \tag{B.9}$$

Then identifying the separate parts of the phase-space variable $\boldsymbol{z}$ as $(\boldsymbol{z}^1, \boldsymbol{z}^2) = (\boldsymbol{r}_p, \boldsymbol{\mathcal{H}}_V)$ enables the relevant part of the correlation to be considered. Specifically, since it is the ensemble average (B.1) involving only the correlation of $\boldsymbol{\mathcal{H}}_V$ with $\frac{\partial}{\partial \mathrm{x}_k}\mathrm{R}_{ji}(\boldsymbol{r}_p)$ that is of interest, it is possible to retrieve this contribution by setting $z_l = z_l^2$ in (B.9). Further, as $\frac{\partial}{\partial \mathrm{x}_k}\mathrm{R}_{ji}(\boldsymbol{r}_p)$ is a function of only $\boldsymbol{r}_p$ and not $\boldsymbol{\mathcal{H}}_V$, the partial derivatives that emerge from the cumulant expansion and act upon $\frac{\partial}{\partial \mathrm{x}_k}\mathrm{R}_{ji}(\boldsymbol{r}_p)$ only make a non-zero contribution to the expansion for $\boldsymbol{z} = \boldsymbol{z}^1$. Restricting attention to these cases extracts from (B.9) the expression

$$\begin{aligned}\left\langle z_l^2 \frac{\partial}{\partial \mathrm{x}_k}\mathrm{R}_{ji}(\boldsymbol{z}^1)\right\rangle \approx \left\langle z_l^2\right\rangle \left\langle \frac{\partial}{\partial \mathrm{x}_k}\mathrm{R}_{ji}(\boldsymbol{z}^1)\right\rangle + \left\langle z_l^{2\prime} z_m^{1\prime}\right\rangle \left\langle \frac{\partial}{\partial \mathrm{z}_m^1}\frac{\partial}{\partial \mathrm{x}_k}\mathrm{R}_{ji}(\boldsymbol{z})\right\rangle \\ + \frac{1}{2}\left\langle z_l^{2\prime} z_m^{1\prime} z_n^{1\prime}\right\rangle \left\langle \frac{\partial}{\partial \mathrm{z}_m^1}\frac{\partial}{\partial \mathrm{z}_n^1}\frac{\partial}{\partial \mathrm{x}_k}\mathrm{R}_{ji}(\boldsymbol{z}^1)\right\rangle \\ + \frac{1}{6}\Big[\left\langle z_l^{2\prime} z_m^{1\prime} z_n^{1\prime} z_q^{1\prime}\right\rangle - \left\langle z_l^{2\prime} z_m^{1\prime}\right\rangle\left\langle z_n^{1\prime} z_q^{1\prime}\right\rangle - \left\langle z_l^{2\prime} z_n^{1\prime}\right\rangle\left\langle z_m^{1\prime} z_q^{1\prime}\right\rangle \\ - \left\langle z_l^{2\prime} z_q^{1\prime}\right\rangle\left\langle z_m^{1\prime} z_n^{1\prime}\right\rangle\Big] \left\langle \frac{\partial}{\partial \mathrm{z}_m^1}\frac{\partial}{\partial \mathrm{z}_n^1}\frac{\partial}{\partial \mathrm{z}_q^1}\frac{\partial}{\partial \mathrm{x}_k}\mathrm{R}_{ji}(\boldsymbol{z}^1)\right\rangle \end{aligned} \tag{B.10}$$

Finally, reinterpreting the phase-space variable $\boldsymbol{z}$ in terms of $\boldsymbol{r}_p$ and $\boldsymbol{\mathcal{H}}_V$ using $(\boldsymbol{z}^1, \boldsymbol{z}^2) = (\boldsymbol{r}_p, \boldsymbol{\mathcal{H}}_V)$, and reshaping $\boldsymbol{\mathcal{H}}_V$ back into the original form of the second order tensor $\boldsymbol{\mathcal{H}}$ gives the required expansion for the ensemble average (B.1) up to the fourth cumulant as

$$\left\langle \mathcal{H}_{kj}\frac{\partial}{\partial \mathrm{x}_k}\mathrm{R}_{ji}(\boldsymbol{r}_p)\right\rangle \approx \left\langle \mathcal{H}_{kj}\right\rangle \left\langle \frac{\partial}{\partial \mathrm{x}_k}\mathrm{R}_{ji}(\boldsymbol{r}_p)\right\rangle + \left\langle \mathcal{H}'_{kj}r'_{p_m}\right\rangle \left\langle \frac{\partial}{\partial \mathrm{r}_m}\frac{\partial}{\partial \mathrm{x}_k}\mathrm{R}_{ji}(\boldsymbol{r}_p)\right\rangle$$
$$+\frac{1}{2}\left\langle \mathcal{H}'_{kj}r'_{p_m}r'_{p_n}\right\rangle \left\langle \frac{\partial}{\partial \mathrm{r}_m}\frac{\partial}{\partial \mathrm{r}_n}\frac{\partial}{\partial \mathrm{x}_k}\mathrm{R}_{ji}(\boldsymbol{r}_p)\right\rangle$$
$$+\frac{1}{6}\Big[\left\langle \mathcal{H}'_{kj}r'_{p_m}r'_{p_n}r'_{p_q}\right\rangle - \left\langle \mathcal{H}'_{kj}r'_{p_m}\right\rangle\left\langle r'_{p_n}r'_{p_q}\right\rangle - \left\langle \mathcal{H}'_{kj}r'_{p_n}\right\rangle\left\langle r'_{p_m}r'_{p_q}\right\rangle$$
$$-\left\langle \mathcal{H}'_{kj}r'_{p_q}\right\rangle\left\langle r'_{p_m}r'_{p_n}\right\rangle\Big]\left\langle \frac{\partial}{\partial \mathrm{r}_m}\frac{\partial}{\partial \mathrm{r}_n}\frac{\partial}{\partial \mathrm{r}_q}\frac{\partial}{\partial \mathrm{x}_k}\mathrm{R}_{ji}(\boldsymbol{r}_p)\right\rangle \tag{B.11}$$

This provides the required description of the interaction between $\boldsymbol{r}_p$ and $\boldsymbol{\mathcal{H}}$ within the expression for $\overline{\boldsymbol{\kappa}}$, and is the result presented in (6.46).

Appendix C

Spatial Derivatives of the Two-Point Fluid Velocity Correlation Tensor in an Isotropic Flow Field

In order to develop models for the expressions that arise within the cumulant expansion (6.46), it is necessary to calculate the higher-order spatial derivatives of the Eulerian two-point two-time correlation tensor $\mathbf{R}\left(\mathbf{x}', t'; \mathbf{x}, t\right)$ as given in (4.25) for the fluctuating particle acceleration $\mathbf{f}\left(\mathbf{x}, t\right)$. Evaluation for the form $\mathbf{f}\left(\mathbf{x}, t\right) = \beta \mathbf{u}'(\mathbf{x}, t)$ associated with the Stokes drag model as given by (4.3) results in

$$\mathrm{R}_{ji}\left(\mathbf{x}', t'; \mathbf{x}, t\right) = \beta^2 \big\langle \mathrm{u}_j\left(\mathbf{x}', t'\right) \mathrm{u}_i\left(\mathbf{x}, t\right) \big\rangle \tag{C.1}$$

To proceed, a specific form of the two-point two-time fluid velocity correlation tensor $\big\langle \mathbf{u}\left(\mathbf{x}', t'\right) \mathbf{u}\left(\mathbf{x}, t\right) \big\rangle$ must be invoked, and assuming an isotropic flow field yields

$$\mathrm{R}_{ji}(\mathbf{x}', t'; \mathbf{x}, t) = \beta^2 u'^2 \left[g(\mathrm{r}, s)\delta_{ji} + \big(f(\mathrm{r}, s) - g(\mathrm{r}, s)\big) \frac{\mathrm{r}_j \mathrm{r}_i}{\mathrm{r}^2} \right] \tag{C.2}$$

where $\mathbf{r} = \mathbf{x} - \mathbf{x}'$ is the spatial separation, $s = t - t'$ is the temporal separation, $\mathrm{r} = |\mathbf{r}|$ is the magnitude of spatial separation, and $f(\mathrm{r}, s)$ and $g(\mathrm{r}, s)$ are the longitudinal and lateral correlation coefficients of the underlying flow field respectively. For a general turbulent flow $f(\mathrm{r}, s)$ and $g(\mathrm{r}, s)$ do not have analytical forms [42], and must be numerically fitted using DNS data, a non-trivial exercise. However, in several common

forms of energy spectrum which are used to initialise turbulent flows that satisfy the full Navier-Stokes equations, a prescribed form of $f(\mathrm{r}, s)$ is used, and it is this approach which is adopted here. Specifically, the work of Batchelor and Townsend [8] on decay in the final period of turbulence determined $f(\mathrm{r}, s)$ to have a self-similar profile in this case, and motivated by this a general Gaussian decorrelation is chosen to represent $f(\mathrm{r}, s)$ in this work

$$f(\mathrm{r}, s) = \exp\left[-\frac{1}{a}\sigma_k^2 \mathrm{r}^2 - \frac{1}{b}\sigma_\omega^2 s^2\right] \tag{C.3}$$

where σ_k and σ_ω are parameters for the rate of decorrelation spatially and temporally respectively, and a and b are constants that can also be used to tune the rate of decorrelation. This choice of longitudinal decorrelation function enables the spatial and temporal decorrelation functions to be written as separate expressions such that $f(\mathrm{r}, s) = f(\mathrm{r})\mathrm{E}_\omega(s)$, where

$$f(\mathrm{r}) = \exp\left[-\frac{1}{a}\sigma_k^2 \mathrm{r}^2\right] \tag{C.4}$$

$$\mathrm{E}_\omega(s) = \exp\left[-\frac{1}{b}\sigma_\omega^2 s^2\right] \tag{C.5}$$

In turn, this enables the two-point two-time correlation tensor $\mathbf{R}(\mathbf{r}, s)$ to be specified as the product of the separate spatial correlations $\mathbf{Q}(\mathbf{r})$ and temporal correlations $\mathrm{E}_\omega(s)$ involved, meaning that $\mathbf{R}\left(\mathbf{x}', t'; \mathbf{x}, t\right)$ decomposes such that

$$\mathrm{R}_{ji}\left(\mathbf{r}, s\right) = \beta^2\, \mathrm{Q}_{ji}(\mathbf{r})\, \mathrm{E}_\omega(s) \tag{C.6}$$

in which $\mathbf{Q}(\mathbf{r})$ is defined according to isotropy by

$$\mathrm{Q}_{ji}(\mathbf{r}) = u'^2 \left[g(\mathrm{r})\delta_{ji} + \big(f(\mathrm{r}) - g(\mathrm{r})\big)\frac{\mathrm{r}_j \mathrm{r}_i}{\mathrm{r}^2}\right] \tag{C.7}$$

With $\mathrm{E}_\omega(s)$ fully determined up to choice of the temporal decorrelation rate, it remains to specify the lateral correlation coefficient $g(\mathrm{r})$ of the flow field. Assuming the flow field is incompressible, $g(\mathrm{r})$ is consequently related to $f(\mathrm{r})$ by the relationship

$$g(\mathrm{r}) = f(\mathrm{r}) + \frac{1}{d-1}\mathrm{r}\frac{\partial}{\partial \mathrm{r}} f(\mathrm{r}) \tag{C.8}$$

in which d is the number of physical spatial dimensions in the system under consideration, valid for $d = \{2, 3\}$. Using the form of $f(\mathrm{r})$ defined in (C.4) then fully determines $g(\mathrm{r})$, with the resultant expression for $\mathbf{Q}(\mathbf{r})$ for this specific choice of $f(\mathrm{r})$ being

$$\mathrm{Q}_{ji}(\mathbf{r}) = u'^2 f(\mathrm{r}) \left\{ \left[1 - \frac{2\sigma_k^2 \mathrm{r}^2}{a(d-1)} \right] \delta_{ji} + \frac{2\sigma_k^2}{a(d-1)} \mathrm{r}_j \mathrm{r}_i \right\} \tag{C.9}$$

The first cumulant in (6.46) requires knowledge of the gradient of $\mathbf{R}(\mathbf{r})$, and since this is purely a spatial gradient the problem can be restricted to the gradient of $\mathbf{Q}(\mathbf{r})$, with the temporal correlation $\mathrm{E}_\omega(s)$ remaining constant. Noting that the definition of $\mathbf{r} = \mathbf{x} - \mathbf{x}'$ implies that by the chain rule the derivative in $\mathbf{r}$ can be substituted for the derivative in $\mathbf{x}$ results in the expression of interest becoming

$$\frac{\partial}{\partial \mathrm{x}_k} \mathrm{R}_{ji}(\mathbf{r}, s) = \beta^2 \frac{\partial}{\partial \mathrm{r}_k} \mathrm{Q}_{ji}(\mathbf{r}) \mathrm{E}_\omega(s) \tag{C.10}$$

The gradient of $\mathbf{Q}(\mathbf{r})$ is calculated by making use of results from tensor analysis

$$\frac{\partial}{\partial \mathrm{r}_k} \left[\mathrm{r} \right] = \frac{\mathrm{r}_k}{\mathrm{r}} \tag{C.11}$$

$$\frac{\partial}{\partial \mathrm{r}_k} \left[\mathrm{r}^2 \right] = 2\mathrm{r}_k \tag{C.12}$$

Following from these, for the specific choice of $f(\mathrm{r})$ in (C.4) we have

$$\frac{\partial}{\partial \mathrm{r}_k} \left[f(\mathrm{r}) \right] = -\frac{2}{a} \sigma_k^2 \mathrm{r}_k f(\mathrm{r}) \tag{C.13}$$

$$\frac{\partial}{\partial \mathrm{r}_k} \left[\mathrm{r}^2 f(\mathrm{r}) \right] = 2\mathrm{r}_k f(\mathrm{r}) - \frac{2}{a} \sigma_k^2 \mathrm{r}^2 \mathrm{r}_k f(\mathrm{r}) \tag{C.14}$$

$$\frac{\partial}{\partial \mathrm{r}_k} \left[\mathrm{r}_j \mathrm{r}_i f(\mathrm{r}) \right] = \mathrm{r}_j \delta_{ik} f(\mathrm{r}) + \mathrm{r}_i \delta_{jk} f(\mathrm{r}) - \frac{2}{a} \sigma_k^2 \mathrm{r}_k \mathrm{r}_j \mathrm{r}_i f(\mathrm{r}) \tag{C.15}$$

Using (C.13) - (C.15), the resultant expression for the gradient of $\mathbf{Q}(\mathbf{r})$ as given in (C.9) is

$$\frac{\partial}{\partial \mathrm{r}_k} \mathrm{Q}_{ji}(\mathbf{r}) = \frac{2}{a(d-1)} u'^2 \sigma_k^2 f(\mathrm{r}) \left\{ \left[\frac{2}{a} \sigma_k^2 \mathrm{r}^2 - (d+1) \right] \mathrm{r}_k \delta_{ji} - \frac{2}{a} \sigma_k^2 \mathrm{r}_k \mathrm{r}_j \mathrm{r}_i + \mathrm{r}_j \delta_{ik} + \mathrm{r}_i \delta_{jk} \right\} \tag{C.16}$$

For the second cumulant in (6.46), the expression $\left\langle \frac{\partial}{\partial \mathrm{r}_m}\frac{\partial}{\partial \mathrm{x}_k}\mathrm{R}_{ji}(\mathbf{r})\right\rangle$ is required. Then making use of (C.10), it is seen that the expression required in the second cumulant is the gradient of $\frac{\partial}{\partial \mathbf{r}}\mathbf{Q}(\mathbf{r})$ as given in (C.16). The results of interest for the given choice of $f(\mathrm{r})$ in this case are

$$\frac{\partial}{\partial \mathrm{r}_l}\left[\mathrm{r}_k f(\mathrm{r})\right] = \delta_{lk} f(\mathrm{r}) - \frac{2}{a}\sigma_k^2 \mathrm{r}_l \mathrm{r}_k f(\mathrm{r}) \tag{C.17}$$

$$\frac{\partial}{\partial \mathrm{r}_l}\left[\mathrm{r}^2 \mathrm{r}_k f(\mathrm{r})\right] = 2\mathrm{r}_l \mathrm{r}_k f(\mathrm{r}) + \mathrm{r}^2 \delta_{lk} f(\mathrm{r}) - \frac{2}{a}\sigma_k^2 \mathrm{r}^2 \mathrm{r}_l \mathrm{r}_k f(\mathrm{r}) \tag{C.18}$$

$$\frac{\partial}{\partial \mathrm{r}_l}\left[\mathrm{r}_k \mathrm{r}_j \mathrm{r}_i f(\mathrm{r})\right] = \mathrm{r}_j \mathrm{r}_i \delta_{lk} f(\mathrm{r}) + \mathrm{r}_k \mathrm{r}_i \delta_{lj} f(\mathrm{r}) + \mathrm{r}_k \mathrm{r}_j \delta_{li} f(\mathrm{r}) - \frac{2}{a}\sigma_k^2 \mathrm{r}_l \mathrm{r}_k \mathrm{r}_j \mathrm{r}_i f(\mathrm{r}) \tag{C.19}$$

Using (C.17) - (C.19), the resultant expression for the gradient of $\frac{\partial}{\partial \mathbf{r}}\mathbf{Q}(\mathbf{r})$ is

$$\begin{aligned}\frac{\partial}{\partial \mathrm{r}_l}\frac{\partial}{\partial \mathrm{r}_k}\mathrm{Q}_{ji}(\mathbf{r}) = \frac{2}{a(d-1)}u'^2\sigma_k^2 f(\mathrm{r})\Bigg\{&\frac{4}{a^2}\sigma_k^4 \mathrm{r}_l \mathrm{r}_k \mathrm{r}_j \mathrm{r}_i + \frac{2}{a}\sigma_k^2\left[(d+3) - \frac{2}{a}\sigma_k^2 \mathrm{r}^2\right]\mathrm{r}_l \mathrm{r}_k \delta_{ji} \\ &- \frac{2}{a}\sigma_k^2\Big[\mathrm{r}_j \mathrm{r}_i \delta_{lk} + \mathrm{r}_k \mathrm{r}_i \delta_{lj} + \mathrm{r}_k \mathrm{r}_j \delta_{li} + \mathrm{r}_l \mathrm{r}_j \delta_{ki} + \mathrm{r}_l \mathrm{r}_i \delta_{kj}\Big] \\ &+ \left[\frac{2}{a}\sigma_k^2 \mathrm{r}^2 - (d+1)\right]\delta_{lk}\delta_{ji} + \delta_{lj}\delta_{ik} + \delta_{li}\delta_{jk}\Bigg\}\end{aligned} \tag{C.20}$$

For the third cumulant in (6.46), the calculation of the expression $\left\langle \frac{\partial}{\partial \mathrm{r}_m}\frac{\partial}{\partial \mathrm{r}_n}\frac{\partial}{\partial \mathrm{x}_k}\mathrm{R}_{ji}(\mathbf{r})\right\rangle$ follows the same procedure, meaning that the gradient of (C.20) is required. The results needed for this step are

$$\begin{aligned}\frac{\partial}{\partial \mathrm{r}_m}\left[\mathrm{r}^2 \mathrm{r}_l \mathrm{r}_k f(\mathrm{r})\right] &= 2\mathrm{r}_m \mathrm{r}_l \mathrm{r}_k f(\mathrm{r}) + \mathrm{r}^2 \mathrm{r}_k \delta_{lm} f(\mathrm{r}) + \mathrm{r}^2 \mathrm{r}_l \delta_{km} f(\mathrm{r}) \\ &\quad - \frac{2}{a}\sigma_k^2 \mathrm{r}^2 \mathrm{r}_m \mathrm{r}_l \mathrm{r}_k f(\mathrm{r})\end{aligned} \tag{C.21}$$

$$\begin{aligned}\frac{\partial}{\partial \mathrm{r}_m}\left[\mathrm{r}_l \mathrm{r}_k \mathrm{r}_j \mathrm{r}_i f(\mathrm{r})\right] &= \mathrm{r}_k \mathrm{r}_j \mathrm{r}_i \delta_{ml} f(\mathrm{r}) + \mathrm{r}_l \mathrm{r}_j \mathrm{r}_i \delta_{mk} f(\mathrm{r}) + \mathrm{r}_l \mathrm{r}_k \mathrm{r}_i \delta_{mj} f(\mathrm{r}) \\ &\quad + \mathrm{r}_l \mathrm{r}_k \mathrm{r}_j \delta_{mi} f(\mathrm{r}) - \frac{2}{a}\sigma_k^2 \mathrm{r}_m \mathrm{r}_l \mathrm{r}_k \mathrm{r}_j \mathrm{r}_i f(\mathrm{r})\end{aligned} \tag{C.22}$$

Using (C.13) - (C.15) and (C.21) - (C.22), the resultant expression for the gradient of $\frac{\partial^2}{\partial \mathbf{r}^2}\mathbf{Q}(\mathbf{r})$ is

$$\frac{\partial}{\partial \mathrm{r}_m}\frac{\partial}{\partial \mathrm{r}_l}\frac{\partial}{\partial \mathrm{r}_k}\mathrm{Q}_{ji}(\mathbf{r}) = \frac{4}{a^2(d-1)}u'^2\sigma_k^4 f(\mathrm{r})\Big\{\frac{2}{a}\sigma_k^2\Big[\mathrm{r}_k\mathrm{r}_j\mathrm{r}_i\delta_{ml} + \mathrm{r}_l\mathrm{r}_j\mathrm{r}_i\delta_{mk}$$
$$+ \mathrm{r}_l\mathrm{r}_k\mathrm{r}_i\delta_{mj} + \mathrm{r}_l\mathrm{r}_k\mathrm{r}_j\delta_{mi} + \mathrm{r}_m\mathrm{r}_j\mathrm{r}_i\delta_{lk} + \mathrm{r}_m\mathrm{r}_k\mathrm{r}_i\delta_{lj} + \mathrm{r}_m\mathrm{r}_k\mathrm{r}_j\delta_{li}$$
$$+ \mathrm{r}_m\mathrm{r}_l\mathrm{r}_j\delta_{ik} + \mathrm{r}_m\mathrm{r}_l\mathrm{r}_i\delta_{jk}\Big] - \frac{4}{a^2}\sigma_k^4\mathrm{r}_m\mathrm{r}_l\mathrm{r}_k\mathrm{r}_j\mathrm{r}_i$$
$$+ \left[(d+3) - \frac{2}{a}\sigma_k^2\mathrm{r}^2\right]\Big[\mathrm{r}_k\delta_{lm}\delta_{ij} + \mathrm{r}_l\delta_{km}\delta_{ij} + \mathrm{r}_m\delta_{lk}\delta_{ij}\Big]$$
$$- \frac{2}{a}\sigma_k^2\left[(d+5) - \frac{2}{a}\sigma_k^2\mathrm{r}^2\right]\mathrm{r}_m\mathrm{r}_l\mathrm{r}_k\delta_{ji} - \Big[\mathrm{r}_m\delta_{lj}\delta_{ik} + \mathrm{r}_m\delta_{li}\delta_{jk}$$
$$+ \mathrm{r}_i\delta_{jm}\delta_{kl} + \mathrm{r}_j\delta_{im}\delta_{kl} + \mathrm{r}_k\delta_{im}\delta_{lj} + \mathrm{r}_i\delta_{km}\delta_{lj} + \mathrm{r}_k\delta_{jm}\delta_{li}$$
$$+ \mathrm{r}_j\delta_{km}\delta_{li} + \mathrm{r}_l\delta_{jm}\delta_{ik} + \mathrm{r}_j\delta_{lm}\delta_{ik} + \mathrm{r}_l\delta_{im}\delta_{jk} + \mathrm{r}_i\delta_{lm}\delta_{jk}\Big]\Big\} \tag{C.23}$$

Finally, the fourth cumulant in (6.46) requires calculation of the expression $\left\langle \frac{\partial}{\partial \mathrm{r}_m}\frac{\partial}{\partial \mathrm{r}_n}\frac{\partial}{\partial \mathrm{r}_q}\frac{\partial}{\partial \mathrm{x}_k}\mathrm{R}_{ji}(\mathbf{r})\right\rangle$, which is the gradient of (C.23). The results used at this stage are

$$\frac{\partial}{\partial \mathrm{r}_n}\left[\mathrm{r}^2\mathrm{r}_m\mathrm{r}_l\mathrm{r}_k f(\mathrm{r})\right] = 2\mathrm{r}_n\mathrm{r}_m\mathrm{r}_l\mathrm{r}_k f(\mathrm{r}) + \mathrm{r}^2\mathrm{r}_l\mathrm{r}_k\delta_{nm}f(\mathrm{r}) + \mathrm{r}^2\mathrm{r}_m\mathrm{r}_k\delta_{nl}f(\mathrm{r})$$
$$+ \mathrm{r}^2\mathrm{r}_m\mathrm{r}_l\delta_{nk}f(\mathrm{r}) - \frac{2}{a}\sigma_k^2\mathrm{r}^2\mathrm{r}_n\mathrm{r}_m\mathrm{r}_l\mathrm{r}_k f(\mathrm{r}) \tag{C.24}$$
$$\frac{\partial}{\partial \mathrm{r}_n}\left[\mathrm{r}_m\mathrm{r}_l\mathrm{r}_k\mathrm{r}_j\mathrm{r}_i f(\mathrm{r})\right] = \mathrm{r}_l\mathrm{r}_k\mathrm{r}_j\mathrm{r}_i\delta_{mn}f(\mathrm{r}) + \mathrm{r}_m\mathrm{r}_k\mathrm{r}_j\mathrm{r}_i\delta_{nl}f(\mathrm{r}) + \mathrm{r}_m\mathrm{r}_l\mathrm{r}_j\mathrm{r}_i\delta_{nk}f(\mathrm{r})$$
$$+ \mathrm{r}_m\mathrm{r}_l\mathrm{r}_k\mathrm{r}_i\delta_{nj}f(\mathrm{r}) + \mathrm{r}_m\mathrm{r}_l\mathrm{r}_k\mathrm{r}_j\delta_{ni}f(\mathrm{r}) - \frac{2}{a}\sigma_k^2\mathrm{r}_n\mathrm{r}_m\mathrm{r}_l\mathrm{r}_k\mathrm{r}_j\mathrm{r}_i f(\mathrm{r}) \tag{C.25}$$

Making use of (C.17) - (C.19) and (C.24) - (C.25), the resultant expression for the gradient of $\frac{\partial^3}{\partial \mathbf{r}^3}\mathbf{Q}(\mathbf{r})$ is

$$
\begin{aligned}
\frac{\partial}{\partial \mathrm{r}_n}\frac{\partial}{\partial \mathrm{r}_m}\frac{\partial}{\partial \mathrm{r}_l}\frac{\partial}{\partial \mathrm{r}_k}\mathrm{Q}_{ji}(\mathbf{r}) = \frac{4}{a^2(d-1)}u'^2\sigma_k^4 f(\mathrm{r})\Bigg\{ & \frac{8}{a^3}\sigma_k^6 \mathrm{r}_n\mathrm{r}_m\mathrm{r}_l\mathrm{r}_k\mathrm{r}_j\mathrm{r}_i \\
& - \frac{4}{a^2}\sigma_k^4\Bigg(\left[\frac{2}{a}\sigma_k^2\mathrm{r}^2 - (d+7)\right]\mathrm{r}_n\mathrm{r}_m\mathrm{r}_l\mathrm{r}_k\delta_{ij} + \mathrm{r}_m\mathrm{r}_l\mathrm{r}_k\mathrm{r}_i\delta_{nj} + \mathrm{r}_n\mathrm{r}_m\mathrm{r}_l\mathrm{r}_i\delta_{kj} \\
& + \mathrm{r}_n\mathrm{r}_k\mathrm{r}_j\mathrm{r}_i\delta_{ml} + \mathrm{r}_n\mathrm{r}_l\mathrm{r}_j\mathrm{r}_i\delta_{mk} + \mathrm{r}_n\mathrm{r}_l\mathrm{r}_k\mathrm{r}_i\delta_{mj} + \mathrm{r}_n\mathrm{r}_l\mathrm{r}_k\mathrm{r}_j\delta_{mi} \\
& + \mathrm{r}_l\mathrm{r}_k\mathrm{r}_j\mathrm{r}_i\delta_{mn} + \mathrm{r}_m\mathrm{r}_k\mathrm{r}_j\mathrm{r}_i\delta_{nl} + \mathrm{r}_m\mathrm{r}_l\mathrm{r}_j\mathrm{r}_i\delta_{nk} + \mathrm{r}_m\mathrm{r}_l\mathrm{r}_k\mathrm{r}_j\delta_{ni} \\
& + \mathrm{r}_n\mathrm{r}_m\mathrm{r}_j\mathrm{r}_i\delta_{kl} + \mathrm{r}_n\mathrm{r}_m\mathrm{r}_k\mathrm{r}_i\delta_{lj} + \mathrm{r}_n\mathrm{r}_m\mathrm{r}_k\mathrm{r}_j\delta_{li} + \mathrm{r}_n\mathrm{r}_m\mathrm{r}_l\mathrm{r}_j\delta_{ki}\Bigg) \\
& + \frac{2}{a}\sigma_k^2\Bigg(\left[\frac{2}{a}\sigma_k^2\mathrm{r}^2 - (d+5)\right]\Big[\mathrm{r}_n\mathrm{r}_k\delta_{lm}\delta_{ij} + \mathrm{r}_n\mathrm{r}_l\delta_{km}\delta_{ij} \\
& + \mathrm{r}_n\mathrm{r}_m\delta_{lk}\delta_{ij} + \mathrm{r}_l\mathrm{r}_k\delta_{mn}\delta_{ij} + \mathrm{r}_m\mathrm{r}_k\delta_{nl}\delta_{ij} + \mathrm{r}_m\mathrm{r}_l\delta_{nk}\delta_{ij}\Big] \\
& + \mathrm{r}_j\mathrm{r}_i\delta_{nk}\delta_{ml} + \mathrm{r}_k\mathrm{r}_i\delta_{nj}\delta_{ml} + \mathrm{r}_k\mathrm{r}_j\delta_{ni}\delta_{ml} + \mathrm{r}_j\mathrm{r}_i\delta_{nl}\delta_{mk} \\
& + \mathrm{r}_l\mathrm{r}_i\delta_{nj}\delta_{mk} + \mathrm{r}_l\mathrm{r}_j\delta_{ni}\delta_{mk} + \mathrm{r}_k\mathrm{r}_i\delta_{nl}\delta_{mj} + \mathrm{r}_l\mathrm{r}_i\delta_{nk}\delta_{mj} \\
& + \mathrm{r}_l\mathrm{r}_k\delta_{ni}\delta_{mj} + \mathrm{r}_k\mathrm{r}_j\delta_{nl}\delta_{mi} + \mathrm{r}_l\mathrm{r}_j\delta_{nk}\delta_{mi} + \mathrm{r}_l\mathrm{r}_k\delta_{nj}\delta_{mi} \\
& + \mathrm{r}_n\mathrm{r}_m\delta_{lj}\delta_{ik} + \mathrm{r}_n\mathrm{r}_m\delta_{li}\delta_{jk} + \mathrm{r}_n\mathrm{r}_i\delta_{jm}\delta_{kl} + \mathrm{r}_n\mathrm{r}_j\delta_{im}\delta_{kl} \\
& + \mathrm{r}_n\mathrm{r}_k\delta_{im}\delta_{lj} + \mathrm{r}_n\mathrm{r}_i\delta_{km}\delta_{lj} + \mathrm{r}_n\mathrm{r}_k\delta_{jm}\delta_{li} + \mathrm{r}_n\mathrm{r}_j\delta_{km}\delta_{li} \\
& + \mathrm{r}_n\mathrm{r}_l\delta_{jm}\delta_{ik} + \mathrm{r}_n\mathrm{r}_j\delta_{lm}\delta_{ik} + \mathrm{r}_n\mathrm{r}_l\delta_{im}\delta_{jk} + \mathrm{r}_n\mathrm{r}_i\delta_{lm}\delta_{jk} \\
& + \mathrm{r}_j\mathrm{r}_i\delta_{mn}\delta_{kl} + \mathrm{r}_m\mathrm{r}_i\delta_{nj}\delta_{kl} + \mathrm{r}_m\mathrm{r}_j\delta_{ni}\delta_{kl} + \mathrm{r}_k\mathrm{r}_i\delta_{nm}\delta_{lj} \\
& + \mathrm{r}_m\mathrm{r}_i\delta_{nk}\delta_{lj} + \mathrm{r}_m\mathrm{r}_k\delta_{ni}\delta_{lj} + \mathrm{r}_k\mathrm{r}_j\delta_{nm}\delta_{li} + \mathrm{r}_m\mathrm{r}_j\delta_{nk}\delta_{li} \\
& + \mathrm{r}_m\mathrm{r}_k\delta_{nj}\delta_{li} + \mathrm{r}_l\mathrm{r}_j\delta_{nm}\delta_{ik} + \mathrm{r}_m\mathrm{r}_j\delta_{nl}\delta_{ik} + \mathrm{r}_m\mathrm{r}_l\delta_{nj}\delta_{ik} \\
& + \mathrm{r}_l\mathrm{r}_i\delta_{nm}\delta_{jk} + \mathrm{r}_m\mathrm{r}_i\delta_{nl}\delta_{jk} + \mathrm{r}_m\mathrm{r}_l\delta_{ni}\delta_{jk}\Bigg) \\
& - \Bigg(\left[\frac{2}{a}\sigma_k^2\mathrm{r}^2 - (d+3)\right]\Big[\delta_{nk}\delta_{lm}\delta_{ij} + \delta_{nl}\delta_{km}\delta_{ij} + \delta_{nm}\delta_{lk}\delta_{ij}\Big] \\
& + \delta_{nm}\delta_{lj}\delta_{ik} + \delta_{nm}\delta_{li}\delta_{jk} + \delta_{ni}\delta_{jm}\delta_{kl} + \delta_{nj}\delta_{im}\delta_{kl} \\
& + \delta_{nk}\delta_{im}\delta_{lj} + \delta_{ni}\delta_{km}\delta_{lj} + \delta_{nk}\delta_{jm}\delta_{li} + \delta_{nj}\delta_{km}\delta_{li} \\
& + \delta_{nl}\delta_{jm}\delta_{ik} + \delta_{nj}\delta_{lm}\delta_{ik} + \delta_{nl}\delta_{im}\delta_{jk} + \delta_{ni}\delta_{lm}\delta_{jk}\Bigg)\Bigg\}
\end{aligned}
\tag{C.26}
$$

In principle further cumulants could be obtained in the expansion (6.46), however (C.26) is the highest order derivative of $\mathbf{Q}(\mathbf{r})$ which can be practically used in simulation post-processing or modelling, thus the limit of including only the first four cumulants in (6.46) is imposed.

In this work $f(\mathrm{r})$ and $\mathrm{E}_\omega(s)$ are both taken to be Gaussian with $a = 2$ and $b = 2$, consistent with the form of $\mathrm{E}_\omega(s)$ given by (5.15) that is used in the KS velocity field constructed in Chapter 5, whilst the flow configuration under consideration is left in general d-dimensional form for $d \in \{2, 3\}$.

Appendix D

Correlation Splitting Results

D.1 Correlation Splitting of the Lagrangian Fluid Velocity Gradient

The aim here is to derive an expression for the fluid velocity gradient along an inertial particle trajectory $\left\langle \nabla \mathbf{u}\left(\boldsymbol{x}_p(t), t\right) \right\rangle_{\mathbf{x},\mathbf{v}}$ via the use of correlation splitting, as required for modelling of the first cumulant in section 6.7.8. To begin with, the PDF $p\left(\mathbf{x}, \mathbf{v}, t\right)$ can be used to write

$$p\left(\mathbf{x}, \mathbf{v}, t\right) \left\langle \nabla \mathbf{u}\left(\boldsymbol{x}_p(t), t\right) \right\rangle_{\mathbf{x},\mathbf{v}} = \left\langle \mathcal{P}\left(\mathbf{x}, \mathbf{v}, t\right) \nabla \mathbf{u}\left(\mathbf{x}, t\right) \right\rangle \tag{D.1}$$

Then manipulation of this average yields

$$\left\langle \mathcal{P}\left(\mathbf{x}, \mathbf{v}, t\right) \frac{\partial \mathrm{u}_i}{\partial \mathrm{x}_l}\left(\mathbf{x}, t\right) \right\rangle = \frac{\partial}{\partial \mathrm{x}_l} \left\langle \mathcal{P}\left(\mathbf{x}, \mathbf{v}, t\right) \mathrm{u}_i\left(\mathbf{x}, t\right) \right\rangle - \left\langle \frac{\partial \mathcal{P}}{\partial \mathrm{x}_l}\left(\mathbf{x}, \mathbf{v}, t\right) \mathrm{u}_i\left(\mathbf{x}, t\right) \right\rangle \tag{D.2}$$

Decomposing the fluid velocity into mean and fluctuating parts produces

$$\left\langle \mathcal{P}\left(\mathbf{x},\mathbf{v},t\right)\frac{\partial \mathrm{u}_i}{\partial \mathrm{x}_l}\left(\mathbf{x},t\right)\right\rangle = \underbrace{\frac{\partial}{\partial \mathrm{x}_l}\left[p\left(\mathbf{x},\mathbf{v},t\right)\overline{\mathrm{u}}_i\left(\mathbf{x},t\right)\right]}_{\boxed{1}} + \underbrace{\frac{\partial}{\partial \mathrm{x}_l}\left[\left\langle \mathcal{P}\left(\mathbf{x},\mathbf{v},t\right)\mathrm{u}_i'\left(\mathbf{x},t\right)\right\rangle\right]}_{\boxed{2}} - \underbrace{\frac{\partial p}{\partial \mathrm{x}_l}\left(\mathbf{x},\mathbf{v},t\right)\overline{\mathrm{u}}_i\left(\mathbf{x},t\right)}_{\boxed{3}} - \underbrace{\left\langle \frac{\partial \mathcal{P}}{\partial \mathrm{x}_l}\left(\mathbf{x},\mathbf{v},t\right)\mathrm{u}_i'\left(\mathbf{x},t\right)\right\rangle}_{\boxed{4}} \tag{D.3}$$

Terms $\boxed{1}$ and $\boxed{3}$ are already closed, term $\boxed{2}$ can be closed using the same correlation splitting procedure outlined in section 6.2.2, whilst term $\boxed{4}$ is the expression of interest in this case.

To proceed, assuming that $\mathbf{u}'\left(\mathbf{x},t\right)$ is a zero-mean stochastic Gaussian field then the Furutsu-Novikov correlation splitting result in (4.10) can be utilised. To keep consistent with the definitions in this thesis, the interpretation used for the zero-mean stochastic field is taken to be $\mathbf{b}\left(\mathbf{x},t\right) = \mathbf{f}\left(\mathbf{x},t\right) = \beta\mathbf{u}'\left(\mathbf{x},t\right)$. Furthermore, since the derivative of $\mathcal{P}\left(\mathbf{x},\mathbf{v},t\right)$ is with respect to only $\mathbf{x}$ and not $\mathbf{v}$, it is helpful to work explicitly with $\mathbf{x}$ and $\mathbf{v}$ rather than the phase-space vector $\boldsymbol{\xi}$ in the following. Therefore correlation splitting is used on $\boxed{4}$ in the form

$$\left\langle \frac{\partial \mathcal{P}}{\partial \mathrm{x}_l}\left(\mathbf{x},\mathbf{v},t\right)\mathrm{f}_i'\left(\mathbf{x},t\right)\right\rangle = \int_{t_0}^{t}\int_{\mathbf{x}'}\int_{\mathbf{v}'}\mathrm{R}_{ij}(\mathbf{x},t;\mathbf{x}',t')\left\langle \frac{\delta}{\delta \mathrm{f}_j(\mathbf{x}',t')}\frac{\partial \mathcal{P}}{\partial \mathrm{x}_l}\left(\mathbf{x},\mathbf{v},t\right)\right\rangle d\mathbf{v}'\,d\mathbf{x}'\,dt' \tag{D.4}$$

Then using the chain rule for functional differentiation yields

$$\begin{aligned}\frac{\delta}{\delta \mathrm{f}_j(\mathbf{x}',t')}\frac{\partial \mathcal{P}}{\partial \mathrm{x}_l}\left(\mathbf{x},\mathbf{v},t\right) &= \frac{\delta x_{p_k}(t)}{\delta \mathrm{f}_j(\mathbf{x}',t')}\frac{\partial}{\partial x_{p_k}}\left[\frac{\partial \mathcal{P}}{\partial \mathrm{x}_l}\left(\mathbf{x},\mathbf{v},t\right)\right] + \frac{\delta v_{p_k}(t)}{\delta \mathrm{f}_j(\mathbf{x}',t')}\frac{\partial}{\partial v_{p_k}}\left[\frac{\partial \mathcal{P}}{\partial \mathrm{x}_l}\left(\mathbf{x},\mathbf{v},t\right)\right] \\ &= -\frac{\delta x_{p_k}(t)}{\delta \mathrm{f}_j(\mathbf{x}',t')}\frac{\partial^2 \mathcal{P}}{\partial \mathrm{x}_k \partial \mathrm{x}_l}\left(\mathbf{x},\mathbf{v},t\right) - \frac{\delta v_{p_k}(t)}{\delta \mathrm{f}_j(\mathbf{x}',t')}\frac{\partial^2 \mathcal{P}}{\partial \mathrm{v}_k \partial \mathrm{x}_l}\left(\mathbf{x},\mathbf{v},t\right)\end{aligned} \tag{D.5}$$

Formally, and consistent with the definitions of the particle response tensor $\boldsymbol{\mathcal{H}}\left[t;t'\right]$ and its derivative $\dot{\boldsymbol{\mathcal{H}}}\left[t;t'\right]$ in (4.27)

$$\frac{\delta x_{p_k}(t)}{\delta \mathrm{f}_j(\mathbf{x}',t')} = \frac{\delta x_{p_k}(t)}{\delta \mathrm{f}_j(\boldsymbol{x}'_p(t'),t')}\,\delta(\mathbf{x}'-\boldsymbol{x}_p(t')) = \mathcal{H}_{kj}\left[t;t'\right]\,\delta(\mathbf{x}'-\boldsymbol{x}_p(t')) \tag{D.6}$$

$$\frac{\delta v_{p_k}(t)}{\delta \mathrm{f}_j(\mathbf{x}',t')} = \frac{\delta v_{p_k}(t)}{\delta \mathrm{f}_j(\boldsymbol{x}'_p(t'),t')}\,\delta(\mathbf{x}'-\boldsymbol{x}_p(t')) = \dot{\mathcal{H}}_{kj}\left[t;t'\right]\,\delta(\mathbf{x}'-\boldsymbol{x}_p(t')) \tag{D.7}$$

Then using (D.6) and (D.7) in (D.5)

$$\begin{aligned}\frac{\delta}{\delta \mathrm{f}_j(\mathbf{x}',t')}\frac{\partial \mathcal{P}}{\partial \mathrm{x}_l}(\mathbf{x},\mathbf{v},t) = &-\mathcal{H}_{kj}\left[t;t'\right]\frac{\partial^2 \mathcal{P}}{\partial \mathrm{x}_k \partial \mathrm{x}_l}(\mathbf{x},\mathbf{v},t)\,\delta(\mathbf{x}'-\boldsymbol{x}_p(t')) \\ &-\dot{\mathcal{H}}_{kj}\left[t;t'\right]\frac{\partial^2 \mathcal{P}}{\partial \mathrm{v}_k \partial \mathrm{x}_l}(\mathbf{x},\mathbf{v},t)\,\delta(\mathbf{x}'-\boldsymbol{x}_p(t'))\end{aligned} \tag{D.8}$$

Accordingly, the closure (D.4) becomes

$$\begin{aligned}&\left\langle \frac{\partial \mathcal{P}}{\partial \mathrm{x}_l}(\mathbf{x},\mathbf{v},t)\,\mathrm{f}'_i(\mathbf{x},t)\right\rangle \\ &= -\left\langle \int_{t_0}^{t}\int_{\mathbf{x}'}\int_{\mathbf{v}'} \mathrm{R}_{ij}(\mathbf{x},t;\mathbf{x}',t')\mathcal{H}_{kj}\left[t;t'\right]\frac{\partial^2 \mathcal{P}}{\partial \mathrm{x}_k \partial \mathrm{x}_l}(\mathbf{x},\mathbf{v},t)\,\delta(\mathbf{x}'-\boldsymbol{x}_p(t'))\,d\mathbf{v}'\,d\mathbf{x}'\,dt'\right\rangle \\ &\quad -\left\langle \int_{t_0}^{t}\int_{\mathbf{x}'}\int_{\mathbf{v}'} \mathrm{R}_{ij}(\mathbf{x},t;\mathbf{x}',t')\dot{\mathcal{H}}_{kj}\left[t;t'\right]\frac{\partial^2 \mathcal{P}}{\partial \mathrm{v}_k \partial \mathrm{x}_l}(\mathbf{x},\mathbf{v},t)\,\delta(\mathbf{x}'-\boldsymbol{x}_p(t'))\,d\mathbf{v}'\,d\mathbf{x}'\,dt'\right\rangle\end{aligned} \tag{D.9}$$

in which the operations of ensemble averaging and integration have been commuted. Evaluation of the integrals over $\mathbf{x}'$ and $\mathbf{v}'$ then produces the simplification

$$\begin{aligned}\left\langle \frac{\partial \mathcal{P}}{\partial \mathrm{x}_l}(\mathbf{x},\mathbf{v},t)\,\mathrm{f}'_i(\mathbf{x},t)\right\rangle = &-\int_{t_0}^{t}\left\langle \mathcal{H}_{kj}\left[t;t'\right]\mathrm{R}_{ji}(\boldsymbol{x}_p(t'),t';\mathbf{x},t)\frac{\partial^2 \mathcal{P}}{\partial \mathrm{x}_k \partial \mathrm{x}_l}(\mathbf{x},\mathbf{v},t)\right\rangle dt' \\ &-\int_{t_0}^{t}\left\langle \dot{\mathcal{H}}_{kj}\left[t;t'\right]\mathrm{R}_{ji}(\boldsymbol{x}_p(t'),t';\mathbf{x},t)\frac{\partial^2 \mathcal{P}}{\partial \mathrm{v}_k \partial \mathrm{x}_l}(\mathbf{x},\mathbf{v},t)\right\rangle dt'\end{aligned} \tag{D.10}$$

where the property $\mathrm{R}_{ij}(\mathbf{x},t;\mathbf{x}',t') = \mathrm{R}_{ji}(\mathbf{x}',t';\mathbf{x},t)$ has also been used. Then manipulation of the derivatives acting on $\mathcal{P}(\mathbf{x},\mathbf{v},t)$ yields

$$
\begin{aligned}
\left\langle \frac{\partial \mathcal{P}}{\partial \mathrm{x}_l}\left(\mathbf{x},\mathbf{v},t\right)\mathrm{f}_i'\left(\mathbf{x},t\right)\right\rangle = &-\frac{\partial^2}{\partial \mathrm{x}_l \partial \mathrm{x}_k}\int_{t_0}^{t}\left\langle \mathcal{H}_{kj}\left[t;t'\right]\mathrm{R}_{ji}(\boldsymbol{x}_p(t'),t';\mathbf{x},t)\mathcal{P}\left(\mathbf{x},\mathbf{v},t\right)\right\rangle dt' \\
&+\frac{\partial}{\partial \mathrm{x}_k}\int_{t_0}^{t}\left\langle \frac{\partial}{\partial \mathrm{x}_l}\Big[\mathcal{H}_{kj}\left[t;t'\right]\mathrm{R}_{ji}(\boldsymbol{x}_p(t'),t';\mathbf{x},t)\Big]\mathcal{P}\left(\mathbf{x},\mathbf{v},t\right)\right\rangle dt' \\
&+\frac{\partial}{\partial \mathrm{x}_l}\int_{t_0}^{t}\left\langle \frac{\partial}{\partial \mathrm{x}_k}\Big[\mathcal{H}_{kj}\left[t;t'\right]\mathrm{R}_{ji}(\boldsymbol{x}_p(t'),t';\mathbf{x},t)\Big]\mathcal{P}\left(\mathbf{x},\mathbf{v},t\right)\right\rangle dt' \\
&-\int_{t_0}^{t}\left\langle \frac{\partial^2}{\partial \mathrm{x}_l \partial \mathrm{x}_k}\Big[\mathcal{H}_{kj}\left[t;t'\right]\mathrm{R}_{ji}(\boldsymbol{x}_p(t'),t';\mathbf{x},t)\Big]\mathcal{P}\left(\mathbf{x},\mathbf{v},t\right)\right\rangle dt' \\
&-\frac{\partial^2}{\partial \mathrm{x}_l \partial \mathrm{v}_k}\int_{t_0}^{t}\left\langle \dot{\mathcal{H}}_{kj}\left[t;t'\right]\mathrm{R}_{ji}(\boldsymbol{x}_p(t'),t';\mathbf{x},t)\mathcal{P}\left(\mathbf{x},\mathbf{v},t\right)\right\rangle dt' \\
&+\frac{\partial}{\partial \mathrm{v}_k}\int_{t_0}^{t}\left\langle \frac{\partial}{\partial \mathrm{x}_l}\Big[\dot{\mathcal{H}}_{kj}\left[t;t'\right]\mathrm{R}_{ji}(\boldsymbol{x}_p(t'),t';\mathbf{x},t)\Big]\mathcal{P}\left(\mathbf{x},\mathbf{v},t\right)\right\rangle dt' \\
&+\frac{\partial}{\partial \mathrm{x}_l}\int_{t_0}^{t}\left\langle \frac{\partial}{\partial \mathrm{v}_k}\Big[\dot{\mathcal{H}}_{kj}\left[t;t'\right]\mathrm{R}_{ji}(\boldsymbol{x}_p(t'),t';\mathbf{x},t)\Big]\mathcal{P}\left(\mathbf{x},\mathbf{v},t\right)\right\rangle dt' \\
&-\int_{t_0}^{t}\left\langle \frac{\partial^2}{\partial \mathrm{x}_l \partial \mathrm{v}_k}\Big[\dot{\mathcal{H}}_{kj}\left[t;t'\right]\mathrm{R}_{ji}(\boldsymbol{x}_p(t'),t';\mathbf{x},t)\Big]\mathcal{P}\left(\mathbf{x},\mathbf{v},t\right)\right\rangle dt'
\end{aligned}
\tag{D.11}
$$

In this expression, the final two terms are identically zero, since neither $\dot{\boldsymbol{\mathcal{H}}}\left[t;t'\right]$ or $\mathbf{R}(\boldsymbol{x}_p(t'),t';\mathbf{x},t)$ contain a dependence of the phase-space velocity $\mathbf{v}$. Then making the interpretation $\mathbf{f}'\left(\mathbf{x},t\right)=\beta\mathbf{u}'\left(\mathbf{x},t\right)$ and extracting the fine-grained PDF $\mathcal{P}\left(\mathbf{x},\mathbf{v},t\right)$ from the averages finally results in

$$\begin{aligned}\left\langle \frac{\partial \mathcal{P}}{\partial \mathrm{x}_l}\left(\mathbf{x},\mathbf{v},t\right)\mathrm{u}_i'\left(\mathbf{x},t\right)\right\rangle =& -\frac{1}{\beta}\frac{\partial^2}{\partial \mathrm{x}_l\partial \mathrm{x}_k}\left[\int_{t_0}^{t}\left\langle \mathcal{H}_{kj}\left[t;t'\right]\mathrm{R}_{ji}(\boldsymbol{x}_p(t'),t';\mathbf{x},t)\right\rangle_{\mathbf{x},\mathbf{v}} dt'\,p\left(\mathbf{x},\mathbf{v},t\right)\right]\\ &+\frac{1}{\beta}\frac{\partial}{\partial \mathrm{x}_k}\left[\int_{t_0}^{t}\left\langle \mathcal{H}_{kj}\left[t;t'\right]\frac{\partial}{\partial \mathrm{x}_l}\mathrm{R}_{ji}(\boldsymbol{x}_p(t'),t';\mathbf{x},t)\right\rangle_{\mathbf{x},\mathbf{v}} dt'\,p\left(\mathbf{x},\mathbf{v},t\right)\right]\\ &+\frac{1}{\beta}\frac{\partial}{\partial \mathrm{x}_l}\left[\int_{t_0}^{t}\left\langle \mathcal{H}_{kj}\left[t;t'\right]\frac{\partial}{\partial \mathrm{x}_k}\mathrm{R}_{ji}(\boldsymbol{x}_p(t'),t';\mathbf{x},t)\right\rangle_{\mathbf{x},\mathbf{v}} dt'\,p\left(\mathbf{x},\mathbf{v},t\right)\right]\\ &-\frac{1}{\beta}\int_{t_0}^{t}\left\langle \mathcal{H}_{kj}\left[t;t'\right]\frac{\partial^2}{\partial \mathrm{x}_l\partial \mathrm{x}_k}\mathrm{R}_{ji}(\boldsymbol{x}_p(t'),t';\mathbf{x},t)\right\rangle_{\mathbf{x},\mathbf{v}} dt'\,p\left(\mathbf{x},\mathbf{v},t\right)\\ &-\frac{1}{\beta}\frac{\partial^2}{\partial \mathrm{x}_l\partial \mathrm{v}_k}\left[\int_{t_0}^{t}\left\langle \dot{\mathcal{H}}_{kj}\left[t;t'\right]\mathrm{R}_{ji}(\boldsymbol{x}_p(t'),t';\mathbf{x},t)\right\rangle_{\mathbf{x},\mathbf{v}} dt'\,p\left(\mathbf{x},\mathbf{v},t\right)\right]\\ &+\frac{1}{\beta}\frac{\partial}{\partial \mathrm{v}_k}\left[\int_{t_0}^{t}\left\langle \dot{\mathcal{H}}_{kj}\left[t;t'\right]\frac{\partial}{\partial \mathrm{x}_l}\mathrm{R}_{ji}(\boldsymbol{x}_p(t'),t';\mathbf{x},t)\right\rangle_{\mathbf{x},\mathbf{v}} dt'\,p\left(\mathbf{x},\mathbf{v},t\right)\right]\end{aligned} \tag{D.12}$$

The result obtained from correlation splitting of term $\boxed{2}$ in (D.3) is that of the standard phase-space diffusion current given by

$$\begin{aligned}\left\langle \mathcal{P}\left(\mathbf{x},\mathbf{v},t\right)\mathrm{u}_i'\left(\mathbf{x},t\right)\right\rangle =& \frac{1}{\beta}\int_{t_0}^{t}\left\langle \mathcal{H}_{kj}\left[t;t'\right]\frac{\partial}{\partial \mathrm{x}_k}\mathrm{R}_{ji}(\boldsymbol{x}_p(t'),t';\mathbf{x},t)\right\rangle_{\mathbf{x},\mathbf{v}} dt'\,p\left(\mathbf{x},\mathbf{v},t\right)\\ &-\frac{1}{\beta}\frac{\partial}{\partial \mathrm{x}_k}\left[\int_{t_0}^{t}\left\langle \mathcal{H}_{kj}\left[t;t'\right]\mathrm{R}_{ji}(\boldsymbol{x}_p(t'),t';\mathbf{x},t)\right\rangle_{\mathbf{x},\mathbf{v}} dt'\,p\left(\mathbf{x},\mathbf{v},t\right)\right]\\ &-\frac{1}{\beta}\frac{\partial}{\partial \mathrm{v}_k}\left[\int_{t_0}^{t}\left\langle \dot{\mathcal{H}}_{kj}\left[t;t'\right]\mathrm{R}_{ji}(\boldsymbol{x}_p(t'),t';\mathbf{x},t)\right\rangle_{\mathbf{x},\mathbf{v}} p\left(\mathbf{x},\mathbf{v},t\right)\,dt'\right]\end{aligned} \tag{D.13}$$

Then substitution of (D.12) and (D.13) into (D.3) along with (D.1), and subsequent cancellation of terms yields

$$
\begin{aligned}
&p\left(\mathbf{x},\mathbf{v},t\right)\left\langle \frac{\partial \mathrm{u}_i}{\partial \mathrm{x}_l}\left(\boldsymbol{x}_p(t),t\right)\right\rangle_{\mathbf{x},\mathbf{v}} = p\left(\mathbf{x},\mathbf{v},t\right)\left\langle \frac{\partial \mathrm{u}_i}{\partial \mathrm{x}_l}\left(\mathbf{x},t\right)\right\rangle \\
&+\frac{1}{\beta}\int_{t_0}^{t}\left\langle \mathcal{H}_{kj}\left[t;t'\right]\frac{\partial^2}{\partial \mathrm{x}_l\partial \mathrm{x}_k}\mathrm{R}_{ji}(\boldsymbol{x}_p(t'),t';\mathbf{x},t)\right\rangle_{\mathbf{x},\mathbf{v}} dt'\, p\left(\mathbf{x},\mathbf{v},t\right) \\
&-\frac{1}{\beta}\frac{\partial}{\partial \mathrm{x}_k}\left[\int_{t_0}^{t}\left\langle \mathcal{H}_{kj}\left[t;t'\right]\frac{\partial}{\partial \mathrm{x}_l}\mathrm{R}_{ji}(\boldsymbol{x}_p(t'),t';\mathbf{x},t)\right\rangle_{\mathbf{x},\mathbf{v}} dt'\, p\left(\mathbf{x},\mathbf{v},t\right)\right] \\
&-\frac{1}{\beta}\frac{\partial}{\partial \mathrm{v}_k}\left[\int_{t_0}^{t}\left\langle \dot{\mathcal{H}}_{kj}\left[t;t'\right]\frac{\partial}{\partial \mathrm{x}_l}\mathrm{R}_{ji}(\boldsymbol{x}_p(t'),t';\mathbf{x},t)\right\rangle_{\mathbf{x},\mathbf{v}} dt'\, p\left(\mathbf{x},\mathbf{v},t\right)\right]
\end{aligned}
\tag{D.14}
$$

The corresponding velocity averaged version of this result in terms of the number density $\rho\left(\mathbf{x},t\right)$ is

$$
\begin{aligned}
&\rho\left(\mathbf{x},t\right)\left\langle \frac{\partial \mathrm{u}_i}{\partial \mathrm{x}_l}\left(\boldsymbol{x}_p(t),t\right)\right\rangle_{\mathbf{x}} = \rho\left(\mathbf{x},t\right)\left\langle \frac{\partial \mathrm{u}_i}{\partial \mathrm{x}_l}\left(\mathbf{x},t\right)\right\rangle \\
&+\frac{1}{\beta}\int_{t_0}^{t}\left\langle \mathcal{H}_{kj}\left[t;t'\right]\frac{\partial^2}{\partial \mathrm{x}_l\partial \mathrm{x}_k}\mathrm{R}_{ji}(\boldsymbol{x}_p(t'),t';\mathbf{x},t)\right\rangle_{\mathbf{x}} dt'\,\rho\left(\mathbf{x},t\right) \\
&-\frac{1}{\beta}\frac{\partial}{\partial \mathrm{x}_k}\left[\int_{t_0}^{t}\left\langle \mathcal{H}_{kj}\left[t;t'\right]\frac{\partial}{\partial \mathrm{x}_l}\mathrm{R}_{ji}(\boldsymbol{x}_p(t'),t';\mathbf{x},t)\right\rangle_{\mathbf{x}} dt'\,\rho\left(\mathbf{x},t\right)\right]
\end{aligned}
\tag{D.15}
$$

In the case of a homogeneous fluid velocity field, this result reduces further to

$$
\left\langle \frac{\partial \mathrm{u}_i}{\partial \mathrm{x}_l}\left(\boldsymbol{x}_p(t),t\right)\right\rangle = \frac{1}{\beta}\int_{t_0}^{t}\left\langle \mathcal{H}_{kj}\left[t;t'\right]\frac{\partial^2}{\partial \mathrm{x}_l\partial \mathrm{x}_k}\mathrm{R}_{ji}(\boldsymbol{x}_p(t'),t';\mathbf{x},t)\right\rangle dt' \tag{D.16}
$$

This then provides an expression for $\left\langle \nabla\mathbf{u}\left(\boldsymbol{x}_p(t),t\right)\right\rangle$ in terms of a dispersion tensor consisting of the standard particle response tensor $\boldsymbol{\mathcal{H}}\left[t;t'\right]$ and two-point two-time correlation tensor $\mathbf{R}(\boldsymbol{x}_p(t'),t';\mathbf{x},t)$ which arise in the PDF kinetic framework, and is the result given by (6.91).

D.2 Correlation Splitting of the One-time Fluctuating Particle Velocity and Fluctuating Lagrangian Fluid Velocity Gradient

The aim here is to develop a closure for the one-time fluctuating particle velocity - fluctuating Lagrangian fluid velocity gradient correlations $\left\langle \boldsymbol{v}_p'(t)\,\nabla\mathbf{u}'(\boldsymbol{x}_p(t),t)\right\rangle_{\mathbf{x}}$ via the use of PDF methods. To begin with, the PDF $p(\mathbf{x},\mathbf{v},t)$ and number density $\rho(\mathbf{x},t)$ can be used to write

$$\begin{aligned}\left\langle \boldsymbol{v}_p'(t)\,\nabla\mathbf{u}'(\boldsymbol{x}_p(t),t)\right\rangle_{\mathbf{x}} &= \frac{1}{\rho(\mathbf{x},t)}\left\langle \varrho(\mathbf{x},t)\,\boldsymbol{v}_p'(t)\,\nabla\mathbf{u}'(\boldsymbol{x}_p(t),t)\right\rangle \\ &= \frac{1}{\rho(\mathbf{x},t)}\int_{\mathbf{v}}\left\langle \mathcal{P}(\mathbf{x},\mathbf{v},t)\left[\boldsymbol{v}_p(t)-\overline{\mathbf{v}}(\boldsymbol{x}_p(t),t)\right]\nabla\mathbf{u}'(\boldsymbol{x}_p(t),t)\right\rangle d\mathbf{v}\end{aligned} \tag{D.17}$$

Then the filtering property of the fine-grained PDF $\mathcal{P}(\mathbf{x},\mathbf{v},t)$ can be used to replace the fluctuating particle velocity $\boldsymbol{v}_p'(t)=\boldsymbol{v}_p(t)-\overline{\mathbf{v}}(\boldsymbol{x}_p(t),t)$ with the fluctuating phase-space velocity $\mathbf{c}(\mathbf{x},t)=\mathbf{v}-\overline{\mathbf{v}}(\mathbf{x},t)$, which is deterministic. Further manipulation then yields

$$\begin{aligned}\left\langle \boldsymbol{v}_p'(t)\,\nabla\mathbf{u}'(\boldsymbol{x}_p(t),t)\right\rangle_{\mathbf{x}} &= \frac{1}{\rho(\mathbf{x},t)}\int_{\mathbf{v}}\left[\mathbf{v}-\overline{\mathbf{v}}(\mathbf{x},t)\right]\left\langle \mathcal{P}(\mathbf{x},\mathbf{v},t)\,\nabla\mathbf{u}'(\boldsymbol{x}_p(t),t)\right\rangle d\mathbf{v} \\ &= \frac{1}{\rho(\mathbf{x},t)}\int_{\mathbf{v}}\mathbf{c}(\mathbf{x},t)\,p(\mathbf{x},\mathbf{v},t)\left\langle \nabla\mathbf{u}'(\boldsymbol{x}_p(t),t)\right\rangle_{\mathbf{x},\mathbf{v}} d\mathbf{v} \\ &= \frac{1}{\rho(\mathbf{x},t)}\int_{\mathbf{v}}\mathbf{c}(\mathbf{x},t)\,p(\mathbf{x},\mathbf{v},t)\left\langle \nabla\mathbf{u}(\boldsymbol{x}_p(t),t)\right\rangle_{\mathbf{x},\mathbf{v}} d\mathbf{v} \\ &\quad -\frac{1}{\rho(\mathbf{x},t)}\int_{\mathbf{v}}\mathbf{c}(\mathbf{x},t)\,p(\mathbf{x},\mathbf{v},t)\,\overline{\nabla\mathbf{u}}(\boldsymbol{x}_p(t),t)\;d\mathbf{v}\end{aligned} \tag{D.18}$$

For the second term, it follows that

$$
\begin{aligned}
&\frac{1}{\rho\left(\mathbf{x},t\right)}\int_{\mathbf{v}}\mathbf{c}\left(\mathbf{x},t\right)p\left(\mathbf{x},\mathbf{v},t\right)\overline{\nabla\mathbf{u}}\left(\boldsymbol{x}_p(t),t\right)\,d\mathbf{v}\\
&=\overline{\nabla\mathbf{u}}\left(\boldsymbol{x}_p(t),t\right)\left[\frac{1}{\rho\left(\mathbf{x},t\right)}\int_{\mathbf{v}}\mathbf{v}p\left(\mathbf{x},\mathbf{v},t\right)\,d\mathbf{v}-\overline{\mathbf{v}}\left(\mathbf{x},t\right)\frac{1}{\rho\left(\mathbf{x},t\right)}\int_{\mathbf{v}}p\left(\mathbf{x},\mathbf{v},t\right)\,d\mathbf{v}\right]\\
&=\overline{\nabla\mathbf{u}}\left(\boldsymbol{x}_p(t),t\right)\left[\overline{\mathbf{v}}\left(\mathbf{x},t\right)-\overline{\mathbf{v}}\left(\mathbf{x},t\right)\right]\\
&=\mathbf{0}
\end{aligned}
$$

Thus the result for (D.18) reduces to

$$
\left\langle \boldsymbol{v}_p'\left(t\right)\nabla\mathbf{u}'\left(\boldsymbol{x}_p(t),t\right)\right\rangle_{\mathbf{x}}=\frac{1}{\rho\left(\mathbf{x},t\right)}\int_{\mathbf{v}}\mathbf{c}\left(\mathbf{x},t\right)p\left(\mathbf{x},\mathbf{v},t\right)\left\langle \nabla\mathbf{u}\left(\boldsymbol{x}_p(t),t\right)\right\rangle_{\mathbf{x},\mathbf{v}}d\mathbf{v} \tag{D.19}
$$

The average $p\left(\mathbf{x},\mathbf{v},t\right)\left\langle \nabla\mathbf{u}\left(\boldsymbol{x}_p(t),t\right)\right\rangle_{\mathbf{x},\mathbf{v}}$ is closed in Appendix D.1, and using the relevant result given by (D.14), (D.19) then accordingly becomes

$$
\begin{aligned}
&\left\langle v_{p_m}'\left(t\right)\frac{\partial \mathrm{u}_i}{\partial \mathrm{x}_l}'\left(\boldsymbol{x}_p(t),t\right)\right\rangle_{\mathbf{x}}\\
&=\underbrace{\frac{1}{\rho\left(\mathbf{x},t\right)}\int_{\mathbf{v}}\mathrm{c}_m\left(\mathbf{x},t\right)p\left(\mathbf{x},\mathbf{v},t\right)\left\langle\frac{\partial \mathrm{u}_i}{\partial \mathrm{x}_l}\left(\mathbf{x},t\right)\right\rangle d\mathbf{v}}_{①}\\
&\quad+\underbrace{\frac{1}{\rho\left(\mathbf{x},t\right)}\int_{\mathbf{v}}\mathrm{c}_m\left(\mathbf{x},t\right)\frac{1}{\beta}\int_{t_0}^{t}\left\langle\mathcal{H}_{kj}\left[t;t'\right]\frac{\partial^2}{\partial \mathrm{x}_l\partial \mathrm{x}_k}\mathrm{R}_{ji}(\boldsymbol{x}_p(t'),t';\mathbf{x},t)\right\rangle_{\mathbf{x},\mathbf{v}}dt'\,p\left(\mathbf{x},\mathbf{v},t\right)\,d\mathbf{v}}_{②}\\
&\quad-\underbrace{\frac{1}{\rho\left(\mathbf{x},t\right)}\int_{\mathbf{v}}\mathrm{c}_m\left(\mathbf{x},t\right)\frac{1}{\beta}\frac{\partial}{\partial \mathrm{x}_k}\left[\int_{t_0}^{t}\left\langle\mathcal{H}_{kj}\left[t;t'\right]\frac{\partial}{\partial \mathrm{x}_l}\mathrm{R}_{ji}(\boldsymbol{x}_p(t'),t';\mathbf{x},t)\right\rangle_{\mathbf{x},\mathbf{v}}dt'\,p\left(\mathbf{x},\mathbf{v},t\right)\right]d\mathbf{v}}_{③}\\
&\quad-\underbrace{\frac{1}{\rho\left(\mathbf{x},t\right)}\int_{\mathbf{v}}\mathrm{c}_m\left(\mathbf{x},t\right)\frac{1}{\beta}\frac{\partial}{\partial \mathrm{v}_k}\left[\int_{t_0}^{t}\left\langle\dot{\mathcal{H}}_{kj}\left[t;t'\right]\frac{\partial}{\partial \mathrm{x}_l}\mathrm{R}_{ji}(\boldsymbol{x}_p(t'),t';\mathbf{x},t)\right\rangle_{\mathbf{x},\mathbf{v}}dt'\,p\left(\mathbf{x},\mathbf{v},t\right)\right]d\mathbf{v}}_{④}
\end{aligned}
\tag{D.20}
$$

Where possible, evaluation of the separate integrals produces

①

$$
\begin{aligned}
&\frac{1}{\rho\left(\mathbf{x},t\right)}\int_{\mathbf{v}}\mathrm{c}_m\left(\mathbf{x},t\right)p\left(\mathbf{x},\mathbf{v},t\right)\left\langle\frac{\partial\mathrm{u}_i}{\partial\mathrm{x}_l}\left(\mathbf{x},t\right)\right\rangle\,d\mathbf{v}\\
&=\left\langle\frac{\partial\mathrm{u}_i}{\partial\mathrm{x}_l}\left(\mathbf{x},t\right)\right\rangle\left[\frac{1}{\rho\left(\mathbf{x},t\right)}\int_{\mathbf{v}}\mathrm{v}_m p\left(\mathbf{x},\mathbf{v},t\right)\,d\mathbf{v}-\overline{\mathrm{v}}_m\left(\mathbf{x},t\right)\frac{1}{\rho\left(\mathbf{x},t\right)}\int_{\mathbf{v}}p\left(\mathbf{x},\mathbf{v},t\right)\,d\mathbf{v}\right]\\
&=0
\end{aligned}
$$

③

$$
\begin{aligned}
&\frac{1}{\rho\left(\mathbf{x},t\right)}\int_{\mathbf{v}}\mathrm{c}_m\left(\mathbf{x},t\right)\frac{1}{\beta}\frac{\partial}{\partial\mathrm{x}_k}\left[\int_{t_0}^{t}\left\langle\mathcal{H}_{kj}\left[t;t'\right]\frac{\partial}{\partial\mathrm{x}_l}\mathrm{R}_{ji}(\boldsymbol{x}_p(t'),t';\mathbf{x},t)\right\rangle_{\mathbf{x},\mathbf{v}}dt'\,p\left(\mathbf{x},\mathbf{v},t\right)\right]\,d\mathbf{v}\\
&=\frac{1}{\beta}\frac{1}{\rho\left(\mathbf{x},t\right)}\int_{\mathbf{v}}\frac{\partial}{\partial\mathrm{x}_k}\left[\mathrm{c}_m\left(\mathbf{x},t\right)\int_{t_0}^{t}\left\langle\mathcal{H}_{kj}\left[t;t'\right]\frac{\partial}{\partial\mathrm{x}_l}\mathrm{R}_{ji}(\boldsymbol{x}_p(t'),t';\mathbf{x},t)\right\rangle_{\mathbf{x},\mathbf{v}}dt'\,p\left(\mathbf{x},\mathbf{v},t\right)\right]\,d\mathbf{v}\\
&\quad-\frac{1}{\beta}\frac{1}{\rho\left(\mathbf{x},t\right)}\int_{\mathbf{v}}\frac{\partial\mathrm{c}_m}{\partial\mathrm{x}_k}\left(\mathbf{x},t\right)\int_{t_0}^{t}\left\langle\mathcal{H}_{kj}\left[t;t'\right]\frac{\partial}{\partial\mathrm{x}_l}\mathrm{R}_{ji}(\boldsymbol{x}_p(t'),t';\mathbf{x},t)\right\rangle_{\mathbf{x},\mathbf{v}}dt'\,p\left(\mathbf{x},\mathbf{v},t\right)\,d\mathbf{v}\\
&=\frac{1}{\beta}\frac{1}{\rho\left(\mathbf{x},t\right)}\frac{\partial}{\partial\mathrm{x}_k}\left[\int_{\mathbf{v}}\mathrm{c}_m\left(\mathbf{x},t\right)\int_{t_0}^{t}\left\langle\mathcal{H}_{kj}\left[t;t'\right]\frac{\partial}{\partial\mathrm{x}_l}\mathrm{R}_{ji}(\boldsymbol{x}_p(t'),t';\mathbf{x},t)\right\rangle_{\mathbf{x},\mathbf{v}}dt'\,p\left(\mathbf{x},\mathbf{v},t\right)\,d\mathbf{v}\right]\\
&\quad-\frac{1}{\beta}\frac{\partial\overline{\mathrm{v}}_m}{\partial\mathrm{x}_k}\left(\mathbf{x},t\right)\int_{t_0}^{t}\left\langle\mathcal{H}_{kj}\left[t;t'\right]\frac{\partial}{\partial\mathrm{x}_l}\mathrm{R}_{ji}(\boldsymbol{x}_p(t'),t';\mathbf{x},t)\right\rangle_{\mathbf{x}}dt'
\end{aligned}
$$

④

$$
\begin{aligned}
&\frac{1}{\rho\left(\mathbf{x},t\right)}\int_{\mathbf{v}}\mathrm{c}_m\left(\mathbf{x},t\right)\frac{1}{\beta}\frac{\partial}{\partial \mathrm{v}_k}\left[\int_{t_0}^{t}\left\langle \dot{\mathcal{H}}_{kj}\left[t;t'\right]\frac{\partial}{\partial \mathrm{x}_l}\mathrm{R}_{ji}(\boldsymbol{x}_p(t'),t';\mathbf{x},t)\right\rangle_{\mathbf{x},\mathbf{v}} dt'\, p\left(\mathbf{x},\mathbf{v},t\right)\right] d\mathbf{v}\\
&=\frac{1}{\beta}\frac{1}{\rho\left(\mathbf{x},t\right)}\int_{\mathbf{v}}\frac{\partial}{\partial \mathrm{v}_k}\left[\mathrm{c}_m\left(\mathbf{x},t\right)\int_{t_0}^{t}\left\langle \dot{\mathcal{H}}_{kj}\left[t;t'\right]\frac{\partial}{\partial \mathrm{x}_l}\mathrm{R}_{ji}(\boldsymbol{x}_p(t'),t';\mathbf{x},t)\right\rangle_{\mathbf{x},\mathbf{v}} dt'\, p\left(\mathbf{x},\mathbf{v},t\right)\right] d\mathbf{v}\\
&\quad-\frac{1}{\beta}\frac{1}{\rho\left(\mathbf{x},t\right)}\int_{\mathbf{v}}\frac{\partial}{\partial \mathrm{v}_k}\left[\mathrm{c}_m\left(\mathbf{x},t\right)\right]\int_{t_0}^{t}\left\langle \dot{\mathcal{H}}_{kj}\left[t;t'\right]\frac{\partial}{\partial \mathrm{x}_l}\mathrm{R}_{ji}(\boldsymbol{x}_p(t'),t';\mathbf{x},t)\right\rangle_{\mathbf{x},\mathbf{v}} dt'\, p\left(\mathbf{x},\mathbf{v},t\right)\, d\mathbf{v}\\
&=\frac{1}{\beta}\frac{1}{\rho\left(\mathbf{x},t\right)}\left[\mathrm{c}_m\left(\mathbf{x},t\right)\int_{t_0}^{t}\left\langle \dot{\mathcal{H}}_{kj}\left[t;t'\right]\frac{\partial}{\partial \mathrm{x}_l}\mathrm{R}_{ji}(\boldsymbol{x}_p(t'),t';\mathbf{x},t)\right\rangle_{\mathbf{x},\mathbf{v}} dt'\, p\left(\mathbf{x},\mathbf{v},t\right)\right]_{\mathbf{v}=-\infty}^{\mathbf{v}=\infty}\\
&\quad-\frac{1}{\beta}\frac{1}{\rho\left(\mathbf{x},t\right)}\int_{\mathbf{v}}\delta_{mk}\int_{t_0}^{t}\left\langle \dot{\mathcal{H}}_{kj}\left[t;t'\right]\frac{\partial}{\partial \mathrm{x}_l}\mathrm{R}_{ji}(\boldsymbol{x}_p(t'),t';\mathbf{x},t)\right\rangle_{\mathbf{x},\mathbf{v}} dt'\, p\left(\mathbf{x},\mathbf{v},t\right)\, d\mathbf{v}\\
&=-\frac{1}{\beta}\int_{t_0}^{t}\left\langle \dot{\mathcal{H}}_{mj}\left[t;t'\right]\frac{\partial}{\partial \mathrm{x}_l}\mathrm{R}_{ji}(\boldsymbol{x}_p(t'),t';\mathbf{x},t)\right\rangle_{\mathbf{x}} dt'
\end{aligned}
$$

where in ④ the first term is equal to zero since $p\left(\mathbf{x},\mathbf{v},t\right)\to 0$ as $\mathbf{v}\to\pm\infty$. Using the results for ①, ③, and ④ in equation (D.20) yields the result

$$
\begin{aligned}
&\left\langle v_{p_m}'\left(t\right)\frac{\partial \mathrm{u}_i{}'}{\partial \mathrm{x}_l}\left(\boldsymbol{x}_p(t),t\right)\right\rangle_{\mathbf{x}}\\
&=\frac{1}{\beta}\frac{1}{\rho\left(\mathbf{x},t\right)}\int_{\mathbf{v}}\mathrm{c}_m\left(\mathbf{x},t\right)\int_{t_0}^{t}\left\langle \mathcal{H}_{kj}\left[t;t'\right]\frac{\partial^2}{\partial \mathrm{x}_l\partial \mathrm{x}_k}\mathrm{R}_{ji}(\boldsymbol{x}_p(t'),t';\mathbf{x},t)\right\rangle_{\mathbf{x},\mathbf{v}} dt'\, p\left(\mathbf{x},\mathbf{v},t\right)\, d\mathbf{v}\\
&\quad-\frac{1}{\beta}\frac{1}{\rho\left(\mathbf{x},t\right)}\frac{\partial}{\partial \mathrm{x}_k}\left[\int_{\mathbf{v}}\mathrm{c}_m\left(\mathbf{x},t\right)\int_{t_0}^{t}\left\langle \mathcal{H}_{kj}\left[t;t'\right]\frac{\partial}{\partial \mathrm{x}_l}\mathrm{R}_{ji}(\boldsymbol{x}_p(t'),t';\mathbf{x},t)\right\rangle_{\mathbf{x},\mathbf{v}} dt'\, p\left(\mathbf{x},\mathbf{v},t\right)\, d\mathbf{v}\right]\\
&\quad+\frac{1}{\beta}\frac{\partial \overline{\mathrm{v}}_m}{\partial \mathrm{x}_k}\left(\mathbf{x},t\right)\int_{t_0}^{t}\left\langle \mathcal{H}_{kj}\left[t;t'\right]\frac{\partial}{\partial \mathrm{x}_l}\mathrm{R}_{ji}(\boldsymbol{x}_p(t'),t';\mathbf{x},t)\right\rangle_{\mathbf{x}} dt'\\
&\quad+\frac{1}{\beta}\int_{t_0}^{t}\left\langle \dot{\mathcal{H}}_{mj}\left[t;t'\right]\frac{\partial}{\partial \mathrm{x}_l}\mathrm{R}_{ji}(\boldsymbol{x}_p(t'),t';\mathbf{x},t)\right\rangle_{\mathbf{x}} dt'
\end{aligned}
\tag{D.21}
$$

The corresponding velocity averaged version of this result is

$$\left\langle v_{p_m}'(t)\,\frac{\partial \mathrm{u}_i'}{\partial \mathrm{x}_l}(\boldsymbol{x}_p(t),t)\right\rangle_{\mathbf{x}} = \frac{1}{\beta}\frac{\partial \overline{\mathrm{v}}_m}{\partial \mathrm{x}_k}(\mathbf{x},t)\int_{t_0}^{t}\left\langle \mathcal{H}_{kj}[t;t']\,\frac{\partial}{\partial \mathrm{x}_l}\mathrm{R}_{ji}(\boldsymbol{x}_p(t'),t';\mathbf{x},t)\right\rangle_{\mathbf{x}} dt' + \frac{1}{\beta}\int_{t_0}^{t}\left\langle \dot{\mathcal{H}}_{mj}[t;t']\,\frac{\partial}{\partial \mathrm{x}_l}\mathrm{R}_{ji}(\boldsymbol{x}_p(t'),t';\mathbf{x},t)\right\rangle_{\mathbf{x}} dt' \tag{D.22}$$

where the integral result for ① is used in which the velocity averaged value of $\mathbf{c}(\mathbf{x},t)$ is zero. In the case of a homogeneous fluid velocity field, this result reduces further to

$$\left\langle v_{p_m}'(t)\,\frac{\partial \mathrm{u}_i'}{\partial \mathrm{x}_l}(\boldsymbol{x}_p(t),t)\right\rangle = \frac{1}{\beta}\int_{t_0}^{t}\left\langle \dot{\mathcal{H}}_{mj}[t;t']\,\frac{\partial}{\partial \mathrm{x}_l}\mathrm{R}_{ji}(\boldsymbol{x}_p(t'),t';\mathbf{x},t)\right\rangle dt' \tag{D.23}$$

This then provides an expression for $\langle \boldsymbol{v}_p'(t)\,\nabla\mathbf{u}'(\boldsymbol{x}_p(t),t)\rangle$ in terms of a dispersion tensor consisting of the standard particle response tensor derivative $\dot{\boldsymbol{\mathcal{H}}}[t;t']$ and two-point two-time correlation tensor $\mathbf{R}(\boldsymbol{x}_p(t'),t';\mathbf{x},t)$ which arise in the PDF kinetic framework.

D.2.1 Closure Consistent with the LHA for the case of Gravitational Settling

Using the result (D.23) and taking the Green's function approximation to $\boldsymbol{\mathcal{H}}[t;t']$ given in (4.65) such that

$$\dot{\boldsymbol{\mathcal{H}}}[t;t'] \approx \dot{\mathbf{H}}[t;t'] = \dot{h}(t,t')\mathbf{I} = \exp\big[-\beta(t-t')\big]\mathbf{I}$$

reduces the closure required to

$$\left\langle v_{p_m}'(t)\,\frac{\partial \mathrm{u}_i'}{\partial \mathrm{x}_l}(\boldsymbol{x}_p(t),t)\right\rangle \approx \frac{1}{\beta}\int_{t_0}^{t}\exp\big[-\beta(t-t')\big]\left\langle \frac{\partial}{\partial \mathrm{x}_l}\mathrm{R}_{mi}(\boldsymbol{x}_p(t'),t';\mathbf{x},t)\right\rangle dt' \tag{D.24}$$

To close this average, in the case of gravitational settling in an isotropic flow, the separation along a particle trajectory can be approximated as $\boldsymbol{r}_p(t';t) \approx \mathbf{r}_0(t';t) = \mathbf{V}_g(t-t')$ as given by (6.63). Then using the approximation

$$\left\langle \frac{\partial}{\partial \mathrm{x}_l}\mathrm{R}_{mi}(\boldsymbol{r}_p)\right\rangle \approx \frac{\partial}{\partial \mathrm{x}_l}\mathrm{R}_{mi}\big(\mathbf{r}_0(t';t)\big)$$

as in (6.64) where the isotropic form of $\frac{\partial}{\partial \mathrm{x}_l}\mathrm{R}_{mi}\big(\mathbf{r}, t-t'\big)\big)$ is given by (C.16) with only the leading order terms in time considered in this case, and further consistent with the LHA replacing the temporal decorrelation function $\mathrm{E}_\omega(t-t')$ with the exponential decorrelation $\exp\big[-1/\tau_{Lp}(t-t')\big]$ produces the closure

$$\left\langle \frac{\partial}{\partial \mathrm{x}_l}\mathrm{R}_{mi}(\boldsymbol{x}_p(t'), t'; \mathbf{x}, t)\right\rangle \approx \frac{1}{d-1}\beta^2 u'^2\sigma_k^2\Big[V_{g_m}\delta_{li} + V_{g_i}\delta_{ml} - (d+1)V_{g_l}\delta_{mi}\Big] \cdot (t-t')\exp\left[-\frac{1}{\tau_{Lp}}(t-t')\right] \tag{D.25}$$

Substitution into (D.24) yields

$$\left\langle v_{p_m}'(t)\frac{\partial \mathrm{u}_i{}'}{\partial \mathrm{x}_l}(\boldsymbol{x}_p(t), t)\right\rangle \approx \frac{1}{d-1}\beta u'^2\sigma_k^2\Big[V_{g_m}\delta_{li} + V_{g_i}\delta_{ml} - (d+1)V_{g_l}\delta_{mi}\Big] \cdot \int_{t_0}^{t}(t-t')\exp\big[-\beta(t-t')\big]\exp\left[-\frac{1}{\tau_{Lp}}(t-t')\right]dt' \tag{D.26}$$

Evaluation of the time integral is tractable due to the use of an exponential decorrelation function, and then taking the limit $t \to \infty$ to obtain the steady-state value finally yields

$$\left\langle v_{p_m}'(t)\frac{\partial \mathrm{u}_i{}'}{\partial \mathrm{x}_l}(\boldsymbol{x}_p(t), t)\right\rangle \approx \frac{1}{d-1}\frac{1}{\beta(1+St_{Lp})^2}u'^2\sigma_k^2\Big[V_{g_m}\delta_{li} + V_{g_i}\delta_{ml} - (d+1)V_{g_l}\delta_{mi}\Big] \tag{D.27}$$

Thus this provides a model for the one-time correlation $\big\langle \boldsymbol{v}_p'(t)\,\nabla\mathbf{u}'(\boldsymbol{x}_p(t), t)\big\rangle$ that direct use of an isotropic assumption for the two-time correlation $\big\langle \boldsymbol{v}_p'(t')\,\nabla\mathbf{u}'(\boldsymbol{x}_p(t), t)\big\rangle$ fails to extract. The approach outlined here can then be used as a basis for modelling these two-time correlations in conjunction with a suitable time decorrelation function $\psi(t-t')$ such that

$$\Big\langle \boldsymbol{v}_p'(t')\,\nabla\mathbf{u}'(\boldsymbol{x}_p(t), t)\Big\rangle \approx \Big\langle \boldsymbol{v}_p'(t)\,\nabla\mathbf{u}'(\boldsymbol{x}_p(t), t)\Big\rangle\psi(t-t')$$

Appendix E

Stability Analysis of the Four-step Explicit Adams-Bashforth Method for the Response Tensor Governing Equation

The general form of a multistep method for numerical solution of the first order system $\dot{Y}_{kl} = f_{kl}(\boldsymbol{Y})$ can be written as [22]

$$Y_{kl}^{(t)} = \sum_{j=1}^{n} \alpha_j Y_{kl}^{(t+1-j)} + \sum_{j=0}^{n} h\beta_j f_{kl}^{(t+1-j)} \tag{E.1}$$

where (t) denotes a discrete time point, and h is the timestep for the numerical method. For the system form $\boldsymbol{\mathcal{G}}[t;t']$ of the response tensor in the case of Stokes drag law, the governing equation is given in (5.31) by

$$\mathcal{G}_{kl}[t;t'] = M_{kr}(t)\mathcal{G}_{rl}[t;t'] \quad , \quad \boldsymbol{M}(t) = \begin{bmatrix} \mathbf{0} & \mathbf{I} \\ \beta\nabla\mathbf{u}^{\top}(\boldsymbol{x}_p(t),t) & -\beta\mathbf{I} \end{bmatrix} \tag{E.2}$$

Further, in the case of the four-step explicit Adams-Bashforth method given by (5.28), the coefficients for (E.1) with $n = 4$ are

$$\alpha_1 = 1\,,\ \alpha_2 = \alpha_3 = \alpha_4 = 0 \tag{E.3}$$

$$\beta_0 = 0\,,\ \beta_1 = \frac{55}{24}\,,\ \beta_2 = -\frac{59}{24}\,,\ \beta_3 = \frac{37}{24}\,,\ \beta_4 = -\frac{9}{24} \tag{E.4}$$

This produces the difference equation with constant coefficients

$$\mathcal{G}_{kl}^{(t+1)} - \left[\delta_{kr} + \frac{55}{24}hM_{kr}\right]\mathcal{G}_{rl}^{(t)} + \frac{59}{24}hM_{kr}\mathcal{G}_{rl}^{(t-1)} - \frac{37}{24}hM_{kr}\mathcal{G}_{rl}^{(t-2)} + \frac{9}{24}hM_{kr}\mathcal{G}_{rl}^{(t-3)} = 0 \tag{E.5}$$

To analyse this equation, it is useful to set $\mathcal{G}_{kl}^{(t)} = z^i\delta_{kl}$ where i is interpreted as an exponent acting upon z. This results in

$$z^{i+1}\delta_{kl} - \left[\delta_{kl} + \frac{55}{24}hM_{kl}\right]z^i + \frac{59}{24}hM_{kl}z^{i-1} - \frac{37}{24}hM_{kl}z^{i-2} + \frac{9}{24}hM_{kl}z^{i-3} = 0 \tag{E.6}$$

To obtain the stability polynomial for AB4 in the case of the linear system (E.2), this equation is divided by $z^{i+1-n} = z^{i-3}$

$$z^4\delta_{kl} - \left[\delta_{kl} + \frac{55}{24}hM_{kl}\right]z^3 + \frac{59}{24}hM_{kl}z^2 - \frac{37}{24}hM_{kl}z + \frac{9}{24}hM_{kl} = 0 \tag{E.7}$$

The solution of this stability polynomial for the timestep h yields

$$h = \frac{-z^4\delta_{kl} + z^3\delta_{kl}}{-\frac{55}{24}M_{kl}z^3 + \frac{59}{24}M_{kl}z^2 - \frac{37}{24}M_{kl}z + \frac{9}{24}M_{kl}} \tag{E.8}$$

The stability of (E.7) is ensured if $|z| < 1$ [22], therefore evaluating (E.8) for $z = \pm 1$ will give the limiting values of the timestep size h

$$z = 1 \quad \Rightarrow \quad h = 0 \tag{E.9}$$

$$z = -1 \quad \Rightarrow \quad h = \frac{-3\delta_{kl}}{10M_{kl}} \tag{E.10}$$

Thus $z = -1$ determines the timestep constraint in this case. Moreover, the limiting factor on timestep size will be the component of $\boldsymbol{M}$ in (E.2), as given by

$\{\mathbf{0}, \mathbf{I}, \beta\nabla\mathbf{u}^\top(\boldsymbol{x}_p(t), t), -\beta\mathbf{I}\}$, which has the largest magnitude. Therefore neglecting the constant blocks $\mathbf{0}$ and $\mathbf{I}$, the constraint that exists on the timestep size for the components of $\boldsymbol{M}$ is given by $M_{kl} = -\max\left(\beta, \beta|\boldsymbol{\nabla}\mathbf{u}^\top(\boldsymbol{x}_p(t), t)|\right)$. Thus this specifies the final condition on the timestep size h in order for the numerical solution of AB4 to remain stable for the system (E.2) as

$$h < \frac{3}{10\ \max\left(\beta, \beta|\boldsymbol{\nabla}\mathbf{u}^\top(\boldsymbol{x}_p(t), t)|\right)} \tag{E.11}$$

which is the result given in (5.32).